École Doctorale
des Sciences de la Vie
et de la Santé
STRASBOURG

Université
de Strasbourg

UNIVERSITE DE STRASBOURG

ÉCOLE DOCTORALE 414-Sciences de la vie et de la santé

INSERM UMR_S1109-Equipe Tumor Biomechanics

THÈSE présentée par

Benjamin MARY

Soutenue le : **20 décembre 2022**

Pour obtenir le grade de : **Docteur de l'Université de Strasbourg**

Discipline : Science de la Vie et de la Santé

Spécialité : Aspect moléculaire et cellulaires de la biologie

Dissecting the impact of hemodynamic forces in uptake, fate and function of circulating tumor extracellular vesicles.

Membres du Jury :

Rapporteur : **Chantal BOULANGER, DR, INSERM U970, Paris**

Rapporteur : **Cécile GAUTHIER-ROUVIÈRE, DR, INSERM UMR5237, Montpellier**

Examinateur : **Catherine STRASSEL, DR, INSERM U1255, Université de Strasbourg**

Examinateur : **Julien SAINT-POL, MCU, Université Jean Perrin, Lens**

Directeur de thèse : **Jacky GOETZ, DR, INSERM U1109, Université de Strasbourg**

Co-superviseur : **Vincent HYENNE, CR, INSERM U1109, Université de Strasbourg**

Table of Contents

Acknowledgments

First, I would like to thank Catherine STRASSEL, Julien SAINT-POL, Chantal BOULANGER and Cécile GAUTHIER-ROUVIERE for having accepted to be part of my thesis jury and review the work I have done during my PhD.
I am grateful to the FRM (Fondation pour la Recherche Médicale) for the fourth-year grant that enabled me to finish my PhD in good conditions.

As one might know, a PhD is not an easy journey. Throughout this adventure I had the opportunity to count on the support of several people that helped me to go through this difficult time and achieve my goal.

I would like to thank Shima and Gautier, who guided my first steps in the amazing worlds of extracellular vesicles and microfluidics.
I am grateful for all the help and support that Nandini gave me these past few years and without whom I would not have been able to do this work.
I thank Katka for her amazing help these last months as well as her support and advice on image analysis.

Je remercie tous les membres de mon équipe qui ont toujours répondu présent lorsque j'avais besoin d'eux, de leurs conseils ainsi que de leur soutien. Merci Olivier, Florent, Naël, Valentin, Amandine, Vincent, Marina et Maria. Je voudrais remercier particulièrement Annabel qui a été une collègue précieuse. Elle m'a non seulement aidé continuellement ces trois dernières années dans mon travail mais l'a également rendu plus agréable au quotidien par son humour et sa personnalité.

Je remercie Jacky d'avoir été un directeur de thèse inspirant en tous point et qui restera toujours un modèle scientifique pour moi.

Tout particulièrement, je voudrais remercier Vincent, qui a été un superviseur formidable, qui m'a toujours soutenu et m'a aidé à reprendre confiance en moi lors de périodes de doutes.

Je suis éternellement reconnaissant envers mes parents, mon père Frédéric, ma mère Corinne ainsi que ma famille, pour m'avoir soutenu moralement et pour toutes leurs attentions durant cette période compliquée que peut être la thèse.

Je remercie mes grands-parents qui, tous, par des manières différentes, m'ont permis d'en arriver là aujourd'hui. J'essaye d'appliquer leurs enseignements et leurs philosophies au quotidien et j'espère qu'ils sont fiers de moi.

Enfin je remercie Alev, mon amour, sans qui rien de tout cela n'aurait été possible, qui me soutient et me supporte chaque jour, qui me permet de ne pas baisser les bras et de continuer à croire en moi.

Merci.

Résumé de thèse en français

Titre en français :
Disséquer l'impact des forces hémodynamiques dans l'internalisation, le destin et la fonction des vésicules extracellulaires tumorales circulantes.

Les **vésicules extracellulaires (VEs)** sont de petites vésicules composées d'une bicouche lipidique d'origine membranaire qui peuvent être sécrétées par n'importe quelle cellule. Elles sont présentes dans tous les fluides corporels (sang, lymphe, urine, fluide cérébrospinal etc) ce qui leur permet de se disséminer à travers tout l'organisme. Ce sont des acteurs importants de la communication intercellulaire autocrine, paracrine et endocrine. Elles transportent différents messagers (ARNm, ARN non-codants, protéines, lipides) qui se transmettent et modifient le phénotype des cellules réceptrice (van Niel et al., 2018; Zomer et al., 2016, 2015). Elles régulent de nombreux processus physiologiques tels : le développement (Gross et al., 2012; Krause et al., 2018), l'immunité (Buzas, 2022; Lundberg et al., 2016; Théry et al., 2002), la physiologie (Whitham et al., 2018); mais également pathologiques tels : les maladies cardiovasculaires (Boulanger et al., 2017), les maladies neurologiques (Ruan et al., 2021; Sardar Sinha et al., 2018) et le cancer (Peinado et al., 2012).

Plus spécifiquement dans le cadre du cancer, il a été montré que les **vésicules extracellulaires (VEs) tumorales** sont sécrétées en plus grandes quantité par les cellules tumorales et sont présentes en abondance dans le sang des patients. Elles exercent principalement des fonctions pro-tumorales localement et peuvent également favoriser **le développement des métastases** en modifiant les **cellules stromales** et **le microenvironnement** à distance de la tumeur primaire. Elle favorisent l'apparition de ce qui est appelé une **niche pré-métastatique** : un site favorable à l'établissement de foyers secondaires (Costa-Silva et al., 2015; Ghoroghi et al., 2021; Hoshino et al., 2015; Peinado et al., 2017).

Malgré leur importance et leur abondance dans la circulation, les études réalisées jusqu'ici sur les vésicules extracellulaires tumorales n'ont que très rarement pris en compte le **caractère dynamique de l'environnement dans lequel elles évoluent**, à savoir le système vasculaire. C'est pourquoi, la compréhension de leur **comportement hémodynamique** et leur **mécanisme d'action dans le système vasculaire** ainsi que dans la progression métastatique restent limitée.

Ainsi, mon projet a eu pour objectif (1) **d'étudier l'impact des forces hémodynamiques**, sur **l'internalisation** des VEs tumorales par l'endothélium ; (2) **d'identifier les mécanismes contrôlant l'internalisation** des VE tumorales circulantes ; (3) d'étudier l'impact des forces hémodynamiques sur le **destin des VE internalisées** et (4) de caractériser **l'effet des VE tumorales circulantes sur l'endothélium.** Afin d'étudier ces processus, j'ai utilisé et adaptés deux modèles complémentaires, l'embryon de **poisson zèbre** (Hyenne et al., 2019) et une approche **microfluidique** (Follain et al., 2018). Ces modèles permettent d'étudier le comportement des VEs dans des conditions dynamiques et physiopathologiques pertinentes *in vivo* et *in vitro*.

Ces deux modèles nous ont permis d'identifier qu'une **vitesse de flux modérée**, correspondant à la vitesse du flux sanguin mesurée dans les lits capillaires (400µm/s), **favorise l'internalisation des vésicules tumorales par les cellules endothéliales**. *In vitro* et *in vivo*, nous avons pu mettre en évidence qu'une absence ou une diminution de la vitesse de flux, respectivement, **diminue significativement l'internalisation des VE** par les cellules endothéliales. Ces résultats suggèrent que la **capacité d'internalisation des VE tumorales** par l'endothélium est, au moins en partie, contrôlés par les contraintes mécaniques auxquelles ils sont soumis. Par ailleurs, nos résultats suggèrent qu'une voie d'endocytose à elle seule ne contrôle pas l'internalisation des vésicules tumorales circulantes mais que, plus probablement, plusieurs mécanismes rentrent en jeu. À titre d'exemple, dans une étude publiée récemment à laquelle j'ai participé (Ghoroghi et al., 2021), nous avons pu mettre en évidence que l'internalisation de VE tumorales est en partie contrôlée par les **molécules d'adhésion à la surface des VEs (CD146)**.

Par ailleurs, nous avons découvert que la présence de **forces hémodynamiques modérées** entraine **l'activation de voies lysosomales** au niveau transcriptionnel dans les **cellules endothéliales** mais également que ces forces **redirige partiellement les vésicules tumorales** internalisées par les cellules endothéliales vers des **compartiments moins acides et potentiellement moins dégradatifs**. Dans leur ensemble, ces résultats suggèrent qu'un flux modéré affecte le destin et le **trafic des VE tumorales internalisées** par l'endothelium. Finalement, des expériences de **séquençage d'ARN** nous ont permis de mettre en évidence que les vésicules tumorales circulantes déclenchent **une réponse pro-angiogénique**

dans ces cellules stimulées par un flux modéré et nous avons confirmé **l'activité pro-angiogénique** de ces VE tumorales dans le modèle du poisson zèbre.

Nos travaux ont permis de démontrer l'importance de l'environnement hémodynamique dans l'**internalisation**, le **trafic** au sein des cellules réceptrices ainsi que la **fonction des vésicules extracellulaires tumorales circulantes**. Bien que certains des mécanismes identifiés nécessitent davantage d'investigations pour mieux comprendre leur fonctionnement complet, nos travaux permettent de mettre en avant le rôle primordial du **flux** dans le comportement de ces **vésicules tumorales circulantes** et **la progression tumorale**. Ce travail, associant l'étude de **forces biomécaniques** et de vésicules extracellulaires pourrait permettre une meilleure compréhension des **mécanismes pro-métastatiques des VE tumorales circulantes** et de leur capacité à favoriser **l'apparition de niche pré-métastatique à distance de leur site de sécrétion**. De façon similaire il pourrait permettre dans le futur d'examiner plus attentivement le rôle des forces hémodynamiques dans **d'autres processus physiopathologiques** régulées par les vésicules extracellulaires et notamment les **maladies cardiovasculaires**.

Ces données, représentant mon projet principal de thèse, sont présentés en détails dans cette thèse, leurs implications, leurs limitations et leur futur développement sont également discutés. Elles font l'objet d'un **manuscrit en cours d'écriture**, intitulé « **Blood flow diverts extracellular vesicles from endothelial degradative compartments to promotes angiogenesis**». Certaines données discutées dans cette thèse proviennent également, d'un autre travail auquel j'ai participé en tant que deuxième auteur, intitulé "**Ral GTPases promote breast cancer metastasis by controlling biogenesis and organ targeting of exosomes**", Ghoroghi, S. *et al. eLife* **10**, e61539 (2021), et d'un chapitre chapitre méthodologique intitulé "**Live tracking of extracellular vesicles in larval zebrafish**", Mary, B., Ghoroghi, S., Hyenne, V. & Goetz, J. G. *Methods in Enzymology* vol. 645 243–275 (Elsevier, 2020) que j'ai rédigé.

Abbreviations

ABCB1: ATP-binding cassette subfamily B member 1
ADAMs: a disintegrin and metalloproteinase
Angpt: Angiopoietin
APC: Antigen Presenting Cells
ARF6: ADP Ribosylation Factor 6
ARRDC1: Arrestin Domain Containing 1
Atg: Autophagy related
ATP: Adenosine triphosphate
BMSCs: Bone marrow-derived Mesenchymal Stromal/Stem Cells
CAF: Cancer Associated Fibroblast
CAM: Cell adhesion molecules
CCL: CC-chemokine ligand
CD: Cluster of Differentiation
CHMP4: Charged Multivesicular Body Protein 4
circRNA: circular RNA
CLEM: Correlative Light and Electron Microscopy
CRP: C-Reactive Protein
CTC: Circulating Tumor Cells
DC: Dendritic cells
DNA: Deoxyribonucleic Acid
DU: Differential Ultracentrifugation
ECM: Extracellular Matrix
EGFR: Epidermal Growth Factor Receptor
EGR1: Early Growth Response-1
EIPA: 5-(N-ethyl-N-isopropyl) amiloride
EMT: Epithelial-to-Mesenchymal Transition
ENDS: Elongated Neutrophil-derived Structures
ER: Endoplasmic Reticulum
EpCam: Epithelial cellular adhesion molecule
EPI: ExoDx Prostate IntelliScore
ERK1/2: Extracellular signal-regulated protein kinase 1/2
ESCRT: Endosomal Sorting Complexes Required for Transport
EVs: Extracellular Vesicles
EX: exosome
FGF: Fibroblast Growth Factor
HIV: Human Immunodeficiency Virus
HLECs: Human Lymphatic Endothelial Cells
hnRNPA2B1: Heterogeneous Nuclear Ribonucleoprotein A2/B1
HSPC: Hematopoietic stem and progenitor cell
ICAM-1: Intercelullar Adhesion Molecules 1
IFN: Interferon

IFNAR1: Interferon Alpha and Beta Receptor Subunit 1
IFP: Interstitial Fluid Pressure
IL-: Interleukin-
ILVs: Intraluminal Vesicles
ITG: Integrins
KLF: Krueppel-like Factor
LBPA: lysobiphosphatidic acid
LEC: Lymphatic Endothelial Cells
LN: Lymph Nodes
LPS: Lipopolysaccharide
MCAM: Melanoma Cell Adhesion Molecule
MDSC: Myeloid-derived Suppressor Cells
MFSD2a: Major Facilitator Superfamily Domain containing protein 2a
MHC: Major Histocompatibility Complex
miRNA: MicroRNA
MMP: Matrix Metalloproteinases
mRNA: messenger RNA
MT1-MMP: membrane-type 1 matrix metalloproteinase
MV: Microvesicle
MVB: Multivesicular Bodies
ncRNA: Noncoding RNA
NF-κB: Nuclear Factor Kappa B
NK: Natural Killer
NP: Nanoparticles
nSMase2: Neutral Sphingomyelinase 2
NTA: Nanoparticle Tracking Analysis
PA: Phosphatidic Acid
PC: Phosphatidylcholine
PDGF: Platelet-derived growth factor
PDL-1: Programmed Death-ligand 1
PE: Phosphatidylethanolamine
PECAM-1: Platelet endothelial cell adhesion molecule-1
PI: Phosphatidylinositol
PI3K: Phosphoinositide 3-kinase
PIEZO-1: Piezo Type Mechanosensitive Ion Channel Component 1
piRNA: Piwi-interacting RNA
PM: Plasma Membrane
PMN: Pre-metastatic Niche
PS: Phosphatidylserine
PSGL-1: P-selectin Glycoprotein Ligand-1
PTEN: Phosphatase and Tensin homolog
RBCEV: Red Blood Cells EV
RNA: Ribonucleic Acid
SEC: Size Exclusion Chromatography

Shh: Sonic Hedgehog
Slco2a1: Solute Carrier Organic Anion Transporter Family Member 2A1
siRNA: Small interfering RNA
SIRT: Sirtuin
SMase: Sphingomyelinases
SNAP23: Synaptosome Associated Protein 23
STAM1/2: Signal-transducing Adaptor Molecule
STAT3: Signal Transducer and Activator of Transcription 3
SYNCRIP: Synaptotagmin Binding Cytoplasmic RNA Interacting Protein
TAM: Tumor-associated Macrophages
tEV: tumor Extracellular Vesicles
TGF-β: Transforming growth factor beta
TLR: Toll-like Receptor
TME: Tumor Microenvironment
TMPs: T cell Microvilli Particles
TNF: Tumor Necrosis Factor
TNFAIP3: TNF Alpha Induced Protein 3
TNFR: Tumor Necrosis Factor Receptor
TRAIL: TNF-related apoptosis-inducing ligands
Treg: Regulatory T
TSG101: Tumor Susceptibility 101
TSPAN: Tetraspanin
VEGF: Vascular Endothelial Growth Factor
VPS: Vacuolar Protein Sorting-associated Protein
VSVG: Vesicular Stomatitis Virus G
VTA1: Vesicle Trafficking 1
WB: Western Blot
YBX1: Y-Box Binding Protein 1

INTRODUCTION

These last decades an increasing number of studies focused on a complex, yet fascinating field of cellular biology, the extracellular vesicles (EVs). They participated to an exponential rise of knowledge about these small vesicles secreted by all cells which act as intercellular messenger. **EVs play role in a plethora of physiological and pathological processes**. In the **first part of my introduction** I will give key examples in which EVs play a critical role in normal as well as pathological situations while focusing at most on long distance effect. Then I will more particularly focus on **cancer** as EVs were shown, not only to be a major actor of intercellular communications in this disease but also to actively participate to the metastatic cascade by delivering their message to distant sites. I will present key examples of their involvement in cancer progression at local as well as distant scale. I will then present what is known about their **secretion, dissemination, uptake and message delivery mechanisms (Part 2)**.

Throughout this journey, the dissemination step via body fluids, notably through blood, is not well understood. Additionally, comprehension of uptake and message delivery mechanisms is also very fragmented. More particularly, the role of **fluidic forces** at work in cardiovascular systems was never investigate in tumor EVs (tEVs) dissemination, uptake and intracellular fate. It is the main subject of my PhD work that I will present in this manuscript. Better comprehension of this biophysical parameter in tEVs biology could help to better characterize their behavior in dynamic environments (**Part 3**). This knowledge could benefit for various field of research as they are involved in many biological phenomenon. More particularly it can help to better understand tEVs-mediated metastatic progression mechanisms and potentially help to unraveled new therapeutic avenues to treat cancer as well.

1. Functional role of EVs in physiology and pathology

1.1. EVs as inter-cell/inter-organ communication mediators

Coordinated communication between cells and between organs is the basis of multicellular organisms' homeostasis maintenance. Evolution gave rise to different mechanisms allowing intercellular and inter-organ interactions. In these mechanisms most of the time, secreted chemical molecules (such as proteins and hormones) act as messengers between cells. To simplify, they bind to their receptors on cell surface and trigger downstream signaling cascades potentially leading to changes in genes expression, cell phenotype and in some cases, modifying organ activity. Autocrine, juxtacrine, paracrine and endocrine signaling are the main processes enabling cells and organs to communicate with each other (**Figure 1**) (Singh and Harris, 2005; Sporn and Roberts, 1985). Autocrine, juxtacrine and paracrine signaling participate to short- and medium range communication, while endocrine signaling is involved in long range communication. Autocrine signaling describes an auto-activation of a cell by its own molecules secreted in the extracellular space and acting on its own membrane receptors (*e.g.* IL-1 and monocytes) (Sporn and Roberts, 1985; Toda et al., 2002). Juxtacrine signalization occurs through cell-cell direct contacts through membrane proteins and junctions (*e.g.* some growth factors) (Anklesaria et al., 1990). Paracrine communication is a mechanism in which secreted molecules can diffuse locally, forming a gradient and affecting neighboring cells at short- and mid- distance (*e.g.* retinoic acid and neurotransmitters) (Molotkov et al., 2006). Finally, endocrine signaling allows the long-range communication between organs. For instance, through this process, hormones travel via body fluids and mediate inter-organ communication. However, long-distance messengers must be adapted to undergo this hazardous journey and avoid degradation/elimination from the body. For example, lipophilic messengers (e.g. cholesterol-derived hormones, eicosanoid acids) must associate with apolipoproteins to solubilize in body fluids and disseminate through the body. In this context, in addition to chemical messengers, previously identified extracellular vesicles (EVs), recently emerged as another important messenger in short- to long-range inter-cellular and even inter-organism communications (Bittel et al., 2021; Thomou et al., 2017).

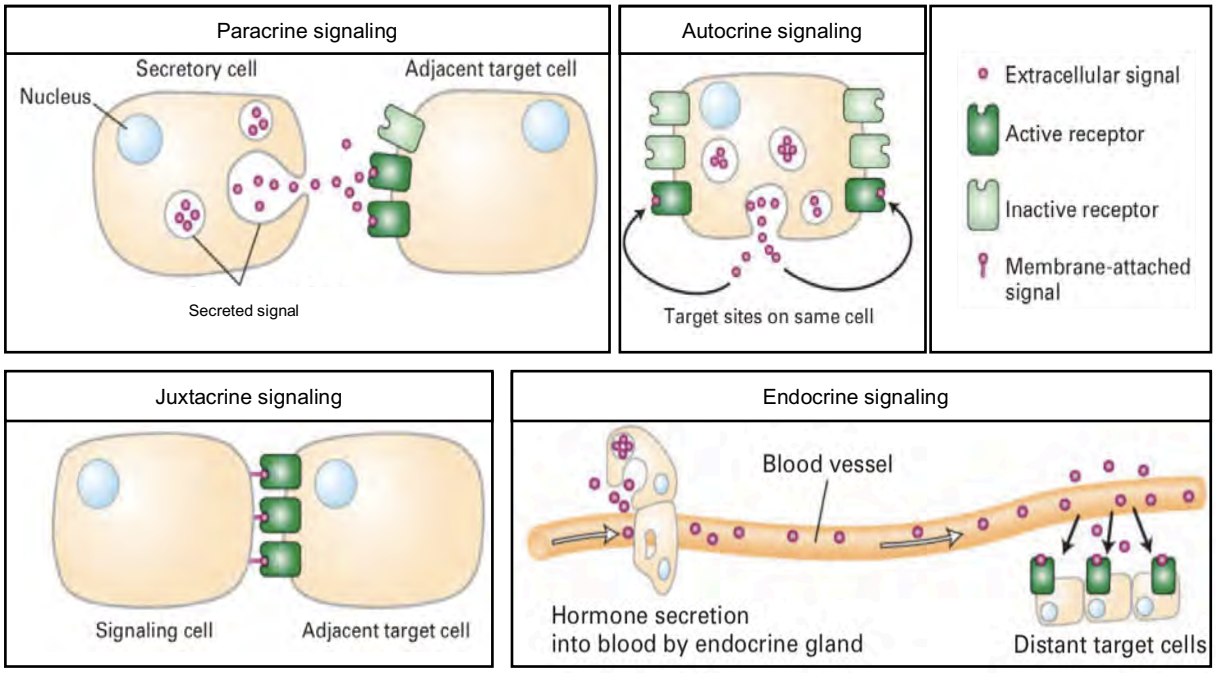

Figure1: The main cell-cell signaling pathways. Paracrine signaling defines exchanges of secreted material between adjacent cells. Autocrine signaling defines auto-activation of a cell with its own secreted material. Juxtacrine signaling defines receptor-ligand based communication between adjacent cells. Endocrine signaling defines dissemination of secreted material through the vascular system between distant cells. Juxtacrine and autocrine signaling occur a short-range, paracrine signaling occurs at short to medium-range (few micrometers), and endocrine signaling occurs at long-range (up to several meters). Adapted from Lodish, Berk, Kaiser, Krieger, Bretscher, Ploegh, Amon, Martin, Molecular Cell Biology 8th edition; W. H. Freeman, 2016.

Extracellular vesicles were observed for the first time more than fifty years ago, and “exosomes” were described 10 years later. However, it is only these last two decades that the multiple functions of extracellular vesicles were more thoroughly investigated (Witwer and Théry, 2019). The capacity to secrete EVs is a common feature shared by all living organisms, from bacteria to eukaryotes and archaea (Toyofuku et al., 2019; Woith et al., 2019). From what we know, EVs can be secreted by all kind of cells, found in all body fluids in human (blood, lymph, urine, cerebrospinal fluids, milk) (García-Silva et al., 2019; Lässer et al., 2011; Norouzi-Barough et al., 2020; Rikkert et al., 2020; Saugstad et al., 2017) and isolated form different ecosystems (Biller et al., 2014; Moros et al., 2021; Schatz and Vardi, 2018) and even found in dust (Dinh et al., 2020).

In 2018, the MISEVs2018 guidelines (Théry et al., 2018) defined EVs as “particles naturally released from the cell that are delimited by a lipid bilayer and cannot replicate, i.e. do not contain a functional nucleus”. This definition includes a variety of particle subpopulations from different cellular origins delimited by lipidic membrane identified during the past decades. They are separated into two families

based on their biogenesis pathways: exosomes, vesicles originating from endosomal origin, and ectosomes (or microvesicles), vesicles coming from the plasma membrane (PM). This second family includes multiple types of vesicles such as exosphere, oncosomes, apoptotic bodies etc.…that will not be discussed in detail here (**Figure 2**). The biogenesis pathway of these two families, their regulation and the composition of different EVs subpopulations will be discussed in more detail later in section **3**. As the EVs community recommends it, the general term “EVs” will be used here to refer to these vesicles, even though some studies cited and discussed here used other terms in their work. This generic term is used to avoid overstatement on the nature of the EVs subpopulation studied which is sometimes difficult to assess.

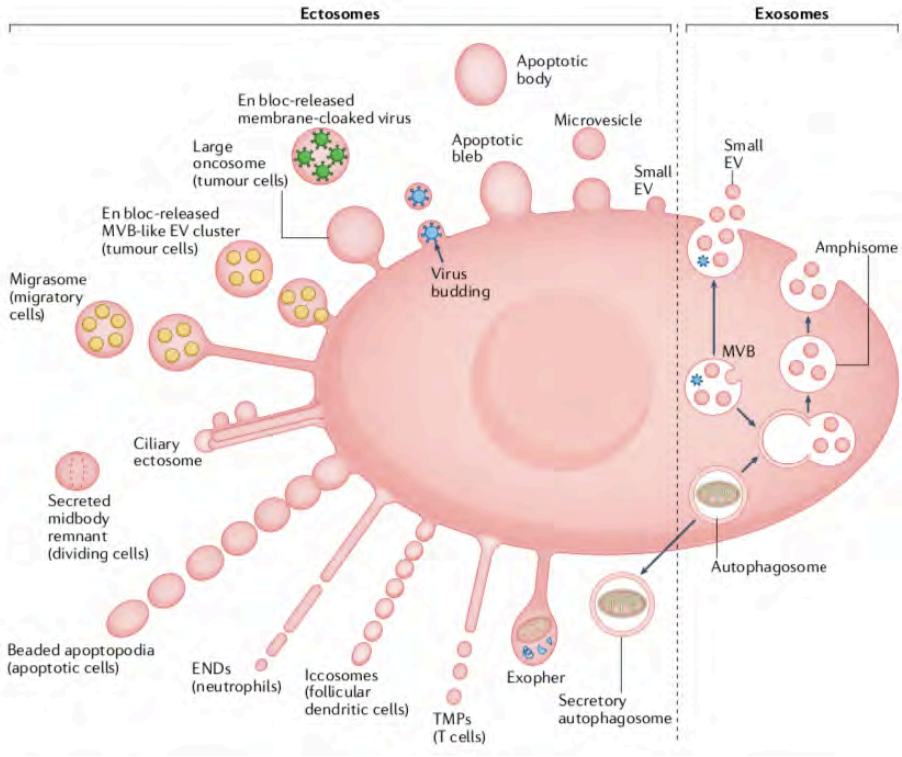

Figure2: The two families of Extracellular Vesicles: the exosomes and the ectosomes/microvesicles. Exosomes are endosome-derived vesicles which come from the release of multivesicular bodies (MVB) or amphisomes contents (i.e., release of intraluminal vesicles (ILV)) into the extracellular space. Amphisomes are intracellular compartments formed after MVB and autophagosome fusion. Ectosomes, also called microvesicles, are plasma membrane derived EVs secreted by membrane budding or blebbing. They include multiple types of vesicles of small (e.g., small ectosomes), medium, and large (e.g., apoptotic bodies) size. Large oncosomes are produced by tumor cells. Migrasome structures are released by migrating cells. Midbodies are remnants structures from cytokinesis. Cilia release specific ectosomes known as ciliary ectosomes. Apoptosis triggers the release of large ectosomes called apoptotic bodies or other type of apoptotic vesicles via beaded apoptopodia and specific protrusions formed by apoptotic cells. Elongated neutrophil-derived structures (ENDs) are generated by rolling neutrophils on the endothelium. Follicular dendritic cells form iccosomes. T cell can form T cell micro-villi particles (TMPs). Exophers contain damaged organelles and protein aggregates. Of note, virus can be secreted through both plasma membrane derived vesicles or MVB secretion. Extracted from Buzas, 2022.

To act at long-range, using endocrine-like signaling, EVs can disseminate through the vascular system and spread into the organism. EVs transport different cargos such as mRNA, miRNA, adhesion molecules, surface receptors, cytosolic proteins as well as lipids, glycans and many other types of RNAs. Their messages can be transmitted to recipient cells, modifying their phenotype as classical messenger do (Kanada et al., 2015; Ridder et al., 2015, 2014; Valadi et al., 2007). Yet, these entities can transport more than only one message to other cells given their cargo diversity. This makes their functions and their mechanisms of action more versatile and more complex compared to classical chemical messengers.

Extracellular vesicles play a role in homeostasis and physiological inter-cellular communication events such as development, metabolism, immunity as well as pathological contexts such as cardiovascular (Boulanger et al., 2017; Coly and Boulanger, 2022; Gomez et al., 2020) and nervous system diseases (Sardar Sinha et al., 2018; You et al., 2022) or cancer (Lucotti et al., 2022). In the next sections I will non-exhaustively describe key roles of EVs in different contexts. In physiological mechanisms I selected examples from development and tissue homeostasis fields as one exemplifies well medium and long-range scale of EVs and the other allows to address the diversity of cellular processes that could be mediated by EVs. In pathological contexts I choose to briefly present EVs involvement in cardiovascular diseases and notably atherosclerosis, as my project is also in relation with the cardiovascular system. Finally, I focused more on cancer and tumor EVs (tEVs) roles in local as well as long distance scales. In both, physiological and pathological contexts, I will briefly present the crucial role of EVs mediated inter-cellular communication regarding the immune system as it plays an essential role in cancer.

1.2 Examples of EVs function in physiological contexts

EVs are key messengers that maintain organisms' basal physiological state. In the next paragraphs examples will be discussed to give an overview of the broad scope of EVs-mediated mechanisms in physiology and homeostasis maintenance.

1.2.a Development

Increasing evidences suggest important roles of EVs in maternal to embryo interactions and developmental processes from oocytes implantation and maturation to embryonic organogenesis. For instance, in mouse models, EVs from embryonic stem cells injected in blastocysts favorize their proper implantation (Desrochers *et al*., 2016) and in bovine models, EVs from uterine flushing facilitate implantation of the fertilized egg in the endometrium (Nakamura *et al*., 2016*;* Kusama *et al.,* 2018). At later stage, it was shown in canine models that EVs from oviduct facilitated the oocytes maturations (Lange-Consiglio *et al.,* 2017).

In embryonic development, EVs are involved in morphogen transport, facilitating their diffusion in the extracellular space (Gustafson and Gammill, 2022; Cruz *et al.,* 2018). This mechanism of diffusion was for instance suggested for Wnt proteins loaded onto EVs in drosophila and human cell models (Gross *et al.,* 2012; Koles *et al.,* 2012). Similarly, vesicular secretion of sonic Hedgehog (Shh) was previously identified as a key actor of left-right determination in mouse embryonic development (Tanaka *et al.,* 2005). More recently, vertebrate Shh morphogen was also found to be secreted into EVs and capable of activating target genes in recipient cells (Vyas *et al.,* 2014).

In organogenesis mechanisms, ex vivo experiments showed that EVs transporting key factor (miRNA and proteins) can serve as a secondary inductive signal for kidney organogenesis (Krause *et al.,* 2018). Additionally, EVs from amniotic fluid stem cells carry a regenerative potential and rescue underdeveloped lungs in rodent models (Antounians *et al.,* 2021). As a last example, in fish, EVs from osteoblasts trigger osteoclast differentiation in the scale (Kobayashi-Sun *et al*., 2020).

Altogether, these examples highlight the multiple roles of EVs in embryonic development as medium to long-range messengers.

1.2.b Immunity

In the last twenty years, increasing number of publications described that EVs play different roles in several innate and adaptive immune processes (Buzas, 2022). Pioneer discoveries showed that B cell-derived and dendritic cell (DC)-derived EVs transport functional major histocompatibility complex (MHC) loaded with peptide and can activate immune response by direct antigen presentation to T cells (Raposo *et al*., 1996; Zitvogel *et al*., 1998) (**Figure 3A**). Few years later, antigen bearing-EVs were shown to mediate an indirect antigen presentation mechanism by transporting antigens and peptides to antigen presenting cells (APC) that are then able to process and present the antigen (Théry et al., 2002) (**Figure 3B**). More recently, a cross-presentation mechanism was identified in which transfer of class I MHC-bearing-EVs, from a donor to an acceptor DC, activate CD8+ T cells (Ruhland et al., 2020) (**Figure 3C**). Antigen cross-presentation was also observed in EVs-mediated transfer of antigen from plasmacytoid-DC to conventional DC for presentation to CD8+ T cells (Fu et al. 2020) (**Figure 3D**) and platelet-derived large EVs were shown to be autonomous in the antigen processing, loading onto MHC class I and activation of naïve CD8+ T cells (Marcoux et al., 2021) (**Figure 3E**).

In addition to antigen presentation functions, EVs were also suggested to be involved in T and B lymphocyte maturation and antibody production. They can carry self-antigen to DC in the thymus for presentation, potentially participating to negative selection of T cells (Skogberg et al. 2015), and thymic epithelial EVs were shown to help maturation of CD4 and CD8 T cells (Lundberg et al., 2016). Additionally, exchanges of CD24 via EVs between B cells was suggested to be involved in B cells maturation in bone marrow (Ayre et al., 2015) and, interestingly, miRNA exchanges from T cells to B was reported to mediate antibody production in germinal center (Fernández-Messina et al., 2020). One of the most recent and fascinating discovery, suggests that EVs regulate the life span of naïve T cells. At the immunological synapse APC can transfer telomeres to T cells via EVs, these telomeres can then fuse with T cell chromosome, rescuing them from senescence, increasing their life span and immune protection (Lanna et al., 2022).

Finally, it was also shown that during pregnancy, placenta-derived EVs carry immunosuppressive molecules allowing the foetus to be tolerated by the mother's immune system (Hedlung et al., 2009; Stenqvist et al., 2013; Kovács et al., 2019).

These examples were purposely selected to highlight the historical discovery of EVs-mediated antigen presentation and EVs-mediated physiological regulation of immunity (i.e. maturation of immune cell and pregnancy) to illustrate EVs capacity to have opposite effects either promoting or downmodulating immune system activity. EVs-mediated immune responses in pathological contexts will be approached in later section.

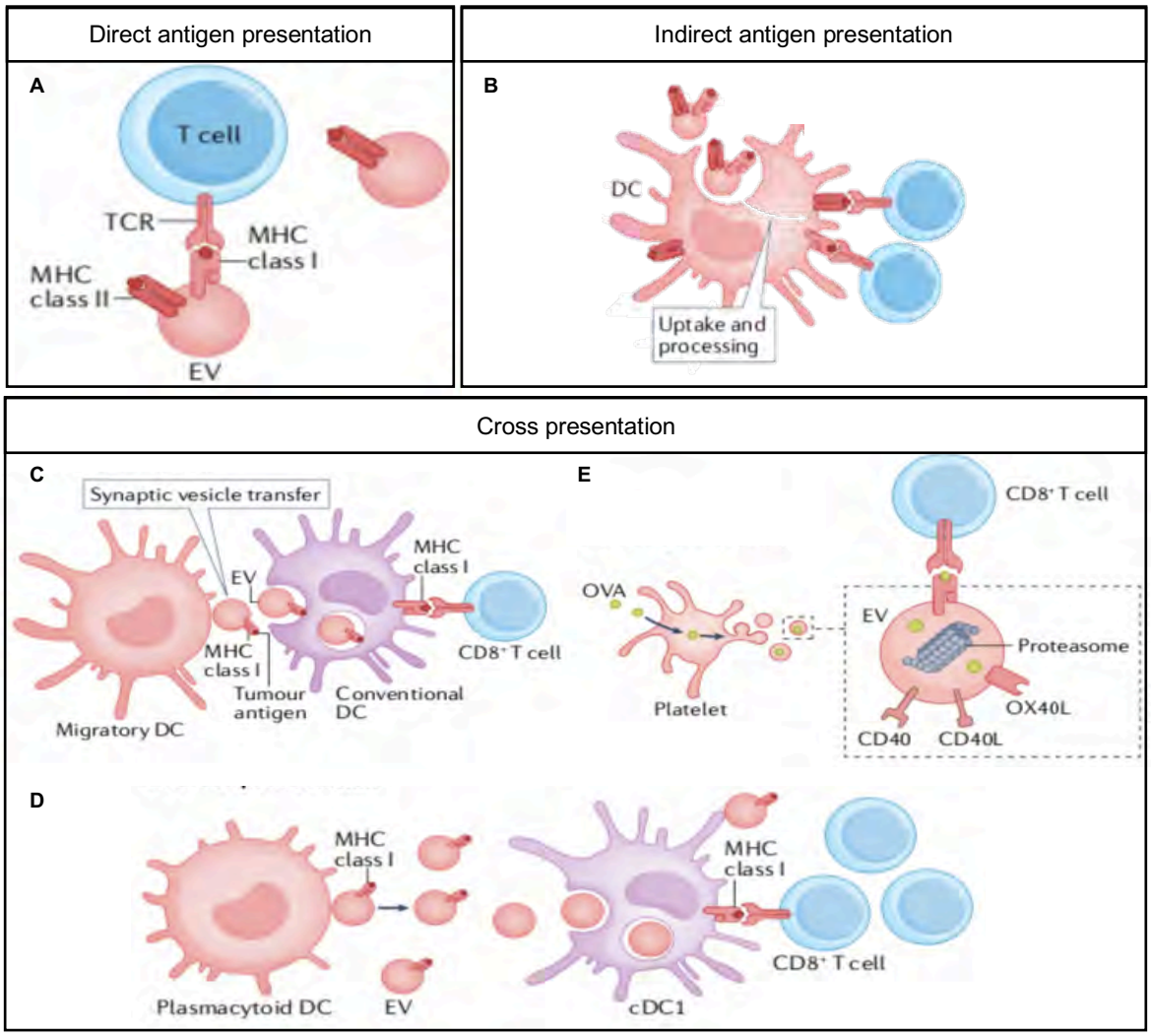

Figure3: Extracellular vesicles-mediated antigen presentation. A) Direct presentation of antigen to T cells via MHC class I loaded with antigen at the surface of EV. B) EV can be internalized by dendritic cells (DC). EV antigens and biomecules can be processed by DC that activate immune cells by indirect presentation. C, D, E) Cross-presentation of MHC via EV. C) Migratory DC from the tumor microenvironment transfer antigens to conventional DC via EV. The second DC activates tumour-specific CD8+ T cells after processing and presentation of EV-transferred peptides. D) Plasmocytoid specialized DC can also secrete EV bearing antigen and trigger activation of CD8+T via cross-presentation of EV-antigens by conventional DC. E) Platelet-derived EVs carry functional machinery to process internalized material (e.g. Ovalbumin OVA), load peptide onto MHC class and present it to T cells and activate it through with the help of co-stimulatory molecules (CD40, CD40L and OX40L) present on their surface. TCR, T cell receptor. Modified from Buzas, 2022.

1.2.c Tissue homeostasis and maintenance

EVs were shown to play important roles in multiple cellular mechanisms involved in tissue homeostasis. The mechanisms in which they are involved have been carefully reviewed recently (Roefs, Sluijter and Vader, 2020) and will not be exhaustively discussed here, but few examples will be presented. Although EVs could play both, beneficial or detrimental effect in tissue maintenance, in this section I will mainly focus on key examples of EVs positive effects to illustrate the broad scope of cell behaviors that EVs can mediate. Of note, EVs were shown to take part in all the six "hallmarks" cellular mechanisms of tissue repair (cell survival, immune modulation, extracellular matrix (ECM) repair, cellular proliferation, cell differentiation, cell migration and angiogenesis) illustrating the omnipresence of EVs in physiological mechanisms (**Figure 4**) (Avalos and Forsthoefel, 2022). For example, bone marrow stem cell- and cardiac progenitor cell-derived EVs were shown to inhibit apoptosis in myocardiac cells (Lai et al., 2010), and EVs from fetal liver-derived supportive stromal cells were shown to promote survival of hematopoietic stem and progenitor cells (HSPC) (Stik et al., 2017). In immune regulation of tissue homeostasis, EVs from macrophages were shown to promote intestinal stem cell regeneration and survival, therefore promoting recovery after injury in mice (Saha et al., 2016). In aging processes and senescence, EVs from young mesenchymal stem cells or fibroblasts were shown to decrease senescence and expand mice life (Dorronsoro *et al*., 2021; Fafián-Labora *et al*., 2020). Conversely, it was shown that EVs from senescent cells activate senescence in target cell through IFN transfer mechanism (Borghesan *et al*., 2019). The positive roles of EVs in regeneration and correct revascularization processes (i.e. skin regeneration) (Wolf *et al*., 2022) and wound healing (Pomatto *et al*., 2021) were also recently highlighted. In addition, it is now known that EVs secreted by stem cells participate to stemness maintenance and stem niche regulation (De Luca *et* al., 2016; Khanh *et al*., 2020; Hur et al., 2021).

EVs recently emerged as an important cue that mediate cell migration and motion in tissue. It has been proposed that cells secrete EVs that bind to the ECM sustainably via their surface molecules, thereby forming a path that following cells could take. In addition, the fact that EVs carry chemoattractive proteins as well as

ECM components and matrix remodeling molecules (e.g. matrix metalloproteinases (MMPs)) enhance their capacity to mediate cell migration in different biological processes (Sung *et al.,* 2015; Kriebel et al., 2018; Brown et al., 2018). Overall, EVs are now considered as an integral part of the ECM, regulating multiple cellular behaviors in physiological processes (Rilla et al., 2019).

Finally, EVs were shown to be a systemic mediator of metabolism. A stunning example is that miRNA present in EVs from adipose tissues can transfer to distant cells and modify metabolism of distant organs (e.g. liver), notably through gene expression regulation. Thereby they participate to systemic long-range EVs-mediated tissue metabolism regulation (Thomou et al., 2017). In addition, it was shown that stressed adipocytes release EVs that can reach the circulation, home to the heart and protect cardiomyocytes from future injuries (e.g. ischemia reperfusion) (Crewe et al., 2021). Overall, EVs disseminating through circulation have a critical impact on organs metabolism, illustrating their importance as messengers at systemic level.

Yet, their role in pathological situations is similarly important. I will discuss significant examples in the next sections.

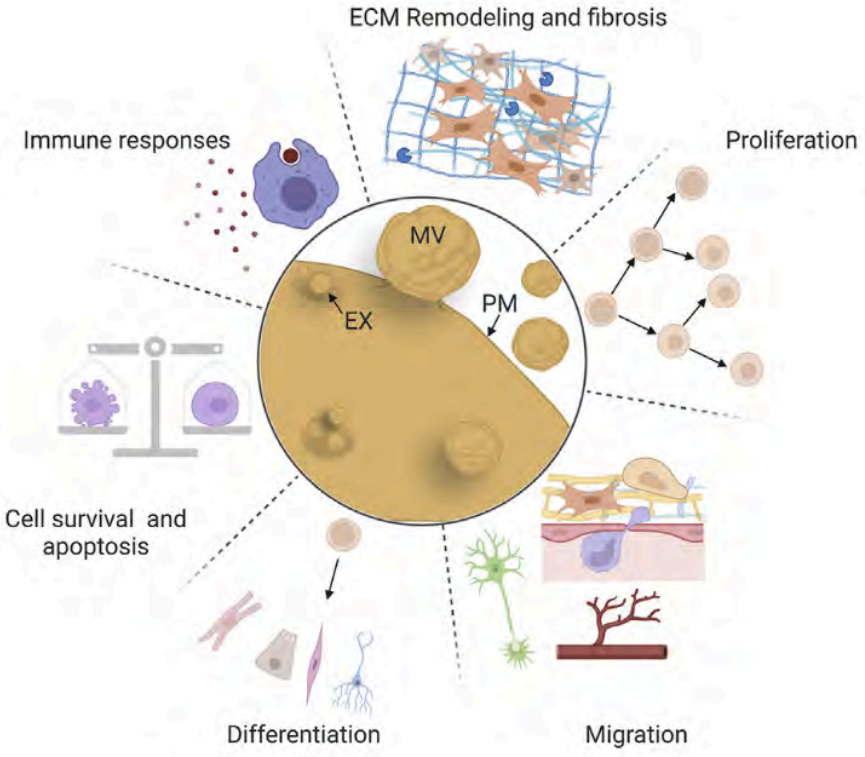

Figure 4: Schemes illustrating EV involvement in the 6 "hallmarks" of mammalian tissue repair and regeneration. These past decades EVs were shown to play a role in each of these cellular behaviours: cell survival, immune responses modulation, ECM remodelling, proliferation, migration, and differentiation. Their involvement in all these cellular processes participate to the maintenance of homeostasis. MV, microvesicles; EX, exosomes; PM, plasma membrane. Extracted from Avalos and Forsthoefel, 2022.

1.3. Role of EVs in pathological contexts

EVs play diverse roles in a plethora of pathological contexts. Although, studies often focus on how EVs facilitate the development of the disease, in some cases EVs participate to the resolution of the abnormal situation. Thus, depending on the context, EVs can be double-sided, playing either enhancer or inhibitor role in pathology progression (Burgelman *et al*., 2021) and raise lot of possibilities as potentials biomarkers to follow diseases progression (Hoshino et al., 2020).

1.3.a Sepsis and inflammation

This double role of EVs is well exemplified in the immunology field, in which EVs either activate and potentialize or decrease immune response to avoid adverse effects.

Besides their important role in antigen presentation EVs were also shown to play a role in innate immune answer and inflammation. For instance, granulocyte-derived EVs can activate monocytes and were associated with poor prognosis in patients in intensive care unit (Danesh et al., 2018). In chronic inflammatory lung disease, activated neutrophil-derived EVs cause lung matrix destruction, supporting progression of the disease (Genschmer et al., 2019), and in mice arthritis models, platelet-derived EVs internalized by neutrophils enhance inflammation (Duchez et al., 2015). Interestingly, it was suggested that EVs associated with C-reactive Protein (CRP) could propagate the inflammation through dissemination of these EVs in the blood (Fendl *et al*, 2021). Overall, EVs were largely identified as actors of chronic inflammatory diseases such as colitis, Crohn's disease, chronic pancreatitis, triggering inflammatory signals such as secretion of IL-1b, IL-6, and CCL-2 and maintaining a global inflammatory state (Lucotti et al., 2022).

However, EVs can also modulate immune response, either for beneficial or detrimental outcomes. For example, macrophages can secret EVs bearing CD14 (the lipopolysaccharide (LPS) co-receptor), which decreases CD14 levels at macrophage membrane thereby affecting pro-inflammatory cytokine production and increasing survival in sepsis (Alarcón-Vila et al., 2020). Similarly, EVs release

from macrophages activated by inflammasome could help to prevent hyperinflammation and its negative systemic consequences (Budden *et al*., 2021). A similar function was identified in polymicrobial infection, where EVs can have a positive effect decreasing macrophage activity and avoiding thereby adverse effects of sepsis (Tu *et al*., 2020). On the contrary, in immune-compromised patients (such as chronic sepsis, HIV patients and Hepatitis C patients), EVs from myeloid-derived suppressor cells (MDSC) drive naïve cell differentiation to immunosuppressive MDSC and inhibit T cell activation participating to the maintenance of a chronic state (Wang et al, 2018b; Alkhateeb et al, 2020; Thakuri et al, 2020).

From a wider perspective, EVs are known to be important in both innate and adaptive immunity displaying microenvironment- and pathology-dependent effects that mediate cross-communication between immune actors at every step of the immune response (Buzas, 2022) and particularly in cancer (Marar et al., 2021).

1.3.b Atherosclerosis and cardiovascular diseases

EVs were shown to either promote the development of cardiovascular disease and atherosclerosis lesions or mediate protective signaling (Boulanger *et al*., 2017; Coly and Boulanger, 2022). On one hand, EVs from atherosclerotic plaque could trigger formation of other plaques at distant sites by dissemination of proinflammatory signals, such as transfer and expression of miR-23a-3p that maintain ERK1/2 phosphorylation and endothelial cell inflammation (Peng *et al*., 2022). Additionally, neutrophil-derived EVs can enhance atherosclerosis by delivering miRNA (miR-155) in arterial endothelial cells that promotes the activation of NF-κB signaling (Gomez *et al*., 2020). In response to atheroprone stimuli, endothelial cell-derived EVs can transfer miRNA-92a to macrophages, leading to atheroprone phenotype macrophages through the downregulation of KLF4 (an essential macrophage polarization regulator), promoting thereby atherosclerotic progression (Chang et al., 2019; Loyer et al., 2014; Coly and Boulanger; 2022). In some cases, EVs produced by cells exposed to inflammation were also shown to have an angiostatic effect, inhibiting the proper revascularization of ischemic arteries (Carter *et al*., 2022). Finally, several EVs-derived cargos were shown to

promote fibrosis in cardiac dysfunctions (Cai et al., 2020; Nie et al., 2018; Govindappa et al., 2020). This is for instance the case of activated CD4+ T cell-derived exosomes that were shown to transfer miR-142-3p to cardiac fibroblasts promoting their activation, proliferation and migration, that ultimately aggravate cardiac fibrosis and dysfunction post-infarction (Cai et al., 2020). Additionally, cardiomyocyte-derived miR-217-containing EVs were shown to be involved in cardiac hypertrophy and cardiac fibrosis (Nie et al., 2018).

On the other hand, it has been shown that EVs can also facilitate recovery in ischemic limb injuries, potentially acting via TGFß signaling and proangiogenic effect (Cavallari *et al*., 2017; Mathiyalagan *et al*., 2017). It was also suggested that they could help cardiac repair after myocardial infarction, notably through their capacity to transfer non-coding RNA. This field of research was well-reviewed in Peters *et al.,* 2020. As an example, EVs derived from endothelial cells expressing KLF2, a transcription factor involved in the regulation of endothelium physiology, were described to promote anti-inflammatory responses, and reduce monocyte recruitment and activation, thereby attenuating myocardial ischemia, potentially via miR-24-3p (Qiao et al., 2020). Overall, the role of EVs in cardiovascular diseases and their recovery is complex and versatile, and the above-mentioned examples highlight once again their different effects depending on EVs subtypes and microenvironmental context.

2. Cancer, metastatic progression and EVs

These last decades, one of the main pathological contexts in which EVs have been extensively studied is cancer. In these diseases tumor-derived EVs (tEVs) were shown to play multiple roles at every step of cancer progression (Lucotti et al., 2022; Kalluri and LeBleu, 2020). After a rapid description of the main characteristics of cancer, I will more precisely discuss the involvement of EVs and particularly their medium to long-range action in cancer. Of note, although studies showed that in some context, EVs and tEVs could inhibit cancer progression (Pucci et al., 2016; Plebanek et al., 2017; Cianciaruso *et al*., 2019; Tokuda et al, 2021), here I will only focus on their pro-tumoral effect and give key examples of tEVs-mediated mechanisms that mediate cancer development at different steps.

2.1. Cancer overview

After heart failure, cancer is the most prevalent cause of death worldwide, supposedly accounting for one in six deaths in 2018 (Bray et al., 2018). Although it includes many different types, the common particularity of cancer is an uncontrolled hyperproliferation of cells (Hanahan and Weinberg, 2011). Cancer can be classified in two main types: liquid cancer (i.e blood cancer) such as lymphoma, leukemia and myeloma, that originate from myeloid or lymphoid cells and do not form a primary tumor mass; and solid cancer (i.e. organ tumors) such as carcinomas and sarcomas, in which proliferative cells form a solid mass in a tissue creating the primary tumor. Carcinomas (i.e. epithelial cancer) are the most common cancers (almost 85%). It can potentially originate from any organ and the outcome of the disease mainly depends on its progression toward metastasis that is responsible for about 90% of cancer-related deaths. Metastasis define the dissemination of cancer cells from a primary tumor to distant organs through body circulatory systems, establishing thereby new tumors in these secondary foci. Metastasis development involves a cascade of complex events that will be detailed hereunder.

More than twenty years ago, Hanahan and Weinberg described six key features of cancer cells that were called the “hallmarks of cancer” (Hanahan and Weinberg, 2000), and 4 additional features were added a decade ago, showing altogether the complexity of cancer disease and recapitulating the general characteristics of cancer (Hanahan and Weinberg, 2011) (**Figure 5**). One of the founding events of a primary tumor formation lies on the genomic instability of a cell or a group of cells which acquire key mutations (randomly or under the effect of mutagenic agents) leading to their transformation from normal cells to malignant cells. However, the external cues and the environmental conditions (e.g. the extracellular matrix, resident immune cells, normal stromal cells), also participate to the tumor formation (Farc and Cristea, 2020). Together, they establish a microenvironment that bears these hallmarks of cancer (**Figure 5**).

1. Genomic instability and mutation
2. Sustained proliferative signaling
3. Evading growth suppressor
4. Avoiding immune destruction

5. Enabling replicative immortality
6. Tumor promoting inflammation
7. Activating invasion and metastasis
8. Inducing angiogenesis
9. Resisting cell death
10. Deregulating cellular energetics

These hallmarks illustrate the fact that tumor cannot be only defined as a mass of cancer cells with intrinsic features but is rather part of a complex ecosystem called the tumor microenvironment (TME) that involves multiple actors playing a role in cancer progression through their interplays. After brief description of main components of TME, the concepts of metastasis and organotropism, and characteristics of pre-metastatic niche (PMN), I will give some examples in which EVs affect cancer in each of these steps.

Figure 5: The hallmarks of Cancer. These hallmarks not only involve intrinsic characteristics of malignant cells but also different contributions of the tumor microenvironment notably the interactions between tumor cells and immune component. They support tumor growth and progression. Adapted from Hanahan and Weinberg, 2011.

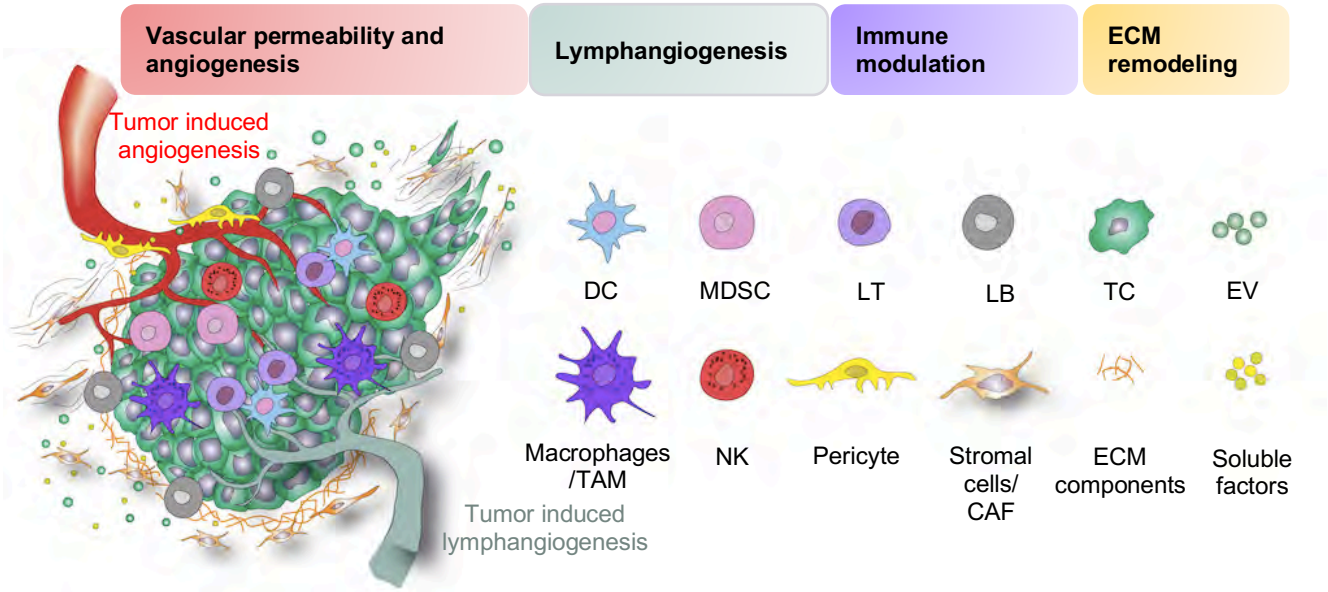

Figure 6. The tumor microenvironment (TME). Scheme of the TME and its main components. The tumor microenvironment involves not only different cancer cells but also multiple other cell types including: stromal, lymphatic endothelial cells and immune cells, as well as a modified extracellular matrix. In this heterogenous microenvironment extracellular vesicles (tumoral or not) together with secreted factors mediate intercellular communication to most of the time support tumor growth. Tumor-induced angiogenesis and lymphangiogenesis, immune suppression and inflammation as well as ECM remodelling participate to the establishment and the growth of the TME.Of note immune cell play a dual role either anti- or pro-tumorigenic. Overall, the tumor microenvironment promotes immune escape of cancer cells. DC: Dendritic cells; MDSC: Myeloid-Derived suppressor cells; LT: Lymphocytes T; LB: Lymphocytes B; TC: Tumor cells; NK: Natural Killer; ECM: Extracellular Matrix. EV: extracellular vesicles

The tumor microenvironment (TME):

The tumor microenvironment is a term used to define the primary mass of proliferative cancer cells and the surroundings of this mass that includes a variety of other cell types (tissue resident cells or recruited by the TME itself), soluble factors (such as growth factors and chemokines), and the extracellular matrix (ECM). The TME participate actively to tumor growth and the progression of the disease, promoting multiple pro-tumorigenic events in which intercellular communication plays a crucial role (Balkwill et al., 2012; Hanahan and Coussens, 2012). Cellular components of the TME use all the different kind of intercellular communication pathways (autocrine, paracrine, juxtacrine) to not only maintain the microenvironment and the proliferation of cancer cells but also their potential dissemination in the body.

Here are some of the main components of the TME which participate to the formation and the maintenance of TME.

- Endothelial cells and pericytes:

As the tumor mass is growing, the cells that are in the center of the mass rapidly lose their access to vascular system and therefore the access of nutrient and oxygen essential for their proliferation. In response to hypoxia, cancer cells as well as pro-

inflammatory cells secrete angiogenic factors such as Vascular Endothelial Growth Factor (VEGF), Fibroblast Growth Factor (FGF) and Platelet-derived Growth Factor (PDGF) that trigger the recruitment of endothelial cells and pericytes enabling thereby neo-angiogenesis supporting tumor growth (Carmeliet and Jain 2011; Farc and Cristea, 2020). Tumor-induced angiogenesis forms disorganized leaky vessels that present abnormal characteristics (in the branching structures and the lumen) and are more permeable (Palma et al., 2017). Consequently, flow is highly perturbed in TME and there is an increased plasma leakage in extracellular space (Follain et al., 2020). Additionally, lymphatic endothelial cells (LEC) and lymphangiogenesis are also stimulated in TME via VEGF-C and VEGF-D signals (Stacker et al., 2014), particularly at the tumor periphery (Pathak et al., 2006). These conditions promote the apparition of a high interstitial fluid pressure (IFP) in the center of the tumor and lower IFP at the periphery, thereby creating a gradient that drives interstitial fluid from the center to the tumor periphery, facilitating its lymphatic drainage (Follain et al., 2020) (**Figure7**). This convective flow is thought to impair drug distribution inside tumor in therapeutic approaches and has been suggested to promote the dissemination of cancer cells (Cornelison et al., 2018; Pereira *et al.,* 2018), tumor-derived soluble factors and importantly, EVs (see section **2.2**), through vascular systems, potentially promoting cancer progression (Follain et al., 2020) (**Figure7**). In the TME, pericytes that normally support the structural integrity of blood vessels, are in less abundance, adding to the overall fragility of newly formed vessels integrity (Balkwill *et al*., 2012). Beside their cancer promoting effect associated to their impact on blood vessel integrity, pericytes can also promote cancer progression through direct and indirect interaction with other stromal cells and cancer cells (Sun et al., 2021; Lechertier et al., 2020). It was recently described that pericyte-derived chemokine (CCL2) promotes tumor cell survival and growth through induction of MEK1-ERK1/2-ROCK2 signaling pathway (Wong et al., 2020). Pericytes were also suggested to have immunosuppressive effects, for instance by recruiting tumor-associated macrophages (Sun et al., 2021)

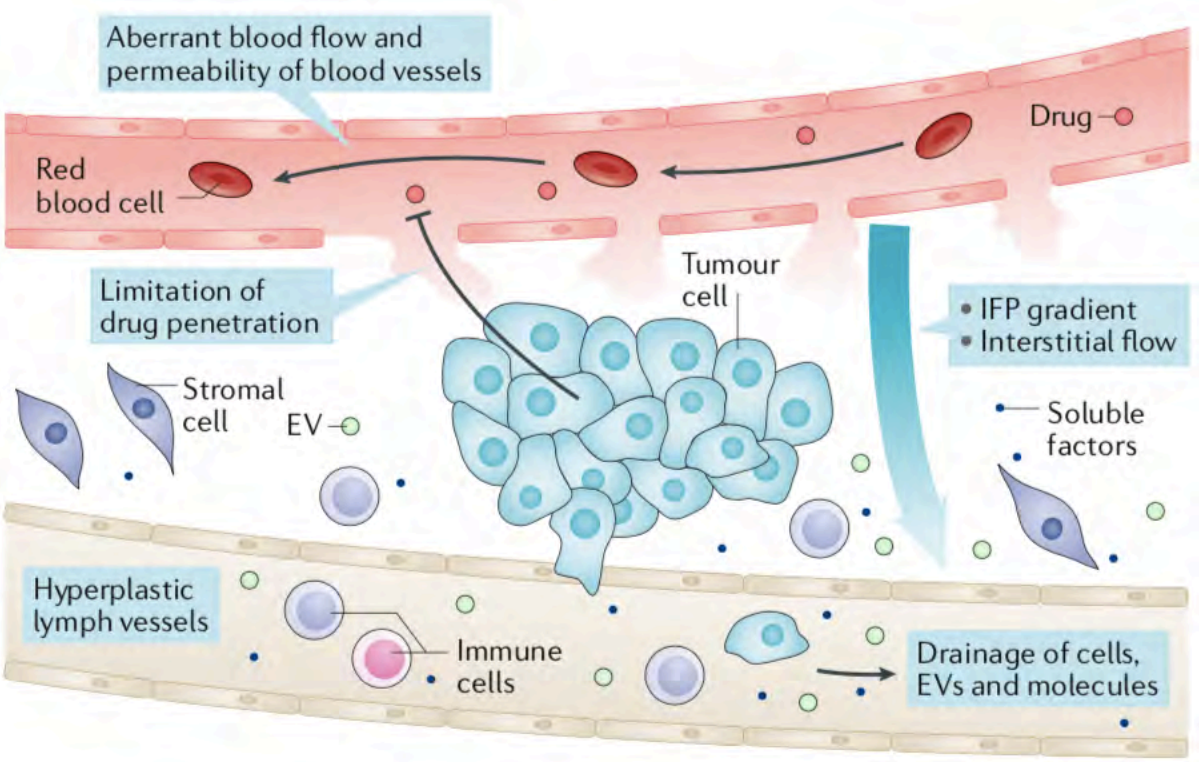

Figure 7: Lymphatic drainage at the tumor site. Aberrant and permeable blood vessels in the tumour microenvironment increase continuous plasma leaking. Intratumoral compression of lymphatic vessels prevents efficient draining of this plasma causing high interstitial fluid pressure (IFP) within the tumour. Tumour-induced lymphangiogenesis enhances lymphatic vessel formation at the tumour periphery, creating a gradient of IFP from the center of the tumour mass toward the periphery. Interstitial fluids and soluble factors that it drains (including tumour derived factors and tEV), reach the lymphatic system driving them to lymph nodes. The lymphatic system will then, recycle lymph, re-injecting it into the blood compartment via the subclavian veins. The gradient of IFP in tumour microenvironment enhance soluble factors and tEVs drainage by lymphatic vessels, which is thought to facilitate their dissemination and their capacity to reach blood compartment. The second route for tEV to reach the blood will be the direct reabsorption of interstitial fluids by blood vessels, which can be facilitate by enhanced permeability and abnormal vessels in the tumor microenvironment. Extracted from Follain et al., 2020

- Immune cells:

Almost all immune cell types (adaptive or innate) can be found in the vicinity of TME, either inside the tumor mass, at the periphery or in draining lymph nodes. Depending on the stage of the disease and the immune cell types considered, they can have contradictory roles either promoting or inhibiting disease progression.

For instance, T lymphocytes involve multiple subtypes that have different, and sometime opposite, effects on tumor progression (Balkwill *et al*., 2012). For instance, cytotoxic CD8+ memory T cells and CD4+ T helper1 are thought to have an anti-tumor effect (Fridman et al. 2012). By contrast, T regulatory (Treg) cells, similarly to CD4+ T helper2 are rather immunosuppressive, decreasing anti-tumor immune response and promoting tumor progression (Ohue and Nishikawa, 2019). Similarly, B cells play

antagonist roles in tumor progression according to their subtypes and to tumor types, thereby correlating with either good or poor prognosis in clinic. On one hand, they have pro-tumorigenic effects promoting for instance angiogenesis through the secretion of Transforming Growth Factor beta (TGFβ) and tumor necrosis factor (TNF), (Schwartz et al., 2016). On the other hand, B cells also have anti-tumor effects for instance by inducing the lysis of cancer cell types via secretion of TNF-related apoptosis-inducing ligands (TRAIL) and granzyme B (Shi et al., 2013).

Innate immunity also plays an important role in TME and involves different actors such as dendritic cells (DC), macrophages and natural killer (NK) cells that all communicate together and with the other components of the TME (Balkwill *et al*., 2012). DC have mainly anti-tumor effects (immune surveillance) and their presence often correlates with good prognosis. Macrophages recruited in the TME, coming from either monocyte precursors or tissue resident macrophages, can undergo modifications and become tumor associated macrophages (TAM). They are usually classified in 2 main subtypes having opposite effects on tumor: “M1” TAM are anti-tumorigenic through the secretion of pro-inflammatory molecules such as IL-12 and TNFα, while “M2” TAM are pro-tumorigenic by triggering angiogenesis through the secretion of VEGF or by modulating anti-tumor immune responses by secreting immune suppressive cytokines (Liu et al., 2020; Biswas and Mantovani, 2010). M1 TAM are usually more abundant in the TME at the beginning of the tumor development, however throughout the establishment of the tumor and its escape from immune surveillance they tend to switch to an M2 phenotype (Quail and Joyce, 2013). However, the M1-M2 classification is highly debated in the immunology field, because the underlying mechanisms and the characteristics of these phenotypes are not well understood and rather plastic. Finally, NK cells present in the TME have the capacity to recognize and directly eliminate cancer cells by secreting granzymes and perforins and are thereby one of the key actors of cancer immune surveillance. However, several factors secreted in the TME such as TGFβ and IL-6 can impair the effector function of NK cells by preventing their activation (Sungur and Murphy, 2014). More recently, unconventional role of these cells was reported. Via Interferon **γ** (IFN **γ**) signaling, NK were shown to promote fibronectin production from melanoma cells which stiffens the ECM and was suggested to prevent metastatic progression (Glasner et al., 2018).

- Cancer associated fibroblasts and Extracellular matrix:

Cancer associated fibroblasts (CAF) represent the most abundant component in the TME. Although the origin of CAF remains poorly understood, several studies described that CAF could derive from different cell types including resident fibroblasts, bone marrow-derived mesenchymal stem cells and endothelial cells (Sahai et al., 2020). CAF promote tumor progression by triggering multiple events including angiogenesis, epithelial-to-mesenchymal transition (EMT), immune response modulation and ECM remodeling (Sahai et al., 2020; Balkwill et al.,2012). Moreover, they are the main producers of ECM molecules, shaping a complex network composed of proteoglycans and fibrous proteins including collagens, fibronectin and laminins. Beside the role of ECM as physical scaffold supporting cells, the remodeling of the extracellular matrix in the TME can promote tumor progression. For instance, ECM can be degraded by proteases including matrix metalloproteinase (MMPs) and a disintegrin and metalloproteinase (ADAMs) secreted by different cell types such as CAF and cancer cells. The proteolytic degradation of ECM molecules can then facilitate cancer cell migration and release ECM-binding soluble signaling molecules (e.g growth factors), leading to their activation (Lu et al., 2011).

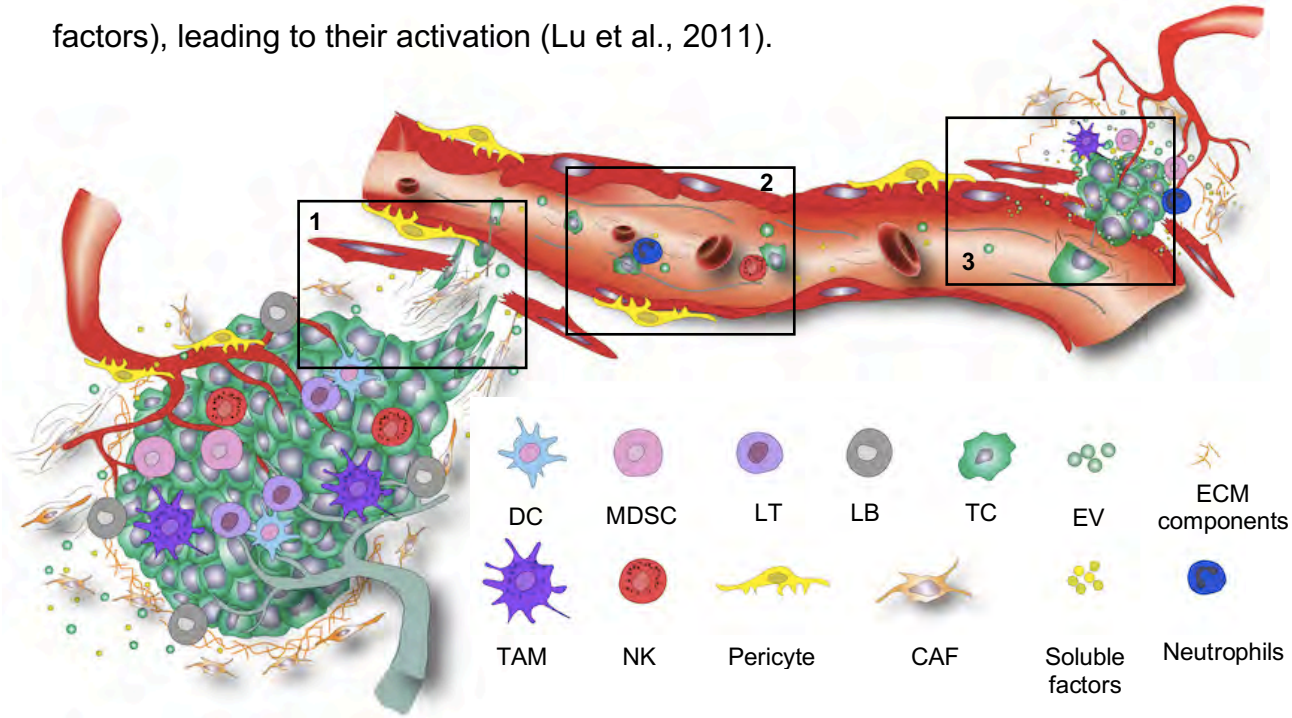

Figure 8: Simplified scheme of the metastatic cascade multiple steps. 1) Malignant cells invade their stroma. They breach through the vascular endothelium via a process called intravasation (enhanced by increased vascular permeability and fragility of at tumor site). 2) In the circulation, part of them survive, avoid immune surveillance and disseminate to distant organs. 3) Circulating Tumor Cells (CTCs) can adhere to vessels walls using adhesion molecules to resist blood flow or mechanically stop due to vessels architecture. Arrested CTC can cross the endothelial barrier (process called extravasation), reach stroma of specific distant site called a pre-metastatic niche (PMN) and form a secondary tumor called metastasis. During PMN and metastasis formation soluble factors and extracellular vesicles play a crucial role, for instance by recruiting cell that will enhance these processes or by remodelling the extracellular matrix. DC: Dendritic cells; MDSC: Myeloid-Derived suppressor cells; LT: Lymphocytes T; LB: Lymphocytes B; TC: Tumor cells; NK: Natural Killer; ECM: Extracellular Matrix. EV: extracellular vesicles.

2.2. The metastatic cascade

The metastatic cascade (**Figure 8**) represents the different steps enabling the progression of cancer disease from an *in situ* primary tumor to the dissemination of cancer cells to distant organs establishing thereby new tumor foci.

- Invasion step:

After the proliferation of initial cancer cells, some of these cells can undergo different processes conferring them migratory and invasive properties. In epithelial tumors one of these processes is called the epithelial-to-mesenchymal transition (EMT) that is triggered by different signaling pathways such as TGFβ and Wnt. One characteristic of this transition is the modulation of cadherin expression, notably the decrease of E-cadherin for the benefit of N-cadherin expression, enhanced expression of metalloproteinases and new repertoire of integrins (Dongre and Weinberg, 2019). In these processes, multiple molecular interactions and chemotactic events mediate tumor cell invasion. However, biomechanical cues such as cell and ECM stiffness, deformability, and, in general, the physical forces (e.g. interstitial fluid pressure) present in the environment play also an important role in the invasion capacities of tumor cells (Follain 2020; Gensbittel et al 2021).

- Intravasation:

Intravasation defines the process by which cancer cells pass through the endothelial barrier (lymphatic or blood vessels) and reach the vascular system. This is facilitated by the leaky vasculature presents in TME and its high permeability. Tumor cells that are present in vessels are called circulating tumor cells (CTC). CTC must survive a lot of different stresses including hemodynamic flow, death by loss of attachment (anoikis), shear stress and immune surveillance by NK cells. While reducing drastically the number of CTC, all these events induce a selective pressure resulting in the survival of the most resistant, resilient and aggressive tumor cells (Follain et al., 2020; Strilic and Offermans 2017).

- Extravasation:

To escape circulation, CTC that survived in the circulation engage contact with the vessel wall to counteract blood flow and mechanical constraints (Osmani et al., 2019), cross the endothelial basal lamina, by diapedesis or endothelial remodeling (Follain et al., 2018), and invade the stroma to potentially form a secondary tumor. Arrest and

extravasation form a complex chain of events that is not totally understood involving not only isolated CTC but also immune cells (e.g. monocytes and neutrophils) (Headley 2016) or clustered CTC. At this step too, the plasticity of tumor cells, the soluble factors present as well as surrounding cells and the modification of the microenvironment will allow part of them to either survive and start proliferating or enter dormancy.

- Organotropism and pre-metastatic niche (PMN) formation:

The fact that CTC do not arrest at totally random sites but rather colonize specific organs depending on the type of cancer is called organotropism (Gao et al., 2019). For example, breast cancer tends to metastasize in bone, lungs, liver, brain or lymph node (Chen et al., 2018). Molecular (i.e. CTC-endothelium interactions) and biophysical cues (hemodynamics forces, flow patterns, vascular architecture, permeability) determine the site of CTC arrest and therefore contribute to organotropism (Follain et al., 2020). Additionally, organotropism is explained by the "seed and soil" theory, proposed in the late XIXth century by Steven Paget (Paget 1989), which states that metastatic outgrowth occurs in organs with favorable microenvironment. Evidences of the past 15 years show that factors, including EVs, secreted by the primary tumor, can modify this microenvironment leading to the formation of the 'pre-metastatic niche' (PMN) in target organs.

The PMN (**Figure 9**) is a microenvironment that underwent series of modifications before the arrival of tumor cells, ultimately supporting cancer cell seeding and proliferation. The establishment and properties of PMNs are still not completely understood for now. Nevertheless, it is known that tumor-derived soluble factors, in particular tumor EVs, are major actors of PMN initiation (EVs will be discussed in a next section). For example, MMP family proteins, Angpt14 and Angpt2 secreted by the primary tumor can trigger the permeabilization of the endothelium and disruption of endothelial cell junctions at distance, initiating PMN formation. This process facilitates the crossing of endothelium barrier by tumor cells (Liu and Cao, 2016). Secreted factors also recruit and activate different types of cells such as myeloid cells and stromal cells (fibroblasts) that in turn can secret pro-inflammatory molecules including TGFβ, MMPs and chemokines, promoting cancer cell seeding and metastasis formation (Liu and Cao, 2016). Immune suppression combined with chronic inflammation at the PMN site favor its establishment and maintenance in time. Additionally, the remodeling of ECM through molecules such as MMPs and deposition

of new ECM constituents including fibronectin and tenascin-C promote also PMN formation (Liu and Cao, 2016) (**Figure9**).

In this cascade of events EVs and particularly tEVs actively participate to the cross-communication between all the actors involved (tumor cells, stromal cells, immune cells, ECM) (Kalluri and LeBleu, 2020; Sheehan and D'Souza-Schorey, 2019). In the following sections, I will give non-exhaustive examples of their roles in cancer disease and illustrate that EVs participate at each step of its progression, from the primary site to the development of metastasis.

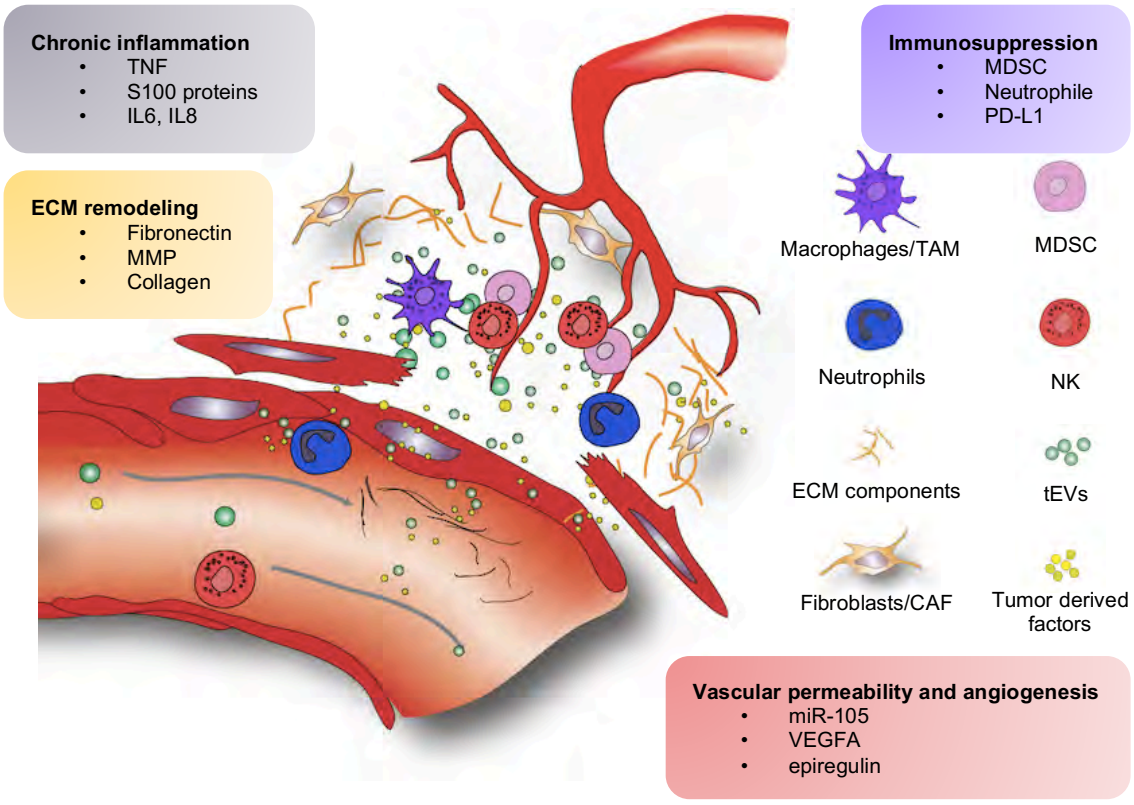

Figure 9. Scheme of the main characteristics of the pre-metastatic niche (PMN). tEV and tumor-derived factors can induced changes in distant environments that contribute to the PMN establishment and subsequent metastatic colonization. tEV were notably identified to fragilize vascular endothelium, induce ECM remodeling, chronic inflammation and immunosuppression in distant sites. MDSC: Myeloid-Derived suppressor cells; TC: NK: Natural Killer; ECM: Extracellular Matrix. tEVs: extracellular vesicles.

2.3 EVs in the primary tumor

Pioneer studies showed that inhibiting tEVs secretion directly decreases cancer progression and metastasis (Bobrie et al., 2012; Peinado et al., 2012; Wang et al., 2014). In parallel, it was shown that tEVs induce changes in phenotype of stromal and epithelial cells (Antonyak et al., 2011, Franzen et al., 2015), endothelial cells (Zhou et al., 2014), and immune cells (e.g. neutrophils) (Hwang et al., 2019) to promote cancer development and communication between all cell types at the primary tumor site (Yan et al 2018). This communication notably promotes horizontal transfer of malignant traits such as migratory, growth capacities or even drug resistance between different populations of tumor cells in the TME (Al-Nadawi *et al*., 2008, Lucotti et al., 2022).

- Vascular permeability and angiogenesis (in TME):

In a seminal study, Skog et al showed that glioma-derived EVs enriched in angiogenic proteins could induce pro-angiogenic behaviors (i.e. formation of tubules) in endothelial cells *in vitro* (Skog et al, 2008). More recently, it was shown that colorectal adenocarcinoma-derived tEVs (from SW480 cells) promote angiogenesis *in vitro* and *in vivo* at the site of injection. They trigger an early growth response-1 (EGR1) activation of the endothelial cells through ERK1/2, JNK dependent signaling enhancing their migratory behavior (Yoon et al., 2014). In addition, it was also reported that Piwi-interacting RNA (piRNA, piRNA-823) transported by tEVs coming from multiple myeloma cells participate not only to angiogenesis activation in endothelial cells in the TMN but also acquisition of malignant traits such as invasiveness and support tumor progression *in vivo* (Li et al 2019). Finally, it was suggested that tEVs produced in hypoxic environments, are even more pro-angiogenic compared to control tEVs, suggesting that tumor environment mediates the production of tEVs with specific features (Mao et al., 2019). Overall, EVs are important transporters of pro-angiogenic factors (e.g. miRNA, ANGPT2, E-cadherin) that can be transmitted to receiving cell (e.g. endothelial cells) or act on the ECM to increase angiogenesis in the primary tumor microenvironment (Umezu et al, 2014; He et al., 2019; Xie et al., 2020; Tang et al. 2018). Although tumor-related angiogenesis forms leaky vessels, tEVs are also able to directly increase vascular permeability by transferring RNA material in endothelial cells, disrupting the cell-cell junctions in the TME (Zhou *et al*., 2014; Tominaga et al., 2015; Treps et al., 2016).

Altogether these studies highlight the role of tEVs in neo-angiogenesis and vascular permeabilization thereby promoting cancer progression at the primary site.

- CAF and EVs mediated communication (in TME):

EVs mediated transfer from CAF to tumor cells support pro-tumoral mechanisms. For instance, CAF-derived EVs can transfer Galectin-1 protein in cancer cells increasing their migration capacities (Toti et al 2021). In addition, miRNA (including miR-21, miR-378e and miR-143) delivered by CAF-derived EVs into breast cancer cell lines increase their stemness, EMT markers and anchorage-independent growth enhancing their aggressiveness (Donnarumma et al., 2017). In breast cancer, CAF-derived EVs can also have an immunosuppressive effect, increasing PD-L1 expression in breast cancer cells via transfer of miR-92 (Dou et al., 2020).

Conversely, tumor EVs can also impact fibroblasts and CAFs. Tumor EVs from gastric cancer can induce the apparition of distinct populations of CAF expressing different chemokine signatures. This participates to the heterogeneity of cancer-associated stromal cells and could support tumor growth (Naito et al., 2019). TGFß signaling plays an important role in EVs-mediated communication between CAF and TME. It was shown that TGFß transferred by bladder tEVs to normal fibroblasts triggers their differentiation into CAF via activation of SMAD pathway (Ringuette Goulet et al., 2018). A recent study showed that mutant p53 protein selectively loaded into tEVs can induce fibroblast differentiation into CAF that supports tumor growth *in vivo* (Ma et al., 2021). Finally, it was also shown that hepatocellular carcinoma EVs induce the transformation of hepatocyte stellate cells into CAF that supports cancer progression (Zhou et al., 2018). Of note, tEVs can also induce fibroblast differentiation into myofibroblast, promoting angiogenesis *in vitro* and tumor growth *in vivo* (Webber et al., 2010; Webber et al., 2015).

- Effect on immunosuppression and Tumor-Associated Macrophages communication (in TME):

At the primary site, tEVs were shown to transfer miRNA (*e.g.* miR1246) to macrophages, that leads to their reprogramming as tumor-associated macrophages (TAM) which secrete TGFß promoting immunosuppression (Cooks *et al*., 2018). Additionally, EVs from osteosarcoma were shown to induce the secretion of TGFß2 by TAM, inducing M2 phenotype and immunosuppressive environment suitable for tumor growth (Wolf-Dennen et al., 2020). Another study showed that in hypoxic lung cancer EVs can transfer miR-103a inducing activation of AKT and STAT3 signaling and

inducing thereby polarization of macrophages into M2 TAM (Hsu et al., 2018). Finally, an interesting study is proposing a new model to explain tEVs spreading (Umakoshi et al., 2019). It shows that TAM can serve as a kind of shuttle for tEVs, helping to transfer tEVs and tEVs-contents in distant stromal cells to enhance the establishment of a pro-tumoral environment.

Besides their effect via TAM, tEVs can enhance the establishment of an immunosuppressive environment through the presence of PD-L1 at their surface that can inactivate T cells (Poggio et al., 2019; Chen et al., 2018). It was suggested that PD-L1 presence at EVs surface is mediated by an Alix protein-dependent secretion pathway in breast cancer cells which also directly inversely impact PD-L1 levels at the plasma membrane of cell. This suggests that cellular- and EVs-associated PD-L1-mediated immunosuppression are closely related but their impact on tumor immunosuppression regarding each other remains to be investigated (Monypenny et al., 2018).

- Effect on extracellular matrix (in TME):

EVs-mediated ECM remodeling can promote local tumor invasion. For instance, tEVs cargo such as membrane-type 1 matrix metalloproteinase (MT1-MMP) facilitate the degradation of ECM, and thereby the invasiveness of cancer cells (Clancy et al., 2015). EVs-associated MMPs were shown to be able to degrade type 1 collagen and gelatin (Hakulinen et al., 2008). Additionally, tEVs secretion mediates the formation of invadopodia, an actin-based structure specialized in invasion that releases proteinases (Hoshino et al., 2013). This study showed an important and synergic link between tEVs secretion, invadopodia formation and maintenance and secretive activity, which generally participate to facilitate tumor cell invasion.

Overall, these examples illustrate the diversity of pro-tumorigenic mechanisms and affected cell types that are mediated by tEVs within the TME.

2.4 EVs-mediated organotropism

- Actors of tEVs organotropism:

The key feature of EVs is their long-range capacity of action by dissemination. Thereby, tEVs research dramatically caught attention when they were described to enhanced PMN establishment and metastatic development (Peinado et al., 2012,

Costa-Silva et al., 2015, Hoshino et al., 2015). As for cancer cells, it has been shown that tEVs biodistribution and accumulation in organs is not a random nor passive process. Their organotropism, similar to CTC, is thought to be regulated by two main features: biophysical cues (e.g. hemodynamic profiles) and chemical/molecular cues. The biophysics aspect and pattern of EVs and tEVs biodistribution and their behavior in body fluids will be discussed in more details later.

tEVs accumulation in organs depends on tEVs origin, their membrane receptor/protein repertoires, and their glycosylation (Hoshino et al., 2015, Wu et al., 2020, Nishida-Aoki et al., 2020) However, it has been reported that, in experimental models the route of tEVs injection also impacts distribution and this limitation would need to be addressed in the future (Gupta et al., 2020).Yet, their biodistribution reflects organ-specific metastatic behavior of their secreting tumor cells (Wu et al., 2020; Gerwing et al., 2020; Peinado et al., 2012; Hoshino et al., 2015; Xu et al., 2018). This organotropism depends on adhesion proteins present on tEVs. For instance, integrins (ITG) α6ß4/ α6ß1 and αVß5 were respectively associated with lung and liver tropism of tEVs, driving subsequent metastasis in these organs (Hoshino et al., 2015; Armacki et al., 2020). Additionally, it was shown that knockdown of lung-tropic proteins (Slco2a1 and CD13) redirects tEVs that normally accumulate in the lung to heart and kidney (Wu et al., 2020). CD44v6 and Tspan8 on pancreatic and colorectal tEVs were shown to mediate the transfer of pro-tumoral characteristics (anti-apoptotic, migratory, invasiveness) to other cells (Wang et al. 2016, Wang et al., 2019). This suggests that different proteins/receptors play a role in tEVs/recipient cell interactions and more details will be given in section **5**.

- Therapeutical approaches:

Some studies already pinpoint the possibility to target these interactions to impact tEVs-mediated progression of cancer. For example, breast cancer-derived tEVs treatment with specific anti-CD9 and anti-CD63 antibodies decreases metastasis burden in lung, lymph node and thoracic cavity, accompanied by an increased antibody treated-tEVs uptake by macrophages. The authors suggest that their treatment could promote tEVs clearance by macrophages thereby counteracting the establishment of metastasis (Nishida-Aoki et al., 2017). This study suggests that targeting surface molecules could help to limit the pro-

metastatic effect of some tEVs. However, for most of the receptors identified their associated ligands remain unknown in the context of tEVs organotropism and PMN formation. Our fragmented knowledge on this subject makes therapeutic application difficult so far.

Overall, these studies highlight the importance of tEVs surface molecules and their accumulation in metastatic-prone organs. Accumulation of tEVs at these sites is most of the time of bad prognosis as tEVs could favor the apparition of the PMN and subsequent metastasis in these locations. Therefore, understanding the molecular actors and the role of fluidic physical forces in tEVs distribution is a fundamental question that needs to be further addressed and constitutes the center of my PhD project.

2.5 Effect of EVs at the future metastatic site

In the same ways as tEVs modify the primary tumor, tEVs can also impact distant site. One major difference is that the effect of tEVs can arise before the arrival of any CTC. Hence, it is admitted that tEVs participate actively to the establishment of the PMN (Costa-Silva et al., 2015; Henrich et al., 2020; Peinado et al., 2017). As tumor secreted factors, tEVs participate to the “soil” preparation, acting on cellular and molecular actors of the metastatic niche. However, it is important to keep in mind that their actions are also likely to take place simultaneously to metastasis growth, once the secondary foci are on development.

- Vascular permeability and angiogenesis (at PMN):

Tumor EVs can weaken the endothelial barrier, increasing its leakiness and permeability at PMN. For instance, tEVs from melanoma cells can increase lung vascular permeability (Peinado et al., 2012) and hepatocellular carcinoma tEVs were shown to reduce VE-cadherin and ZO-1 expressions in non-cancerous region of the liver (Yokota et al, 2021). Different non-coding RNAs transported by tEVs (e.g. miR-105, miR-25-3p, miR-181c, circRNA) were shown to mediate this increases vascular permeability in breast, colorectal, brain and pancreatic metastasis models (Zhou et al., 2014; Zeng 2018; Tominaga et al. 2015, Li et al., 2018). In addition to RNA, protein cargo, such as semaphorine3A, epiregulin,

VEGFA were also shown to increase vessel permeability via tEVs transfer (Treps et al., 2016; Treps et al., 2017; Yang et al., 2017).

tEVs also induce neo-angiogenesis and lymphangiogenesis at distant sites before the arrival of CTC, for instance in lymph nodes (García-Silva et al., 2021). For instance, tEVs cargo CEMIP, VEGF and epiregulin were shown to trigger angiogenesis and endothelial remodeling in brain and lung PMN (Rodrigues et al., 2019; Treps et al., 2017; Yang et al., 2017). In addition, miR-221-3p from cervical squamous carcinoma cell-derived EVs was shown to promotes lymph node lymphangiogenesis by inhibiting vasohibin-1 in human lymphatic endothelial cells (HLECs) and enhance metastasis (Zhou et al. 2019).

Overall, increased permeability, neo-angiogenesis and lymphangiogenesis (Stacker et al., 2014) participate to tumor cell dissemination and these newly formed vessels display structural and functional defects promoting subsequent CTC extravasation and invasion at future metastatic sites.

- CAF and EVs mediated communication (at PMN):

tEVs can regulate CAF at PMN. Studies identified that tEVs from hepatocellular carcinoma can transform fibroblast to CAF in the lung by using a miRNA (miR-1247-3p) dependent mechanism, β1-integrin/NF-κB signaling pathway (Fang et al., 2018). Moreover, CAF-derived tEVs from the primary site participate to the niche establishment and maintenance. It was shown that CAF-derived tEVs activate resident lung fibroblasts at distant site, enabling matrix remodeling, facilitating PMN formation and subsequent metastasis in lung (Kong et al., 2019).

Other cells can also be modified through tEVs-mediated signaling. It was shown that prostate cancer tEVs, breast cancer tEVs or EGFR-loaded gastric cancer tEVs can respectively modify bone marrow stromal cells, osteoblasts, osteoclasts and liver stromal cells, promoting bone or liver metastasis (Dai et al., 2019; Li et al., 2019; Yuan et al., 2021; Zhang et al., 2017). Recent study reported that tEVs from melanoma cells can educate normal lung cells, downregulate type I interferon receptor and cholesterol 25-hydroxylase which promotes PMN formation and melanoma lung metastasis (Ortiz et al., 2019).

- Effect on the inflammation and immunosuppression (in PMN):

Overall, it was shown that tEVs at the PMN trigger signaling cascades that induce the establishment of an inflammatory environment attracting tumor supporting cells. For instance, tEVs from metastatic melanoma cells increase the

expression of TNF, S100A8 and S100A9 in lung PMN (Peinado et al., 2012). These molecules activate pro-inflammatory gene signatures in lung fibroblasts and astrocytes, promoting lung and brain metastasis, respectively (Gener Lahav et al., 2019). Another recent study showed that in colorectal cancer, primary tumors secrete ITG beta-like 1-enriched tEVs in circulation that stimulates an NF-κß signaling pathway which activates fibroblasts and induces the secretion of pro-inflammatory cytokines (IL-6, IL-8) in distant organs, contributing to PMN formation (Ji et al., 2020).

Besides inflammation, tEVs also mediate recruitment of immune cells at the PMN to promote an immunosuppressive environment. For instance, pancreatic cancer derived tEVs were reported to induce the recruitment of macrophages and granulocytes in liver participating to PMN establishment (Costa-Silva *et al*., 2015). Moreover, it was found that tEVs also promote the accumulation of myeloid-derived suppressor cells (MDSC), directly inhibiting T-cell growth and decreasing NK cell cytotoxicity in PMN (Wen et al. 2016). Additionally, it was reported that melanoma tEVs contain small nuclear RNA that can promote PMN in the lung through TLR3 activation and the release of cytokines leading to the recruitment of neutrophils. These neutrophils can alter their polarization displaying then tumor promoting effects (Liu et al. 2016). Besides tEVs role in the recruitment of immune cells within the PMN, they also play a role in the immune escape. Similarly, to what was described for the primary TME, PD-L1-mediated immunosuppression also impacts PMN. It was found that systemic presence of PD-L1 onto EVs from the circulation positively correlates with metastatic burden in patients. Hence, PD-L1 from EVs in the circulation impairs immune response and enhances metastasis formation (Chen et al., 2018).

Altogether, the inflammatory status of PMN combined with the establishment of an immunosuppressive environment mediated by tEVs, participate to the formation of a permissive “soil” for secondary tumor formation, survival, and growth.

- Effect on extracellular matrix:

Once tEVs reach the PMN, they can remodel the ECM network (Mu et al. 2013; Medeiros et al. 2020). Besides their capacity to transport MMP and degrade the matrix (Sung et al., 2021), EVs can also carry ECM molecules such as fibronectin and transfer it to recipient cells or to the new environment (Antonyak et al., 2011; Sung et al., 2015), modifying the PMN. They can also alter secretion of ECM

molecules by ECM producer cells. For instance, tEVs containing mutant p53, modify fibroblast phenotype to produce abnormal ECM with different organization and composition (Novo et al, 2018). EVs from pancreatic cancer cells contribute to ECM remodeling at the liver PMN by transferring migration inhibitory factor (MIF) to Kupffer cells inducing release of TGF-β, which in turn promotes collagen I deposition and production of fibronectin by hepatic stellate cells. (Costa-Silva et al. 2015). Another study from the same group also showed that the uptake of breast cancer EVs by lung fibroblasts stimulates their activation and fibronectin secretion (Hoshino et al. 2015).

These studies highlighted the important role of tEVs in ECM remodeling at PMN which supports tumor cell invasion, seeding, resistance to apoptosis and, ultimately, enhances metastasis development.

These selected examples illustrate well the various aspects of EVs in physiological and pathophysiological contexts and particularly their action at distance from the secreting site. In cancer, this feature is paramount for their involvement in PMN establishment at distance from the primary tumor (Gao et al., 2021). A last but, striking example, is the capacity of breast cancer cell tEVs to reprogram glucose metabolism in non-tumor cells at distant sites (i.e. lung and brain). TEVs decrease their capacity to uptake glucose, increasing available nutrients for subsequent cancer cells, thereby, promoting PMN establishment and metastasis (Fong et al., 2015).

While I tried to give an overview of their function through selected examples (particularly their role at distance), there are multiple other cellular processes regulated by long-range tEVs communication. Yet, the different underlying mechanisms involved are not well known. Depending on the secreting cells, EVs can have antagonist roles in given context which makes their study even more difficult. For instance, they are also involved in tumor dormancy and were described to trigger both, maintenance and awaking processes on tumor cells (Ono et al., 2014; Bliss et al., 2016; Walker et al., 2019). Better understanding of these mechanisms could shed light on tumor cell immune escape and cancer relapse after years of latency, which is one of the major issues in this disease. In addition, EVs functions can also differ from the one attributed to their parent cells. For instance, if TAM are usually considered as pro-tumorigenic (because of their

immunosuppressive properties), their EVs could have on the contrary tendency to activate immune response by stimulating T cell activation and proliferation, suggesting opposite roles between TAM and TAM-derived EVs (Cianciaruso *et al*., 2019). These differences are thought to be closely linked to their origins and their biogenesis processes. The diversity of EVs populations is correlated with the diversity of production and secretion pathways that are better understood and characterized each year.

3. Extracellular Vesicles biogenesis and secretion

3.1. Terminology

The name “Extracellular vesicles” refers to a wide variety of vesicles composed by a lipidic membrane from cell origin and with a diameter that varies between 10nm to several µm. Recently, the name “extracellular particles” was proposed to include non-vesicular nanoparticles produced by cells such as the recently identified exomer subpopulation. As I previously explained the main subtypes of EVs and their origin (**Figure 2**), in the following section, I will briefly discuss the different biogenesis mechanisms and their regulation. I will use the term “EVs” to generally refer to vesicles, the term exosomes to refer to endosomes-derived vesicles and microvesicles (MV) to refer to plasma membrane derived veiscles, as it is advised by the community in the MISEVs recommendation (Théry et al., 2018).

3.2. Biogenesis and secretion

Exosomes biogenesis depends on multivesicular body (MVB) formation and regulation in secreting cells. The MVB is a late endosome formed during maturation of the endolysosomal pathway, which can ultimately fuse with lysosomes for degradation (Scott et al., 2014). Its characteristic structure is easily recognizable on electronic microscopy images (**Figure 10**). During MVB formation, small invaginations bud within the lumen and form the intraluminal vesicles (ILV). Thus, ILV (future EVs) cargo proteins depend on their trafficking to late endosome. Part of these proteins are coming from Golgi apparatus after post-translational modifications, from plasma membrane after internalization and recycling, or from

cytoplasm. In the context of EVs secretion, MVB are redirected to the plasma membrane, fuse with the plasma membrane and release ILV in the extracellular space, which become exosomes.

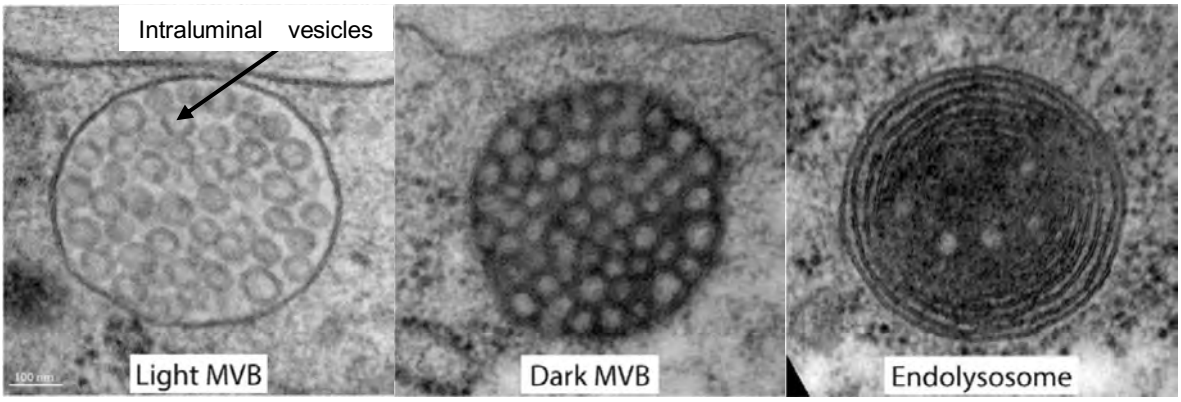

Figure10: Different types of MVBs and endolysosome seen by electron microscopy in the worm *C. elegans*. Specific structures of intracellular compartments are seen: intraluminal vesicles in MVB and multiple membrane containing endolysosome. Extracted from Hyenne et al., 2015.

The formation of ILV is controlled by ESCRT-dependent pathways and ESCRT-independent pathway (Kowal et al., 2014; Van Niel et al., 2018; Mathieu et al., 2019). ESCRT machineries are groups of proteins formed by regulated assembly sequence of several subunits that makes up the ESCRT complex. In ESCRT-dependent pathway, ESCRT-0 (STAM1/2, HGS), -I (TSG101), -II (VPS22), -III (CHMP4), Alix, VPS4, VTA1 and eventually syndecan, syntenin and VPS32 proteins are sequentially recruited. A regulated cascade of events involving these proteins controls protein sorting in ILV and their formation in the MVB (Baeitti et al., 2012; Schöneberg et al., 2017; Wenzel et al., 2018). It was shown that impacting expression of these machinery components not only modulates exosome secretion, but also affects their cargo load (Colombo et al., 2013; Larios et al., 2020), showing the role of these molecules in both biogenesis and cargo sorting of exosomes (**Figure 11**).

ESCRT-independent pathways were identified since depletion of all ESCRT complexes does not totally impair ILV formation (Stuffers et al., 2009). Other molecules/proteins maintain and control the production of exosomes in absence of ESCRT complexes. For instance, the tetraspanin CD63 (Stuffers et al., 2009; Edgar et al., 2014; Van Niel et al., 2011) and the small GTPase Rab31 (Wei et al., 2021)

participate to ILV formation and CD9, CD82, CD81 (van Niel et al., 2018; Chairoungdua et al., 2010; Luga et al., 2012) are more dedicated to sorting of proteins in late endosomes/ILV. Of note, Ral-1 in C. elegans, a Ras related GTPase homolog to Ral proteins in mammals, was also identified to play a role in ILV generation, MVB transport and EVs secretion (Hyenne et al., 2015). Similarly, sphingomyeline, ceramide, lysobiphosphatidic acid (LBPA), and lipid-raft play a role in different biogenesis mechanisms described as lipid-dependent biogenesis pathways (Trajkovic et al., 2008; Kajimoto et al., 2013; Valapala et al., 2011; Egea-Jimenez and Zimmermann, 2018; Larios et al., 2020; Wei et al 2021). Although Syndecan, Syntenin, and Alix proteins were shown to take part in ESCRT-dependent mechanisms in ILV formation and cargo sorting (Baietti et al., 2012; Larios et al., 2020), they also function independently of ESCRTcomplexes, through the syndecan-syntenin-alix pathway (Friand et al., 2015; Ghossoub et al., 2014; Leblanc et al., 2020) in which tetraspanin TSPAN6 negatively regulates exosome biogenesis (Ghossoub et al., 2020). (**Figure 11**).

Once ILVs are formed, MVBs can be transported to the plasma membrane in a process controlled by various small GTPases (**Figure 11**). Rab27a and Rab27b (Ostrowski et al., 2010; Bobrie et al., 2012; Mathieu et al., 2019) as well as Rab11 and Rab35 (Savina et al., 2005; Hsu et al., 2010) regulate MVB transport, docking and tethering to the plasma membrane, thereby mediating ILV secretion. More recently, Rab39 GTPase was shown to control specifically basolateral secretion of exosomes, and Rab37 apical release in canine kidney epithelial cells (Matsui et al., 2022).

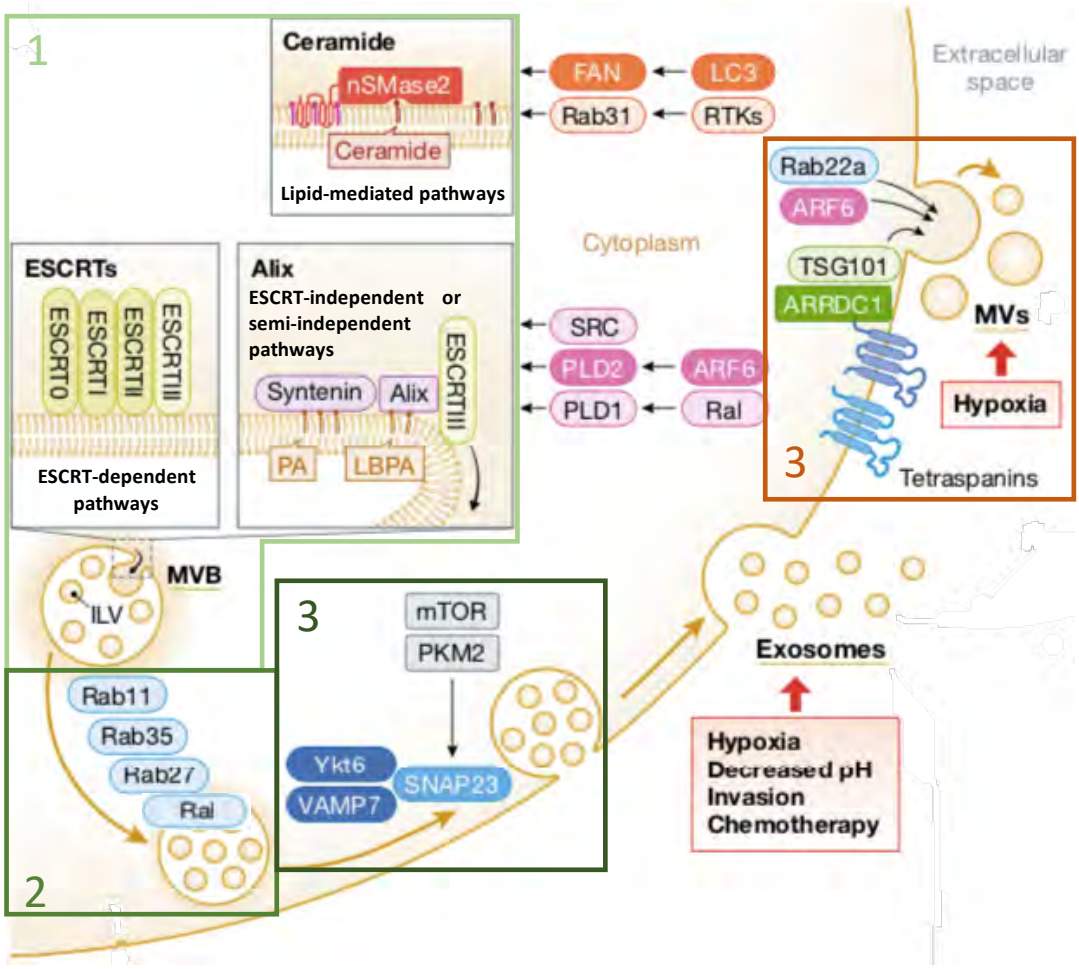

Figure 11: Biogenesis of endosomes-derived extracellular vesicles (exosomes) and plasma membrane-derived vesicles (microvesicles, MV). Exosomes biogenesis follows a sequence of events: 1. Loading and sorting of protein cargo into EV, 2. Transport to the plasma membrane and 3. Release by fusion of the MVB with plasma membrane. Biogenesis of microvesicles requires membrane curvature mediated by cytosqueleton components and budding of the plasma membrane. Modified from Lucotti et al., 2022.

The last step of exosomes release is the fusion of MVB with plasma membrane. SNARE (soluble N-ethylmaleimide-sensitive fusion attachment protein receptor, R-SNARE and Q-SNARE) complex mediates membrane fusion events between compartments (Yoon and Munson, 2018). Logically, they were also shown to mediate MVB fusion at the plasma membrane (Koles et al., 2012; van Niel et al., 2018; Verweij et al., 2018). For instance, Vamp7, YKT6, SNAP23 as well as syntaxine 4 and syntaxine 5 play a role in EVs release at the plasma membrane in human cell lines and *C. elegans* (Palmulli and van Niel 2018; van Niel et al., 2018 ; Verweij et al., 2018; Hyenne et al., 2015). There is still a lack of knowledge about how MVB redirection to plasma membrane and ILV release are regulated.

Cytoskeleton components could play an important role in these mechanisms (e.g. in MVB docking at plasma membrane) as they regulate organelle positioning and trafficking inside cells (Granger et al., 2014). For instance, MVB move along microtubules and actin regulation controls EVs secretion. Cortactin, together with Rab27a and coronin1b, were shown to mediate MVB and plasma membrane interaction and EVs secretion (Sinha et al., 2016) (**Figure 11**).

In addition to biogenesis pathways, the balance between secretion and degradation regulates EVs secretion. Along the endolysosomal pathway, endosome acidification increases and ultimately late-endosomes/MVB fuse with lysosomes for degradation, forming the endolysosome compartment (**Figure 10**). It was suggested that EVs biogenesis pathway includes mechanisms to escape this degradative fate. For instance, knockdown or disruption of V-ATPase protein impairs the acidification of MVB and increases EVs release (Kozik et al., 2013; Guo et al., 2017). Similarly, pharmacological inhibition of degradation (e.g. by the use of bafilomycin A) also increases EVs secretion (Edgar et al., 2016; Villarroya-Beltri et al., 2016). In addition, V-ATPase regulation on MVB by neutral sphingomyelinase 2 can decrease acidification and increase EVs secretion (Choezom and Gross, 2022). Interestingly, it was shown that impairing lysosomal function via inhibition of MEK/ERK pathway increases EVs release in cancer cells, suggesting that lysosomal and degradation escape is a mechanism used by cancer cells to release more EVs (Hikita et al., 2022). Moreover, loss of sirtuin 1 expression in breast cancer cells decreases lysosomal acidification and MVB targeting to degradation. Consequently, these cancer cells release EVs with a unique cargo that can promote cancer progression (Latifkar et al., 2019). Overall, recent discoveries suggest that EVs secretion could be tightly linked to MVB acidification and degradation through the endolysosomal pathways. However, this mechanism is still not well understood.

Compared to exosomes, mechanisms that control ectosomes/microvesicles (MV) budding from plasma membrane are less known. Outward budding and membrane scission depend on specific lipids families and enzymes. MVs arise from membrane domains rich in ceramide and cholesterol that facilitate membrane curvature (i.e. lipid-raft) (Sedgwick & D'Souza-Schorey, 2018). For instance, cholesterol depletion decreases MV release (del Conde et al., 2005). Additionally, enzymes regulating lipids such as flippase, floppases, scramblases or SMase family enzyme (acid sphingomyelinase, A-SMase) also mediate membrane

curvature by rearrangement of lipids in the membrane, thus affecting MV formation and secretion (Al-Nedawi et al., 2008; Piccin et al. 2007; Bianco et al., 2009). More recently, it was shown that the glycocalyx is also playing a role in membrane curvature, participating to MV release (Shurer et al., 2019).

Cytoskeleton regulators and cell cortex activity are also important in MV generation. For instance, ARF6 and RhoA/ROCK signaling control actin contractility at the periphery of the cell to facilitate MV secretion (Muralidharan-Chari et al., 2009; Li et al., 2012; Sedgwick et al., 2015). Additionally, Rab35 together with ARF6 regulates fascin proteins that control actin bundling and MV formation (Clancy et al., 2019) and finally ESCRT-I subunit (TSG101) was shown to interact with ALIX and ARRDC1 proteins at the vicinity of the plasma membrane controlling MV release (Nabhan et al., 2012). Interestingly, hypoxia was shown to trigger MV release in Rab22a dependent mechanism (Wang et al., 2014) opening questions for hypoxia-induced release of MV in tumor (Clancy et al., 2021). Overall, current knowledge about MV biogenesis shows that plasma membrane lipids and the cytoskeleton are the two main actors of MV biogenesis. However, it will need more studies to fully understand their regulatory mechanisms.

Despite recent discoveries, key questions remain largely unanswered in EVs biogenesis (exosomes and microvesicles). Firstly, the link between the various biogenesis mechanisms and the diversity of EVs subpopulations secreted by one single cell or by different cells is not understood. Secondly, there is no clear idea on how cell state and extracellular signals control biogenesis pathways and/or sorting mechanisms. Thirdly, if EVs biogenesis mechanisms seem to be quite conserved between species (e.g. in yeast, drosophila or *C. elegans* (Linnemannstöns et al., 2022; Hyenne et al., 2015)), yet we do not know how one particular pathway is favored compared to another in different contexts/organisms/cells. Finally, it is thought that biogenesis/cargo sorting pathways impact the subsequent function of EVs once secreted, but this link is not understood yet.

3.3. EVs composition and sorting mechanisms

- Exosomes cargo sorting:

Besides their membrane lipids, EVs contain proteins (including receptors and surface molecules), enzymes and nucleic acids (**Figure 12**). Their cargo content dictates their interactions and their effect on receiving cells as well as on the ECM (Mu et al., 2013). The cargo can differ depending on EVs origin/subpopulation (Haraszty et al., 2016; Kowal et al., 2016; Jeppesen et al., 2019), pathophysiological state of the secreting cells (Hurwitz et al., 2016; Min et al., 2019; Hoshino et al., 2020) or the metabolic state of the organism (Whitham et al., 2018; Zhang et al., 2021). For instance, in cancer research, comparison of protein load in EVs is done to identify distinct EVs proteomes between patients and healthy donors (Hurwitz et al., 2016; Hoshino et al., 2020). Additionally, this kind of studies showed that differential protein expression in EVs does not reflect similar variations in the secreting cells. This supports the idea of selective packaging of cargo into EVs (Hurwitz et al., 2016).

Protein loading into EVs, particularly into exosomes but not exclusively, are thought to be mediated by tetraspanins (CD9, CD63, CD81), integrins, syntenin as well as ESCRT proteins and Alix (van Niel et al. 2018; Andreu and Yáñez-Mó 2014; Latysheva et al., 2006; Baietti et al., 2012). They control not only the budding of ILV inside MVB but also loading of proteins inside future exosomes. More recently, it has been suggested that SIRT proteins (SIRT1 and SIRT2) participate to exosome biogenesis and cargo sorting (Li et al., 2019; Latifkar et al., 2019; Lee et al., 2019). Interestingly, Rab31 controls EGFR loading into exosomes after its phosphorylation during ILV formation (Wei et al., 2021), and TSG101 also controls E-cadherin recruitment to exosomes through interaction with a late-domain motif in E-cadherin tail (Bänfer et al., 2022). Additionally, post-translational modifications (e.g. ubiquitination, SUMOylation, phosphorylation glycosylation) also mediate cargo sorting into EVs (Anand et al., 2019; Carnino et al., 2020).

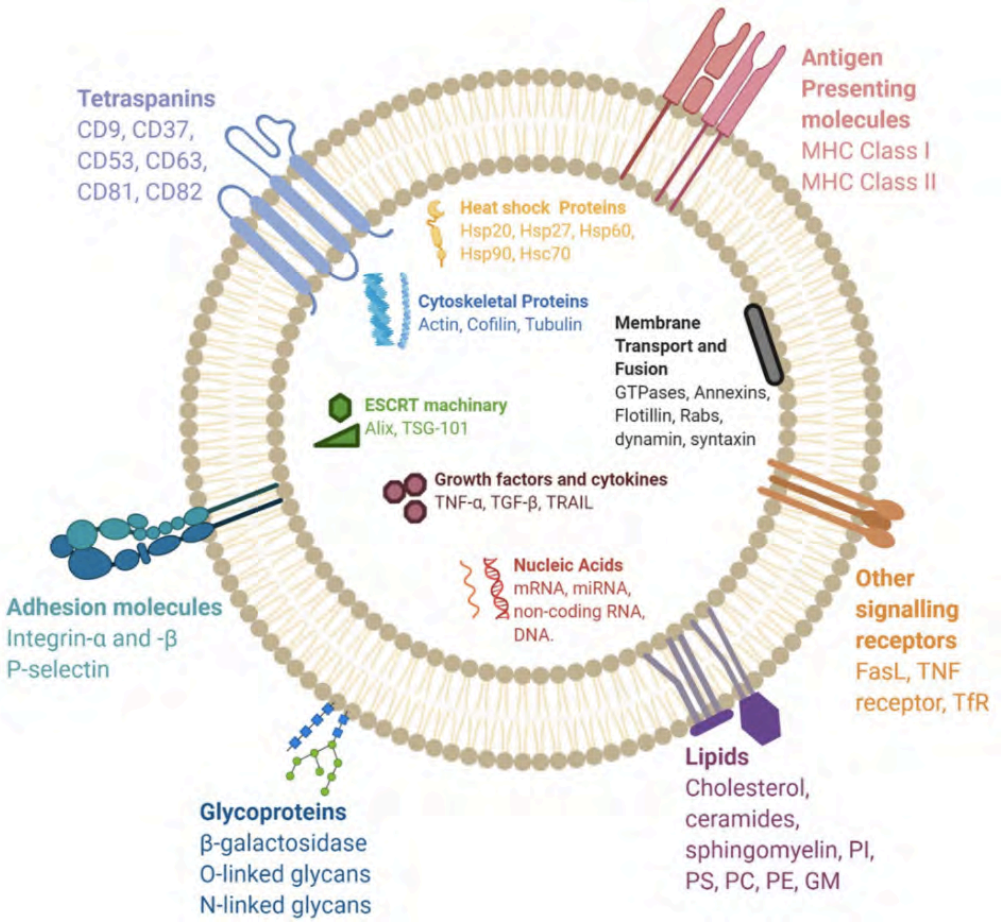

Figure 12: Composition of Extracellular Vesicles (EVs). Multiple cargos can be transported via EV. This scheme represents an overview of the different molecules identified as EV cargo, their respective presence in EV differ depending on their secreting cells and the type of EV subpopulation. EV can contain transmembrane proteins (e.g., tetraspanins, glycoproteins and adhesion molecules), cytosolic proteins (e.g. heat shock proteins (Hsp), cytoskeletal proteins, ESCRT components, cytokines) and multiple lipids (e.g. cholesterol, ceramides, sphingomyelin, phosphatidylinostol (PI), phosphatidylserine (PS), phosphatidylcholine (PC), phosphatidylethanolamine (PE)). Finally, they can also transport mRNA, miRNA, non-coding RNA in their lumen (of note, DNA cargo could be mainly associated with tumor derived EV). Hsc = Heat shock cognate; TSG = tumor suspectibility gene; TNF = tumor necrosis factor; TGF = Transforming growth factor; TRAIL = TNF-related apoptosis-inducing ligand; FasL = Fas ligand; TfR = Transferrin receptor. Extracted from Gurung et al., 2021.

Nucleic acids are also present in EVs. Presence of DNA in endosome-derived EVs is still debated, as well as its localization (inside or outside EVs) (Lázaro-Ibáñez et al., 2019) and their consideration as co-isolated contaminant products rather than a proper EVs cargo (Mateescu et al., 2017; Jeppesen et al., 2019). However, it could be different in cancer context, as more proofs supporting DNA as a functional tEVs cargo were reported these last years (Maire et al., 2021; Lucotti et al., 2022). In contrast, RNA and non-coding RNA cargo are more documented. There is a large diversity of nature (mRNA, miRNA, ncRNA, RNA fragments etc…) and function of these RNA (O'brien et al., 2020). Although, functional RNA transfer

and its effect on receiving cells is now quite documented in different contexts, a paradox remains, since only an extremely low quantity of RNA, and particularly miRNA, is packed into EVs (Li et al 2014; Chevillet et al., 2014; Wei et al., 2017). Yet, similarly to proteins, RNA cargo in EVs do not necessarily reflects RNA contain of their corresponding secreting cells, suggesting active RNA sorting mechanisms in EVs (Leidal et al., 2020). Various proteins, such as nSMase2 (Kosaka et al., 2013), hnRNPA2B1 ribonucleotide (Villarroya-Beltri et al., 2013), YBX1 RNA-binding protein (Shurtleff et al., 2017), Ras-MECK network and AGO2 (McKenzie et al., 2016) or SYNCRIP (Santangelo et al., 2016) were shown to control RNA sorting into EVs via specific RNA targeting sequences. Interestingly it was reported that, in cancer cells, miRNA sorting into EVs can be regulated by different pathways, either selective or non-selective, supporting the idea that a unique cell can produce different EVs populations with different cargo load (Temoche-diaz et al., 2019). Recently, it was shown that small sequences of miRNA control their sorting into EVs (EXOmotifs) or retention into cells (CELLmotifs). The two RNA-binding proteins Alyref and Fus were shown to control the loading of miRNA into EVs (Garcia-Martin et al., 2022). Although, this study brought key insights in the field, RNA sorting into EVs is still far from being totally understood.

Lastly, lipids present in EVs membrane (e.g. phosphatidylcholine (PC), phosphatidylserine (PS), phosphatidylethanolamine (PE), phosphatidylinositol (PI), phosphatidic acid (PA), cholesterol, ceramides GM3, sphyngomyeline, glycosphingolipids) play an important role in vesicles formation, structure, membrane curvature, trafficking and release (Skotland et al., 2020; Skotland et al., 2019). Interestingly, it has been shown that there is a specific enrichment in some lipids (cholesterol, PS, PA) and low levels of other (PC, PI) in EVs compared to cells, suggesting a specific selection of lipids (Skotland et al., 2020). However, the mechanism regulating their incorporation into EVs during vesicle formation remains unknown.

- microvesicles cargo sorting:

The mechanisms regulating cargo sorting into ectosomes (MV) are even less understood. However, some key actors were identified. For instance, TSG101 mediates MV release and T cell receptor loading in T cell MV (Choudhuri et al, 2014). Additionally, VAMP3 (a SNARE protein) (together with CD9) and a complex between ARF6 and Exportin5, were identified in tumor cells to control loading of

proteins (notably matrix metalloprotease) and nucleic acid (miRNA) respectively, into MV (Clancy et al, 2015; Clancy et al, 2019). In addition, the small GTPase Rab22a was found to colocalize with MV in formation, controlling cargo loading into hypoxic cancer cells (Wang et al., 2014). Another study found that a 25-nucleotide motif sequence containing short CTGCC sequence in mRNA could mediate their sorting into MV (Bolukbasi et al., 2012). Cytosolic protein loading into MV requires interactions between cargo protein and plasma membrane at lipid-rafts location. Thus, the post-translational modifications that control protein anchorage at the plasma membrane also control their sorting into MV (van Niel et al., 2018). Yet the exact mechanisms that control nucleic acid addressing to plasma membrane and loading into MV is far from being understood entirely.

Identification of EVs cargo and its composition is of uppermost importance as it will define EVs capacity to interact with their environment and receiving cells, controlling the organotropism of EVs, their interaction with other molecular actors, their capacity to disseminate through body fluids and reach their receiving cells/organs, and ultimately their function at these targeted sites.

4. EVs dissemination, body fluids and biomechanics

4.1 Joining the circulation

After their secretion, EVs are directly exposed to the extracellular space. Their repertoire of cargo molecules allows them to interact with their surroundings. For instance, the MMP that they transport can affect the remodeling of the ECM (Hakulinen et al., 2008; Mu et al., 2013). In addition, tEVs mediate the secretion, recruitment and regulation of ECM proteins such as laminins, collagen, fibronectine and tenascine C (Antonyak et al., 2011; Hoshino et al., 2013; Sun et al., 2021). This feature has dramatic consequences for tumor cell invasiveness at the primary and PMN site (cf section **2**). How EVs are transported from their secretion site to body fluids remains poorly known, specifically for EVs secreted by deep cell layer in poorly vascularized regions. In the case of tEVs, the aberrant vasculature (i.e. permeabilized and fragile) of the TME, could favor their dissemination inside vascular system. Additionally, the interstitial fluid pressure gradient in the tumor (cf **Figure 7**) could enhance tEVs drainage toward peripheral lymphatic vessels (Follain et al., 2020). Thus, two main

routes could mediate tEVs dissemination at long range scale: the tumoral lymphatic drainage of interstitial fluids and their passage in blood flow via dysfunctional and permeable vessels (Broggi et al., 2019; García-Silva et al., 2019; Maus et al., 2019). Additionally, a more exotic hypothesis could be that EVs use cellular shuttle to reach circulation. As described before, TAM can transfer tumor cell-EVs components to other cells of the TME (Umakoshi et al., 2019). However, proper “re-secretion” of intact tEVs was not described in this study, rather a transfer of material through macrophage membrane blebs (Umakoshi et al., 2019). This hypothesis is for now quite conjectural but also very interesting and will be discussed later in section **5**.

In the following sections I will discuss EVs present in body fluids and refer to them as “**circulating EVs**” by opposition to EVs that act at a local range, near their site of secretion. For the sake of brevity, I will describe lymph and blood EVs, although EVs are present in other body fluids (urine, milk, sweat, saliva, tears etc…) in human and animal models (Karimi *et al*., 2018; Yáñez-Mó et al., 2015); Butler, Abdelhamed, & Kurre, 2018; Hoshino et al., 2020, Rikkert et al., 2020, García-Silva et al., 2019, Lässer et al., 201; Zhao *et al*., 2020). I will mainly focus on circulating EVs in the context of cancer. EVs levels are usually elevated in the body fluids of cancer patients (Hoshino et al., 2020; Rikkert et al., 2020; García-Silva et al., 2019) such that it was suggested that this parameter could be used for diagnosis (Sabbagh et al., 2020).

4.2 EVs in lymph and lymphoid organs

In organs, interstitial fluid present in between cells is drained by the lymphatic system, filtered by lymph node, becomes lymph and is reinjected into the circulatory system. Interstitial fluid drains many different components coming from cell secretions and cell debris, including soluble factors and more importantly EVs, that could eventually accumulate in lymph nodes and lymph. Thereby, because of the biophysical and directional properties of the lymphatic system, when EVs are drained by the lymph, they first encounter lymphatic vessels and lymphoid organs and therefore likely to accumulate there. This is facilitated by the interstitial pressure in solid tumors (see **Figure 7**) (Swartz and Fleury, 2007; Cornelison *et al*., 2018). On one hand, these mechanical properties and flow direction of the lymphatic system facilitate tEVs interactions with immune cells present in lymphatic drainage organs (Pucci et al., 2016). These interactions can promote antigen presenting cells to activate immune

response via EVs-mediated antigen transport (Théry et al 2002), facilitating immune surveillance (Pucci et al., 2016). On the other hand, accumulation of tEVs in these location makes lymphatic system and lymphoid organs an early site for PMN and subsequent metastasis formation (Hood *et al*., 2011). Supporting this hypothesis, studies showed an increased accumulation of melanoma tEVs bearing tumorigenic markers in lymph and lymphoid organs than in blood (García-Silva et al., 2019; Broggi et al., 2019) and adenocarcinoma, gastric and colorectal cancer tEVs were shown to induce PMN formation in lymph nodes (Jung et al., 2009; Liu et al., 2016; Sun et al., 2019). For instance, tEVs expressing CD97 increase the expression of CD55, CD44v6, CD151, CD46 and EpCam in LN thereby enhancing cell proliferation, migration and invasion at this site, supporting the establishment of PMN (Liu et al., 2016). These studies, and others, support the idea that lymph nodes, as the first draining organs, are privileged locations of tEVs accumulation and tEVs-mediated PMN formation. Hence, the lymphatic flow direction would be one of the biophysical parameters that mediate EVs and tEVs biodistribution, controlling apparition of PMN and secondary tumors (Maus et al., 2019). However, accumulation of tEVs in the LN does not impair necessarily their further dissemination and it is known that tEVs can trigger PMN and metastasis formation beyond sentinel lymph nodes, in other more distant organs (Maus et al., 2019; Broggi et al., 2019). It suggests that lymphatic circulation could participate to tEVs-mediated PMN formation in lymph nodes, but also that lymphatic drainage is not the only (biophysical) parameter that mediates tEVs organotropism, in addition to presumably not being the only route of dissemination.

4.3. EVs in blood

The blood circulatory system is also an important reservoir of EVs from various origins. Depending on the studies, blood was shown to contain between10^9 to 10^{12} EVs/mL (Johnsen et al., 2019). This concentration varies depending on (patho)physiological parameters such as physical exercise (Whitham *et al.,* 2018; Zhang et al., 2021; Denham and Spencer, 2020), disease (notably cancer) (Peinado *et al*., 2012; Boulanger et al., 2017; Sabbagh et al., 2021), gender (Toth et al., 2007; Nielsen et al. 2014) and balance between EVs secretion and clearance (Imai et al., 2015; Matsumoto et al., 2020). In normal condition, circulatory EVs are mostly coming from vascular cells. Erythrocytes and platelets (Karimi et al., 2018; Flaumenhaft et al.,

2010), and monocytes and endothelial cells (Nielsen et al. 2014) were identified as main producers of circulating EVs. However, it is possible to isolate circulating EVs from other origins in blood, notably from tumor cells or stromal cells in cancer. Indeed, tEVs are found in high quantities in blood samples of cancer patients and it is associated with poor prognosis (Hoshino et al., 2020). For instance, it has been shown that the concentration of glioblastoma circulating EVs in plasma was higher in patients compared to healthy donor or patients with other brain lesions (Osti et al 2019). This concentration decreased upon surgery and tumor removal suggesting that plasma circulating EVs in the case of glioblastoma can originate from tumor or tumor-associated stromal cells.

Within the vasculature, EVs can interact with various cell types and blood components and affect the homeostasis of vascular tracts and notably the coagulation processes. For instance, pancreatic, glioblastoma and breast carcinoma tEVs transport pro-coagulant factors (Tissue Factor, P-selectin glycoprotein ligand-1(PSGL-1), podoplanin) and trigger thrombogenic events when interacting with platelets or neutrophils (Thomas et al., 2009; Tawil et al., 2021; Gomes et al., 2017; Leal et al., 2017). Although platelet aggregation is known for being involved in the formation of PMN (Lucotti et al., 2019), the role of EVs in this mechanism remains to be elucidated. However, it was shown that, metastatic tEVs can trigger low-density lipoproteins aggregation and tEVs uptake by monocytes, potentially affecting PMN formation by immunomodulatory events (Busatto et al., 2020). Overall, circulating tEV interaction with other cells (and notably the endothelium) is thought to be mediated by cell adhesion molecules (CAM). For instance, glycoproteins, ITG and other (e.g. ICAM-1) were shown to mediate circulating tEV interactions within the blood compartment (Jerabkova-Roda et al., 2022).

4.4. EVs biodistribution

Despite their relative stability fluids in absence of cells, several papers reported that circulating EVs have a rather short half-life in circulation. In mice, the majority of exogenously injected EVs are cleared from circulation after 2 to 10 min (Morishita et al 2015, Lai et al., 2014, Takahashi et al., 2013). It is explained by their rapid accumulation in two main receiving cell types: patrolling monocytes and endothelial cells (Imai et al., 2015; Kamerkar et al., 2017; Verweij et al., 2019). This can be in part

explained by the presence of specific CAM at the surface of circulating EVs. In cancer, tEVs biodistribution reflects the same organotropism as the secreting tumor cells when they form metastasis (Wen et al., 2016; Xu et al., 2018, Gerwing et al., 2020; Wu et al., 2020). Interestingly, injected EVs do not arrest at the first capillary bed they encounter, but rather colonize specific organ depending on EVs origin, showing a contribution of specific EVs factors (Gupta et al., 2020; Wiklander et al., 2015). As discussed before, EVs biodistribution depends on surface molecule repertoire such as ITG (e.g. α6β4/ α6β1 and αvβ5) and tetraspanins (TSPAN8 and CD151) (Hoshino et al., 2015; Yue et al., 2015; Wang et al., 2016; Wu et al., 2020; Armacki et al., 2020; Gerwing et al., 2020) as well as surface glycans and glycosylation status of proteins (Nishida-Aoki et al., 2020; Williams et al., 2019). Similarly, EVs adhesion molecules affect their uptake by monocytes. The presence of the transmembrane protein CD47 at the surface of EVs, for instance, precluded their internalization by monocytes (Kamerkar et al., 2017). Importantly, these CAM-mediated interactions dictate the function of circulating tEV. For example, CD44 and ICAM-1 at the surface of tEV were shown to mediate their capacity to form PMN (Jung et al., 2009; Zhang et al., 2022). Overall, EVs adhesion receptors play an important role in tEVs/cells interactions and mediate organotropism, biodistribution and function, although the ligands of these receptors are mostly unknown.

In addition to these mechanisms, it is possible that biomechanical forces, blood flow and vascular pattern also contribute to EVs organotropism and distribution similarly to the effect they have on CTCs. Our team and others previously showed that hemodynamic forces, together with sequential adhesive events, tune CTC arrest and metastasis formation (Follain et al., 2018; Osmani et al., 2019; Follain et al., 2021; Follain et al., 2020 Massagué et al., 2016). Particularly, our team identified a flow-dependent mechanism called endothelial remodeling that mediate CTC extravasation (Follain et al. 2018). Interestingly, while reduced flow promotes CTC arrest it decreases their extravasation capacities by impairing endothelial remodeling. On the contrary, increased flow decreases CTC arrest whereas it promotes CTC extravasation. Therefore, the permissive range identified in this study describes an intermediate flow allowing both CTC arrest and extravasation. This study showed for the first time that hemodynamic forces impact CTC intravascular arrest and extravasation, guiding thereby CTC and determining their homing. As CTC show many similarities with circulating tEV regarding adhesive properties (Jerabkova-Roda

et al., 2022), it is possible that flow-dependent processes also affect circulating tEV biodistribution, arrets and ultimately, uptake. In addition, several studies showed that hemodynamic forces (flow speed and shear stress) affect the uptake of synthetic nanoparticles (NP) of similar diameter to EVs (Bhowmick et al., 2012; Han et al., 2012; Han et al., 2015). Thus, a balance between molecular and hemodynamic factors could also control EVs distribution in the vasculature. Yet, the implication of hemodynamics in EVs biodistribution remains poorly investigated. Only one study, published at the end of my thesis, address this question (Qin et al., 2022). I will detail this study, as well as the NP ones in the discussion. Nevertheless, studying the role of hemodynamics on the uptake of circulating EVs by endothelial cells require to understand how endothelial cells respond to flow forces.

4.5 Hemodynamic sensing by endothelium

In response to fluid shear stress, the shape of endothelial cells is modified, cells elongate and orientate along the flow direction. A variety of apical membrane molecules and microdomains are involved in transducing and converting shear stress into intracellular signals leading to the activation of multiple downstream signaling pathways (Yamamoto and Ando, 2018). Among others one can cite ion channels, the glycocalyx, adhesion molecules and the primary cilia (Ando and Yamamoto, 2013; Tanaka et al., 2021). Tzima and colleagues showed that PECAM-1, VE-cadherin and VEGFR2 constitute a mechanosensory complex sufficient to transduce shear stress by triggering integrin pathway activation and downstream events that mediate endothelial cell alignment in direction of flow (Tzima et al., 2005). Several studies showed that shear stress induces the remodeling of actin cytoskeleton and is associated with modifications of intercellular junctions as well as focal adhesions (Inglebert et al., 2020; Tanaka et al., 2020; Thi et al., 2004). For instance, endothelial cell elongation and alignment requires actin assembly at one end of the stress fibers, leading to their growth, fusion with neighboring stress fibers and their reorientation, ultimately leading to their protrusion from cell membrane (Noria et al., 2004). The endothelial glycocalyx was described as another mechanism enabling the transduction of shear stress and the adaptation of endothelial cells to this stress (Thi et al., 2004; Tanaka et al., 2020; Wang et al., 2020). Several studies described that upon shear stress exposure, the endothelial glycocalyx undergoes organizational adaptive

changes through the synthesis of major glycocalyx structural components (e.g heparan sulfate, hyaluronan) and associated with actin cytoskeleton modification (Wang et al., 2020; Zeng and Tarbell 2014). Mechanosensitive channels have also been proposed as early shear stress transducers. It was for instance shown that potassium and calcium channels are flow-sensitive channels that trigger nitric oxide production leading to vasodilation and ultimately decrease wall shear stress (Ahn et al., 2017; Gerhold and Schwartz, 2016). Endothelial primary cilia are non-motile organelles protruding from cell apical membrane and have been described to play a role in fluid shear sensing by transducing extracellular fluid shear into intracellular signaling. It was shown that the absence of primary cilia in endothelial cells reduces cytosolic calcium and nitric oxide production that is triggered by fluid shear stress (Nauli et al., 2008; Gerhold and Schwartz, 2016).

4.6. Technical limitations for circulating EVs studies

Although circulating EVs gained attention these past years, their *in vivo* study remains challenging due to the difficulties to monitor them dynamically in circulatory system. It is particularly difficult to follow with precision a population of EVs throughout an organism and its accumulation in organs. Thereby, the organotropism and behavior of these circulatory EVs in fluids is poorly understood. To date, in cancer and tEVs research, no *in vivo* model allows to follow entirely and document the fate of tEVs, from their secretion by an endogenous growing tumor, through their journey to vascular system, their accumulation in distant organs up to the development of metastasis in this organ afterwards. Injection of pre-labelled EVs with lipophilic dyes in mice/model organisms is commonly used to track tEVs *in vivo* (Wiklander et al., 2015; Wen et al., 2016; Peinado et al, 2012; Costa-Silva et al, 2015; Hoshino et al, 2015; Rodrigues et al, 2019). However, the amount of labelled EVs injected, the potential aggregation of the dyes and their fluorescent half-life, are important limitations and it questions the physiological relevance of these models. Moreover, to correctly identify organs where EVs accumulate, mice sacrifice and organ removal is necessary (Wiklander et al., 2015; Hoshino et al., 2015), thus precluding dynamic *in vivo* imaging. To overcome these limitations, several studies used fusion proteins to follow biodistribution of circulating tEVs using fluorescent, bioluminescence or radioactivity reporters (Suetsugu et al, 2013; Takahashi et al., 2013; Lai et al., 2014; Morishita et al, 2015,

Lai et al 2015; Hikita et al, 2018; Zaborowski et al., 2019; Wang et al, 2020). Overall, these studies show that injected or endogenous EVs and tEVs accumulate rapidly in the spleen, liver, lungs, pancreas and the gastro-intestinal tracts, and to lesser extent in the heart, brain and muscles of mice. Many different types of tEVs were also described to accumulate in the bone marrow, however the proportion in which tEVs accumulate in these organs/tissues are dependent of EVs-types, methods of injection and EVs quantities (Gupta et al., 2020). Interestingly, it has been reported that the biodistribution of small EVs can be affected by the physiological state (for example sepsis) of the individual (Mirzaaghasi et al., 2021). This characteristic should be considered in the study of tEVs biodistribution since tumoral burden could affect this behavior. As another approach, intravital imaging in rodent could be a good way to visualize EVs *in vivo*. Yet, it is not an easy handling technic and depends on the localization of optical windows (van der Vos et al., 2016; Zomer et al., 2015). Another approach is to use the Cre/Lox system in mice models to visualize EVs dissemination and investigate the biodistribution of floxed EV reporter (Ridder et al., 2014; Ridder et al., 2015; Zomer et al., 2015; Kur et al., 2020; Bittel 2021). With this approach, leukocytes, neurons, microglia, and endothelial cells were shown not only to uptake tEVs but also to express fluorescence suggesting a proper reconstitution of the Cre/Lox system and proper transfer of tEVs cargo in the targeted tissue (Ridder et al, 2015; Kur et al., 2020; Bittel 2021). Additionally, it was shown that melanoma tEVs can efficiently transfer Cre RNA in lymph nodes, lungs, and spleen allowing recombination and expression of the fluorescent reporter enabling to follow tEVs biodistribution (Zomer et al., 2015). Although these technics allow to study the fate of circulating EVs at the organism scale in mice, they do not allow to investigate easily circulating EVs behavior at single vesicle or single receiving level and high spatio-temporal resolution, highlighting the importance of developing alternative approaches and models.

4.7. Circulating tEVs as diagnosis marker

As circulating EVs can now be isolated relatively easily form body fluid samples and their content analyzed by lipidomic, proteomic or transcriptomic approaches, they were suggested to be a powerful tool to detect diseases and classify diseases stage, notably in cancer (Zhou et al., 2020; Hoshino et al., 2020; Lucotti et al., 2022). It was suggested that the overall plasmatic concentration in EVs (independently of their

origin) could be used in clinical diagnosis (e.g. in glioblastoma) (Sabbagh et al., 2020), as well as the precise analysis of circulating EV cargo composition. For instance, RNA or protein signature in circulating EVs isolated from patients' blood sample could help the detection of different types of cancer such as nasopharyngeal carcinoma, hepatocellular carcinoma, non-small cell lung cancer or breast cancer (Ye et al., 2014, Sohn et al., 2015, Liu et al., 2017, Keup et al., 2018, Koi et al., 2020; Hoshino et al., 2020). A recent study proposed a rapid and feasible procedure allowing the characterization of circulating EVs from serum of multiple myeloma patients and their use as biomarker (Laurenzana et al., 2021). However, despite an increasing number of publications describing circulating tEVs as potential cancer marker, only few have been approved for clinical use to my knowledge. As an example, the non-invasive ExoDx Prostate (IntelliScore) (EPI) test has been developed and tested in clinic to detect specific RNA in urinary exosome. It allows to stratified high from low-grade prostate cancer and avoid unnecessary medical examination and biopsy (McKiernan et al., 2018; Margolis et al., 2022). The development of diagnostic tool can be limited by several reasons. Among others the difficulty to properly purify circulating EVs populations from body fluids and to remove unwanted contaminants (such as lipoproteins). Additionally, the heterogeneity of EVs cargo seen in different individuals also restrains diagnostic tool development. Interestingly, it has been suggested that the lymphatic exudate of melanoma patients could be a better source of biomarker than blood, specially at early stages (Broggi et al., 2019; García-Silva et al 2019).

Altogether, it appears that finding more specific markers, or molecular signature as well as improving protocols for EVs isolation are needed to completely understand the variation of circulating EVs concentration and cargos upon cancer progression and metastatic outgrowth.

5. EVs uptake and intracellular fate

5.1. Uptake mechanisms

Until I started my PhD, EVs uptake had never been studied in flow conditions. Therefore, everything I am describing hereafter come from studies performed in static conditions. The first step in EVs uptake is the initial interaction/recognition between EVs and receiving cells. Whether EVs uptake is mostly a specific or a random

mechanism remains to be fully addressed. However, the specificity of EVs-cell interactions and cell-targeting behavior of EVs observed in many studies support a specific process. For instance, EVs derived from oligodendrocytes are specifically internalized by microglia but not by neurons (Fitzner et al., 2011). Inversely, amyloid precursor protein-carrying EVs from neuroblastoma cells preferentially accumulate in neurons compared to glial cells (Laulagnier et al., 2017).

EVs-cell interactions are usually either mediated by direct ligand-receptor binding or are indirect, with adhesion of EVs to cell-adjacent ECM molecules (e.g. fibronectin, collagen-I, laminin) facilitating EVs uptake at given sites by specific cells (Clayton et al., 2004; Sung et al., 2015; Hoshino et al., 2015; Purushothaman et al., 2016). These interactions happen at the plasma membrane but can also occur at specialized structures such as filopodia (Heusermann et al., 2016). Moreover, it was suggested that the dynamic of EVs-cell interaction varies depending on the type of receiving cells (e.g. between microglia and astrocytes) (Prada et al., 2016). In this study the fact that microglial cells are macrophages could explain this difference of uptake. Supporting this, it was shown that macrophages actively internalize EV through phagocytosis (Feng et al., 2010). Additionally, it was shown that lower temperature decreases EVs uptake, showing that EVs uptake is an active process requiring energy (Escrevente et al., 2011; Christianson et al., 2013).

Treatment of EVs or receiving cells by proteinase K was described to decrease EVs uptake, showing that surface adhesion molecules mediate binding of EVs to specific receiving cells, thus controlling receptor mediated EVs uptake (Escrevente et al., 2011). As it was previously mentioned, the presence of some proteins at the surface of EVs could inhibit their uptake. This is for instance the case of CD47, an ITG-associated transmembrane protein that can trigger phagocytosis-inhibiting signal (Kamerkar et al., 2017). Inversely, other key receptors mediate and promote EVs uptake, such as lectins, integrin (e.g. α4 or β4) and tetraspanins (TSPAN8) (Rana et al., 2012; Hoshino et al., 2015; Yue et al., 2015). For instance, complexes formed by these adhesive molecules at EVs surface (e.g. Tspan8-CD49d (ITGα4)) mediate proper binding and uptake of rat adenocarcinoma tEVs by endothelial cells (Nazarenko et al., 2010). Additionally, glypican 1 and glycoprotein CD44 were shown to participate to EVs uptake (Gonda et al., 2019; Melo et al., 2015) as well as the overall glycosylation status of EVs surface proteins and glycan (Nishida-Aoki et al., 2020; Williams et al., 2019). Surface molecules on receiving cells also play a role in EVs-cell

interactions. Interestingly, heparan sulfate proteoglycans at the surface of receiving cells, but not at the surface of EVs, favor tEVs uptake in glioblastoma cells and epithelial cells (Chinese Hamster Ovary cells, CHO cells) (Christianson et al., 2013). Going further, a comprehensive study recently showed that it is ITGβ3 on tEVs that interacts with heparan sulfate proteoglycans on receiving cells to mediate tEVs internalization and intercellular communication in breast cancer model (Fuentes et al., 2020). Nevertheless, most of the time corresponding ligands at the surface of cells often failed to be identified. Better understanding of their nature and identity would greatly improve our understanding of EVs-cell interactions.

Beside receptor-dependent/ mechanisms, receptor-independent pathways also play a role in EVs endocytosis and are usually associated with unspecific uptake events. For instance, macropinocytosis was described to control EVs uptake in bone marrow-derived mesenchymal stromal cells (BMSCs), human pancreatic adenocarcinoma and HeLa cells (Tian et al., 2014; Kamerkar et al., 2017; Nakase et al., 2015; Costa-Verdera et al., 2017). Using different pharmacological treatments to inhibit vacuolar acidification with alkalinizing drugs, it was shown that macropinocytosis is also involved in oligodendrocytes-EVs uptake by microglia (Fitzner et al., 2011). Interestingly in this study, inhibition of dynamin 1 and 2 using dynasore also decreases EVs uptake by microglial cells, suggesting involvement of clathrin-dependent endocytosis as well. Dynamin and clathrin-dependent EVs uptake were also previously observed in BMSCs (Tian et al., 2014) and was confirmed more recently in HeLa cells (Roberts-Dalton et al., 2017).

EVs internalization can also go through clathrin-independent mechanisms. For instance, caveolae-mediated EVs uptake was described in epithelial cells (Nanbo et al., 2013) but the role of caveolin-1, important in clathrin-independent endocytosis, is still not clear and can have both negative and positive effect in EVs uptake (Costa-Verdera et al., 2017; Svensson et al., 2013; Nanbo et al., 2013). Additionally, the use of Methyl-β-cyclodextrine to remove cholesterol and alter membrane lipid microdomains was shown to reduce EVs internalization in endothelial cells suggesting the implication of lipid-raft-mediated endocytosis (Svensson et al., 2013). Importantly, it was shown that intact actin cytoskeleton is needed for proper EVs uptake as cytochalasin D and latrunculin treatment of cells inhibit glioblastoma-derived EVs internalization by parental cell (Svensson et al., 2013) and leukemia-derived EVs internalization by macrophages (Feng et al., 2010). Finally, genistein was used to

inhibit clathrin-independent endocytosis and reduced EVs uptake by human carcinoma and Hela cells (Horibe et al., 2018; Costa Verdera et al., 2017).

Overall, almost all the main endocytic pathways, including clathrin-dependent or independent pathways, were described to play a role in EVs uptake, at least partially (Mulcahy et al., 2014; Adem et al., 2019) (**Figure 13)**. However, depending on the origin of EVs and the receiving cell types, results were different from one study to the other. Hence, mechanisms that drive the choice of the endocytic pathways remains unknown and could depend on many parameters (EVs size, CAM repertoire, type or physiological state of receiving cell). This multiplicity of possible endocytic pathways also complicates the study of the molecular actors require for EVs internalization, actin cytoskeleton coordination and membrane regulation during this process.

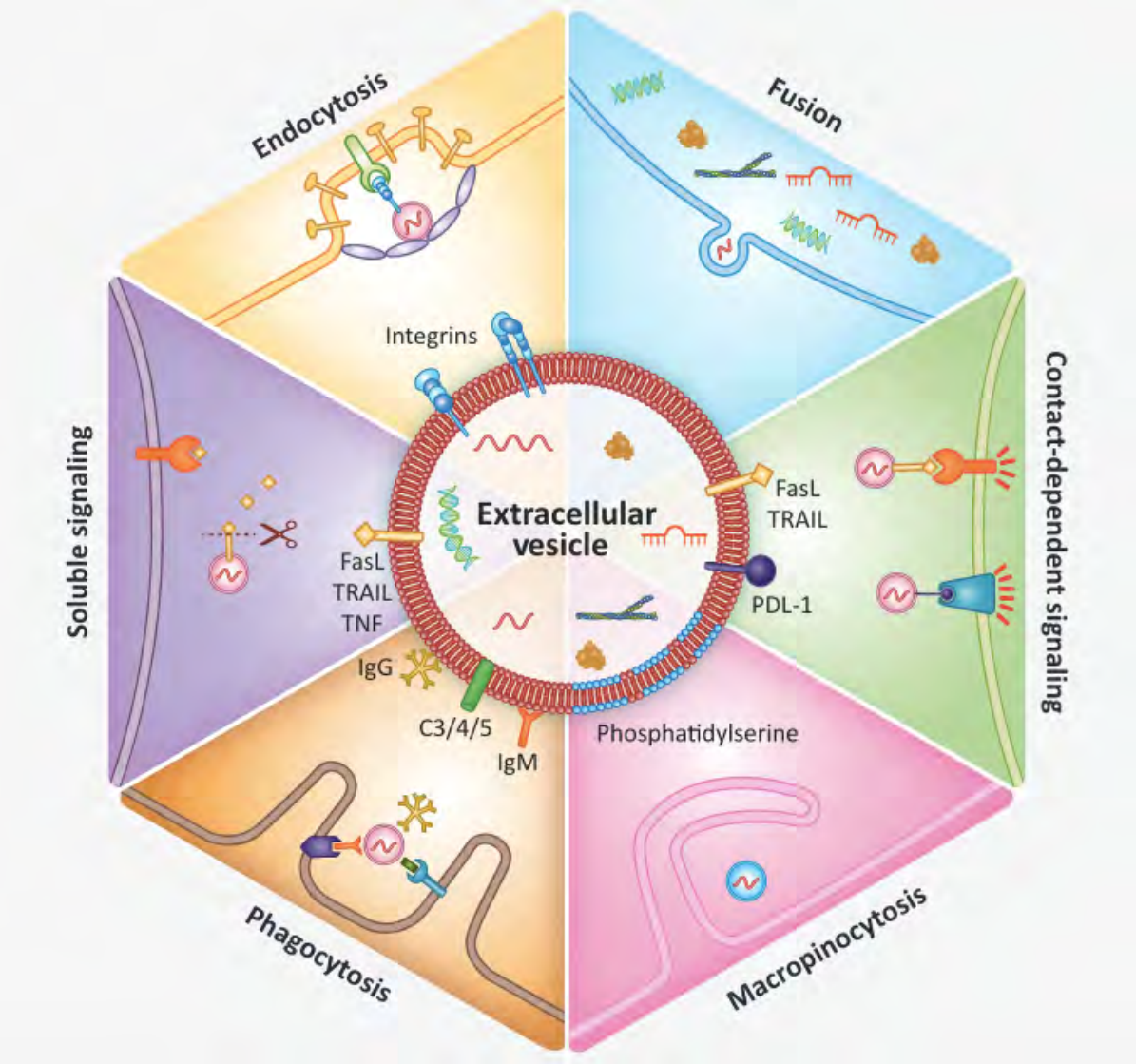

Figure13: Extracellular Vesicles uptake.
Interactions between EV and recipient cells can lead to several outcomes. Fusion events can happen, releasing EV contents directly into the cell cytosol. A simple contact between EV and cells can also triggers signaling (e.g. through cytokines present at the surface of EV, or specific ligands such as PD-L1). Several pathways of receptor-mediated endocytosis were identified in EV uptake. Among them phagocytosis (most probably via complement-related proteins) and integrin-mediated endocytosis. In addition, membrane lipids were shown to mediate micropinocytosis dependant EV uptake. Finally, soluble forms of EV surface cargo can also triggers signaling, yet with less efficiency. Abbreviation: PDL-1, programmed death-ligand 1. Extracted from Adem et al., 2019.

5.2. EVs intracellular fate and message delivery

5.2.a EVs at cell surface

After binding with receiving cell membrane, EVs can have different fates. They can fuse directly with plasma membrane (PM) releasing their luminal contents directly into the cytosol (Del Conde et al., 2005; Montecalvo et al., 2012). For instance, it was shown that melanoma tEVs can fuse with PM of human melanoma cells suggesting a paracrine signaling effect in tumor (Parolini et al., 2009). Fusion between EVs and PM lipidic bilayers results in the integration of EVs lipids and trans-membrane proteins in the plasma membrane of the receiving cells, participating to lipid regulation and exchange between secreting and receiving cells (Record et al., 2014) (**Figure 13**). It was suggested that EVs-cell fusion at the PM is mediated by the interaction between syncytin-2 and the receptor Major Facilitator Superfamily Domain 2a (MFSD2a) (Prada and Meldolesi, 2016). However, PM fusion seems to be more restricted to larger vesicles (e.g. PM-derived EVs) which show limited internalization because of their size (Kanada et al., 2015; Del Conde et al., 2005). Of note, it was suggested that low pH in tumor microenvironment could enhance fusion events (Parolini et al., 2009). This would mean that environmental as well as physiological parameters dictate EVs way of entry in recipient cells. Yet, this hypothesis remains to be demonstrated. EVs-cell contact only could also directly trigger signaling pathways from the cell surface. This suggests that internalization or even cargo transfer is not always essential for EVs function (Sato et al., 2019; Ko et al., 2019).

However, most studies show that EVs are mainly internalized in receiving cells (Mulcahy et al., 2014; van Niel et al., 2018; Tian et al., 2013). At this point, internalized EVs can either: 1) follow the endolysosomal pathway and be degraded in lysosomal compartment 2) escape from endosome compartments and deliver their content in the cytoplasm or 3) be re-secreted by the cell (**Figure 14**). In the next paragraphs I will discuss these three mechanisms and their regulation.

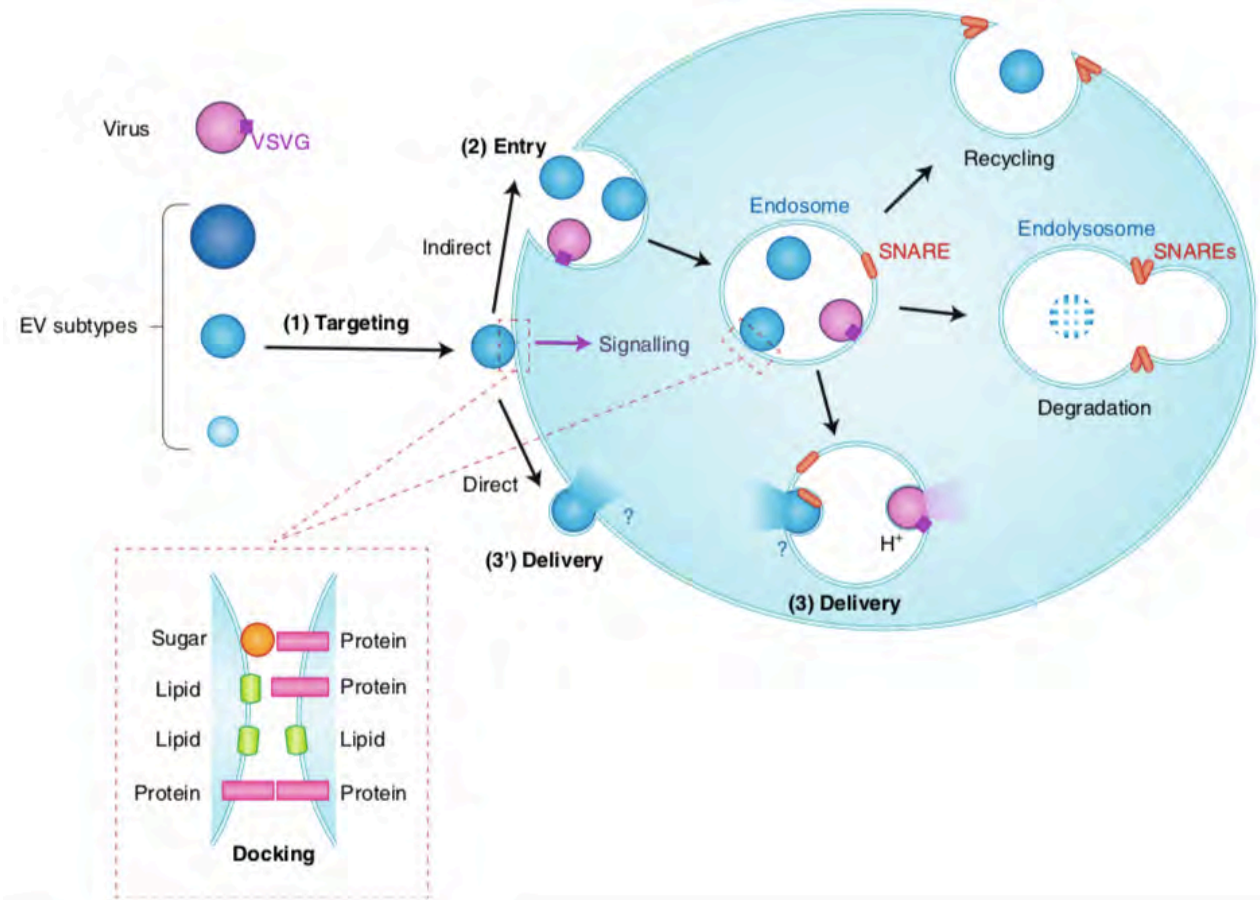

Figure14: The different fates of internalized EVs. (1) EVs tether to recipient cell membrane most of the time through specific molecular interactions involving membrane-exposed proteins, sugars or lipids (inset). (2) Studies showed that EVs are globally trafficking via the endolysosomal pathway and accumulate in endolysosomes. At this point three fates are possible. i) acidification of the endolysosome trigger the degradation of internalized EV. ii) EVs undergo endosomal escape by mechanisms that are still poorly understood, releasing their content in recipient cell cytosol. (3) At this time it is the main hypothesis to explain functional EV message delivery to recipient cells after internalization. iii) Lastly, EVs might also be recycled and re-secreted or targeted to the lysosome for degradation. (3′) The alternative route of EV content delivery to the acceptor cell is fusion with the plasma membrane and cytosolic cargo release. Yet this mechanism could be more specific to plasma-membrane derive EV (microvesicles) rather than endosome-derived EV (exosomes). Extracted from Mathieu et al., 2019.

5.2.b EVs and the endolysosomal pathway

After uptake, internalized EVs accumulate in intracellular compartments of the endocytic pathway. First in early endosomes which will mature in late endosomes and multivesicular bodies (MVB). MVB can then fuse with lysosomal compartments, targeting their content (including internalized EVs and newly formed ILV) towards degradation (van Niel et al., 2018). Colocalization of fluorescently labelled EVs with early then late endosomal compartments showed that substantial part of internalized EVs follows this endolysosomal route, to finally accumulate in late endosomal-lysosomal compartment in perinuclear regions (Chen et al., 2016; Tian et al., 2010; Tian et al., 2013; Tian et al., 2014; Costa-Verdera et al., 2017). For instance, LysoTracker probe, that labels acidic compartments (i.e; lysosomes), allowed to demonstrate colocalization of internalized EVs and lysosome in living cells (Tian et al., 2013).

Accumulation in lysosomal acidic compartments over time suggests that, after internalization, intact EVs progressively move forward to degradative processes, impairing efficient transfer of their message/cargos because of biomolecule degradation. Indeed, inside endolysosomal compartments hydrolysis will degrade internalized material to recycle biomolecules. Thereby, the degradation of internalized EVs can also provide lipids, proteins and nutrients to recipient cells and notably starving cancer cells (Zhao et al., 2016). Overall, lysosomal catabolism participates to EVs-mediated trophic support of receiving cells. Lysosomal compartments are not simple degradative organelles but can also recycle bioactive material of EVs origin, support membrane regulation, participate to signaling, cell metabolism and even secretion processes (Ballabio and Bonifacino 2020). Hence, the degradation of EVs inside lysosome does not mean that EVs would have no effect on recipient cells and accumulation of EVs inside these compartments should not be considered as a non-functional EVs destination (Verweij et al., 2019; Mathieu et al., 2019).

Several studies show that internalized EVs can also follow a different fate, escape from degradation and deliver their cargo to receiving cells. For instance, EVs-mediated transfer of miRNA (miR-21) was shown to decrease expression of TGFβ receptor II (TGFβRII) in BMSCs (Tian et al., 2014). Similarly, using a Cre-Lox reported system, EVs were shown to functionally transfer mRNA to neurons (Ridder et al., 2014)

or cells in the tumor microenvironment in glioma and carcinoma mice models (Ridder et al., 2015). The same approach was used to show transfer of RNA from malignant mammary tumor cells to less malignant cells locally and at distance in mice (Zomer et al., 2015). Likewise, transfer of proteins between glioma cells (Al-Nedawi et al., 2008) and in the nervous system (Korkut et al., 2013) were observed, as well as transfer of Galectin-1 between fibroblast and cancer cells and angiopoietin 2 between cancer cells and endothelial cells (Xie et al., 2020). Overall, EVs-mediated transfer of functional nucleic acid and proteins also implies that EVs cargo escape from degradation and reach the cytosol or an environment suitable for its translation/use by the recipient cell.

Although, the precise mechanisms controlling EVs escape and/or capacity to deliver their message into the cytosol is not well described, it is thought that back-fusion occurs between the EVs membrane and the endosomal membrane leading to cargo release in the cytosol. It was suggested that EVs fusion events are more likely to occur in endosomes rather than at the plasma membrane (Bonsergent and Lavieu, 2019; Joshi et al., 2020; Yao et al., 2018; Costafreda et al., 2020). Back-fusion could be controlled by membrane lipids, such as cholesterol, phosphatydilserine, or lysobiphosphatidic acid (LBPA) (Del Conde., 2005; Joshi et al., 2020; Yao et al., 2018). Alternatively, it could involve protein-based mechanisms, similar to the processes used by virus with fusogenic proteins as vesicular stomatitis virus G glycoproteins (VSVG) (Van Dongen et al., 2016). Of note, this protein is extensively used for EVs bioengineering as it facilitates cargo transfer (Somiya and Kuroda., 2021). Although decrease in pH is commonly associated with degradation processes and endosome maturation towards lysosome, low pH inside endosomes has also been suggested to enhance back-fusion mechanism and EVs cargo release (Parolini et al., 2009; Montecalvo et al., 2012). This hypothesis was confirmed more recently, showing that fusion events in endosomes are triggered by endosomal acidification (Bonsergent and Lavieu, 2019; Joshi et al., 2020). Hence, acidification of intracellular compartments could be a key feature in EVs biology, controlling events from their biogenesis to their secretion, to their degradation or their back fusion with endosomal membrane. As for now, back fusion still deserves more work, in particular to characterize the time scale, the frequency, the precise localization (i.e. the type of endosomes) and the molecular regulators involved.

Alternative mechanisms of cargo transfer were described. For instance, it was suggested that EVs cargo could escape degradation and be transferred in the

endoplasmic reticulum (ER). Indeed, during their maturation, EVs-containing endosomes were shown to contact ER before their fusion with lysosomes, through a process called ER scanning (Heusermann et al., 2016). Alternatively, EVs could escape degradation by retrograde trafficking from the endolysosomal pathway to the trans-Golgi network. (Gurung et al, 2021). Finally, a study suggests that EVs cargos could be directly transferred into the nucleus of the recipient cell when late endosomes and the nuclear envelope interact during endolysosomal maturation (Santos et al., 2018). However, all these alternative routes remain to be confimed.

Overall, membrane fusion between EVs and endosomal compartment is still considered as prevalent mechanism that mediate the release of endocytosed EVs cargo into cytosol, their capacity to transfer their message and ultimately their function on receiving cells. However, the proportion of EVs undergoing degradation or cargo transfer and the mechanisms regulating this balance are not known.

5.3. Recycling and re-secretion

The last possible fate for endocytosed EVs beside degradation or escape from endosomal compartment is their potential re-secretion. This mechanism is assimilated to transcytosis as it could allow the endocytosis of EVs at one pole of the cell and its exocytosis at another location (potentially the opposite pole). Since the classical endolysosomal pathway includes the maturation of late endosome into MVB, it is possible that part of internalized EVs may rejoin secretory pathways and be recycled and released again in the extracellular space (Van Niel et al., 2018; Mathieu et al., 2019; Kalluri and Lebleu, 2020) (**Figure 14**). In a striking study, it was reported that breast cancer cells (MDA-MB-231) can uptake fibroblast $CD81^{+}$ EVs, load Wnt11 onto these EVs and re-secrete them to enhance breast cancer cell motility by Wnt11 signaling, promoting thereby metastasis (Luga et al., 2012). The recycling and re-secretion of internalized EVs was also reported to allow EV breaching through an intact blood brain barrier using transcytosis in brain endothelial cells (Morad et al., 2019). Notably, the authors showed that internalized EV could colocalize with Rab11+ recycling compartments (Takahashi et al., 2012). Interestingly, they also showed that part of the internalized EV is still trafficking toward degradative route in endolysosomes. This suggests that different populations of internalized EV could be

sorted into different endocytic pathways to be either degraded or recycled (Morad et al., 2019).

Overall, these studies strongly suggested that EVs recycling and re-secretion could happen in different context. Nevertheless, whether it is only specific subpopulations of EVs that are recycled remain to be fully demonstrated. For instance, trophoblastic EVs were reported to colocalize more with Rab5+ and EEA1+ early endosomes rather than lysosomal compartments, suggesting a selective route of recycling for these EVs (Vargas et al., 2014). Finally, the precise molecular regulation of EVs recycling and transcytosis remains to be characterized.

Altogether, these studies highlight that various molecular and biophysical signal can impact the function, trafficking and regulation of organelles, and thereby potentially EVs fate and functions. However, the impact of biophysical signals remains poorly investigated. For example, as EVs uptake and internalization has been almost exclusively studied in static condition, or at least usually neglecting biomechanical constraints of EVs environment, it would be of great importance to study how hemodynamic forces could impact circulating EVs uptake and function.

Aims of the project

Background:

As I presented it in the introduction, EVs contribute to cell cross-communication locally but also between distant organs, participating in various physiological and pathological processes. In cancer, tumor EVs, released in large amount by cancer cells, are found in abundance in blood samples from patients, and were shown to be involved in multiple events promoting cancer progression (Osti et al., 2019 (Henrich et al., 2020; Hyenne et al 2019, Peinado et al. 2017, Costa-Silva et al., 2015, Hoshino et al., 2015). Thus, it appears essential to understand the behavior and the fate of circulating EVs. Despites recent advances in this field, we still do not have a clear idea of the fate of circulating tEVs after clearance from vessels. Part of them, but not the totality, accumulate in specific organ/location in experimental set-up (namely, injection of exogenous EVs), but, at vesicle scale, circulating tEVs destination and fate in complex circulatory system remains quite obscure. Partly, because of incomplete understanding of molecular interactions controlling circulating tEVs biodistribution and organotropism in hemodynamic systems and even less insights on biomechanical parameters that could impact it. Consequently, we do not know how biophysics affect tEVs-mediated pre-metastatic niche formation. **During my PhD, I aimed to develop new models adapted to the study of circulating EVs and to understand their fate and function in receiving cells.**

Our previous work on CTCs showed that a permissive range of flow not only enables the stable arrest of CTC on vessel wall through integrin-mediated adhesion (Follain et al. 2018; Osmani et al., 2019), but also promotes extravasation of CTC by a process called endothelium remodeling (Follain et al. 2018). My working hypothesis is that tEVs, in similar fashion, exploit both molecular as well as biophysical parameters to, not only disseminate through the vascular system but also potentially mediate PMN formation. Better understanding of these two aspects might help to predict arrest pattern of tEVs more efficiently and modify it to interfere with metastatic cascade and cancer progression.

Project:

My PhD project aimed to investigate the role of biomechanical cues in tEVs uptake, intracellular trafficking and function in endothelial recipient cells. I focused on endothelial cells, on one hand because they are an important EVs recipient cell type. Different types of endothelium (cardiac, brain, venous) were shown to be able to uptake EVs (Zwi-Dantsis et al., 2020; Morad et al., 2019; He et al., 2019). Importantly, the vasculature in non-pathological context was also shown to display important EVs uptake (Verweij *et al.,* Dev Cell 2019). On the other hand, because the endothelium represents the first barrier to circulating tumor cell invasion in distant organs and circulating tEVs-mediated modifications of the endothelium greatly impact PMN formation and metastatic progression (cf Introduction section **1**). The first part of my work participated to the establishment of *in vitro* and *in vivo* experimental models (i.e. microfluidic approach and use of the zebrafish embryo) for the study of tEVs, their uptake, their intracellular trafficking and their function in dynamic conditions. These models allowed me to investigate key questions that remain poorly understood in circulating tEVs biology. My goals were to: (1) **study** the role of **hemodynamic forces on circulating EVs uptake** by recipient cells. (2) **Identify** the **endocytic pathways and the receptors involved in circulating EVs uptake**. EVs were shown to be internalized through different endocytic pathways. However, these mechanisms were mostly studies in *in vitro* static assays. (3) **Determine** whether the dynamic environment of circulating EVs affects the **trafficking of internalized EVs inside receiving cells and their targeting to specific endocytic compartments**. Indeed, the environment in which internalized EVs end up (mostly compartments of the endolysosomal pathway) determine their capacity to deliver messages. (4) **Investigate** how combined exposure of hemodynamic flow and circulating tEVs affects **endothelial cell phenotypes**. Various effect of tEVs on endothelium were reported in the literature (e.g. endothelial disruption, pro-angiogenic effect). However, endothelial response to tEVs exposure in relevant context including realistic biomechanical parameters had not been explored.

Therefore, the main goals of my PhD project can be summarized in the following five axis:

1. **Development of *in vitro* and *in vivo* models for the study of circulating tEVs**
2. **Impact of flow forces on tEVs utpake**
3. **Mechanisms of circulating tEVs uptake**
4. **Effect of flow on intracellular compartments and tEVs fate**
5. **Effect of flow on tEVs message delivery and its consequences on endothelial cell phenotype**

Models to investigate circulating tEVs

In the last decades, several studies investigated tEVs distribution and uptake by endothelial cells and their consequences on endothelium *in vitro* and *in vivo* (Skog et al., 2008; Svensson et al., 2013; Zhou et al., 2014; Morad et al., 2019; Xie et al., 2020; Tominaga et al., 2015; Yokota et al., 2021; Yang et al., 2017; Zeng et al., 2018). However, until recently, as I started my PhD project, studies usually done *in vitro* in transwell assays or *in vivo* by injection of tEVs in the circulation never considered the biophysical aspect of the hemodynamic forces.

In addition, at that time, limitations of existing models prevented study of tEVs in dynamic environments such as the circulatory system. Although, development of new tools allowed visualization of EVs and detection of efficient EVs cargo transfer *in vivo*, either by injection of fluorescent EVs labelled by lipidic dyes, with fusion proteins or by recombination events in Cre/lox systems (Wiklander 2015; Hoshino et al., 2015; van der Vos et al., 2016; Abels et al., 2019; Ridder et al., 2014; Zomer et al., 2015; Lai et al., 2015), detection of circulating EVs directly into circulatory vessels and dynamic recording of their behavior was still quite challenging. More specifically, they displayed major drawbacks to investigate the link between hemodynamic profiles, tEVs biodistribution and consequences of their uptake on endothelial cells at almost-single-particle resolution scale (e.g. control of hemodynamic forces in the mice is complicated).

Hence, during the first part of my PhD, I contributed to develop two models (one *in vitro* and on *in vivo*) adapted to the study of tEVs in biophysically relevant conditions and investigate key questions on circulating tEVs. In the next paragraphs I will present these two models.

An *in vitro* microfluidic system

Microfluidic device was previously used in our lab to investigate CTC dynamic behavior and mechanisms of arrest (Follain et al., 2018, Osmani et al., 2019). Although microfluidic and flow chambers were previously used in *in vitro* studies of nanoparticle distribution and uptake (Han et al., 2012, Han et al., 2015, Charwat et al., 2018; Gomez-Garcia et al., 2018), it was not used to study circulating tEVs uptake and fate in endothelial cells at that time. I adapted it to the study of circulating EVs, allowing me to precisely tune flow speed parameters and perfuse fluorescently labelled tumor EVs on an endothelial monolayer. This microfluidic system enabled to reproduce physiological hemodynamic conditions of small vessels in which tEVs accumulate. Hence, the use of microfluidic devices allowed me to better control the environment of circulating tEVs and analyze the fate of tEVs once they are internalized.

An *in vivo* model: the zebrafish embryo

At the beginning of my PhD, I participated to the establishment of the zebrafish embryo as a good model to study circulating EVs *in vivo*. Using the advantages of the zebrafish embryo, our team, in parallel with the one of Guillaume van Niel, published founder papers demonstrating the power of the zebrafish embryo in the study of circulating EVs, their biodistribution, their behavior as well as their function *in vivo*, with live imaging and correlative light electron microscopy (CLEM) techniques (Hyenne et al., 2019; Verweij et al., 2019). I had the opportunity to participate to this work and be co-author on this paper we published in 2019. In addition, technics and protocols used in this work (i.e. exogenous injection of tEVs inside zebrafish vasculature) were detailed in a chapter method in which I am first author and published one year after (Mary et al., 2020). Based on this work, I could use this model for my own project. For instance, this model allowed me to measure flow speed in different regions of the vascular tracks based on red blood cell displacement and correlate flow speed profiles with injected labelled tEVs distribution in the vascular system.

Overall, I used the microfluidic model and the zebrafish embryo together to thoroughly investigate the link between hemodynamics and tEVs uptake, fate and function in endothelial cells.

RESULTS

1. The zebrafish embryo: a model to study circulating tEVs

At the beginning of my thesis, live imaging of tEVs in circulatory system *in vivo* at almost-single-particle resolution was still quite challenging due to the small size of EVs and the difficulty to limit background signals (Verweij et al., 2021). The worm *C. elegans* and the fly *D. melanogaster* were previously used to visualize EVs at the organ or vesicles scale *in vivo* (Verweij et al., 2021). However, these two are not appropriate to model tEVs biodistribution in complex mammalian circulatory systems. Despite, improvements made in mice models (Wiklander 2015; Hoshino et al., 2015; van der Vos et al., 2016; Abels et al., 2019; Ridder et al., 2014; Zomer et al., 2015), detection of EVs at the vesicle scale was still limited in terms of depth and tissue/organ and most of the time big amount of EVs, and sacrifice for *ex-vivo* harvesting of organs were necessary (Men et al., 2019). Although these models had their own advantages, their limitations did not allow live detection and recording of circulating tEVs in the vascular system, their interactions and their function on recipient cells.

Upon my arrival in the lab, we used the zebrafish embryo model to overcome several limitations of previous models and make possible the study of hemodynamics in tEVs biology. First, the transparency of zebrafish embryos autofluorescence in live imaging approaches is crucial and enable the detection of fluorescently labelled EVs (either with dye or genetically) at vesicle scale in living tissues. Moreover, the reduce size of the animal facilitate its compatibility with high resolutive optical systems. Secondly, the zebrafish embryo rapidly develops a complex and stereotyped vasculature as well as an innate immune system (i.e. presence of myeloid cells in the vascular system within 48h post fertilization). In addition, vessels of different sizes as well as arterial and venous regions that show different flow speeds, reproduce biophysical characteristics of human and mice arterioles, venules and capillary beds (Follain et al., 2020). Overall, zebrafish embryo vascular system allows to model human vasculature and study EVs circulation along vascular tracts in innate immune competent environment. In addition, as it was previously used by our lab (Follain et al., 2018), it is easily possible to modify heart rate and thus, tune blood flow speed in the embryo. This facilitates the study of hemodynamic forces *in vivo*. Finally, 82% of human disease-related genes are conserved between human and zebrafish (Howe et al., 2013). This genes conservation makes the zebrafish a powerful model to study

different human diseases such as cancer, cardiovascular, gastrointestinal, kidney or even neurodegenerative diseases upstream of using mice models directly (Verweij et al., 2019). For instance, zebrafish embryo was used in our lab to investigate key steps of the metastatic cascade (i.e. extravasation of tumor cells, CTC arrest) (Follain et al., 2018; Osmani et al., 2019) and by others to model human cancer in fish (Cagan et al., 2019; Brown et al., 2017). At this time, simultaneously with the lab of Guillaume van Niel, in Paris, we continued to exploit advantages of the zebrafish organism to adapt this model to the study and live imaging of circulating EVs at high spatio-temporal resolution and vesicle scale.

On one hand, in a thorough study, the group of Guillaume van Niel, described the journey of endogenous EVs, produced by the yolk syncitial layer, from their secretion by a syntenin-dependent mechanism, to their dissemination into the circulatory tracks and their accumulation inside macrophages and endothelial cells in potential lysosomal compartments (Verweij et al., 2019).

On the other hand, our lab developed a different, yet complementary approach, based on injection of exogenous tumor EVs or tumor cells labelled with a brighter, less aggregation-prone, more stable lipophilic dye (Collot et al., 2019) (i.e. MemBright, now commercialized under the name of MemGlow). We aimed to track tEVs at high resolutive scale in complex hemodynamic context and better document the behavior, the fate and the potential function of circulating tEVs *in vivo* (Hyenne et al., 2019). We showed that:

- Zebrafish melanoma EVs share a high percentage of proteins with human melanoma EVs.
- Exogenously injected tEVs can be followed at high spatiotemporal resolution and vesicle scale. Additionally, their hotspot of arrest corresponds to the caudal vein region with low flow speed profiles.
- tEVs in movement follow a Poiseuille distribution in zebrafish bloodstream, showing that circulating tEVs go slower in the vicinity of the endothelium than at the center of the vessel.
- tEVs are massively and rapidly internalized by endothelial cells and patrolling macrophages (but not neutrophils) and seem to accumulate in lysosomal compartments.

- tEVs trigger phenotype switch in these macrophages from an M2 to an M1 signature. This supports the long-distance action of tEVs circulating in the vascular system.
- Education of the embryo by pre-injection of tEVs facilitates metastatic progression upon subsequent injection of tumor cells.

This work participates to the establishment of the zebrafish embryo as a model to study tEVs in hemodynamic conditions at a good resolutive scale. Additionally, it illustrates the relevance of this model to reproduce late stage of the metastatic cascade induced by circulating tEVs and notably their capacity to enhance metastatic formation.

See Annexe: Study the fate of tumor extracellular vesicles at high spatiotemporal resolution using the zebrafish embryo

- **Hyenne et al., 2019**

2. A versatile protocol compatible with different applications

In the research paper published in 2019 (Hyenne et al, 2019), we highlighted the power of the zebrafish as a model for circulating tEVs research and the study of tEVs long-distance action which can (i) modify the phenotype of immune cells (e.g. macrophages) and (ii) support growth of metastasis. Subsequently to this work, we published a method article, in which I am first author, that describes in detail our tEVs injection protocol and discuss its applications.

We wrote in detailed manner all the key steps of our approach. The aims were to focus on specific aspects of our protocol, share our expertise and suggest different ideas of applications. We demonstrated the versatility and simplicity of exogenous injection of EVs in different transgenic zebrafish lines, its advantages (e.g. EVs labelling possibilities, EVs population and quantity control) and gave examples of its multiple applications. In this chapter we discussed:

- Our isolation protocols: differential ultracentrifugation (DU) size exclusion chromatography (SEC).
- EVs labelling: lipophilic dye, MemGlow (Collot et al., 2019) and genetically labelled fluorescent tEVs (e.g. Syntenin2-GFP-EVs from zebrafish melanoma cells).
- Our quantification method: nanoparticle tracking analysis methodology (NTA).
- Zebrafish injection method: advice to increase efficiency (localization, quantities).

Additionally, we suggested and provided examples of:

- Imaging and analysis workflow: high speed scanning and object-based tracking (tEVs and RBC).
- Complementary analysis: spatiotemporal analysis of object in movement, visualization of tEVs in intracellular compartments by Lysotracker or CLEM approaches.
- Functional assay: priming of metastatic niche.

We stressed that all the technics addressed in this method chapter can be adapted in different contexts according to experimental goals and should definitively not be only restricted to cancer research.

Live tracking of extracellular vesicles in larval zebrafish

- **Mary et al., 2020**

CHAPTER FOURTEEN

Live tracking of extracellular vesicles in larval zebrafish

Benjamin Mary[a,b,c,†], **Shima Ghoroghi**[a,b,c,†], **Vincent Hyenne**[a,b,c,d,*], **and Jacky G. Goetz**[a,b,c,*]

[a]INSERM UMR_S1109, Strasbourg, France
[b]Université de Strasbourg, Strasbourg, France
[c]Fédération de Médecine Translationnelle de Strasbourg (FMTS), Strasbourg, France
[d]CNRS, SNC 5055, Strasbourg, France
*Corresponding authors: e-mail address: hyenne@unistra.fr; jacky.goetz@inserm.fr

Contents

Abstract

Formerly considered as insignificant cell debris, extracellular vesicles (EVs) have emerged as potent mediators of cell-cell communication, both in proximity and at distance from the producing cell. EVs are transported in body fluids and can be internalized by specific distant cells to ultimately deliver a functional message. Despite their striking importance in many physiological and pathological contexts, the exact mechanisms by

† These authors contributed equally.

Methods in Enzymology, Volume 645
ISSN 0076-6879
https://doi.org/10.1016/bs.mie.2020.07.013

which EVs impose local and distant modifications of the microenvironment *in vivo* remain to be fully understood. We realized that some conceptual gaps are direct consequences of the difficulty to visualize the shuttling and targeting of EVs in real time *in vivo*. The zebrafish larvae offered attractive features for live tracking of EVs, within circulating fluids. Here, we describe the experimental procedures that we have built for dissecting the dissemination of EVs at high spatio-temporal resolution *in vivo*.

1. Introduction

Over the past 20 years, extracellular vesicles (EVs) became central mediators of cell-cell communication in various physiologic contexts, such as development, reproduction, metabolism or neurology (Yáñez-Mó et al., 2015). They also contribute to the progression of multiple pathologies, such as immune deficiencies, cardiovascular disorders, infectious disease, or cancer. These multi-tasking cellular products can also behave as protecting soldiers from bacterial toxins and thus combat infection (Keller et al., 2020). EVs are heterogeneous vesicles secreted by all cell types with diameters ranging from a few nanometers to several micrometers. They can be found in most, if not all human body fluids (blood, lymph, urine, milk, sweat, saliva, tears and others) (Bakhshandeh, Kamaleddin, & Aalishah, 2016; Yáñez-Mó et al., 2015). Their lipid bilayer ensures protection of their cargo, which is composed of mRNAs, non-coding RNAs, proteins and, in the case of some tumor EVs, DNA (Balaj et al., 2011; Lázaro-Ibáñez et al., 2019). The repertoire of molecules that EVs carry depends on their cellular and sub-cellular origin as well as their species of origin and the physiological state of secreting cells (Karimi et al., 2018; Zhao et al., 2020). EVs are heterogeneous by nature. A single cell can secrete a wide variety of EVs-subpopulations (Kowal et al., 2016) that are likely to convey a functional heterogeneity. EVs act within short, medium and distant ranges. They function as paracrine and autocrine factors and can alter the behavior of cells, and the associated microenvironment, in close proximity. For instance, EVs rearrange the extracellular matrix, thereby promoting invadopodia formation and cell migration, close to the site of secretion (Hoshino et al., 2013). EVs also communicate at the scale of an organ through the dissemination of morphogen factors beyond the reach of diffusion gradient of soluble molecules (Gross, Chaudhary, Bartscherer, & Boutros, 2012; Matusek et al., 2014). Finally, and most interestingly for this protocol, EVs also act within long range. They can disseminate in the organism through body fluids, thereby

contributing to cross-organ communication and ultimately, act as endocrine factors (Butler, Abdelhamed, & Kurre, 2018). The most striking examples probably come from cancer studies suggesting that EVs secreted by a primary tumor can exploit the blood circulation to reach distant organs and locally modify the microenvironment to promote future metastasis (Adem, Vieira, & Melo, 2020; Costa-Silva et al., 2015; Hoshino et al., 2015; Peinado et al., 2012). However, some black boxes remain concerning the origin, shuttling behavior, destination and functional impact of the large amounts of EVs present in our body fluids (ranging around 10^{10} EVs per ml in blood (Johnsen, Gudbergsson, Andresen, & Simonsen, 2019)). EVs found in body fluids have several cellular origins (Flaumenhaft, Mairuhu, & Italiano, 2010; Karimi et al., 2018). In blood, their concentration depends on several parameters, that can be physiological (Whitham et al., 2018) or pathological (*i.e.,* Cancer or cardiovascular diseases Peinado et al., 2012; Boulanger, Loyer, Rautou, & Amabile, 2017), and counter-balanced by rapid clearance (Matsumoto et al., 2020). However, how single EV (or population of EVs) use, respond and exploit body fluids remains to be elucidated. Circulating EVs can now be sampled, isolated and analyzed in multiple ways, revealing their contents and their origin (Nielsen, Beck-Nielsen, Andersen, & Handberg, 2014; Zhao et al., 2020). We reasoned that understanding their fate and their function would greatly benefit from animal models adapted to the imaging of small objects in complex environments like circulatory systems *in vivo*.

Microscopic visualization of circulating EVs in realistic pathophysiological situations *in vivo* still faces major challenges (Verweij, Hyenne, Van Niel, & Goetz, 2019). Imaging nano-sized objects as single particles depend on both subcellular resolution and brightness of the labeling objects (*i.e.,* EVs) so that one can distinguish EVs from the potential autofluorescence background. Furthermore, because some body fluids such as blood circulate at high-speed, high-speed sampling is needed to study the dynamic of circulating EVs with microscopy. Finally, the animal model used should allow deep, non-invasive access to internal organs and be compatible with the expression of fluorescent markers in tissue-specific cell lines in order to identify EVs receiving cells and organs. In rodents, different strategies, based on bioluminescence, lipophilic dyes, or transgenic expression of EVs fluorescent markers have been developed (Hyenne, Lefebvre, & Goetz, 2017). It is now possible to track the biodistribution of labeled EVs injected into the circulation at the whole animal scale (Hoshino et al., 2015; Lai et al., 2014; Wiklander et al., 2015). However, these approaches often require *ex vivo* imaging and do not allow to investigate

the circulating EVs behavior at the high spatio-temporal resolution, towards single EV detection. To overcome these limitations, several groups developed intravital imaging of EVs in mice (Lai et al., 2015; van der Vos et al., 2016; Zomer et al., 2015). Although they provide unique observations of EVs in their natural microenvironment, the complexity of these procedures prevents high-throughput imaging and are often not compatible with a high sampling of EVs shuttling in body fluids. Alternatively, the zebrafish larvae meets all requirements for in-depth, high-speed analysis of circulating EVs.

Indeed, over the past years, zebrafish larvae emerged as a unique animal model to study physiological and pathological circulating EVs at unprecedented spatiotemporal resolution (Verweij, Hyenne, et al., 2019). It offers several advantages for non-invasive analysis *in vivo*. Zebrafish embryos develop a stereotype vasculature (and blood circulation) and a maturing immune system within 48 h. Its translucent body allows simple *in vivo* non-invasive imaging and it is easily amenable to all types of confocal and high-speed microscopy. This model easily tolerates genetic manipulation to express fluorescent proteins in specific cell populations within zebrafish tissues. Overall, zebrafish presents a high level of genetic and physiologic homology with humans and can be used to model a large number of human diseases (cancer, cardiovascular, neurological, *etc*...). More particularly, it reproduces a relevant physiological environment for the study of circulating EVs (Hyenne et al., 2019; Verweij, Hyenne, et al., 2019; Verweij, Revenu, et al., 2019). Detection of fluorescent EVs, labeled with either lipophilic dyes or by transgenic expression of fluorescent markers within secreting cells is favored by transparent larvae. Zebrafish internal organs are easily accessible by confocal microscopy thus, 3D analysis of regions where EVs arrest and accumulate is within reach. Moreover, high-speed imaging allows to follow circulating EVs dynamic at single-particle scale in fish vasculature, and transgenic zebrafish lines are used to visualized EVs/cells interaction *in vivo*. Finally, we exploited this model to perform an extensive analysis of circulating EVs and describe their hemodynamic behavior *in vivo* in both physiological and pathological conditions (Hyenne et al., 2019; Verweij, Revenu, et al., 2019).

In this chapter, we describe a simple but detailed procedure (Hyenne et al., 2019), from isolation and labeling of EVs to intravascular injection and imaging in the zebrafish larvae. The versatility of our experimental approach offers the possibility to study exogenous EVs of different origins and pathological conditions, for instance from human samples, and to compare their respective roles and hemodynamic behavior once they have

reached the circulation. Despite the advantages of using zebrafish for studying tumor EVs, there are some limitations that are important and need to be addressed (such as difference in maintenance temperature and/or molecular and cellular process conservation between species) when studying human pathophysiology. Nevertheless, the zebrafish has proven very useful in different fields of human medical research (tissue regeneration, cardiovascular diseases, cancer progression) and could pave the way for later validation in mammalian models. In particular, it is suitable to study the dissemination of tumor EVs, document their arrest and internalization, as well as their capacity to cross the endothelium and induce local phenotypic changes.

2. EVs isolation and labeling

EVs are generally isolated from conditioned cell culture media or from various body fluids such as blood plasma, urine, saliva, breast milk, semen, and amniotic fluid. There are several methods available to isolate EVs including ultracentrifugation-based methods, size-based techniques, immune affinity, precipitation and microfluidic (Karimi et al., 2018; Willms, Cabañas, Mäger, Wood, & Vader, 2018; Yang et al., 2020). Here, we will describe two approaches that we found suitable for a subsequent labeling approach: differential centrifugation (UC) (Théry, Amigorena, Raposo, & Clayton, 2006) and size exclusion chromatography (SEC). The latter has no deleterious effect on EVs' integrity, and better preserves their functionality (Mol, Goumans, Doevendans, Sluijter, & Vader, 2017; Stranska et al., 2018). A schematic illustration of UC and SEC methods are shown in Fig. 1C. Upon isolation, we characterize EVs to confirm the presence, size and concentration of EVs in the preparation (physical characterization), but also to assess EV purity and content (molecular characterization) (Théry et al., 2018). Isolation is followed by characterization of EVs population. In this chapter, we will describe the basic quantification of EVs size and concentration by nanoparticle tracking analysis (NTA). Finally, we will detail a procedure for EV fluorescent labeling. While several strategies have been developed to fluorescently label EVs (Chuo, Chien, & Lai, 2018), the post-isolation labeling with fluorescent lipophilic dyes remains the most versatile and rapid approach to label EVs. They, such as PKH-26, PKH-67, DiO, DiL, Dir or MemBright, are inserted into EVs lipid bilayer (Collot et al., 2018; Hood, Roman, & Wickline, 2011; Hoshino et al., 2015; Takahashi et al., 2013). Due to their lipophilic nature, these dyes have been shown to have multiple drawbacks, including non-specific labeling, altered biodistribution, and

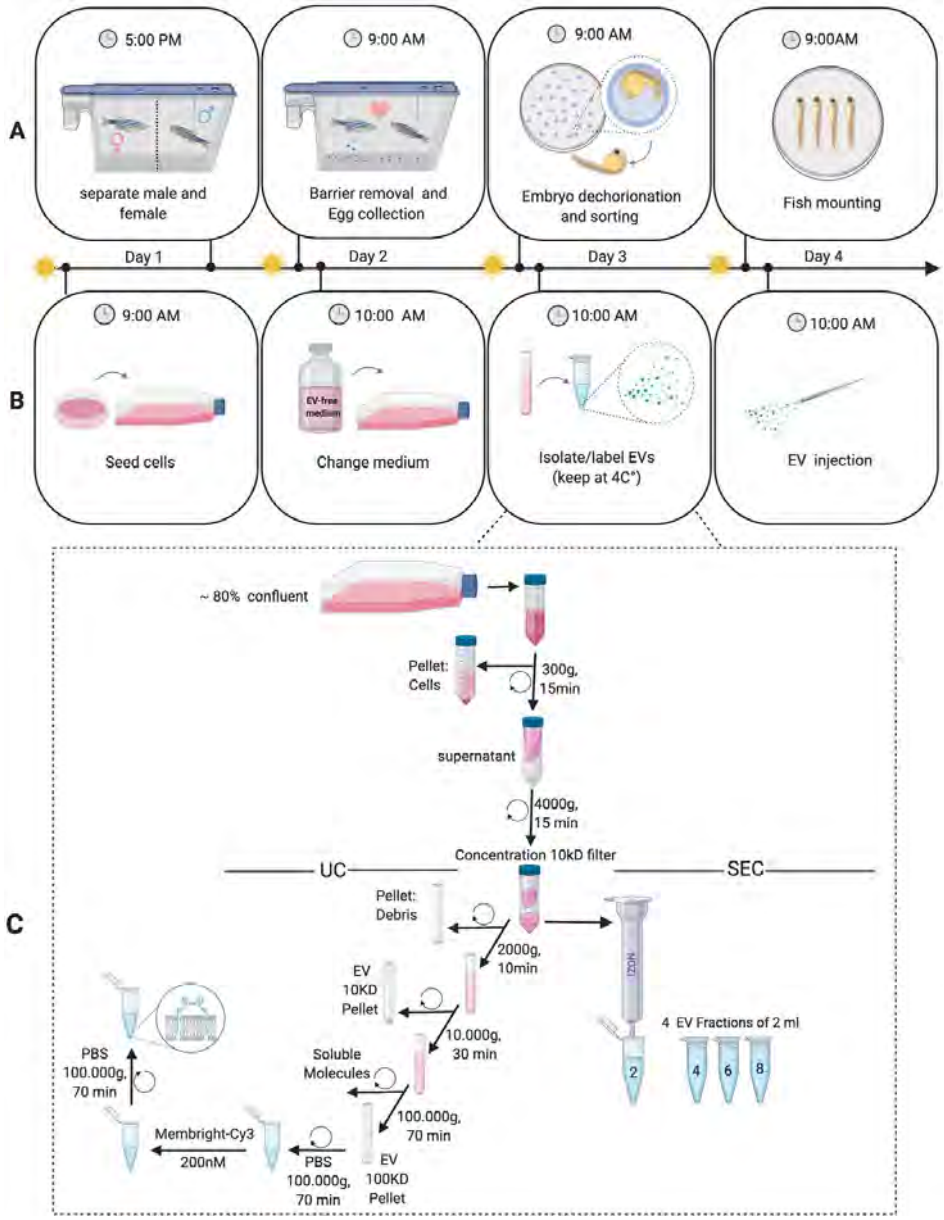

Fig. 1 Parallel zebrafish embryo and EV preparation. A schematic illustration of the parallel workflow timeline required for zebrafish embryo generation (A) and EV isolation and labeling (B and C).

presence of additional artifacts (Takov, Yellon, & Davidson, 2017). However, they remain very useful and unique tools for labeling of EVs from all origins and can be trusted when used with appropriate controls (Simonsen, 2019). As an alternative strategy, EV proteins can be fused to fluorescent proteins and expressed in EV-producing cells (Corso, 2019; Görgens et al., 2019).

This allows to visualize unique subpopulations of EVs and can also be used to track EVs from a genetically engineered cell or zebrafish lines, as we have done for endogenous zebrafish EVs (Verweij, Hyenne, et al., 2019; Verweij, Revenu, et al., 2019). Here, we present both strategies: genetically labeled EVs isolated from zebrafish melanoma cells (Zmel1) expressing syntenin2-GFP and post-isolation labeling of EVs with MemBright. MemBrights are recently developed cyanine-based membrane probes (Cy3, Cy5 or Cy7), bearing alkyl chains and zwitterionic groups (Collot et al., 2018). These probes have unique properties that provide high brightness and specificity to labeled-EVs in addition to preventing fluorescent self-aggregation (Hyenne et al., 2019). In addition, MemBright can be used to co-inject different types of EVs labeled with different colors (Cy3, Cy5), which allows us to compare different EV population (or origin) and track their specific behavior, fate and function. As a control, PBS is incubated with MemBright in a similar way as we labeled EVs, analyzed by NTA and injected into zebrafish larvae.

2.1 Equipment and reagents

- Centricon Plus-70 centrifugal filter (10k, Millipore).
- Beckman tubes thinwall polypropylene (17mL).
- Ultracentrifuge (Beckman XL-70, equipped with at SW28 and 70Ti rotors).
- Size exclusion chromatography column (iZon qEV2).
- ZetaView apparatus (Particle Metrix, Meerbusch, Germany) for NTA.
- Alignment suspension for NTA measurement (Particle Metrix, Meerbusch, Germany).
- MemBright-Cy3 or Cy5 (Collot et al., 2018).
- PBS solution (Dutscher X0520-500; 0.2μm filtered using a pore filtration unit (Stericup Merck)).
- EV free medium, obtained by ultracentrifugation of classical culture media for 20h at 100000g during (Beckman XL-70 centrifuge, rotor70Ti) to eliminate EVs present in FBS. The supernatant is collected and filtered at 0.22μm (Stericup Merck).
- Cells lines. Here, we use Zmel1 melanoma cells (Heilmann et al., 2015) and Zmel1 cells expressing Syntenin2-GFP (Hyenne et al., 2019). Depending on the cell type and the growth rate of EVs producing cells, the number of cells seeded 48h before EV isolation could differ. Usually, EVs are isolated when cell confluency reaches 80%.

2.2 EV isolation

2.2.1 Isolation by ultracentrifugation

1. Culture cells in the EV free medium for 24 h before collecting conditioned medium (see Fig. 1).
2. Transfer supernatant media from a cell culture flask (~80% confluent) to a 50 mL falcon, and centrifuge at 300 × *g* for 15 min at 4 °C. Keep the supernatant for further processing
3. Concentrate supernatant in 15 mL using a Centricon Plus-70 centrifugal filter (10 k; Millipore)
   - Add supernatant to sample filter cup and spin at up to 4000 × *g* until the desired concentration is achieved.
   - Typical spin time is 15–20 min, depending on solute type and concentration.
4. Centrifuge concentrated medium at 2000 × *g* for 10 min at 4 °C. Keep the supernatant for further processing.
5. Centrifuge supernatant at 10,000 × *g* for 30 min at 4 °C, discard 10 K pellet (large-sized EVs). Keep the supernatant for further processing. Note that in this protocol, large-sized EVs that mainly include microvesicles are discarded because we mainly focused on the effect and characterization of small tumor EVs (exosomes).
6. Centrifuge supernatant medium at 100,000 × *g* for 70 min at 4 °C and the 100 K pellet (small-sized EVs) is kept for further processing.
7. Wash pellet with 15 mL of 1 × PBS, centrifuge at 100,000 × *g* for 70 min at 4 °C.
8. Resuspend the EV pellet in 50 μL of 1 × PBS by gentle pipetting.
9. Use isolated EVs immediately or store at 4 °C in the dark to use the next day.

2.2.2 Isolation by size-exclusion chromatography (SEC)

1. Collect and concentrate conditioned medium similarly to Section 2.2.1 (Steps 1–3) but with a final volume of 2 mL.
2. Rinse the SEC columns with 50 mL of PBS, twice.
3. Apply 2 mL of the concentrated extracellular medium on top of qEV column (Izon Science).
4. Fill the column with PBS and collect 2 mL fractions. At this step, the concentration of EVs in each fraction should be analyzed, for instance using NTA analysis. Depending on the experiments, single fractions can be used, or multiple fractions can be pooled.

5. Centrifuge single or pooled fractions for 1 h at 100,000 × *g*, 4 °C.
6. Resuspend the EV pellet in 50 μL of 1 × PBS by gentle pipetting.
7. Alternatively, single or pooled fractions can be concentrated using an Amicon Ultra-4 10 kDa centrifugal filter device (Merck Millipore).
8. Use isolated EVs immediately or store at 4 °C in the dark to use the next day.

2.3 EV labeling

1. Use fresh EVs isolated by ultracentrifugation or SEC (see Section 2.2). As a control, use a similar volume of particle-free PBS (0.2 μm filtered).
2. Incubate isolated EVs, or control PBS with MemBright-Cy3 or Cy5 at 200 nM (final concentration) in PBS.
3. Mix continuously for 30 s by gentle pipetting.
4. Let stand at room temperature in the dark for 30 min.
5. Rinse labeled EVs in 15 mL of PBS and centrifuged at 100,000 × *g* for 70 min at 4 °C.
6. Carefully aspirate the supernatant which contains the excess unbound dye.
7. Resuspend the EV pellet in 50 μL of 1 × PBS by gentle pipetting.
8. To ensure the highest possible fluorescent intensity, use labeled EVs a soon as possible or store at 4 °C in the dark.

2.4 EV quantification and size measurement

1. Dilute EVs samples before analysis in particle-free PBS (0.2 μm filtered) to obtain a concentration within the recommended measurement range ($1–10 \times 10^9$ particles/mL), corresponding to dilutions from 1:100 to 1:100,000 depending on the initial sample concentration.
2. Start the program and flush the cell channel with distilled water prior to measurement.
3. To align the foci of the laser and microscope, inject the alignment suspension, containing polystyrene particles, into the NTA instrument.
4. Inject the EV suspension into the channel and start the measurement.
5. Save the measurement and based on that adjust the EV sample to have the ideal concentrations for zebrafish injections which is between 10^9 and 10^{10} EVs per mL.

Since freezing is sought to alter EVs pellet (Cheng, Zeng, Han, & Xia, 2019) we recommend using only fresh EVs for fish injections. EV pellets are either used right after isolation or the next morning. In any case, EV pellets are never frozen and are kept at 4 °C, protected from the light, for a maximum

duration of 1 week. To coordinate EVs isolation with fish breeding and embryo production, we use an optimized organizational timeline developed to save maximum time for experimentation (Fig. 1B). In this workflow, EV isolation and fish breeding protocols are followed in parallel. Starting from day 1 EVs isolation takes 3 days and zebrafish larvae are ready for injection in the morning of the fourth day of the protocol which corresponds to 2 dpf for zebrafish larvae (Fig. 1).

3. Zebrafish embryo handling and injection

Intravascular injection of EVs in zebrafish larvae is an easy-handling protocol based on a previously described method of tumor cell injection (Follain, Osmani, Fuchs, et al., 2018; Follain, Osmani, Azevedo, et al., 2018). Zebrafish fluorescent transgenic zebrafish strains allow to identify specific cell types and can be adapted to the user's need (see Section 3.3). When EVs are labeled with Membright-Cy5 or Membright-Cy3, these strains offer the possibility to dissect cell types that are targeted by EVs once they reach their final destination within the circulatory system. Once EVs samples are collected, characterized and labeled in particle-free PBS, they are ready to be injected in the larvae. Larvae are anesthetized and immobilized in an agarose drop to facilitate injection of a few nanoliters of EVs solution under the stereomicroscope using a nanoinjector. This methodology (*i.e.,* intravascular injection of EVs) can also be used for educating metastatic niches (Hyenne et al., 2019) as it had been done in murine models (Costa-Silva et al., 2015; Peinado et al., 2012).

3.1 Reagents

- DANIEAU: stock solution 30 ×: H_2O + 1740 mM NaCL, 21 mM KCl, 12 mM $MgSO_4$, 18 mM$Ca(NO_3)_2$, 150 mM HEPES, pH at 7.6
- PTU: 1-phenyl-2-thiourea (Merck KGaA P7629): stock solution (50 ×): 10 mM in DANIEAU (0.3 ×) solution
- Tricain (ethyl-3-aminobenzoate-methanesulfonate): stock solution (25 ×): 16.25 mM in DANIEAU (0,3 ×)/PTU (1 ×) solution
- Low melting point agarose 0.8% (m/v): melt at 80 °C cool down and maintain at 40 °C during the procedure
- Mineral oil

3.2 Equipment

- 10 cm petri dish
- Plastic pipette
- Thin tweezers (Electron Microscopy Sciences 5,SA-78320-5)
- 35 cm glass-bottomed petri dish (ref: 35 mm Dish | No. 1.0 Coverslip | 20 mm Glass 9. Diameter | Uncoated-P35G-1.0-20-C)
- Stereomicroscope: Leica M205 FA equipped with a fluorescent excitation lamp (Mercury short-arc reflector lamp, EL6000), a GFP filter (Ex. 450–490/Em. 500–550), an ET-C filter (Ex. 533–557/Em. 570–640), a plan APO objective 20× (10450028) and a camera (DFC3000 G)
- Capillary glass (Drummond scientific company—Item# 3-000-203-G/X)
- Capillary puller (Sutter Instrument P-1000)
- Nanoinjector (Drummond Scientific Nanoject II Auto-Nanoliter Injector)

3.3 Biological materials

- Labeled EVs in PBS at an ideal concentration of 10^{10} particles/mL (Section 2).
- Basically, any fish line can be used in this model depending on the biology that is tested. We provide a non-exhaustive list of transgenic lines commonly used in our lab (Table 1). This list is non-exhaustive and can be extended depending on the cell type or biological pathway that is studied.
- Zebrafish, *Danio rerio,* fluorescent transgenic lines: in our case, we mostly use the following strains:
  - *Tg(Fli1a::eGFP)* and *Tg(Fli1a::RFP)* stably expressing GFP and RFP proteins respectively in endothelial cells.
  - *Tg(mpeg::GFP)* stably expressing GFP in myeloid cells (macrophages and monocytes are visualized at this stage of development).
  - Double transgenic lines *Tg(Fli1a::Gal4 Uas::RFP, mpeg::GFP)* that express RFP in endothelial cells and GFP in myeloid cells at the same time.

    These transgenes are expressed in fish with a golden background, which are mutated for the gene slc24a5 and present a delayed pigmentation in their early developmental stage (Lamason et al., 2005). Note that we also use these transgenic fish lines in Casper background, which is a mutant fish strain homozygous for two genes, $roy^{-/-}$ and $nacre^{-/-}$, that control pigmentation. These fish lack melanocytes and iridophores and are translucent even in adulthood (White et al., 2008).

Table 1 Zebrafish transgenic lines.

Genetic background	Name of transgenic line	Fluorophore	Tissue/Cell type	References
Golden (Lamason et al., 2005) or Casper (White et al., 2008)	*Tg(Fli1a: eGFP)*	GFP	Endothelial cells	Lawson and Weinstein (2002)
Golden (Lamason et al., 2005) or Casper (White et al., 2008)	*Tg(mpeg: GFP)*	GFP	Myeloid cells (macrophages and monocytes)	Ellett, Pase, Hayman, Andrianopoulos, and Lieschke (2011)
Golden (Lamason et al., 2005) or Casper (White et al., 2008)	*Tg(Fli1a: Gal4, Uas: RFP, mpeg: GFP)*	RFP and GFP	Endothelial cells and myeloid cells (macrophages and monocytes)	Herwig et al. (2011); Ellett et al. (2011); Hyenne et al. (2019)
Golden (Lamason et al., 2005)	*Tg(mpo: eGFP)*	GFP	Neutrophils	Yuan et al. (2011)
Golden (Lamason et al., 2005)	*Tg(mpeg: mcherry/TNF α:eGFP)*	mCherry and GFP	Myeloid cells (Red) and TNFα-secreting macrophages (Green)	Nguyen-Chi et al. (2015)
Casper (White et al., 2008)	*Tg (Flk: eGFP; Gata1: RFP)*	GFP and RFP	Endothelium and red blood cells	Home-made
Casper (White et al., 2008)	*Tg(gata1: dsRed)*	dsRed	Red blood cells	Traver et al. (2003)

- Other fish strains are commonly used like: *Tg(mpo::eGFP)* which expresses GFP in neutrophils, *Tg(mpeg::mcherry/TNFα::eGFP)* which expresses mcherry in macrophages and GFP in TNF α-secreting macrophages (Nguyen-Chi et al., 2015), (Casper) *Tg (Flk::eGFP; Gata1::RFP)* expressing GFP in the endothelium and RFP in red blood cells or *Tg(gata1:dsRed)* expressing dsRed in red blood cells.

All animal procedures were performed in accordance with French and European Union animal welfare guidelines and supervised by the local ethics committee (Animal facility #A6748233; APAFIS #2018092515234191).

3.4 Zebrafish lines handling and embryo preparation

3.4.1 Zebrafish handling

1. Prepare 0.3× DANIEAU solution using the stock solution (Section 3.1.)
2. Collect the fertilized eggs after mating in 10 cm petri dish and kept in DANIEAU (0.3×) solution at 28 °C for the first 24 h post-fertilization (hpf).
3. Sort the positive embryos 24 hpf with a stereomicroscope M205 FA Leica.
4. Put embryos in DANIEAU (0.3×) solution with 200 μM of PTU (1-phenyl-2-thiourea Merck KGaA P7629) to inhibit melanogenesis (Karlsson, von Hofsten, & Olsson, 2001). Embryos remain in this DANIEAU (0.3×)/PTU(1×) solution over the course of the experiment.
5. Mechanically dechorionate embryo with precaution using a thin tweezer before immobilization.

3.4.2 Zebrafish immobilization

1. At 48 hpf, anesthetize zebrafish larvae with DANIEAU(0.3×)/PTU (1×) solution containing 650 μM of tricaine (DANIEAU(0.3×)/PTU (1×)/Tricain(1×) solution).
2. Carefully put larvae in a low melting point 0.8% agarose drop also containing 650 μM of tricaine on a glass-bottomed petri dish compatible with imaging (Fig. 2B). We use 35 mm MatTek microwell petri dish No.1.0 Coverslip, 14 mm glass diameter, uncoated. Larvae are all aligned in the same direction on their flank at the bottom of the agarose drop using tweezers before agarose solidifies. After 5 min agarose should be solidified and the fish immobilized in the petri dish.
3. Add DANIEAU(0.3×)/PTU(1×) solution in the petri dish.

3.4.3 Preparations for larvae injection

1. Pull 0.53 mm diameter glass needles with a capillary puller (Sutter Instrument P-1000) in order to obtain capillaries with a tip of approximately 10 μm of diameter (Fig. 2A).

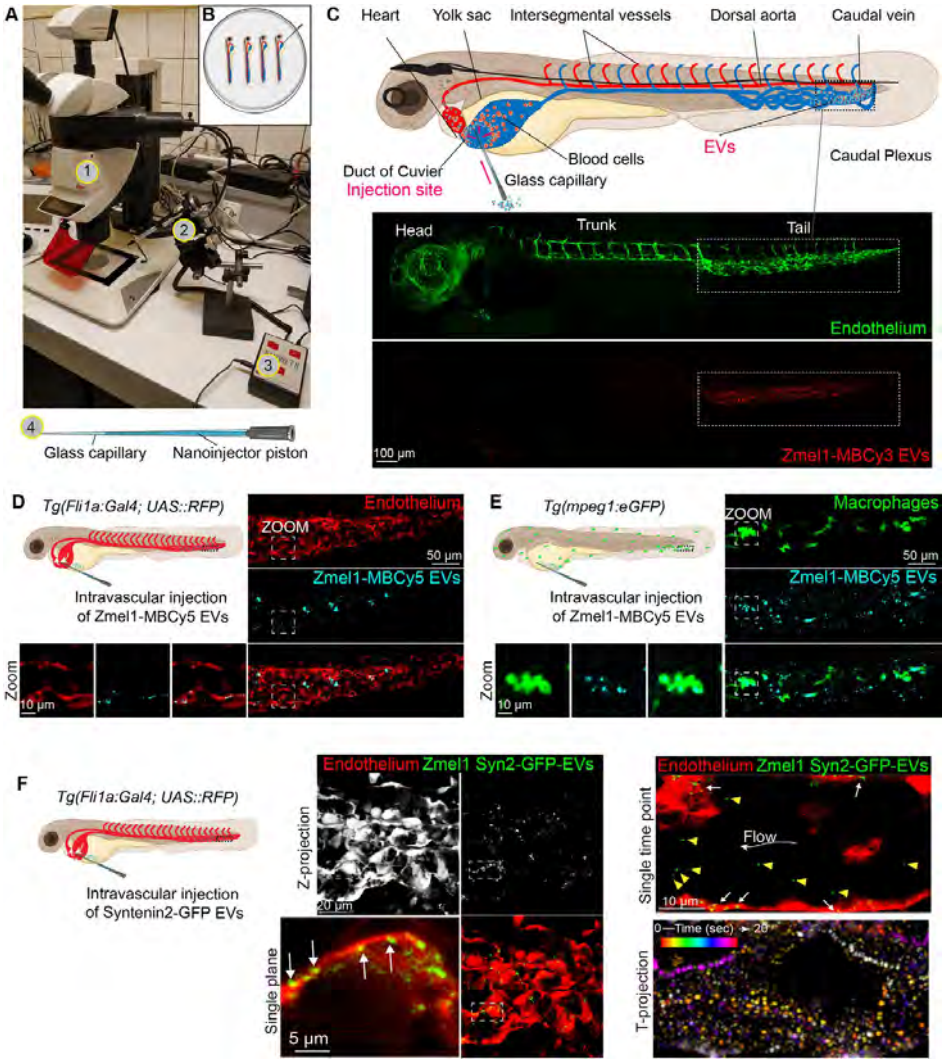

Fig. 2 EV injection and imaging in zebrafish larvae. (A) Equipment required for EVs injection in zebrafish larvae 1: Stereomicroscope, 2: Nanoinjector, 3: Injection control unit, 4: Scheme of glass capillary. (B) Schematic representation of 48 hpf larvae embedded in agarose and mounted in a glass-bottom petri dish. (C) Upper panel: Schematic representation of a 48 hpf zebrafish larvae showing the site of EVs injection (duct of Cuvier) and their main site of arrest (caudal plexus). Bottom panels: Confocal images of Fli1a::eGFP larvae injected with Membright Cy3 labeled Zmel EVs. (D) Schematic representation and confocal images of the caudal plexus of Fli1a::Gal4 UAS::RFP larvae injected with Membright Cy5 Zmel EVs. Large field of view: Z-stack. Zoom: single plane. (E) Schematic representation and confocal images of the caudal plexus of Mpeg::GFP larvae injected with Membright Cy5 Zmel EVs. Large field of view: Z-stack. Zoom: single plane. (F) Schematic representation and confocal images of the caudal plexus of Fli1a::Gal4 UAS::RFP larvae injected with Zmel EVs expressing the fusion protein syntenin2-GFP. Middle panels: Z-projection and single plane images showing arrested and internalized EVs in endothelial cells. Right panels: EVs circulating in the caudal vein at a single time point (upper panel). Temporal projection representing EVs movements (lower panel). *Panel C: from Hyenne, V., Ghoroghi, S., Collot, M., Bons, J., Follain, G., Harlepp, S., Mary, B., Bauer, J., Mercier, L., Busnelli, I., Lefebvre, O., Fekonja, N., Garcia-Leon, M.J., Machado, P., Delalande, F., López, A.A., Silva, S.G., Verweij, F.J., van Niel, G., Djouad, F., Peinado, H., Carapito, C., Klymchenko, A.S., Goetz, J.G., 2019. Studying the fate of tumor extracellular vesicles at high spatiotemporal resolution using the zebrafish embryo. Developmental Cell 48, 554–572.e7. https://doi.org/10.1016/j.devcel.2019.01.014.*

2. Break the tip of the capillary with tweezers to obtain the thinnest capillary tip that can pierce through the yolk sac.
3. Fill the needle with mineral oil using a syringe. It is important to avoid the presence of any bubbles inside the needle as it could affect the quality and reproducibility of the injection. The needle is mounted on a nanoinjector (Drummond Scientific Nanoject II Auto-Nanoliter Injector) (Fig. 2 A2) which allows injecting between 2.3 nL and 69 nL of a solution with a speed of 46 nL/s (fast) or 23 nL/s (slow). The nanoinjector piston is pushed up to two-third of the needle length in order to have enough available volume to aspirate the solution containing the EVs (Fig. 2A).
4. Put 5 μL of fluorescent EVs suspension in 1 × PBS on a parafilm paper placed under the stereomicroscope.
5. Fill the capillary of EV suspension. Avoid air bubbles in the capillary.

3.5 Larvae injection

1. Place the petri dish containing aligned larvae mounted in agarose under the stereomicroscope with their yolk facing the injector and the tip of the needle (Fig. 2B).
2. Gently insert the capillary in the duct of Cuvier, which connects the yolk vasculature to the heart (Fig. 2C). The needle's tip is placed in the vicinity of the circulating blood cell in the blood vessel right under the epidermis that cover the yolk sac.
3. Inject between 23.0 nL and 36.8 nL of EVs, depending on the concentration of EVs and the number of particles you want to inject, in one single injection. Best results are obtained with $5e10^5$ to $1e10^6$ particles per injection. During injection, blood cells that are displaced by the injected volume and pumped by the heartbeat can be visualized under the stereomicroscope (Fig. 2C). These movements are used as readout to control the efficacy of the injection. It is important to ensure that the injected volume is pumped by the heart during injection in order to avoid that the solution of EVs leaks out of the circulatory tract by the wound made by the capillary. Doing so will allow reproducible injections.

4. *In vivo* imaging of circulating EVs in zebrafish larvae: Applications

Once a series of 8–16 larvae are injected, they can be imaged with any microscope allowing fast imaging, ideally with optimal resolution (spinning

disk, single-plane illumination (SPIM), confocal microscopy, etc…). These microscopes should ideally be equipped with a thermostatic chamber heated at 28 °C. Here, we will describe high spatio-temporal imaging of EVs using confocal microscopy (Leica SP5/SP8 equipped with a resonant scanner). Alternatively, spinning disk microscopy proved to be equally efficient (Verweij, Hyenne, et al., 2019; Verweij, Revenu, et al., 2019) and SPIM should in theory also allow non-invasive imaging of circulating EVs over a long period of time (Follain, Mercier, Osmani, Harlepp, & Goetz, 2017). In the next sections, we provide specific microscopy procedures to track: (1) circulating EVs, (2–3) individual EVs right after injection, (4) freshly arrested EVs (5) EVs uptake and (6) the functional consequences of dispersion of tumor EVs. We also show how these procedures can be adapted to the multi-color simultaneous imaging of different EV populations (Hyenne et al., 2019). These imaging sessions are focused on the caudal plexus area of the zebrafish vasculature, which proves to be a perfect region for optimal imaging parameters (speed and resolution). This region is thin and thus easily accessible with single-photon imaging. Furthermore, it is a hotspot for the arrest of circulating tumor cells (Follain, Osmani, Fuchs, et al., 2018; Follain, Osmani, Azevedo, et al., 2018) and EVs (Hyenne et al., 2019).

4.1 Equipment

- Microscope: TCS inverted SP5 with HC PL APO 20 × /0.7 IMM CORR CS objective (Leica) or upright SP8 confocal microscope with an HC FLUOTAR L 25 × /0.95 W VISIR objective (Leica), equipped with a resonant scanner and a thermostatic chamber (28 °C).
- Softwares: SP5/SP8 microscope is equipped with the Leica LAS_AF software version INK 2.7.3.9723. The FIJI/Image J software is used for further image analysis.
- Imaris: Fast tracking of EVs can be performed and rendered using the tracking tool of Imaris.

4.2 Imaging and analysis protocols

4.2.1 High-speed imaging for hemodynamic profiling of circulating EVs

High-speed imaging is mandatory to reveal the accurate hemodynamic profiles of populations of fluorescently labeled EVs in the zebrafish vasculature. Here, we provide examples of how one can reach high-speed

confocal microscopy that is suited for imaging and tracking circulating EVs in the blood flow of zebrafish larvae (as published in Hyenne et al., 2019).

1. Place the glass-bottom petri dish containing zebrafish larvae under the microscope right after injection. Larvae can be either imaged using an inverted or an upright confocal microscope.
2. Use transmitted light and overall fluorescence to focus, if desired, on the caudal plexus region where most of the EVS would accumulate (see Verweij, Hyenne, et al., 2019; Verweij, Revenu, et al., 2019; Hyenne et al., 2019). Such region can be of course adapted to the needs of the study. Imaging at several magnifications is recommended to fully characterize the vascular region of interest with optical sectioning.
3. Lasers are set according to the dyes (Membright, *etc.*) and the transgenic zebrafish strain that are used. We usually use Membright-Cy3 or -Cy5 labeled EVs injected in *Tg(Fli1a::eGFP)*, *Tg(mpeg1::eGFP)* or *Tg(Fli1a::Gal4; UAS::RFP)* fish, respectively, to identify circulating EVs in the vasculature (Fig. 2C–E). Note that the same protocol is used for genetically engineered fluorescent EVs (Fig. 2F). Transmitted light imaging is also used to record and track the displacement of circulating red blood cells (RBCs). Alternatively, one can use the *Tg(gata1::dsRed)* zebrafish line to track circulating RBCs using fluorescence (see Goetz et al., 2014; Hyenne et al., 2019). Finally, two populations of EVs can be imaged simultaneously, for instance, population #1 labeled with MemBright-Cy3, co-injected with population #2 labeled with MemBright-Cy5 in *Tg(Fli1a::eGFP)* fish.
4. Use a resonant scanner (Leica) to reach a frequency of 80–100 frames per second in order to capture the motion of EVs in circulation. This could imply to reduce the image pixel size to 512×32 pixels, for example, focusing on a single arterial or venous vessel. We usually rotate the acquisition region so that a single vessel/vascular region would fit within a 512×32 pixels window (Fig. 3A).
5. Acquire only one Z plane inside the selected vascular region with a pinhole >1 airy unit to capture EVs moving slightly out of the focal plane, for 1 min (Fig. 3A) at optimal scanning speed (to reach 80–100 frames/s, which should allow capturing RBCs and EVs flowing in the dorsal aorta of a 2dpf larvae). RBCs can be imaged at the same time by transmitted light, or by fluorescence using transgenic fish with fluorescent erythrocytes (Gata1::dsRed for instance).

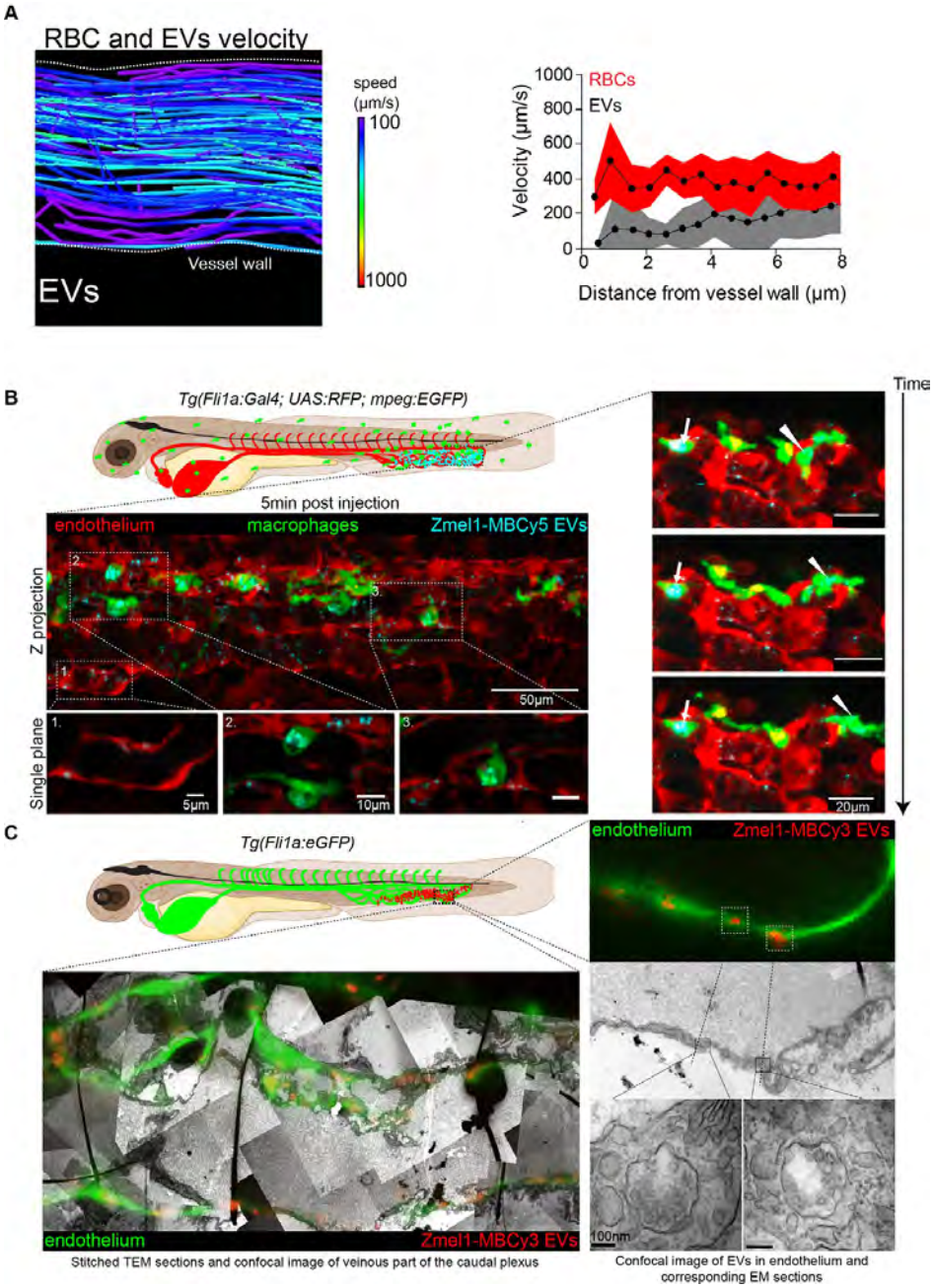

Fig. 3 Dynamic behavior of circulating EVs and fate of internalized EVs. (A) Membright Cy3 4T1 EVs and red blood cells (RBC) tracking in zebrafish caudal plexus: tracking of individual 4T1 EVs in the caudal vein. Right histogram: EVs and RBC velocities (y axis: µm/s) *versus* distance to vessel wall (x axis: µm). (B) Schematic representation and confocal images of double transgenic fish (Fli1a::Gal4 UAS::RFP mpeg::eGFP) injected with Membright Cy5 Zmel EVs. Left panels: 3D stack of caudal plexus region. Zoom: single planes. Right panels: time-lapse showing macrophages (GFP) having internalized

(Continued)

4.2.2 Image analysis

Once movies are recorded, we use FIJI (or Imaris tracking modules) to track RBCs and EVs in motion and process the images. We provide here one possible workflow to analyze these images. We recommend referring to the Imaris tracking modules for optimal tracking parameters and will detail below how we reach accurate tracking of flowing EVs and RBCs using FIJI plugins.

4.2.2.1 Tracking of RBCs

1. Enhance the contrast of the whole stack. Depending on the quality of the image, the Gaussian Blur or Unsharp mask FIJI filters can be used.
2. Execute a Z-projection with average intensity option and subtract the obtained image to the stack. The remaining stack should only display RBCs.
3. Make a binary image of the resulting stack.
4. Apply a bandpass filter with the correct values to remove the background noise and keep only the RBCs.
5. Analyze the obtain stack with the Mosaic 2D/3D particle tracker plugin. For each frame, the position of each blood cell is obtained, and the velocities of each individual track can be visualized (Fig. 3A).

4.2.2.2 Tracking of EVs

1. Use an appropriate threshold to improve the quality of the images (flowing EVs).
2. Make binary images and invert the stack.

Fig. 3—Cont'd Membright Cy5-Zmel EVs (cyan) and moving along the endothelium (red). Arrows: macrophage inside the vasculature. Arrowheads: macrophage carrying EVs and moving outside the vasculature. (C) Schematic representation and illustrative images of a CLEM experiment on a Fli1a:eGFP larvae injected with Membright Cy3-Zmel EVs (Upper left). Lower left panel: superposition of the region of interest imaged with confocal and with electron microscopy. Bottom right panels: Same endothelial region imaged with confocal and with electron microscopy. Magnified areas show that this region contains multivesicular endosomes, which could be the compartments containing internalized EVs. *Panel A: Adapted from Hyenne, V., Ghoroghi, S., Collot, M., Bons, J., Follain, G., Harlepp, S., Mary, B., Bauer, J., Mercier, L., Busnelli, I., Lefebvre, O., Fekonja, N., Garcia-Leon, M.J., Machado, P., Delalande, F., López, A.A., Silva, S.G., Verweij, F.J., van Niel, G., Djouad, F., Peinado, H., Carapito, C., Klymchenko, A.S., Goetz, J.G., 2019. Studying the fate of tumor extracellular vesicles at high spatiotemporal resolution using the zebrafish embryo. Developmental Cell 48, 554–572.e7. https://doi.org/10.1016/j.devcel.2019.01.014.*

3. Use the 2D spot enhancing Filter plugin.
4. Use the stack obtained to make another binarization.
5. Use the Mosaic 2D/3D particle tracker plugin. The position of each EV for each frame is obtained, thus their velocity can be plotted on the image (Fig. 3A).

4.2.2.3 Spatio-temporal analysis of EVs and RBCs within blood vessels

An important parameter to dissect the hemodynamic profiles of EVs is their exact location, and subsequent velocity, within blood vessels when flowing. We previously analyzed the velocity of EVs according to their position within the vessel (Hyenne et al., 2019). Here, we provide a detailed procedure for performing such analysis.

1. Delineate the endothelial wall using the transmitted light (or GFP fluorescence from a *Tg(Fli1a:eGFP)* larvae, and extract the coordinates (into an excel or csv table).
2. Using the temporal analysis of RBCs and EVs velocities (Sections 4.2.2.1 and 4.2.2.2.), extract the coordinates of EVs and RBCs over time.
3. Calculate all the possible distances "d" between EVs (or RBCs) positions (X_{EV} and Y_{EV} or X_{RBC} and Y_{RBC}, respectively) and the closest position of the endothelium (X_{endo} and Y_{endo}).
4. Use these following equations to calculate "d":

$$d = \sqrt{(X_{EV} - X_{endo})^2 + (Y_{EV} - Y_{endo})^2} \text{ or}$$

$$d = \sqrt{(X_{RBC} - X_{endo})^2 + (Y_{RBC} - Y_{endo})^2}$$

5. Keep the smallest distances "d" for each EVs or RBC position.
6. This procedure allows to plot the velocities of RBCs and EVs as a function of the distance from the endothelial wall (Fig. 3A) and thus their position within the vessel.

Such detailed analysis allowed us to make the first hemodynamic profiling of circulating EVs in the zebrafish vasculature (Hyenne et al., 2019). We found that EVs follow a Poiseuille repartition during the circulation in zebrafish vessels. They display high velocity in the middle of the vessel and reduced velocity in the vicinity of endothelial walls, where they drastically slow down and engage rolling and adhesion behaviors. To go further in the analysis of circulating EVs and their interactions with their microenvironment, we complement the dynamic analysis of EVs in movement with fine 3D imaging of arrested EVs in the caudal plexus.

4.2.3 Dissect the mechanisms of EVs arrest with 3D volume imaging

In order to prime metastatic niches (Peinado et al., 2017), circulating EVs are believed to first target specific vascular regions and get internalized by endothelial cells or patrolling macrophages present in the circulation. Whether this is an active or passive process remains to be determined. We provide here means to accurately characterize the intravascular arrest behavior of circulating EVs *in vivo*. Such analysis is based on volume imaging of the zebrafish vasculature concomitantly with arrested EVs. Doing so, we discovered that the vast majority of artificially introduced tumor EVs display a flow-dependent arrest behavior and preferentially stop in low flow venous compartments of the zebrafish vasculature, only 10 min after injection (Hyenne et al., 2019). We also identified the main cell types taking up EVs in zebrafish: endothelial cells and patrolling macrophages. This protocol can also be adapted to image two populations of EVs concomitantly. It could therefore allow comparing simultaneously different profiles of the arrest of natural subpopulations of EVs (*e.g.,* microvesicles and exosomes) or of engineered EVs (*e.g.,* expressing or not an adhesion receptor).

1–3. The three first steps -1. -2. -3. are common with the protocols described in Section 4.2.1.

4. Use a pinhole of 1 airy unit and a z-step of 0.5 μm, acquire an optical confocal section of the entire caudal plexus (Fig. 2D and F, Fig. 3B). Several resolutions can be used and we, for example, apply 512×512 or 1024×1024 pixels imaging (or 512×256, 1024×350 pixels) which are imaging parameters (size) that allow optimal EVs and vasculature imaging (Fig. 2D and E).

5. Perform a maximum intensity Z projection of the stack to visualize the overall distribution of EVs in the caudal plexus. Such analysis allows to attribute EV arrest position with respect to the vessel identity and flow parameters (see Hyenne et al., 2019; Verweij, Hyenne, et al., 2019).

6. Single planes of the stack are selected to confirm the internalization of fluorescent EVs in fish cells (Fig. 2D–F, Fig. 3B).

When combined with imaging acquisition parameters allowing to accurately determine hemodynamic profiles (see Section 3.3), such an analysis allows to correlate hotspots of the arrest of EVs with vascular flow profiles. In addition, this protocol allows to identify the cells internalizing circulating EVs. For example, we routinely inject EVs labeled with Membright dyes in *Tg(Fli1a::eGFP), Tg(mpeg1::eGFP), Tg(Fli1a::Gal4; UAS::RFP)* or *Tg(Fli1a::Gal4; UAS::RFP; mpeg1::GFP)* fish lines (Fig. 2C–F, Fig. 3) as we had identified that patrolling

macrophages, in addition to endothelial cells, are massively engulfing circulating EVs (Hyenne et al., 2019; Verweij, Hyenne, et al., 2019) (Fig. 2D and E, Fig. 3B). Finally, this protocol can be used to compare the preferential arrest sites and target cells of two populations of EVs simultaneously. In this case, two populations of EVs will be labeled with two different dyes in parallel and mixed at the same concentration right before injection in zebrafish larvae (Hyenne et al., 2019).

4.2.4 Visualization of circulating EVs arrest and uptake

Depending on the source of EVs and the identity of the receiving cell, many different mechanisms of EV arrest and uptake have been described. They include direct fusion between EVs and the receiving cell plasma membrane, phagocytosis, macropinocytosis, clathrin-dependent and independent endocytosis and receptor mediated endocytosis. The arrest and internalization of circulating EVs can now be visualized *in vivo* in zebrafish larvae. It can be used to directly test the involvement of a particular EV receptor or to compare the arrest and uptake of different populations of EVs.

1–3. The three first steps -1. -2. -3. are common with the protocols described in Section 4.2.1.

4. Note that for this protocol, it is essential to start imaging right after injection, as quickly as possible, since most of the circulating EVs get internalized in less than 10 min.

5. Make a xyzt time-lapse of the cell of interest. Of note, different settings can be used depending on the dynamic of the internalization. As an example, we previously used the following settings: Short time lapses at 5–10 Z stacks per minute for 1 min with a z-step of 0.5 mm; long time lapses at 1 Z stack per minute for 1 h with a z-step of 2 mm; short time-lapses at 3–8 images per second on single Z planes (Hyenne et al., 2019).

This protocol allowed us to capture events of internalization by endothelial cells and macrophages (Fig. 3B right panel) (Hyenne et al., 2019). Our analysis identified two different mechanisms of EVs uptake by macrophages *in vivo*: endocytosis and a mechanism similar to filopodia surfing (Heusermann et al., 2016; Hyenne et al., 2019). Furthermore, this protocol can be used to track the trafficking of EVs within the receiving cells, from the initial entry of EVs, to their storage compartment.

4.2.5 Identification of the compartments storing internalized EVs

After uptake, EVs are usually trafficked to late endosomes-lysosomes, where they will deliver their cargo or be degraded. Zebrafish larvae are well adapted

to study the fate of circulating EV once they are internalized. Indeed, as zebrafish larvae are permeable, it is possible to visualize the late endosomes-lysosomes by simply adding lysotracker to zebrafish incubating medium.

The following labeling protocol can be added to the protocols Sections 4.2.3 or 4.2.4 described above:

- Add lysoTracker (Thermofisher Scientific) at 5 μM in the DANIEAU medium for 2 h before EVs injection

Another way to study the fate of circulating EVs in zebrafish with the high spatial resolution is to use correlative light electron microscopy (CLEM) (Fig. 3C). Since this protocol has been described elsewhere (Follain, Osmani, Fuchs, et al., 2018; Goetz, Monduc, Schwab, & Vermot, 2015; Hyenne et al., 2019), we will briefly describe the main steps. Living zebrafish larvae are imaged at different magnifications after EVs internalization, with labeling allowing visualization of EVs and a specific cell type (endothelial cells or macrophages for instance) as well as additional anatomical landmarks. Larvae are fixed and processed for serial electron microscopy analysis, using previously described protocols (Follain, Osmani, Fuchs, et al., 2018; Goetz et al., 2015; Hyenne et al., 2019). Using recorded anatomic landmarks, such as the architecture of the vasculature in the caudal plexus, the cell of interest can be retrieved (Fig. 3C). It is then possible to image and reconstruct the 3D volume of the cell of interest at high resolution by serial section electron microscopy or tomography.

These approaches (with their associated protocols described above (in particular Sections 4.2.3 or 4.2.4)) can be instrumental to identify the fate of internalized EVs. In the future, it could contribute to the understanding of the mechanisms of EV cargo transfer.

4.2.6 Functional assay: Priming of metastatic niches

EVs are known to induce phenotypic changes in multiple physiologic and pathologic contexts. The zebrafish larvae can be used to capture these phenotypes in real time and correlate them with the uptake of EVs. While many other possibilities will likely arise in different fields in the coming years, we provide here an example of a functional assay aiming to determine the pro-metastatic potential of tumor EVs. Many studies in mice revealed that intravenous injection of tumor EVs increases the metastatic growth of tumor cells subsequently injected into the circulation (Costa-Silva et al., 2015; Peinado et al., 2012). Here, we detail a protocol allowing to directly image the events occurring after the initial arrival of tumors EVs. In this assay, zebrafish melanoma EVs (Zmel1 EVs) are injected into larvae circulation before the

injection and tracking of Zmel1 td-tomato cells. As a control for EVs, we initially used 100 nm polystyrene beads, but complementary controls should use EVs from non-tumoral cells (*e.g.,* Zebrafish fibroblasts AB9). Afterward, tumor cell growth is monitored over time using longitudinal imaging.

1. Inject a control concentration of (in our case Zmel EVs, 100 nm polystyrene beads (phosphorex) as a control) into the circulation of zebrafish larvae at 32 hpf
2. 14 h after EVs injection, inject tumor cells corresponding to the tEVs secreting cells, in our case, Zmel1 td-Tomato melanoma cells. Tumor cells are prepared as previously described (Follain, Osmani, Fuchs, et al., 2018). Briefly, cells are detached, and a cell suspension is prepared in their culture medium at a 10^8 cells/mL. Between 27.6 and 32 nL of the cell suspension is injected into the fish vasculature.
3. Image the zebrafish caudal plexus with a confocal microscope at different time points to record tumor cells survival and colonization. In our case 24 h, 48 h and 7 days after tumor cell injection (Fig. 4B). Larvae are mounted for imaging and replaced in their growing medium, according to the procedure. Note that in this experiment we use beads as control, in previous work we added a supplemental control injecting EVs coming from zebrafish fibroblasts (AB9 cell line) (Hyenne et al., 2019).

The zebrafish transparency allows to easily visualize the arrest of tumor cells in the circulation at a single cell level (Fig. 4B left panels), to follow extravasation of tumor cells at different time-points (Fig. 4B middle and right panels) and their outgrowth and invasion of surrounding tissues (Fig. 4B right panels).

5. Conclusions

As research in circulating extracellular vesicles grows with developments in diagnosis, biomaterials or fundamental biology, appropriate models are crucial to dissect their behavior in physiologic and pathologic conditions *in vivo*. Unfortunately, a majority of *in vitro* studies have not yet taken into account the hemodynamic environment which circulating EVs use to disseminate and execute their functions. In addition, classical *in vivo* models (such as mice) do not allow to precisely follow EVs dynamics in body fluids. On the contrary, intravascular injection of EVs within the zebrafish larvae allows a non-invasive visualization of individual EVs dispersion, uptake and interactions with cells in the physiological environment of a circulatory system. This methodology is compatible with every type of EVs isolation

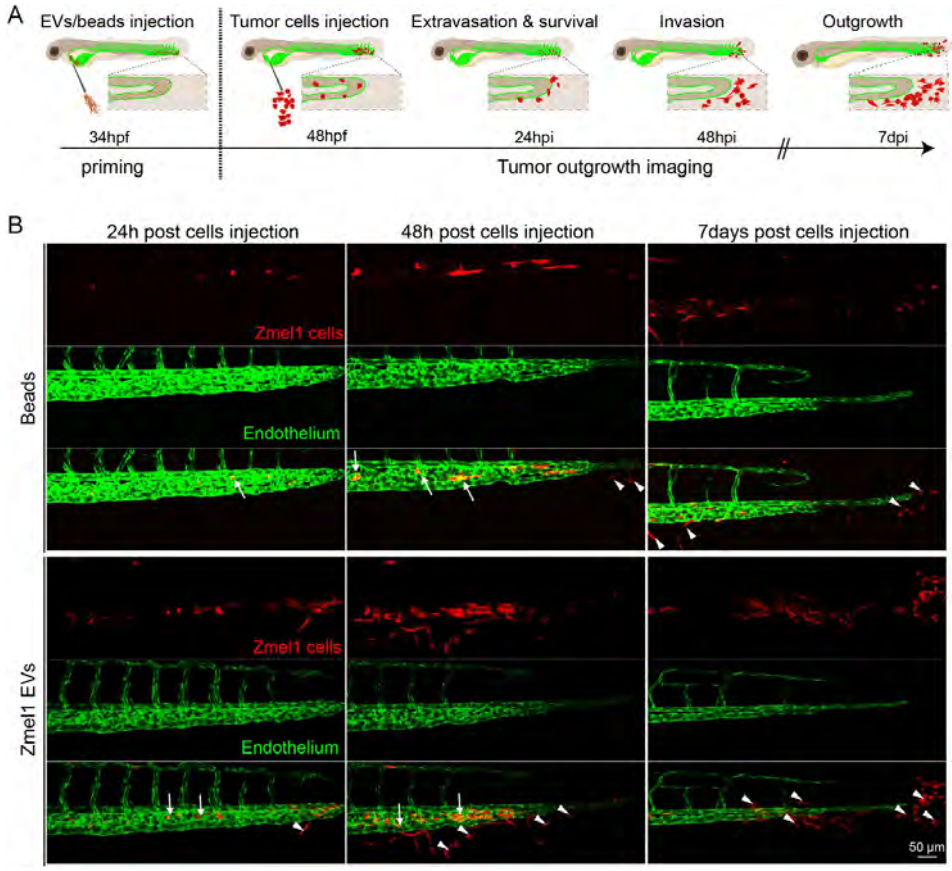

Fig. 4 Example of a functional EVs experiment in zebrafish. (A) Schematic representation a priming experiment protocol in zebrafish. EVs or 100 nm beads are injected in 34 hpf larvae. Tumor cells are injected in 48 hpf larvae. Tumor cell survival and colonization is followed at different time-points. Hptci: hours post tumor cell injection. (B) Confocal images of a representative priming experiment. The growth of Zmel1 tdTomato cells is imaged in Flie1a:eGFP fish at three different time-points after tumor EVs or beads treatments. Arrows: intravascular cells, arrowheads: extravascular cells.

protocol, requires minimum material and basic imaging setup. Ultimately, it is currently the best model to investigate EVs hemodynamics behavior, attachment, uptake and endocytosis by specific cell types *in vivo* (Hyenne et al., 2019; Verweij, Hyenne, et al., 2019).

The methodology described within this chapter is likely to provide fertile grounds for increasing our knowledge and address several important questions:

(1) *How do EVs disseminate through body fluids?* To escape their secreting site and reach distant receiving cells, EVs often need to cross the endothelial barriers. Two processes, transcytosis and endothelial leakage have been

described (Matsumoto et al., 2017; Tominaga et al., 2015). However, the articulation of the two processes and their underlying molecular mechanism remains to be unraveled *in vivo*. In zebrafish, injection of pre-labeled EVs with appropriate dyes, combined with CLEM imaging, could allow to image EVs leaving the blood circulation with high levels of details (Hyenne et al., 2019). High-resolution visualization of EVs inside and outside the zebrafish vasculature will help to understand if EVs reach distant cells as isolated vesicles or if other cells (*e.g.,* macrophages) can help EVs to cross the endothelial barrier (Fig. 3B arrowheads). Furthermore, using CD63-pHLuorin tool (a pH sensitive GFP fused to the CD63 EV marker that is fluorescent only in non-acidic compartments) in zebrafish larvae (Verweij, Hyenne, et al., 2019; Verweij, Revenu, et al., 2019) allows visualizing EVs diffusing from their secreting site and helps to understand how EVs cross the endothelial barrier to reach the circulation. Therefore, zebrafish larvae can be used to track the journey of EVs from their secretion site to their target cells, *via* the blood circulation.

(2) *Which mechanisms control EVs organotropism and uptake?* It is thought that the repertoire of adhesion molecules present on the surface EVs is responsible for specific interactions between EVs and receiving cells, ultimately leading to EVs internalization and cargo delivery. Several molecules, such as integrins (Hoshino et al., 2015), tetraspanins (Nazarenko et al., 2010; Rana, Claas, Kretz, Nazarenko, & Zoeller, 2011; Rana, Yue, Stadel, & Zöller, 2012), heparan sulfate proteoglycans (Purushothaman et al., 2016) and lectins (Barrès et al., 2010; Bruno et al., 2009) have been shown to mediate the interaction between EVs and receiving cells. However, the relative importance and the interplay of these molecules is unknown. Zebrafish model allows comparing and visualizing *in vivo* interaction and internalization of different populations of EVs bearing different membrane proteins. Therefore, it offers the possibility to test the individual or combined role of specific adhesion molecules in circulating EVs arrest and uptake. Furthermore, because pharmacological approaches and genetic manipulation are easily performed in the zebrafish, one can dissect endocytic pathways that control EVs uptake *in vivo* and test pathways previously identified *in vitro* like clathrin-dependent endocytosis or micropinocytosis (Nakase, Kobayashi, Takatani-Nakase, & Yoshida, 2015; Tian et al., 2014). The zebrafish larvae provides a relevant model to test these pathways in realistic physiological environments where hemodynamics forces are taken into account.

(3) *What are the consequences of EVs uptake?* The dynamic of the phenotypic changes induced by EVs uptake on a receiving cell are not fully understood. This is in part due to the lack of appropriate models allowing to visualize the impact of EVs on receiving cells *in vivo*. However, zebrafish larvae offers the possibility to directly correlate the number and timing of EVs uptake to modifications of the phenotype of an individual receiving cell. Various tools could be developed to investigate this question. For instance, we have shown that tumor EVs activate the expression of TNF-α in macrophages in zebrafish (Hyenne et al., 2019). This transgenic line, *Tg(mpeg::mcherry, TNF-α::GFP)* (Nguyen-Chi et al., 2015) can now be used to dissect precisely the consequences of EVs uptake on macrophages phenotypic switch. Similar approaches adapted to other fields of biology could easily be developed in zebrafish. For instance, genetic reporters, such as the Cre-Lox system, which are available in zebrafish (Carney & Mosimann, 2018), could be used to visualize EVs cargo delivery, similarly to what has been done in mice (Zomer et al., 2015).

Finally, we think that the zebrafish model could be a great asset in various fields of EVs research. Indeed, zebrafish models have been developed in several domains (Gut, Reischauer, Stainier, & Arnaout, 2017; Kirchberger, Sturtzel, Pascoal, & Distel, 2017; Torraca & Mostowy, 2018; White, Rose, & Zon, 2013; Xi, Noble, & Ekker, 2011) where circulating tEVs play instrumental roles, such as cancer biology, cardiovascular diseases, neurodegenerative disorders or pathogenic diseases. Therefore, these fields could strongly benefit from studying the role of EVs in zebrafish, which could increase our knowledge on EVs biology in addition to accelerate the development of therapeutic strategies and clinical trials.

Acknowledgments

We thank all members of the Goetz Lab for helpful discussions. We are indebted to Kerstin Richter and Francesca Peri (EMBL, Heidelberg, Germany) as well as to Pauline Hanns and Claudia Lengerke (University Hospital Basel, Switzerland) for supplying zebrafish embryos during the early stages of this work. We are grateful to Camille Hergott and Gregory Khelifi for zebrafish care. We are grateful to R. White (MSKCC, New York, USA) for the Zmel1 (native and tdTomato) cells, as well as to Pascale Zimmerman (CRCM, Marseille, France) for the Syntenin-2 construct. This work was supported by a fellowship from the French Ministry for Research to BM, and by a fellowship from the IDEX (University of Strasbourg) and ARC (Association pour le Recherche sur le Cancer) to SG, by grants from La Ligue contre le Cancer, Canceropole Grand-Est, INCa (EVRALTIC) and Plan Cancer (VESMATIC) to VH and JGG, and by institutional funds from University of Strasbourg, INSERM to JGG.

References

Adem, B., Vieira, P. F., & Melo, S. A. (2020). Decoding the biology of exosomes in metastasis. *Trends in Cancer*, *6*, 20–30. https://doi.org/10.1016/j.trecan.2019.11.007.

Bakhshandeh, B., Kamaleddin, M., & Aalishah, K. (2016). A comprehensive review on exosomes and microvesicles as epigenetic factors. *CSCR*, *12*, 31–36. https://doi.org/10.2174/1574888X11666160709211528.

Balaj, L., Lessard, R., Dai, L., Cho, Y.-J., Pomeroy, S. L., Breakefield, X. O., et al. (2011). Tumour microvesicles contain retrotransposon elements and amplified oncogene sequences. *Nature Communications*, *2*, 180. https://doi.org/10.1038/ncomms1180.

Barrès, C., Blanc, L., Bette-Bobillo, P., André, S., Mamoun, R., Gabius, H.-J., et al. (2010). Galectin-5 is bound onto the surface of rat reticulocyte exosomes and modulates vesicle uptake by macrophages. *Blood*, *115*, 696–705. https://doi.org/10.1182/blood-2009-07-231449.

Boulanger, C. M., Loyer, X., Rautou, P.-E., & Amabile, N. (2017). Extracellular vesicles in coronary artery disease. *Nature Reviews. Cardiology*, *14*, 259–272. https://doi.org/10.1038/nrcardio.2017.7.

Bruno, S., Grange, C., Deregibus, M. C., Calogero, R. A., Saviozzi, S., Collino, F., et al. (2009). Mesenchymal stem cell-derived microvesicles protect against acute tubular injury. *JASN*, *20*, 1053–1067. https://doi.org/10.1681/ASN.2008070798.

Butler, J. T., Abdelhamed, S., & Kurre, P. (2018). Extracellular vesicles in the hematopoietic microenvironment. *Haematologica*, *103*, 382–394. https://doi.org/10.3324/haematol.2017.183335.

Carney, T. J., & Mosimann, C. (2018). Switch and trace: Recombinase genetics in zebrafish. *Trends in Genetics*, *34*, 362–378. https://doi.org/10.1016/j.tig.2018.01.004.

Cheng, Y., Zeng, Q., Han, Q., & Xia, W. (2019). Effect of pH, temperature and freezing-thawing on quantity changes and cellular uptake of exosomes. *Protein & Cell*, *10*, 295–299. https://doi.org/10.1007/s13238-018-0529-4.

Chuo, S. T.-Y., Chien, J. C.-Y., & Lai, C. P.-K. (2018). Imaging extracellular vesicles: Current and emerging methods. *Journal of Biomedical Science*, *25*, 91. https://doi.org/10.1186/s12929-018-0494-5.

Collot, M., Fam, T. K., Ashokkumar, P., Faklaris, O., Galli, T., Danglot, L., et al. (2018). Ultrabright and Fluorogenic probes for multicolor imaging and tracking of lipid droplets in cells and tissues. *Journal of the American Chemical Society*, *140*, 5401–5411. https://doi.org/10.1021/jacs.7b12817.

Corso, G., Heusermann, W., Trojer, D., Görgens, A., Steib, E., Voshol, J., et al. (2019). Systematic characterization of extracellular vesicle sorting domains and quantification at the single molecule – single vesicle level by fluorescence correlation spectroscopy and single particle imaging. *Journal of Extracellular Vesicles*, *8*(1), 1663043.

Costa-Silva, B., Aiello, N. M., Ocean, A. J., Singh, S., Zhang, H., Thakur, B. K., et al. (2015). Pancreatic cancer exosomes initiate pre-metastatic niche formation in the liver. *Nature Cell Biology*, *17*, 816–826. https://doi.org/10.1038/ncb3169.

Ellett, F., Pase, L., Hayman, J. W., Andrianopoulos, A., & Lieschke, G. J. (2011). mpeg1 promoter transgenes direct macrophage-lineage expression in zebrafish. *Blood*, *117*, e49–e56. https://doi.org/10.1182/blood-2010-10-314120.

Flaumenhaft, R., Mairuhu, A., & Italiano, J. (2010). Platelet- and megakaryocyte-derived microparticles. *Seminars in Thrombosis and Hemostasis*, *36*, 881–887. https://doi.org/10.1055/s-0030-1267042.

Follain, G., Mercier, L., Osmani, N., Harlepp, S., & Goetz, J. G. (2017). Seeing is believing – Multi-scale spatio-temporal imaging towards *in vivo* cell biology. *Journal of Cell Science*, *130*, 23–38. https://doi.org/10.1242/jcs.189001.

Follain, G., Osmani, N., Azevedo, A. S., Allio, G., Mercier, L., Karreman, M. A., et al. (2018). Hemodynamic forces tune the arrest, adhesion, and extravasation of circulating tumor cells. *Developmental Cell*, *45* 33–52.e12. https://doi.org/10.1016/j.devcel.2018.02.015.

Follain, G., Osmani, N., Fuchs, C., Allio, G., Harlepp, S., & Goetz, J. G. (2018). *Using the zebrafish embryo to dissect the early steps of the metastasis Cascade. In A. Gautreau (Ed.), Cell Migration* (pp. 195–211). New York, NY: Methods in Molecular Biology. Springer New York. *https://doi.org/10.1007/978-1-4939-7701-7_15*.

Goetz, J. G., Monduc, F., Schwab, Y., & Vermot, J. (2015). Using correlative light and Electron microscopy to study zebrafish vascular morphogenesis. In C. M. Nelson (Ed.), *Tissue morphogenesis, Methods in Molecular Biology* (pp. 31–46). New York, NY: Springer New York. https://doi.org/10.1007/978-1-4939-1164-6_3.

Goetz, J. G., Steed, E., Ferreira, R. R., Roth, S., Ramspacher, C., Boselli, F., et al. (2014). Endothelial cilia mediate low flow sensing during zebrafish vascular development. *Cell Reports*, *6*, 799–808. https://doi.org/10.1016/j.celrep.2014.01.032.

Görgens, A., Bremer, M., Ferrer-Tur, R., Murke, F., Tertel, T., et al. (2019). Optimisation of imaging flow cytometry for the analysis of single extracellular vesicles by using fluorescence-tagged vesicles as biological reference material. *Journal of Extracellular Vesicles*, *8*(1), 1587567.

Gross, J. C., Chaudhary, V., Bartscherer, K., & Boutros, M. (2012). Active Wnt proteins are secreted on exosomes. *Nature Cell Biology*, *14*, 1036–1045. https://doi.org/10.1038/ncb2574.

Gut, P., Reischauer, S., Stainier, D. Y. R., & Arnaout, R. (2017). Little fish, big data: Zebrafish as a model for cardiovascular and metabolic disease. *Physiological Reviews*, *97*, 889–938. https://doi.org/10.1152/physrev.00038.2016.

Heilmann, S., Ratnakumar, K., Langdon, E. M., Kansler, E. R., Kim, I. S., Campbell, N. R., et al. (2015). A quantitative system for studying metastasis using transparent zebrafish. *Cancer Research*, *75*, 4272–4282. https://doi.org/10.1158/0008-5472.CAN-14-3319.

Herwig, L., Blum, Y., Krudewig, A., Ellertsdottir, E., Lenard, A., Belting, H.-G., et al. (2011). Distinct Cellular Mechanisms of Blood Vessel Fusion in the Zebrafish Embryo. *Current Biology*, *21*, 1942–1948. https://doi.org/10.1016/j.cub.2011.10.016.

Heusermann, W., Hean, J., Trojer, D., Steib, E., von Bueren, S., Graff-Meyer, A., et al. (2016). Exosomes surf on filopodia to enter cells at endocytic hot spots, traffic within endosomes, and are targeted to the ER. *The Journal of Cell Biology*, *213*, 173–184. https://doi.org/10.1083/jcb.201506084.

Hood, J. L., Roman, S. S., & Wickline, S. A. (2011). Exosomes released by melanoma cells prepare sentinel lymph nodes for tumor metastasis. *Cancer Research*, *71*(11), 3792–3801.

Hoshino, A., Costa-Silva, B., Shen, T.-L., Rodrigues, G., Hashimoto, A., Tesic Mark, M., et al. (2015). Tumour exosome integrins determine organotropic metastasis. *Nature*, *527*, 329–335. https://doi.org/10.1038/nature15756.

Hoshino, D., Kirkbride, K. C., Costello, K., Clark, E. S., Sinha, S., Grega-Larson, N., et al. (2013). Exosome secretion is enhanced by invadopodia and drives invasive behavior. *Cell Reports*, *5*, 1159–1168. https://doi.org/10.1016/j.celrep.2013.10.050.

Hyenne, V., Ghoroghi, S., Collot, M., Bons, J., Follain, G., Harlepp, S., et al. (2019). Studying the fate of tumor extracellular vesicles at high spatiotemporal resolution using the zebrafish embryo. *Developmental Cell*, *48*, 554–572.e7. https://doi.org/10.1016/j.devcel.2019.01.014.

Hyenne, V., Lefebvre, O., & Goetz, J. G. (2017). Going live with tumor exosomes and microvesicles. *Cell Adhesion & Migration*, *11*, 173–186. https://doi.org/10.1080/19336918.2016.1276694.

Johnsen, K. B., Gudbergsson, J. M., Andresen, T. L., & Simonsen, J. B. (2019). What is the blood concentration of extracellular vesicles? Implications for the use of extracellular

vesicles as blood-borne biomarkers of cancer. *Biochimica et Biophysica Acta, Reviews on Cancer*, *1871*, 109–116. https://doi.org/10.1016/j.bbcan.2018.11.006.

Karimi, N., Cvjetkovic, A., Jang, S. C., Crescitelli, R., Hosseinpour Feizi, M. A., Nieuwland, R., et al. (2018). Detailed analysis of the plasma extracellular vesicle proteome after separation from lipoproteins. *Cellular and Molecular Life Sciences*, *75*, 2873–2886. https://doi.org/10.1007/s00018-018-2773-4.

Karlsson, J., von Hofsten, J., & Olsson, P.-E. (2001). Generating transparent zebrafish: A refined method to improve detection of gene expression during embryonic development. *Marine Biotechnology*, *3*, 0522–0527. https://doi.org/10.1007/s1012601-0053-4.

Keller, M. D., Ching, K. L., Liang, F.-X., Dhabaria, A., Tam, K., Ueberheide, B. M., et al. (2020). Decoy exosomes provide protection against bacterial toxins. *Nature*, *579*, 260–264. https://doi.org/10.1038/s41586-020-2066-6.

Kirchberger, S., Sturtzel, C., Pascoal, S., & Distel, M. (2017). Quo natas, danio?—recent progress in modeling Cancer in zebrafish. *Frontiers in Oncology*, 7, 186. https://doi.org/10.3389/fonc.2017.00186.

Kowal, J., Arras, G., Colombo, M., Jouve, M., Morath, J. P., Primdal-Bengtson, B., et al. (2016). Proteomic comparison defines novel markers to characterize heterogeneous populations of extracellular vesicle subtypes. *Proceedings National Academy of Sciences United States of America*, *113*, E968–E977. https://doi.org/10.1073/pnas.1521230113.

Lai, C. P., Kim, E. Y., Badr, C. E., Weissleder, R., Mempel, T. R., Tannous, B. A., et al. (2015). Visualization and tracking of tumour extracellular vesicle delivery and RNA translation using multiplexed reporters. *Nature Communications*, *6*, 7029. https://doi.org/10.1038/ncomms8029.

Lai, C. P., Mardini, O., Ericsson, M., Prabhakar, S., Maguire, C. A., Chen, J. W., et al. (2014). Dynamic biodistribution of extracellular vesicles *in Vivo* using a multimodal imaging reporter. *ACS Nano*, *8*, 483–494. https://doi.org/10.1021/nn404945r.

Lamason, R. L., Mohideen, M. A. P. K., Mest, J. R., Wong, A. C., Norton, H. L., Aros, M. C., et al. (2005). SLC24A5, a putative cation exchanger, affects pigmentation in zebrafish and humans. *Science*, *310*, 1782–1786. https://doi.org/10.1126/science.1116238.

Lawson, N. D., & Weinstein, B. M. (2002). In Vivo Imaging of Embryonic Vascular Development Using Transgenic Zebrafish. *Developmental Biology*, *248*, 307–318. https://doi.org/10.1006/dbio.2002.0711.

Lázaro-Ibáñez, E., Lässer, C., Shelke, G. V., Crescitelli, R., Jang, S. C., Cvjetkovic, A., et al. (2019). DNA analysis of low- and high-density fractions defines heterogeneous subpopulations of small extracellular vesicles based on their DNA cargo and topology. *Journal of Extracellular Vesicles*, *8*, 1656993. https://doi.org/10.1080/20013078.2019.1656993.

Matsumoto, J., Stewart, T., Sheng, L., Li, N., Bullock, K., Song, N., et al. (2017). Transmission of α-synuclein-containing erythrocyte-derived extracellular vesicles across the blood-brain barrier via adsorptive mediated transcytosis: Another mechanism for initiation and progression of Parkinson's disease? *Acta Neuropathologica Communications*, *5*, 71. https://doi.org/10.1186/s40478-017-0470-4.

Matsumoto, A., Takahashi, Y., Chang, H. Y., Wu, Y. W., Yamamoto, A., Ishihama, Y., et al. (2020). Blood concentrations of small extracellular vesicles are determined by a balance between abundant secretion and rapid clearance. *Journal of Extracellular Vesicles*, *9*, 1696517. https://doi.org/10.1080/20013078.2019.1696517.

Matusek, T., Wendler, F., Polès, S., Pizette, S., D'Angelo, G., Fürthauer, M., et al. (2014). The ESCRT machinery regulates the secretion and long-range activity of Hedgehog. *Nature*, *516*, 99–103. https://doi.org/10.1038/nature13847.

Mol, E. A., Goumans, M.-J., Doevendans, P. A., Sluijter, J. P. G., & Vader, P. (2017). Higher functionality of extracellular vesicles isolated using size-exclusion chromatography

compared to ultracentrifugation. *Nanomedicine: Nanotechnology, Biology and Medicine*, *13*, 2061–2065. https://doi.org/10.1016/j.nano.2017.03.011.

Nakase, I., Kobayashi, N. B., Takatani-Nakase, T., & Yoshida, T. (2015). Active macropinocytosis induction by stimulation of epidermal growth factor receptor and oncogenic Ras expression potentiates cellular uptake efficacy of exosomes. *Scientific Reports*, *5*, 10300. https://doi.org/10.1038/srep10300.

Nazarenko, I., Rana, S., Baumann, A., McAlear, J., Hellwig, A., Trendelenburg, M., et al. (2010). Cell surface Tetraspanin Tspan8 contributes to molecular pathways of exosome-induced endothelial cell activation. *Cancer Research*, *70*, 1668–1678. https://doi.org/10.1158/0008-5472.CAN-09-2470.

Nguyen-Chi, M., Laplace-Builhe, B., Travnickova, J., Luz-Crawford, P., Tejedor, G., Phan, Q. T., et al. (2015). Identification of polarized macrophage subsets in zebrafish. *eLife*, *4*, e07288 https://doi.org/10.7554/eLife.07288.

Nielsen, M. H., Beck-Nielsen, H., Andersen, M. N., & Handberg, A. (2014). A flow cytometric method for characterization of circulating cell-derived microparticles in plasma. *Journal of Extracellular Vesicles*, *3*, 20795. https://doi.org/10.3402/jev.v3.20795.

Peinado, H., Alečković, M., Lavotshkin, S., Matei, I., Costa-Silva, B., Moreno-Bueno, G., et al. (2012). Melanoma exosomes educate bone marrow progenitor cells toward a pro-metastatic phenotype through MET. *Nature Medicine*, *18*, 883–891. https://doi.org/10.1038/nm.2753.

Peinado, H., Zhang, H., Matei, I. R., Costa-Silva, B., Hoshino, A., Rodrigues, G., et al. (2017). Pre-metastatic niches: Organ-specific homes for metastases. *Nature Reviews Cancer*, *17*, 302–317.

Purushothaman, A., Bandari, S. K., Liu, J., Mobley, J. A., Brown, E. E., & Sanderson, R. D. (2016). Fibronectin on the surface of myeloma cell-derived exosomes mediates exosome-cell interactions. *The Journal of Biological Chemistry*, *291*, 1652–1663. https://doi.org/10.1074/jbc.M115.686295.

Rana, S., Claas, C., Kretz, C. C., Nazarenko, I., & Zoeller, M. (2011). Activation-induced internalization differs for the tetraspanins CD9 and Tspan8: Impact on tumor cell motility. *The International Journal of Biochemistry & Cell Biology*, *43*, 106–119. https://doi.org/10.1016/j.biocel.2010.10.002.

Rana, S., Yue, S., Stadel, D., & Zöller, M. (2012). Toward tailored exosomes: The exosomal tetraspanin web contributes to target cell selection. *The International Journal of Biochemistry & Cell Biology*, *44*, 1574–1584. https://doi.org/10.1016/j.biocel.2012.06.018.

Simonsen, J. B. (2019). Pitfalls associated with lipophilic fluorophore staining of extracellular vesicles for uptake studies. *Journal of Extracellular Vesicles*, *8*, 1582237. https://doi.org/10.1080/20013078.2019.1582237.

Stranska, R., Gysbrechts, L., Wouters, J., Vermeersch, P., Bloch, K., Dierickx, D., et al. (2018). Comparison of membrane affinity-based method with size-exclusion chromatography for isolation of exosome-like vesicles from human plasma. *Journal of Translational Medicine*, *16*, 1. https://doi.org/10.1186/s12967-017-1374-6.

Takahashi, Y., Nishikawa, M., Shinotsuka, H., Matsui, Y., Ohara, S., Imai, T., et al. (2013). Visualization and in vivo tracking of the exosomes of murine melanoma B16-BL6 cells in mice after intravenous injection. *Journal of Biotechnology*, *165*(2), 77–84.

Takov, K., Yellon, D. M., & Davidson, S. M. (2017). Confounding factors in vesicle uptake studies using fluorescent lipophilic membrane dyes. *Journal of Extracellular Vesicles*, *6*(1), 1388731.

Théry, C., Amigorena, S., Raposo, G., & Clayton, A. (2006). Isolation and characterization of exosomes from cell culture supernatants and biological fluids. *Current Protocols in Cell Biology*, *30*, 3.22.1–3.22.29. https://doi.org/10.1002/0471143030.cb0322s30.

Tian, T., Zhu, Y.-L., Zhou, Y.-Y., Liang, G.-F., Wang, Y.-Y., Hu, F.-H., et al. (2014). Exosome uptake through Clathrin-mediated endocytosis and macropinocytosis and mediating miR-21 delivery. *The Journal of Biological Chemistry*, *289*, 22258–22267. https://doi.org/10.1074/jbc.M114.588046.

Tominaga, N., Kosaka, N., Ono, M., Katsuda, T., Yoshioka, Y., Tamura, K., et al. (2015). Brain metastatic cancer cells release microRNA-181c-containing extracellular vesicles capable of destructing blood–brain barrier. *Nature Communications*, *6*, 6716. https://doi.org/10.1038/ncomms7716.

Torraca, V., & Mostowy, S. (2018). Zebrafish infection: From pathogenesis to cell biology. *Trends in Cell Biology*, *28*, 143–156. https://doi.org/10.1016/j.tcb.2017.10.002.

Traver, D., Paw, B. H., Poss, K. D., Penberthy, W. T., Lin, S., & Zon, L. I. (2003). Transplantation and in vivo imaging of multilineage engraftment in zebrafish bloodless mutants. *Nature Immunology*, *4*, 1238–1246. https://doi.org/10.1038/ni1007.

van der Vos, K. E., Abels, E. R., Zhang, X., Lai, C., Carrizosa, E., Oakley, D., et al. (2016). Directly visualized glioblastoma-derived extracellular vesicles transfer RNA to microglia/macrophages in the brain. *Neuro-Oncology*, *18*, 58–69. https://doi.org/10.1093/neuonc/nov244.

Verweij, F. J., Hyenne, V., Van Niel, G., & Goetz, J. G. (2019). Extracellular vesicles: Catching the light in zebrafish. *Trends in Cell Biology*, *29*, 770–776. https://doi.org/10.1016/j.tcb.2019.07.007.

Verweij, F. J., Revenu, C., Arras, G., Dingli, F., Loew, D., Pegtel, D. M., et al. (2019). Live tracking of inter-organ communication by endogenous exosomes in vivo. *Developmental Cell*, *48* 573–589.e4. https://doi.org/10.1016/j.devcel.2019.01.004.

White, R., Rose, K., & Zon, L. (2013). Zebrafish cancer: The state of the art and the path forward. *Nature Reviews Cancer*, *13*, 624–636. https://doi.org/10.1038/nrc3589.

White, R. M., Sessa, A., Burke, C., Bowman, T., LeBlanc, J., Ceol, C., et al. (2008). Transparent adult zebrafish as a tool for in vivo transplantation analysis. *Cell Stem Cell*, *2*, 183–189. https://doi.org/10.1016/j.stem.2007.11.002.

Whitham, M., Parker, B. L., Friedrichsen, M., Hingst, J. R., Hjorth, M., Hughes, W. E., et al. (2018). Extracellular vesicles provide a means for tissue crosstalk during exercise. *Cell Metabolism*, *27* 237–251.e4. https://doi.org/10.1016/j.cmet.2017.12.001.

Wiklander, O. P. B., Nordin, J. Z., O'Loughlin, A., Gustafsson, Y., Corso, G., Mäger, I., et al. (2015). Extracellular vesicle in vivo biodistribution is determined by cell source, route of administration and targeting. *Journal of Extracellular Vesicles*, *4*, 26316. https://doi.org/10.3402/jev.v4.26316.

Willms, E., Cabañas, C., Mäger, I., Wood, M. J. A., & Vader, P. (2018). Extracellular vesicle heterogeneity: Subpopulations, isolation techniques, and diverse functions in Cancer progression. *Frontiers in Immunology*, *9*, 738. https://doi.org/10.3389/fimmu.2018.00738.

Xi, Y., Noble, S., & Ekker, M. (2011). Modeling Neurodegeneration in Zebrafish. *Current Neurology and Neuroscience Reports*, *11*, 274–282. https://doi.org/10.1007/s11910-011-0182-2.

Yáñez-Mó, M., Siljander, P. R.-M., Andreu, Z., Zavec, A. B., Borràs, F. E., Buzas, E. I., et al. (2015). Biological properties of extracellular vesicles and their physiological functions. *Journal of Extracellular Vesicles*, *4*, 27066. https://doi.org/10.3402/jev.v4.27066.

Yang, D., Zhang, W., Zhang, H., Zhang, F., Chen, L., Ma, L., et al. (2020). Progress, opportunity, and perspective on exosome isolation - efforts for efficient exosome-based theranostics. *Theranostics*, *10*, 3684–3707. https://doi.org/10.7150/thno.41580.

Yuan, H., Zhou, J., Deng, M., Zhang, Y., Chen, Y., Jin, Y., et al. (2011). Sumoylation of CCAAT/enhancer–binding protein α promotes the biased primitive hematopoiesis of zebrafish. *Blood*, *117*, 7014–7020. https://doi.org/10.1182/blood-2010-12-325712.

Zhao, F., Cheng, L., Shao, Q., Chen, Z., Lv, X., Li, J., et al. (2020). Characterization of serum small extracellular vesicles and their small RNA contents across humans, rats, and mice. *Scientific Reports*, *10*, 4197. https://doi.org/10.1038/s41598-020-61098-9.

Zomer, A., Maynard, C., Verweij, F. J., Kamermans, A., Schäfer, R., Beerling, E., et al. (2015). In vivo imaging reveals extracellular vesicle-mediated Phenocopying of metastatic behavior. *Cell*, *161*, 1046–1057. https://doi.org/10.1016/j.cell.2015.04.042.

3. The role of hemodynamics forces on circulating tEVs and endothelium interactions

The two complementary models presented before allowed me to decipher the fate of circulating tEVs. During my PhD, my main work aimed at (i) investigate the potential correlation between flow speed and tEVs accumulation in endothelial recipient cells *in vivo*; (ii) explore if biophysical cues of the circulation (i.e. hemodynamic forces) affect circulating tEVs trafficking inside recipient endothelial cells; (iii) study combined effects of tEVs internalization and presence of hemodynamic forces on endothelial cell phenotype.

Using both, the zebrafish embryo and a microfluidic approach, together with my colleagues Nandini Asokan, we found that the presence of a moderate flow, similar to the one in small vessels (e.g. venules) and corresponding to the area where circulating tEVs arrest *in vivo*, have a significant impact on circulating tEVs biology. This supports the idea that hemodynamic is indeed an important factor to consider while studying circulating tEVs (e.g. their biodistribution and their function). We showed that:

- Venous moderate flow speed *in vivo* and similar range of flow speed *in vitro* (400µm/s) enhance tEVs internalization by endothelial cells.
- *in vivo*, there is an inverted correlation between flow speed and tEVs accumulation in endothelial cells (i.e. high arterial flow speed decreases tEVs accumulation, low venous flow speed increases it).
- *In vitro* and *in vivo*, absence or decrease of flow speed respectively, reduces tEVs internalization by endothelial cells.
- *In vitro* and *in vivo* flow speed regulates tEVs redirection toward less acidic compartments in endothelial cells.
- *In vitro*, presence of moderate flow speed increases colocalization of tEVs with Rab14+ compartments.
- *In vitro* and *in vivo*, tEVs treatment associated with a relevant hemodynamic environment activates pro-angiogenic mechanisms.

Overall, our work showed the importance of the hemodynamic environment in circulating tEVs biology. Biophysical forces tune the internalization, the trafficking as well as the function of tEVs inside endothelial cells. Further investigations will be

needed to entirely characterize some mechanisms identified in this work. Nonetheless, it could pave the way for further research about circulating tEVs behavior in circulation and more importantly in tumor progression and the apparition of PMN. Additionally, it could also bring lights on the importance of the hemodynamic part of EVs biology in other pathophysiological processes mediated by EVs such as cardiovascular disease.

Blood flow diverts circulating extracellular vesicles from endothelial degradation to promote angiogenesis

- **Mary et al., 2022 (in preparation)**

Blood flow diverts extracellular vesicles from endothelial degradative compartments to promote angiogenesis

B. Mary[1,2,3,4], N. Asokan[1,2,3,4], K. Jerabkova-Roda[1,2,3,4], A. Larnicol[1,2,3,4], I. Busnelli[1,2,3,4], T. Stemmelen[5,6], A. Pichot[5,6], A. Molitor[5,6], R Carapito[1,2,3], O Lefebvre[1,2,3], JG Goetz[1,2,3*], and V Hyenne[1,2,3,4,7*]

[1]INSERM UMR S1109, Tumor Biomechanics, Strasbourg, France
[2]Université de Strasbourg, Strasbourg, France
[3]Fédération de Médecine Translationnelle de Strasbourg (FMTS), Strasbourg, France
[4]Équipe labellisée Ligue Contre le Cancer
[5]Laboratoire d'ImmunoRhumatologie Moléculaire, Plateforme GENOMAX, Institut national de la santé et de la recherche médicale (INSERM)
UMR$_S$1109, $Institut thématique interdisciplinaire (ITI) de Médecine de Précision de Strasbourg Transplant ex NG, Faculté de Médecine, Fédération Hospitalo-Universitaire OMICARE, Fédération de Médecine Translationnelle de Strasbourg (FMTS), Université de Strasbourg, Strasbourg, France$
[6]Service d'Immunologie Biologique, Plateau Technique de Biologie, Pôle de Biologie, Nouvel Hôpital Civil, Hôpitaux Universitaires de Strasbourg, 1 Place de l'Hôpital, 67091, Strasbourg, France
[7]CNRS SNC5055, Strasbourg, France
[*]Equal contribution

Extracellular vesicles released by tumors (tEVs) disseminate via circulatory networks and promote microenvironmental changes in distant organs favouring metastatic seeding. Despite their abundance in the bloodstream, how hemodynamics affect the function of circulating tEVs remains unsolved. We experimentally tuned flow profiles in vitro (microfluidics) and in vivo (zebrafish) and demonstrated that efficient uptake of tEVs occurs in endothelial cells subjected to capillary-like hemodynamics. Such flow profiles partially reroute internalized tEVS towards Rab14-positive endosomes, which are non-acidic and non-degradative, suggesting that endothelial mechanosensing allows to divert tEVs from degradation. Subsequently, tEVs promote the expression of pro-angiogenic transcription factors in flow-stimulated endothelial cells and favor vessel sprouting in zebrafish. Altogether, we demonstrate that capillary-like flow profiles potentiate the pro-tumoral function of circulating tEVs by promoting their uptake and rerouting their trafficking. We propose that tEVs contribute to pre-metastatic niche formation by exploiting endothelial mechanosensing in specific vascular regions with permissive flow profiles.

extracellular vesicles, endothelium, hemodynamics, metastasis

Correspondence: ***hyenne@unistra.fr jacky.goetz@inserm.fr***

Introduction

Inter-organ communication is instrumental in maintaining systemic homeostasis, coordinating metabolic response to environmental challenges or reacting to diseased tissue. It can be mediated by hormones, cytokines, but also by more recently described and more complex structures belonging to the heterogenous family of extracellular vesicles (EVs). These small vesicles (30nm-5µm diameter) transport bioactive molecules (RNAs, lipid, proteins) between distant organs by traveling through circulatory networks (Yáñez-Mó et al., 2015; Cheng and Hill, 2022). In cancer, as the disease becomes systemic and progresses from primary to secondary sites, EVs actively contribute to organ cross-talk and thereby impact both primary tumor growth and metastatic spreading. Tumor EVs (tEVs) released by primary tumors, spread via blood or lymphatic circulation and reach distant organs where they alter the microenvironment in multiple ways (Kalluri and LeBleu, 2020; Marar et al., 2021). By joining future metastatic organs before tumor cells arrival, tEVs modify its cellular and extracellular composition and create a pre-metastatic niche favorable to metastasis formation (Peinado et al., 2017; Ghoroghi et al., 2021a). While the changes induced by tEVs on distant organs started to be unraveled over the past years, the transit of EVs from the circulation to the new organ are very poorly described. By contrast, the behavior of circulating tumor cells in the vasculature is better understood (Follain et al., 2020b). For instance, it is now well established that blood flow forces directly impact the arrest, extravasation and metastatic capacities of circulating tumor cells (Follain et al., 2020a). It is therefore possible that hemodynamics affects the abilities of tEVs to alter distant organs and form pre-metastatic niches. Furthermore, hemodynamics strongly affects the biology of the endothelium, which, together with patrolling monocytes, takes up most of circulating EVs (Morishita et al., 2015; Imai et al., 2015; Takahashi et al., 2013; Hyenne et al., 2019). For instance hemodynamic forces alter endothelial shape and cytoskeleton organization (Li et al., 2005), but also endosomal pathways, as they regulate endothelial autophagy (Vion et al., 2017). Flow shear forces also directly impact the capacity of endothelial cells to take up material flowing in the circulation, such as ions, proteins or nanoparticles (Han et al., 2015, 2012; Tarbell, 2010). Therefore, we speculated that hemodynamics would impact the fate and trafficking of internalized tEVs. To test this possibility, we studied the initial steps of tEVs settling in pathophysiologic models properly reproducing the hemodynamic environment. We combined an in vivo model, the zebrafish embryo, that we adapted to the study of tEVs (Hyenne et al., 2019; Verweij et al., 2019), together with an in vitro microfluidics models where a monolayer of endothelial cells can be challenged with flow of a tunable speed (Follain et al., 2018).

Our results show that hemodynamics has a major impact on EVs fate and function as it promotes EVs uptake, alters their trafficking in endothelial cells by inducing a partial lysosomal escape and enhances their pro-angiogenic function.

Results and Discussion

Blood flow tune endothelial uptake of circulating tEVs To determine the influence of hemodynamics on the dissemination of circulating tEVs, we took advantage of the zebrafish embryo that we previously described (Hyenne et al., 2019). At 48h post-fertilization, the zebrafish embryo is composed of a complex vascular network suited to real-time imaging of circulating EVs (Verweij et al., 2021, 2019; Hyenne et al., 2019). When injected in the duct of cuvier, injected EVs quickly disseminate through the bloodstream and reach the caudal plexus via the dorsal aorta (Fig.1a and Hyenne et al. 2019). While the dorsal aorta carries circulating tEVs at relatively high flow velocities, these quickly return in venous compartments characterized by low flow velocities. Interestingly, when assessing which vascular regions were preferably targeted by tEVs, we observed that both endothelial cells and patrolling macrophages of low flow regions efficiently internalized circulating tEV (Hyenne et al., 2019). In order to better dissect such observation, we carefully and concomitantly measured blood flow velocities and endothelial accumulation of circulating tEVs (Fig.1A). To do so, we isolated tEVs from 4T1 mouse mammary tumor cells by differential centrifugation, labeled them with a stable and bright lipophilic dye that we previously characterized, the MemGlow (formerly known as MemBright) (Hyenne et al., 2019) and injected them in the circulation of zebrafish embryos (Mary et al., 2020). We analyzed four vascular regions that are representatives of the flow profiles found in the caudal plexus and plotted the amount of tEVs internalized by endothelial cells with respect to the flow velocities (Figure 1A). We observed a significant inverse correlation between flow profiles and endothelial accumulation of tEVs : while accumulation of tEVs is maximal in venous regions with 400 µm/s flow velocity, it is significantly reduced in arterial regions where flow exceeds/reaches 600 µm/s in average. In order to confirm that flow profiles directly control the uptake of tEVs, we experimentally and pharmacologically tuned blood flow velocities in the ZF embryo and quantified the resulting tEVs uptake in a common vascular region (caudal vein). Decreasing flow velocities with lidocaine (that reduces pacemaker activity of the heart (Figure 1B, left) as previously described (Follain et al., 2018)) lead to a significant decrease of tEVs uptake by endothelial cells (Figure 1B). Conversely, increasing the heart pacemaker activity using IBMX (that increases pacemaker activity of the heart (Figure 1C, left) as previously described (Follain et al., 2018)) results in a slight albeit non-significant increase in tEVs uptake in the veinous endothelium (Figure 1C). To confirm these in vivo data suggesting that tEVs uptake is mostly efficient at permissive flow profiles of 400 µm/s, we exploited in vitro microfluidics system, which allow for a precise and homogenous control of flow regimes. Similarly, we measured the internalization of fluorescent tEVs perfused on a monolayer of endothelial cells and observed that tEVs accumulate more efficiently in endothelial cells subjected to a 400 µm/s flow speed (when compared to static, no flow conditions). Altogether, our in vitro and in vivo experiments demonstrate that endothelial cells most efficiently accumulate tEVs when subjected to flow velocities of 400 µm/s. We propose that binding and arrest of tEVs at the endothelial surface are prevented when flow velocities exceed the permissive value of 400 µm/s while both uptake and trafficking of tEVs would be impaired, through mechanosensing, at low flow velocities. Interestingly, we had observed EVs rolling on the surface of the endothelium of zebrafish embryos at this flow velocity (Hyenne et al., 2019). In addition a velocity of 400 µm/s favors the arrest of circulating tumor cells (Follain 2018) and is the average flow speed measured in small capillaries from organs that are prone to metastasis such as human liver or mouse brains (Follain et al., 2020b). Nevertheless, hemodynamics cannot be the sole explanation for such behavior and we and others had shown that endothelial targeting of tEVs also relies on specific adhesion receptors present at their surface, such as integrins or CD146/MCAM (Hoshino et al., 2015; Ghoroghi et al., 2021b). Therefore, efficient binding of tEVs to the endothelial surface occurs when adhesion-prone tEVs exploit permissive flow profiles. Interestingly, similar observations were made with synthetic nanoparticles as their uptake by endothelial cells is higher at venous-like low shear stress than in static conditions, but decreases at higher arterial-like shear stress in a receptor-dependent manner (Han et al., 2012, 2015; Chen et al., 2020; Lin et al., 2010). Therefore, is it likely that the destination of circulating EVs relies on the combined effect of hemodynamics and receptor-ligand interactions.

Circulating tEVs are partially re-routed to alternative non-acidic and non-degradative RAB14 positive compartments We then aimed to characterize the fate of circulating tEVs in flow-stimulated endothelial cells. To investigate the trafficking routes exploited by tEVs, we generated vHUVECs endothelial cell lines stably expressing fluorescent markers of early (mCherry-Rab5), late (mEmerald-Rab7) and recycling endosomes (eGFP-Rab11) as well as late endosome-lysosomes (RFP-Lamp1). We tracked the internalization of fluorescently labelled tEVs by live imaging and quantified their colocalization with endosomal markers after 3h using an automated image analysis pipeline (see material and methods). We found that internalized EVs mostly colocalize with LAMP1 positive compartments and, to a lesser extent with Rab5 and Rab7 (Fig.2A and Fig.S1). Flow had no effect on the distribution of tEVs among these endosomal markers suggesting that endothelial mechanosensing had no impact on the general internalization routes used by tEVs. Since accumulation of circulating tEVs in LAMP1 positive compartments suggests that they end up in degradative compartments, we wondered whether flow could divert tEVs from degradative machineries. We first labeled degradative compartments in endothelial cells using the Magic Red membrane permeant probe, which rapports the activity of the lysosomal protease cathepsin B. While most of the inter-

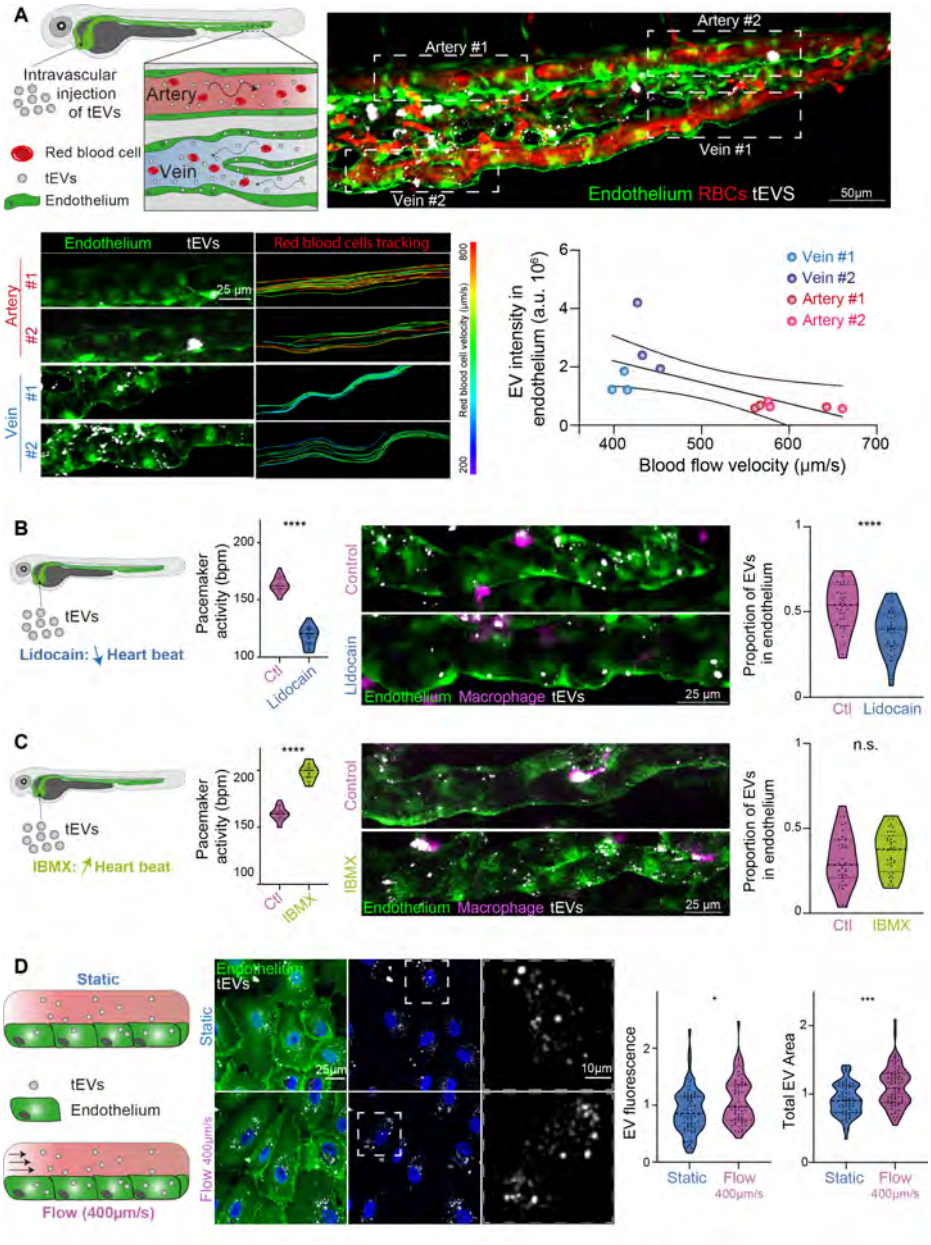

Fig. 1. Blood flow tune the uptake of circulating tEVs by endothelial cells A) Description of the experimental setup: 2 days post-fertilization transgenic (Fli1:GFP (endothelium) Gata1:dsRed (red blood cells -RBCs) zebrafish embryos are injected intravascularly with Memglow-Cy5-labeled 4T1 EVs and imaged in the caudal plexus after 3h (right, Z projection). Velocities of individual circulating RBCs are tracked and fluorescent EV signal internalized in the endothelium is measured in four indicated regions per fish (2 aortic and 2 veinous). Bottom left: representative images of the four regions showing EVs within the endothelium (Z projections) and RBCs tracks with a color code representing velocities. Bottom right: graph showing the correlation between internalized EVs and RBC velocities in the same region (n= 3 embryos). B-C) Memglow-Cy5-labeled 4T1 EVs are injected intravascularly in Fli1:GFP (GFP endothelium) embryos with decreased (B) or increased (C) heart pacemaker activity with respectively lidocaine and IBMX. Left graphs display pacemaker activities (1 dot: 1 fish). Middle: representative images, single planes. Right graph represents the proportion of fluorescent EVs within the endothelium (1 dot: 1 fish; Lidocain: n=36 per condition, three independent experiments; p<0,0001 Student T-test; IBMX: n=39 per condition, three independent experiments, p=0,11). D) Memglow-Cy5-labeled 4T1 EVs are perfused on HUVECs endothelial monolayer labeled with Memglow 488 in static or flow conditions (400m/s) and imaged by confocal after 3h. Representative images and quantification of internalized EVs showing increase in EV total area, in EV total fluorescence (1 dot: 1 field of view; experiment performed in quadruplicate).

nalized tEVs accumulate in Magic Red positive compartments, flow significantly reduced the proportion of tEVs found in CathepsinB-positive structures (Fig. 2B) suggesting that internalized EVs are partially redirected to non-

degradative compartments upon flow mechanosensing. Since the degradative activity of lysosomes hydrolases relies on the acidic luminal pH (Perera and Zoncu, 2016), we next probed the pH of EV-containing compartments by exploiting the pH sensitive reporter pHluorin. When anchored on EVs external membrane via an insertion in the extracellular domain of the tetraspanin CD63, such construct, which is also fused to pH insensitive mScarlet at its intracellular C-terminal end (Sung et al., 2020), allows to probe the pH of the compartments targeted by tEVs. We generated tumor cells expressing CD63-pHluorin-Scarlet and validated that these cells can secrete pH sensitive fluorescent EVs (data not shown and Fig.2C). The ratio of green (PhLuorin) towards red (mScarlett) fluorescence was then used to probe the pH of tEVs' environment. When pH-sensor tEVs were perfused on endothelial cells, we again observed striking differences in endothelial cells subjected to flow. We found that flow drastically increases the pHluorin/mScarlet ratio suggesting that endothelial mechanosensing can change the trafficking routes of internalized tEVs and reroute them towards more neutral compartments (Fig. 2C). Together, these results show that internalized tEVs are in part diverted to less acidic and less degradative compartments when endothelial cells are cultured under flow. In order to identify such compartments, we focused on Rab14, a Rab GTPase known for being localized in LAMP1 positive late endosomes, in addition to other compartments (Hoffman et al., 2022). Among other functions, Rab14 is involved in intracellular virus and pathogen trafficking towards late endo-lysosomes (Kyei et al., 2006; Okai et al., 2015; Kuijl et al., 2013). Importantly, Rab14 also controls the transit of internalized material toward non-acidic LAMP1 positive compartments (Trofimenko et al., 2021). Therefore, we stably expressed GFP-Rab14 in endothelial cells and assessed their proximity to internalized tEVs. While internalized EVs are often found in close proximity of Rab14 positive independently of flow, the proportion of EVs within the lumen of Rab14 positive compartments is significatively increased in flow-stimulated endothelial cells. Altogether, our results show that the presence of a moderate flow speed partially switches EVs trafficking toward Rab14 positive non-acidic and non-degradative compartments suggesting that endothelial mechanosensing of flow would prevent tEVs from degradation. To validate our observations in vivo, we injected CD63-pHluorin-mScarlet tEVs in the circulation of zebrafish embryos where the flow speed was pharmacologically manipulated. We measured the pHluorin/mScarlet ratio of tEVs internalize in a single vessel (caudal vein) as performed in Fig.1 and observed that the pHluorin/mScarlet ratio was reduced in embryos with decreased flow velocities, suggesting that EVs accumulate in more acidic compartments under low flow velocity (Fig.2F). Conversely, increasing blood flow velocity with IBMX increases the pHluorin/mScarlet ratio, suggesting that tEVs tend to accumulate in less acidic compartments in endothelial cells facing higher flow speed (Fig.2G). Altogether, our combined in vitro and in vivo data show that circulating EVs follow a different trafficking route depending on hemodynamic forces applied on endothelial cells. At moderate or high velocities, internalized EVs are partially rerouted towards non-acidic compartments suggesting that the fate of tEVs, and their function, is strictly controlled by the mechano-sensing abilities of the endothelium. Flow-dependent trafficking of internalized EVs could determine the proportion of EVs undergoing lysosomal degradation or allowed to transfer their cargo through back-fusion in endosomes. However, since both processes rely on endosomal acidification (Bonsergent et al., 2021; Joshi et al., 2020), the extent to which tEVs escape lysosomal degradation could relate to alternative fate, such as endothelial transcytosis which allows EVs to cross the blood-brain barrier (Morad et al., 2019).

Blood flow promotes lysosomal pathways in endothelial cells Endothelial cells have exceptional mechanosensing abilities that orchestrate multiple cellular fonctions (Fang et al., 2019; Freund et al., 2012). Having observed that flow re-directs tEVs towards non-degradative compartments, we wondered whether this resulted from a broad re-organization of endosomal trafficking in flow-stimulated endothelial cells. To address this question, we simply analyzed endolysosomal trafficking in flow-stimulated endothelial cells, in absence of EVs. We first compared transcriptional response using RNAseq in endothelial cells subjected to 400 µm/s or not. Interestingly, such flow profiles significantly favor the transcription of genes associated with lysosomal pathways (Fig. 3A). When probing the endolysosomal pathway using fluorescent dyes, we oberved that flow increases the number of lysotracker positive compartments, whose area was decreased (Fig.3B). When carefully assessing inner trafficking compartments using electron microscopy, we confirmed that flow significantly increases the number of endolysosomes, which displayed a smaller size (Fig.3C). Finally, to gain insight into the functionality of those compartments, we quantified the cathepsin B activity using the Magic Red dye. We observed that not only the number of Magic Red positive compartment is increased, but their intensity is also higher (Fig.3D). This result suggests that endothelial cells sensing flow profiles that are permissive to tEVs uptake also increase their lysosomal degradative activity, which is regulated by pH. Interestingly, the RNAseq analysis further revealed that flow-stimulated endothelial cells could turn on genes involved in the regulation of lysosomal pH (Fig.3A). Among them, the proton exchanger NHE9 is known to limit endosome luminal acidification (Kondapalli et al., 2015). When flow-stimulated endothelial cells stably expressing NHE9-mCherry were incubated with fluorescent tEVs, we observed that most of them ended up in NHE9-positive compartments, independently of flow (Fig.S2). Altogether, these experiments show that flow profiles that do favor tEVs uptake and re-routing also promote endolysosomal degradative pathways. Therefore, the re-routing of EVs toward non-degradative compartments does not solely result from a mechano-transduction pathway that adjusts lysosomal pathways, but more likely reflects a flow-dependent EV specific switch in trafficking route.

Blood flow and circulating tEVs cooperate to favor angio-

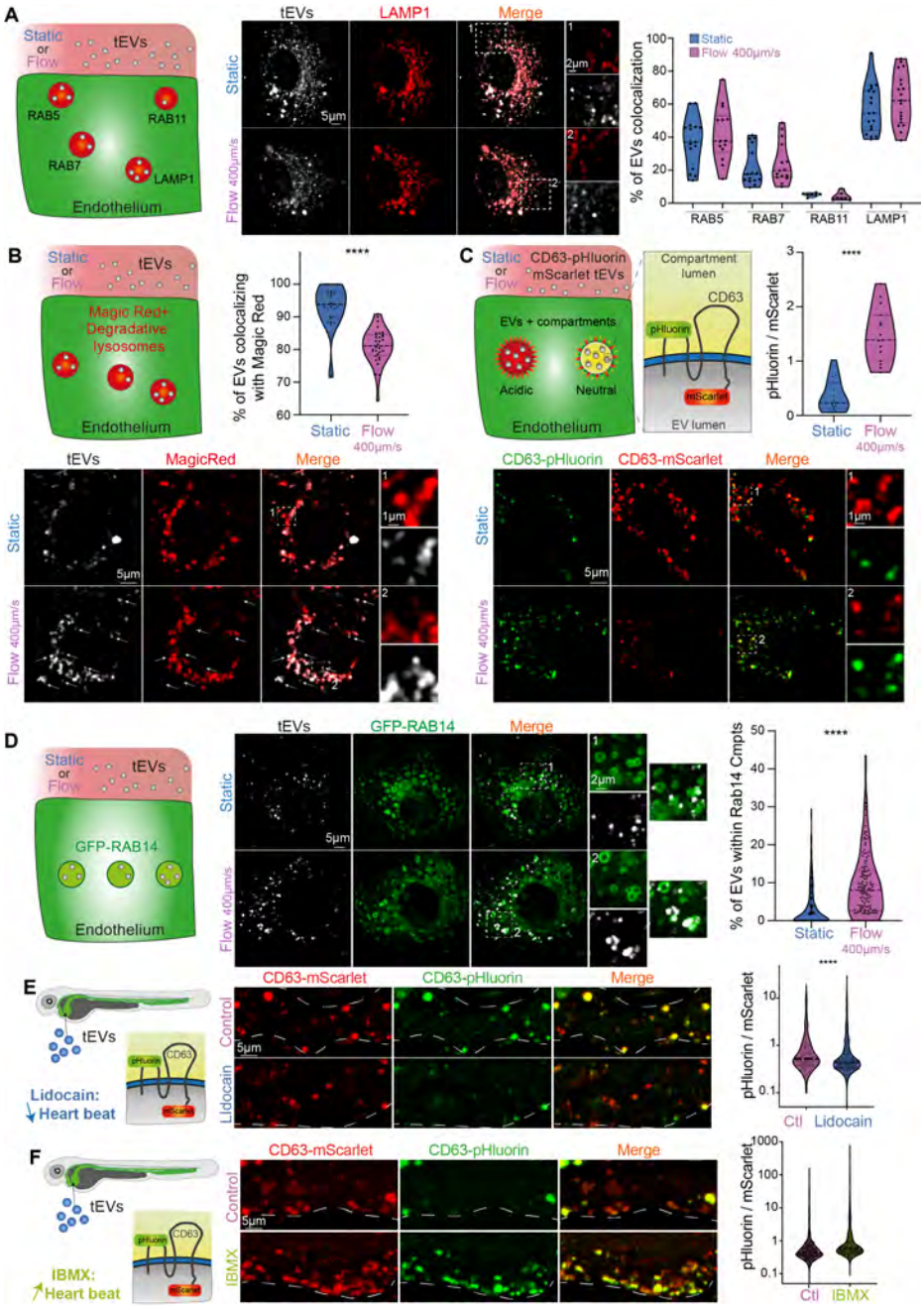

Fig. 2. Blood flow induces a switch in tEVs trafficking towards RAB14 positive non- degradative and non-acidic compartments. A) In vitro, internalized EVs co-localize more efficiently with LAMP1 than RAB5, RAB7 and RAB11 in endothelial cells cultured under flow. Memglow-Cy5 labeled EVs were perfused on vHUVECs cells stably expressing FP-RAB5,7,11 or LAMP1 cultured in flow or static conditions and imaged by spinning disk after 3h (single plane representative images). Automated colocalization (Kruskal-Wallis, one dot= one cell, n=7-20). B) Decreased accumulation of circulating tEVs in degradative compartments in endothelial cells cultured under flow. Memglow-Cy5 labeled EVs were perfused on HUVECs cultured in flow or static conditions and labeled using Magic Red to stain compartments with cathepsin B activity. Representative spinning disk single plane images (Manual quantification, one dot=one cell, n=30, Mann Whitney, p<0,0001). C) tEVs accumulate in less acidic compartments when endothelial cells are cultured under flow. CD63-pHluorin-mScarlet 4T1 EVs were perfused on HUVECs cultured in flow or static condition and imaged by spinning disk after 3h (single plane representative images). Graph represents the pHluorin/mScarlet ratio (one dot = one field of view, n=15, Mann Whitney, p<0,0001). D) tEVs show increased accumulation in Rab14 positive compartments in endothelial cells cultured under flow. Memglow-Cy5 labeled EVs were perfused on vHUVECs cells stably expressing GFP-RAB14 cultured in flow or static conditions and imaged by spinning disk after 3h (single plane representative images). Manual and automated quantifications show increased colocalization in flow conditions (Stats). E-F) In zebrafish embryos, modulating flow speed alters EV destination. CD63-pHluorin-mScarlet 4T1 EVs were injected in wild-type zebrafish embryos treated with lidocaine (E) or IBMX (F) to respectively decrease or increase heart beat rates and flow velocity. Representative Z projections showing EVs accumulation in the endothelium (visualized by transmitted light and represented with a white dashed line) 3h post-injection. (Right graph represents the pHluorin/mScarlet ratio, one dot = one Z plane, n>500, Mann Whitney, p<0,0001).

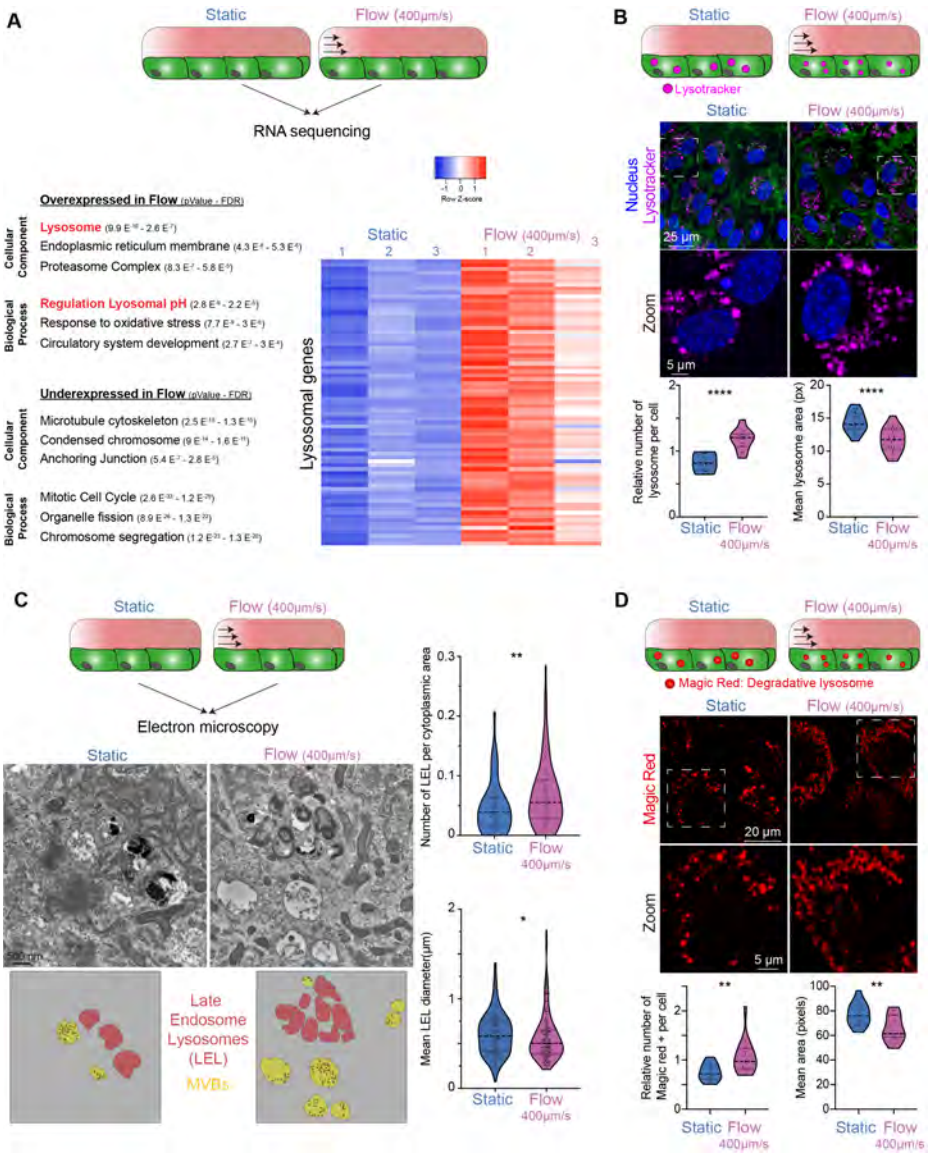

Fig. 3. Blood flow upregulates lysosomal pathway. A) RNA sequencing of HUVEC cells cultured under a moderate flow speed reveals an enrichment in genes associated with lysosomal regulation. Transcriptomics was performed on HUVEC cells cultured in static or flow conditions. Differentially expressed GO terms are listed. Heat map shows the expression of the 73 genes associated with lysosomes GO term and dysregulated between static and flow conditions. B-C) Increased number of lysosomes in endothelial cells cultured under flow and observed by photonic (B) and electronic microscopy (C). HUVEC cells were cultured in static or flow conditions, labeled with Memglow 488, Nucblue and lysotracker to visualize cells, nuclei and lysosomes respectively and imaged by confocal as shown on representative single planes. Left graph represents the relative number of lysosomes per cell and right graph the mean area per lysosome. (one dot is one field of view, n=20, p<0,0001, Student T-test) C) Representative electron microscopy images of HUVEC cells cultured in flow and static conditions and schematic representation of late endosome lysosome (LEL, red) and MVBs (yellow). Graphs show an increase in the number of LEL per cytoplasmic surface (one dot represents one field of view; n=121 and 125 fields of view respectively; p=0,0028 Mann Whitney) and a decrease in their average diameter in HUVEC cells cultured under flow (one dot represents one LEL; n=166 and 178 LELs respectively; p=0,015 Mann Whitney). D) Increase in degradative compartments in HUVEC cells upon flow treatment. HUVEC cells were cultured in static or flow conditions, labeled Magic Red to visualize compartments with cathepsin B activity and imaged by confocal as shown on representative single planes. Left graph represents the relative number of magic red positive compartment per cell (1 dot: 1 cell; p=0,0025 T-test) and right graph the mean area of these compartments. (1 dot is 1 field of view, 0,049 Mann Withney)

genesis Having demonstrated that blood flow favor both the uptake and lysosomal escape of tEVs, we wondered whether they might tune endothelial response. We first interrogated to what extent blood flow and tEVs would cooperate and impact transcriptional programs of targeted endothelial cells. Interestingly, the endothelial transcriptome was differentially impacted by EVs in static and flow condition. While the number of genes dysregulated by tEVs is similar in static and flow, their identity differs: Genes whose transcription was impacted when tEVs were internalized by flow-stimulated edothelial cells remain unaltered when tEVs were internalized in static endothelial cells (Fig.4A). This demonstrates that endothelial cells respond differently to EVs when subjected to flow. As tEVs escape lysosomal compartments in such conditions, this suggests that such re-routing allows tEVs cargo delivery that ultimately tunes gene expression. Among the genes upregulated by tEVs in flow-stimulated endothelial cells, we found several pro-angiogenic transcription factors, such as ID1, ID2, ID3, Hey1, Hey2, MAFB, Runx1 and HES1 (Benezra et al.; Fischer et al., 2004; Morioka et al., 2014; Kitagawa et al., 2013). We further identified genes that are reminiscent of two pro-angiogenic signaling pathways, Notch (HEY1, HEY2, HES1, JAG1) and TGFß (Smad6, Smad7, Bambi, PMEPA1, Nog). Altogether, we demonstrate here that (blood) flow and tEVs cooperate to favor lysosomal escape allowing tEVs to promote a pronounced pro-angiogeneic transcriptional program in endothelial cells. Interestingly, endothelial EVs were shown to activate the Notch pathway in endothelial cells, resulting in increased expression of HEY1 and HEY2 and formation of capillary-like structures in vitro and in vivo (Sheldon et al., 2010). In addition, activation of the TGFß pathway in endothelial cells promotes inflammation and endothelial permeabilisation (Chen et al., 2019). Interestingly, our tEVs contain several regulators of the TGFß pathway (Smad5, Smurf2, etc.) (Ghoroghi et al., 2021b), including TGFß type II receptor, whose presence on tEVs is sufficient to activate the TGF pathway in receiving cells and correlates with metastasis (Xie et al.). While pro-angiogenic programs, which could possibly be activated by the Notch and TGFß pathways, require a concerted action of flow and tEVs uptake in endothelial cells, whether they impact the angiogenic activity of endothelial cells remained unsolved. To test the relevance of such gene signature in vivo, we adapted a well-established experimental tumor angiogenesis assay in zebrafish embryos (Nicoli and Presta, 2007) to investigate whether tEVs could impact endothelial response in realistic hemodynamic conditions. To this end, we assessed the ability of i.v injected and circulating tEVs to promote the formation of neo-sprouts from existing subintestinal vessels in embryos bearing a tumor mass. When embryos are injected with tEVs, the tumor-induced sprouting is potentiated with an increased number of neo-vascular sprouts per embryo (Fig.4B). Importantly, tEVs also increase the percentage of embryos bearing tumor-induced endothelial sprouts when compared to embryos injected with PBS. These results confirm that circulating tEVs promote tumor-induced neo-angiogenesis in vivo. While tumor EVs were previously shown to promote angiogenesis in vitro (Todorova et al., 2017), our results suggest that such effect can be potentiate by hemodynamic forces of perfused vessels. As a consequence, we expect circulating tEVs to favour the formation of neo-vascular sprouts in capillary-like vessels that are prone, from an hemodynamics stand-point, to favor arrest of CTCs (Follain, 2018). The formation of new and abnormal blood vessels could constitute a first step in the creation of pre-metastatic niches, leading to the subsequent recruitment of specific immune populations and ultimately favoring homing of circulating tumor cells (Peinado et al., 2017). We have recently shown that endothelial cells also hijack a flow-stimulated pro-angiogenic transcriptional program to perform intravascular remodeling that favors the extravasation of arrested CTCs (Follain et al., 2018, 2021). It is tempting to speculate that tEVs could mediate such intravascular remodeling, whose dependence on flow forces is also established (Follain et al., 2018). Finally, one could expect that the induction of neo-sprouts by circulating tEVs could sustain the growth of metastatic foci that have colonized distant organs.

Overall, our work demonstrates for the first time that the fate and function of EVs flowing in the bloodstream and on their way to shape pre-metastatic niches is tightly linked to hemodynamic forces as well as mechanosensing abilities of the endothelium. We provide here the first evidence that flow-sensing endothelial cells divert internalized tEVs from lysosomal degadation, which is at the basis of a potential change in their fate. We further identified permissive flow regimes where EVs uptake by endothelial cells is optimal. Such regimes not only favor the uptake and lysosomal escape of tEVs, they also allow the arrest of CTCs that precedes metastatic extravasation and outgrowth (Follain et al., 2020a, 2018). In endothelial cells subjected to such flow regimes, internalized EVs are partially rerouted to non-acidic and non-degradative RAB14 positive compartments (Fig.4C) with direct and functional consequences on their angiogenic potential. In conclusion, hemodynamics potentiate the functional impact of tEVs on endothelial cells towards a pro-angiogenic response which ultimately shapes pre-metastatic niches and metastatic outgrowth.

Methods

Cell culture 4T1 cells were cultured in RPMI-1640 medium complemented with 10per cent Foetal Bovine Serum (FBS, Hyclone) and 1per cent penicillin/streptomycin (PS, 100U/ml, Gibco). HUVEC cells (Human Umbilical Vein Endothelial Cell, Promocell) were grown in Endothelial Growth Medium (ECGM, Promocell) complemented with supplemental mix (SupplementMix, Promocell) and 1per cent PS. VeravecTM HUVECs human endothelial cells (Angiocrine Biosciences), referred here as vHUVECs, were cultured in ECGM MV2 (Promocell) complemented with 20per cent of FBS and 1per cent PS. For all the microfluidic experiments, HUVECs or vHUVECs were used before passage number 4. HEK293T cells were grown in DMEM (Gibco) complemented with 10per cent FBS and 1per cent PS. All cell lines

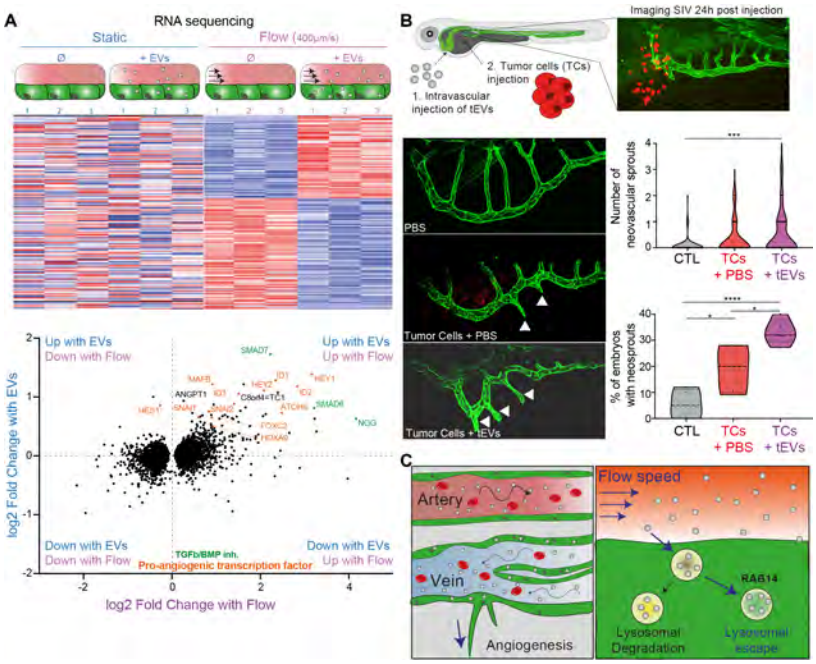

Fig. 4. Circulating tumor EVs and blood flow cooperate to promote angiogenesis A) RNA sequencing reveals an enrichment in pro-angiogenic pathways in HUVEC cells cultured under a moderate flow speed and treated with 4T1 EVs. Transcriptomics was performed on HUVEC cells cultured in static or flow conditions and treated with 4T1 EVs or PBS for 24h. Heat map shows that the genes differentially expressed upon EV treatment in flow condition are not deregulated in static conditions. The lower graph shows differentially expressed genes. Pro-angiogenic transcription factors (orange) and members of the TGFb/BMP pathway (green) are highlighted. B) Tumor EVs promote angiogenesis in vivo. Zebrafish embryos were injected with 4T1 EVs or PBS and subsequently with 4T1 tumor cells (TCs). Representative confocal images show neovascular sprouts in the sub-intestinal vessels (SIV)24h post-tumor cell injection. The number of neovascular sprouts and the percentage of embryos with neovascular sprouts were quantified. C) model explaining the fate and function of circulating tumor EVs: low flow speed promotes EVs uptake by endothelial cells followed by partial lysosomal escape and rerouting in RAB14 positive compartments. As a consequence, tumor EVs induce a pro-angiogenic response.

were maintained at 37C and 5per cent CO2 and verified for the absence of mycoplasma by PCR on a regular basis.

Stable cell line generation Lentivirus containing the following constructs were produced in HEK293T cells using JetPRIME (Polyplus, FRANCE) transfection: pLSFFV-mCherry-Rab5A, pLSFFV-RFP-LAMP1, pLSFFV-mEmerald-Rab7A, pLSFFV-eGFP-Rab11A, pLSFFV-GFP-Rab14 (gift from N. Vitale, INCI, Strasbourg, France), pLSFFV-NHE9-mCherry (gift from K. C. Kondapalli, Michigan-Dearborn University, USA), pLSFFV-pHluorin-CD63-mScarlet (gift from A. M. Weaver, Vanderbilt University, USA). vHuvec or 4T1 cells were infected by lentivirus in the presence of 5µg/mL polybrene (Sigma) followed by antibiotic selection (Puromycin at 1µg/mL or blasticidin at 5µg/mL).

EVs isolation and labelling For EV isolation, cells were cultured at sub-confluency in EV depleted medium for 24h. EV depleted medium was prepared using 2X complete medium, centrifuged at 100,000g for 20h (Optima XE-90 ultracentrifuge - Beckman Coulter) to eliminate EVs from FBS. Supernatant was then filtered at 0,22µm (Millipore) and adjusted to 1X. EVs were isolated using differential ultracentrifugation protocols as described previously (Hyenne et al., 2015, 2019). The pellets obtained at the final step of 100,000g centrifugation were resuspended in sterile PBS1X. When needed, EVs were labeled using 200nM of MemGlow-Cy5 (Cytoskeleton Inc.) lipidic dye between the 1st and the 2nd 100 000g ultracentrifugation as described previously. Following the EV isolation, their number and size distribution were measured by ZetaView NTA (PMX-120-12B-R2 – Particle Metrix). EVs were stored at 4°C and used within 24h.

Microfluidics experiments For microfluidic experiments, IBIDI® µ-slides with 1 (µ-Slide I 0.4 Luer ibiTreat: 1.5 polymer coverslip) or 6 (µ-Slide VI 0.4 ibiTreat: 1.5 polymer coverslip) channels were coated with fibronectin (SIGMA) for 1 hour and seeded with 100 000 or 50 000 cells per channel respectively. Once endothelial cells reached confluency, the channels were either maintained in static conditions or continuously perfused under a flow of 400µm.s-1 for 17h using a Reglo Digital MS-CA 2/12 peristaltic pump. EVs were then either applied on the static cells or perfused continuously under flow at a concentration of 108 particles/ml. After 3h of EV perfusion, channels were removed from the flow, and washed 3 times with fresh ECGM and 3 times with ECGM/Hoechst 33342 (NucBlue™ ThermoFisher). After 10min incubation, cells were washed twice with ECGM/HEPES 20mM before imaging. To assess lysosome number or Cathespin-B activity, endothelial cells were incubated after EV perfusion with Lysotracker Deep Red (Thermo Fisher Scientific) diluted at 50nM or MagicRed dye (Bio-Rad) diluted at 1:260 respectively for 1h. When needed,

cells were incubated with MemGlow-488 (Cytoskeleton Inc.) at 200nM to label the plasma membrane.

Photon microscopy Cells were imaged live in chambers thermostated at 37°C with 5 per cent CO2. Imaging was performed using an Olympus Spinning Disk with 60X objective or with an SP5 confocal (Leica) with a 63X objective (N.A. 1.25). Zebrafish embryos were imaged live at 28°C with a SP5 confocal equipped with a HC PL APO 20X/0,7 IMM objective (Leica) or with a Olympus Spinning Disk with a 30X objective. Image analysis and processing were performed using the Fiji software. Cell Profiler 4.2.1 was used to analyze the immunofluorescent images, one Z plane for each field of view. Prior to CellProfiler analysis, Fiji was used to process the individual channels (TopHat 50 filter for the compartment and Despecle + GaussianBlur 1 filter for the EV channel. Objects (EVs and compartment marker) were identified in CellProfiler based on the intensity thresholding. Objects were considered colocalized if distance between their centers was 4 pixels. The percentage of EV colocalization with given compartment was calculated as a ratio of colocalized EV objects to the total number of EV objects times 100.

Electron microscopy Electron microscopy: Chemical fixation: Cells were fixed with 2,5 per cent glutaraldehyde (GA)/2,0 per cent paraformaldehyde (PFA) (Electron Microscopy Sciences) in 0.1M NaCac buffer (pH 7.4) at room temperature for 2h, then rinsed in 0.1M NaCac buffer (pH 7.4) (Electron Microscopy Sciences) and post-fixed with 1 per cent OsO4 (Electron Microscopy Sciences) and 0.8 per cent K3Fe(CN)6 (Sigma-Aldrich) for 1h at room temperature. Then, samples were rinsed in 0.1M NaCac buffer (pH 7.4) followed by a distilled water rinse and stained with 1 per cent uranyl acetate, overnight at 4°C sheltered from the light. The samples were stepwise dehydrated in Ethanol (50 per cent x10min, 70 per cent x10min, 95 per cent x15min and 100 per cent 3x10min), infiltrated in a graded series of Epon (Ethanol 100 per cent/Epon 3/1, 1/1) 1h and kept in Ethanol 100per cent/Epon 1/3 overnight at room temperature. The following day, samples were placed in pure Epon 3 x1h and polymerized at 60°C 48h. 100 nm thin sections were collected in 200 copper mesh grids and data set was acquired with a TEM Hitachi 7500 TEM, with 80 kV beam voltage, and the 8-bit images were obtained with a Hamamatsu camera C4742-51-12NR. The number of MVBs and lysosomes per surface of cytoplasm were quantified using the Fiji software. MVBs and lysosomes were distinguished based on their morphology: MVBs have one or more ILVs and lysosomes contain ILVs but are also electron dense and contain irregular membrane curls.

Intravascular injection of tEVs in zebrafish embryos Zebrafish embryos were obtained from the following strains: Tg(fli1a:eGFP), Tg(Fli :LA-eGFP), Tg(Fli1:Gal4; UAS: RFP), Casper Tg(Gata1:RFP; flk:GFP). Embryos were maintained at 28°C in Danieau 0.3X medium, supplemented with 1-Phenyl-2-thiourea (PTU, Sigma-Aldrich) after 24 h post fertilization (hpf). All injection experiments were carried out at 48 hpf and imaged between 48 hpf and 72 hpf. All animal procedures were performed in accordance with French and European Union animal welfare guidelines and supervised by local ethics committee (Animal facility A6748233; APAFIS 2018092515234191). At 48 hpf, zebrafish (ZF) embryos were dechorionated and mounted on a 0.8per cent low melting agarose pad containing 650 µM tricaine (ethyl-3-aminobenzoate-methanesulfonate). Embryos were injected intravascularly in the duct of Cuvier with 27,6 nL of Membright Cy5- labeled EVs (at 1010 EVs/ml) Labeled tEVs (4T1Nat-MemGlowCy5-EV or 4T1CD63pHluorinmScarlet-EV) with a Nanoject microinjector 2 (Drummond) under a M205 FA stereomicroscope (Leica) as described previously (Mary et al., 2020; Hyenne et al., 2019).

Blood flow mapping For flow speed mapping, we injected MemGlow labelled 4T1 EVs in Tg (kdrl:EGFP; gata1:DsRed) embryos in Casper background at 48hpf. 30 min post injection, we recorded short time-lapses in 4 different regions in the zebrafish caudal plexus (two in the dorsal aorta and two in the venous area). For each region, we recorded 30s time-lapses (17ms time interval) at single focal plane with flowing red blood cells (RBC). Flow speed was measured by tracking RBC in each region with IMARIS software. tEVs (Cy5) accumulation in endothelial cells (GFP) was measured by IMARIS for each region.

Pharmacological blood flow tuning IBMX (3-Isobutyl-1-Methylxanthin - Merck) and lidocaine (Brand ?) were directly added to the embryo water (Danieau/PTU solution) containing ZF embryos at the concentration of 100µM in DMSO for 20h and at the concentration of 640µM in EtOH for 2h respectively. Control embryos were treated with similar amount of DMSO or EtOH accordingly. Embryos were then mounted and maintained in fresh solutions of drugs until the end of the experiment. Heartbeat of the embryos were recorded as short time-lapses with a Stereomicroscope (Leica M205 FA). Heartbeats were manually counted on kymographs.

In vivo Angiogenesis assay For angiogenesis assay, PTU treated Tg(Fli :LA-eGFP) dechorionated embryos were either uninjected (control) or injected with PBS or with 4T1 Memglow-labeled EVs at 36 hpf intravascularly. At 48 hpf, PBS injected and EV injected embryos received 4T1-tDT tumor cell injection (volume- 18 nl containing 100-150 cells) in the perivitelline space. 24 hpi of tumor cells embryos were imaged by spinning Disk focusing on the sub-intestinal vein (SIV) plexus (that spans the dorso-lateral part of the yolk) as described in (Hen et al., 2015). The number of newly formed vascular sprouts were manually counted.

Transcriptomic analyses RNA extraction and sequencing Total RNA was extracted using RNeasy Mini Kit (Qiagen, Hilden, Germany) and RNA integrity was assessed by Bioanalyzer (total RNA Pico Kit, 2100 Instrument, Agilent Technologies, Paolo Alto, USA). SMART-Seq® HT PLUS Kit (Takara, Kusatsu, Japan) was used to build mRNA libraries. Libraries were pooled and sequenced (single-end, 75bp) on a NextSeq500 using the NextSeq 500/550 High Output Kit v2 according to the manufacturer's instructions (Illumina Inc., San Diego, CA, USA).

Analysis of RNA-sequence reads: Identification of differ-

entially expressed genes Sequence reads were mapped on the human hg19 genome using STAR (Dobin et al., 2013) to obtain a BAM file (Binary Alignment Map). Raw read counts were determined as an abundance matrix with the HTseq-count tool of the Python package HTSeq (Anders et al., 2015). Trimmed Mean of M-values normalization (TMM) was applied using the EdgeR package (Robinson et al., 2010). A voom transformation was applied to the data that were then fitted into a linear model using weighted least squares for each gene with limma package (Ritchie et al., 2015). Finally, a contrast matrix was created and differential expressions were computed. Up- and down-regulated genes were selected based on adjusted p-values < 0.05 and fold-changes > 1.5. Functional enrichment analyses were performed using STRING v11 (Szklarczyk et al., 2019).

Statistical analyses All experiments were performed and results were analyzed in at least three independent experiments. Statistical analysis of the results was done using GraphPad Prism (Software version 9.0). Normality of the data was confirmed using Shapiro-Wilkson test and accordingly different statistical tests were used as described in legends. For data that do not follow gaussian distribution, Mann-Whitney or Krustal-Wallis tests (Dunn's post-test analysis) were used. Illustrations of the statistical analyses were displayed in the figures as the mean +/- standard deviation (SD). p-Values smaller than 0.05 were considered as statistically significant. *, p<0.05, **, p<0.01, ***, p<0.001, ****, p<0.0001.

Acknowledgements We thank all members of the Goetz Lab for helpful discussions, in particular Florent Colin for careful reading, Pascal Kessler from the PICSTRA platform, as well as Gregory Khelifi and Camille Hergott for animal care. This work was supported by a fellowship from La Ligue COntre le Cancer to M.M.; by grants from La Ligue contre le Cancer, Canceropole Grand-Est, INCa (PLBIO19-291), Plan Cancer (Nanotumor) and Roche to J.G.G.; and by institutional funds from University of Strasbourg and INSERM to JGG.

Author Contributions BM and NA performed most experiments, with help from KJR (image analysis), AL (molecular biology, cell line generation), and OL (molecular biology, cell line generation). Electron microscopy processing and analysis was performed by IB and VH. TS, AP, AM and RC performed RNA sequencing and analysis. JGG and VH supervised and designed the project. JGG (with help from VH) was responsible for funding the project. JGG and VH wrote the manuscript with insights from all authors.

Bibliography

Benezra, R., S. Rafii, and D. Lyden. 2001. The Id proteins and angiogenesis. Oncogene. 20:8334–8341. doi:10.1038/sj/onc/1205160.

Bonsergent, E., E. Grisard, J. Buchrieser, O. Schwartz, C. Théry, and G. Lavieu. 2021. Quantitative characterization of extracellular vesicle uptake and content delivery within mammalian cells. Nat. Commun. 12:1–11. doi:10.1038/s41467-021-22126-y.

Chen, P.Y., L. Qin, G. Li, Z. Wang, J.E. Dahlman, J. Malagon-Lopez, S. Gujja, N.A. Cilfone, K.J. Kauffman, L. Sun, H. Sun, X. Zhang, B. Aryal, A. Canfran-Duque, R. Liu, P. Kusters, A. Sehgal, Y. Jiao, D.G. Anderson, J. Gulcher, C. Fernandez-Hernando, E. Lutgens, M.A. Schwartz, J.S. Pober, T.W. Chittenden, G. Tellides, and M. Simons. 2019. Endothelial TGF-β signalling drives vascular inflammation and atherosclerosis. Nat. Metab. 2019 19. 1:912–926. doi:10.1038/S42255-019-0102-3.

Chen, Y.Y., A.M. Syed, P. MacMillan, J. V. Rocheleau, and W.C.W. Chan. 2020. Flow Rate Affects Nanoparticle Uptake into Endothelial Cells. Adv. Mater. 32:1–7. doi:10.1002/adma.201906274.

Cheng, L., and A.F. Hill. 2022. Therapeutically harnessing extracellular vesicles. Nat. Rev. Drug Discov. 2022 215. 21:379–399. doi:10.1038/S41573-022-00410-W.

Fang, Y., D. Wu, and K.G. Birukov. 2019. Mechanosensing and Mechanoregulation of Endothelial Cell Functions. Compr. Physiol. 9:873. doi:10.1002/CPHY.C180020.

Fischer, A., N. Schumacher, M. Maier, M. Sendtner, and M. Gessler. 2004. The Notch target genes Hey1 and Hey2 are required for embryonic vascular development. doi:10.1101/gad.291004.

Follain, G., D. Herrmann, S. Harlepp, V. Hyenne, N. Osmani, S.C. Warren, P. Timpson, and J.G. Goetz. 2020b. Fluids and their mechanics in tumour transit: shaping metastasis. Nat. Rev. Cancer. 20:107–124. doi:10.1038/s41568-019-0221-x.

Follain, G., N. Osmani, A. Sofia, G. Allio, L. Mercier, M.A. Karreman, G. Solecki, M.G. Leon, O. Lefebvre, N. Fekonja, C. Hille, V. Chabannes, G. Dollé, T. Metivet, F. Der Hovsepian, C. Prud'Homme, A. Pichot, N. Paul, R. Carapito, S. Bahram, B. Ruthensteiner, A. Kemmling, S. Siemonsen, T. Schneider, J. Fiehler, M. Glatzel, F. Winkler, Y. Schwab, K. Pantel, S.S. Harlepp, J.G. Goetz, A.S. Azevedo, G. Allio, L. Mercier, M.A. Karreman, G. Solecki, M.J. Garcia Leòn, O. Lefebvre, N. Fekonja, C. Hille, V. Chabannes, G. Dollé, T. Metivet, F. Der Hovsepian, C. Prudhomme, A. Pichot, N. Paul, R. Carapito, S. Bahram, B. Ruthensteiner, A. Kemmling, S. Siemonsen, T. Schneider, J. Fiehler, M. Glatzel, F. Winkler, Y. Schwab, K. Pantel, S.S. Harlepp, and J.G. Goetz. 2018. Hemodynamic forces tune the arrest, adhesion and extravasation of circulating tumor cells. Dev. Cell. 45:33-52.e12. doi:10.1016/j.devcel.2018.02.015.

Freund, J.B., J.G. Goetz, K.L. Hill, and J. Vermot. 2012. Fluid flows and forces in development: functions, features and biophysical principles. doi:10.1242/dev.085902.

Ghoroghi, S., B. Mary, N. Asokan, J.G. Goetz, and V. Hyenne. 2021a. Tumor extracellular vesicles drive metastasis (it's a long way from home). FASEB BioAdvances. 3:930–943. doi:10.1096/FBA.2021-00079.

Ghoroghi, S., B. Mary, A. Larnicol, N. Asokan, A. Klein, N. Osmani, I. Busnelli, F. Delalande, N. Paul, S. Halary, F. Gros, L. Fouillen, A.-M. Haeberle, C. Royer, C. Spiegelhalter, G. André-Grégoire, V. Mittelheisser, A. Detappe, K. Murphy, P. Timpson, R. Carapito, M. Blot-Chabaud, J. Gavard, C. Carapito, N. Vitale, O. Lefebvre, J.G. Goetz, and V. Hyenne. 2021b. Ral GTPases promote breast cancer metastasis by controlling biogenesis and organ targeting of exosomes. Elife. doi:10.7554/elife.61539.

Han, J., V. V. Shuvaev, P.F. Davies, D.M. Eckmann, S. Muro, and V.R. Muzykantov. 2015. Flow shear stress differentially regulates endothelial uptake of nanocarriers targeted to distinct epitopes of PECAM-1. J. Control. Release. 210:39–47. doi:10.1016/j.jconrel.2015.05.006.

Han, J., B.J. Zern, V. V. Shuvaev, P.F. Davies, S. Muro, and V. Muzykantov. 2012. Acute and chronic shear stress differently regulate endothelial internalization of nanocarriers targeted to platelet-endothelial cell adhesion molecule-1. ACS Nano. 6:8824–8836. doi:10.1021/nn302687n.

Hen, G., J. Nicenboim, O. Mayseless, L. Asaf, M. Shin, G. Busolin, R. Hofi, G. Almog, N. Tiso, N.D. Lawson, and K. Yaniv. 2015. Venous-derived angioblasts generate organ-specific vessels during zebrafish embryonic development. doi:10.1242/dev.129247.

Hoffman, H.K., R.S. Aguilar, A.R. Clark, N.S. Groves, N. Pezeshkian, M.M. Bruns, and S.B. van Engelenburg. 2022. Endocytosed HIV-1 Envelope Glycoprotein Traffics to Rab14 + Late Endosomes and Lysosomes to Regulate Surface Levels in T-Cell Lines . J. Virol. 96. doi:10.1128/JVI.00767-22.

Hoshino, A., B. Costa-Silva, T.-L. Shen, G. Rodrigues, A. Hashimoto, M. Tesic Mark, H. Molina, S. Kohsaka, A. Di Giannatale, S. Ceder, S. Singh, C. Williams, N. Soplop, K. Uryu, L. Pharmer, T. King, L. Bojmar, A.E. Davies, Y. Ararso, T. Zhang, H. Zhang, J. Hernandez, J.M. Weiss, V.D. Dumont-Cole, K. Kramer, L.H. Wexler, A. Narendran, G.K. Schwartz, J.H. Healey, P. Sandstrom, K. Jørgen Labori, E.H. Kure, P.M. Grandgenett, M.A. Hollingsworth, M. de Sousa, S. Kaur, M. Jain, K. Mallya, S.K. Batra, W.R. Jarnagin, M.S. Brady, O. Fodstad, V. Muller, K. Pantel, A.J. Minn, M.J. Bissell, B.A. Garcia, Y. Kang, V.K. Rajasekhar, C.M. Ghajar, I. Matei, H. Peinado, J. Bromberg, and D. Lyden. 2015. Tumour exosome integrins determine organotropic metastasis. Nature. 1–19. doi:10.1038/nature15756.

Hyenne, V., A. Apaydin, D. Rodriguez, C. Spiegelhalter, S. Hoff-Yoessle, M. Diem, S. Tak, O. Lefebvre, Y. Schwab, J.G. Goetz, and M. Labouesse. 2015. RAL-1 controls multivesicular body biogenesis and exosome secretion. J. Cell Biol. 211:27–37. doi:10.1083/jcb.201504136.

Hyenne, V., S. Ghoroghi, M. Collot, J. Bons, G. Follain, S. Harlepp, B. Mary, J. Bauer, L. Mercier, I. Busnelli, O. Lefebvre, N. Fekonja, M.J. Garcia-Leon, P. Machado, F. Delalande, A.A. López, S.G. Silva, F.J. Verweij, G. van Niel, F. Djouad, H. Peinado, C. Carapito, A.S. Klymchenko, and J.G. Goetz. 2019. Studying the Fate of Tumor Extracellular Vesicles at High Spatiotemporal Resolution Using the Zebrafish Embryo. Dev. Cell. 48:554-572.e7. doi:10.1016/j.devcel.2019.01.014.

Imai, T., Y. Takahashi, M. Nishikawa, K. Kato, M. Morishita, T. Yamashita, A. Matsumoto, C. Charoenviriyakul, and Y. Takakura. 2015. Macrophage-dependent clearance of systemically administered B16BL6-derived exosomes from the blood circulation in mice. J. Extracell. vesicles. 4:26238. doi:10.3402/jev.v4.26238. Joshi, B.S., M.A. de Beer, B.N.G. Giepmans, and I.S. Zuhorn. 2020. Endocytosis of Extracellular Vesicles and Release of Their Cargo from Endosomes. ACS Nano. doi:10.1021/acsnano.9b10033.

Kalluri, R., and V.S. LeBleu. 2020. The biology, function, and biomedical applications of exosomes. Science (80-.). 367. doi:10.1126/science.aau6977. Kitagawa, M., M. Hojo, I. Imayoshi, M. Goto, M. Ando, T. Ohtsuka, R. Kageyama, and S. Miyamoto. 2013. Hes1 and Hes5 regulate vascular remodeling and arterial specification of endothelial cells in brain vascular development. Mech. Dev. 130:458–466. doi:10.1016/J.MOD.2013.07.001.

Kondapalli, K.C., J.P. Llongueras, V. Capilla-González, H. Prasad, A. Hack, C. Smith, H. Guerrero-Cázares, A. Quiñones-Hinojosa, and R. Rao. 2015. A leak pathway for luminal protons in endosomes drives oncogenic signalling in glioblastoma. Nat. Commun. 6. doi:10.1038/ncomms7289. Kuijl, C., M. Pilli, S.K. Alahari, H. Janssen, P.S. Khoo, K.E. Ervin, M. Calero, S. Jonnalagadda, R.H. Scheller, J. Neefjes, and J.R. Junutula. 2013. Rac and Rab GTPases dual effector Nischarin regulates vesicle maturation to facilitate survival of intracellular bacteria. EMBO J. 32:713–727. doi:10.1038/EMBOJ.2013.10.

Kyei, G.B., I. Vergne, J. Chua, E. Roberts, J. Harris, J.R. Junutula, and V. Deretic. 2006. Rab14 is critical for maintenance of Mycobacterium tuberculosis phagosome maturation arrest. EMBO J. 25:5250–5259. doi:10.1038/SJ.EMBOJ.7601407.

Li, Y.S.J., J.H. Haga, and S. Chien. 2005. Molecular basis of the effects of shear stress on vascular endothelial cells. J. Biomech. 38:1949–1971. doi:10.1016/J.JBIOMECH.2004.09.030.

Lin, A., A. Sabnis, S. Kona, S. Nattama, H. Patel, J.F. Dong, and K.T. Nguyen. 2010. Shear-regulated uptake of nanoparticles by endothelial cells and development of endothelial-targeting nanoparticles. J. Biomed. Mater. Res. Part A. 93A:833–842. doi:10.1002/JBM.A.32592.

Marar, C., B. Starich, and D. Wirtz. 2021. Extracellular vesicles in immunomodulation and tumor progression. Nat. Immunol. 22:560–570. doi:10.1038/s41590-021-00899-0.

Mary, B., S. Ghoroghi, V. Hyenne, and J.G. Goetz. 2020. Live tracking of extracellular vesicles in larval zebrafish. In Methods in Enzymology.

Morad, G., C. V. Carman, E.J. Hagedorn, J.R. Perlin, L.I. Zon, N. Mustafaoglu, T.E. Park, D.E. Ingber, C.C. Daisy, and M.A. Moses. 2019. Tumor-Derived Extracellular Vesicles Breach the Intact Blood-Brain Barrier via Transcytosis. ACS Nano. 13:13853–13865. doi:10.1021/acsnano.9b04397.

Morioka, T., M. Sakabe, T. Ioka, T. Iguchi, K. Mizuta, M. Hattammaru, C. Sakai, M. Itoh, G.E. Sato, A. Hashimoto, M. Fujita, K. Okumura, M. Araki, M. Xin, R.A. Pedersen, M.F. Utset, H. Kimura, and O. Nakagawa. 2014. An Important Role of Endothelial Hairy-Related Transcription Factors in Mouse Vascular Development. doi:10.1002/dvg.22825.

Morishita, M., Y. Takahashi, M. Nishikawa, K. Sano, K. Kato, T. Yamashita, T. Imai, H. Saji, and Y. Takakura. 2015. Quantitative analysis of tissue distribution of the B16BL6-derived exosomes using a streptavidin-lactadherin fusion protein and Iodine-125-Labeled biotin derivative after intravenous injection in mice. J. Pharm. Sci. 104:705–713. doi:10.1002/jps.24251.

Nicoli, S., and M. Presta. 2007. The zebrafish/tumor xenograft angiogenesis assay. Nat. Protoc. 2:2918–2923. doi:10.1038/nprot.2007.412.

Okai, B., N. Lyall, N.A.R. Gow, J.M. Bain, and L.P. Erwig. 2015. Rab14 regulates maturation of macrophage phagosomes containing the fungal pathogen Candida albicans and outcome of the host-pathogen interaction. Infect. Immun. 83:1523–1535. doi:10.1128/IAI.02917-14.

Peinado, H., H. Zhang, I.R. Matei, B. Costa-Silva, A. Hoshino, G. Rodrigues, B. Psaila, R.N. Kaplan, J.F. Bromberg, Y. Kang, M.J. Bissell, T.R. Cox, A.J. Giaccia, J.T. Erler, S. Hiratsuka, C.M. Ghajar, and D. Lyden. 2017. Pre-metastatic niches: organ-specific homes for metastases. Nat. Rev. Cancer. 17:302–317. doi:10.1038/nrc.2017.6.

Perera, R.M., and R. Zoncu. 2016. The Lysosome as a Regulatory Hub. Annu. Rev. Cell Dev. Biol. 32:223–253. doi:10.1146/annurev-cellbio-111315-125125.

Sheldon, H., E. Heikamp, H. Turley, R. Dragovic, P. Thomas, C.E. Oon, R. Leek, M. Edelmann, B. Kessler, R.C.A. Sainson, I. Sargent, J.L. Li, and A.L. Harris. 2010. New mechanism for Notch signaling to endothelium at a distance by Delta-like 4 incorporation into exosomes. Blood. 116:2385–2394. doi:10.1182/BLOOD-2009-08-239228.

Sung, B.H., A. von Lersner, J. Guerrero, E.S. Krystofiak, D. Inman, R. Pelletier, A. Zijlstra, S.M. Ponik, and A.M. Weaver. 2020. A live cell reporter of exosome secretion and uptake reveals pathfinding behavior of migrating cells. Nat. Commun. 11:1–15. doi:10.1038/s41467-020-15747-2.

Szklarczyk, D., A.L. Gable, D. Lyon, A. Junge, S. Wyder, J. Huerta-Cepas, M. Simonovic, N.T. Doncheva, J.H. Morris, P. Bork, L.J. Jensen, and C. Von Mering. 2019. STRING v11: Protein-protein association networks with increased coverage, supporting functional discovery in genome-wide experimental datasets. Nucleic Acids Res. doi:10.1093/nar/gky1131.

Takahashi, Y., M. Nishikawa, H. Shinotsuka, Y. Matsui, S. Ohara, T. Imai, and Y. Takakura. 2013. Visualization and in vivo tracking of the exosomes of murine melanoma B16-BL6 cells in mice after intravenous injection. J. Biotechnol. 165:77–84. doi:10.1016/j.jbiotec.2013.03.013.

Tarbell, J.M. 2010. Shear stress and the endothelial transport barrier. Cardiovasc. Res. 87:320. doi:10.1093/CVR/CVQ146.

Tian, T., Y.L. Zhu, F.H. Hu, Y.Y. Wang, N.P. Huang, and Z.D. Xiao. 2013. Dynamics of exosome internalization and trafficking. J. Cell. Physiol. doi:10.1002/jcp.24304.

Todorova, D., S. Simoncini, R. Lacroix, F. Sabatier, and F. Dignat-George. 2017. Extracellular Vesicles in Angiogenesis. Circ. Res. 120:1658–1673. doi:10.1161/CIRCRESAHA.117.309681.

Trofimenko, E., Y. Homma, M. Fukuda, and C. Widmann. 2021. The endocytic pathway taken by cationic substances requires Rab14 but not Rab5 and Rab7. Cell Rep. 37. doi:10.1016/J.CELREP.2021.109945.

Verweij, F., L. Balaj, C. Boulanger, D. Carter, E. Compeer, G. D'Angelo, S. El Andaloussi, J. Goetz, J.C. Gross, V. Hyenne, E.-M. Krämer-Albers, C.P. Lai, X. Loyer, A. Marki, S. Momma, E. Nolte-'t Hoen, M. Pegtel, H. Peinado, G. Raposo, K. Rilla, H. Tahara, C. Théry, M. van Royen, R. Vandenbroecke, A. Wehman, K. Witwer, Z. Wu, R. Wubbolts, and G. van Niel. 2021. The power of imaging to understand Extracellular Vesicle biology in vivo. Nat. Methods. In press. Verweij, F.J., V. Hyenne, G. Van Niel, and J.G. Goetz. 2019. Extracellular Vesicles: Catching the Light in Zebrafish. Trends Cell Biol. 29:770–776. doi:10.1016/j.tcb.2019.07.007.

Vion, A.C., M. Kheloufi, A. Hammoutene, J. Poisson, J. Lasselin, C. Devue, I. Pic, N. Dupont, J. Busse, K. Stark, J. Lafaurie-Janvore, A.I. Barakat, X. Loyer, M. Souyri, B. Viollet, P. Julia, A. Tedgui, P. Codogno, C.M. Boulanger, and P.E. Rautou. 2017. Autophagy is required for endothelial cell alignment and atheroprotection under physiological blood flow. Proc. Natl. Acad. Sci. U. S. A. doi:10.1073/pnas.1702223114.

Xie, F., X. Zhou, P. Su, H. Li, Y. Tu, J. Du, C. Pan, X. Wei, M. Zheng, K. Jin, L. Miao, C. Wang, X. Meng, H. van Dam, P. ten Dijke, L. Zhang, and F. Zhou. Breast cancer cell-derived extracellular vesicles promote CD8 + T cell exhaustion via TGF-β type II receptor signaling. doi:10.1038/s41467-022-31250-2.

Yáñez-Mó, M., P.R.-M. Siljander, Z. Andreu, A.B. Zavec, F.E. Borràs, E.I. Buzas, K. Buzas, E. Casal, F. Cappello, J. Carvalho, E. Colás, A. Cordeiro-da Silva, S. Fais, J.M. Falcon-Perez, I.M. Ghobrial, B. Giebel, M. Gimona, M. Graner, I. Gursel, M. Gursel, N.H.H. Heegaard, A. Hendrix, P. Kierulf, K. Kokubun, M. Kosanovic, V. Kralj-Iglic, E.-M. Krämer-Albers, S. Laitinen, C. Lässer, T. Lener, E. Ligeti, A. Linē, G. Lipps, A. Llorente, J. Lötvall, M. Manček-Keber, A. Marcilla, M. Mittelbrunn, I. Nazarenko, E.N.M. Nolte-'t Hoen, T.A. Nyman, L. O'Driscoll, M. Olivan, C. Oliveira, É. Pállinger, H.A. Del Portillo, J. Reventós, M. Rigau, E. Rohde, M. Sammar, F. Sánchez-Madrid, N. Santarém, K. Schallmoser, M.S. Ostenfeld, W. Stoorvogel, R. Stukelj, S.G. Van der Grein, M.H. Vasconcelos, M.H.M. Wauben, and O. De Wever. 2015. Biological properties of extracellular vesicles and their physiological functions. J. Extracell. vesicles. 4:27066. doi:10.3402/jev.v4.27066.

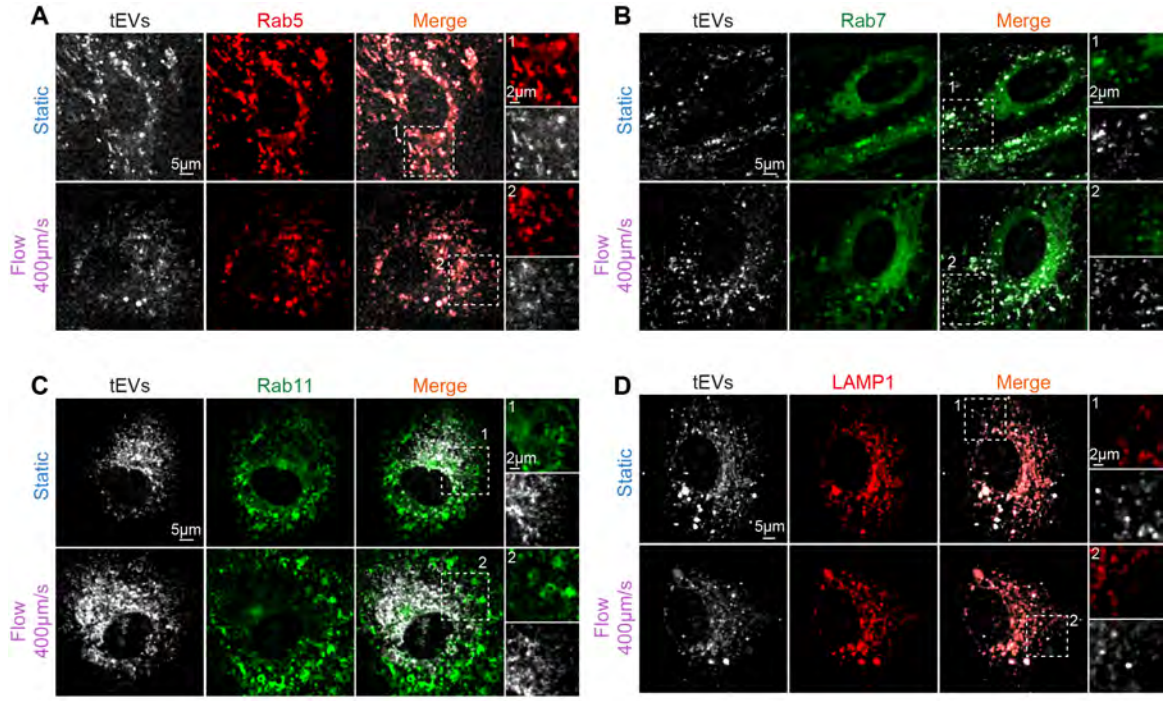

Supplementary Figure 1: tEVs trafficking in endothelial cells in flow and static conditions

Fig. 5. Supplementary Figure 1: tEVs trafficking in endothelial cells in flow and static conditions. Representative confocal images (single plane) of internalized EVs in vHUVECs cells cultured in flow or static conditions and expressing either mCherry-RAB5 (A), mEmerald-RAB7 (B), eGFP-RAB11 (C), or RFP-LAMP1 (D).

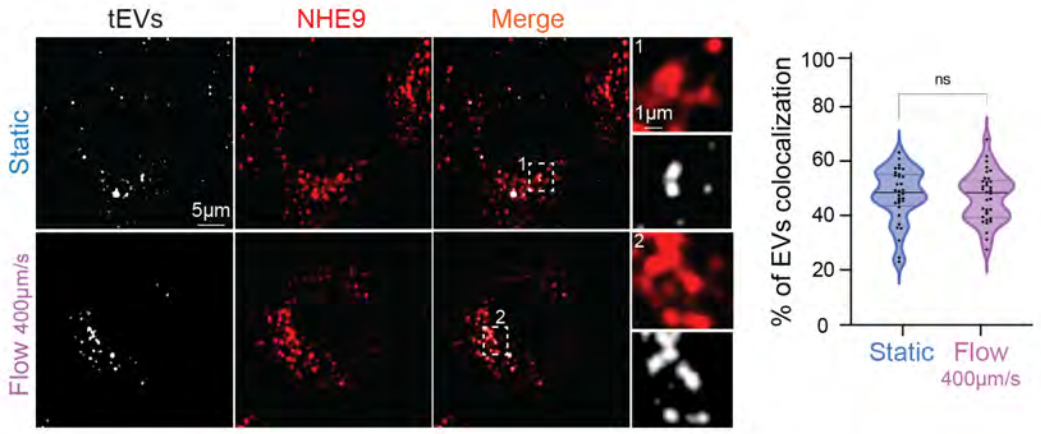

Supplementary Figure 2: tEVs accumulate in NHE9 positive compartments

Fig. 6. Supplementary Figure 2: tEVs accumulate in NHE9 positive compartments. Representative confocal images (single plane) of internalized EVs in vHUVECs cells cultured in flow or static conditions and expressing NHE9- mCherry. Colocalization was quantified using an automated pipeline.

4. The role of tEVs secretion pathway in metastatic progression

During my PhD I also participated to another project that identified a new role of Ral GTPase in tEVs biogenesis and breast cancer metastasis. Although there is now numerous evidences of the pro-tumoral role of tEVs in metastatic progression and notably their capacity to enhance PMN formation (Wortzel et al., 2019), the link between their origin and their deleterious functions is still not well understood.

This work explored the role of small GTPases, RalA and RalB, in the biogenesis and cargo loading of tEVs in murine breast cancer model. We found that:

- Ral GTPases control tEVs biogenesis, their formation and secretion levels through a phospholipase D-dependent pathway controlling MVB homeostasis.
- In mice, RalA and RalB promote lung metastasis of breast cancer cells.
- Proteomic analysis showed that these GTPases control the cargo loading of specific proteins and RNAs inside tEVs.
- Specific loading of the adhesion molecule CD146/MCAM mediated by Ral GTPases in tEVs mediates their organotropism capacities.
- CD146/MCAM is one of the actors responsible of the lung tropism and pro-metastatic effect of these tEVs.

Overall, this study identified RalA and B as new regulators of tEVs biogenesis and release. In addition, it identified CD146/MCAM as an important mediator of breast cancer tEVs organotropism which mediates the pro-tumoral effect of these tEVs. This work highlighted the link between origin, biogenesis pathway and pro-metastatic effect of tEVs, and could even support further therapeutic investigations targeting RalA/B or CD146/MCAM in mammalian model.

Ral GTPases promotes metastases by controlling biogenesis and organ colonization of exosomes

- **Ghoroghi et al., 2021**

RESEARCH ARTICLE

Ral GTPases promote breast cancer metastasis by controlling biogenesis and organ targeting of exosomes

Shima Ghoroghi[1,2,3], Benjamin Mary[1,2,3], Annabel Larnicol[1,2,3], Nandini Asokan[1,2,3], Annick Klein[1,2,3], Naël Osmani[1,2,3], Ignacio Busnelli[1,2,3], François Delalande[4], Nicodème Paul[2,3,5], Sébastien Halary[6], Frédéric Gros[1,2,3], Laetitia Fouillen[7], Anne-Marie Haeberle[8], Cathy Royer[9], Coralie Spiegelhalter[10], Gwennan André-Grégoire[11,12], Vincent Mittelheisser[1,2,3,13], Alexandre Detappe[13,14], Kendelle Murphy[15,16], Paul Timpson[15,16], Raphaël Carapito[2,3,5], Marcel Blot-Chabaud[17], Julie Gavard[11,12], Christine Carapito[4], Nicolas Vitale[8], Olivier Lefebvre[1,2,3], Jacky G Goetz[1,2,3†*], Vincent Hyenne[1,2,3,18†*]

[1]INSERM UMR_S1109, Tumor Biomechanics, Strasbourg, France; [2]Université de Strasbourg, Strasbourg, France; [3]Fédération de Médecine Translationnelle de Strasbourg (FMTS), Strasbourg, France; [4]Laboratoire de Spectrométrie de Masse BioOrganique (LSMBO), IPHC UMR 7178, CNRS, Université de Strasbourg, Strasbourg, France; [5]INSERM UMR_S1109, Genomax, Strasbourg, France; [6]CNRS, UMR 7245 MCAM, Muséum National d'Histoire Naturelle de Paris, Paris, France; [7]Université de Bordeaux, CNRS, Laboratoire de Biogenèse Membranaire, UMR 5200, Villenave d'Ornon, France; [8]Centre National de la Recherche Scientifique, Université de Strasbourg, Institut des Neurosciences Cellulaires et Intégratives, Strasbourg, France; [9]Plateforme Imagerie In Vitro, CNRS UPS 3156, Strasbourg, France; [10]IGBMC Imaging Center CNRS (UMR7104)/ INSERM (U1258)/ Université de Strasbourg, Illkirch, France; [11]Team SOAP, CRCINA, INSERM, CNRS, Université de Nantes, Université d'Angers, Nantes, France; [12]Integrated Center for Oncology, ICO, St-Herblain, France; [13]Nanotranslational laboratory, Institut de Cancérologie Strasbourg Europe, Strasbourg, France; [14]Équipe de synthèse pour l'analyse (SynPA), Institut Pluridisciplinaire Hubert Curien (IPHC), UMR7178, CNRS/Université de Strasbourg, Strasbourg, France; [15]Vincent's Clinical School, Faculty of Medicine, University of New South Wales, Sydney, Australia; [16]The Kinghorn Cancer Centre, Garvan Institute of Medical Research, Sydney, Australia; [17]C2VN, INSERM 1263, Inrae 1260, Aix-Marseille Université, Marseille, France; [18]CNRS SNC5055, Strasbourg, France

***For correspondence:** jacky.goetz@inserm.fr (JGG); hyenne@unistra.fr (VH)

†These authors contributed equally to this work

Competing interests: The authors declare that no competing interests exist.

Funding: See page 23

Received: 28 July 2020
Accepted: 05 January 2021
Published: 06 January 2021

Reviewing editor: Erica A Golemis, Fox Chase Cancer Center, United States

Abstract Cancer extracellular vesicles (EVs) shuttle at distance and fertilize pre-metastatic niches facilitating subsequent seeding by tumor cells. However, the link between EV secretion mechanisms and their capacity to form pre-metastatic niches remains obscure. Using mouse models, we show that GTPases of the Ral family control, through the phospholipase D1, multivesicular bodies homeostasis and tune the biogenesis and secretion of pro-metastatic EVs. Importantly, EVs from RalA or RalB depleted cells have limited organotropic capacities *in vivo*and are less efficient in promoting metastasis. RalA and RalB reduce the EV levels of the adhesion molecule MCAM/CD146, which favors EV-mediated metastasis by allowing EVs targeting to the lungs. Finally, RalA, RalB, and MCAM/CD146, are factors of poor prognosis in breast cancer

patients. Altogether, our study identifies RalGTPases as central molecules linking the mechanisms of EVs secretion and cargo loading to their capacity to disseminate and induce pre-metastatic niches in a CD146-dependent manner.

Introduction

The communication between tumor cells and their neighboring stromal cells is essential to sustain tumor growth and promote invasion and metastasis (**Becker et al., 2016**; **Follain et al., 2020**). Notably, this communication allows tumors to indoctrinate their microenvironment and switch the phenotypes of various cell types, such as endothelial cells, fibroblasts, or immune cells to the benefit of tumor growth, invasion, immune escape and metastasis. Such communication occurs with organs distant of the primary tumors and favors the formation of pre-metastatic niches where the modified microenvironment can help settling metastatic tumor cells (**Peinado et al., 2017**). Seeding of this favorable metastatic environment can be mediated by soluble molecules (**Kaplan et al., 2005**; **Wang et al., 2017**) or by extracellular vesicles (EVs) secreted by tumor cells (**Costa-Silva et al., 2015**; **Hoshino et al., 2015**; **Jung et al., 2009**; **Peinado et al., 2012**). EVs are lipid bilayered vesicles of nanometric diameters containing a complex mixture of RNA and protein cargoes, including a repertoire of surface receptors (**Mathieu et al., 2019**). They can be directly secreted from the plasma membrane and called microvesicles or originate from an endosomal compartment, the multi-vesicular body (MVB), and then called exosomes (**van Niel et al., 2018**). The levels of circulating tumor EVs tend to correlate with tumor progression (**Baran et al., 2010**; **Galindo-Hernandez et al., 2013**; **Logozzi et al., 2009**). Accordingly, inhibition of key components of the EV secretion machinery often correlates with decreased metastasis (**Hyenne et al., 2017**). For instance, Rab27a, which directs exosome secretion by controlling the docking of MVBs to the plasma membrane (**Ostrowski et al., 2010**), promotes breast and melanoma tumor growth and metastasis in mice (**Bobrie et al., 2012**; **Peinado et al., 2012**) and predicts poor survival in human pancreatic cancer (**Wang et al., 2015**). In addition to the levels of secreted tumor EVs, their content, and in particular their set of surface adhesion proteins equally orchestrates metastasis formation. For instance, the presence of tetraspanins CD151 and Tspan8 on the surface of pancreatic adenocarcinoma EVs favors metastasis in rats by enhancing their adhesive capacities and controlling their biodistribution (**Yue et al., 2015**). Moreover, integrin receptors exposed by tumor EVs dictate their organotropism and thereby tune/control the seeding of a premetastatic niche in specific and distant organ (**Hoshino et al., 2015**). Therefore, accumulating evidence show that both the levels and the content of secreted tumor EVs are instrumental in promoting metastasis.

However, the molecular mechanisms coordinating these processes remain elusive. In particular, how the machinery governing EV secretion can impact the pro-metastatic properties of tumor EVs deserves in-depth characterization. To address this issue, we focused on the members of the Ral family, RalA and RalB (collectively referred to as RalA/B), acting downstream of RAS and promoting metastasis of different tumor types in both mice and human (**Gentry et al., 2014**; **Yan and Theodorescu, 2018**). We recently found that these versatile proteins are evolutionarily conserved regulators of exosome secretion (**Hyenne et al., 2015**). We originally observed that, in the nematode *C. elegans*, the Ral GTPase ortholog RAL-1 controls exosome secretion by acting on the biogenesis of MVBs. Importantly, we further showed that RalA/B modulate the levels of secreted EVs in models that are relevant to human breast cancer (**Hyenne et al., 2015**) suggesting that these GTPases could influence disease progression through EVs release. Here, we exploited 4T1 cells, an aggressive mammary tumor model that mimics human triple-negative breast cancer (**Kaur et al., 2012**) to further decipher how RalA/B tune EV secretion mechanisms and thereby control metastatic progression of the disease.

In this study, we first provide a detailed dissection of the impact of the Ral GTPases on EV secretion levels and unravel the mechanisms by which they control the homeostasis of MVBs. We have discovered that RalA/B directly acts through the phospholipase D1 (PLD1), which, as we show, also promotes EVs secretion, to favor the maturation of MVBs. We further demonstrate that RalA and RalB promote lung metastasis without affecting the invasive potential of breast carcinoma. Importantly, RalA/B are crucial for the organ targeting of tumor EVs, and, as a consequence, for the seeding of pre-metastatic niches. Finally, we identify the adhesion protein CD146/MCAM as a key EV

cargo controlled by RalA and RalB and demonstrate that it conveys, in part, the pro-metastatic function to EVs by controlling the lung tropism of breast cancer EVs.

Results

RalA and RalB control exosome secretion levels through the homeostasis of MVBs

We have previously shown that RalA and RalB control EV secretion in aggressive 4T1 mammary tumor cells (***Hyenne et al., 2015***) that reliably mimics the aggressive phenotype of human triple-negative breast cancer. We thus built on this relevant tumor model and decided to test the hypothesis that RalA and RalB could orchestrate pro-metastatic functions by tuning the molecular mechanisms driving the secretion levels and nature of EVs. We first confirmed our initial observations with the nanoparticle-tracking analysis (NTA) of EVs released by 4T1 cells and isolated by ultracentrifugation (100,000 g pellet). Stable depletion of RalA or RalB by shRNA reduces by 40% the amount of secreted EVs (***Figure 1a***, ***Figure 1—figure supplement 1a***), with no impact on their average size (***Figure 1—figure supplement 1b***). RBC8 and BQU57, two previously described specific chemical inhibitors of Ral GTPases (***Yan et al., 2014***) significantly reduced EV secretion levels in mouse and human mammary tumor cell lines (4T1, MDA-MB231, D2A1, and MCF7 cells) as well as in two other cancer cell lines, human melanoma (A375) and pancreatic carcinoma (Panc1) cells (***Figure 1b*** and ***Figure 1—figure supplement 1c***). Together with evidence previously obtained in *Caenorhabditis elegans* (***Hyenne et al., 2015***), this demonstrates that the mechanisms by which RalA/B GTPases tune EV secretion levels are conserved throughout evolution and are notably at play in various cancer cell lines.

To better understand how Ral GTPases could impact EVs secretion, we first characterized their intracellular distribution in 4T1 cells. Endogenous RalA and RalB localize mostly within CD63-positive endosomal compartments (MVBs and late endosomes), as well as at the plasma membrane (***Figure 1c***). Similarly, GFP-tagged RalA and RalB localize both in late endosomal compartments positive for Lysotracker and at the plasma membrane (***Figure 1c***). Therefore, in 4T1 cells, Ral GTPases localize both at biogenesis sites of microvesicles (plasma membrane) and exosomes (MVBs). To further determine whether Ral GTPases affect MVBs as previously observed in *C. elegans*, we performed thorough electron microscopy (EM) analysis of endosomal compartments in 4T1 cells. In a first analysis of cells that were processed upon chemical fixation, we quantified the densities of (i) MVBs and (ii) endolysosomes, as well as (iii) the diameter of MVBs, (iv) the number and (v) the diameter of intraluminal vesicles (ILVs) per MVB. Strikingly, we found RalA or RalB depletion leads to a 40% decrease in the number of MVB per cytoplasmic surface in 4T1 cells (***Figure 1d*** and ***Figure 1—figure supplement 2a***), with no impact on the density of endolysosomes (***Figure 1—figure supplement 2b***). Further analysis of Lysotracker-positive compartments using FACS confirmed that RalA/B depletion has no significant effect on the late endosome-lysosome pathway (***Figure 1—figure supplement 2c***). Besides, EM analysis revealed no differences in ILV numbers per MVB surface (***Figure 1—figure supplement 2d***), nor in MVB diameters (***Figure 1—figure supplement 2e***). However, since chemical fixation is known to affect the morphology of endosomal compartments, we took our EM analysis one step forward by implementing high-pressure freezing (HPF) of cells, which better preserves the ultrastructure of endosomes (***Klumperman and Raposo, 2014***). A similar decrease in the number of MVBs per cytoplasmic surface in RalA and RalB knockdown cells was observed in these conditions (***Figure 1—figure supplement 2a***). Upon HPF, we further observed a slight decrease in the number of ILVs per MVB surface (***Figure 1—figure supplement 2d***) that could be, in part, explained by a slight increase in MVB diameters (***Figure 1—figure supplement 2e***). In conclusion, depletion of either RalA or RalB significantly reduces MVB number, while the remaining MVBs are slightly bigger. Overall, thorough EM analysis of intracellular compartments using both chemical fixation and HPF clearly demonstrates that both RalA and RalB control MVB homeostasis in breast mammary tumor cells.

A RalA/B-PLD1-PA axis governs exosome biogenesis

We further investigated the molecular mechanisms controlling MVB homeostasis downstream of RalA/B GTPases. We decided to focus on phospholipases D (PLDs), which catalyzes the hydrolysis of

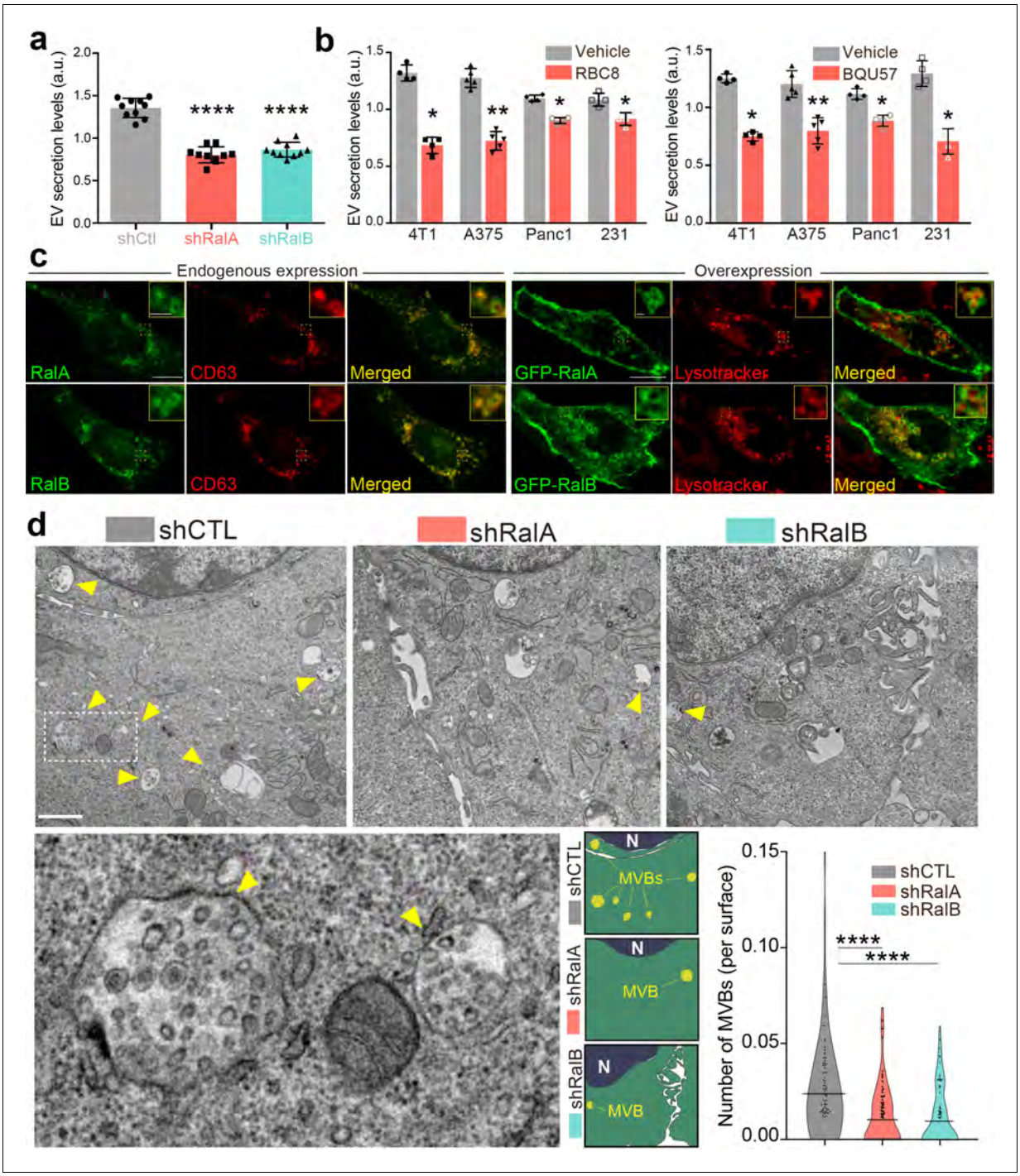

Figure 1. RalA and RalB control exosome secretion and multi-vesicular body (MVB) homeostasis. (**a–b**) Nanoparticle tracking analysis of extracellular vesicles (EVs) isolated by ultracentrifugation (100,000 g pellet) from the supernatant of shCtl, shRalA, or shRalB 4T1 cells (**a**) or from various cell types treated with Ral inhibitors RBC8 (**b**, left) or BQU57 (**b**, right). 231: MDA-MB-231 cells. Each dot represents one experiment (a: 10 independent

Figure 1 continued on next page

Figure 1 continued

experiments; One-Way Anova followed by Bonferroni's Multiple Comparison Test; b: four to five independent experiments, Mann Whitney test). (**c**) Representative confocal images of 4T1 cells showing endogenous expression of RalA, RalB, and CD63 by immunofluorescence (left) and overexpression of GFP-RalA and GFP-RalB in cells incubated with Lysotracker (right). Scale bar: 10 μm; zoom: 2 μm. (**d**) Representative electron micrographs of 4T1 shCtl, shRalA and shRalB cells, with zoom on MVBs; Scale bar: 1 μm; zoom: 200 nm. Violin plots show quantification of the number of MVB per cytoplasm surface. Each dot represents one field of view; horizontal bars represent the average (76–88 fields of view; Kruskal-Wallis test followed by Dunn's Multiple Comparison Test).

The online version of this article includes the following figure supplement(s) for figure 1:

Figure supplement 1. Ral knockdown efficiency and impact on EV secretion.

Figure supplement 2. Electron microscopy analysis of endosomes in the absence of RalA or RalB (**a-b**).

phosphatidylcholine (PC) into phosphatidic acid (PA), for three reasons: (1) PLD1 and PLD2 are two well-known targets of RalA and RalB (***Jiang et al., 1995***; ***Luo et al., 1998***; ***Vitale et al., 2005***), (2) PLD2 controls exosome secretion in breast cancer cells (***Ghossoub et al., 2014***), and (3) PLDs impact cancer progression (***Bruntz et al., 2014***). We first verified that both PLD1 and PLD2 are expressed in 4T1 cells by RT-qPCR (***Figure 2—figure supplement 1a***). In the absence of efficient anti-PLD antibody for immunofluorescence, we decided to assess the subcellular localization of PLD-GFP fusion proteins. PLD1 mostly localizes to endosomal compartments positive for RalA, RalB, and lysotracker, whereas PLD2 mostly localizes to the plasma membrane (***Figure 2a*** and ***Figure 2—figure supplement 1b***). Therefore, we tested whether PLDs could function downstream of RalA/B to control MVBs homeostasis and exosome secretion using two chemical inhibitors, CAY10593 for PLD1 and CAY10594 for PLD2 (***Lewis et al., 2009***; ***Scott et al., 2009***). EM analysis of 4T1 cells revealed that inhibition of PLD1, but not of PLD2, induces a 40% decrease in the number of MVBs per cytoplasmic surface (***Figure 2b***). This phenotype is consistent with PLDs respective localizations and suggests that PLD1 functions in the RalA/B exosome secretion pathway. Further NTA analysis of treated cells showed that both inhibitors reduce EV secretion levels in 4T1 cells (***Figure 2c***), suggesting that both PLD isoforms regulate EV secretion potentially through distinct mechanisms. Importantly, PLD1 inhibition fully phenocopies the effect of RalA/B GTPases depletion, both on the cellular density of MVBs and on the level of EV secretion. To determine whether PLD1 acts downstream of RalA/B, we looked at its localization in the absence of RalA or RalB. Confocal analysis revealed that in 40% of shRalA or shRalB cells, PLD1 is uniformly cytoplasmic instead of being endosomal (***Figure 2d***). By contrast, RalA/B depletion had no major impact on PLD2 localization at the plasma membrane (also its trafficking might be altered) (***Figure 2—figure supplement 1c***). This shows that RalA/B GTPases are required for PLD1 localization on endosomes. To further investigate if PLD activity is involved in Ral GTPases-dependent EV secretion, we performed a lipidomic analysis of secreted EVs. As PLD converts PC into PA, we focused on these two lipid species. Importantly, RalA/B depletion significantly reduces the PA/PC ratio of secreted EVs (***Figure 2e***). In particular, the PA/PC ratio made of mono- and di-unsaturated lipid species (36:1, 36:2, 38:1, and 38:2), known to be PLD product/target, respectively, showed a tendency to be decreased although not reaching statistical significance (***Figure 2—figure supplement 1d***). This further implies that PLD's main product, PA, plays a crucial role in MVB homeostasis. Altogether, these results suggest that Ral GTPases control PLD1 localization on MVBs, which is required for local PA accumulation and ultimately for MVB homeostasis and exosome secretion (***Figure 2f***).

RalA and RalB promote metastasis non-cell autonomously

Having identified RalA and RalB as important regulators of EV secretion in breast cancer cells, we next investigated whether such a function could impact metastasis. At first, we analyzed public databases to interrogate a potential correlation between RalA/B expression levels and metastatic progression. Using a large cohort of breast cancer patients with metastatic progression from the Cancer Genome Atlas (TCGA), we found that high expression of either RalA or RalB is significantly correlated with reduced survival (***Figure 3a***). Automated quantification of RalA/B expression levels by immunohistochemistry in primary tumors of breast cancer patients unraveled overexpression of both proteins in tumors from patients with metastasis (***Figure 3b***). These results prompted us to investigate in depth the role of RalA/B in a syngeneic mouse model of aggressive breast cancer, which is highly relevant to the human pathology.

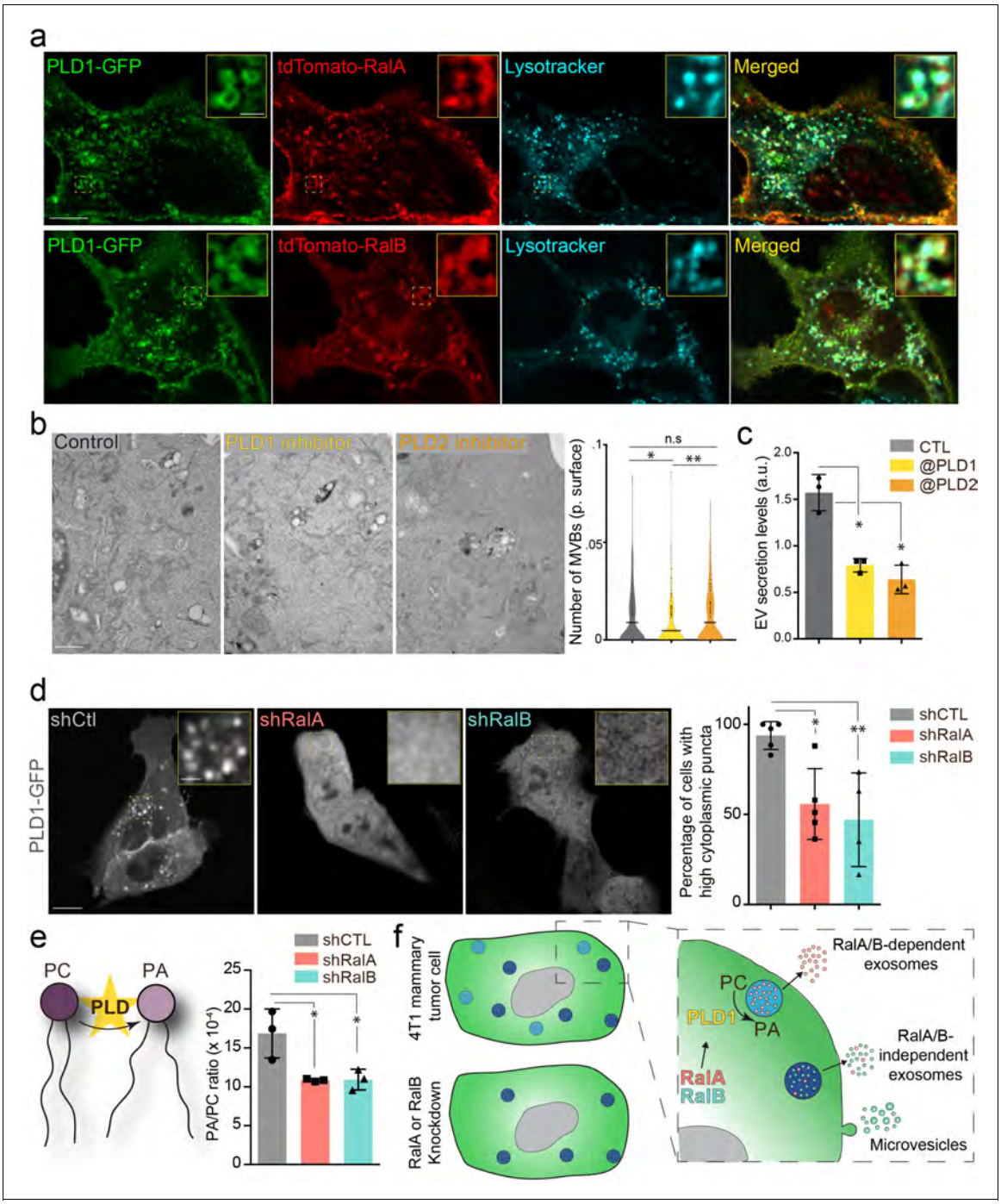

Figure 2. The RalA/B-PLD1-PA axis governs exosome secretion. (**a**) Representative confocal images of 4T1 cells co-transfected with PLD1-GFP and tdTomato-RalA (upper panels) or tdTomato-RalB (lower panels) and incubated with Lysotracker. Scale bar: 10 µm; zoom: 2 µm. (**b**) Electron microscopy analysis of 4T1 cells treated with PLD1 or PLD2 inhibitor. Scale bar: 1 µm. Violin plots show quantification of the number of multi-vesicular body (MVB) per cytoplasmic surface. Each dot represents one field of view; horizontal bar represents the average (180–194 fields of view; Kruskal-Wallis test

Figure 2 continued on next page

Figure 2 continued

followed by Dunn's Multiple Comparison Test). (**c**) Nanoparticle tracking analysis of extracellular vesicles (EVs) isolated by ultracentrifugation (100,000 g pellet) from the supernatant of 4T1 cells treated with PLD1 (CAY10593) or PLD2 (CAY10594) inhibitor. Each dot represents one experiment (three independent experiments; One-Way Anova permutation test followed by fdr multi-comparison permutation test). (**d**) Representative confocal images of shControl, shRalA and shRalB 4T1 cells transfected with PLD1-GFP. Scale bar: 10 μm; zoom: 2 μm. Graph shows the percentage of cells with high (>5) number of PLD1-GFP cytoplasmic puncta. (Each dot represents one experiment. Five independent experiments; Number of cells analyzed: shCtl (136), shRalA (170), shRalB (244); Kruskal-Wallis test followed by Dunn's Multiple Comparison Test). (**e**) Quantification of the Phosphatidic Acid (PA) / PhosphatidylCholine (PC) ratio in EVs isolated from shControl, shRalA, and shRalB cells (each dot represents one experiment; three independent experiments; One-Way Anova permutation test followed by fdr multi-comparison permutation test; fdr <0.1). (**f**) Model showing how RalA and RalB could control PLD1 localization on MVBs, thereby inducing the PA accumulation on MVBs, promoting MVB homeostasis and controlling exosome secretion.

The online version of this article includes the following figure supplement(s) for figure 2:

Figure supplement 1. PLD1 and PLD2 in 4T1 cells.

Therefore, we conducted a careful and exhaustive longitudinal analysis of metastatic progression of mammary tumors in syngeneic Balb/c mice. Briefly, 4T1 cells depleted or not for RalA or RalB were orthotopically grafted in mammary ducts, and several criteria were tracked over time. First, RalA and RalB have antagonist effects on tumor growth measured in vivo over time and ex vivo after 41 days: while RalA depletion significantly increased tumors growth, RalB depletion induced the opposite effect when compared to control tumors (***Figure 3c***). Neither RalA, nor RalB affected apoptosis, using caspase3 as a read-out (***Figure 3—figure supplement 1a–b***). In contrast, 4T1 cells depleted of RalA and RalB show increased growth rate *in vitro* and a decreased proportion of cells in sub-G1 phase of the cell cycle (***Figure 3—figure supplement 1c–d***). A similar increase in proliferation rates was observed *in vivo* in the absence of RalA (***Figure 3d***). Therefore, while depletion of RalA favors *in vivo* tumor growth by enhancing 4T1 proliferation potential, it is likely that additional non-cell autonomous factors are responsible for the decreased tumor growth observed upon RalB depletion.

We obtained the most striking result when carefully assessing the lung metastasis burden of these mice after 41 days. We measured the number and the surface covered by metastatic foci in serial lung sections and observed that RalA or RalB depletion in mammary tumors drastically reduced their metastatic potency (***Figure 3e***). When compared to the tumor growth rate, the most dramatic reduction of metastasis was observed in the case of RalA depletion. These experiments show that although RalA and RalB have antagonist effects on primary tumors, they both promote metastasis. To dissect this phenotype, we tested whether RalA or RalB could impact inherent cell migration and invasion potential of 4T1 cells, as it had been reported for RalB (***Oxford et al., 2005***; ***Zago et al., 2018***). We performed 2D (***Figure 3f***) and 3D (***Figure 3g***) *in vitro* invasion assays and observed no effect of RalA or RalB expression levels on motility potential of 4T1 cells. Therefore, RalA/B seem to promote metastasis independently of cell invasion and are likely to promote metastasis of aggressive breast cancer cells non-cell autonomously by inducing pro-metastatic micro-environmental changes.

RalA- and RalB-dependent EVs induce endothelial permeability

Since RalA and RalB promote metastasis independently of their cell-intrinsic properties, we wondered whether they could control secreted factors that are likely to induce micro-environmental alterations. In addition to EVs, tumor cells secreted soluble factors can promote metastasis by modulating the microenvironment, notably by promoting the formation of a metastatic niche (***Ombrato et al., 2019***). To test this possibility, we examined the impact of RalA and RalB on the soluble secretome of 4T1 cells. Depletion of RalA or RalB had no drastic effect on the soluble factors secreted by 4T1 cells (***Figure 3—figure supplement 2***). However, the secretion of one protein known to promote metastasis (***Ombrato et al., 2019***), WISP1/CCN4, is significantly decreased in shRalA/B cells (***Figure 3—figure supplement 2***). Thus, RalA and RalB are likely to enhance metastatic potency by promoting the secretion of EVs and possibly as well through WISP1/CCN4. Furthermore, in addition to enhancing the levels of secreted EVs, RalA/B could alter their functionality. To test this possibility, we challenged the pro-tumoral function of RalA/B EVs in an in vitro functional assay.

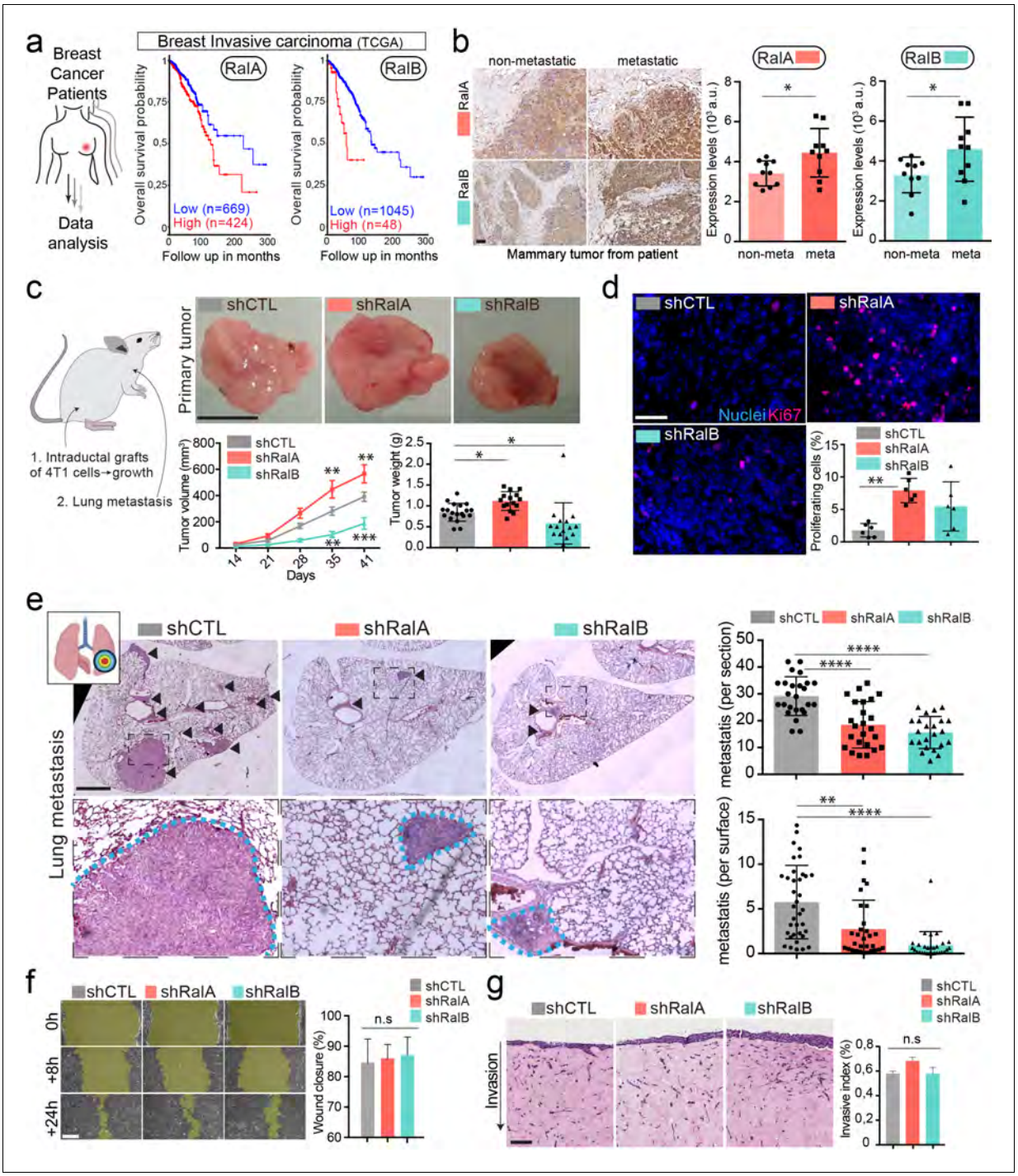

Figure 3. RalA and RalB promote lung metastasis in a non-cell autonomous fashion. (**a**) Kaplan-Meier curve, obtained from TCGA 1097 cohort, showing the survival probability of patients with tumor breast invasive carcinoma having high or low RalA (pvalue: 5.15 e-03; pAdj: 1.35e-01) or RalB (pvalue: 1.77 e-05; pAdj: 5.99e-03) expression levels. (**b**) Representative images of immunohistochemistry against RalA or RalB performed on mammary primary

Figure 3 continued on next page

Figure 3 continued

tumors from patients with or without metastasis. Scale bar: 500 μm Graphs represent automated scoring of DAB staining. Each dot represents one patient; 10 patients per group; Student t-test. (**c**) Orthotopic injection of shControl, shRalA, and shRalB 4T1 cells in syngenic mice. Representative images of primary tumors at day 41. Scale bar: 1 cm. Graphs showing the primary tumor growth over time (Left) and the primary tumor weight at day 41. Each dot represents one mouse. (Two independent experiments; Left: Two-way Anova followed by Bonferonni post-test, Right: Kruskal-Wallis test followed by Dunn's Multiple Comparison Test). (**d**) Representative images of primary tumors stained with anti-Ki67 antibody. Scale bar: 50 μm. Graph indicates the % of Ki67-positive nuclei. Each dot represents one mouse. (six mice taken from two independent experiments; Kruskal-Wallis test followed by Dunn's Multiple Comparison Test. (**e**) Analysis of lung metastasis in mice from the orthotopic experiment presented in (**c**). Representative images of lung sections (Day 41) stained with hematoxilin eosin. Scale bar: 1 mm. Graphs show the number of metastatic foci per section (upper, One-Way Anova followed by Bonferroni's Multiple Comparison Test) and the metastatic surface per lung surface (lower; Kruskal-Wallis test followed by Dunn's Multiple Comparison Test). Each dot represents one section **f**) Pictures of wound healing closure at different time points. Scale bar: 150 μm. Graph represents the percentage of wound closure at 16 hr (three independent experiments; Kruskal-wallis test followed by Dunn's multiple comparison test). (**g**) Pictures of 3D invasion assay after 15 days. Graph represents the invasive index. Scale bar: 100 μm.
The online version of this article includes the following figure supplement(s) for figure 3:

Figure supplement 1. Proliferation and apoptosis of 4T1 cells and tumors.
Figure supplement 2. Soluble secretome of 4T1 shControl cells compared to 4T1 shRalA or 4T1 shRalB cells (three independent experiments; One-Way Anova permutation test followed with pairwise permutation test with fdr correction).

Since tumor EVs are known to induce vascular permeability in the vicinity of tumors as well as in distant organs (***Tominaga et al., 2015***; ***Treps et al., 2016***; ***Zhou et al., 2014***), we tested the capacity of RalA/B dependent EVs to promote endothelial permeability *in vitro*. When added to a monolayer of endothelial cells, 4T1 EVs increased its permeability in a dose-dependent manner (***Figure 3—figure supplement 1e***). We then tested the impact of EV content on vascular permeability by subjecting endothelial cells to similar amounts of EVs derived from 4T1 cells expressing or not RalA/B. Interestingly, endothelial monolayers became less permeable when treated with a similar amount of EVs derived from shRalA or shRalB cells. Similarly, such EVs fail to disrupt adherent and tight junctions by contrast to EVs derived from 4T1 control cells (***Figure 4b***) suggesting that EVs from RalA/B knockdown cells have reduced pro-permeability abilities. Therefore, depletion of RalA/B reduces secretion levels of EVs and leads to the secretion of EVs whose effect on vascular leakiness is hampered. The important observation that vascular permeability could be reduced upon depletion of RalA or RalB, and with a similar amount of EVs, prompted us to further dissect whether RalA or RalB could tune the priming of pre-metastatic niches.

RalA and RalB dependent EVs are pro-metastatic and lung tropic

Here, we thus explored whether RalA and RalB synergistically impact the pro-metastatic functions of EVs by tuning their secretion levels as well as their content. Since on one hand RalA and RalB positively control the levels and the functionality of secreted tumor EVs (***Figures 1*** and ***4a***), and on the other hand they promote metastasis (***Figure 3***), we tested a direct impact of RalA/B-dependent EVs on the promotion of lung metastasis. For this, we decided to directly assess the role of 4T1 EVs in priming lung metastatic niches in vivo, as previously described for other tumor EVs (***Costa-Silva et al., 2015***; ***Hoshino et al., 2015***; ***Peinado et al., 2012***; ***Zhou et al., 2014***). Priming of lungs with control EVs significantly enhances lung metastasis over 14 days when compared to PBS (***Figure 4c***). In striking contrast, priming of mouse lungs with a similar number of EVs derived from Ral-depleted cells did not promote metastasis. This key experiment demonstrates that RalA/B confer pro-metastatic functions to EVs, in addition to controlling their secretion levels. Indeed, the decreased metastasis observed in absence of RalA/B can result from either drastically reduced EVs secretion or diminished pro-metastatic potential of EVs. To unravel why EVs from RalA/B-depleted cells are unable to promote metastasis, we first determined their capacity to efficiently reach the lungs and prime pre-metastatic niches by tracking the dissemination of fluorescently labeled EVs that were injected in the blood circulation of Balb/c mice. We found that 1 hr after injection 4T1 EVs mostly accumulate in the lungs, as well as the liver and brain (***Figure 4d*** and ***Figure 4—figure supplement 1a***). These three organs are the main metastatic organs of 4T1 cells, and breast carcinoma, showing that the organotropism of 4T1 EVs mirrors the metastatic organotropism of their parental cells and further validates the relevance of our model to human pathology (***Kaur et al., 2012***; ***Lou et al., 2008***). Through a careful analysis of cell types that internalize EVs in these conditions, we

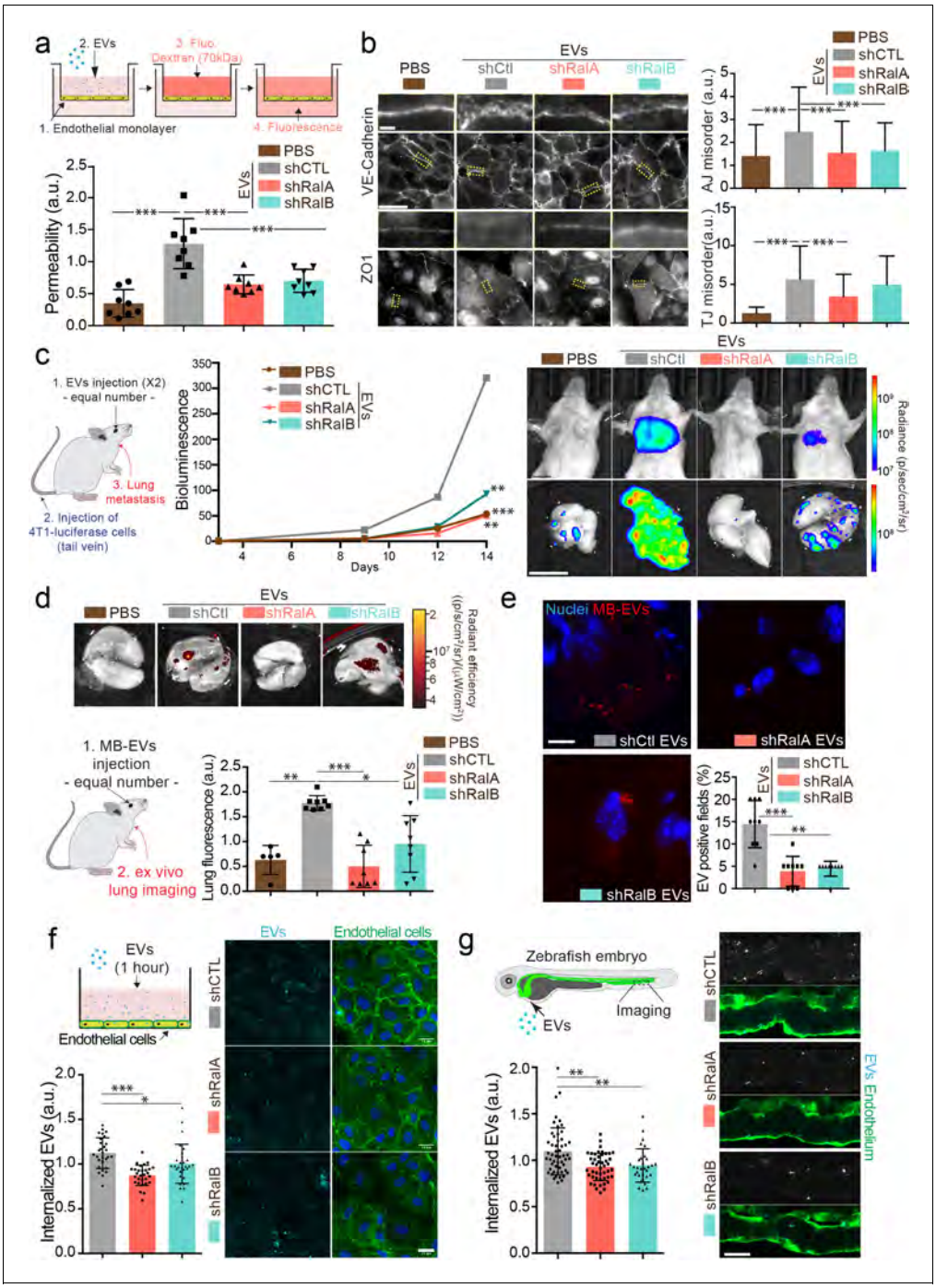

Figure 4. RalA and RalB control lung tropism of pro-metastatic tumor extracellular vesicles (EVs). (**a**) Effect of a similar amount of EVs on HUVEC monolayer permeability *in vitro*. The graph represents the normalized amount of fluorescent dextran that crossed the endothelial barrier. Each dot represents one experiment (eight independent experiments; One-Way Anova followed by Bonferroni's Multiple Comparison Test). (**b**) Representative epifluorescence images of VE-cadherin (upper panels) and ZO1 (Lower panel) stainings on HUVECS cells treated with similar amounts of EVs. Scale bar:

Figure 4 continued on next page

Figure 4 continued

20 μm; zoom: 2 μm. Graphs represent the disorganization of adherent (up) and tight (low) junctions (Three independent experiments; up; Kruskal-Wallis test followed by Dunn's Multiple Comparison Test). (**c**) Metastasis priming experiment, Balb/c mice are first injected twice with tumor equal number of EVs (1.5×10^8 EVs), then intravenously with 4T1 luciferase cells and metastasis is then followed over time. Graph shows metastasis progression over time in mice pre-injected with PBS, or with equal number of EVs from shControl, shRalA or shRalB cells (7–10 mice per group; merge of two independent experiments; Two-way Anova followed by Bonferonni multiple comparison post test; stars indicate statistically significant differences at day 14). Right: *In vivo* and *ex vivo* representative images of mice and lungs at day 14. Scale bars: 1 cm. (**d–e**) Lung accumulation of equal number of fluorescent-labeled EVs ($3\ 10^8$ EVs), from shControl, shRalA or shRalB cells injected intravenously. (**d**) Representative ex vivo images and graph showing the total lung fluorescence 1 hr post-injection. Each dot represents one mouse. (Eight mice taken from two independent experiments; Kruskal-Wallis test followed by Dunn's Multiple Comparison Test.) (**e**) Representative confocal lung sections images and graph showing the percentage of EVs-positive fields. Each dot represents one section (three mice; Kruskal-Wallis test followed by Dunn's Multiple Comparison Test). Scale bar: 5 μm. (**f–g**) Arrest and internalization of equal number of EVs from shControl, shRalA, and shRalB cells on endothelial cells *in vitro* and *in vivo*. (**f**) Representative confocal Z-stacks of equal number of EVs after 1 hr or incubation with HUVEC monolayer. Scale bar: 25 μm. Each dot represents one field of view (each dot represents one field of view from three independent experiments; Kruskal-Wallis test followed by Dunn's Multiple Comparison Test). (**g**) Representative confocal Z-stacks the caudal plexus of Tg(Fli1:GFP) zebrafish embryos, where GFP is expressed in the endothelium, injected with similar number of EVs and imaged right after injection. Each dot represents one zebrafish (31–53 embryos from four independent experiments; Kruskal-Wallis test followed by Dunn's Multiple Comparison Test). Scale bar: 20 μm.

The online version of this article includes the following figure supplement(s) for figure 4:

Figure supplement 1. 4T1 extracellular vesicles (EVs) organotropism.

observed that 4T1 EVs mostly accumulate in endothelial cells, macrophages, and fibroblasts of the lung parenchyma (***Figure 4—figure supplement 1b***). Importantly, EVs derived from RalA- or RalB-depleted cells failed to efficiently reach the lungs, even though similar amounts were injected in all conditions (***Figure 4d,e***). Similar results were observed for EVs reaching the liver (***Figure 4—figure supplement 1c***). Hence, we can conclude at this stage that RalA/B control the pro-metastatic properties of EVs by tuning their ability to reach vascular regions and local parenchyma and efficiently reach metastatic organs, thereby modulating the formation of a pre-metastatic niche.

The latter results raised the exciting hypothesis that metastasis impairment could be, in part, explained by a general defect in adhesion of circulating EVs at the vascular wall. We recently showed that EVs target specific vascular regions by first arresting at the surface of endothelial cells (***Hyenne et al., 2019***). We used two complementary models that allow careful tracking of single EVs and assessed early events of EVs internalization in endothelial cells. Using microfluidics, we found that internalization of 4T1 EVs within endothelial cells is decreased after 1 hr when they originate from RalA/B-depleted cells (***Figure 4f***). Similarly, upon tracking of fluorescent EVs injected in the circulation of zebrafish embryos, we observed that endothelial arrest/internalization of EVs from RalA/B knockdown cells is significantly hampered (***Figure 4g***). Altogether, these experiments suggest that RalA/B knockdown significantly reduced the adhesive properties of EVs to the endothelium, establishing a potential link with their failure to accumulate in mice lungs. Furthermore, our results support a model in which RalA/B GTPases, in addition to promoting EV secretion, also control the pro-metastatic function of these EVs, likely by modulating their content.

RalA/B promote CD146 EV loading for efficient lung targeting and pre-metastatic niche priming

These functional experiments (***Figure 4***) suggest that the content of EVs can directly influence metastasis formation and that such content is likely to be impacted by RalA/B. Therefore, we carried out a careful and thorough molecular comparison of the cargo content of EVs derived from RalA/B-tuned cells. We first analyzed the RNA content of EVs using RNAseq and found that a large proportion of the RNAs present in EVs from shRal cells were different from the control (30–50%) (***Figure 5a***; ***Supplementary file 1***). Accordingly, GO terms associated with mRNA enriched in each EV type showed important differences in biological processes, molecular function, or cellular components (***Figure 5—figure supplement 1***). In addition, EVs from shRalA cells differed from control or shRalB EVs in the nature of the RNA they contain, as shRalA EVs showed an important increase in non-coding RNA (***Figure 5b***). Overall, this experiment reveals that RalA/B have a profound impact on the content of RNA in 4T1 EVs.

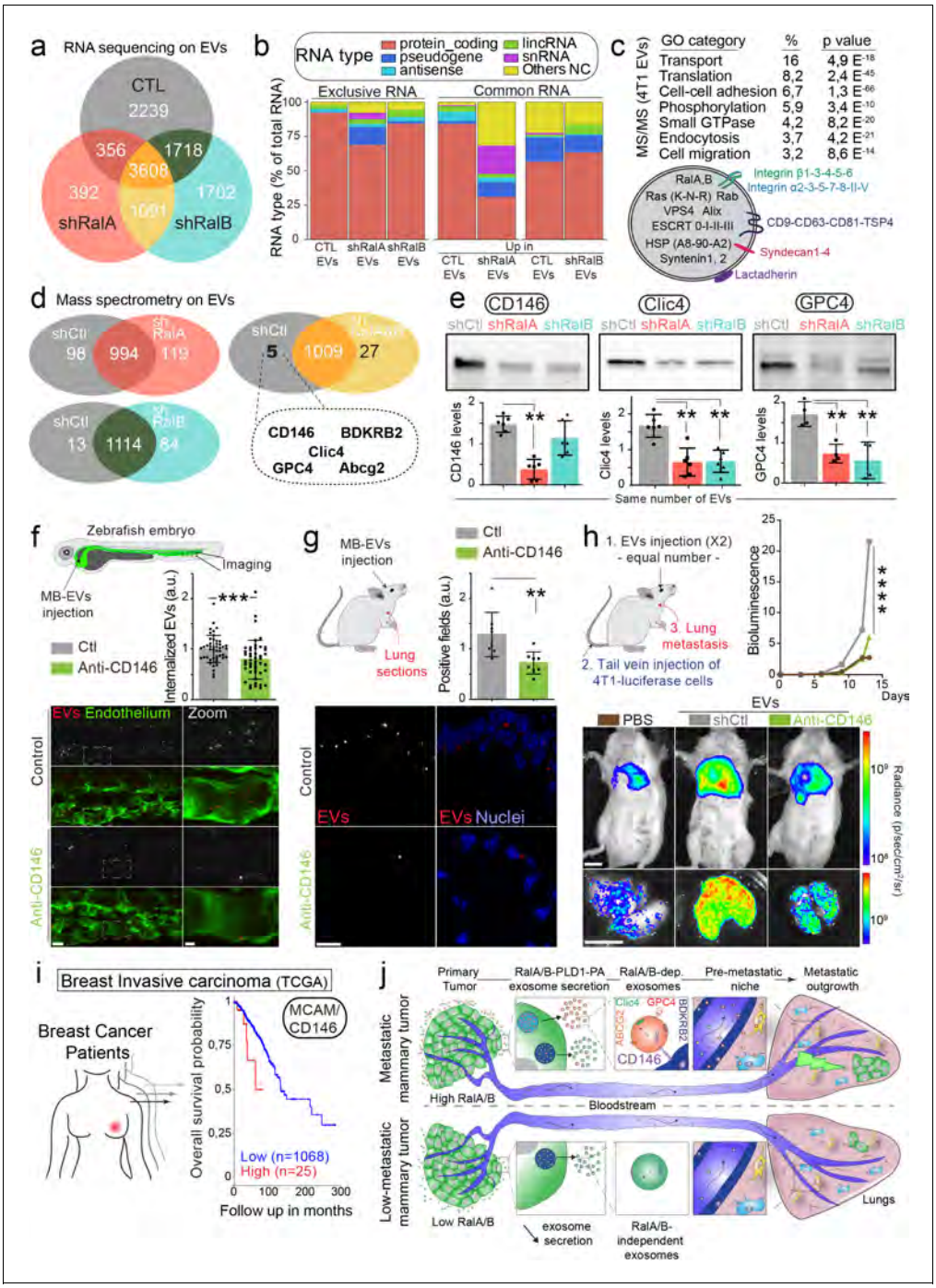

Figure 5. CD146/MCAM is under-expressed in RalA/B knockdown extracellular vesicles (EVs) and mediates their lung tropism. (**a**) Venn diagram representing the RNA present in the EVs isolated from shControl, shRalA or shRalB cells (with a minimum of 10 reads per sample; RNA sequencing performed in triplicate). (**b**) Type of RNA associated identified in EVs isolated from shControl, shRalA, or shRalB cells. Left: RNA exclusively present in one type of EVs. Right: enriched RNAs (log2 fold change >2; p(adj.)<0,05). (**c**) GO terms of the proteins identified in EVs isolated from 4T1 cells by

Figure 5 continued on next page

Figure 5 continued

ultracentrifugation (100,000 g pellet) and illustration of some proteins known to be present in EVs. (**d**) Comparison of the protein content of EVs isolated from shControl, shRalA, and shRalB cells. The venn diagram represents proteins having different expression levels (Mass spectrometry performed in triplicate; FDR < 1%). (**e**) Analysis of the expression of CD146/MCAM, Clic4, and Glypican4 in EVs isolated from shControl, shRalA and shRalB cells by western blots. Each dot represents one experiment (four to six independent experiments; Kruskal-Wallis test followed by Dunn's Multiple Comparison Test). (**f–g**) Arrest, internalization, and organotropism of EVs treated with an anti-CD146 antibody and injected in the circulation of zebrafish embryos (**f**) or mouse (**g**). (**f**) Representative confocal Z-stacks the caudal plexus of Tg(Fli1:GFP) zebrafish embryos, where GFP is expressed in the endothelium, injected with equal number of EVs and imaged right after injection. Scale bar: 20 μm; Zoom scale bar: 5 μm. Each dot represents one zebrafish (46 embryos from four independent experiments; Mann Whitney test). (**g**) Representative confocal images of lung sections and graph showing the percentage of EVs-positive fields. Scale bar: 10 μm. Each dot represents one mouse (eight mice from two independent experiments; Mann Whitney test). (**h**) Metastasis priming experiment, Balb/c mice are injected twice with tumor equal number of EVs (1.5×10^8 EVs), pre-incubated with CD146 blocking antibody or isotype control, and then intravenously injected with 4T1 luciferase cells and metastasis is followed over time. Graph shows metastasis progression over time (14 mice per group; merge of two independent experiments; Two-Way Anova followed by Bonferonni multiple comparison post-test; stars indicate statistically significant differences at day 14). *In vivo* and *ex vivo* representative images of mice and lungs at day 14. Scale bars: 1 cm. (**i**) Kaplan-Meier curve, obtained from TCGA 1097 cohort, showing the survival probability of patients with tumor breast invasive carcinoma having high or low MCAM/CD146 expression levels (pvalue: 3.42 e-02; pAdj: 5.67e-01). (**j**) Model describing the role of RalA/B-dependent EVs in metastatic formation.

The online version of this article includes the following figure supplement(s) for figure 5:

Figure supplement 1. RNA content of extracellular vesicles (EVs) from shControl, shRalA, and shRalB cells.

Figure supplement 2. 4T1 cells and extracellular vesicles (EVs) express CD146/MCAM long isoform.

We further analyzed the protein content of 4T1 EVs by mass spectrometry. As shown in ***Figure 5c*** and 4T1 EVs contain a large number of proteins usually found in small EVs (77 of the top 100 proteins from Exocarta are found in 4T1 EVs; ***Supplementary file 2***), such as tetraspanins, integrins, ESCRT proteins or small GTPases, such as RalA/B themselves. Importantly, many of these proteins are known to localize to endosomes, suggesting that some of these EVs are bona fide exosomes. Unexpectedly, comparison of the proteome of EVs secreted by RalA or RalB knockdown cells did not reveal major differences, as no protein is exclusive to one type of EVs. Instead, a small proportion of proteins showed differential expression levels (***Figure 5d***; ***Supplementary file 2***). Regarding their protein content, we noted that EVs from control cells are closer to EVs from shRalB cells (97 proteins with differential expression) than to EVs from shRalA cells (217 proteins with differential expression). We then focused on the five proteins over-expressed in EVs from shCtl cells compared to both EVs from shRalA and EVs from shRalB cells. These proteins are CD146/MCAM, Clic4, Glypican 4, BDKRB2, and Abcg2. We verified the expression levels of CD146/MCAM, Clic4 and Glypican4 by western blot of identical number of EVs (***Figure 5e***). While Clic4 and Glypican4 are significantly under-expressed in EVs from shRalA or shRalB cells, the long isoform of CD146/MCAM (***Figure 5—figure supplement 2a***) showed a significant decrease in EVs from shRalA cells, and a tendency to decrease in EVs from shRalB cells, which was confirmed by anti-CD146 ELISA (***Figure 5—figure supplement 2b***). The hypothesis that Ral GTPases could control CD146 EV loading is further sustained by colocalization analysis. Indeed, by immunofluorescence, we observed that CD146 localizes both at the plasma membrane and in CD63-positive MVB/late endosomes in 4T1 cells, similarly to Ral GTPases (***Figure 5—figure supplement 2c***). Altogether, content analysis reveals that depletion of either RalA or RalB deeply affects the EV RNA loading and changes the levels of several key proteins.

We next interrogated whether the impact of RalA/B on the lung targeting and priming potential of EVs could be explained by its effect on the EV levels of MCAM/CD146. MCAM/CD146 (also known as Mel-CAM, Muc18, S-endo1, Gicerin) is an adhesion receptor overexpressed in various cancer types, including breast cancer, where it was shown to promote invasion and tumor progression (***Garcia et al., 2007***; ***Zeng et al., 2011***; ***Zeng et al., 2012***). In addition, MCAM/CD146 is present on endothelial cells where it mediates the adhesion of several cell types, including the transendothelial migration of monocytes (***Bardin et al., 2009***). Given, the known function of MCAM/CD146 in cell adhesion (***Wang and Yan, 2013***), we hypothesized that it may, at least in part, be responsible for the lung tropism defects observed with EVs derived from RalA/B-depleted cells. To test the involvement of MCAM/CD146 in EVs adhesion, we treated 4T1 EVs with an anti-mouse MCAM/CD146 blocking antibody before injection in zebrafish or mouse circulation. EVs pretreated with MCAM/

CD146 blocking antibody failed to successfully arrest on endothelial walls of zebrafish embryos (*Figure 5f*) and inefficiently reached the lungs in our mouse model (*Figure 5g*). Finally, we assessed the functional role of EV-bound CD146 in priming of pre-metastatic niches. To do this, 4T1 EVs were pre-treated with MCAM/CD146 blocking antibody (or with an isotype control) and injected intravenously, preceding tail-vein injection of 4T1 luciferase cells. Blocking CD146 on EVs significantly reduced their pro-metastatic potential. Therefore, inhibition of MCAM/CD146 precludes their lung accumulation and the subsequent formation of metastasis and thereby phenocopies RalA/B knockdown. These results demonstrate that MCAM/CD146, whose presence at the surface of EVs is tuned by RalA/B, is, at least partly responsible of the adhesion and lung tropism of 4T1 EVs. It further explains why EVs from RalA knockdown cells, which have reduced levels of MCAM/CD146, fail to reach the lungs efficiently. The pro-metastatic role of MCAM/CD146 is further confirmed by the analysis of a human cohort of breast cancer showing that its high expression is associated with worsened prognosis (*Figure 5h*). Altogether, our work demonstrates that RalA/B, by controlling MVB homeostasis, promote the secretion CD146-enriched EVs, whose lung tropism sustains efficient metastasis (*Figure 5i*).

Discussion

The therapeutic limitations of breast cancer metastasis warrant a deeper understanding of its molecular machinery. Our findings highlight the exosome-mediated priming of metastatic niches by Ral GTPases as a critical requisite for lung metastasis during breast cancer progression. We show that RalA and RalB promote the secretion of exosomes by maintaining a high number of multi-vesicular bodies, likely through the PLD1-PA axis. Furthermore, we demonstrate that RalGTPases favor the secretion of CD146-rich exosomes, which accumulate in metastatic organs, notably in lungs, where they establish premetastatic niches (*Figure 5i*). Finally, we show that high levels of RalA and RalB correlated with poor prognosis suggesting a unified mechanism for human breast cancer metastasis.

This work, together with our previous study of RAL-1 in *C. elegans* (*Hyenne et al., 2015*), establishes Ral GTPases as major evolutionarily conserved mediators of exosome secretion. Our experiments suggest that RalA/B contribute to exosome secretion in several tumor cell lines, of different origins, implying that they might function pleiotropically over various cancers. Our results suggest that RalA/B and their effector PLD1 affect the levels of secreted exosomes by tuning the levels of cytoplasmic MVBs. While Ral GTPases, partially localized at the plasma membrane, could also affect microvesicle secretion, our data indicate that they function in exosome biogenesis upstream of PLD1. Similarly, a direct correlation between MVB density and levels of secreted EVs was recently suggested by studies showing that chemical or electric stimulation of MVB biogenesis results in increased EV secretion (*Kanemoto et al., 2016*; *Yang et al., 2020*). The formation of MVBs results from dramatic biochemical transformations of endosomes involving multiple protein and lipid switches (*Huotari and Helenius, 2011*; *Scott et al., 2014*). Understanding the steps at which RalA/B and PLD affect this endosome maturation program is critical and remains to be fully deciphered. Our results from mice and *C. elegans* suggest that biogenesis of ILVs, which is a key step in MVB maturation and the initial phase of the exosome secretion pathway, could as well be controlled by RalA/B. Our work further identifies PLD as an effector acting downstream of Ral to control exosome secretion. Whether other Ral effectors contribute to EV secretion remains to be addressed. Interestingly, while PLD2 was found to impact exosome secretion by governing ILV biogenesis in a different breast carcinoma cell line (*Ghossoub et al., 2014*), our data rather suggest that PLD1 controls exosome biogenesis in 4T1 cells. Indeed, PLD1 localizes on MVBs and its inhibition, but not the inhibition of PLD2, decreases MVB density. Nevertheless, it should be noted that we measured EV secretion levels and MVB density based on PLD inhibition at previously-published high concentrations of the inhibitors (compared to their respective IC50) and that off-target effect can not be ruled out. By contrast, PLD2 is essentially localized at the plasma membrane of 4T1 cells and its inhibition reduces EV secretion suggesting that PLD2 could rather promote microvesicle secretion in 4T1 cells. Therefore, we speculate that RalA/B-PLD1 control ILV biogenesis in 4T1 cells, possibly through the regulation of PA levels. Alternatively, they could impact the homeostasis of a subclass of MVBs, for instance by controlling their stability or their degradation.

Priming of metastatic niches by (soluble or) EV-mediated factors takes central stages in cancer progression (*Gao et al., 2019*; *Peinado et al., 2017*) and identification of molecular machineries

that underlie this condition could point to new therapeutic or diagnostic targets. Our study demonstrates that Ral GTPases enhance the formation of lung metastasis in mouse models, by promoting the secretion of exosomes within primary tumors, while RalA/B expression levels correlates with metastasis in human breast cancer. While the pro-tumoral activity of Ral GTPases was so far mostly attributed to their capacity to promote anchorage-independent cell growth (for RalA) or cell invasion (for RalB) (**Yan and Theodorescu, 2018**), we now show that Ral GTPases have additional non-cell autonomous functions, and that these functions are important contributors to metastasis. Indeed, in 4T1 cells, depletion of either RalA or RalB alters the levels, content and functionality of secreted EVs, without decreasing cell migration or proliferation. Depending on the cell type or the biological process, RalA and RalB can display redundant, synergistic or even antagonist activities (**Gentry et al., 2014**). Since RalA and RalB mostly share similar phenotypes regarding EV secretion, content and function, they likely function in the same pathway. Interestingly, both Ral proteins appear to be essential for exosome secretion, revealing that their functions are not fully redundant. Therefore, both GTPases are required for the generation of a specific subpopulation of EVs with enhanced pro-metastatic properties and further work is needed to fully unravel the downstream molecular pathways. With this work, RalA and RalB add to the list of proteins known to control exosome secretion and to affect tumor progression, such as Rab27a (**Bobrie et al., 2012**; **Kren et al., 2020**; **Peinado et al., 2012**), Alix (**Monypenny et al., 2018**), syntenin (**Das et al., 2019**), and components of the ESCRT machinery (**Mattissek and Teis, 2014**). These studies demonstrate that the number of EVs secreted by a primary tumor is an essential element determining the efficiency of metastasis. However, it is important to keep in mind that all these proteins regulating EV trafficking, including RalA/B, contribute to tumor progression through both exosome dependent and exosome independent functions. Altogether, despite pointing to additional functions of RAL GTPases, our study is the first to identify new molecular machinery from its function in EV biogenesis up to its pro-metastatic function in breast cancer lung metastasis.

Priming of metastatic niches by EVs has, so far, mostly been attributed to increased levels of pro-metastatic EVs with pro-metastatic functions (**Becker et al., 2016**; **Bobrie et al., 2012**; **Peinado et al., 2012**). In addition to controlling the levels of secreted EVs, we show that RalA/B affect their function by enhancing their capacity to induce endothelial permeability *in vitro* and pre-metastatic niches *in vivo*. These two observations could be linked, as RalA/B-dependent EVs could promote endothelial permeability locally in the primary tumor or at distance in lungs, thereby favoring both tumor intravasation and extravasation. Content analysis revealed that RalA/B control the identity and levels of RNAs and proteins present in secreted EVs. Interestingly, Ras, which is known to activate RalA/B (**Gentry et al., 2014**), also controls the protein and RNA cargo of tumor EVs (**Cha et al., 2015**; **Demory Beckler et al., 2013**; **McKenzie et al., 2016**), although its effect on the levels of secreted EVs is unclear (**Demory Beckler et al., 2013**; **McKenzie et al., 2016**). As McKenzie and collaborators identified a MEK-ERK-Ago2 pathway downstream of Ras (**McKenzie et al., 2016**), it would be interesting to determine how this pathway connects with the Ral-PLD-PA axis described in our study. Among the few proteins significantly enriched in RalA/B-dependent EVs, we identified CD146, a molecule known to modulate cell-cell adhesion (**Wang and Yan, 2013**). We showed, using functional inhibition, that CD146 present on pro-metastatic EVs controls their lung targeting efficiency thereby impacting their biodistribution and niche-promoting function. Accordingly, we and others show that high expression of CD146 correlates with poor prognosis in human breast carcinoma (**Garcia et al., 2007**; **Zeng et al., 2012**). CD146 functions as an adhesion molecule involved in homophilic and heterophilic interactions (**Wang and Yan, 2013**), promoting for instance monocyte transmigration (**Bardin et al., 2009**). CD146 can perform trans-homophilic interactions via its immunoglobulin-like extracellular domain (**Taira et al., 1994**; **Taira et al., 2005**). It also binds to extracellular matrix proteins or other transmembrane proteins, such as VEGFR2 (**Wang and Yan, 2013**). Therefore, it is tempting to speculate that CD146 affects the biodistribution and organ targeting efficiency of circulating tumor EVs by mediating their interaction with specific ligands present on the luminal side of endothelial cells of metastatic organs. Other adhesion molecules, such as integrins and tetraspanins were shown to affect the biodistribution of tumor EVs and ultimately the formation of metastasis (**Hoshino et al., 2015**; **Yue et al., 2015**). Therefore, it is likely that the combination of these receptors at the surface of tumor EVs, combined with the differential expression of their ligands on endothelial cells throughout the organism will dictate their homing. More work will be needed to characterize this organ specific EV zip code and to identify relevant endothelial ligands

for circulating EVs and develop inhibitory strategies to impair their arrest and uptake at metastatic sites. In addition, the presence of other cell types in the circulation, such as patrolling monocytes, which take up large amounts of circulating EVs, could also contribute to the accumulation of tumor EVs in specific organs (**Hyenne et al., 2019**; **Plebanek et al., 2017**). Finally, other factors, such as the vascular architecture and hemodynamic patterns could be involved (**Follain et al., 2020**; **Hyenne et al., 2019**) and the interplay between these mechanical cues and the surface repertoire of metastatic EVs should be a fertile ground for future research. Precisely dissecting the mechanisms by which tumor EVs reach specific organs would allow to understand the priming of premetastatic niches.

Overall, our study identifies RalA/B GTPases as a novel molecular machinery that regulates the formation and shedding of pro-metastatic EVs. We also discovered CD146 as an EV cargo whose targeting could inspire new therapeutic strategies to impact the progression of metastatic breast cancer.

Materials and methods

Cell culture

The establishment of 4T1 cell lines stably expressing shRNA against RalA, RalB, or a scramble sequence has been described previously (**Hyenne et al., 2015**). 4T1-Luciferase (RedLuc) cells were purchased from Perkin-Elmer. All 4T1 cell lines were cultured in RPMI-1640 medium, completed with 10% fetal bovine serum (FBS, Hyclone) and 1% penicillin-streptomycin (PS) (GIBCO). 4T1 shRNA cell lines were maintained in medium containing 1 µg/ml puromycin, except during experiments, and regularly checked for the stability of knockdown by western blots. Human Umbilical Vein Endothelial Cells (HUVEC) (PromoCell) were grown in ECGM (PromoCell) supplemented with a supplemental mix (PromoCell C-39215) and 1% PS. Human A375 melanoma and human MDA-MB-231, MCF7 and SKBR3 breast cancer (ATCC) cell lines were grown in high-glucose Dulbecco's modified Eagle's Medium (DMEM, Gibco Invitrogen Corporation) supplemented with 10% (FBS) and 1% PS. D2A1 cell were grown in high-glucose Dulbecco's modified Eagle's Medium (DMEM, Gibco Invitrogen Corporation) supplemented with 5% (FBS), 5% new born calf serum, 1% non-essential amino acids, and 1% PS. Human Panc-1 pancreatic adenocarcinoma cell line was grown in RPMI-1640 supplemented with 10% FBS, and 50 µg/ml gentamicin sulfate (Gibco/Life Technologies). All cell lines were cultured in a humidified atmosphere containing 5% CO_2 at 37˚C and checked regularly for absence of mycoplasma by PCR (VenorGeM, Clinisciences).

Plasmid transfections

Cells at 50–70% confluency were transfected with 1 µg of plasmid using JetPRIME (PolyPlus, Illkirch, France) according to the manufacturer's instructions. The following plasmids were used: pGFP-PLD1, pGFP-PLD2 (**Corrotte et al., 2006**), pLenti CMV:tdtomato-RalA, and pLenti CMV:tdtomato-RalB.

Drug treatment

Cells were incubated with the following drugs in the appropriate medium: RalA/B inhibitors BQU57 (10 µM; Sigma) and RBC8 (10 µM; Sigma), PLD1 inhibitor CAY10593 (10 µM; Santa Cruz Biotechnology) or PLD2 inhibitor CAY10594 (10 µM; Santa Cruz Biotechnology). Cells were treated for 18 hr before processing for EV isolation or cell analysis.

qRT-PCR analysis

Total RNA was extracted from cells using TRI Reagent (Molecular Research Center) according to the manufacturer's instructions. For qRT-PCR, RNA was treated with DNase I and reverse transcribed using the High-Capacity cDNA RT Kit. qRT-PCR was performed using the Power SYBR Green PCR Master Mix or TaqMan Gene Expression Master Mix using a 7500 Real-Time PCR machine (Applied Biosystems). All compounds were purchased from Life Technologies (St Aubin, France). Data were normalized using a Taqman mouse probe against GADPH as endogenous control (4333764T, Life Technology) and fold induction was calculated using the comparative Ct method (-ddCt).

Western blot

Cell or EV extracts were denatured in Laemmli buffer and incubated at 95˚C for 10 min. 10 µg of protein extract (for cell lysates) or equal number of EVs (8.50×10^8 EVs per lane, measured by NTA) were loaded on 4–20% polyacrylamide gels (Bio-Rad Laboratories, Inc). The following antibodies were used: CD9 (Rat, 553758; BD Biosciences), RalA (mouse, 610221; BD Biosciences), RalB (mouse, 04037; Millipore), Glypican 4 (Rabbit, PA5-97801; Thermo Fisher Scientific), antibodies specifically recognizing the short and long isoforms of CD146 were previously described (***Kebir et al., 2010***), Clic4 (mouse, 135739; Santa Cruz Biotechnology), α-tubulin (mouse, CP06; Millipore) and Secondary horseradish peroxidase-linked antibodies: anti-Rat (GE healthcare; NA935), anti-Mouse (GE healthcare; NA 931) and anti-rabbit (GE healthcare; NA934). Acquisitions were performed using a PXi system (Syngene). Intensities were measured using the Fiji software.

Elisa

Elisa was performed according to the manufacture's instruction (RayBiotech) by loading equal number of EVs (7×10^8 - 9.5×10^9) per well (two experiments in triplicate).

Electron microscopy

Chemical fixation

Cells were fixed with 2.5% glutaraldehyde/2.0% paraformaldehyde (PFA) (Electron Microscopy Sciences) in 0.1M Cacodylate buffer at room temperature for 2 hr, then rinsed in 0.1M Cacodylate buffer (Electron Microscopy Sciences) and post-fixed with 1% OsO4 (Electron Microscopy Sciences) and 0.8% $K_3Fe(CN)_6$ (Sigma-Aldrich) for 1 hr at 4˚C. Then, samples were rinsed in 0.1M Cacodylate buffer followed by a water rinse and stained with 1% uranyl acetate, overnight at 4˚C. The samples were stepwise dehydrated in Ethanol (50%, 70% 2 × 10 min, 95% 2 × 15 min and 100% 3 × 15 min), infiltrated in a graded series of Epon (Ethanol100%/Epon 3/1, 1/1, 1 hr) and kept in Ethanol100%/Epon 1/3 overnight. The following day, samples were placed in pure Epon and polymerized at 60˚C. One hundred nm thin sections were collected in 200 copper mesh grids and imaged with a Philips CM12 transmission electron microscope operated at 80 kV and equipped with an Orius 1000 CCD camera (Gatan).

High-pressure freezing

HPF was performed using an HPF COMPACT 03 high pressure freezing machine (Wohlwend), using 3 mm diameter Aclar film disks (199 um thickness), as cell carriers. Subsequent freeze substitution in acetone was performed using an automatic FS unit (Leica AFS), including 0.25% OsO4 staining, and Epon embedding. Sections were contrasted on grids with 1% uranyl acetate followed with 0,4% lead citrate (Sigma-Aldrich). Imaging was performed similarly to chemical fixation.

The number of MVBs and lysosomes per surface of cytoplasm were quantified using the Fiji software. MVBs and lysosomes were distinguished based on their morphology: MVBs have one or more ILVs and lysosomes contain ILVs but are also electron dense and contain irregular membrane curls.

FACS analysis

For cell cycle analysis, 10^6 cells were fixed using the FoxP3 Staining Kit (00-5523-00 eBioscience) for 30 min at room temperature in the dark. Samples were then resuspended in permeabilization buffer containing 20 µg of RNase A (R6513 Sigma) and 1 µg of propidium iodide (PI) (130-093-233 Miltenyi Biotech) for 30 min. PI fluorescence was analyzed using a BD Accuri C6 cell analyzer with BD CSampler Analysis Software. Results were analyzed with FlowJo software version 10 (TreeStar).

For lysosomal analysis, confluent cells were incubated with 1 µM Lysotracker Green DND 26 (L7526-Thermo Fischer) diluted in complete RPMI medium for 30 min at 37˚C. Cells were then detached by addition of TrypLE (12604021, ThermoFischer), washed in PBS 2% (v/v) FCS, and stained with 0.1 µM DAPI in PBS 2% (v/v) FCS immediately before analysis. Samples were processed on a Gallios Flow Cytometer (Beckman Coulter). Dead cells and doublets were excluded from analysis respectively by the selection of DAPI negative cells and co-analysis of integral vs time-of-flight side scatter signals. Data were analyzed on FlowJo software (BD Bioscience). Mean Fluorescence intensities (MFI) of lysotracker in each condition were normalized by performing a ratio with MFI of an unstained condition in the same channel.

Migration assays

For 2D migration assays, 4T1 mammary tumor cells were plated on 35 mm plastic dishes (six-well plates) and grown for 2 days until reaching 90% confluence. The cells were then grown for 16 hr in serum-free medium before wounding of the monolayer by scraping from the middle of the plate. Cells were incubated in complete RPMI medium and sequential images of the wound were collected with a ×10 objective at 0, 8, and 24 hr after wounding. Percentage of wound closure over time was analyzed and quantified using the Fiji software.

3D Organotypic invasion assays were conducted as previously described (***Timpson et al., 2011***; ***Vennin et al., 2017***). Briefly, rat tail tendon collagen was extracted with 0.5 mol/L acetic acid to a concentration of 2.5 mg/ml. A total of 8.4×10^4 telomerase immortalized fibroblasts (TIFs) were embedded into the neutralized collagen in the presence of 1 x MEM and 8.8% FBS. Matrices were allowed to contract over a 12-day period in DMEM (1% P/S, 10% FBS). Following contraction TIFs were removed with puromycin (2 µg/ml) for 72 hr before 8×10^4 4T1 cells were seeded on the contracted matrices and allowed to grow to confluence for 48 hr in RPMI (1% P/S, 10% FBS). The matrices were then transferred to an air-liquid interface on a metal grid and cells allowed to invade for 15 days with media changes every 2 days. Following the invasion, organotypic matrices were fixed in 10% buffered formalin and processed for histochemical analysis. The invasive index was measured in three representative fields of view per matrix with three matrices per replicate for three replicates.

$$\text{Invasive Index} = \frac{\text{Number of cells} > 200\ \mu\text{m depth}}{\text{Cells on top of the matrix}}$$

In vitro permeability assay

Transwell filter inserts (pore size 1.0 µm, 12 mm diameter, polyester membrane, Corning, New York, USA) were coated with fibronectin (10 µg/ml; Sigma). Then, HUVECs were seeded (0.3×10^6 cells/well) and grown on transwell filters for 48 hr until reaching confluency. Confluent monolayers of HUVEC cells were treated with similar amounts (10–100 µg) of 4T1-EVs, PBS (as a negative control) or with 100 ng/ml TNF-α (as a positive control) overnight. FITC-dextran (MW ~70,000; Sigma) was added to the top well at 25 mg/ml for 20 min at 37˚C, and fluorescence was measured in the bottom well using a fluorescence plate reader (Berthold Tris Star 2; 485 nm excitation and 520 nm emission). Cells were washed for three times and were fixed for immunofluorescence (described below).

Secretome analysis

Cell culture supernatants were collected and centrifuged for 15 min at 300 g. Supernatants were incubated with Mouse XL Cytokine Array membranes (R and D Systems) according to the manufacturers' instructions. Three independent experiments were performed. Intensities were measured using the Fiji software.

In vitro proliferation assay

Briefly, cells were seeded in 96-well plates at the density of 2000 cells per well with 200 µl of complete culture medium and cultured for 24, 48, and 72 hr at 37˚C. Culture medium without cells was used as the blank control group. To avoid the edge effect, the peripheral wells were filled with sterile PBS. For the proliferation test, a total of 20 µl MTS solution was added to each well, followed by incubation for 2 hr at 37˚C. Optical density was measured at 490 nm using a Berthold Tristar device.

EVs isolation and characterization

Cells were cultured in EV-depleted medium (obtained by overnight ultracentrifugation at 100,000 g, using a Beckman, XL-70 centrifuge with a 70Ti rotor) for 24 hr before supernatant collection. The extracellular medium was concentrated using a Centricon Plus-70 centrifugal filter (10 k; Millipore) and EVs were isolated by successive centrifugation at 4˚C: 15 min at 300 g, 10 min at 2000 g, 30 min at 10,000 g and 70 min at 100,000 g (using a Beckman XL-70 centrifuge with a SW28 rotor). EVs pellets were washed in PBS, centrifuged again at 100,000 g for 70 min, resuspended in PBS and stored at 4˚C. For all functional experiments, EVs were used immediately after isolation or stored overnight at 4˚C and injected the next day. For content analysis, EVs were frozen at −80˚C. After EV isolation, EVs numbers and size distribution were measured by NTA using a ZetaView (Particle Metrix, Meerbusch, Germany).

For *in vivo* mouse experiments, EVs were isolated the using the iZON qEV2 size exclusion column (Izon science, Cambridge MA) according to the manufacturer's instructions. After rinsing the columns with PBS, 2 ml of concentrated extracellular medium were applied on top of a qEV column (Izon Science) and 6 ml fractions were collected. For organotropism experiments, four EV-rich fractions (F2, F4, F6, and F8) were pooled, then ultracentrifuged for 1 hr at 100,000 ×g, 4˚C with a SW28 rotor in a Beckman XL-70 centrifuge or concentrated using an Amicon Ultra-4 10 kDa centrifugal filter device (Merck Millipore). Pellets were resuspended in 500 µl PBS. For priming experiment, the most EV-rich fraction was used (F4).

For fluorescent labeling, isolated EVs were incubated with MemBright-Cy3 or Cy5 (**Collot et al., 2018**) at 200 nM (zebrafish) and 500 nM (mice) (final concentration) in PBS for 30 min at room temperature in the dark. Labeled EVs were then rinsed in 15 ml of PBS, centrifuged at 100,000 g with a SW28 rotor in a Beckman XL-70 centrifuge and pellets were resuspended in 50 µl PBS. EVs were used immediately after isolation or stored for a maximum of one night at 4˚C before use.

Mass spectrometry-based proteomics experiments

Sample preparation of EVs Proteins. A total of 20 mg samples were denatured at 95˚C for 5 min in Laemmli buffer and concentrated in one stacking band using a 5% SDS-PAGE gel. The gel was fixed with 50% ethanol/3% phosphoric acid and stained with colloidal Coomassie Brilliant Blue. The gel bands were cut, washed with ammonium hydrogen carbonate and acetonitrile, reduced and alkylated before trypsin digestion (Promega). The generated peptides were extracted with 60% acetonitrile in 0.1% formic acid followed by a second extraction with 100% acetonitrile. Acetonitrile was evaporated under vacuum and the peptides were resuspended in 10 µl of H20% and 0.1% formic acid before nanoLC-MS/MS analysis.

NanoLC-MS/MS analysis. NanoLC-MS/MS analyses were performed on a nanoACQUITY Ultra-Performance LC system (Waters, Milford, MA) coupled to a Q-Exactive Plus Orbitrap mass spectrometer (ThermoFisher Scientific) equipped with a nanoelectrospray ion source. The solvent system consisted of 0.1% formic acid in water (solvent A) and 0.1% formic acid in acetonitrile (solvent B). Samples were loaded into a Symmetry C18 precolumn (0.18 × 20 mm, 5 µm particle size; Waters) over 3 min in 1% solvent B at a flow rate of 5 µl/min followed by reverse-phase separation (ACQUITY UPLC BEH130 C18, 200 mm x 75 µm id, 1.7 µm particle size; Waters) using a linear gradient ranging from 1% to 35% of solvent B at a flow rate of 450 nl/min. The mass spectrometer was operated in data-dependent acquisition mode by automatically switching between full MS and consecutive MS/MS acquisitions. Survey full scan MS spectra (mass range 300–1800) were acquired in the Orbitrap at a resolution of 70K at 200 m/z with an automatic gain control (AGC) fixed at 3.10^6 and a maximal injection time set to 50 ms. The 10 most intense peptide ions in each survey scan with a charge state $\geq$2 were selected for fragmentation. MS/MS spectra were acquired at a resolution of 17.5K at 200 m/z, with a fixed first mass at 100 m/z, AGC was set to 1.10^5, and the maximal injection time was set to 100 ms. Peptides were fragmented by higher energy collisional dissociation with a normalized collision energy set to 27. Peaks selected for fragmentation were automatically included in a dynamic exclusion list for 60 s. All samples were injected using a randomized and blocked injection sequence (one biological replicate of each group plus pool in each block). To minimize carry-over, a solvent blank injection was performed after each sample. EVs mass spectrometry was performed in triplicate.

Data interpretation. Raw MS data processing was performed using MaxQuant software1 v1.6.7.0 (**Cox et al., 2014**). Peak lists were searched against a database including *Mus musculus* protein sequences extracted from SwissProt (09-10-2019; 17 007 sequences, Taxonomy ID = 10 090). MaxQuant parameters were set as follows: MS tolerance set to 20 ppm for the first search and five ppm for the main search, MS/MS tolerance set to 40 ppm, maximum number of missed cleavages set to 1, Carbamidomethyl (C) set as a fixed modification, Oxidation (M) and Acetyl (Protein N-term) set as variable modifications. False discovery rates (FDR) were estimated based on the number of hits after searching a reverse database and were set to 1% for both peptide spectrum matches (with a minimum length of seven amino acids) and proteins. All other MaxQuant parameters were set as default. Protein intensities were used for label-free quantification. The imputation of the missing values (DetQuantile imputation) and differential data analysis were performed using the open-source ProStaR software (**Wieczorek et al., 2017**). A Limma moderated t-test was applied on the dataset to perform

differential analysis. The adaptive Benjamini-Hochberg procedure was applied to adjust the p-values and FDR values under 1% were achieved.

Complete dataset has been deposited to the ProteomeXchange Consortium via the PRIDE partner repository5 with the dataset identifier PXD020180 (**Deutsch et al., 2020**).

RNA sequencing

EV pellets were treated with proteinase K (0.05 µg/µl) for 10 min at 37˚C. Roche Cocktail Inhibitor was then added to the sample for 10 min at room temperature followed by incubation at 85˚C for 5 min. Samples were then incubated with RNase A (0.5 µg/µl) for 20 min at 37˚C to degrade unprotected RNA. Total RNAs of isolated EVs was extracted using TRI Reagent (Molecular Research Center). Total RNA Sequencing libraries were prepared with SMARTer Stranded Total RNA-Seq Kit v2 - Pico Input Mammalian (TaKaRa) according to the manufacturer's instructions. Libraries were pooled and sequenced (paired-end 2*75 bp) on a NextSeq500 using the NextSeq 500/550 High Output Kit v2 according to the manufacturer's instructions (Illumina, San Diego, CA, USA). Raw sequencing data generated by the Illumina NextSeq500 instrument were mapped to the mouse reference genome using the hisat2 software (**Kim et al., 2015**). For every sample, quality control was carried out and assessed with the NGS Core Tools FastQC (http://www.bioinformatics.babraham.ac.uk/projects/fastqc/). Read counts were generated with the htseq-count tool of the Python package HTSeq (**Anders et al., 2015**). Differential analysis was performed by the DESEQ2 (**Love et al., 2014**) package of the Bioconductor framework. Detection of significantly up- and down-regulated genes between pairs of conditions based on their log2FC and functional enrichment analyses were performed using STRING v11 (**Szklarczyk et al., 2019**). EVs RNA sequencing was performed in triplicate.

Lipidomics

EVs were extracted with 2 ml of chloroform/methanol 2/1 v/v and 1 ml water, sonicated for 30 s, vortexed, and centrifuged. Lower organic phase was transferred to a new tube, the upper aqueous phase was re-extracted with 2 ml chloroform. Organic phases were combined and evaporated to dry. Lipid extracts were resuspended in 50 µl of eluent A. Synthetics internals lipid standards (PA 14:1/17:0, PC 17:0/14:1 and PS 17:0/17:0) from Avanti Polar Lipids was added. LC-MS/MS (MRM mode) analyses were performed with a MS model QTRAP 6500 (ABSciex) coupled to an LC system (1290 Infinity II, Agilent). Analyses were achieved in the negative (PA) and in positive (PC) mode; nitrogen was used for the curtain gas (set to 20), gas 1 (set to 20) and gas 2 (set to 10). Needle voltage was at − 4500 or 5500 V without needle heating; the declustering potential was adjusted set at − 172 V or + 40 V. The collision gas was also nitrogen; collision energy is set to − 46 or + 47 eV. The dwell time was set to 30 ms. Reversed phase separations were carried out at 50˚C on a Luna C8 150 × 1 mm column, with 100 Å pore size, 5 µm particles (Phenomenex). Eluent A was isopropanol/CH_3OH/H_2O (5/1/4) +0.2% formic acid+0.028% NH_3 and eluent B was isopropanol+0.2% formic acid+0.028% NH_3. The gradient elution program was as follows: 0–5 min, 30–50% B; 5–30 min, 50–80% B; 31–41 min, 95% B; 42–52 min, 30% B. The flow rate was set at 40 µl/min; 15 µl sample volumes were injected. The areas of LC peaks were determined using MultiQuant software (v3.0, ABSciex) for PA and PC quantification. EVs lipid analysis was performed in triplicate.

Animal experiments

All animals were housed and handled according to the guidelines of INSERM and the ethical committee of Alsace, France (CREMEAS) (Directive 2010/63/EU on the protection of animals used for scientific purposes). Animal facility agreement number: #C67-482-33. Experimental license for mice: Apafis #4707–20 l6032416407780; experimental license for zebrafish: Apafis #16862–2018121914292754.

Mouse experiments

Six- to 8-week-old female BalB/c mice (Charles River) were used in all experiments.

Orthotopic breast tumor experiments: Syngenic BalB/c mice were injected in the left fourth mammary gland with 250,000 4T1 mammary tumor cells stably expressing either scramble control shRNA, RalA shRNA, or RalB shRNA and diluted in 50 µl PBS. When tumors became palpable, tumor volume

was assessed by caliper measurements using the formula (width^2 × length)/2 (mm^3) twice a week for 41 days. At the endpoint of the experiment, tumors and lungs were harvested, weighted, and fixed in formaldehyde. Alternatively, organs were embedded in OCT and frozen at −80˚C. In this case, lungs were inflated with OCT before dissection.

Priming experiments

Mice were injected retro-orbitally with 1.5 × 10^8 EVs isolated from 4T1-shControl, shRalA and shRalB cells. Two injections of EVs were performed 2 days apart. PBS was used as a negative control. Subsequently, 4T1-luciferase cells (90.000) were injected via tail vein one day after EV pre-conditioning. After cells injection, the extent of lung metastasis was measured every 3 days for 12 days using non-invasive imaging with IVIS Lumina III (Perkin Elmer). In brief, a D-luciferin solution (purchased from Perkin Elmer and used at 150 mg/kg, according to manufacturer's instructions) was injected intraperitoneally to the isofluorane (Zoetis) anesthetized mice. 5 min after luciferin injection, a bioluminescence image was acquired with an IVIS Lumina III (Perkin Elmer) imaging system and then analyzed using the Living Image software (Perkin Elmer). The rate of total light emission of the lung metastatic area was calculated and expressed as radiance photons counted during the whole acquisition time (5 min) and normalized to the initial radiance photon (photon/second/cm^2/sr) measured immediately after 4T1- luciferase cells injection for each mouse (t0).

EV biodistribution

Mice were injected via retro-orbital venous sinus with 1–4 × 10^8 MenBright-Cy3-labeled EVs freshly isolated from 4T1-shControl, shRalA, and shRalB cells. PBS was used as a negative control. Mice were sacrificed 1 hr post-injection to quantify the fluorescence intensity of the organs ex vivo with IVIS Lumina III (Perkin Elmer). Average of fluorescent photons per lung were quantify as radiant efficiency [photon/second/cm^2/sr] / [µW/cm^2]. For experiment testing the role of CD146 in EV biodistribution, isolated EVs were incubated with CD146 blocking antibody (EPR3208; Abcam; 12 µg/ml) for 30 min at room temperature before injection. For metastasis priming experiments, CD146 was blocked similarly and a rabbit IgG isotype was used as control (Abcam) at an equivalent concentration.

Zebrafish experiments

At 48 hr post-fertilization (hpf), Tg(Fli1 :GFP) zebrafish embryos were dechorionated and mounted in 0.8% low melting point agarose pad containing 650 mM of tricaine (ethyl-3-aminobenzoate-methanesulfonate). Embryos were injected in the duct of Cuvier with 27.6 nl of Membright Cy5-labeled EVs (at 10^{10} EVs/ml) freshly isolated from 4T1-shControl, shRalA, and shRalB cells with a Nanoject microinjector 2 (Drummond) under a M205 FA stereomicroscope (Leica), using microforged glass capillaries (25–30 mm inner diameter) filled with mineral oil (Sigma). Embryos were imaged with confocal right after injection. For experiment testing the role of CD146, 4T1-isolated EVs were incubated with CD146 blocking antibody (12 µg/ml) for 30 min at room temperature before injection.

Tissue section and staining

Mouse lungs were incubated overnight in 4% PFA, dehydrated in 100% ethanol for 24 hr, embedded in paraffin, cut in 7-µm-thick sections, dewaxed and rehydrated with 100% Toluene (two washes of 15 min) then incubated in 100–70% alcohol solutions (10 min each) followed by final staining with hematoxylin (Surgipath) for 5 min and washing with tap water. Sections were further processed with differentiation solution (1% HCl in absolute ethanol, for 7 s), followed by washing under tap water for 10 min. Sections were then incubated in eosin (Harris) for 10 s, rinsed and dehydrated in 70–100% alcohol baths with rapid dips in each bath before a final wash in toluene for 15 min and embedded in Eukitt solution (Sigma). Two random distanced sections taken in each of the five lung were analyzed for each mouse. Stitching imaging was performed using an AxioImager (Zeiss) with a ×10 objective. Metastatic surfaces and whole lung surfaces were measured using the Fiji software.

Caspase 3/7 assay

Mouse tumor samples stored at −80˚C are disrupted in a buffer containing Tris HCl pH 7.5, 50 mM, NaCl 150 mM, NP40 1% + Protease Inhibitors cocktail (Complete from Roche) in the presence of 4

zirconium beads, using the Precellis system (Bertin instruments) with two pulses (10'') at 5000 rpm. Protein concentration was measured using Bradford kit (BioRad) and 5 µg was analyzed using the Caspase 3/7 glo kit (Promega) according to manufacturer's instructions. Photons production generated by the luciferase was measured using a luminometer (Berthold Tris Star 2).

Immunofluorescence

For immunofluorescence on cultured cells, cells were fixed with 4% PFA for 15 min, permeabilized in PBS-Triton 0.1% (Sigma) for 10 min and incubated in 5% normal goat serum for 1 hr. The following primary antibodies were used: ZO-1 (Rabbit, 61–7300; Thermo Fisher Scientific), VE-Cadherin (mouse, 348502; BioLegend), CD63 (rat, D623-3; MBL), RalA (mouse, 610221; BD), RalB (mouse, 04037; Millipore), CD146 (Mouse, P1H12, Thermofisher). The following secondary antibodies were used: goat anti-mouse/rat/rabbit coupled with Alexa Fluor 488, Alexa 555, or Alexa 647 (Invitrogen). Cells were mounted with DAPI-containing Vectashield (Vector Laboratories).

For immunofluorescence on tissue sections, tissues were cut in 7-µm-thick sections, dewaxed for paraffin-embedded tissues and air-dried for frozen tissues. Sections were incubated first in 5% normal goat serum for 2 hr in a humidified container. The following antibodies were used: CD31 (Mouse, 37–0700; Thermo Fisher Scientific), S100A4 A gift from Nona Ambartsumian (Institut for Cancer Biology, Copenhagen, DK-2100, Denmark.), F4/80 (Rat, ab6640; abcam), rabbit monoclonal antibody against Ki67 (Rabbit, RM-9106-S0; Thermo Fisher Scientific), and caspase-3 (Mouse, 966S1; Cell Signaling Technology). Secondary antibodies were similar to the ones used with cells. Nuclei were stained with DAPI (Sigma).

Imaging and analysis

Imaging on fixed samples. Tissue and cell sections were imaged with a Zeiss Imager Z2 with a ×40 objective (N.A. 1.4) or with an SP5 confocal (Leica) with a ×63 objective (N.A. 1.25). Image analysis and processing were performed using the Fiji software. For endothelial adherent and tight junction analysis, 10 random junctions were analyzed per image (five images per sample) measuring junction width. For Ki67 and Caspase3 imaging, 15 random fields of view were quantified per sample. For EVs imaging, 40–60 random fields of view were imaged on three to four sections per mouse.

Live-cell imaging. For live-cell imaging, cells were seeded on 3.5 cm diameter glass-bottom dishes (MatTek Corporation, Ashland, MA) pre-coated with fibronectin (10 µg/ml; Sigma). Nuclei were labeled with NucBlue Live Ready Probe (Life Technologies, Grand Island, NY). In some experiments, cells were incubated with Lysotracker Deep Red (Thermo Fisher Scientific) at 1 µM for 30 min before imaging. Cells were imaged by confocal microscopy (SP5, Leica) equipped with a thermostated chamber at 37˚C with 5% CO_2. Image analysis and processing were performed using the Fiji software.

HUVEC cells were seeded in fibronectin (10 µg/ml; Sigma) pre-coated glass bottom culture chambers (LabTek I, Dutscher 055082). Confluent cells were incubated with 2×10^8 MemBright-labeled EVs in ECGM EV-free medium for 1 hr. Nucleus were labeled using NucBlue (Life Technologies, Grand Island, NY). Cells were imaged by confocal microscopy (SP5 Leica) in a thermostated chamber at 37˚C with 5% CO_2.

Zebrafish imaging: Confocal imaging was performed on the caudal plexus of zebrafish embryos right after injection with an inverted TCS SP5 with HC PL APO 20X/0,7 IMM Corr CS objective (Leica). Image analysis and processing were performed using the Fiji software.

Human samples

Human databases: Kaplan-Meier survival curves and statistical analysis of overall survival and gene expression was assessed on the TCGA breast invasive carcinoma cohort (1097 patients) using data generated by the TCGA Research Network: https://www.cancer.gov/tcga.

Immunohistochemistry

Paraffin sections of 4 µm from metastasic and non-metastasic breast tumours were obtained from CRB-Tumorothèque of the Institut de Cancérologie de l'Ouest (ICO, Saint-Herblain, France) (***Heymann et al., 2020***). Immunohistochemsitry was performed using RalA (BD Transduction #610222, 1/100) and RalB (Sigma WH0005899, 1/400) antibodies on MicroPICell facility (Nantes,

France) Citrate buffer pH6 was used for antigen retrieval 20 min at 96˚C (Target Retrieval solution low pH, Dako) and DAB and Hematoxylin staining were revealed using ImPath detection kit (DAB OB Sensitive Detection Kit, ImPath). Whole slides were scanned on Hamamatsu scanner using Nanozoomer Digital Pathology software. Automated computer quantification of DAB staining in perinuclear zones (brown intensity measurement) after automatic nuclei detection with hematoxylin staining in the whole biopsies was performed using Qupath open source software for digital pathology image analysis (***Bankhead et al., 2017***) on MicroPICell platform (Nantes, France). Quantification was further confirmed by manual blinded arbitrary scoring of DAB brown intensity in tumoral zones was performed using a score of 1 for low staining to score of 3 for intense staining.

Statistical analyses

All results were confirmed in at least two independent experiments. Statistical significance of results was analyzed using the GraphPad Prism program version 5.04. The Shapiro-Wilk normality test was used to confirm the normality of the data. The statistical difference of Gaussian data sets was analyzed using the Student unpaired two-tailed t test, with Welch's correction in case of unequal variances and the one-way ANOVA test followed by a Bonferonni multiple comparison post-test was used for multiple data comparison. For data not following a Gaussian distribution, the Mann-Whitney test was used, and the Kruskal-Wallis test followed by Dunn's Multiple Comparison post-test was used for multiple data comparison. Two Way Anova was used to compare more than one parameters followed by Bonferonni post-test. For analyzing data containing only three measurements, One-Way Anova permutation test followed pairwise permutation test with false detection rate (fdr) correction, using R software (version 3.6.2) was used. Illustrations of these statistical analyses are displayed as the mean +/- standard deviation (SD). p-Values smaller than 0.05 were considered as significant. *, $p<0.05$, **, $p<0.01$, ***, $p<0.001$, ****, $p<0.0001$.

Acknowledgements

We thank all members of the Goetz Lab for helpful discussions, in particular Florent Colin for careful reading, as well as Gregory Khelifi and Camille Hergott for animal care. We thank the CRB-Tumorothèque of the Institut de Cancérologie de l'Ouest (ICO, Saint-Herblain, France) and the Cellular and Tissular Imaging Core Facility of Nantes University MicroPICell (SFR-Santé, Nantes, France). We thank Mayeul Collot and Andrey Klymchenko (UMR 7021) for providing the MemBright dye. We thank Monique Dontenwill (CNRS 7213, Strasbourg, France) and Hector Peinado (CNIO, Madrid Spain) for help and discussions. This work was supported by a fellowship from IDEX (University of Strasbourg) and ARC (Association pour le Recherche sur le Cancer) to SG; by grants from La Ligue contre le Cancer, Canceropole Grand-Est, INCa (PLBIO19-291), Plan Cancer (Nanotumor) and Roche to JGG; and by institutional funds from University of Strasbourg and INSERM to JGG, and ANR (to CC, French Proteomics Infrastructure ProFI, ANR-10-INBS-08–03; to NV, ANR-19-CE44-0019). The Metabolome Bordeaux facility was supported by the grant MetaboHUB-ANR-11-INBS-0010. PT and KM were supported by Suttons, Sydney Catalyst, NHMRC, Cancer Council NSW, Cancer Institute NSW and by an Avner Pancreatic Cancer Foundation and Len Ainsworth Pancreatic Research Funds. BM and VM are supported by fellowships from the French Ministry of Science (MESRI).

Additional information

Funding

Funder	Grant reference number	Author
Institut National Du Cancer	PLBIO19-291	Jacky G Goetz
Ligue Contre le Cancer		Jacky G Goetz
Canceropôle Grand Est	Exosomics	Jacky G Goetz
Plan Cancer	Vesmatic	Jacky G Goetz
Roche		Jacky G Goetz
Agence Nationale de la Re-	ANR-10-INBS-08-03	Christine Carapito

cherche		
Agence Nationale de la Recherche	ANR-19-CE44-0019	Nicolas Vitale
Agence Nationale de la Recherche	ANR-11-INBS- 0010	Laetitia Fouillen
Association pour la Recherche sur le Cancer		Shima Ghoroghi
French ministry of Science		Benjamin Mary Vincent Mittelheisser
Suttons		Kendelle Murphy Paul Timpson
Sydney catalyst		Kendelle Murphy Paul Timpson
NHMRC		Kendelle Murphy Paul Timpson
Cancer Council NSW		Kendelle Murphy Paul Timpson
Pancreatic Cancer Action		Kendelle Murphy Paul Timpson
Pancreatic cancer resource		Kendelle Murphy Paul Timpson
University of Strasbourg		Jacky G Goetz
Region Est	Exosomics	Jacky G Goetz
Inserm		Jacky G Goetz

The funders had no role in study design, data collection and interpretation, or the decision to submit the work for publication.

Author contributions

Shima Ghoroghi, Benjamin Mary, Formal analysis, Investigation, Methodology; Annabel Larnicol, Investigation, Methodology; Nandini Asokan, Annick Klein, Naël Osmani, Ignacio Busnelli, Anne-Marie Haeberle, Cathy Royer, Coralie Spiegelhalter, Vincent Mittelheisser, Investigation; François Delalande, Nicodème Paul, Frédéric Gros, Laetitia Fouillen, Gwennan André-Grégoire, Kendelle Murphy, Formal analysis, Investigation; Sébastien Halary, Data curation, Formal analysis; Alexandre Detappe, Paul Timpson, Supervision; Raphaël Carapito, Christine Carapito, Nicolas Vitale, Formal analysis, Supervision; Marcel Blot-Chabaud, Resources; Julie Gavard, Resources, Formal analysis, Supervision; Olivier Lefebvre, Data curation, Formal analysis, Supervision, Investigation; Jacky G Goetz, Conceptualization, Formal analysis, Supervision, Funding acquisition, Investigation, Writing - original draft, Project administration, Writing - review and editing; Vincent Hyenne, Conceptualization, Data curation, Formal analysis, Supervision, Funding acquisition, Investigation, Methodology, Writing - original draft, Writing - review and editing

Author ORCIDs

Shima Ghoroghi https://orcid.org/0000-0002-5715-4559
Benjamin Mary https://orcid.org/0000-0003-0815-842X
Nandini Asokan https://orcid.org/0000-0003-0505-6487
Naël Osmani https://orcid.org/0000-0003-1195-753X
François Delalande https://orcid.org/0000-0003-3590-9874
Nicodème Paul https://orcid.org/0000-0003-4680-3012
Frédéric Gros https://orcid.org/0000-0002-6252-4323
Laetitia Fouillen http://orcid.org/0000-0002-1204-9296
Coralie Spiegelhalter https://orcid.org/0000-0001-6372-1647
Alexandre Detappe https://orcid.org/0000-0001-9364-1621
Julie Gavard https://orcid.org/0000-0002-7985-9007

Christine Carapito https://orcid.org/0000-0002-0079-319X
Olivier Lefebvre https://orcid.org/0000-0001-9130-9174
Jacky G Goetz https://orcid.org/0000-0003-2842-8116
Vincent Hyenne https://orcid.org/0000-0002-1254-2814

Ethics

Human subjects: Paraffin sections of 4 µm from metastasic and non-metastasic breast tumours were obtained from CRB-Tumorothèque of the Institut de Cancérologie de l'Ouest (ICO, Saint-Herblain, France) (Heymann et al., 2020). Patients were diagnosed and treated at ICO (Integrated Center for Oncology, St Herblain) for metastatic and non-metastatic breast cancers. Samples were processed and included in the CRB-Tumorothèque ICO upon donor agreement and informed consent. Samples and related information are destroyed at the request of the donor. The CRB-Tumorothèque ICO have been declared to and authorized by the French Research Ministry (Declaration Number: DC-2018-3321). This declaration includes approval by a research ethics committee (CPP "Comité de protection des personnes"), in accordance with the French legislation of the Public Health Code.
Animal experimentation: All animals were housed and handled according to the guidelines of INSERM and the ethical committee of Alsace, France (CREMEAS) (Directive 2010/63/EU on the protection of animals used for scientific purposes). Animal facility agreement number: C67-482-33. Experimental license for mice: Apafis 4707-20l6032416407780; experimental license for zebrafish: Apafis 16862-2018121914292754.

Decision letter and Author response

Decision letter https://doi.org/10.7554/eLife.61539.sa1
Author response https://doi.org/10.7554/eLife.61539.sa2

Additional files

Supplementary files

- Supplementary file 1. EVs RNA analysis. Sheet a: RNAs overexpressed in EVs from 4T1 shCtl cells Vs EVs from shRalA cells Sheet b: RNAs overexpressed in EVs from 4T1 shRalA cells Vs EVs from shCtl cells Sheet c: RNAs overexpressed in EVs from 4T1 shCtl cells Vs EVs from shRalB cells Sheet d: RNAs overexpressed in EVs from 4T1 shRalB cells Vs EVs from shCtl cells

- Supplementary file 2. EVs proteomic analysis. Sheet a: Proteins identified in EVs from 4T1 shCtl cells Sheet b: Proteins overexpressed in EVs from 4T1 shCtl cells Vs EVs from shRalA cells Sheet c: Proteins overexpressed in EVs from 4T1 shRalA cells Vs EVs from shCtl cells Sheet d: Proteins overexpressed in EVs from 4T1 shCtl cells Vs EVs from shRalB cells Sheet e: Proteins overexpressed in EVs from 4T1 shRalB cells Vs EVs from shCtl cells Sheet f: Proteins overexpressed in EVs from 4T1 shCtl cells Vs EVs from shRalA cells and EVs from shRalB cells

Data availability

Sequencing and mass spectrometry data have been deposited in the EV-Track database.

The following previously published dataset was used:

Author(s)	Year	Dataset title	Dataset URL	Database and Identifier
The Cancer Genome Atlas Network	2012	Comprehensive molecular portraits of human breast tumours	https://www.cancer.gov/tcga	TCGA breast invasive carcinoma cohort (1097 patients), 10.1038/nature11412

References

Anders S, Pyl PT, Huber W. 2015. HTSeq–a Python framework to work with high-throughput sequencing data. *Bioinformatics* **31**:166–169. DOI: https://doi.org/10.1093/bioinformatics/btu638, PMID: 25260700

Bankhead P, Loughrey MB, Fernández JA, Dombrowski Y, McArt DG, Dunne PD, McQuaid S, Gray RT, Murray LJ, Coleman HG, James JA, Salto-Tellez M, Hamilton PW. 2017. QuPath: open source software for digital pathology image analysis. *Scientific Reports* **7**:5. DOI: https://doi.org/10.1038/s41598-017-17204-5, PMID: 29203879

Baran J, Baj-Krzyworzeka M, Weglarczyk K, Szatanek R, Zembela M, Barbasz J, Czupryna A, Szczepanik A, Zembala M. 2010. Circulating tumour-derived microvesicles in plasma of gastric Cancer patients. Cancer immunology. *Immunotherapy* **59**:841–850. DOI: https://doi.org/10.1007/s00262-009-0808-2

Bardin N, Blot-Chabaud M, Despoix N, Kebir A, Harhouri K, Arsanto JP, Espinosa L, Perrin P, Robert S, Vely F, Sabatier F, Le Bivic A, Kaplanski G, Sampol J, Dignat-George F. 2009. CD146 and its soluble form regulate monocyte transendothelial migration. *Arteriosclerosis, Thrombosis, and Vascular Biology* **29**:746–753. DOI: https://doi.org/10.1161/ATVBAHA.108.183251, PMID: 19229070

Becker A, Thakur BK, Weiss JM, Kim HS, Peinado H, Lyden D. 2016. Extracellular vesicles in Cancer: cell-to-cell mediators of metastasis. *Cancer Cell* **30**:836–848. DOI: https://doi.org/10.1016/j.ccell.2016.10.009, PMID: 27960084

Bobrie A, Krumeich S, Reyal F, Recchi C, Moita LF, Seabra MC, Ostrowski M, Théry C. 2012. Rab27a supports exosome-dependent and -independent mechanisms that modify the tumor microenvironment and can promote tumor progression. *Cancer Research* **72**:4920–4930. DOI: https://doi.org/10.1158/0008-5472.CAN-12-0925, PMID: 22865453

Bruntz RC, Lindsley CW, Brown HA. 2014. Phospholipase D signaling pathways and phosphatidic acid as therapeutic targets in Cancer. *Pharmacological Reviews* **66**:1033–1079. DOI: https://doi.org/10.1124/pr.114.009217, PMID: 25244928

Cha DJ, Franklin JL, Dou Y, Liu Q, Higginbotham JN, Demory Beckler M, Weaver AM, Vickers K, Prasad N, Levy S, Zhang B, Coffey RJ, Patton JG. 2015. KRAS-dependent sorting of miRNA to exosomes. *eLife* **4**:e07197. DOI: https://doi.org/10.7554/eLife.07197, PMID: 26132860

Collot M, Ashokkumar P, Anton H, Boutant E, Faklaris O, Galli T, Mély Y, Danglot L, Klymchenko AS. 2018. MemBright: a family of fluorescent membrane probes for advanced cellular imaging and neuroscience. *Cell Chemical Biology* **26**:9. DOI: https://doi.org/10.1016/j.chembiol.2019.01.009

Corrotte M, Chasserot-Golaz S, Huang P, Du G, Ktistakis NT, Frohman MA, Vitale N, Bader MF, Grant NJ. 2006. Dynamics and function of phospholipase D and phosphatidic acid during phagocytosis. *Traffic* **7**:365–377. DOI: https://doi.org/10.1111/j.1600-0854.2006.00389.x, PMID: 16497229

Costa-Silva B, Aiello NM, Ocean AJ, Singh S, Zhang H, Thakur BK, Becker A, Hoshino A, Mark MT, Molina H, Xiang J, Zhang T, Theilen TM, García-Santos G, Williams C, Ararso Y, Huang Y, Rodrigues G, Shen TL, Labori KJ, et al. 2015. Pancreatic Cancer exosomes initiate pre-metastatic niche formation in the liver. *Nature Cell Biology* **17**:816–826. DOI: https://doi.org/10.1038/ncb3169, PMID: 25985394

Cox J, Hein MY, Luber CA, Paron I, Nagaraj N, Mann M. 2014. Accurate proteome-wide label-free quantification by delayed normalization and maximal peptide ratio extraction, termed MaxLFQ. *Molecular & Cellular Proteomics* **13**:2513–2526. DOI: https://doi.org/10.1074/mcp.M113.031591, PMID: 24942700

Das SK, Sarkar D, Emdad L, Fisher PB. 2019. *MDA-9/Syntenin: An Emerging Global Molecular Target Regulating Cancer Invasion and Metastasis*. Elsevier Inc.

Demory Beckler M, Higginbotham JN, Franklin JL, Ham AJ, Halvey PJ, Imasuen IE, Whitwell C, Li M, Liebler DC, Coffey RJ. 2013. Proteomic analysis of exosomes from mutant KRAS Colon cancer cells identifies intercellular transfer of mutant KRAS. *Molecular & Cellular Proteomics* **12**:343–355. DOI: https://doi.org/10.1074/mcp.M112.022806, PMID: 23161513

Deutsch EW, Bandeira N, Sharma V, Perez-Riverol Y, Carver JJ, Kundu DJ, García-Seisdedos D, Jarnuczak AF, Hewapathirana S, Pullman BS, Wertz J, Sun Z, Kawano S, Okuda S, Watanabe Y, Hermjakob H, MacLean B, MacCoss MJ, Zhu Y, Ishihama Y, et al. 2020. The ProteomeXchange consortium in 2020: enabling "big data" approaches in proteomics. *Nucleic Acids Research* **48**:gkz984. DOI: https://doi.org/10.1093/nar/gkz984

Follain G, Herrmann D, Harlepp S, Hyenne V, Osmani N, Warren SC, Timpson P, Goetz JG. 2020. Fluids and their mechanics in tumour transit: shaping metastasis. *Nature Reviews Cancer* **20**:107–124. DOI: https://doi.org/10.1038/s41568-019-0221-x, PMID: 31780785

Galindo-Hernandez O, Villegas-Comonfort S, Candanedo F, González-Vázquez MC, Chavez-Ocaña S, Jimenez-Villanueva X, Sierra-Martinez M, Salazar EP. 2013. Elevated concentration of microvesicles isolated from peripheral blood in breast Cancer patients. *Archives of Medical Research* **44**:208–214. DOI: https://doi.org/10.1016/j.arcmed.2013.03.002, PMID: 23506723

Gao Y, Bado I, Wang H, Zhang W, Rosen JM, Zhang XH. 2019. Metastasis organotropism: redefining the congenial soil. *Developmental Cell* **49**:375–391. DOI: https://doi.org/10.1016/j.devcel.2019.04.012, PMID: 31063756

Garcia S, Dalès JP, Charafe-Jauffret E, Carpentier-Meunier S, Andrac-Meyer L, Jacquemier J, Andonian C, Lavaut MN, Allasia C, Bonnier P, Charpin C. 2007. Poor prognosis in breast carcinomas correlates with increased expression of targetable CD146 and c-Met and with proteomic basal-like phenotype. *Human Pathology* **38**:830–841. DOI: https://doi.org/10.1016/j.humpath.2006.11.015, PMID: 17316758

Gentry LR, Martin TD, Reiner DJ, Der CJ. 2014. Ral small GTPase signaling and oncogenesis: more than just 15minutes of fame. *Biochimica Et Biophysica Acta (BBA) - Molecular Cell Research* **1843**:2976–2988. DOI: https://doi.org/10.1016/j.bbamcr.2014.09.004

Ghossoub R, Lembo F, Rubio A, Gaillard CB, Bouchet J, Vitale N, Slavík J, Machala M, Zimmermann P. 2014. Syntenin-ALIX exosome biogenesis and budding into multivesicular bodies are controlled by ARF6 and PLD2. *Nature Communications* **5**:3477. DOI: https://doi.org/10.1038/ncomms4477, PMID: 24637612

Heymann D, Kerdraon O, Verriele V, Verhille E, Veron V, Vitre M, Delmas F, Henry C, Gouy Y, Amiand M, Bard J-M. 2020. Centre de ressources Biologiques-Tumorothèque: bioresources and associated clinical data dedicated to translational research in oncology at the institut de cancérologie de l'Ouest, France. *Open Journal of Bioresources* **7**:62. DOI: https://doi.org/10.5334/ojb.62

Hoshino A, Costa-Silva B, Shen TL, Rodrigues G, Hashimoto A, Tesic Mark M, Molina H, Kohsaka S, Di Giannatale A, Ceder S, Singh S, Williams C, Soplop N, Uryu K, Pharmer L, King T, Bojmar L, Davies AE, Ararso Y, Zhang T, et al. 2015. Tumour exosome integrins determine organotropic metastasis. *Nature* **527**:329–335. DOI: https://doi.org/10.1038/nature15756, PMID: 26524530

Huotari J, Helenius A. 2011. Endosome maturation. *The EMBO Journal* **30**:3481–3500. DOI: https://doi.org/10.1038/emboj.2011.286, PMID: 21878991

Hyenne V, Apaydin A, Rodriguez D, Spiegelhalter C, Hoff-Yoessle S, Diem M, Tak S, Lefebvre O, Schwab Y, Goetz JG, Labouesse M. 2015. RAL-1 controls multivesicular body biogenesis and exosome secretion. *Journal of Cell Biology* **211**:27–37. DOI: https://doi.org/10.1083/jcb.201504136

Hyenne V, Lefebvre O, Goetz JG. 2017. Going live with tumor exosomes and microvesicles. *Cell Adhesion & Migration* **11**:173–186. DOI: https://doi.org/10.1080/19336918.2016.1276694, PMID: 28135898

Hyenne V, Ghoroghi S, Collot M, Bons J, Follain G, Harlepp S, Mary B, Bauer J, Mercier L, Busnelli I, Lefebvre O, Fekonja N, Garcia-Leon MJ, Machado P, Delalande F, López AA, Silva SG, Verweij FJ, van Niel G, Djouad F, et al. 2019. Studying the fate of tumor extracellular vesicles at high spatiotemporal resolution using the zebrafish embryo. *Developmental Cell* **48**:554–572. DOI: https://doi.org/10.1016/j.devcel.2019.01.014, PMID: 30745140

Jiang H, Luo JQ, Urano T, Frankel P, Lu Z, Foster DA, Feig LA. 1995. Involvement of ral GTPase in v-Src-induced phospholipase D activation. *Nature* **378**:409–412. DOI: https://doi.org/10.1038/378409a0, PMID: 7477381

Jung T, Castellana D, Klingbeil P, Cuesta Hernández I, Vitacolonna M, Orlicky DJ, Roffler SR, Brodt P, Zöller M. 2009. CD44v6 dependence of premetastatic niche preparation by exosomes. *Neoplasia* **11**:1093–1105. DOI: https://doi.org/10.1593/neo.09822, PMID: 19794968

Kanemoto S, Nitani R, Murakami T, Kaneko M, Asada R, Matsuhisa K, Saito A, Imaizumi K. 2016. Multivesicular body formation enhancement and exosome release during endoplasmic reticulum stress. *Biochemical and Biophysical Research Communications* **480**:166–172. DOI: https://doi.org/10.1016/j.bbrc.2016.10.019, PMID: 27725157

Kaplan RN, Riba RD, Zacharoulis S, Bramley AH, Vincent L, Costa C, MacDonald DD, Jin DK, Shido K, Kerns SA, Zhu Z, Hicklin D, Wu Y, Port JL, Altorki N, Port ER, Ruggero D, Shmelkov SV, Jensen KK, Rafii S, et al. 2005. VEGFR1-positive haematopoietic bone marrow progenitors initiate the pre-metastatic niche. *Nature* **438**:820–827. DOI: https://doi.org/10.1038/nature04186, PMID: 16341007

Kaur P, Nagaraja GM, Zheng H, Gizachew D, Galukande M, Krishnan S, Asea A. 2012. A mouse model for triple-negative breast Cancer tumor-initiating cells (TNBC-TICs) exhibits similar aggressive phenotype to the human disease. *BMC Cancer* **12**:120. DOI: https://doi.org/10.1186/1471-2407-12-120

Kebir A, Harhouri K, Guillet B, Liu JW, Foucault-Bertaud A, Lamy E, Kaspi E, Elganfoud N, Vely F, Sabatier F, Sampol J, Pisano P, Kruithof EK, Bardin N, Dignat-George F, Blot-Chabaud M. 2010. CD146 short isoform increases the proangiogenic potential of endothelial progenitor cells in vitro and in vivo. *Circulation Research* **107**:66–75. DOI: https://doi.org/10.1161/CIRCRESAHA.109.213827, PMID: 20448216

Kim D, Langmead B, Salzberg SL. 2015. HISAT: a fast spliced aligner with low memory requirements. *Nature Methods* **12**:357–360. DOI: https://doi.org/10.1038/nmeth.3317, PMID: 25751142

Klumperman J, Raposo G. 2014. The complex ultrastructure of the endolysosomal system. *Cold Spring Harbor Perspectives in Biology* **6**:a016857. DOI: https://doi.org/10.1101/cshperspect.a016857, PMID: 24851870

Kren N, Michaud D, Bagchi S, Greene K, Pylayeva-Gupta Y. 2020. Rab27a plays a dual role in metastatic propensity of pancreatic Cancer. *Scientific Reports* **10**:e64248-1. DOI: https://doi.org/10.1038/s41598-020-64248-1

Lewis JA, Scott SA, Lavieri R, Buck JR, Selvy PE, Stoops SL, Armstrong MD, Brown HA, Lindsley CW. 2009. Design and synthesis of isoform-selective phospholipase D (PLD) inhibitors. part I: impact of alternative halogenated privileged structures for PLD1 specificity. *Bioorganic & Medicinal Chemistry Letters* **19**:1916–1920. DOI: https://doi.org/10.1016/j.bmcl.2009.02.057, PMID: 19268584

Logozzi M, De Milito A, Lugini L, Borghi M, Calabrò L, Spada M, Perdicchio M, Marino ML, Federici C, Iessi E, Brambilla D, Venturi G, Lozupone F, Santinami M, Huber V, Maio M, Rivoltini L, Fais S. 2009. High levels of exosomes expressing CD63 and caveolin-1 in plasma of melanoma patients. *PLOS ONE* **4**:e5219. DOI: https://doi.org/10.1371/journal.pone.0005219, PMID: 19381331

Lou Y, Preobrazhenska O, auf dem Keller U, Sutcliffe M, Barclay L, McDonald PC, Roskelley C, Overall CM, Dedhar S. 2008. Epithelial-mesenchymal transition (EMT) is not sufficient for spontaneous murine breast Cancer metastasis. *Developmental Dynamics* **237**:2755–2768. DOI: https://doi.org/10.1002/dvdy.21658, PMID: 18773493

Love MI, Huber W, Anders S. 2014. Moderated estimation of fold change and dispersion for RNA-seq data with DESeq2. *Genome Biology* **15**:550. DOI: https://doi.org/10.1186/s13059-014-0550-8, PMID: 25516281

Luo JQ, Liu X, Frankel P, Rotunda T, Ramos M, Flom J, Jiang H, Feig LA, Morris AJ, Kahn RA, Foster DA. 1998. Functional association between arf and RalA in active phospholipase D complex. *PNAS* **95**:3632–3637. DOI: https://doi.org/10.1073/pnas.95.7.3632, PMID: 9520417

Mathieu M, Martin-Jaular L, Lavieu G, Théry C. 2019. Specificities of secretion and uptake of exosomes and other extracellular vesicles for cell-to-cell communication. *Nature Cell Biology* **21**:9–17. DOI: https://doi.org/10.1038/s41556-018-0250-9, PMID: 30602770

Mattissek C, Teis D. 2014. The role of the endosomal sorting complexes required for transport (ESCRT) in tumorigenesis. *Molecular Membrane Biology* **31**:111–119. DOI: https://doi.org/10.3109/09687688.2014.894210, PMID: 24641493

McKenzie AJ, Hoshino D, Hong NH, Cha DJ, Franklin JL, Coffey RJ, Patton JG, Weaver AM. 2016. KRAS-MEK Signaling Controls Ago2 Sorting into Exosomes. *Cell Reports* **15**:978–987. DOI: https://doi.org/10.1016/j.celrep.2016.03.085

Monypenny J, Milewicz H, Flores-Borja F, Weitsman G, Cheung A, Chowdhury R, Burgoyne T, Arulappu A, Lawler K, Barber PR, Vicencio JM, Keppler M, Wulaningsih W, Davidson SM, Fraternali F, Woodman N, Turmaine M, Gillett C, Franz D, Quezada SA, et al. 2018. ALIX regulates Tumor-Mediated immunosuppression by controlling EGFR activity and PD-L1 presentation. *Cell Reports* **24**:630–641. DOI: https://doi.org/10.1016/j.celrep.2018.06.066, PMID: 30021161

Ombrato L, Nolan E, Kurelac I, Mavousian A, Bridgeman VL, Heinze I, Chakravarty P, Horswell S, Gonzalez-Gualda E, Matacchione G, Weston A, Kirkpatrick J, Husain E, Speirs V, Collinson L, Ori A, Lee JH, Malanchi I. 2019. Metastatic-niche labelling reveals parenchymal cells with stem features. *Nature* **572**:603–608. DOI: https://doi.org/10.1038/s41586-019-1487-6, PMID: 31462798

Ostrowski M, Carmo NB, Krumeich S, Fanget I, Raposo G, Savina A, Moita CF, Schauer K, Hume AN, Freitas RP, Goud B, Benaroch P, Hacohen N, Fukuda M, Desnos C, Seabra MC, Darchen F, Amigorena S, Moita LF, Thery C. 2010. Rab27a and Rab27b control different steps of the exosome secretion pathway. *Nature Cell Biology* **12**:19–30. DOI: https://doi.org/10.1038/ncb2000, PMID: 19966785

Oxford G, Owens CR, Titus BJ, Foreman TL, Herlevsen MC, Smith SC, Theodorescu D. 2005. RalA and RalB: antagonistic relatives in Cancer cell migration. *Cancer Research* **65**:7111–7120. DOI: https://doi.org/10.1158/0008-5472.CAN-04-1957, PMID: 16103060

Peinado H, Alečković M, Lavotshkin S, Matei I, Costa-Silva B, Moreno-Bueno G, Hergueta-Redondo M, Williams C, García-Santos G, Ghajar C, Nitadori-Hoshino A, Hoffman C, Badal K, Garcia BA, Callahan MK, Yuan J, Martins VR, Skog J, Kaplan RN, Brady MS, et al. 2012. Melanoma exosomes educate bone marrow progenitor cells toward a pro-metastatic phenotype through MET. *Nature Medicine* **18**:883–891. DOI: https://doi.org/10.1038/nm.2753, PMID: 22635005

Peinado H, Zhang H, Matei IR, Costa-Silva B, Hoshino A, Rodrigues G, Psaila B, Kaplan RN, Bromberg JF, Kang Y, Bissell MJ, Cox TR, Giaccia AJ, Erler JT, Hiratsuka S, Ghajar CM, Lyden D. 2017. Pre-metastatic niches: organ-specific homes for metastases. *Nature Reviews Cancer* **17**:302–317. DOI: https://doi.org/10.1038/nrc.2017.6, PMID: 28303905

Plebanek MP, Angeloni NL, Vinokour E, Li J, Henkin A, Martinez-Marin D, Filleur S, Bhowmick R, Henkin J, Miller SD, Ifergan I, Lee Y, Osman I, Thaxton CS, Volpert OV. 2017. Pre-metastatic Cancer exosomes induce immune surveillance by patrolling monocytes at the metastatic niche. *Nature Communications* **8**:e01433-3. DOI: https://doi.org/10.1038/s41467-017-01433-3

Scott SA, Selvy PE, Buck JR, Cho HP, Criswell TL, Thomas AL, Armstrong MD, Arteaga CL, Lindsley CW, Brown HA. 2009. Design of isoform-selective phospholipase D inhibitors that modulate cancer cell invasiveness. *Nature Chemical Biology* **5**:108–117. DOI: https://doi.org/10.1038/nchembio.140

Scott CC, Vacca F, Gruenberg J. 2014. Endosome maturation, transport and functions. *Seminars in Cell & Developmental Biology* **31**:2–10. DOI: https://doi.org/10.1016/j.semcdb.2014.03.034

Szklarczyk D, Gable AL, Lyon D, Junge A, Wyder S, Huerta-Cepas J, Simonovic M, Doncheva NT, Morris JH, Bork P, Jensen LJ, Mering CV. 2019. STRING v11: protein-protein association networks with increased coverage, supporting functional discovery in genome-wide experimental datasets. *Nucleic Acids Research* **47**:D607–D613. DOI: https://doi.org/10.1093/nar/gky1131, PMID: 30476243

Taira E, Takaha N, Taniura H, Kim CH, Miki N. 1994. Molecular cloning and functional expression of Gicerin, a novel cell adhesion molecule that binds to neurite outgrowth factor. *Neuron* **12**:861–872. DOI: https://doi.org/10.1016/0896-6273(94)90338-7, PMID: 8161457

Taira E, Kohama K, Tsukamoto Y, Okumura S, Miki N. 2005. Gicerin/CD146 is involved in neurite extension of NGF-treated PC12 cells. *Journal of Cellular Physiology* **204**:632–637. DOI: https://doi.org/10.1002/jcp.20365, PMID: 15880440

Timpson P, Mcghee EJ, Erami Z, Nobis M, Quinn JA, Edward M, Anderson KI. 2011. Organotypic collagen I assay: a malleable platform to assess cell behaviour in a 3-Dimensional context. *Journal of Visualized Experiments* **13**:e3089. DOI: https://doi.org/10.3791/3089

Tominaga N, Kosaka N, Ono M, Katsuda T, Yoshioka Y, Tamura K, Lötvall J, Nakagama H, Ochiya T. 2015. Brain metastatic Cancer cells release microRNA-181c-containing extracellular vesicles capable of destructing blood-brain barrier. *Nature Communications* **6**:6716. DOI: https://doi.org/10.1038/ncomms7716, PMID: 25828099

Treps L, Edmond S, Harford-Wright E, Galan-Moya EM, Schmitt A, Azzi S, Citerne A, Bidère N, Ricard D, Gavard J. 2016. Extracellular vesicle-transported Semaphorin3A promotes vascular permeability in glioblastoma. *Oncogene* **35**:2615–2623. DOI: https://doi.org/10.1038/onc.2015.317, PMID: 26364614

van Niel G, D'Angelo G, Raposo G. 2018. Shedding light on the cell biology of extracellular vesicles. *Nature Reviews Molecular Cell Biology* **19**:213–228. DOI: https://doi.org/10.1038/nrm.2017.125, PMID: 29339798

Vennin C, Chin VT, Warren SC, Lucas MC, Herrmann D, Magenau A, Melenec P, Walters SN, Del Monte-Nieto G, Conway JR, Nobis M, Allam AH, McCloy RA, Currey N, Pinese M, Boulghourjian A, Zaratzian A, Adam AA, Heu C, Nagrial AM, et al. 2017. Transient tissue priming via ROCK inhibition uncouples pancreatic Cancer progression, sensitivity to chemotherapy, and metastasis. *Science Translational Medicine* **9**:eaai8504. DOI: https://doi.org/10.1126/scitranslmed.aai8504, PMID: 28381539

Vitale N, Mawet J, Camonis J, Regazzi R, Bader M-F, Chasserot-Golaz S. 2005. The small GTPase RalA controls exocytosis of large dense core secretory granules by interacting with ARF6-dependent phospholipase D1. *Journal of Biological Chemistry* **280**:29921–29928. DOI: https://doi.org/10.1074/jbc.M413748200

Wang Q, Ni Q, Wang X, Zhu H, Wang Z, Huang J. 2015. High expression of RAB27A and TP53 in pancreatic Cancer predicts poor survival. *Medical Oncology* **32**:372. DOI: https://doi.org/10.1007/s12032-014-0372-2, PMID: 25428385

Wang D, Sun H, Wei J, Cen B, DuBois RN. 2017. CXCL1 Is Critical for Premetastatic Niche Formation and Metastasis in Colorectal Cancer. *Cancer Research* **77**:3655–3665. DOI: https://doi.org/10.1158/0008-5472.CAN-16-3199

Wang Z, Yan X. 2013. CD146, a multi-functional molecule beyond adhesion. *Cancer Letters* **330**:150–162. DOI: https://doi.org/10.1016/j.canlet.2012.11.049

Wieczorek S, Combes F, Lazar C, Giai Gianetto Q, Gatto L, Dorffer A, Hesse A-M, Couté Y, Ferro M, Bruley C, Burger T. 2017. DAPAR & ProStaR: software to perform statistical analyses in quantitative discovery proteomics. *Bioinformatics* **33**:135–136. DOI: https://doi.org/10.1093/bioinformatics/btw580

Yan C, Liu D, Li L, Wempe MF, Guin S, Khanna M, Meier J, Hoffman B, Owens C, Wysoczynski CL, Nitz MD, Knabe WE, Ahmed M, Brautigan DL, Paschal BM, Schwartz MA, Jones DN, Ross D, Meroueh SO, Theodorescu D. 2014. Discovery and characterization of small molecules that target the GTPase ral. *Nature* **515**:443–447. DOI: https://doi.org/10.1038/nature13713, PMID: 25219851

Yan C, Theodorescu D. 2018. RAL GTPases: biology and potential as therapeutic targets in Cancer. *Pharmacological Reviews* **70**:1–11. DOI: https://doi.org/10.1124/pr.117.014415, PMID: 29196555

Yang Z, Shi J, Xie J, Wang Y, Sun J, Liu T, Zhao Y, Zhao X, Wang X, Ma Y, Malkoc V, Chiang C, Deng W, Chen Y, Fu Y, Kwak KJ, Fan Y, Kang C, Yin C, Rhee J, et al. 2020. Large-scale generation of functional mRNA-encapsulating exosomes via cellular nanoporation. *Nature Biomedical Engineering* **4**:69–83. DOI: https://doi.org/10.1038/s41551-019-0485-1

Yue S, Mu W, Erb U, Zöller M. 2015. The tetraspanins CD151 and Tspan8 are essential exosome components for the crosstalk between Cancer initiating cells and their surrounding. *Oncotarget* **6**:2366–2384. DOI: https://doi.org/10.18632/oncotarget.2958, PMID: 25544774

Zago G, Veith I, Singh MK, Fuhrmann L, De Beco S, Remorino A, Takaoka S, Palmeri M, Berger F, Brandon N, El Marjou A, Vincent-Salomon A, Camonis J, Coppey M, Parrini MC. 2018. RalB directly triggers invasion downstream ras by mobilizing the wave complex. *eLife* **7**:e40474. DOI: https://doi.org/10.7554/eLife.40474, PMID: 30320548

Zeng GF, Cai SX, Wu GJ. 2011. Up-regulation of METCAM/MUC18 promotes motility, invasion, and tumorigenesis of human breast Cancer cells. *BMC Cancer* **11**:113. DOI: https://doi.org/10.1186/1471-2407-11-113, PMID: 21450088

Zeng Q, Li W, Lu D, Wu Z, Duan H, Luo Y, Feng J, Yang D, Fu L, Yan X. 2012. CD146, an epithelial-mesenchymal transition inducer, is associated with triple-negative breast Cancer. *PNAS* **109**:1127–1332. DOI: https://doi.org/10.1073/pnas.1111053108, PMID: 22210108

Zhou W, Fong MY, Min Y, Somlo G, Liu L, Palomares MR, Yu Y, Chow A, O'Connor ST, Chin AR, Yen Y, Wang Y, Marcusson EG, Chu P, Wu J, Wu X, Li AX, Li Z, Gao H, Ren X, et al. 2014. Cancer-secreted miR-105 destroys vascular endothelial barriers to promote metastasis. *Cancer Cell* **25**:501–515. DOI: https://doi.org/10.1016/j.ccr.2014.03.007, PMID: 24735924

This study, to which I contributed, mainly on the CD146/MCAM axis and fish experiments, was highlighted in a small article that I wrote in a French journal (Médecine/Science) where we discussed our findings and their significance in cancer research as well as in tEVs biology.

Les vesicules extracellulaires tumorales favorisent la formation de niches pre-métastatiques

- **Mary et al., Med/Sci 2021**

médecine/sciences 2021 ; 37 : 1116-8

Les vésicules extracellulaires tumorales favorisent la formation de niches pré-métastatiques

Benjamin Mary[1,2,3,5], Shima Ghoroghi[1,2,3,5], Jacky G. Goetz[1,2,3,5*], Vincent Hyenne[1-5*]

[1]Biomécanique des tumeurs (*Tumor biomechanics*), Inserm UMRS1109, Strasbourg, France.
[2]Université de Strasbourg, Strasbourg, France.
[3]Fédération de médecine translationnelle de Strasbourg (FMTS), Strasbourg, France.
[4]CNRS, SNC5055, Strasbourg, France.
[5]Équipe labellisée par la Ligue contre le cancer.
*Co-derniers auteurs
hyenne@unistra.fr

Vésicules extracellulaires et cancer

La communication entre les cellules tumorales et les cellules stromales façonne un microenvironnement permissif à la progression métastatique. Les vésicules extracellulaires favorisent cet échange en modifiant le comportement de cellules qu'elles ciblent, stimulant ainsi la progression de la tumeur, mais également la formation de métastases [1]. Lorsqu'elles sont sécrétées par les cellules tumorales, les vésicules extracellulaires peuvent stimuler localement la prolifération, l'invasion ou la résistance aux traitements anti-tumoraux des cellules tumorales voisines [1]. Elles peuvent également agir sur des cellules non tumorales du microenvironnement et, par exemple, promouvoir la néo-vascularisation de la tumeur ou activer les fibroblastes résidents, modifiant ainsi la composition de la matrice extracellulaire. Elles jouent, par ailleurs, un rôle crucial dans la réponse immunitaire anti-tumorale, et peuvent l'activer en servant, par exemple, de source d'antigènes tumoraux ou, au contraire, peuvent favoriser « l'évasion » immunitaire de la tumeur en inhibant les lymphocytes T ou en réduisant la cytotoxicité des cellules NK (*natural killer*) [2]. Outre cette action locale, les vésicules extracellulaires tumorales agissent également à distance de la tumeur primaire, dans des organes ou des tissus qu'elles atteignent en empruntant les circulations sanguine ou lymphatique. Elles pré-conditionnent ainsi de futurs organes à recevoir des métastases, avant même l'arrivée des cellules tumorales, en formant des niches pré-métastatiques [3]. Ces niches, qui favorisent l'arrivée et la croissance de cellules tumorales, donc l'implantation de métastases, présentent des caractéristiques communes : des barrières endothéliales fragiles et poreuses, une activation des cellules stromales, un recrutement de cellules myéloïdes et un microenvironnement globalement pro-inflammatoire et immunosuppresseur [2, 3]. Si ce nouveau paradigme impliquant les vésicules extracellulaires dans le développement métastasique est porteur d'espoir sur un plan diagnostique voire thérapeutique, de nombreuses zones d'ombre limitent encore sa compréhension et freinent son exploitation. Par exemple, si la fonction pro-métastatique de certains cargos (protéines et micro-ARN) présents dans les vésicules extracellulaires tumorales a été rapportée [1, 3], l'identité moléculaire du contenu des vésicules extracellulaires induisant l'apparition des niches pré-métastatiques est encore mal connue. On ignore également la nature précise des mécanismes permettant l'accumulation de ces cargos dans les vésicules extracellulaires et la sécrétion de ces vésicules par les cellules de la tumeur primaire. Par ailleurs, alors que les niches pré-métastatiques et les métastases se forment dans des organes déterminés, qui varient selon le type tumoral, on comprend encore mal les processus qui régissent cette spécificité [3]. Comprendre les mécanismes de la biodistribution des vésicules extracellulaires tumorales pourrait aider à expliquer ce phénomène. De manière générale, une meilleure compréhension de ces processus et des molécules mises en jeu permettrait de mieux détecter et combattre la formation de métastases, une étape critique de l'agressivité d'une tumeur cancéreuse. Sonder le répertoire moléculaire des vésicules extracellulaires par des biopsies liquides permettrait de développer des outils pour détecter la maladie plus tôt et entreprendre des approches thérapeutiques ciblées.

Notre équipe de recherche vient d'apporter un éclairage nouveau sur ces questions en identifiant une nouvelle voie de biogenèse des vésicules extracellulaires tumorales et en décrivant, par une approche moléculaire « multi-modèle », son implication dans la formation de niches pré-métastatiques dans le contexte du cancer du sein métastatique [4].

Vignette (© Guillaume van Niel, Aurélie di Cicco, Graça Raposo, Daniel Levy).

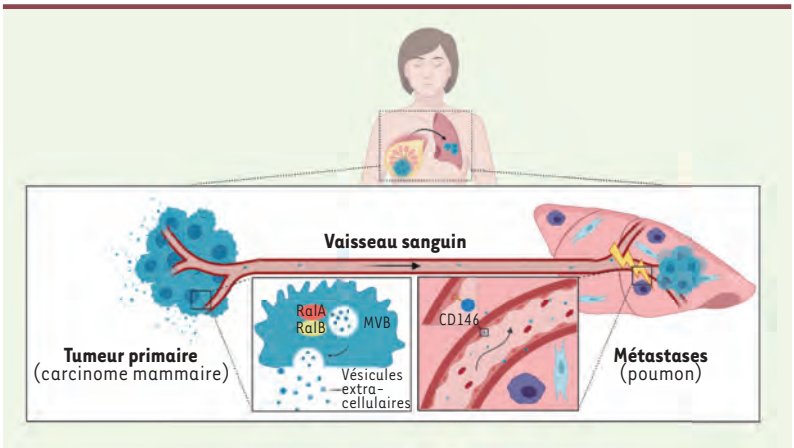

Figure 1. ***Modèle expliquant le rôle des GTPases Ral dans la sécrétion d'exosomes tumoraux et dans la formation de niches pré-métastatiques.*** Les GTPases RalA et RalB contrôlent la densité de corps multivésiculaires (*multivesicular body*, MVB) dans les cellules tumorales et la sécrétion de vésicules extracellulaires par ces cellules. Elles contrôlent également le chargement de CD146 dans les vésicules extracellulaires, une protéine d'adhérence qui favorise leur accumulation dans les organes destinés à recevoir des métastases et la formation de niches pré-métastatiques (figure créée sur BioRender.com).

Biogenèse des vésicules extracellulaires tumorales

Bien que représentant un ensemble très hétérogène, les vésicules extracellulaires sont classées en deux catégories selon leur voie de biogenèse : exosomes ou microvésicules. Les exosomes proviennent de la sécrétion des vésicules intraluminales présentes au sein d'un endosome tardif particulier, le corps multi-vésiculaire. Lorsque celui-ci fusionne avec la membrane plasmique de la cellule, les vésicules intraluminales sécrétées dans le milieu extracellulaire sont alors appelées exosomes [5] *(Figure 1)*. Les microvésicules, quant à elles, proviennent du bourgeonnement de la membrane plasmique de la cellule [5]. Certains mécanismes moléculaires contrôlant la sécrétion des vésicules extracellulaires tumorales et participant directement à la formation de métastases ont été récemment identifiés [1, 5]. Par exemple, la GTPase Rab27a permet l'ancrage des corps multivésiculaires à la membrane plasmique, et contrôle ainsi la sécrétion d'exosomes, ce qui favorise notamment les métastases de carcinomes mammaires et de mélanomes chez la souris [6, 7]. Afin de mieux comprendre comment la sécrétion de vésicules extracellulaires contrôle l'apparition de métastases, nous avons choisi de nous concentrer sur les GTPases RalA et RalB car nous avions préalablement mis en évidence le rôle de leur orthologue, RAL-1, dans la sécrétion d'exosomes chez le nématode *Caenorhabditis elegans* [8]. Ces protéines étaient alors connues pour leur fonction dans différents processus cellulaires (sécrétion, migration, prolifération, etc.) et pour leur rôle pro-tumoral dans plusieurs types de cancers [9]. Pour évaluer leur importance dans les processus de métastases induits par les vésicules extracellulaires, nous avons étudié les effets de l'inhibition de l'expression de ces GTPases dans un modèle de carcinome mammaire murin particulièrement agressif [4]. Ce modèle cellulaire, appelé 4T1[1], mime fidèlement, après injection à des souris BALB/c, la maladie humaine (cancer du sein « triple négatif ») et permet de réaliser des études de tumorigenèse et de métastases expérimentales dans un contexte syngénique. Nous avons constaté que la réduction de l'expression de RalA ou de RalB (par la technique de shARN [*short hairpin RNA*]), ou leur inhibition pharmacologique, diminuent la sécrétion des vésicules extracellulaires tumorales. Les inhibiteurs chimiques des GTPases Ral diminuent également la sécrétion de vésicules extracellulaires par d'autres types de cellules tumorales (cellules de mélanome et de carcinome pancréatique), ce qui indique que la fonction de ces protéines n'est pas restreinte au cancer du sein. Une analyse subcellulaire des organelles a également permis de montrer que RalA et RalB affectent la sécrétion d'exosomes en contrôlant la densité cellulaire des corps multi-vésiculaires *(Figure 1)* [4]. Ainsi, nous avons mis en évidence une nouvelle voie de sécrétion d'exosomes tumoraux dépendant des GTPases Ral, pour laquelle il conviendra de déterminer comment elle s'articule avec les mécanismes de biogenèse des exosomes décrits précédemment [5].

Vésicules extracellulaires tumorales et niche pré-métastatique

Afin d'évaluer l'importance de cette voie de sécrétion d'exosomes dans la progression tumorale et la formation de métastase, nous avons entrepris d'injecter les cellules 4T1 dans la glande mammaire de souris syngéniques immunocompétentes. Alors que les GTPases RalA et RalB perturbent la croissance des tumeurs primaires de manière opposée, toutes deux sont requises pour la formation de métastases pulmonaires. On retrouve d'ailleurs une expression plus élevée de ces GTPases chez des patientes atteintes de cancer du sein et présentant des métastases [4, 9]. Les résultats que nous avons obtenus montrent ainsi, d'une part, que les GTPases Ral contrôlent la sécrétion d'exosomes tumoraux et, d'autre part, que ces GTPases sont nécessaires à la formation de métastases. Afin d'établir un lien

[1] 4T1 est une lignée cellulaire de cancer du sein dérivée du tissu de la glande mammaire de souris BALB/c.

entre ces deux phénotypes, nous avons évalué la capacité des vésicules extracellulaires tumorales à induire la formation de niches pré-métastatiques dans un modèle de métastases expérimentales chez la souris. Nous avons observé que les vésicules extracellulaires issues de cellules dans lesquelles l'expression des GTPases Ral a été inhibée perdent leur potentiel pro-métastatique. Ces vésicules perdent également la capacité de cibler les organes destinés à recevoir des métastases (le foie et le poumon), une propriété essentielle à la formation des niches pré-métastatiques. Les GTPases Ral sont donc nécessaires à la sécrétion d'une sous-population de vésicules extracellulaires capables de cibler efficacement un organe destiné à recevoir des métastases et d'y former des niches pré-métastatiques.

Nous avons ensuite analysé le contenu des vésicules extracellulaires tumorales par une approche « multi-omique ». Nous avons observé que les GTPases Ral contrôlent le contenu de ces vésicules en protéines, en ARN (ARNm et ARN non-codants) et en lipides. Une découverte majeure de cette analyse comparative a été l'identification d'une protéine d'adhérence intercellulaire, CD146 (aussi appelée MCAM pour molécule d'adhérence cellulaire du mélanome), dont l'enrichissement dans les vésicules extracellulaires tumorales dépend des GTPases Ral *(Figure 1)*. L'inhibition de CD146 à l'aide d'un anticorps anti-CD146 a montré que cette protéine est nécessaire au ciblage pulmonaire de ces vésicules ainsi qu'à la formation de niches prémétastatiques. L'identification de CD146 dans ce contexte vient s'ajouter à celle des tétraspanines (TSPAN8 et CD151) et des couples d'intégrines ($\alpha6\beta4$, $\alpha_v\beta4$ et $\alpha6\beta1$), dont l'impact sur l'accumulation des vésicules extracellulaires tumorales dans des organes spécifiques et sur la formation de niches pré-métastatiques a été établi [10, 11]. Ces découvertes suggèrent que la combinaison de l'expression de molécules d'adhérence à la surface de vésicules extracellulaires détermine leur capacité à s'accumuler dans un organe déterminé. Décrypter cette combinaison de récepteurs et en identifier les ligands permettraient de développer des thérapies ciblées bloquant les étapes initiales de la formation des niches pré-métastatiques, ce qui constituerait un outil innovant et d'action précoce dans la lutte contre la formation de métastases.

Conclusion

Nos travaux, que nous présentons ici dans le cadre du numéro thématique de *médecine/sciences* dédié aux vésicules extracellulaires, ont donc permis de mettre en évidence une nouvelle voie de biogenèse d'exosomes tumoraux dépendant des GTPases RalA et RalB. Nous avons montré que cette voie contrôle l'enrichissement des vésicules extracellulaires tumorales en certaines molécules cargos étroitement liées à leur capacité pro-métastatique (en particulier la protéine CD146). D'autres cargos (ARN, protéines, etc.) de ces vésicules contribuent cependant également à la mise en place des niches pré-métastatiques [1, 3], mais leur rattachement à des voies de sécrétion particulières dans les cellules tumorales reste à déterminer. L'identification simultanée de molécules pro-métastatiques portées par les vésicules extracellulaires et de leurs mécanismes moléculaires de sécrétion respectifs permettrait l'élaboration de stratégies thérapeutiques ciblées « à double-tranchant », en agissant à la fois sur la quantité et sur l'identité des vésicules extracellulaires tumorales. Une meilleure connaissance des marqueurs moléculaires présents à la surface de ces vésicules pourrait finalement favoriser l'émergence de nouveaux outils diagnostiques multimoléculaires à partir de biopsies liquides réalisées chez les patients. ◊

Ral-dependent tumor extracellular vesicles induce premetastatic niches in secondary organs

REMERCIEMENTS

Ce travail a été soutenu par des bourses individuelles de l'IDEX (université de Strasbourg), de l'Association pour la recherche sur le cancer (ARC) et de la Fondation pour la recherche médicale (FRM) pour BM et SG, par des financements obtenus par JGG et VH auprès de la Ligue contre le cancer, le Cancéropôle Grand-Est, l'INCa (PLBIO19-291) et le Plan cancer (Nanotumor and Vesmatic), ainsi que par des financements institutionnels de l'université de Strasbourg et de l'Inserm accordés à JGG.

LIENS D'INTÉRÊT

Les auteurs déclarent n'avoir aucun lien d'intérêt concernant les données publiées dans cet article.

RÉFÉRENCES

1. Xu R, Rai A, Chen M, *et al.* Extracellular vesicles in cancer: implications for future improvements in cancer care. *Nat Rev Clin Oncol* 2018 ; 15 : 617-38.
2. Marar C, Starich B, Wirtz D. Extracellular vesicles in immunomodulation and tumor progression. *Nat Immunol* 2021 ; 22 : 560-70.
3. Peinado H, Zhang H, Matei IR, *et al.* Pre-metastatic niches: organ-specific homes for metastases. *Nat Rev Cancer* 2017 ; 17 : 302-17.
4. Ghoroghi S, Mary B, Larnicol A, *et al.* Ral GTPases promote breast cancer metastasis by controlling biogenesis and organ targeting of exosomes. *eLife* 2021 ; 10 : e61539.
5. Niel G van, D'Angelo G, Raposo G. Shedding light on the cell biology of extracellular vesicles. *Nat Rev Mol Cell Biol* 2018 ; 19 : 213-28.
6. Bobrie A, Krumeich S, Reyal F, *et al.* Rab27a supports exosome-dependent and -independent mechanisms that modify the tumor microenvironment and can promote tumor progression. *Cancer Res* 2012 ; 72 : 4920-30.
7. Peinado H, Alečković M, Lavotshkin S, *et al.* Melanoma exosomes educate bone marrow progenitor cells toward a pro-metastatic phenotype through MET. *Nat Med* 2012 ; 18 : 883-91.
8. Hyenne V, Apaydin A, Rodriguez D, *et al.* RAL-1 controls multivesicular body biogenesis and exosome secretion. *J Cell Biol* 2015 ; 211 : 27-37.
9. Yan C, Theodorescu D. RAL GTpases: Biology and potential as therapeutic targets in cancer. *Pharmacol Rev* 2018 ; 70 : 1-11.
10. Hoshino A, Costa-Silva B, Shen T-L, *et al.* Tumour exosome integrins determine organotropic metastasis. *Nature* 2015 ; 1-19.
11. Yue S, Mu W, Erb U, *et al.* The tetraspanins CD151 and Tspan8 are essential exosome components for the crosstalk between cancer initiating cells and their surrounding. *Oncotarget* 2015 ; 6 : 2366-84.

TIRÉS À PART

V. Hyenne

5. tEVs and the metastatic cascade

In addition to our own research project and papers, together with my colleagues Shima GHOROGHI and Nandini ASOKAN, we recently published a review article describing what is currently known about the role of tEVs in metastatic progression. We recapitulated what was known at that time on tEVs fate from their secretion to their dissemination through body fluids and their involvement in the formation of pre-metastatic sites. This review focuses on key steps during tEVs' journey through organisms, and notably what is known concerning their escape of the primary tumor site and the mechanisms that can drive their organotropism and their dissemination in circulation. In addition, we described known mechanisms by which tEVs facilitate PMN formation such as their pro-angiogenesis and permeabilization effect, their capacity to remodel the ECM and to mediate immune cells response.

Tumor extracellular vesicles drive metastasis (it's a long way from home)

- **S. Ghoroghi, B. Mary, N. Asokan, FASEB 2021**

Received: 3 July 2021 | Accepted: 27 July 2021

DOI: 10.1096/fba.2021-00079

REVIEW

FASEB BioAdvances WILEY

Tumor extracellular vesicles drive metastasis (it's a long way from home)

Shima Ghoroghi[1,2,3,4] | **Benjamin Mary**[1,2,3,4] | **Nandini Asokan**[1,2,3,4] | **Jacky G. Goetz**[1,2,3,4] | **Vincent Hyenne**[1,2,3,4,5]

[1]Tumor Biomechanics, INSERM UMR_S1109, Strasbourg, France

[2]Université de Strasbourg, Strasbourg, France

[3]Fédération de Médecine Translationnelle de Strasbourg (FMTS), Strasbourg, France

[4]Equipe Labellisée Ligue Contre le Cancer, Strasbourg, France

[5]CNRS, SNC5055, Strasbourg, France

Correspondence
Vincent Hyenne, Université de Strasbourg, Strasbourg, France.
Email: hyenne@unistra.fr

Funding information
IDEX; ARC (Association pour le Recherche sur le Cancer); FRM (Fondation pour la Recherche Médicale); La Ligue contre le Cancer; Canceropole Grand-Est; INCa, Grant/Award Number: PLBIO19-291; Plan Cancer; University of Strasbourg; INSERM

This article is part of the Extracellular Vesicles and Homeostasis Special Collection.

Abstract

Among a plethora of functions, extracellular vesicles released by primary tumors spread in the organism and reach distant organs where they can induce the formation of a premetastatic niche. This constitutes a favorable microenvironment for circulating tumor cells which facilitates their seeding and colonization. In this review, we describe the journey of extracellular vesicles (EVs) from the primary tumor to the future metastatic organ, with a focus on the mechanisms used by EVs to target organs with a specific tropism (i.e., organotropism). We then highlight important tumor EV cargos in the context of premetastatic niche formation and summarize their known effects on extracellular matrix remodeling, angiogenesis, vessel permeabilization, resident cell activation, recruitment of foreign cells, and ultimately the formation of a pro-inflammatory and immuno-tolerant microenvironment. Finally, we discuss current experimental limitations and remaining opened questions in light of metastatic diagnosis and potential therapies targeting PMN formation.

KEYWORDS

extracellular vesicles, metastasis, microenvironment, premetastatic niche

1 | INTRODUCTION

Cancer is among the most common causes of morbidity and mortality worldwide, and the vast majority of cancer-related death is due to metastasis rather than primary tumors.[1] Thus, the limitations of anti-metastasic treatments require a deeper understanding of the complex stepwise process of tumor cell dissemination toward target organs in order to design innovative therapies.[2] Metastasis is a highly inefficient process as only a very

Shima Ghoroghi, Benjamin Mary and Nandini Asokan are co-authors.

Jacky G. Goetz and Vincent Hyenne are co-authors.

small proportion of tumor cells escaping primary tumors are able to successfully form micrometastatic foci in distant organs.[3,4] As they leave the primary tumor, tumor cells face hostile environments with specific and distinct properties: they need to resist harsh forces of blood or lymph shear stress, cross endothelial barriers, evade immune surveillance, settle, and finally proliferate in territories where micro-environmental properties are often distinct from their site of origin.[2,5] It is now well established that metastatic success relies on the capacity of tumor cells to adapt to these variations through cellular and metabolic plasticity. Over the past decade, however, this paradigm evolved with the identification of tumor-released factors able to modify the microenvironment at future metastatic sites before tumor cell arrival. These novel tumor-induced microenvironments are referred to as premetastatic niches (PMNs) and defined by their capacity to facilitate metastasis of circulating tumor cells (CTCs) arriving subsequently.[6] The discovery of PMNs refreshed the "seed and soil" theory established by Stephen Paget in 1889, who proposed that metastasis succeeds in organs where the local microenvironment (the soil) is favorable for tumor cells seeding and colonization (the seed).[7] It appears now that the soil can be fertilized by various types of tumor-secreted factors (reviewed in Refs [6,8]), such as growth factors,[9] cytokines,[10] and extracellular vesicles (EVs), which constitute the focus of this review.

Over the past 10 years, several studies demonstrated that tumor EVs have the capacity to spread away from the primary tumor though body fluids and reach distant organs where they can induce the formation of PMNs. EVs regroup a heterogenous collection of secreted vesicles with diameters ranging from a few nm to several μm, containing various cargos (RNAs, lipids, and proteins) and responding to a plethora of names (exosomes, microvesicles, oncosomes, and much more).[11–13] Conceptually, EVs present the advantage of harboring combinations of molecules with potential signaling properties protected or inserted within a resistant lipid bilayer.[14] Multiple evidences now show that EVs can carry functional cargo and modify the microenvironment by affecting the phenotype of their receiving cells or by altering the organization of the extracellular matrix (ECM).[14–17] Importantly, recent studies reported the capacity of EVs to mediate the communication between distant organs in several physiologic and pathologic contexts.[18–21] This raises an exciting functional potential for the high amounts of EVs present in all body fluids (average concentration 10^9 EVs/ml in human blood with important variations[22]). However, it is important to acknowledge that at this stage, the fate and function of most EVs naturally present in body fluids are far from being understood.

It is now firmly established that tumor-secreted EVs can impact multiple aspects of tumor progression such as proliferation, invasion, drug resistance, endothelial permeability, or immune response.[17,23,24] Their high heterogeneity is likely to explain the diversity of their function, their range of action (local or distant), and ultimately their impact on tumor progression (pro- or anti-tumoral). In this review, we will describe the common features of PMNs and explain how tumor EVs, and their cargo, contribute to their formation. We will discuss the diagnostic and therapeutic consequences of EVs function in PMN formation and highlight the important remaining questions (see Table 1, outstanding questions).

2 | GLOBAL FEATURES OF PREMETASTATIC NICHES

PMNs are characterized by a number of key modifications of the tissue architecture, composition, and metabolism, which facilitate CTCs arrival and expansion. So far, PMNs have been essentially described in rodent models and direct evidences of the PMNs existence in human are rare and mostly observed in sentinel lymph nodes and lungs.[6,25–27] This can be explained by the difficulty to obtain patients tissue samples from future metastatic sites. Nevertheless, PMNs have been observed in future metastatic organs of mice bearing orthotopic primary

TABLE 1 Outstanding questions

Do tumor EV subtypes and EV content evolve as tumor grows?
What is the frequency of EV release from primary tumors during tumor progression and what is the proportion of secreted EVs able to reach PMN?
Are intratumoral regions/clones identical in secreting EVs (levels and cargo)?
What is the dynamic of EVs and CTCs arrival on metastatic sites?
What is the relative contribution of EVs and other tumor-derived secreted factors to PMN?
What are the tissue-specific ligands driving EV organotropism and how can we identify them?
Once metastasis has formed, is there a permanent bi-directional exchange of EVs between primary, secondary, or tertiary tumor sites?
To what extent, do the stromal/non-tumor EVs contribute to the formation of PMN and eventually metastasis?
Are the tumor EV-induced re-programming of stromal cells a transient feature in the PMN or stable over time?
What is the balance between pro- and anti-metastatic EVs secreted by tumor cells and how can it be tuned?
What is the best strategy to target blood-borne EVs when treating metastasis?

tumors.[28–31] For instance, bone marrow lesions were observed in mice bearing mammary breast tumors, before the arrival of tumor cells.[28] However, most of our knowledge on PMN formation emerged from mouse models where PMN is induced by injection of tumor-secreted factors. Such experimental approaches provide direct evidence for the function of PMN promoting factors and opportunities to dissect the first steps of PMN formation. However, these approaches also contain inherent limits when compared to the real pathophysiologic situation, since they often rely on the repeated bolus injection of high amounts of tumor-derived factors, which unlikely mimic their natural release.

PMNs have been described in different organs such as lungs, liver, brain, lymph nodes, and bone marrow, with various associated primary tumor types (breast, pancreatic, colorectal cancer, and melanoma...).[6] The initial alteration of PMNs is believed to take place at the entry gates of the target organ, the blood vessels, which is the most efficient route for long distance communication. Several studies report the disruption of endothelial junctions, breakdown of vascular basement membranes, and ultimately permeabilization of the endothelium before the arrival of CTCs.[32,33] It is tempting to speculate that initial permeabilization of the endothelium by tumor-secreted factors triggers a positive feedback loop promoting the increased accumulation of such factors in the target organ and finally facilitating CTC extravasation. Other key features of the PMN are the activation of resident stromal cells, (such as fibroblasts or myeloid cells) and the recruitment of new cells (such as bone marrow-derived cells (BMDCs) or neutrophils) from other organs, by tumor-secreted factors.[6,34] These changes in cell phenotypes and populations will alter the homeostasis of the tissue on multiple levels: promotion of ECM remodeling, alteration of cell metabolism,[29] and triggering of a pro-inflammatory[33,35,36] and immunosuppressive environment.[33,37] ECM remodeling can be orchestrated by resident cells as fibroblasts or macrophages or by newly recruited myeloid cells.[9,31,38,39] It occurs either through the deposition of new ECM components or through the alteration of pre-existing ones (such as fibronectin, periostin, or versican among others).[9,30,31,40,41] Altered ECM composition and organization can then promote the recruitment of BMDCs as well as the homing of CTCs to the PMN.[33,34,38,42] These events are likely to constitute a second positive feedback loop contributing to the reinforcement of PMNs, as recruited BMDCs will contribute to ECM remodeling which will further promote BMDC recruitment. Finally, the activation of resident cells and recruitment of novel cells will induce the formation of a pro-inflammatory and immunosuppressive microenvironment, which will actively contribute to efficient PMN formation.[35,38,43–47]

Formation of this complex pre-metastatic environment results from the interplay between various types of tumor-secreted soluble molecules and heterogenous tumor-derived EVs. Importantly, additional external factors, such as aging, infection, cancer treatment, or surgery could directly contribute to PMN evolution. Our review is focused on the role of tumor EVs in PMN formation, but they likely function in close relationship with tumor-derived and tumor-independent factors. The journey of EVs toward the PMN is a multistep process, involving their secretion from tumor cells, their travel in blood and lymphatic circulation, their accumulation in distant organs, usually following a non-random pattern (organotropism), their exit from circulation, and their uptake by recipient cells where they prime the PMN formation (Figure 1).

3 | LEAVING THE PRIMARY TUMOR

The capacity of tumor cells to secrete high levels of pro-metastatic EVs clearly correlates with their ability to metastasize from a primary tumor.[34,48,49] For instance, depletion of genes involved in EV secretion, such as Rab27a, nSMase2, RalA, or RalB in aggressive tumor cells leads to a decrease in both the levels of secreted EVs in vitro and metastasis in vivo.[34,50–53] Importantly, the content of released EVs might even be more relevant for PMN formation than their actual number. Indeed, several studies showed that injection of an equal number of tumor EVs with different contents has different impact on PMN formation.[35,38,52] However, the heterogeneity of tumor EVs composition, in addition to the variety of documented EVs sub-populations, is far from being fully elucidated (see Table 1, outstanding questions). Therefore, it will be essential to characterize precisely the content and the amount of released EVs along tumor progression in order to define the identity of EV subtypes that directly contribute to PMN formation (see Table 1, outstanding questions). The secretion of pro-metastatic EVs is likely to vary as tumor progresses, depending on the primary tumor microenvironment. For instance, EVs secreted by tumor cells cultured in hypoxic conditions have enhanced capacities to promote PMN formation.[54,55] Importantly, the secretion of pro-metastatic EVs is enhanced when tumor cells are exposed to chemotherapeutic treatments, revealing that attempts to inhibit primary tumor can actually result in PMN priming and increased metastasis.[56,57]

Independently of their heterogeneity, the dynamics of EV release by tumors have been poorly described in vivo so far (see Table 1, outstanding questions), as it remains technically challenging to track EVs from their secretion to their uptake. It is likely that tumor EVs are

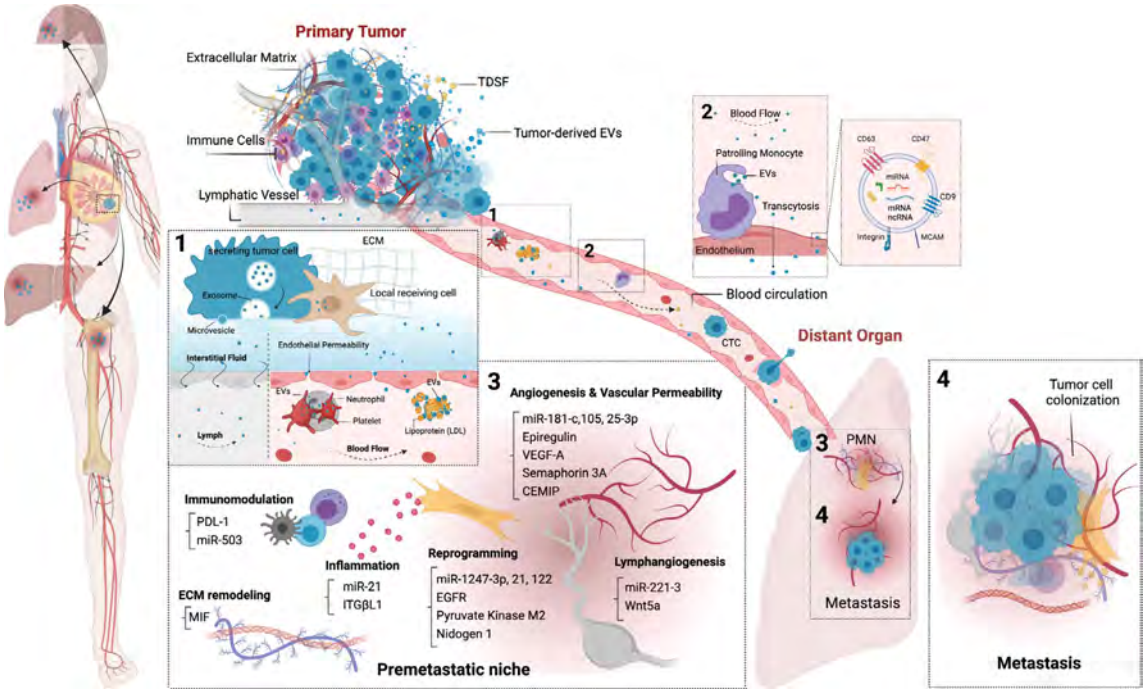

FIGURE 1 Tumor extracellular vesicles prime premetastatic niches. The journey of EVs from the primary tumor to the future metastatic organ is a multistep process initiated with the secretion of tumor-derived EVs and other tumor-derived soluble factors (TDSF) from the primary tumor. 1. Upon secretion, tumor-derived EVs leave the primary tumor and travel through the blood and lymphatic circulation, where they interact with blood components like neutrophils, endothelial cells, platelets, low-density lipoproteins (LDL), and other immune cells. These interactions affect blood homeostasis, enhance the uptake of tumor EVs by distinct recipient cells, and could induce endothelial permeabilization, thereby promoting the formation of premetastatic niche (PMN). 2. Tumor EVs are further taken up by patrolling monocytes and endothelial cells and some of the tumor EVs pass through the impermeable endothelial cells within the tissue by transcytosis. Uptake of tumor EVs by these recipient cells can directly impact the PMN formation. Inset shows a magnified tumor EV, that are encapsulated by a lipid bilayer, containing various biomolecules such as DNA, RNA, proteins as well glycans, specialized receptors at their surface (CD47, CD9, and CD63), and several adhesion proteins such as integrins and MCAM. 3. *Key features of the PMN*. Highlighted are the key features of the PMN and their associated tumor EV cargos that actively contribute to efficient PMN formation. Upon internalization by distinct recipient cells, tumor EVs deliver their cargo, induce phenotypic changes in them, thereby promoting ECM remodeling, reprogramming cell metabolism, inducing immunomodulation, angiogenesis and vascular permeability, lymphangiogenesis, and also triggering pro-inflammatory molecules. All these salient features eventually promote PMN formation. 4. Following the PMN formation, circulating tumor cells (CTCs) eventually reach the PMN and colonize in the new tissue, leading to metastasis. Highlighted in the far left, is the human women model demonstrating organotrophic metastasis, where primary breast tumor-secreted EVs prime PMN at distant organs such as lungs, brain, liver, and bone. Created with BioRender.com

secreted very early, akin to metastatic tumor cells,[58] and thereby prime PMNs before tumors can be diagnosed. Key experiments performed in mice using the Cre-lox system revealed that tumor EV transfer occurs not only at short distance between neighboring cells within the primary tumor mass but also with cells located in distant organs.[59,60] Release of EVs from the primary tumor must account for random movements in interstitial fluids, interactions with the ECM, and uptake by neighbor cells. Indeed, EVs, which often express ECM adhesion and degradation proteins at their surface, were shown to interact with distinct types of matrix and eventually remodel their organization.[40,61,62] Therefore, it is possible that only a small proportion of secreted tumor EVs reach the circulation and spread in the organism. The retention of some EVs within the primary tumors might select a sub-population of spreading EVs with specific adhesive properties. Tumor EVs can be found in blood and lymphatic circulation[63,64] (Figure 1). How they safely reach circulation has not been firmly demonstrated, but it can be speculated that they are transported by interstitial fluids to reach lymphatic vessels. Indeed, in tumors, high interstitial fluid pressure induces a convective flow from blood vessels toward the lymphatic vessels.[65] Besides,

tumor EVs could benefit from abnormally permeabilized blood vessels characteristic of tumors to reach the blood circulation.[66] Interestingly, tumor EVs bearing PMN markers are more concentrated in lymph than in blood from melanoma patients.[63,64] Besides, mice experiments revealed that lymphatic vessels are essential for tumor EVs spreading.[64] Finally, adenocarcinoma, melanoma, or gastric cancer EVs can induce PMN formation in lymph nodes.[67–69] These data suggest that tumor EVs could exploit different routes to reach distant organs and initiate PMN formation. Similarly, tumor cells can in some cases first reach the lymph node, form a first metastatic foci and then transfer to the blood circulation to seed secondary metastasis in more distant organs.[70–72] Whether tumor EVs can follow similar routes ahead of tumor cells and induce a first PMN in lymph nodes and a second one in more distant organs remains to be properly demonstrated. Therefore, in the future, a proper description of the temporal and spatial dynamics of tumor EV spreading away from primary tumors will be instrumental to properly understand the initial steps of PMN formation (see Table 1, outstanding questions).

4 | BEHAVIOR IN CIRCULATION

It is now established that tumor EVs circulate in blood and lymph vessels of cancer patients, alongside non-tumor EVs.[63,73,74] Regardless of their origin, an increase in the levels of circulating EVs or in the amount of protein per EV was reported in lymph and blood circulation of cancer patients.[34,63,75–77] Part of this increase could be directly attributed to the presence of a primary tumor rather than an indirect systemic effect, since surgical removal of the tumor tends to decrease the global levels of circulating EVs as shown for glioblastoma.[75] However, the precise proportion of tumor EVs in the circulation, and even more importantly, the proportion of tumor EVs able to induce or contribute to PMN formation are unknown. As tumor-derived EVs are 20 times more abundant than CTCs in the circulation of metastatic patients[78] a hunt for EV-associated cancer biomarkers was launched over the past years. It allowed the identification of tens of novel potential diagnosis targets, which can either be single RNAs or proteins or more complex molecular signatures.[48,79–81] Even if the clinical validation of most of these findings is still awaited, the molecular signatures carried by circulating EVs could eventually provide identification of specific cancer types, progression stages, or predict therapeutic response. In addition, the molecular study of circulating EVs in patients body fluids, if correlated with metastasis formation could contribute to a better understanding of PMNs in humans.

Despite being stable for days in serum, EVs' half-life in the circulation remain low.[82,83] Indeed, reports in mice and zebrafish show that exogenous EVs have a very short half-life (2–10 min) in the blood circulation.[82,84–86] This short circulating time is mostly explained by the rapid uptake of circulating EVs by patrolling monocytes and endothelial cells.[83,84,87] In circulation, EVs are subjected to a highly dynamic environment, defined by important biomechanical forces with unknown consequences on their biology.[5] Recently, the use of zebrafish embryo, an emerging model in cancer biology,[88–91] allowed the first in vivo description of circulating endogenous and exogenous EVs with high spatio-temporal resolution.[21,84] The distribution of circulating EVs in blood vessels follow the Poiseuille law: they circulate faster in the center of the vessel than on its margins, where they can eventually be seen rolling on the surface of the endothelium. This reduced velocity at the margin of the vessel likely drives their uptake by endothelial cells.

5 | INTERACTION WITH BLOOD COMPONENTS

Circulating tumor EVs can also interact with several blood components, such as circulating immune cells, lipoproteins, platelets, or endothelial cells, but probably not with circulating red blood cells[84,92,93] (Figure 1). These interactions can have direct consequences on blood homeostasis. For instance, several reports show that tumor EVs transport pro-coagulant factors such as tissue factor, PSGL-1, or podoplanin and promote thrombosis through interactions with platelets or with neutrophils.[94–97] The pro-thrombotic activity of tumor EVs appears to vary depending on the subtype of EV and the stage of the secreting tumor cell.[96,98] While platelet aggregation correlates with PMN formation,[99] the role of tumor EVs in this process has not yet been investigated. In addition to platelets, EVs from brain metastasis (originating from breast cancer and melanoma cells), were shown to interact with blood low-density lipoproteins and to trigger their aggregation.[92] This interaction enhances the uptake of EVs by monocytes and could, therefore, potentially affect PMN formation.

The uptake of circulating tumor EVs by endothelial cells and patrolling monocytes can directly impact PMN formation (Figure 1). Indeed, several studies report that tumor EVs induce permeabilization of the endothelium,[93,100,101] which could constitute a first step in PMN formation.[32,33] Patrolling monocytes are mostly considered anti-metastatic through their capacity to take up tumor-derived material and promote the recruitment and activation of natural killer cells.[102] Indeed, the uptake of EVs from non-metastatic tumor cells by patrolling

monocytes prevents the establishment of a PMN in the lung.[103] Similarly, in lymph nodes, sub-capsular macrophages block tumor EVs dissemination and limit tumor progression.[104] Accordingly, anti-tumor EVs induced the accumulation of patrolling monocytes to the lungs, thereby inhibiting metastasis.[105] Therefore, while the uptake of circulating tumor EVs by endothelial cells seems to mostly promote PMN formation, their uptake by patrolling monocytes prevents it. Along this line, EVs which are the most efficient at inducing PMN formation could have the capacity to escape patrolling monocytes surveillance. This could be achieved by specialized receptors at the surface of EVs, as for instance, the glycoprotein CD47 limits their uptake by patrolling monocytes.[87] Alternatively, PMN-efficient EVs could be taken up by patrolling monocyte and modify their phenotype to the benefit of PMN formation, for instance, by promoting TNF-α expression and inducing a pro-inflammatory environment.[84]

Altogether, these studies suggest that the interactions of tumor EVs with various circulating factors have direct consequences on PMN formation.

6 | ORGAN TARGETING

Deciphering the mechanisms controlling the biodistribution of tumor EVs is essential to understand the early steps of PMN formation. To date, this question has been mostly tackled by tracking pre-labeled exogenous EVs injected as a bolus in mouse circulation. This approach has some limitations since the injection site and the labeling method of EVs can impact their biodistribution.[106,107] Nevertheless, a recent study showed that prostate cancer EVs injected in the circulation reach the bone marrow similar to CD63-GFP EVs secreted by orthotopic grafted tumor cells.[108] Importantly, EVs from different cell types tend to accumulate in different organs and in general injected EVs do not arrest at the first capillary bed they encounter, suggesting the existence of specific targeting or retention mechanisms.[106] Indeed, an increasing number of studies demonstrated the existence of tumor EVs organotropism by showing that they accumulate preferentially in the organs where their secreting cells mostly form metastasis.[35,46,52,109,110] Similar to tumor cell organotropism, tumor EV organotropism could be dictated by a balance between hemodynamics, vascular patterns, and intrinsic adhesive properties.[5,111] Accordingly, circulating EVs were shown to accumulate mostly in vascular regions with a low blood flow speed in zebrafish embryo.[21,84] However, the precise contribution of hemodynamics in EVs biodistribution has not been elucidated yet. In contrast, several adhesion proteins, such as integrins, MCAM/CD146, and tetraspanins Tspan8 and CD151 were shown to mediate EV biodistribution and PMN fo rmation.[35,52,110,112–114] Depletion of these receptors or inhibition of their adhesive properties alters EVs biodistribution and their capacity to form PMNs in mice models. For example, the presence of integrin β_4 on breast tumor EVs is necessary for their lung accumulation.[35] Strikingly, forced expression of integrin β_4 on tumor EVs which normally accumulate in bones is sufficient to promote their lung tropism.[35] In addition to the identity of these adhesion proteins, their posttranslational modifications could contribute to EV organotropism, since the global levels of glycosylation on EVs were recently shown to impact their biodistribution.[115] Although this has not been formally demonstrated yet, the combination of adhesion molecules present at the surface of tumor EVs may define a zip-code for EV organotropism. Supporting this hypothesis, it was shown that the co-expression of a tetraspanin (Tspan8) with an integrin (ITGα_4) defines the novel biodistribution of pancreatic adenocarcinoma EVs in rats.[116] Importantly, although ligands of integrins, tetraspanins, or CD146 have been characterized in various contexts, their identity in EV organotropism and PMN formation has not been revealed. This is a crucial question since the receptor-mediated EV organotropism hypothesis implies the existence of organ-specific differentially enriched ligands (see Table 1, outstanding questions). Finally, while CTCs and immune cells often exploit low and high affinity receptors to engage and subsequently stabilize their adhesion,[117,118] more work is needed to identify whether such scenario is at play for EVs.

7 | MECHANISMS OF PMN PRIMING BY TUMOR EVS

Once they have reached their target organ, tumor EVs initiate most of the microenvironmental changes observed in PMNs and described earlier (Figure 1). In this section, we will review the mechanisms triggered by tumor EVs, identify the major EV cargos, and describe the subsequent chain of events leading to PMN formation.

7.1 | Vascular permeability and angiogenesis

Tumor EVs internalized by endothelial cells were reported to promote endothelial permeability through different molecular pathways triggered by their miRNAs or protein cargos. For instance, miRNAs miR-105 and miR-25-3p, respectively, present in EVs from breast or colorectal cancer cells, induce a direct or indirect decrease in the expression of tight junction components, which

leads to endothelial permeability, PMN formation, and ultimately to increased metastasis in the liver, lung, and brain of mice.[101,119] Another miRNA, miR-181c, present in EVs from breast cancer metastatic cells, downregulates the actin regulator PDPK1 and disrupts endothelial cell–cell junctions in the blood–brain barrier, thereby leading to an increased brain metastatic.[93] Besides, several tumor EV protein cargos, such as semaphorin3A, epiregulin, or VEGF-A are responsible for blood vessel permeability in distant organs.[100,120,121]

In addition, tumor-derived EVs facilitate PMN formation by promoting angiogenesis in distant organs in the absence of tumor cells.[121–123] For instance, several EV cargos, such as CEMIP, epiregulin, or VEGF-A have the capacity to induce vascular remodeling in brain or lung PMNs.[120,121,123] CEMIP-induced angiogenesis leads to the formation of pro-inflammatory peri-vascular niches where colonizing tumor cells accumulate.[123] Similar to their action on blood vessels, tumor EVs can affect lymphatic vessels and promote lymphangiogenesis in lymph nodes.[124–126] For instance, miR-221-3p enriched in EVs derived from cervical squamous carcinoma cells, induces the downregulation of the lymphangiogenesis inhibitor vasohibin-1 in lymphatic endothelial cells, thereby promoting lymph PMN and metastasis.[125] A more indirect role was described for EVs from colorectal cancer cells, which can induce the expression of VEGF-C by macrophages in an IRF-2-dependent manner. In turn VEGF-C promotes remodeling of the lymphatic network and subsequently facilitates lymph node metastasis.[124] Wnt5a present in EVs from gastric cancer activates the YAP transcription factor in bone marrow-derived mesenchymal stem cells, leading to enhanced lymphangiogenesis and PMN formation.[126] Altogether, these studies show that various cargos present in EVs from different tumor origins tune the vascular and lymphatic systems at multiple future metastatic sites.

7.2 | Matrix remodeling

Increased endothelial permeability would allow circulating EVs to cross more easily the endothelial barrier and accumulate in the target organ. In addition, tumor EVs can be transported throughout impermeable endothelial vessels by transcytosis and be released within the tissue.[127] Tumor EVs contain multiple adhesion receptors and matrix metalloproteases which allow them to bind different types of ECMs and directly alter their composition and their organization in PMNs.[40,112] In addition, tumor EVs indirectly induce matrix remodeling by activating resident cells. For instance, breast cancer or pancreatic ductal adenocarcinoma EVs activate lung fibroblasts and promote fibronectin secretion and reorganization.[31,35] Similarly, tumor EVs RNA cargos promote Toll-like receptor3 (TLR3)-dependent secretion of fibronectin by lung alveolar epithelial cells.[43] Costa-Silva and colleagues described a complete cascade of events starting with pancreatic cancer EVs and ending in the reorganization of three ECM components (vitronectin, Tenascin C, and fibronectin) and the formation of a pro-inflammatory microenvironment.[38] In brief, macrophage migration inhibitory factor (MIF) contained in tumor EVs induces the secretion of TGF-β by Kupffer cells, which in turn promotes the production of fibronectin by hepatic stellate cells and ultimately the recruitment of bone marrow-derived macrophages to the liver.[38] Moreover, osteosarcoma EVs-associated TGFβ1, upon internalization by lung fibroblasts-induced pulmonary fibroblast differentiation and upregulated variety of ECM components that promoted invasive competence of these cells and tumor progression in distant PMN.[128] Interestingly, depending on the tumor subtype they come from, breast cancer EVs can induce different compositions of ECM in lung PMNs.[30] Therefore, tumor EVs are clear regulators of ECM remodeling in PMNs. This can directly affect the cell composition of PMNs by contributing to the recruitment of various immune cells[42] and favoring tumor cell colonization.

7.3 | Activation of tissue-resident cells

As described above, activation of fibroblasts or macrophages by tumor EVs can lead to ECM modification remodeling. In addition, tumor EVs can modify the cytokine and growth factor secretion pattern of resident stromal cells. EVs from hepatocellular carcinoma, for instance, can induce the activation of cancer-associated fibroblasts (CAFs) in the lung PMN through two different mechanisms: via miR-1247-3p and the activation of NF-κB signaling pathway[129] or by Nidogen 1 and TNFR1 secretion.[130] CAF activation results in the secretion of pro-inflammatory cytokines which contribute to PMN establishment.[129,131] Activation of resident fibroblasts by tumor EVs could induce a positive feedback loop, as CAFs EVs can further promote PMN formation in lungs.[132] Other resident cells can be activated by tumor EVs, depending on the organ. In bone marrow, for instance, the transfer of pyruvate kinase M2 from prostate cancer EVs to bone marrow stromal cells leads to an increased secretion of CXCL12, which sustains prostate cancer cell growth and metastasis.[108] Likewise, the transfer of miR-21 from breast cancer EVs to osteoclasts triggers their differentiation and activation, favoring the establishment of bone metastasis in breast cancer model.[133] In the liver, EGFR-loaded EVs drive the expression of hepatocyte growth factor (HGF) in stromal cells, which further promotes liver metastasis.[134]

In addition, recent studies showed that tumor EVs contain regulators of metabolism and have the capacity to modulate the metabolism in PMNs.[29] For instance, miR-122 downregulates the glycolytic enzyme pyruvate kinase in lung stromal cells during breast cancer metastasis. The decrease of glucose uptake by stromal cells results in an increase in nutrient availability for tumor cells, thereby promoting metastasis.[29]

7.4 | Pro-inflammatory environment

EV-dependent activation of resident cells (and recruited immune cells) induces the formation of a pro-inflammatory microenvironment in various PMNs[34,35,38,135] For example, the arrival of melanoma EVs to the lungs favors the expression of pro-inflammatory molecules TNF, S100A8 and S100A9, which lead to BMDCs recruitment to the lung PMNs.[34] A similar increase of S100 proteins was observed in lung and liver PMNs.[35] In addition, secretion of pro-inflammatory cytokines can be induced by tumor EVs.[131,135,136] For instance, secretion of the IL6 by resident macrophages is increased by miR-21 containing tEVs from colorectal cancer cells in liver PMNs.[136] IL6 and IL8 can also be secreted by fibroblasts activated by integrin beta-like 1 enriched EVs from colorectal cancer cells through a TNFAIP3-mediated NF-κβ signaling pathway.[131] Altogether, EVs orchestrate the formation of an inflammatory environment that is a hallmark of PMN.

7.5 | Cells recruitment to PMN

Another important hallmark of PMNs consists in the recruitment of cells from other organs. Originally, pioneer work from the group of D. Lyden demonstrated that inflammation in PMNs leads to the recruitment of BMDCs.[34] Since then, different types of immune cells were shown to be recruited to PMNs. For instance, monocytes can be recruited to PMNs by tumor EV-induced upregulation of CCL2 in resident macrophages or endothelial cells.[57,137] Additionally, activation of alveolar epithelial cells by small nuclear RNA melanoma EVs leads to an enhanced secretion of cytokines which promotes neutrophil recruitment to the lung PMN.[43] Neutrophils can suppress anti-tumor immunity, create an inflammatory microenvironment, retain CTCs in the organ vasculature, and promote their colonization.[138–141]

7.6 | Immunomodulation

Tumor EVs have antagonist effects on the immune system, as they can both deliver tumor antigens to antigen presenting cells, thereby activating the immune system, but also suppress the anti-tumor immune response by targeting various immune cells.[24] While most studies focused on primary tumors, some evidences show that tumor EVs modulate both innate and adaptative immunity in PMN.[34,46,104,142] For instance, breast cancer EVs promote the accumulation of BMDCs, directly inhibit T-cell growth, and decrease Natural killer (NK) cell cytotoxicity leading to the formation of an immunosuppressive environment in lung PMN.[46] Interestingly, intravital imaging revealed that extravasating tumor cells release large EVs which are taken up by different myeloid cells arriving sequentially at the metastatic site. This EV uptake induces phenotypic changes in receiving immune cells and promotes metastasis.[143] Besides tumor EVs have the capacity to mediate immune suppression, notably through the PD-1–PD-L1 axis.[24] Indeed, metastatic melanoma EVs carrying programmed death-ligand 1 (PD-L1) on their surface have the capacity to inhibit anti-tumoral CD8 T-cell function and promote tumor progression.[144] A recent study suggests that breast cancer EVs carrying miR-503 promote the M1–M2 conversion of microglia, which results in enhanced PD-L1 expression and suppression of local immunity in brain metastasis.[145] Overall, the balance between pro- and anti-tumor roles of EVs on distant immune cell populations remains to be fully investigated as it could open novel therapeutic avenues.

8 | CONCLUSIONS

Although the understanding of PMNs considerably progressed since their initial description in 2005, a large number of fundamental questions remain opened (see Table 1, outstanding questions).

First of all, the existence of PMNs implies that tumor-secreted factors, including EVs, reach distant organs before the arrival of CTCs. Although the exact timing and dynamics have not been solved, some experiments using orthotopic primary tumors show the localization of tumor EVs and/or distant microenvironmental changes happening before tumor cells could be detected.[28,29,31,108] However, this sequence of events has not been firmly proven in a relevant orthotopic spontaneous tumor model. This is important in particular because tumor cell spreading to future metastatic sites was shown to be an early event in several types of cancer.[146–148] While early disseminating CTCs mostly enter dormancy,[149] it could be speculated that disseminating tumor EVs instead or in addition to altering the distant microenvironment before tumor cell arrival, are also able to help awakening rare dormant tumor cells already present on site. This is appealing since dormant cell often reside in perivascular niches,[150] where

they would be in good position to receive circulating EVs and soluble factors. Interestingly, recent studies showed that EVs from stromal cells have the capacity to mediate tumor cell dormancy.[151–155] Whether EVs shed by primary tumors can also perturb tumor cell dormancy remains to be explored, yet such discoveries would provide exciting treatment options for counteracting the major issue of tumor cell dormancy. More generally, determining the relative dynamics of EVs and cell release from primary tumors is essential for the definition and the understanding of PMN formation, but also to design adapted therapeutic strategies.[156]

Along the same line, it will be essential to describe the dynamics of EVs release during tumor progression, and its impact on driving efficient PMNs. Notably, whether tumor EVs continue to land to metastatic sites once metastasis has started is not known, yet this is likely to happen. While metastatic growth surely benefits from permanent feeding by EVs released from the primary tumor, metastatic outgrowth might feedback on the primary tumor, akin to metastatic cells. Indeed, the communication between primary and secondary tumor sites is not unidirectional as tumor cells from metastasis can recolonize primary tumors, in a process called tumor self-seeding.[157] In addition, tumor cells were shown to redisseminate from metastatic to tertiary sites[158] raising the possibility that EVs from metastatic foci can prime additional PMNs. Interestingly, studies report that tumor EVs, either injected in the circulation or co-incubated with tumor cells before injection, promote tumor self-seeding in mice.[159,160] If it is not known yet whether EVs from metastatic sites can target primary tumors, Zomer and colleagues made elegant use of in vivo imaging to show that two distinct primary tumor sites can exchange EVs.[60] Such intravital imaging of EVs shuttling in relevant metastasis models would undoubtedly help addressing these issues and increase our understanding of the (bio)genesis of PMNs.[60,104,161,162]

PMN formation is induced by a complex interplay of soluble molecules and EVs, whose precise orchestration remains to be understood. For this, it will be essential to characterize the heterogeneity of EVs released by primary tumors, as they have antagonist effects on PMN formation, notably by inducing differential immune responses. It would be particularly interesting to link EVs heterogeneity to intratumor heterogeneity which is a key driver of therapy resistance and metastasis[163] and to document the impact of EVs released in this difficult context of therapy resistance. In addition, while significant progress has been made in understanding the identity and position of cells that have metastatic potential within tumors, whether similar regions and cellular identity correlated with EV secretion potential and function would be an exciting area of research (see Table 1, outstanding questions). It will be equally important to fully characterize EVs secreted by non-tumoral cells, which populate, react, and participate to tumor growth, as they also play a significant role in PMN formation.[132,164] Additionally, exogenous EVs, such as bovine milk-derived EVs, could directly impact metastasis.[165] Finally, tumor-secreted EVs are not always sufficient to induce PMN formation and require the additional contribution of tumor-secreted factors.[128] Therefore, the relative contribution of tumor released soluble factors and EVs and their potential cooperation will have to be studied in detail (see Table 1, outstanding questions). Interestingly, the interaction between tumor EVs and cytokines, in particular CCL2, was recently shown to modify their organotropism, the formation of PMNs, and finally lung metastasis.[142]

While several clinical trials aiming to block PMN formation are already undergoing,[6] a fine understanding of the contribution of tumor EVs to PMN formation could pave the way for novel therapeutic approaches. For instance, it could be possible to inhibit EV secretion from primary tumors, since this approach decreases metastasis in mice.[34,50–53] Alternatively, tuning the balance of pro- versus anti-tumoral EVs released by tumor cells could improve the anti-tumoral immune response (see Table 1, outstanding questions). Another exciting, yet tricky, possibility would be to target and stop tumor EVs in the circulation. In a recent study, Nishida-Aoki and colleagues showed that intravenous injection of anti-humanCD9 or anti-humanCD63 antibodies decreases lung metastasis in mice bearing orthotopic breast xenografts.[166] Therefore, the identification of tumor EVs-specific surface proteins would allow to distinguish them from non-tumoral ones and would constitute ideal candidates for such therapeutic approaches. Finally, targeting the mechanisms of pro-metastatic tumor EVs uptake by resident stromal cells constitutes a promising possibility to prevent metastasis, as shown in mice where reserpine suppresses tumor EV uptake and disrupts PMN formation.[167]

Altogether, tumor EVs are central players in PMN formation and constitute diagnostic and therapeutic targets to detect and treat metastasis progression.

ACKNOWLEDGMENTS

This work was supported by fellowships from IDEX (University of Strasbourg), ARC (Association pour le Recherche sur le Cancer), and FRM (Fondation pour la Recherche Médicale) to SG and BM; by grants from La Ligue contre le Cancer, Canceropole Grand-Est, INCa (PLBIO19-291), Plan Cancer (Nanotumor and Vesmatic) to VH and JGG; and by institutional funds from the University of Strasbourg and INSERM to JGG.

CONFLICT OF INTEREST

None.

AUTHOR CONTRIBUTIONS

All authors contributed to writing and editing the review.

ORCID

Vincent Hyenne https://orcid.org/0000-0002-1254-2814

REFERENCES

1. Dillekås H, Rogers MS, Straume O. Are 90% of deaths from cancer caused by metastases? *Cancer Med*. 2019;8:5574-5576.
2. Lambert AW, Pattabiraman DR, Weinberg RA. Emerging biological principles of metastasis. *Cell*. 2017;168:670-691.
3. Luzzi KJ, MacDonald IC, Schmidt EE, et al. Multistep nature of metastatic inefficiency dormancy of solitary cells after successful extravasation and limited survival of early micrometastases. *Am J Pathol*. 1998;153:865-873.
4. Cameron MD, Schmidt EE, Kerkvliet N, et al. Temporal progression of metastasis in lung: cell survival, dormancy, and location dependence of metastatic inefficiency. *Can Res*. 2000;60:2541-2546.
5. Follain G, Herrmann D, Harlepp S, et al. Fluids and their mechanics in tumour transit: shaping metastasis. *Nat Rev Cancer*. 2020;20:107-124.
6. Peinado H, Zhang H, Matei IR, et al. Pre-metastatic niches: organ-specific homes for metastases. *Nat Rev Cancer*. 2017;17:302-317.
7. Paget S. The distribution of secondary growths in cancer of the breast. *Lancet*. 1889;133:571-573.
8. Liu Y, Cao X. Characteristics and significance of the pre-metastatic niche. *Cancer Cell*. 2016;30:668-681.
9. Kaplan RN, Riba RD, Zacharoulis S, et al. VEGFR1-positive haematopoietic bone marrow progenitors initiate the pre-metastatic niche. *Nature*. 2005;438:820-827.
10. Qian B-Z, Li J, Zhang H, et al. CCL2 recruits inflammatory monocytes to facilitate breast-tumour metastasis. *Nature*. 2011;475:222-225.
11. Fabbiano F, Corsi J, Gurrieri E, Trevisan C, Notarangelo M, D'Agostino VG. RNA packaging into extracellular vesicles: an orchestra of RNA-binding proteins? *J Extracell Vesicles*. 2020;10(2).
12. van Niel G, D'Angelo G, Raposo G. Shedding light on the cell biology of extracellular vesicles. *Nat Rev Mol Cell Biol*. 2018;19(4):213-228.
13. Skotland T, Hessvik NP, Sandvig K, Llorente A. Exosomal lipid composition and the role of ether lipids and phosphoinositides in exosome biology. *J Lipid Res*. 2019;60:9-18.
14. Mathieu M, Martin-Jaular L, Lavieu G, Théry C. Specificities of secretion and uptake of exosomes and other extracellular vesicles for cell-to-cell communication. *Nat Cell Biol*. 2019;21:9-17.
15. Yáñez-Mó M, Siljander P-M, Andreu Z, et al. Biological properties of extracellular vesicles and their physiological functions. *J Extracel Vesicles*. 2015;4:27066.
16. Boulanger CM, Loyer X, Rautou PE, Amabile N. Extracellular vesicles in coronary artery disease. *Nat Rev Cardiol*. 2017.
17. Kalluri R, LeBleu VS. The biology, function, and biomedical applications of exosomes. *Science*; 2020;367.
18. Kur IM, Prouvot PH, Fu T, et al. Neuronal activity triggers uptake of hematopoietic extracellular vesicles in vivo. *PLoS Biol*. 2020.
19. Thomou T, Mori MA, Dreyfuss JM, et al. Adipose-derived circulating miRNAs regulate gene expression in other tissues. *Nature*. 2017;542:450-455.
20. Whitham M, Parker BL, Friedrichsen M, et al. Extracellular vesicles provide a means for tissue crosstalk during exercise. *Cell Metab*. 2018;27:237-251.e4.
21. Verweij FJ, Revenu C, Arras G, et al. Live tracking of inter-organ communication by endogenous exosomes in vivo. *Dev Cell*. 2019;48:573-589.e4.
22. Johnsen KB, Gudbergsson JM, Andresen TL, Simonsen JB. What is the blood concentration of extracellular vesicles? Implications for the use of extracellular vesicles as blood-borne biomarkers of cancer. *Biochim Biophys Acta Rev Cancer*. 2019;1871:109-116.
23. Sheehan C, D'Souza-Schorey C. Tumor-derived extracellular vesicles: molecular parcels that enable regulation of the immune response in cancer. *J Cell Sci*. 2019;132(20).
24. Marar C, Starich B, Wirtz D. Extracellular vesicles in immunomodulation and tumor progression. *Nat Immunol*. 2021;22:560-570.
25. Matsuura K, Yamaguchi Y, Ueno H, Osaki A, Arihiro K, Toge T. Maturation of dendritic cells and T-cell responses in sentinel lymph nodes from patients with breast carcinoma. *Cancer*. 2006;106(6):1227-1236.
26. Qian C-N, Berghuis B, Tsarfaty G, et al. Preparing the "'soil'": the primary tumor induces vasculature reorganization in the sentinel lymph node before the arrival of metastatic cancer cells. *Cancer Res*. 2006;66:10365-10376.
27. Chung MK, Do I-G, Jung E, et al. Lymphatic vessels and high endothelial venules are increased in the sentinel lymph nodes of patients with oral squamous cell carcinoma before the arrival of tumor cells. *Oncol*. 2012;19:1595-1601.
28. Cox TR, Rumney RMH, Schoof EM, et al. The hypoxic cancer secretome induces pre-metastatic bone lesions through lysyl oxidase. *Nature*. 2015;522:106-110.
29. Fong MY, Zhou W, Liu L, et al. Breast-cancer-secreted miR-122 reprograms glucose metabolism in premetastatic niche to promote metastasis. *Nat Cell Biol*. 2015;17:183-194.
30. Medeiros B, Goodale D, Postenka C, et al. Triple-negative primary breast tumors induce supportive premetastatic changes in the extracellular matrix and soluble components of the lung microenvironment. *Cancers*. 2020;12.
31. Novo D, Heath N, Mitchell L, et al. Mutant p53s generate pro-invasive niches by influencing exosome podocalyxin levels. *Nature Communications*. 2018;9.
32. Huang Y, Song N, Ding Y, et al. Pulmonary vascular destabilization in the premetastatic phase facilitates lung metastasis. *Can Res*. 2009;69:7529-7537.
33. Yan HH, Pickup M, Pang Y, et al. Gr-1+CD11b+ myeloid cells tip the balance of immune protection to tumor promotion in the premetastatic lung. *Cancer Res*. 2010;70(15):6139-6149.
34. Peinado H, Alečković M, Lavotshkin S, et al. Melanoma exosomes educate bone marrow progenitor cells toward a pro-metastatic phenotype through MET. *Nat Med*. 2012;18:883-891.

35. Hoshino A, Costa-Silva B, Shen T-L, et al. Tumour exosome integrins determine organotropic metastasis. *Nature*. 2015;1-19.
36. Hiratsuka S, Watanabe A, Sakurai Y, et al. The S100A8–serum amyloid A3–TLR4 paracrine cascade establishes a pre-metastatic phase. *Nature Cell Biol*. 2008;10(11):1349-1355.
37. Kowanetz M, Wu X, Lee J, et al. Granulocyte-colony stimulating factor promotes lung metastasis through mobilization of Ly6G+Ly6C+ granulocytes. *Proc Natl Acad Sci U S A*. 2010;107(50):21248-21255.
38. Costa-Silva B, Aiello NM, Ocean AJ, et al. Pancreatic cancer exosomes initiate pre-metastatic niche formation in the liver. *Nature Cell Biol*. 2015;17(6):816–826.
39. Gao D, Joshi N, Choi H, et al. Myeloid progenitor cells in the premetastatic lung promote metastases by inducing mesenchymal to epithelial transition. *Cancer Res*. 2012;72(6):1384-1394.
40. Mu W, Rana S, Zöller M. Host matrix modulation by tumor exosomes promotes motility and invasiveness. *Neoplasia*. 2013;15:875-887.
41. Wang Z, Xiong S, Mao Y, et al. Periostin promotes immunosuppressive premetastatic niche formation to facilitate breast tumour metastasis. *J Pathol*. 2016;239:484-495.
42. Erler JT, Bennewith KL, Cox TR, et al. Hypoxia-induced lysyl oxidase is a critical mediator of bone marrow cell recruitment to form the premetastatic niche. *Cancer Cell*. 2009;15:35-44.
43. Liu Y, Gu Y, Han Y, et al. Tumor exosomal RNAs promote lung pre-metastatic niche formation by activating alveolar epithelial TLR3 to recruit neutrophils. *Cancer Cell*. 2016;30:243-256.
44. Seubert B, Grünwald B, Kobuch J. Tissue inhibitor of metalloproteinases (TIMP)-1 creates a premetastatic niche in the liver through SDF-1/CXCR4-dependent neutrophil recruitment in mice. *Hepatology*. 2015;61(1):238-248.
45. Casbon AJ, Reynau D, Park C, et al. Invasive breast cancer reprograms early myeloid differentiation in the bone marrow to generate immunosuppressive neutrophils. *Proc Natl Acad Sci USA*. 2015;112:E566-E575.
46. Wen SW, Sceneay J, Lima LG, et al. The biodistribution and immune suppressive effects of breast cancer-derived exosomes. *Can Res*. 2016;76:6816-6827.
47. Sharma SK, Chintala NK, Vadrevu SK, Patel J, Karbowniczek M, Markiewski MM. Pulmonary alveolar macrophages contribute to the premetastatic niche by suppressing antitumor T cell responses in the lungs. *J Immunol*. 2015;194:5529-5538.
48. Melo SA, Luecke LB, Kahlert C, et al. Glypican-1 identifies cancer exosomes and detects early pancreatic cancer. *Nature*. 2015;523:177-182.
49. Sabbagh Q, Andre-Gregoire G, Guevel L, Gavard J. Vesiclemia: counting on extracellular vesicles for glioblastoma patients. *Oncogene*. 2020;39:6043-6052.
50. Bobrie A, Krumeich S, Reyal F, et al. Rab27a supports exosome-dependent and -independent mechanisms that modify the tumor microenvironment and can promote tumor progression. *Can Res*. 2012;72:4920-4930.
51. Kosaka N, Iguchi H, Hagiwara K, Yoshioka Y, Takeshita F, Ochiya T. Neutral sphingomyelinase 2 (nSMase2)-dependent exosomal transfer of angiogenic micrornas regulate cancer cell metastasis. *J Biol Chem*. 2013;288:10849-10859.
52. Ghoroghi S, Mary B, Larnicol A, et al. Ral GTPases promote breast cancer metastasis by controlling biogenesis and organ targeting of exosomes. *eLife*. 2021;10:e61539.
53. Guo J, Duan Z, Zhang C, et al. Mouse 4T1 breast cancer cell-derived exosomes induce proinflammatory cytokine production in macrophages via miR-183. *J Immunol*. 2020;205:2916-2925.
54. Deep G, Jain A, Kumar A, et al. Exosomes secreted by prostate cancer cells under hypoxia promote matrix metalloproteinases activity at pre-metastatic niches. *Molecular*. 2020;59(3):323-332.
55. Umezu T, Tadokoro H, Azuma K, Yoshizawa S, Ohyashiki K, Ohyashiki JH. Exosomal miR-135b shed from hypoxic multiple myeloma cells enhances angiogenesis by targeting factor-inhibiting HIF-1. *Blood*. 2014;124:3748-3757.
56. Wills CA, Liu X, Chen L, et al. Chemotherapy-induced upregulation of small extracellular vesicle-associated PTX3 accelerates breast cancer metastasis. *Cancer Res*. 2021;81(2):452-463.
57. Keklikoglou I, Cianciaruso C, Güç E, et al. Chemotherapy elicits pro-metastatic extracellular vesicles in breast cancer models. *Nat Cell Biol*. 2019;21(2):190-202.
58. Harper KL, Sosa Sosa M, Entenberg D, et al. *Mechanism of Early Dissemination and Metastasis in Her2+ Mammary Cancer*. Nature Publishing Group; 2016.
59. Ridder K, Sevko A, Heide J, et al. Extracellular vesicle-mediated transfer of functional RNA in the tumor microenvironment. *OncoImmunology*. 2015;4:e1008371.
60. Zomer A, Maynard C, Verweij FJ, et al. In vivo imaging reveals extracellular vesicle-mediated phenocopying of metastatic behavior. *Cell*. 2015;161:1046-1057.
61. Sung BH, Ketova T, Hoshino D, Zijlstra A, Weaver AM. Directional cell movement through tissues is controlled by exosome secretion. *Nat Commun*. 2015;6:7164.
62. Hoshino D, Kirkbride K, Costello K, et al. Exosome secretion is enhanced by invadopodia and drives invasive behavior. *Cell Rep*. 2013;5:1159-1168.
63. García-Silva S, Benito-Martín A, Sánchez-Redondo S, et al. Use of extracellular vesicles from lymphatic drainage as surrogate markers of melanoma progression and BRAF V600E mutation. *J Exp Med*. 2019;jem.20181522.
64. Broggi MAS, Maillat L, Clement CC, et al. Tumor-associated factors are enriched in lymphatic exudate compared to plasma in metastatic melanoma patients. *J Exp Med*. 2019;216(5):1091-1107.
65. Swartz MA, Fleury ME. Interstitial flow and its effects in soft tissues. *Annu Rev Biomed Eng*. 2007;9(1):229-256.
66. Ganss R. Tumour vessel remodelling: new opportunities in cancer treatment. *Vasc Biol*. 2020;2(1):R35-R43.
67. Jung T, Castellana D, Klingbeil P, et al. CD44v6 dependence of premetastatic niche preparation by exosomes. *Neoplasia*. 2009;11:1093-1105.
68. Hood JL, San RS, Wickline SA. Exosomes released by melanoma cells prepare sentinel lymph nodes for tumor metastasis. *Can Res*. 2011;71:3792-3801.
69. Liu D, Li C, Trojanowicz B, et al. CD97 promotion of gastric carcinoma lymphatic metastasis is exosome dependent. *Gastric Cancer*. 2016;19:754-766.
70. Brown M, Assen FP, Leithner A, et al. Lymph node blood vessels provide exit routes for metastatic tumor cell dissemination in mice. *Science*. 2018;359(6382):1408-1411.
71. Naxerova K, Reiter JG, Brachtel E, et al. Origins of lymphatic and distant metastases in human colorectal cancer. *Science*. 2017;357(6346):55-60.

72. Pereira ER, Kedrin D, Seano G, et al. Lymph node metastases can invade local blood vessels, exit the node, and colonize distant organs in mice. *Science*. 2018;359:1403-1407.
73. Notarangelo M, Zucal C, Modelska A, et al. Ultrasensitive detection of cancer biomarkers by nickel-based isolation of polydisperse extracellular vesicles from blood. *EBioMedicine*. 2019;43:114-126.
74. Baran J, Baj-Krzyworzeka M, Weglarczyk K, et al. Circulating tumour-derived microvesicles in plasma of gastric cancer patients. *Cancer Immunol Immunother*. 2010;59:841-850.
75. Osti D, Del Bene M, Rappa G, et al. Clinical significance of extracellular vesicles in plasma from glioblastoma patients. *Clin Cancer Res*. 2019;25(1):266-276.
76. Cappello F, Logozzi M, Campanella C, et al. Exosome levels in human body fluids: a tumor marker by themselves? *Eur J Pharm Sci*. 2017;96:93-98.
77. Logozzi M, De Milito A, Lugini L, et al. High levels of exosomes expressing CD63 and caveolin-1 in plasma of melanoma patients. *PLoS ONE*. 2009;4.
78. Nanou A, Miller MC, Zeune LL, et al. Tumour-derived extracellular vesicles in blood of metastatic cancer patients associate with overall survival. *Br J Cancer*. 2020;122:801-811.
79. Hoshino A, Kim HS, Bojmar L, et al. Extracellular vesicle and particle biomarkers define multiple human cancers. *Cell*. 2020;182:1044-1061.e18.
80. Laurenzana I, Trino S, Lamorte D, et al. Analysis of amount, size, protein phenotype and molecular content of circulating extracellular vesicles identifies new biomarkers in multiple myeloma. *International J Nanomed*. 2021;16:3141-3160.
81. Keup C, Mach P, Aktas B, et al. RNA profiles of circulating tumor cells and extracellular vesicles for therapy stratification of metastatic breast cancer patients. *Clin Chem*. 2018;64(7):1054-1062.
82. Morishita M, Takahashi Y, Nishikawa M, et al. Quantitative analysis of tissue distribution of the B16BL6-derived exosomes using a streptavidin-lactadherin fusion protein and Iodine-125-Labeled biotin derivative after intravenous injection in mice. *J Pharm Sci*. 2015;104:705-713.
83. Imai T, Takahashi Y, Nishikawa M, et al. Macrophage-dependent clearance of systemically administered B16BL6-derived exosomes from the blood circulation in mice. *J Extracell Vesicles*. 2015;4:26238.
84. Hyenne V, Ghoroghi S, Collot M, et al. Studying the fate of tumor extracellular vesicles at high spatiotemporal resolution using the zebrafish embryo. *Dev Cell*. 2019;48:554-572.e7.
85. Lai CP, Mardini O, Ericsson M, et al. Dynamic biodistribution of extracellular vesicles in vivo using a multimodal imaging reporter. *ACS Nano*. 2014;8:483-494.
86. Takahashi Y, Nishikawa M, Shinotsuka H, et al. Visualization and in vivo tracking of the exosomes of murine melanoma B16-BL6 cells in mice after intravenous injection. *J Biotechnol*. 2013;165:77-84.
87. Kamerkar S, LeBleu VS, Sugimoto H, et al. Exosomes facilitate therapeutic targeting of oncogenic KRAS in pancreatic cancer. *Nature*. 2017;546(7659):498-503.
88. Verweij FJ, Hyenne V, Van Niel G, Goetz JG. Extracellular vesicles: catching the light in zebrafish. *Trends Cell Biol*. 2019;29:770-776.
89. Cagan RL, Zon LI, White RM. Modeling cancer with flies and fish. *Dev Cell*. 2019;49:317-324.
90. Mary B, Ghoroghi S, Hyenne V, Goetz JG. Live tracking of extracellular vesicles in larval zebrafish. *Methods Enzymol*. 2020;645:243-275.
91. Osmani N, Goetz JG. Multiscale imaging of metastasis in zebrafish. *Trends Cancer*. 2019;5:766-778.
92. Busatto S, Yang Y, Walker SA, et al. Brain metastases-derived extracellular vesicles induce binding and aggregation of low-density lipoprotein. *J Nanobiotechnology*. 2020;18(1).
93. Tominaga N, Kosaka N, Ono M, et al. Brain metastatic cancer cells release microRNA-181c-containing extracellular vesicles capable of destructing blood–brain barrier. *Nat Commun*. 2015;6:6716.
94. Thomas GM, Panicot-Dubois L, Lacroix R, Dignat-George F, Lombardo D, Dubois C. Cancer cell-derived microparticles bearing P-selectin glycoprotein ligand 1 accelerate thrombus formation in vivo. *J Exp Med*. 2009;206:1913-1927.
95. Tawil N, Bassawon R, Meehan B, et al. Glioblastoma cell populations with distinct oncogenic programs release podoplanin as procoagulant extracellular vesicles. *Blood Adv*. 2021;5(6):1682-1694.
96. Gomes FG, Sandim V, Almeida VH, et al. Breast-cancer extracellular vesicles induce platelet activation and aggregation by tissue factor-independent and -dependent mechanisms. *Thromb Res*. 2017;159:24-32.
97. Leal AC, Mizurini DM, Gomes T, et al. Tumor-derived exosomes induce the formation of neutrophil extracellular traps: implications for the establishment of cancer-associated thrombosis. *Sci Rep*. 2017;7.
98. Durrieu L, Bharadwaj A, Waisman DM. Analysis of the thrombotic and fibrinolytic activities of tumor cell–derived extracellular vesicles. *Blood Adv*. 2018;2(10):1054-1065.
99. Lucotti S, Cerutti C, Soyer M, et al. Aspirin blocks formation of metastatic intravascular niches by inhibiting platelet-derived COX-1/thromboxane A2. *J Clinical Investigation*. 2019;129:1845-1862.
100. Treps L, Edmond S, Harford-Wright E, et al. Extracellular vesicle-transported Semaphorin3A promotes vascular permeability in glioblastoma. *Oncogene*. 2016;35:2615-2623.
101. Zhou W, Fong MY, Min Y, et al. Cancer-secreted miR-105 destroys vascular endothelial barriers to promote metastasis. *Cancer Cell*. 2014;25:501-515.
102. Hanna RN, Cekic C, Sag D, et al. Patrolling monocytes control tumor metastasis to the lung. *Science*. 2015;350:985-990.
103. Plebanek MP, Angeloni NL, Vinokour E, et al. Pre-metastatic cancer exosomes induce immune surveillance by patrolling monocytes at the metastatic niche. *Nature Communications*. 2017;8.
104. Pucci F, Garris C, Lai CP, et al. SCS macrophages suppress melanoma by restricting tumor-derived vesicle-B cell interactions. *Science*. 2016;352(6282):242-246.
105. Schuldner M, Dörsam B, Shatnyeva O, et al. Exosome-dependent immune surveillance at the metastatic niche requires BAG6 and CBP/p300-dependent acetylation of p53. *Theranostics*. 2019;9:6047-6062.
106. Gupta D, Liang X, Pavlova S, et al. Quantification of extracellular vesicles *in vitro* and *in vivo* using sensitive bioluminescence imaging. *J Extacell Vesicles*. 2020;9.
107. Wiklander OPB, Nordin JZ, O'Loughlin A, et al. Extracellular vesicle in vivo biodistribution is determined by cell source, route of administration and targeting. *J Extracell Vesicles*. 2015;4:26316.

108. Dai J, Escara-Wilke J, Keller JM, et al. Primary prostate cancer educates bone stroma through exosomal pyruvate kinase M2 to promote bone metastasis. *J Exp Med*. 2019;216:2883-2899.
109. Gerwing M, Kocman V, Stölting M, et al. Tracking of tumor cell-derived extracellular vesicles in vivo reveals a specific distribution pattern with consecutive biological effects on target sites of metastasis. *Mol Imaging Biol*. 2020;22:1501-1510.
110. Wu AYT, Sung YC, Chen YJ, et al. Multiresolution imaging using bioluminescence resonance energy transfer identifies distinct biodistribution profiles of extracellular vesicles and exomeres with redirected tropism. *Adv Sci*. 2020;7(19):2001467.
111. Massagué J, Obenauf AC. Metastatic colonization by circulating tumour cells. *Nature*. 2016;529:298-306.
112. Yue S, Mu W, Erb U, Zöller M. The tetraspanins CD151 and Tspan8 are essential exosome components for the crosstalk between cancer initiating cells and their surrounding. *Oncotarget*. 2015;6:2366-2384.
113. Wang Z, von Au A, Schnölzer M, Hackert T, Zöller M. CD44v6-competent tumor exosomes promote motility, invasion and cancer-initiating cell marker expression. *Oncotarget*. 2016.
114. Armacki M, Polaschek S, Waldenmaier M, et al. Protein kinase D1, reduced in human pancreatic tumors, increases secretion of small extracellular vesicles from cancer cells that promote metastasis to lung in mice. *Gastroenterol*. 2020;159(3):1019-1035.e22.
115. Nishida-Aoki N, Tominaga N, Kosaka N, Ochiya T. Altered biodistribution of deglycosylated extracellular vesicles through enhanced cellular uptake. *J Extracell Vesicles*. 2020;9(1):1713527.
116. Rana S, Yue S, Stadel D, Zöller M. Toward tailored exosomes: the exosomal tetraspanin web contributes to target cell selection. *Int J Biochem Cell Biol*. 2012;44:1574-1584.
117. Osmani N, Follain G, García León MJ, et al. Metastatic tumor cells exploit their adhesion repertoire to counteract shear forces during intravascular arrest. *Cell Rep*. 2019;28:2491-2500.e5.
118. Vestweber D. How leukocytes cross the vascular endothelium. *Nat Rev Immunol*. 2015;15:692-704.
119. Zeng Z, Li Y, Pan Y, et al. Cancer-derived exosomal miR-25-3p promotes pre-metastatic niche formation by inducing vascular permeability and angiogenesis. *Nature Communications*. 2018;9.
120. Treps L, Perret R, Edmond S, Ricard D, Gavard J. Glioblastoma stem-like cells secrete the pro-angiogenic VEGF-A factor in extracellular vesicles. *J Extracell Vesicles*. 2017;6:1359479.
121. Yang W-W, Yang L-Q, Zhao F, et al. Epiregulin promotes lung metastasis of salivary adenoid cystic carcinoma. *Theranostics*. 2017;7:3700-3714.
122. Grange C, Tapparo M, Collino F, et al. Microvesicles released from human renal cancer stem cells stimulate angiogenesis and formation of lung premetastatic niche. *Can Res*. 2011;71:5346-5356.
123. Rodrigues G, Hoshino A, Kenific CM, et al. Tumour exosomal CEMIP protein promotes cancer cell colonization in brain metastasis. *Nat Cell Biol*. 2019;21:1403-1412.
124. Sun B, Zhou Y, Fang Y, Li Z, Gu X, Xiang J. Colorectal cancer exosomes induce lymphatic network remodeling in lymph nodes. *Int J Cancer*. 2019;145:1648-1659.
125. Zhou C-F, Ma J, Huang L, et al. Cervical squamous cell carcinoma-secreted exosomal miR-221-3p promotes lymphangiogenesis and lymphatic metastasis by targeting VASH1. *Oncogene*. 2019;38:1256-1268.
126. Wang M, Zhao X, Qiu R, et al. Lymph node metastasis-derived gastric cancer cells educate bone marrow-derived mesenchymal stem cells via YAP signaling activation by exosomal Wnt5a. *Oncogene*. 2021;40(12):2296-2308.
127. Morad G, Carman CV, Hagedorn EJ, et al. Tumor-derived extracellular vesicles breach the intact blood-brain barrier via transcytosis. *ACS Nano*. 2019;13:13853-13865.
128. Mazumdar A, Urdinez J, Boro A, et al. Exploring the role of osteosarcoma-derived extracellular vesicles in pre-metastatic niche formation and metastasis in the 143-b xenograft mouse osteosarcoma model. *Cancers*. 2020;12(11):3457.
129. Fang T, Lv H, Lv G, et al. Tumor-derived exosomal miR-1247-3p induces cancer-associated fibroblast activation to foster lung metastasis of liver cancer. *Nature Communications*. 2018;9.
130. Mao X, Keong Tey S, Yeung LS, et al. Nidogen 1-enriched extracellular vesicles facilitate extrahepatic metastasis of liver cancer by activating pulmonary fibroblasts to secrete tumor necrosis factor receptor 1. *Adv Sci*. 2020;7(21):2002157.
131. Ji Q, Zhou L, Sui H, et al. Primary tumors release ITGBL1-rich extracellular vesicles to promote distal metastatic tumor growth through fibroblast-niche formation. *Nature Communications*. 2020;11(1).
132. Kong J, Tian H, Zhang F, et al. Extracellular vesicles of carcinoma-associated fibroblasts creates a pre-metastatic niche in the lung through activating fibroblasts. *Mol Cancer*. 2019;18.
133. Yuan X, Qian N, Ling S, et al. Breast cancer exosomes contribute to pre-metastatic niche formation and promote bone metastasis of tumor cells. *Theranostics*. 2021;11:1429-1445.
134. Zhang H, Deng T, Liu R, et al. Exosome-delivered EGFR regulates liver microenvironment to promote gastric cancer liver metastasis. *Nature Communications*. 2017;8.
135. Lahav TG, Adler O, Zait Y, et al. Melanoma-derived extracellular vesicles instigate proinflammatory signaling in the metastatic microenvironment. *International J Cancer*. 2019;145:2521-2534.
136. Shao Y, Chen T, Zheng X, et al. Colorectal cancer-derived small extracellular vesicles establish an inflammatory premetastatic niche in liver metastasis. *Carcinogenesis*. 2018;39:1368-1379.
137. Zhang H, Yu Y, Zhou L, et al. Circulating tumor microparticles promote lung metastasis by reprogramming inflammatory and mechanical niches via a macrophage-dependent pathway. *Cancer Immunol Res*. 2018;6(9):1046-1056.
138. Bald T, Quast T, Landsberg J, et al. Ultraviolet-radiation-induced inflammation promotes angiotropism and metastasis in melanoma. *Nature*. 2014;507:109-113.
139. Coffelt SB, Kersten K, Doornebal CW, et al. IL17-producing γδ T cells and neutrophils conspire to promote breast cancer metastasisdV performed the experiments Europe PMC Funders Group. *Nature*. 2015;522:345-348.
140. Cools-Lartigue J, Spicer J, Najmeh S, Ferri L. Neutrophil extracellular traps in cancer progression. *Cell Mol Life Sci*. 2014;71:4179-4194.
141. Wculek SK, Malanchi I. Neutrophils support lung colonization of metastasis-initiating breast cancer cells Europe PMC Funders Group. *Nature*. 2015;528:413-417.
142. Lima LG, Ham S, Shin H, et al. Tumor microenvironmental cytokines bound to cancer exosomes determine uptake by cytokine receptor-expressing cells and biodistribution. *Nature Communications*. 2021;12.

143. Headley MB, Bins A, Nip A, et al. Visualization of immediate immune responses to pioneer metastatic cells in the lung. *Nature*. 2016;531:513-517.
144. Chen G, Huang AC, Zhang W, et al. Exosomal PD-L1 contributes to immunosuppression and is associated with anti-PD-1 response. *Nature*. 2018;560(7718):382-386.
145. Xing F, Liu Y, Wu S-Y, et al. Loss of XIST in breast cancer activates MSN-c-Met and reprograms microglia via exosomal miRNA to promote brain metastasis. *Cancer Research*. 2018;78(15):4316-4330.
146. Hosseini H, Obradovic MMS, Hoffmann M, et al. Early dissemination seeds metastasis in breast cancer. *Nature*. 2016;540(7634):552-558.
147. Rhim AD, Mirek ET, Aiello NM, et al. EMT and dissemination precede pancreatic tumor formation. *Cell*. 2012;148:349-361.
148. Hüsemann Y, Geigl JB, Schubert F, et al. Systemic spread is an early step in breast cancer. *Cancer Cell*. 2008;13:58-68.
149. Eyles J, Puaux A-L, Wang X, et al. Tumor cells disseminate early, but immunosurveillance limits metastatic outgrowth, in a mouse model of melanoma. *J Clin Investig*. 2010;120(6):2030-2039.
150. Goddard ET, Bozic I, Riddell SR, Ghajar CM. Dormant tumour cells, their niches and the influence of immunity. *Nat Cell Biol*. 2018;20(11):1240-1249.
151. Sandiford OA, Donnelly RJ, El-Far MH, et al. Mesenchymal stem cell-secreted extracellular vesicles instruct stepwise dedifferentiation of breast cancer cells into dormancy at the bone marrow perivascular region. *Can Res*. 2021;81:1567-1582.
152. Walker ND, Elias M, Guiro K, et al. Exosomes from differentially activated macrophages influence dormancy or resurgence of breast cancer cells within bone marrow stroma. *Cell Death Dis*. 2019;10.
153. Sansone P, Savini C, Kurelac I, et al. Packaging and transfer of mitochondrial DNA via exosomes regulate escape from dormancy in hormonal therapy-resistant breast cancer. *Proc Natl Acad Sci USA*. 2017;114:E9066-E9075.
154. Bliss SA, Sinha G, Sandiford OA, et al. Mesenchymal stem cell-derived exosomes stimulate cycling quiescence and early breast cancer dormancy in bone marrow. *Can Res*. 2016;76:5832-5844.
155. Ono M, Kosaka N, Tominaga N, et al. Exosomes from bone marrow mesenchymal stem cells contain a microRNA that promotes dormancy in metastatic breast cancer cells. *Science signaling*. 2014;7:ra63.
156. Xu R, Rai A, Chen M, Suwakulsiri W, Greening DW, Simpson RJ. Extracellular vesicles in cancer—implications for future improvements in cancer care. *Nature Rev Clin Oncol*. 2018;15:617-638.
157. Kim MY, Oskarsson T, Acharyya S, et al. Tumor self-seeding by circulating cancer cells. *Cell*. 2009;139:1315-1326.
158. Borriello L, Condeelis J, Entenberg D, Oktay MH. Breast cancer cell re-dissemination from lung metastases—a mechanism for enhancing metastatic burden. *J Clin Med*. 2021;10:2340.
159. Huang H, Zheng X, Cai C, et al. Exosomes derived from breast cancer lung metastasis subpopulations promote tumor self-seeding. *Biochem Biophys Res Comm*. 2018;503:242-248.
160. Liu H, Chen W, Zhi X, et al. Tumor-derived exosomes promote tumor self-seeding in hepatocellular carcinoma by transferring miRNA-25-5p to enhance cell motility. *Oncogene*. 2018;37:4964-4978.
161. Van Rheenen J, Scheele CLGJ. Intravital microscopy to illuminate cell state plasticity during metastasis. *Curr Opin Cell Biol*. 2021;2021:28-35.
162. Verweij F, Balaj L, Boulanger C, et al. The power of imaging to understand Extracellular Vesicle biology in vivo. *Nature Methods*. 2021;in press.
163. González-Silva L, Quevedo L, Varela I. Tumor functional heterogeneity unraveled by scRNA-seq technologies. *Trends in Cancer*. 2020;6:13-19.
164. Zhang L, Zhang S, Yao J, et al. Microenvironment-induced PTEN loss by exosomal microRNA primes brain metastasis outgrowth. *Nature*. 2015;527:100-104.
165. Samuel M, Fonseka P, Sanwlani R, Oral administration of bovine milk-derived extracellular vesicles induces senescence in the primary tumor but accelerates cancer metastasis. *Nature Communications*. 2021;12.
166. Nishida-Aoki N, Tominaga N, Takeshita F, Sonoda H, Yoshioka Y, Ochiya T. Disruption of circulating extracellular vesicles as a novel therapeutic strategy against cancer metastasis. *Mol Ther*. 2017.
167. Ortiz A, Gui J, Zahedi F, et al. An interferon-driven oxysterol-based defense against tumor-derived extracellular vesicles. *Cancer Cell*. 2019;35:33-45.e6.

How to cite this article: Ghoroghi S, Mary B, Asokan N, Goetz JG, Hyenne V. Tumor extracellular vesicles drive metastasis (it's a long way from home). *FASEB BioAdvances*. 2021;00:1–14. https://doi.org/10.1096/fba.2021-00079

DISCUSSION

Current model suggests that tEVs from the primary tumor reach the circulation, diffuse in the organism, enhance PMN establishment at distant and mediate subsequent metastatic formation (Henrich et al., 2020; Costa-Silva et al., 2015, Hoshino et al., 2015; Peinado et al. 2017). However, this model still holds lot of black boxes and specifically on the involvement of hemodynamic forces on EVs distribution and function.

Hence my work during my PhD aimed at adapting live imaging models to study circulating tEVs and investigate the role of hemodynamics forces on tEVs uptake, fate and function on recipient cells and more particularly on endothelial cells.

More particularly my work participated to the development of the zebrafish embryo as a good model to study circulating tEVs and their consequence on metastatic progression. In addition, I adapted a microfluidic system to study tEVs in a relevant hemodynamic context at the intracellular level. These two models allowed me to show that flow forces importantly impact tEVs uptake (mediated in part by the presence of the receptor CD146/MCAM at the surface of tEVs) and fate inside endothelial cells, notably by a marked redirection of internalized tEVs toward less acidic compartments. In addition, my results suggest that presence of flow forces could also potentiate the function of tEVs onto endothelial cells, supporting a pro-angiogenetic signature upon combined stimulation by flow plus tEVs.

Setting-up new models to study circulating EVs

Zebrafish

At the beginning of my thesis, despite development of new tools allowing visualization of EVs distribution in different models (worm, drosophila, mice) (Verweij et al., 2021), accumulation pattern and fate of circulating tEVs *in vivo* were still difficult to study. Overall, circulating tEVs destinations and behavior in complex circulatory system were quite obscure. To overcome limitations that previous models exhibited, we took advantages of the zebrafish model to study circulating tEVs in relevant hemodynamic environment. Zebrafish had been previously used to investigate EVs-mediated delivery of anticancer drugs through the blood-brain barrier (Yang et al., 2015). However, in this study, proper visualization of EVs in vivo was absent as well as reliable proofs of EVs interactions, effect on recipient cells and effective delivery of drugs into the brain. In addition, transgenic zebrafish lines were used to follow the

uptake of endogenous CD63-GFP+ neurons-EVs by brain endothelial cells, the transfer of miRNA-132and its effect on brain vasculature (Xu et al., 2017). Nonetheless, here as well, there was no visualization of EVs in circulation and no EVs-mediated long distance communication event was reported.

On our side, we took advantage of zebrafish transparency to dynamically follow tEVs in live imaging at vesicle and high spatiotemporal scale (Hyenne et al., 2019). Additionally, we documented the distribution pattern and behavior of circulating tEVs and identified recipient cell type. Moreover, we demonstrated that exogenous injection of tEVs in the zebrafish could be used to model the effect of circulating tEVs in later stage of the metastatic cascade in relevant hemodynamics conditions at high resolutive scales. This work, together with one of Guillaume Van Niel's team that simultaneously published a thorough study on circulating EVs in zebrafish, although in a non-pathological model, could help to sustainably anchor the zebrafish embryo as a state-of-the-art model for dynamic study of circulating EVs (Hyenne et al., 2019; Verweij et al, 2019).

Our protocol (published recently in a method chapter (Mary et al., 2020)) relies on exogenous injection of tEVs in the duct of Cuvier. However, in mice the route of EVs injection affects their biodistribution (Gupta et al., 2020). In zebrafish, the back-to-back comparison between endogenous release (Verweij et al., 2019) and exogenous injections of EVs (Hyenne et al., 2019) showed similar pattern of distribution and interactions with recipient cells. It supports that in the zebrafish, exogenous injection of EVs at concentration which is in the physiologic range, reproduces quite accurately endogenous behavior of circulating EVs. The use of lipidic dyes that incorporate into membranes of cells or EVs (DiD, PKH or CellMask) often comes with drawbacks such as unbound dye, unspecific labelling, aggregation, unequal labelling of different subpopulations of EVs or longer half-life than EVs. Hence, it is recommended to limit the concentration of dye used, to properly remove free dye and to complement their use with other labelling approaches (Verweij et al., 2021). To overcome these limitations, we used a new generation of cyanine-based lipidic dye (Memglow=MemBright) that reported to be brighter, to trigger less aggregation, to be more stable in membrane (less leakage) and that can be used at lower concentration (Collot et al., 2019). In addition, we used genetically labelled tEVs (Syntenin2-GFP-EVs and CD63-pHluorin-mScarlet-EVs (Sung et al., 2020)) that confirmed our results obtained with tEVs labelled with dyes.

The two methods of labelling were used with success in both our models (zebrafish and microfluidics) and showed similar pattern of distribution. When EVs arrest we can observe discrete spots, which could correspond to single vesicles as well as larger intracellular clusters, which correspond to multiple EVs stored in the same compartment. Due to diffraction limit of classical optical microscopy, we cannot assume that single spot detected in the zebrafish embryo or in the microfluidic system are indeed all single vesicles. However, synthetic nanoparticle of 100nm diameter have a similar apparent size as labeled EVs. It would be interesting to assess in which proportion detected spots, *in vitro* and *in vivo*, correspond to either single vesicles or small aggregates. Possibilities include the use of super-resolution imaging techniques to overcome the diffraction limit (Follain et al., 2017) and the use of correlative light-electron microscopy (CLEM) approaches to differentiate single or aggregated circulating tEVs internalization in different compartments of endothelial cells *in vivo* (e.g. by adapting previously used technics done in macrophages (Hyenne et al., 2019)) and *in vitro*. This might be possible with specific constructs, such as CD63-GFP-Apex2, allowing genetic labelling of small EVs to detect them in both photonic and electronic systems (Lam et al., 2015).

Microfluidics

With microfluidic channels, I reproduced quite accurately the positive effect of specific hemodynamic conditions on uptake and trafficking of circulating tEVs. This model could be used to explore other range of flow *in vitro*, for example higher flow speed mimicking arterial flow. In addition, this approach could be also be improved to investigate other flow types such as oscillatory or disturbed flow as opposed to laminar flow. However, one limitation of this system is that it does not reproduce the three-dimensional environment of circulating tEVs. Additionally, it does not allow to reproduce the small internal diameter of the smaller vessels *in vivo*. As a consequence, it is not possible to reproduce high shear stress, while maintaining relevant flow speeds in our system (see later). Thereby microfluidics should be complemented with other approaches.

Another important aspect of our in vitro studies relies in the choice of the endothelial cells. We choose to use HUVEC and VERAHUVEC cells, as they are commonly used and can be considered as generic endothelial cells. However, it is likely that they have

different properties than endothelial cells of specific tissues and types of vessels. Ideally, our project should be pursued with venous capillary endothelial cells, as the permissive flow regimes we identified is more likely present in small venules. Additionally, we could use mouse brain BEnd.3 endothelial cells to investigate more in detail potential transcytosis events.

According to me combining these two models allows to overcome their individual limitations (i.e. limited intracellular resolution for the zebrafish and only partial reproduction of cardiovascular complexity for microfluidics) and could greatly improve study of circulating EVs fate inside the cardiovascular system.

Model homology and EV heterogeneity

In those models, I principally used heterologous systems (mouse breast carcinoma tEVs, human endothelial cells and zebrafish). In the lab, our experimental pipeline consists in identifying fundamental mechanisms in heterologous zebrafish or microfluidic models and ultimately confirm them in a mouse homologous model of breast cancer. This approach previously led to important breakthrough in CTC biology and tEV-mediated metastasis, showing its robustness (Follain et al., 2018, 2021; Ghoroghi et al., 2021). In the case of EVs, efficient transfer of nucleic materials was shown to be possible between mouse and human cells (Valadi et al., 2007). Altogether it supports that the fundamental mechanisms that I described during my thesis could be shared between these species and our heterologous models still maintain their relevance. However, heterologous models also have some limitations that will need to be addressed in the future. For example, do the different species body temperatures (28° C instead of 37) have an impact on our model of mouse tEVs distribution in zebrafish embryo? Does it impact their uptake? It is possible as temperature was shown to impact EVs uptake in recipient cells. However, in our cases we found that zebrafish tEVs (Zmel1 tEVs) (Hyenne et al., 2019) showed the same pattern of distribution and internalization than mouse tEVs (4T1 tEVs). Nevertheless, a side-by-side comparison of internalization rate between zebrafish tEVs and mouse tEVs would be important. Overall, the results discussed here could certainly benefit from reproduction in homologous model.

Another level of complexity comes from EVs heterogeneity. I used either heterogenous sub-populations of EVs isolated by ultracentrifugation or CD63 positive

EVs fused to pHluorin. Although, both groups of EVs partially accumulate in non-degradative endosomes upon flow treatment, we can not exclude that different tEVs subpopulations are differentially affected by flow-mediated mechanisms (uptake and trafficking). Systematic comparison of subpopulations of tEVs could help to better characterize the specificities of the processes we discovered.

Hemodynamic parameters control circulating tEVs biodistribution

During my PhD I investigated how fluid-based mechanical properties could affect circulating tEVs. My work, done with colleagues, showed that tEVs accumulation in endothelial cells is enhanced in venous regions of the vasculature, where blood flow is reduced (around 400µm/s). In addition, we documented a correlation between flow speed (measured by displacement of red blood cells) and tEVs accumulation in endothelial cells, accumulation of tEVs being inversely correlated with flow speed. The fact that higher flow speed region (i.e. arteries) show less tEVs accumulation than venous area suggested that, similarly to CTC, tEVs arrest need a permissive range of flow and that hemodynamic cues indeed play a role in tEVs biodistribution. Interestingly, we found that in this venous area, reducing blood flow *in vivo* or an absence of flow *in vitro* decreased tEVs accumulation inside endothelial cells. This suggested that flow speed-mediated mechanism of circulating tEVs uptake is not only a passive event. In this case the absence of tEVs movement would have increased uptake. On the contrary, in the microfluidic system we observed a positive effect of moderate flow on tEVs uptake by endothelial cells, reproducing what we saw in the zebrafish in the venous area.

Altogether my results suggest that along the cardiovascular system of vertebrates, variation of flow speed and hemodynamic regimes will greatly affect circulating tEVs accumulation in endothelial cells and a window of permissive flow regimes could exists. Hence, flow forces could either, inhibit circulating tEVs uptake by endothelium in arterial regions where flow speed is more important, or enhance it in flow permissive regions such as venous area or capillaries. These hypotheses still need to be studied in more complex system using a mouse model for example and inhibitory and promoting aspects of blood flow should be better characterized in the future.

Effect of flow speed and shear stress on EVs uptake: a mechanical explanation

A simplistic mechanical explanation of the beneficial effect of moderate blood flow, could be that reduced speed enhance the number of circulating tEVs-endothelium interactions. Conversely, high flow speed regimes, would be too fast to allow, significant proportion of interactions and stable adhesion events capable of counteracting the mechanics of stream flow. Supporting this, the Poiseuille distribution of tEVs inside the venous area, shows that circulating tEVs at the vicinity of vessels border are slower and even exhibit rolling behavior of tEVs at the endothelium surface reminiscent of immune cell behavior (Hyenne et al., 2019). This margination of small objects at vessel walls, which was also documented for synthetic nanoparticles (Toy et al., 2011; Müller et al., 2015) and endogenous circulating EVs (Verweij et al., 2019), increases interaction time between tEVs and endothelium, and could facilitate potential ligand/receptor interactions that control their uptake (Hyenne et al., 2019). Indeed, it is known that surface receptors mediate tEVs organotropism and accumulation in target organs, notably integrins (Hoshino et al., 2015). During my PhD, we showed that CD146/MCAM, is a key tEVs surface cargo that mediates, in part, 4T1-tEVs accumulation in endothelial cells and at lungs PMN and affects metastatic progression (Ghoroghi et al., 2021). Although we showed that CD146-mediated interactions take place in the vascular system, we do not know if these interactions are flow-dependent or how flow forces regulate them. In addition, we still ignore the identity of CD146 ligand on the endothelium. CD146 at EVs surface could perform homophilic interactions with endothelial CD146 or heterophilic interactions with various membrane proteins (i.e. VEGFR2 or Netrin-1) or extracellular matrix proteins (Wang and Yan, 2015). These interactions could allow the arrest of circulating tEVs and their uptake by recipient cells at flow permissive areas in the vascular system.

Interestingly, studies using nanoparticles (NP) similar in size with EVs, showed that reduced flow speed which is, in experimental settings, linked to reduced wall shear stress (i.e. the force exerted by blood flow on the endothelium walls per area unit and depending on flow speed), also enhanced NP uptake by endothelial cells. On the contrary, increasing shear stress reduced the uptake of NP (Han et al., 2012; Bhowmick et al., 2012) and liposome (Kusunose et al., 2013) by endothelial cells. More

recently, it was reported that shear stress in the range of 1,8 dyn/cm^2 favor NP uptake whereas a shear stress of 10 dyn/cm^2 restricts it (Charwat et al., 2018). Overall, this past decade, papers tend to show that low shear stress (more or less < 5dyn/cm^2) enhances NP internalization by endothelial cells and higher shear stress (> 5 (+/-1) dyn/cm^2) decrease it (Lin et al., 2009; Bhowmick et al., 2012; Han et al. 2012; Tan et al., 2019; Chen et al., 2020). This was also confirmed in vivo in mice and zebrafish models, arteries showing less NP accumulation than venules and/or capillaries (Gomez-Garcia et al., 2018; Han et al., 2012). Importantly for us, it was reported that shear stress on the endothelial walls of caudal ventral vein in larvae varies between 0,016 to 3,4 dyn/cm^2 with an average of 1 dyn/cm^2 (Gomez-Garcia et al., 2018). In our microfluidic system, a flow speed of 400µm/s previously measured in the venous area of the zebrafish and used in our *in vitro* system, corresponds to a shear stress of 0,5 (+/- 0,2) dyn/cm^2. Overall, this suggests that our microfluidic system reproduces rather accurately the conditions of the zebrafish model and that circulating tEVs accumulation in dynamic environment phenocopies results previously obtained for NP. However, in our case we did not properly investigate the inverted correlation between increased shear stress and tEVs accumulation in endothelial cells in vitro. The reason is that we decided to focus on flow speed measured in the zebrafish embryo at the tEVs hotspot of arrest (i.e. the venous area) (Hyenne et al., 2019; Mary et al., 2022). Fortunately, reproducing accurate zebrafish venous flow speed while maintaining relevant shear stress conditions in vitro is possible. However, mimicking higher shear stress (i.e. > 5dyn/cm^2) implies to increase flow speed too much *in vitro*, to the point that it would be irrelevant compared to the flow speed measured not only in venules but also in arterioles of the zebrafish larvae. All studies investigating hemodynamic parameters are facing the same dilemma (i.e. reproduction and control of the flow speed or reproduction and control of the shear stress?) and, to my knowledge, studying both at the same time in physiologically relevant conditions *in vitro* is hardly achievable.

Concerning EVs, at the beginning of my thesis, no study investigated these questions. However, in a paper published at the end of my thesis, in 2022, using both in vitro microfluidic and *in vivo* models (zebrafish and mice), it was reported that low magnitude hemodynamic forces and shear stress produced by laminar (<5dyn/cm^2) or oscillatory flow (0.5 ± 4 dyn/cm^2) facilitated endothelial uptake of Red Blood Cells EVs (RBCEVs) compared to higher shear stress produced by high laminar flow speed (12 to 25 dyn/cm^2) *in vitro* (Qin et al., 2022). The authors reproduced these results in

zebrafish and in mice (using a left carotid ligation model in mice) showing that RBCEVs preferentially accumulate in endothelial cells in area of low magnitude flow forces or oscillatory flow/perturbed flow (Qin et al., 2022). These findings mirrored nanoparticle behavior in zebrafish and microfluidic models, where NP mostly accumulate in regions with low shear stress (i.e. venous), disturbed or non-laminar flow speed (Gomez-Garcia et al., 2018). Similarly to reduced flow speed, authors suggested that disturbed flow increases the number of interactions between EVs (or NP) and endothelium, facilitating the accumulation of particles in endothelium. Supporting this, in zebrafish, our results together with those on RBCEVs and NP showed increased accumulation in branched capillaries localized between the dorsal aorta and vein in the caudal plexus, where flow speed and shear stress drop and are highly perturbed (Quin et al., 2022; Gomez-Garcia et al., 2018; Verweij et al., 2019; Hyenne et al., 2019). Although we did not investigate disturbed flow regimes in our models, it was reported that at low flow regime/shear stress magnitudes (around 1dyn/cm^2) there is no significant difference of NP uptake by endothelial cells between laminar or disturbed flow profiles (Gomez-Garcia et al., 2018). This suggests that our models, at low flow speed range, maintain their relevancy. In addition, it could be possible that at higher shear stress (and potentially higher flow speed) disturbance of the flow play a crucial role in circulating EVs interactions with endothelium but might be less important at reduced shear stress scale as lower flow velocity already promotes interactions between EVs (or particles) and endothelial cells.

Altogether, these results on RBCEVs and NP, support our findings and confirmed that tumor EVs show similar behavior and dissemination pattern than nanoparticles and normal RBCEVs in dynamic environments *in vitro* and *in vivo*. Our results, suggest that circulating tEVs accumulate in low flow speed and low shear stress regions in vivo.

Effect of flow speed on EVs uptake: a biological response

In addition to acting on the interactions between EVs and the endothelial surface, mechanical sensing could trigger an endothelial response that promotes circulating tEVs uptake. However, our RNA sequencing analysis of endothelial cells cultivated under flow failed to identify specific candidates related to flow sensing. In the future it will be necessary to identify which endothelium mechanoreceptors are involved in flow-related internalization of circulating tEVs (either inhibitory or promoting effect). To add

to the complexity of these mechanisms, mechanoreceptors would likely differ between different types of endothelial cells, different areas of the vasculature and upon different mechanical stresses (Gray and Stroka, 2017). Among others, primary cilium, glycocalyx, PECAM-1, mechanosensitive ion-channels (e.g. PIEZO-1), tyrosine kinase receptors, VE-cadherin or VEGF receptors are thought to be involved in endothelial cell mechanosensing (Gray and Stroka, 2017; Fang et al., 2019).

NP studies suggested that PECAM-1 at the surface of endothelial cells as well as lipid raft domains could play a role in the mechanosensing of flow. This could subsequently activate RhoA/ROCK dependent endocytosis pathways (also involving src kinases) and mediate internalization of antibody-coated NP by endothelium supporting an active involvement of actin cytoskeleton in this mechanism in flow mediated endocytosis (Han et al., 2015). A well-known feature of endothelial response to flow is the apparition of aligned actin stress fibers (Wong et al., 1983). Numerous studies on flow mediated NP uptake suggest that limited range of flow could recruit actin cytoskeleton and enhance NP uptake, while on the contrary, high and continuous flow speed (and shear stress) would lead to the formation of stress fibers and inhibit NP uptake (Han et al., 2012; Bhowmick et al., 2012; Han et al., 2015; Chen et al., 2020). In our case, it would be interesting to explore whether formation of actin stress fibers in the fish endothelial cells, depending on the area (e.g. artery versus veins), correlates with the different accumulations of circulating tEVs.

Additionally, it was shown that endothelial primary cilium is a structure specialized in low flow sensing in the zebrafish larvae and can trigger calcium-mediated signaling, regulating angiogenesis (Goetz et al., 2014). This organelle could play a role in flow-mediated circulating tEVs uptake by endothelial cells. Supporting this hypothesis, it was shown that cilium curvature enhances clathrin- and dynamin-dependent receptor-mediated and fluid-phased endocytosis (Raghavan et al., 2014). However, this was observed in renal proximal tubule cells and internalized cargo tested were albumin and dextran, not NP or EVs. Of note, the flow conditions used in this study recapitulated the range of shear present in venous area of the zebrafish larvae. Involvement of endothelial primary cilium in flow-mediated tEVs uptake remains to be investigated. The recent finding that endogenous circulating EVs are internalized in zebrafish endothelial cells via a dynamin dependent pathway could pair with this model (Verweij et al., 2019).

Finally, despite changes in lysosomal activity-related genes, our *in vitro* transcriptomic analysis did not show any significative upregulation of genes associated with endocytic pathways. Nonetheless, post-transcriptional modifications could regulate the uptake of circulating tEVs. Along this line, our lab reported that the presence of moderate flow enhanced localization of the secreted extracellular matrix protein fibronectin to the luminal side of endothelial cells *in vivo* and *in vitro*, without affecting its expression level (Osmani et al 2019). Interestingly it was suggested that heparan sulfate proteoglycan interactions with fibronectin is a key actor of tEVs adhesion, uptake and function onto endothelial cells (Purushothaman et al., 2016). Although, in these studies, fibronectin is described to be on EVs surface, it is reasonable to think that interaction can work the other way round. Endothelial cells heparan sulfate proteoglycan would bind fibronectin lying at the luminal side of endothelium in the zebrafish and subsequent circulating tEVs could bind luminal fibronectin via their own heparan sulfate proteoglycans, facilitating uptake by endothelial cells. Although, this hypothesis remains to be tested, it could explain, maybe a part of flow related circulating tEVs uptake.

Overall, we still need further investigations to dissect the particularities of positive and inhibitory effect of flow regimes on circulating tEVs uptake. (i) Mechanical receptors, (ii) adhesion molecules involved, (iii) endocytic pathways, and (iv) exact limits of permissive flow speed regimes (min and max), are among the questions that remain to be answered.

Circulating tEVs and endocytic pathways

The identification of endocytic pathways that control circulating tEVs uptake by endothelial cells is essential. Static experiment previously identified many different pathways controlling EVs uptake (Mulcahy et al., 2014). According to the literature it appears that nearly all common endocytic pathways were at least once described to play a role in EVs uptake by recipient cells. It is reasonable to think that, indeed the type of EVs (and its repertoire of surface molecules) as well as the type of recipient cells could impact the endocytic pathway involved. However, no study investigated dependency of endocytic pathway regarding dynamic environment. Therefore, in addition to the identification of CD146 as an important receptor for circulating tEVs uptake, I used a pharmacological approach to identify pathways involved in tEVs

uptake in dynamic condition (**Figure 15**). I used the Dynasore (dynamin inhibitor) to inhibit clathrin-mediated endocytosis (Fitzner et al., 2011; Roberts-Dalton et al., 2017), the genistein (tyrosine kinase inhibitor, PI3K) supposed to inhibit clathrin-independent endocytosis (Horibe et al., 2018; Costa-Verdera et al., 2017), and the Bafilomycin A that inhibits V-ATPases, vesicular acidification and supposedly micropinocytosis (Fitzner et al., 2011) in the microfluidic system. Interestingly, in dynamic environment none of these treatments significantly decrease tEVs uptake compared to control cells (although some tendencies could be seen). These results differ from previous studies showing involvement of these pathways in EVs uptake (Fitzner et al., 2011; Roberts-Dalton et al., 2017; Costa-Verdera et al., 2017) and particularly in endogenous EVs uptake by endothelial cells *in vivo* (Verweij et al., 2019). For instance, dynamin and clathrin-dependent endocytosis were showed to control endogenous circulating EVs uptake, via scavenger receptors, by endothelial cells in the zebrafish embryo (yet, using another drug, pyrimidin-7) (Verweij et al., 2019). The difference of EVs population, recipient cells type and models (*in vivo* versus *in vitro*) in my system compared to the previous studies could explain the different results.

The fact that none of the drug alone significantly affected circulating tEVs uptake could mean that endocytic pathways differ in static and dynamic conditions. Alternatively, it could illustrate the existence of compensatory mechanisms in dynamic conditions. Therefore, it would be interesting to test the co-depletion of several pathways. In addition, it would be interesting to test other processes, such as lipid raft-mediated endocytosis (with Methyl-ß-cyclodextrin, Filipine or Simvastatin for example) or caveolae-related processes as they were shown to respectively promote EVs uptake by endothelial cells (Svensson et al., 2013) and flow-mediated NP uptake (Han et al., 2012, Han et al., 2015). Similarly, we could test macropinocytosis (using 5-(N-ethyl-N-isopropyl) amiloride (EIPA)) that can be regulated by shear stress (Davies et al., 1984; Raghavan et al., 2014) and controls EVs uptake by macrophages (Kamerkar et al., 2017) and brain endothelial cells (Morad et al., 2019).

Although we did not find a clear answer on which general endocytic pathway control circulating tEVs uptake, microfluidic approaches could be combined with zebrafish to screen multiple drugs (or other approaches such as antibody-mediated blocking) interfering with EVs uptake in dynamic conditions. In this context, it would also be interesting to use genetically labelled tEVs with specific subpopulation markers (e.g. CD63-GFP-tEVs) to better characterize endocytosis of precise tEVs subpopulation.

Finally, we observed that all endothelial cells present in the same monolayer do not internalize tEVs with the same efficiency (data not shown here). Interestingly, it was previously observed that different types of endothelial cells (from different origins but also within a same population) also internalized nanoparticles with different efficiency and only distinct subpopulations are the main internalizing cells (Aliyandi et al., 2020; Kingston et al., 2021; Åberg et al., 2021). This heterogeneity is not well understood but could reflect heterogeneity in the repertoire of surface receptors that are involved in interactions with EVs. Understanding the ligand/receptors interactions involved in circulating tEVs uptake might help to resolve this question.

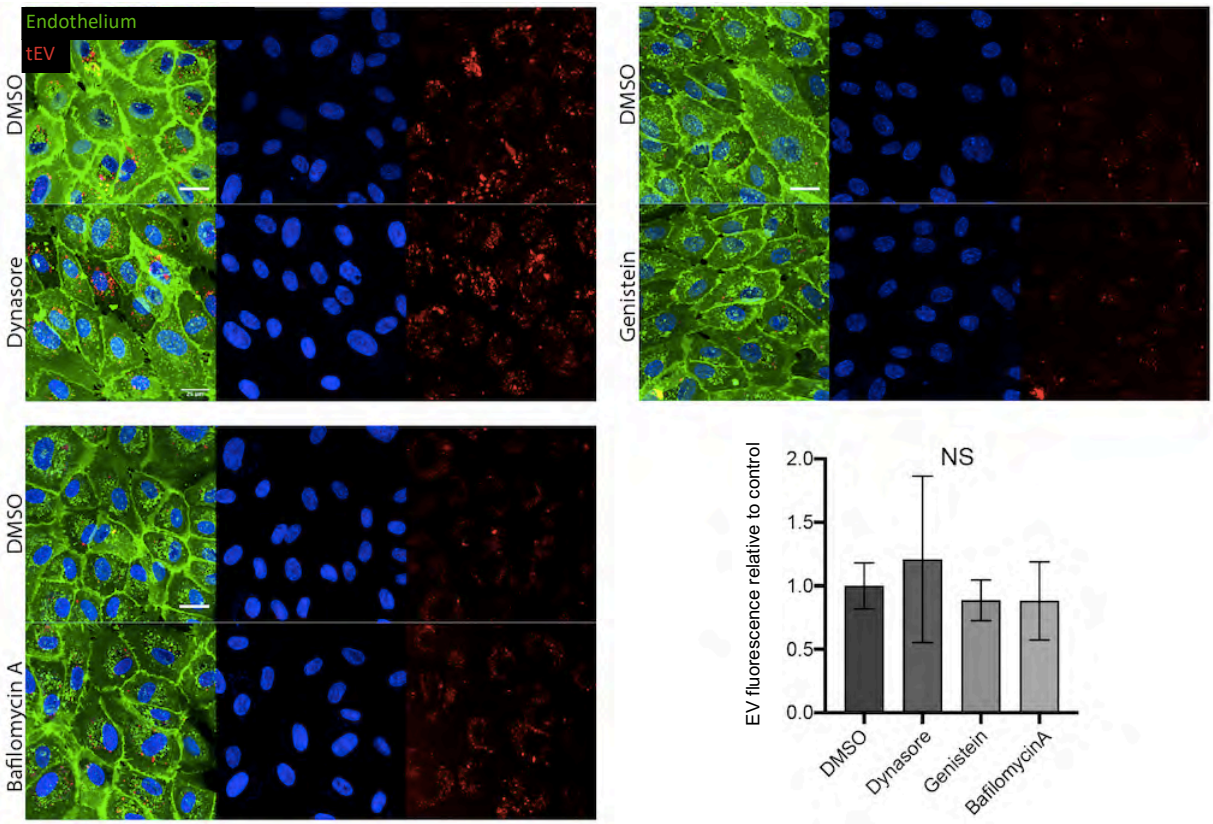

Figure 15: Pharmacological treatment of endothelial cells in dynamic condition. Memglow-Cy5-labeled 4T1 EVs are perfused on HUVECs endothelial monolayer labeled with Memglow 488 in flow condition (400m/s) and treated for 30min with the indicated drug before adding tEV. Drug is present in the system during the perfusion time. Images are taken by confocal microscopy after 3h of perfusion and after three wash steps with PBS and a final wash with endothaliall medium. Scale bar 25µm. Representative images and quantification of internalized tEV from two independent experiments for a total of twenty fields of view per condition minimum normalized to tEV fluorescence in the CTRL condition (DMSO). Kruskal-Wallis statistical test. Results showed no significant differences bewteen CTRL condition and treated cells.

To summarize, our results suggest that all along the vascular system, as the flow forces greatly vary, endothelial uptake of tEVs will also varies. It seems that regions with reduced flow speed and shear stress as well as area of perturbed flow will be hotspots of arrest for tEVs in endothelial cells. These regions also correspond to the

regions of arrest of CTCs. Biodistribution of circulating tEVs is, on one hand, controlled by hemodynamics cues and on the other hand, by receptors/ligand interactions. The exact nature of the flow sensors and endocytic pathways involved still have to be deciphered. Whether this permissive flow will also be more suitable for endothelial crossing by transcytosis (similarly to CTC extravasation which is increased by permissive flow regimes (Follain et al., 2018)), remains to be investigated. Yet, these new insights on circulating tEVs distribution in a vascular system could greatly help to better understand and predict potential localization of tEVs-induced pre-metastatic niche formation.

Circulating tEVs intracellular trafficking and fate: degradation or functional cargo delivery?

In addition to a better understanding of flow forces impact on circulating tEVs internalization by endothelial cells, my work also contributed to better characterize the fate of internalized tEVs inside these recipient cells. I have shown that that presence of a moderate flow partially redirects circulating tEVs to less acidic and potentially less degradative compartments positive for Lamp1+, Rab14+ and NHE9+.

The small GTPase Rab14 appears as a specific marker of EVs trafficking under flow. It was shown to control trafficking of intracellular pathogens toward late endosomes-lysosomes and to be present on different endosomes including Lamp1 positive compartments (Hoffman et al., 2022). Importantly, Rab14 is also part of an alternative endocytic pathway, not sensitive to the classical endocytosis inhibitors (phosphoinositide 3-kinase (PI3K) inhibitors). This pathway, controls uptake of cationic substances and redirects them to non-acidic and potentially non degradative Lamp1 positive compartments (Trofimenko et al., 2021). Yet, EVs have a negative zeta potential due to the presence of anionic lipids (Verweij et al., 2019; Midekessa et al., 2020). However, this does not exclude that part of internalized tEVs, in our case, can be redirected toward Rab14+ compartments after their uptake. At this stage two hypothesis remain, either (i) in permissive range of flow circulating tEVs enter in endothelial cells via classical endocytosis (including dynamin-dependent mechanisms) and then part of them is redirected toward RAB14+ Lamp1+ compartments; or (ii) flow activates this different endocytic pathway and trigger the endocytosis of some circulating tEVs through this unconventional pathway.

At this stage, we still do not have a clear idea on how presence of flow could mediate (and potentially activate) this unconventional endocytosis pathway. In addition, we do not know how EVs zeta potential could impact their uptake and fate or if presence of hemodynamic forces could affect their charge. Finally, our results suggest that CD63+ populations of extracellular vesicles can undergo this redirection toward RAB14+ Lamp1+ compartments as the pHsensitive probe fuse to this tetraspanin was used to identified it. Nevertheless, whether this flow-dependent redirection toward less acidic, less degradative compartments is similar for different subpopulations of EVs (tEVs or EVs) remains to be investigated.

Interestingly, our RNA sequencing, electron microscopy, lysotracker and cathepsin B experiments rather support a global activation of lysosomal and degradative activity in endothelial cells treated by moderate flow speed. Therefore, we suggest that moderate flow can both, affects global activation of the endolysosomal pathway and at the same time be responsible of a flow dependent EVs specific redirection during their intracellular trafficking. In addition, although we detected an upregulation of endolysosomal compartments number, we also noticed their decrease in size upon moderate flow treatment. It has been suggested that size of lysosomal compartments could be a readout of lysosomal differential functioning (Araujo et al., 2020). Thereby, it could be interesting to investigate with better resolutive approaches (for example CLEM), whether upon flow, circulating tEVs are redirected towards endolysosomal compartments of different sizes and if this is linked to different pH levels.

Overall, the redirection of circulating tEVs towards less acidic and less degradative compartments could greatly impact their capacity to deliver their message to receiving cells and therefore affect their function on endothelial cells. On one hand, acidification of endolysosomal compartments is required for activity of lysosome hydrolases and therefore its degradative function (Ballabio and Bonifacino, 2020). On the other hand, it has also been suggested that acidification allows efficient EVs cargo release into recipient cells cytosol supposedly via back-fusion of EVs and endosome membranes (Joshi et al., 2020; Bonsergent et al., 2021). Another recent study showed that pH-sensitive and pH-insensitive liposomes can be both internalized by brain endothelial cells via classical endolysosomal pathway but undergo different fates (Reginald-Opara et al., 2022). PH-sensitive ones could preferentially release their cargo into the cell cytosol, potentially through back fusion with acidic endolysosomal compartments.

Conversely, pH-insensitive liposomes treated endothelial cells showed increased retention of these liposomes inside endolysosomal compartments. Authors suggested that part of them can be exocytosed together with endogenous EVs as intact liposomes (the other part being fused with endogenous EVs), illustrating a transcytosis event. This study suggests that pH levels in endosomal compartments mediates the fate of internalized particles (degradation, cargo transfer or re-secretion) (Reginald-Opara et al., 2022). Of note, other studies already showed the capacity of endothelial cells to redirect part of internalized EV toward re-secretion fate. This mechanism was suggested to mediate transcytosis events and EVs crossing of the blood brain barrier (Morad et al. 2019). However, potential re-secretion remains to be investigated in our models.

Overall, this alternate trafficking in presence of flow could really modify tEVs capacity to deliver their message to endothelial cells. To investigate this question, during my thesis I tried to adapt to my microfluidic model, a bioluminescent assay, developed to monitor EVs cargo transfer to receiving cells via cytoplasmic release (Somiya and Kuroda, 2021). This bioluminescent reporter assay is based on a split-luciferase called NanoBit system. EVs secreting cells (in my case 4T1 cells) express a small luminescent tag (HiBit) that can complement a large subunit of luciferase (LgBit) expressed in recipient cells (in my case Huvec or vHUVEC) and induce detectable luminescent signal. I controlled that the transient co-expression of the two parts of the luciferase (HiBit and LgBit) in endothelial cells (HUVEC) was able to produce detectable luminescence in 96-wells plate and in microfluidic channels (luminescence detected by plate reader and IVIS Spectrum *in vivo* imaging system respectively) (**Figure 16A and 16B**). In a parallel control, I transiently expressed LgBit construct in stable 4T1-HiBit cells and detected correct level of luminescence (Data not shown). Together these results showed that the complementation between HiBit and LgBit is able to produce luminescence. The HiBit tag was fused with either the VSVG protein, or with peptides described to favor EVs targeting: the CAAX sequence and the EXOSignal sequence (Garcia-Martin et al., 2022) to increase EVs loading. I treated HUVEC cells transiently expressing LgBit construct with different amount of 4T1-Hibit-EVs or with PBS but none of the concentrations allowed detection of luminescence after 6h of treatment (**Figure 16A graph**). I tried a similar approach in microfluidic channels seeded with vHUVEC cells stably expressing LgBit construction fused with a GFP proteins to confirm presence of the LgBit subunit. Yet, here again,

even high concentrations of 4T1-HiBit-EVs did not give any bioluminescent signal significantly different from the control condition treated with PBS (**Figure 16C**). However, I could not detect VSVG in EVs (**Figure 16D-E**) (and I had no way to verify the presence of CAAX-HiBit or EXOSignal-Hibit) suggesting an inefficient loading of Hibit in EVs. This could explain the impossibility to complement LgBit subunit upon EVs treatment of LgBit expressing vHUVEC. Therefore, I was unable to validate the split-luciferase assay in my system. In the future it will be necessary to adapt new EVs cargo delivery reporter assay in our microfluidic system (Bonsergent et al., 2021). This would allow to determine whether the presence of flow affects capacity of tEVs to transfer their messages to recipient cells.

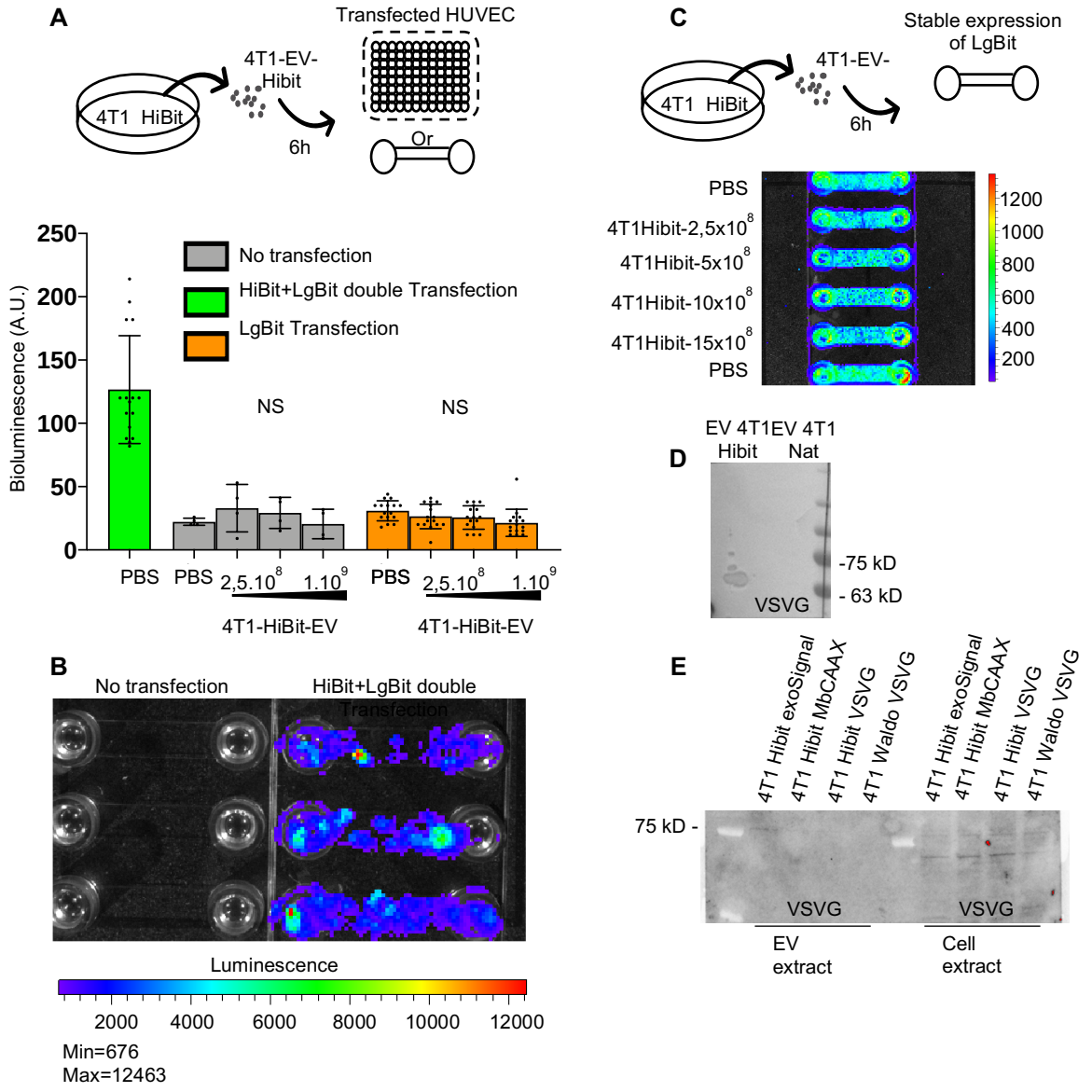

Figure 16: Split-luciferase reporter assay. A) Huvec cells transiently expressing LgBit subunit are treated with different concentrations of tEV (in particles/mL) produced by Hibit expressing 4T1 cells (4T1-HiBit-EV). PBS treatment and double transient transfection of Hibit and LgBit subunits in Huvec cells are used as negative and positive controls respectively. Bioluminscence is detected by plate reader. B) Double transient transfection of HiBit and LgBit in Huvec cells seeded in microfluidic channel compared to untransfected cells. C) Different treatments of stably expressing LgBit vHuvec cells with 4T1-Hibit-EV or PBS. D and E) Western Blot of VSVG proteins tEVs (D) or tEVs and cell extracts (E) from native 4T1 cells or stable 4T1 cell lines expressing different HiBit constructs.

Circulating tEVs function on endothelium; potential effect on PMN formation

Since tEVs can have a huge impact on endothelium biology (see introduction), we decided to explore circulating tEVs effect in functional studies. We previously showed in priming experiments, that circulating tEVs enhanced metastatic formation but did not provide further evidence of an explanatory mechanism. I investigated more thoroughly the impact of circulating EVs on the endothelium by transcriptomics. While the treatment with tEVs affects endothelial gene expression in both cases (in static and in flow condition), the signature is significantly different. Our results showed that a combined treatment with flow and tEVs activates an overexpression of transcription factors associated with pro-angiogenic activity (e.g. ID1, ID2, ID3, MAFB, Runx1 and HES1) and genes belonging to two signaling pathways, Notch and TGFß, known to promote angiogenesis (Sheldon et al., 2010; Achyut and Yang, 2011; Costanza et al., 2017). While still very hypothetical, this differential tEVs response upon flow treatment could indeed support that presence of a moderate flow tune tEVs function on endothelium and do it via several potential mechanisms. First, we can imagine that redirection toward less degradative compartments increases tEVs half-life inside recipient cells, potentializing their opportunity to deliver their message in endothelium either through cargo transfer or via direct signaling from endosomes. Interestingly, both Notch and TGFß pathways can be activated either directly from the plasma membrane or from within endosomes. This was shown for EV bearing inactive forms of TGFß that become active inside endosomes compartments, activating endosomal TGFß receptors (Shelke et al., 2019). To test this hypothesis, we could perform time-lapse analysis of circulating tEVs inside endothelial cells (for example with the CD63pHlurinmSacrlet construction) and monitor their residency time on different compartments. Second, since acidification of endolysosomal compartments promotes EVs cargo transfer (Bonsergent et al., 2021, Joshi et al., 2020), we can imagine that upregulation of lysosomal pathways, acidity regulators and increased number of LysoTracker and Cathepsin B positive compartments, potentially enhance efficiency of tEVs message delivery.

The pro-angiogenic signature induced by the combined action of EVs and blood flow is closely related to Notch and TGFß pathways (e.g. Hey1, Hey2, JAG1, Smad6, Smad7, Bambi, PMEPA, Nog) which are known to be involved in EV-mediated angiogenesis events (Sheldon et al., 2010; Achyut and Yang, 2011; Costanza et al.,

2017). In addition, TGFß activation also increases inflammation and permeabilization in the endothelium (Chen et al., 2019). In our case, we do not know which potential tEV cargo can trigger this endothelial response. Yet, we know, through proteomic analysis (Ghoroghi et al., 2021) that our tEV, contain TGFß regulators such as Smad5, Smurf2 and notably TGFß type II receptor. The later was shown to be transferred via tEV and sufficient to activate TGFß pathway in recipient cells and impact metastasis (Xie et al., 2022). We found that Smad6 and Smad7 are upregulated in our model. These two proteins have an inhibitory effect of the canonical TGFß pathway. However, activation of the TGFß pathway can lead to increased Smad6 and Smad7 expression via negative feedback loop. Besides, TGFß signaling also includes non-canonical pathways that involve different actors (Achyut and Yang, 2011; Costanza et al., 2017). Thereby, it will be interesting to test in our model the activation of the TGFß pathway, not only by investigating the phosphorylation of Smad2/3 proteins which are the main regulators of the canonical pathway, but also the phosphorylation status of non-canonical pathways components (e.g AKT).

Using an adapted and established tumor-induced angiogenesis assay (Nicoli and Presta, 2007), we confirmed this pro-angiogenic activity of circulating tEVs *in vivo* in the zebrafish model. Our results showed that injection of tEVs in zebrafish-bearing tumor mass promotes formation of neo-vascular sprouts from sub-intestinal vessels compared to PBS injections. While pro-angiogenic activity of tEVs was already shown *in vitro* and *in vivo (*Todorova et al., 2017), we confirmed their effect in a relevant hemodynamic context. Additionally, our results suggest that this environment could favor this tEV-mediated pro-angiogenic activity. In this model, it is possible that tumor-derived factor could synergically function with the injected circulating tEVs to potentialize this pro-angiogenic activity. This hypothesis is compatible with our results showing less neo-sprouts when zebrafish are only injected with PBS.

An increased angiogenic activity is one of the characteristics of the PMN. Hence, circulating tEVs, at a distant site, could trigger an angiogenic activity supporting PMN formation (Peinado et al., 2017). Additionally, hemodynamic forces enhance circulating tEVs arrest at the same location they induce endothelial remodeling and facilitate CTC extravasation through the highjack of pro-angiogenic program in endothelial cells (Follain et al., 2018, 2021). tEV are known actors of tumor-related endothelial regulation (Kugeratski et al., 2022). Thereby, we suggest that, at these sites, circulating tEVs could support this endothelial remodeling and CTC

extravasation, via their own pro-angiogenic activity. Finally, tumor-induced newly formed vessels are usually more permeable and abnormal. Thereby, it is possible that disturbed and low flow regimes created locally by these vessels or sprouts could increase later tEV accumulation. This could potentialize their effect, enhancing further vessel formation and ultimately could facilitate the subsequent vascularization of secondary foci, supporting metastatic growth. This could also happen after the formation of a secondary tumor, allowing their nutrient supply.

Altogether the work done during my PhD showed for the first time that the low flow profiles together with the molecular interactions between circulating tEVs and endothelium mediates arrest, uptake and functions of circulating tEVs. Therefore, circulating tEVs-mediated function will vary depending on the vasculature region. In addition, the zebrafish model (notably the venous region) reproduces quite well hemodynamic profiles (in terms of flow speed and shear stress) that can be measured in mice and human lungs, liver, brain or bone marrow (Follain et al., 2020). Notably in these organs, we can find low speed/shear regions matching hemodynamic parameters that I identified in my work as optimal for circulating tEVs arrest and uptake. Interestingly, these organs/regions are also hotspots of circulating tEVs arrest and PMN formation in animal models (Smyth et al., 2015; Fong et al., 2015; Xu et al., 2018), supporting our findings. Further investigations will be needed to entirely characterize underlying mechanisms in flow mediated effects identified in this work. Nonetheless, it could pave the way for further research about circulating tEVs behavior in circulation and more importantly in tumor progression and the apparition of PMN. Additionally, it could also bring lights on the importance of the hemodynamic part of EVs biology in other pathophysiological processes mediates by EVs.

BIBLIOGRAPHY

Abels, E.R., Maas, S.L.N., Nieland, L., Wei, Z., Cheah, P.S., Tai, E., Kolsteeg, C.-J., Dusoswa, S.A., Ting, D.T., Hickman, S., El Khoury, J., Krichevsky, A.M., Broekman, M.L.D., Breakefield, X.O., 2019. Glioblastoma-Associated Microglia Reprogramming Is Mediated by Functional Transfer of Extracellular miR-21. Cell Reports 28, 3105-3119.e7. https://doi.org/10.1016/j.celrep.2019.08.036

Åberg, C., Piattelli, V., Montizaan, D., Salvati, A., 2021. Sources of variability in nanoparticle uptake by cells. Nanoscale 13, 17530–17546. https://doi.org/10.1039/D1NR04690J

Achyut, B.R., Yang, L., 2011. Transforming Growth Factor-β in the Gastrointestinal and Hepatic Tumor Microenvironment. Gastroenterology 141, 1167–1178. https://doi.org/10.1053/j.gastro.2011.07.048

Adem, B., Vieira, P.F., Melo, S.A., 2020. Decoding the Biology of Exosomes in Metastasis. Trends in Cancer 6, 20–30. https://doi.org/10.1016/j.trecan.2019.11.007

Ahn, S.J., Fancher, I.S., Bian, J.-T., Zhang, C.X., Schwab, S., Gaffin, R., Phillips, S.A., Levitan, I., 2017. Inwardly rectifying K^+ channels are major contributors to flow-induced vasodilatation in resistance arteries: Kir contributes to FIV in resistance arteries. J Physiol 595, 2339–2364. https://doi.org/10.1113/JP273255

Alarcón-Vila, C., Baroja-Mazo, A., de Torre-Minguela, C., Martínez, C.M., Martínez-García, J.J., Martínez-Banaclocha, H., García-Palenciano, C., Pelegrin, P., 2020. CD14 release induced by P2X7 receptor restricts inflammation and increases survival during sepsis. eLife 9, e60849. https://doi.org/10.7554/eLife.60849

Aliyandi, A., Satchell, S., Unger, R.E., Bartosch, B., Parent, R., Zuhorn, I.S., Salvati, A., 2020. Effect of endothelial cell heterogeneity on nanoparticle uptake. International Journal of Pharmaceutics 587, 119699. https://doi.org/10.1016/j.ijpharm.2020.119699

Alkhateeb, T., Bah, I., Kumbhare, A., Youssef, D., Yao, Z.Q., McCall, C.E., Gazzar, M.E., 2020. Long Non-Coding RNA Hotairm1 Promotes S100A9 Support of MDSC Expansion during Sepsis 22.

Al-Nedawi, K., Meehan, B., Micallef, J., Lhotak, V., May, L., Guha, A., Rak, J., 2008. Intercellular transfer of the oncogenic receptor EGFRvIII by microvesicles derived from tumour cells. Nat Cell Biol 10, 619–624. https://doi.org/10.1038/ncb1725

Anand, S., Samuel, M., Kumar, S., Mathivanan, S., 2019. Ticket to a bubble ride: Cargo sorting into exosomes and extracellular vesicles. Biochimica et Biophysica Acta (BBA) - Proteins and Proteomics 1867, 140203. https://doi.org/10.1016/j.bbapap.2019.02.005

Ando, J., Yamamoto, K., 2013. Flow detection and calcium signalling in vascular endothelial cells. Cardiovascular Research 99, 260–268. https://doi.org/10.1093/cvr/cvt084

Andreu, Z., YÃ¡Ã±ez-MÃ^3, M., 2014. Tetraspanins in Extracellular Vesicle Formation and Function. Front. Immunol. 5. https://doi.org/10.3389/fimmu.2014.00442

Anklesaria, P., Teixidó, J., Laiho, M., Pierce, J.H., Greenberger, J.S., Massagué, J., 1990. Cell-cell adhesion mediated by binding of membrane-anchored transforming growth factor alpha to epidermal growth factor receptors promotes cell proliferation. Proc. Natl. Acad. Sci. U.S.A. 87, 3289–3293. https://doi.org/10.1073/pnas.87.9.3289

Antonyak, M.A., Li, B., Boroughs, L.K., Johnson, J.L., Druso, J.E., Bryant, K.L., Holowka, D.A., Cerione, R.A., 2011. Cancer cell-derived microvesicles induce transformation by transferring tissue transglutaminase and fibronectin to recipient cells. Proceedings of the National Academy of Sciences 108, 4852–4857. https://doi.org/10.1073/pnas.1017667108

Antounians, L., Catania, V.D., Montalva, L., Liu, B.D., Hou, H., Chan, C., Matei, A.C., Tzanetakis, A., Li, B., Figueira, R.L., da Costa, K.M., Wong, A.P., Mitchell, R., David, A.L., Patel, K., De Coppi, P., Sbragia, L., Wilson, M.D., Rossant, J., Zani, A., 2021. Fetal lung underdevelopment is rescued by administration of amniotic fluid stem cell extracellular vesicles in rodents. Sci. Transl. Med. 13, eaax5941. https://doi.org/10.1126/scitranslmed.aax5941

Araujo, M.E.G., Liebscher, G., Hess, M.W., Huber, L.A., 2020. Lysosomal size matters. Traffic 21, 60–75. https://doi.org/10.1111/tra.12714

Armacki, M., Polaschek, S., Waldenmaier, M., Morawe, M., Ruhland, C., Schmid, R., Lechel, A., Tharehalli, U., Steup, C., Bektas, Y., Li, H., Kraus, J.M., Kestler, H.A., Kruger, S.,

Ormanns, S., Walther, P., Eiseler, T., Seufferlein, T., 2020. Protein Kinase D1, Reduced in Human Pancreatic Tumors, Increases Secretion of Small Extracellular Vesicles From Cancer Cells That Promote Metastasis to Lung in Mice. Gastroenterology 159, 1019-1035.e22. https://doi.org/10.1053/j.gastro.2020.05.052
Avalos, P.N., Forsthoefel, D.J., 2022. An Emerging Frontier in Intercellular Communication: Extracellular Vesicles in Regeneration. Front. Cell Dev. Biol. 10, 849905. https://doi.org/10.3389/fcell.2022.849905
Baietti, M.F., Zhang, Z., Mortier, E., Melchior, A., Degeest, G., Geeraerts, A., Ivarsson, Y., Depoortere, F., Coomans, C., Vermeiren, E., Zimmermann, P., David, G., 2012. Syndecan–syntenin–ALIX regulates the biogenesis of exosomes. Nat Cell Biol 14, 677–685. https://doi.org/10.1038/ncb2502
Balkwill, F.R., Capasso, M., Hagemann, T., 2012. The tumor microenvironment at a glance. Journal of Cell Science 125, 5591–5596. https://doi.org/10.1242/jcs.116392
Ballabio, A., Bonifacino, J.S., 2020. Lysosomes as dynamic regulators of cell and organismal homeostasis. Nat Rev Mol Cell Biol 21, 101–118. https://doi.org/10.1038/s41580-019-0185-4
Bänfer, S., Kutscher, S., Fleck, F., Dienst, M., Preußer, C., Pogge von Strandmann, E., Jacob, R., 2022. Late domain dependent E-cadherin recruitment into extracellular vesicles. Front. Cell Dev. Biol. 10, 878620. https://doi.org/10.3389/fcell.2022.878620
Bhowmick, T., Berk, E., Cui, X., Muzykantov, V.R., Muro, S., 2012. Effect of flow on endothelial endocytosis of nanocarriers targeted to ICAM-1. Journal of Controlled Release 157, 485–492. https://doi.org/10.1016/j.jconrel.2011.09.067
Bianco, F., Perrotta, C., Novellino, L., Francolini, M., Riganti, L., Menna, E., Saglietti, L., Schuchman, E.H., Furlan, R., Clementi, E., Matteoli, M., Verderio, C., 2009. Acid sphingomyelinase activity triggers microparticle release from glial cells. EMBO J 28, 1043–1054. https://doi.org/10.1038/emboj.2009.45
Biller, S.J., Schubotz, F., Roggensack, S.E., Thompson, A.W., Summons, R.E., Chisholm, S.W., 2014. Bacterial Vesicles in Marine Ecosystems. Science 343, 183–186. https://doi.org/10.1126/science.1243457
Biswas, S.K., Mantovani, A., 2010. Macrophage plasticity and interaction with lymphocyte subsets: cancer as a paradigm. Nat Immunol 11, 889–896. https://doi.org/10.1038/ni.1937
Bittel, M., Reichert, P., Sarfati, I., Dressel, A., Leikam, S., Uderhardt, S., Stolzer, I., Phu, T.A., Ng, M., Vu, N.K., Tenzer, S., Distler, U., Wirtz, S., Rothhammer, V., Neurath, M.F., Raffai, R.L., Günther, C., Momma, S., 2021. Visualizing transfer of microbial biomolecules by outer membrane vesicles in microbe-host-communication in vivo. Journal of Extracellular Vesicles 10. https://doi.org/10.1002/jev2.12159
Bliss, S.A., Sinha, G., Sandiford, O.A., Williams, L.M., Engelberth, D.J., Guiro, K., Isenalumhe, L.L., Greco, S.J., Ayer, S., Bryan, M., Kumar, R., Ponzio, N.M., Rameshwar, P., 2016. Mesenchymal Stem Cell–Derived Exosomes Stimulate Cycling Quiescence and Early Breast Cancer Dormancy in Bone Marrow. Cancer Research 76, 5832–5844. https://doi.org/10.1158/0008-5472.CAN-16-1092
Bobrie, A., Krumeich, S., Reyal, F., Recchi, C., Moita, L.F., Seabra, M.C., Ostrowski, M., Thery, C., 2012. Rab27a Supports Exosome-Dependent and -Independent Mechanisms That Modify the Tumor Microenvironment and Can Promote Tumor Progression. Cancer Research 72, 4920–4930. https://doi.org/10.1158/0008-5472.CAN-12-0925
Bolukbasi, M.F., Mizrak, A., Ozdener, G.B., Madlener, S., Ströbel, T., Erkan, E.P., Fan, J.-B., Breakefield, X.O., Saydam, O., 2012. miR-1289 and “Zipcode”-like Sequence Enrich mRNAs in Microvesicles. Molecular Therapy - Nucleic Acids 1, e10. https://doi.org/10.1038/mtna.2011.2
Bonsergent, E., Grisard, E., Buchrieser, J., Schwartz, O., Théry, C., Lavieu, G., 2021. Quantitative characterization of extracellular vesicle uptake and content delivery within mammalian cells. Nat Commun 12, 1864. https://doi.org/10.1038/s41467-021-22126-y
Bonsergent, E., Lavieu, G., 2019. Content release of extracellular vesicles in a cell-free extract. FEBS Lett 593, 1983–1992. https://doi.org/10.1002/1873-3468.13472

Borghesan, M., Fafián-Labora, J., Eleftheriadou, O., Carpintero-Fernández, P., Paez-Ribes, M., Vizcay-Barrena, G., Swisa, A., Kolodkin-Gal, D., Ximénez-Embún, P., Lowe, R., Martín-Martín, B., Peinado, H., Muñoz, J., Fleck, R.A., Dor, Y., Ben-Porath, I., Vossenkamper, A., Muñoz-Espin, D., O'Loghlen, A., 2019. Small Extracellular Vesicles Are Key Regulators of Non-cell Autonomous Intercellular Communication in Senescence via the Interferon Protein IFITM3. Cell Reports 27, 3956-3971.e6. https://doi.org/10.1016/j.celrep.2019.05.095

Boulanger, C.M., Loyer, X., Rautou, P.-E., Amabile, N., 2017. Extracellular vesicles in coronary artery disease. Nat Rev Cardiol 14, 259–272. https://doi.org/10.1038/nrcardio.2017.7

Bray, F., Ferlay, J., Soerjomataram, I., Siegel, R.L., Torre, L.A., Jemal, A., 2018. Global cancer statistics 2018: GLOBOCAN estimates of incidence and mortality worldwide for 36 cancers in 185 countries. CA: A Cancer Journal for Clinicians 68, 394–424. https://doi.org/10.3322/caac.21492

Broggi, M.A.S., Maillat, L., Clement, C.C., Bordry, N., Corthésy, P., Auger, A., Matter, M., Hamelin, R., Potin, L., Demurtas, D., Romano, E., Harari, A., Speiser, D.E., Santambrogio, L., Swartz, M.A., 2019. Tumor-associated factors are enriched in lymphatic exudate compared to plasma in metastatic melanoma patients. Journal of Experimental Medicine 216, 1091–1107. https://doi.org/10.1084/jem.20181618

Brown, H.K., Schiavone, K., Tazzyman, S., Heymann, D., Chico, T.J., 2017. Zebrafish xenograft models of cancer and metastasis for drug discovery. Expert Opinion on Drug Discovery 12, 379–389. https://doi.org/10.1080/17460441.2017.1297416

Brown, M., Johnson, L.A., Leone, D.A., Majek, P., Vaahtomeri, K., Senfter, D., Bukosza, N., Schachner, H., Asfour, G., Langer, B., Hauschild, R., Parapatics, K., Hong, Y.-K., Bennett, K.L., Kain, R., Detmar, M., Sixt, M., Jackson, D.G., Kerjaschki, D., 2018. Lymphatic exosomes promote dendritic cell migration along guidance cues. Journal of Cell Biology 217, 2205–2221. https://doi.org/10.1083/jcb.201612051

Budden, C.F., Gearing, L.J., Kaiser, R., Standke, L., Hertzog, P.J., Latz, E., 2021. Inflammasome-induced extracellular vesicles harbour distinct RNA signatures and alter bystander macrophage responses. Journal of Extracellular Vesicles 10. https://doi.org/10.1002/jev2.12127

Burgelman, M., Vandendriessche, C., Vandenbroucke, R.E., 2021. Extracellular Vesicles: A Double-Edged Sword in Sepsis. Pharmaceuticals 14, 829. https://doi.org/10.3390/ph14080829

Busatto, S., Yang, Y., Walker, S.A., Davidovich, I., Lin, W.-H., Lewis-Tuffin, L., Anastasiadis, P.Z., Sarkaria, J., Talmon, Y., Wurtz, G., Wolfram, J., 2020. Brain metastases-derived extracellular vesicles induce binding and aggregation of low-density lipoprotein. J Nanobiotechnol 18, 162. https://doi.org/10.1186/s12951-020-00722-2

Butler, J.T., Abdelhamed, S., Kurre, P., 2018. Extracellular vesicles in the hematopoietic microenvironment. Haematologica 103, 382–394. https://doi.org/10.3324/haematol.2017.183335

Buzas, E.I., 2022. The roles of extracellular vesicles in the immune system. Nat Rev Immunol. https://doi.org/10.1038/s41577-022-00763-8

Cagan, R.L., Zon, L.I., White, R.M., 2019. Modeling Cancer with Flies and Fish. Developmental Cell 49, 317–324. https://doi.org/10.1016/j.devcel.2019.04.013

Cai, L., Chao, G., Li, W., Zhu, J., Li, F., Qi, B., Wei, Y., Chen, S., Zhou, G., Lu, X., Xu, J., Wu, X., Fan, G., Li, J., Liu, S., 2020. Activated CD4+ T cells-derived exosomal miR-142-3p boosts post-ischemic ventricular remodeling by activating myofibroblast. Aging 12, 7380–7396. https://doi.org/10.18632/aging.103084

Carmeliet, P., Jain, R.K., 2011. Molecular mechanisms and clinical applications of angiogenesis. Nature 473, 298–307. https://doi.org/10.1038/nature10144

Carnino, J.M., Ni, K., Jin, Y., 2020. Post-translational Modification Regulates Formation and Cargo-Loading of Extracellular Vesicles. Front. Immunol. 11, 948. https://doi.org/10.3389/fimmu.2020.00948

Carter, N., Mathiesen, A.H., Miller, N., Brown, M., Colunga Biancatelli, R.M.L., Catravas, J.D., Dobrian, A.D., 2022. Endothelial cell-derived extracellular vesicles impair the

angiogenic response of coronary artery endothelial cells. Front. Cardiovasc. Med. 9, 923081. https://doi.org/10.3389/fcvm.2022.923081
Cavallari, C., Ranghino, A., Tapparo, M., Cedrino, M., Figliolini, F., Grange, C., Giannachi, V., Garneri, P., Deregibus, M.C., Collino, F., Rispoli, P., Camussi, G., Brizzi, M.F., 2017. Serum-derived extracellular vesicles (EVs) impact on vascular remodeling and prevent muscle damage in acute hind limb ischemia. Sci Rep 7, 8180. https://doi.org/10.1038/s41598-017-08250-0
Chairoungdua, A., Smith, D.L., Pochard, P., Hull, M., Caplan, M.J., 2010. Exosome release of β-catenin: a novel mechanism that antagonizes Wnt signaling. Journal of Cell Biology 190, 1079–1091. https://doi.org/10.1083/jcb.201002049
Chang, Y.-J., Li, Y.-S., Wu, C.-C., Wang, K.-C., Huang, T.-C., Chen, Z., Chien, S., 2019. Extracellular MicroRNA-92a Mediates Endothelial Cell–Macrophage Communication. ATVB 39, 2492–2504. https://doi.org/10.1161/ATVBAHA.119.312707
Charwat, V., Olmos Calvo, I., Rothbauer, M., Kratz, S.R.A., Jungreuthmayer, C., Zanghellini, J., Grillari, J., Ertl, P., 2018. Combinatorial in Vitro and in Silico Approach To Describe Shear-Force Dependent Uptake of Nanoparticles in Microfluidic Vascular Models. Anal. Chem. 90, 3651–3655. https://doi.org/10.1021/acs.analchem.7b04788
Chen, C.C., Liu, L., Ma, F., Wong, C.W., Guo, X.E., Chacko, J.V., Farhoodi, H.P., Zhang, S.X., Zimak, J., Ségaliny, A., Riazifar, M., Pham, V., Digman, M.A., Pone, E.J., Zhao, W., 2016. Elucidation of Exosome Migration Across the Blood–Brain Barrier Model In Vitro. Cel. Mol. Bioeng. 9, 509–529. https://doi.org/10.1007/s12195-016-0458-3
Chen, P.-Y., Qin, L., Li, G., Wang, Z., Dahlman, J.E., Malagon-Lopez, J., Gujja, S., Cilfone, N.A., Kauffman, K.J., Sun, L., Sun, H., Zhang, X., Aryal, B., Canfran-Duque, A., Liu, R., Kusters, P., Sehgal, A., Jiao, Y., Anderson, D.G., Gulcher, J., Fernandez-Hernando, C., Lutgens, E., Schwartz, M.A., Pober, J.S., Chittenden, T.W., Tellides, G., Simons, M., 2019. Endothelial TGF-β signalling drives vascular inflammation and atherosclerosis. Nat Metab 1, 912–926. https://doi.org/10.1038/s42255-019-0102-3
Chen, W., Hoffmann, A.D., Liu, H., Liu, X., 2018. Organotropism: new insights into molecular mechanisms of breast cancer metastasis. npj Precision Onc 2, 4. https://doi.org/10.1038/s41698-018-0047-0
Chen, Y.Y., Syed, A.M., MacMillan, P., Rocheleau, J.V., Chan, W.C.W., 2020. Flow Rate Affects Nanoparticle Uptake into Endothelial Cells. Adv. Mater. 32, 1906274. https://doi.org/10.1002/adma.201906274
Chevillet, J.R., Kang, Q., Ruf, I.K., Briggs, H.A., Vojtech, L.N., Hughes, S.M., Cheng, H.H., Arroyo, J.D., Meredith, E.K., Gallichotte, E.N., Pogosova-Agadjanyan, E.L., Morrissey, C., Stirewalt, D.L., Hladik, F., Yu, E.Y., Higano, C.S., Tewari, M., 2014. Quantitative and stoichiometric analysis of the microRNA content of exosomes. Proc. Natl. Acad. Sci. U.S.A. 111, 14888–14893. https://doi.org/10.1073/pnas.1408301111
Choezom, D., Gross, J.C., 2022. Neutral sphingomyelinase 2 controls exosome secretion by counteracting V-ATPase-mediated endosome acidification. Journal of Cell Science 135, jcs259324. https://doi.org/10.1242/jcs.259324
Choudhuri, K., Llodrá, J., Roth, E.W., Tsai, J., Gordo, S., Wucherpfennig, K.W., Kam, L.C., Stokes, D.L., Dustin, M.L., 2014. Polarized release of T-cell-receptor-enriched microvesicles at the immunological synapse. Nature 507, 118–123. https://doi.org/10.1038/nature12951
Christianson, H.C., Svensson, K.J., van Kuppevelt, T.H., Li, J.-P., Belting, M., 2013. Cancer cell exosomes depend on cell-surface heparan sulfate proteoglycans for their internalization and functional activity. Proc. Natl. Acad. Sci. U.S.A. 110, 17380–17385. https://doi.org/10.1073/pnas.1304266110
Cianciaruso, C., Beltraminelli, T., Duval, F., Nassiri, S., Hamelin, R., Mozes, A., Gallart-Ayala, H., Ceada Torres, G., Torchia, B., Ries, C.H., Ivanisevic, J., De Palma, M., 2019. Molecular Profiling and Functional Analysis of Macrophage-Derived Tumor Extracellular Vesicles. Cell Reports 27, 3062-3080.e11. https://doi.org/10.1016/j.celrep.2019.05.008

Clancy, J.W., Schmidtmann, M., D'Souza-Schorey, C., 2021. The ins and outs of microvesicles. FASEB BioAdvances 3, 399–406. https://doi.org/10.1096/fba.2020-00127

Clancy, J.W., Sedgwick, A., Rosse, C., Muralidharan-Chari, V., Raposo, G., Method, M., Chavrier, P., D'Souza-Schorey, C., 2015. Regulated delivery of molecular cargo to invasive tumour-derived microvesicles. Nat Commun 6, 6919. https://doi.org/10.1038/ncomms7919

Clancy, J.W., Zhang, Y., Sheehan, C., D'Souza-Schorey, C., 2019. An ARF6–Exportin-5 axis delivers pre-miRNA cargo to tumour microvesicles. Nat Cell Biol 21, 856–866. https://doi.org/10.1038/s41556-019-0345-y

Clayton, A., Turkes, A., Dewitt, S., Steadman, R., Mason, M.D., Hallett, M.B., n.d. Adhesion and signaling by B cell-derived exosomes: the role of integrins 3.

Collot, M., Ashokkumar, P., Anton, H., Boutant, E., Faklaris, O., Galli, T., Mély, Y., Danglot, L., Klymchenko, A.S., 2019. MemBright: A Family of Fluorescent Membrane Probes for Advanced Cellular Imaging and Neuroscience. Cell Chemical Biology 26, 600-614.e7. https://doi.org/10.1016/j.chembiol.2019.01.009

Colombo, M., Moita, C., van Niel, G., Kowal, J., Vigneron, J., Benaroch, P., Manel, N., Moita, L.F., Théry, C., Raposo, G., 2013. Analysis of ESCRT functions in exosome biogenesis, composition and secretion highlights the heterogeneity of extracellular vesicles. Journal of Cell Science jcs.128868. https://doi.org/10.1242/jcs.128868

Coly, P., Boulanger, C.M., 2022. Role of extracellular vesicles in atherosclerosis: An update. J Leukocyte Bio 111, 51–62. https://doi.org/10.1002/JLB.3MIR0221-099R

Cooks, T., Pateras, I.S., Jenkins, L.M., Patel, K.M., Robles, A.I., Morris, J., Forshew, T., Appella, E., Gorgoulis, V.G., Harris, C.C., 2018. Mutant p53 cancers reprogram macrophages to tumor supporting macrophages via exosomal miR-1246. Nat Commun 9, 771. https://doi.org/10.1038/s41467-018-03224-w

Cornelison, R.C., Brennan, C.E., Kingsmore, K.M., Munson, J.M., 2018. Convective forces increase CXCR4-dependent glioblastoma cell invasion in GL261 murine model. Sci Rep 8, 17057. https://doi.org/10.1038/s41598-018-35141-9

Costa Verdera, H., Gitz-Francois, J.J., Schiffelers, R.M., Vader, P., 2017. Cellular uptake of extracellular vesicles is mediated by clathrin-independent endocytosis and macropinocytosis. Journal of Controlled Release 266, 100–108. https://doi.org/10.1016/j.jconrel.2017.09.019

Costafreda, M.I., Abbasi, A., Lu, H., Kaplan, G., 2020. Exosome mimicry by a HAVCR1–NPC1 pathway of endosomal fusion mediates hepatitis A virus infection. Nat Microbiol 5, 1096–1106. https://doi.org/10.1038/s41564-020-0740-y

Costanza, B., Umelo, I., Bellier, J., Castronovo, V., Turtoi, A., 2017. Stromal Modulators of TGF-β in Cancer. JCM 6, 7. https://doi.org/10.3390/jcm6010007

Costa-Silva, B., Aiello, N.M., Ocean, A.J., Singh, S., Zhang, H., Thakur, B.K., Becker, A., Hoshino, A., Mark, M.T., Molina, H., Xiang, J., Zhang, T., Theilen, T.-M., García-Santos, G., Williams, C., Ararso, Y., Huang, Y., Rodrigues, G., Shen, T.-L., Labori, K.J., Lothe, I.M.B., Kure, E.H., Hernandez, J., Doussot, A., Ebbesen, S.H., Grandgenett, P.M., Hollingsworth, M.A., Jain, M., Mallya, K., Batra, S.K., Jarnagin, W.R., Schwartz, R.E., Matei, I., Peinado, H., Stanger, B.Z., Bromberg, J., Lyden, D., 2015. Pancreatic cancer exosomes initiate pre-metastatic niche formation in the liver. Nat Cell Biol 17, 816–826. https://doi.org/10.1038/ncb3169

Crewe, C., Funcke, J.-B., Li, S., Joffin, N., Gliniak, C.M., Ghaben, A.L., An, Y.A., Sadek, H.A., Gordillo, R., Akgul, Y., Chen, S., Samovski, D., Fischer-Posovszky, P., Kusminski, C.M., Klein, S., Scherer, P.E., 2021. Extracellular vesicle-based interorgan transport of mitochondria from energetically stressed adipocytes. Cell Metabolism 33, 1853-1868.e11. https://doi.org/10.1016/j.cmet.2021.08.002

Cruz, L., Romero, J.A.A., Iglesia, R.P., Lopes, M.H., 2018. Extracellular Vesicles: Decoding a New Language for Cellular Communication in Early Embryonic Development. Front. Cell Dev. Biol. 6, 94. https://doi.org/10.3389/fcell.2018.00094

Dai, J., Escara-Wilke, J., Keller, J.M., Jung, Y., Taichman, R.S., Pienta, K.J., Keller, E.T., 2019. Primary prostate cancer educates bone stroma through exosomal pyruvate kinase M2 to promote bone metastasis. Journal of Experimental Medicine 216, 2883–2899. https://doi.org/10.1084/jem.20190158

Danesh, A., Inglis, H.C., Abdel-Mohsen, M., Deng, X., Adelman, A., Schechtman, K.B., Heitman, J.W., Vilardi, R., Shah, A., Keating, S.M., Cohen, M.J., Jacobs, E.S., Pillai, S.K., Lacroix, J., Spinella, P.C., Norris, P.J., 2018. Granulocyte-Derived Extracellular Vesicles Activate Monocytes and Are Associated With Mortality in Intensive Care Unit Patients. Front. Immunol. 9, 956. https://doi.org/10.3389/fimmu.2018.00956

Davies, P.F., Dewey, C.F., Bussolari, S.R., Gordon, E.J., Gimbrone, M.A., 1984. Influence of hemodynamic forces on vascular endothelial function. In vitro studies of shear stress and pinocytosis in bovine aortic cells. J. Clin. Invest. 73, 1121–1129. https://doi.org/10.1172/JCI111298

De Luca, L., Trino, S., Laurenzana, I., Simeon, V., Calice, G., Raimondo, S., Podestà, M., Santodirocco, M., Di Mauro, L., La Rocca, F., Caivano, A., Morano, A., Frassoni, F., Cilloni, D., Del Vecchio, L., Musto, P., 2016. MiRNAs and piRNAs from bone marrow mesenchymal stem cell extracellular vesicles induce cell survival and inhibit cell differentiation of cord blood hematopoietic stem cells: a new insight in transplantation. Oncotarget 7, 6676–6692. https://doi.org/10.18632/oncotarget.6791

De Palma, M., Biziato, D., Petrova, T.V., 2017. Microenvironmental regulation of tumour angiogenesis. Nat Rev Cancer 17, 457–474. https://doi.org/10.1038/nrc.2017.51

del Conde, I., Shrimpton, C.N., Thiagarajan, P., López, J.A., 2005. Tissue-factor–bearing microvesicles arise from lipid rafts and fuse with activated platelets to initiate coagulation. Blood 106, 1604–1611. https://doi.org/10.1182/blood-2004-03-1095

Denham, J., Spencer, S.J., 2020. Emerging roles of extracellular vesicles in the intercellular communication for exercise-induced adaptations. American Journal of Physiology-Endocrinology and Metabolism 319, E320–E329. https://doi.org/10.1152/ajpendo.00215.2020

Desrochers, L.M., Bordeleau, F., Reinhart-King, C.A., Cerione, R.A., Antonyak, M.A., 2016. Microvesicles provide a mechanism for intercellular communication by embryonic stem cells during embryo implantation. Nat Commun 7, 11958. https://doi.org/10.1038/ncomms11958

Dinh, N.T.H., Lee, Jaewook, Lee, Jaemin, Kim, S.S., Go, G., Bae, S., Jun, Y.I., Yoon, Y.J., Roh, T., Gho, Y.S., 2020. Indoor dust extracellular vesicles promote cancer lung metastasis by inducing tumour necrosis factor-α. Journal of Extracellular Vesicles 9, 1766821. https://doi.org/10.1080/20013078.2020.1766821

Dongre, A., Weinberg, R.A., 2019. New insights into the mechanisms of epithelial–mesenchymal transition and implications for cancer. Nat Rev Mol Cell Biol 20, 69–84. https://doi.org/10.1038/s41580-018-0080-4

Donnarumma, E., Fiore, D., Nappa, M., Roscigno, G., Adamo, A., Iaboni, M., Russo, V., Affinito, A., Puoti, I., Quintavalle, C., Rienzo, A., Piscuoglio, S., Thomas, R., Condorelli, G., 2017. Cancer-associated fibroblasts release exosomal microRNAs that dictate an aggressive phenotype in breast cancer. Oncotarget 8, 19592–19608. https://doi.org/10.18632/oncotarget.14752

Dorronsoro, A., Santiago, F.E., Grassi, D., Zhang, T., Lai, R.C., McGowan, S.J., Angelini, L., Lavasani, M., Corbo, L., Lu, A., Brooks, R.W., Garcia-Contreras, M., Stolz, D.B., Amelio, A., Boregowda, S.V., Fallahi, M., Reich, A., Ricordi, C., Phinney, D.G., Huard, J., Lim, S.K., Niedernhofer, L.J., Robbins, P.D., 2021. Mesenchymal stem cell-derived extracellular vesicles reduce senescence and extend health span in mouse models of aging. Aging Cell 20. https://doi.org/10.1111/acel.13337

Dou, D., Ren, X., Han, M., Xu, X., Ge, X., Gu, Y., Wang, X., 2020. Cancer-Associated Fibroblasts-Derived Exosomes Suppress Immune Cell Function in Breast Cancer via the miR-92/PD-L1 Pathway. Front. Immunol. 11, 2026. https://doi.org/10.3389/fimmu.2020.02026

Duchez, A.-C., Boudreau, L.H., Naika, G.S., Bollinger, J., Belleannée, C., Cloutier, N., Laffont, B., Mendoza-Villarroel, R.E., Lévesque, T., Rollet-Labelle, E., Rousseau, M., Allaeys, I., Tremblay, J.J., Poubelle, P.E., Lambeau, G., Pouliot, M., Provost, P., Soulet, D., Gelb, M.H., Boilard, E., 2015. Platelet microparticles are internalized in neutrophils via the concerted activity of 12-lipoxygenase and secreted phospholipase A_2 -IIA. Proc. Natl. Acad. Sci. U.S.A. 112. https://doi.org/10.1073/pnas.1507905112

Edgar, J.R., Eden, E.R., Futter, C.E., 2014. Hrs- and CD63-Dependent Competing Mechanisms Make Different Sized Endosomal Intraluminal Vesicles: Mechanisms of Intraluminal Vesicle Formation. Traffic 15, 197–211. https://doi.org/10.1111/tra.12139

Edgar, J.R., Manna, P.T., Nishimura, S., Banting, G., Robinson, M.S., 2016. Tetherin is an exosomal tether. eLife 5, e17180. https://doi.org/10.7554/eLife.17180

Egea-Jimenez, A.L., Zimmermann, P., 2018. Phospholipase D and phosphatidic acid in the biogenesis and cargo loading of extracellular vesicles. Journal of Lipid Research 59, 1554–1560. https://doi.org/10.1194/jlr.R083964

Escrevente, C., Keller, S., Altevogt, P., Costa, J., 2011. Interaction and uptake of exosomes by ovarian cancer cells. BMC Cancer 11, 108. https://doi.org/10.1186/1471-2407-11-108

Fafián-Labora, J.A., Rodríguez-Navarro, J.A., O'Loghlen, A., 2020. Small Extracellular Vesicles Have GST Activity and Ameliorate Senescence-Related Tissue Damage. Cell Metabolism 32, 71-86.e5. https://doi.org/10.1016/j.cmet.2020.06.004

Fang, J., Zhang, Z., Shang, L., Luo, Y., Lin, Y., Yuan, Y., Zhuang, S., 2018. Hepatoma cell-secreted exosomal microRNA-103 increases vascular permeability and promotes metastasis by targeting junction proteins. Hepatology 68, 1459–1475. https://doi.org/10.1002/hep.29920

Fang, T., Lv, H., Lv, G., Li, T., Wang, C., Han, Q., Yu, L., Su, B., Guo, L., Huang, S., Cao, D., Tang, L., Tang, S., Wu, M., Yang, W., Wang, H., 2018. Tumor-derived exosomal miR-1247-3p induces cancer-associated fibroblast activation to foster lung metastasis of liver cancer. Nat Commun 9, 191. https://doi.org/10.1038/s41467-017-02583-0

Fang, Y., Wu, D., Birukov, K.G., 2019. Mechanosensing and Mechanoregulation of Endothelial Cell Functions, in: Terjung, R. (Ed.), Comprehensive Physiology. Wiley, pp. 873–904. https://doi.org/10.1002/cphy.c180020

Farc, O., Cristea, V., 2020. An overview of the tumor microenvironment, from cells to complex networks (Review). Exp Ther Med 21, 96. https://doi.org/10.3892/etm.2020.9528

Fendl, B., Weiss, R., Eichhorn, T., Linsberger, I., Afonyushkin, T., Puhm, F., Binder, C.J., Fischer, M.B., Weber, V., 2021. Extracellular vesicles are associated with C-reactive protein in sepsis. Sci Rep 11, 6996. https://doi.org/10.1038/s41598-021-86489-4

Feng, D., Zhao, W.-L., Ye, Y.-Y., Bai, X.-C., Liu, R.-Q., Chang, L.-F., Zhou, Q., Sui, S.-F., 2010. Cellular Internalization of Exosomes Occurs Through Phagocytosis. Traffic 11, 675–687. https://doi.org/10.1111/j.1600-0854.2010.01041.x

Fernández-Messina, L., Rodríguez-Galán, A., de Yébenes, V.G., Gutiérrez-Vázquez, C., Tenreiro, S., Seabra, M.C., Ramiro, A.R., Sánchez-Madrid, F., 2020. Transfer of extracellular vesicle-micro RNA controls germinal center reaction and antibody production. EMBO Rep 21. https://doi.org/10.15252/embr.201948925

Fitzner, D., Schnaars, M., van Rossum, D., Krishnamoorthy, G., Dibaj, P., Bakhti, M., Regen, T., Hanisch, U.-K., Simons, M., 2011. Selective transfer of exosomes from oligodendrocytes to microglia by macropinocytosis. Journal of Cell Science 124, 447–458. https://doi.org/10.1242/jcs.074088

Flaumenhaft, R., Mairuhu, A., Italiano, J., 2010. Platelet- and Megakaryocyte-Derived Microparticles. Semin Thromb Hemost 36, 881–887. https://doi.org/10.1055/s-0030-1267042

Follain, G., Herrmann, D., Harlepp, S., Hyenne, V., Osmani, N., Warren, S.C., Timpson, P., Goetz, J.G., 2020. Fluids and their mechanics in tumour transit: shaping metastasis. Nat Rev Cancer 20, 107–124. https://doi.org/10.1038/s41568-019-0221-x

Follain, G., Mercier, L., Osmani, N., Harlepp, S., Goetz, J.G., 2017. Seeing is believing – multi-scale spatio-temporal imaging towards *in vivo* cell biology. J Cell Sci 130, 23–38. https://doi.org/10.1242/jcs.189001

Follain, G., Osmani, N., Azevedo, A.S., Allio, G., Mercier, L., Karreman, M.A., Solecki, G., Garcia Leòn, M.J., Lefebvre, O., Fekonja, N., Hille, C., Chabannes, V., Dollé, G., Metivet, T., Hovsepian, F.D., Prudhomme, C., Pichot, A., Paul, N., Carapito, R., Bahram, S., Ruthensteiner, B., Kemmling, A., Siemonsen, S., Schneider, T., Fiehler, J., Glatzel, M., Winkler, F., Schwab, Y., Pantel, K., Harlepp, S., Goetz, J.G., 2018. Hemodynamic Forces Tune the Arrest, Adhesion, and Extravasation of Circulating Tumor Cells. Developmental Cell 45, 33-52.e12. https://doi.org/10.1016/j.devcel.2018.02.015

Follain, G., Osmani, N., Gensbittel, V., Asokan, N., Larnicol, A., Mercier, L., Garcia-Leon, M.J., Busnelli, I., Pichot, A., Paul, N., Carapito, R., Bahram, S., Lefebvre, O., Goetz, J.G., 2021. Impairing flow-mediated endothelial remodeling reduces extravasation of tumor cells. Sci Rep 11, 13144. https://doi.org/10.1038/s41598-021-92515-2

Fong, M.Y., Zhou, W., Liu, L., Alontaga, A.Y., Chandra, M., Ashby, J., Chow, A., O'Connor, S.T.F., Li, S., Chin, A.R., Somlo, G., Palomares, M., Li, Z., Tremblay, J.R., Tsuyada, A., Sun, G., Reid, M.A., Wu, X., Swiderski, P., Ren, X., Shi, Y., Kong, M., Zhong, W., Chen, Y., Wang, S.E., 2015. Breast-cancer-secreted miR-122 reprograms glucose metabolism in premetastatic niche to promote metastasis. Nat Cell Biol 17, 183–194. https://doi.org/10.1038/ncb3094

Franzen, C.A., Blackwell, R.H., Todorovic, V., Greco, K.A., Foreman, K.E., Flanigan, R.C., Kuo, P.C., Gupta, G.N., 2015. Urothelial cells undergo epithelial-to-mesenchymal transition after exposure to muscle invasive bladder cancer exosomes. Oncogenesis 4, e163–e163. https://doi.org/10.1038/oncsis.2015.21

Friand, V., David, G., Zimmermann, P., 2015. Syntenin and syndecan in the biogenesis of exosomes: Syndecan-syntenin pathway in exosome biogenesis. Biol. Cell 107, 331–341. https://doi.org/10.1111/boc.201500010

Fridman, W.H., Pagès, F., Sautès-Fridman, C., Galon, J., 2012. The immune contexture in human tumours: impact on clinical outcome. Nat Rev Cancer 12, 298–306. https://doi.org/10.1038/nrc3245

Fu, C., Peng, P., Loschko, J., Feng, L., Pham, P., Cui, W., Lee, K.P., Krug, A.B., Jiang, A., 2020. Plasmacytoid dendritic cells cross-prime naive CD8 T cells by transferring antigen to conventional dendritic cells through exosomes. Proc. Natl. Acad. Sci. U.S.A. 117, 23730–23741. https://doi.org/10.1073/pnas.2002345117

Fuentes, P., Sesé, M., Guijarro, P.J., Emperador, M., Sánchez-Redondo, S., Peinado, H., Hümmer, S., Ramón y Cajal, S., 2020. ITGB3-mediated uptake of small extracellular vesicles facilitates intercellular communication in breast cancer cells. Nat Commun 11, 4261. https://doi.org/10.1038/s41467-020-18081-9

Gao, J., Li, S., Xu, Q., Zhang, X., Huang, M., Dai, X., Liu, L., 2021. Exosomes Promote Pre-Metastatic Niche Formation in Gastric Cancer. Front. Oncol. 11, 652378. https://doi.org/10.3389/fonc.2021.652378

Gao, Y., Bado, I., Wang, H., Zhang, W., Rosen, J.M., Zhang, X.H.-F., 2019. Metastasis Organotropism: Redefining the Congenial Soil. Developmental Cell 49, 375–391. https://doi.org/10.1016/j.devcel.2019.04.012

Garcia-Martin, R., Wang, G., Brandão, B.B., Zanotto, T.M., Shah, S., Kumar Patel, S., Schilling, B., Kahn, C.R., 2022. MicroRNA sequence codes for small extracellular vesicle release and cellular retention. Nature 601, 446–451. https://doi.org/10.1038/s41586-021-04234-3

García-Silva, S., Benito-Martín, A., Nogués, L., Hernández-Barranco, A., Mazariegos, M.S., Santos, V., Hergueta-Redondo, M., Ximénez-Embún, P., Kataru, R.P., Lopez, A.A., Merino, C., Sánchez-Redondo, S., Graña-Castro, O., Matei, I., Nicolás-Avila, J.Á., Torres-Ruiz, R., Rodríguez-Perales, S., Martínez, L., Pérez-Martínez, M., Mata, G., Szumera-Ciećkiewicz, A., Kalinowska, I., Saltari, A., Martínez-Gómez, J.M., Hogan, S.A., Saragovi, H.U., Ortega, S., Garcia-Martin, C., Boskovic, J., Levesque, M.P.,

Rutkowski, P., Hidalgo, A., Muñoz, J., Megías, D., Mehrara, B.J., Lyden, D., Peinado, H., 2021. Melanoma-derived small extracellular vesicles induce lymphangiogenesis and metastasis through an NGFR-dependent mechanism. Nat Cancer 2, 1387–1405. https://doi.org/10.1038/s43018-021-00272-y

García-Silva, S., Benito-Martín, A., Sánchez-Redondo, S., Hernández-Barranco, A., Ximénez-Embún, P., Nogués, L., Mazariegos, M.S., Brinkmann, K., Amor López, A., Meyer, L., Rodríguez, C., García-Martín, C., Boskovic, J., Letón, R., Montero, C., Robledo, M., Santambrogio, L., Sue Brady, M., Szumera-Ciećkiewicz, A., Kalinowska, I., Skog, J., Noerholm, M., Muñoz, J., Ortiz-Romero, P.L., Ruano, Y., Rodríguez-Peralto, J.L., Rutkowski, P., Peinado, H., 2019. Use of extracellular vesicles from lymphatic drainage as surrogate markers of melanoma progression and BRAFV600E mutation. Journal of Experimental Medicine 216, 1061–1070. https://doi.org/10.1084/jem.20181522

Gener Lahav, T., Adler, O., Zait, Y., Shani, O., Amer, M., Doron, H., Abramovitz, L., Yofe, I., Cohen, N., Erez, N., 2019. Melanoma-derived extracellular vesicles instigate proinflammatory signaling in the metastatic microenvironment. Int. J. Cancer 145, 2521–2534. https://doi.org/10.1002/ijc.32521

Gensbittel, V., Kräter, M., Harlepp, S., Busnelli, I., Guck, J., Goetz, J.G., 2021. Mechanical Adaptability of Tumor Cells in Metastasis. Developmental Cell 56, 164–179. https://doi.org/10.1016/j.devcel.2020.10.011

Genschmer, K.R., Russell, D.W., Lal, C., Szul, T., Bratcher, P.E., Noerager, B.D., Abdul Roda, M., Xu, X., Rezonzew, G., Viera, L., Dobosh, B.S., Margaroli, C., Abdalla, T.H., King, R.W., McNicholas, C.M., Wells, J.M., Dransfield, M.T., Tirouvanziam, R., Gaggar, A., Blalock, J.E., 2019. Activated PMN Exosomes: Pathogenic Entities Causing Matrix Destruction and Disease in the Lung. Cell 176, 113-126.e15. https://doi.org/10.1016/j.cell.2018.12.002

Gerhold, K.A., Schwartz, M.A., 2016. Ion Channels in Endothelial Responses to Fluid Shear Stress. Physiology 31, 359–369. https://doi.org/10.1152/physiol.00007.2016

Gerwing, M., Kocman, V., Stölting, M., Helfen, A., Masthoff, M., Roth, J., Barczyk-Kahlert, K., Greune, L., Schmidt, M.A., Heindel, W., Faber, C., König, S., Wildgruber, M., Eisenblätter, M., 2020. Tracking of Tumor Cell–Derived Extracellular Vesicles In Vivo Reveals a Specific Distribution Pattern with Consecutive Biological Effects on Target Sites of Metastasis. Mol Imaging Biol 22, 1501–1510. https://doi.org/10.1007/s11307-020-01521-9

Ghoroghi, S., Mary, B., Asokan, N., Goetz, J.G., Hyenne, V., 2021a. Tumor extracellular vesicles drive metastasis (it's a long way from home). FASEB BioAdvances fba.2021-00079. https://doi.org/10.1096/fba.2021-00079

Ghoroghi, S., Mary, B., Larnicol, A., Asokan, N., Klein, A., Osmani, N., Busnelli, I., Delalande, F., Paul, N., Halary, S., Gros, F., Fouillen, L., Haeberle, A.-M., Royer, C., Spiegelhalter, C., André-Grégoire, G., Mittelheisser, V., Detappe, A., Murphy, K., Timpson, P., Carapito, R., Blot-Chabaud, M., Gavard, J., Carapito, C., Vitale, N., Lefebvre, O., Goetz, J.G., Hyenne, V., 2021b. Ral GTPases promote breast cancer metastasis by controlling biogenesis and organ targeting of exosomes. eLife 10, e61539. https://doi.org/10.7554/eLife.61539

Ghossoub, R., Chéry, M., Audebert, S., Leblanc, R., Egea-Jimenez, A.L., Lembo, F., Mammar, S., Le Dez, F., Camoin, L., Borg, J.-P., Rubinstein, E., David, G., Zimmermann, P., 2020. Tetraspanin-6 negatively regulates exosome production. Proc. Natl. Acad. Sci. U.S.A. 117, 5913–5922. https://doi.org/10.1073/pnas.1922447117

Ghossoub, R., Lembo, F., Rubio, A., Gaillard, C.B., Bouchet, J., Vitale, N., Slavík, J., Machala, M., Zimmermann, P., 2014. Syntenin-ALIX exosome biogenesis and budding into multivesicular bodies are controlled by ARF6 and PLD2. Nat Commun 5, 3477. https://doi.org/10.1038/ncomms4477

Glasner, A., Levi, A., Enk, J., Isaacson, B., Viukov, S., Orlanski, S., Scope, A., Neuman, T., Enk, C.D., Hanna, J.H., Sexl, V., Jonjic, S., Seliger, B., Zitvogel, L., Mandelboim, O., 2018. NKp46 Receptor-Mediated Interferon-γ Production by Natural Killer Cells

Increases Fibronectin 1 to Alter Tumor Architecture and Control Metastasis. Immunity 48, 107-119.e4. https://doi.org/10.1016/j.immuni.2017.12.007
Goetz, J.G., Steed, E., Ferreira, R.R., Roth, S., Ramspacher, C., Boselli, F., Charvin, G., Liebling, M., Wyart, C., Schwab, Y., Vermot, J., 2014. Endothelial Cilia Mediate Low Flow Sensing during Zebrafish Vascular Development. Cell Reports 6, 799–808. https://doi.org/10.1016/j.celrep.2014.01.032
Gomes, F.G., Sandim, V., Almeida, V.H., Rondon, A.M.R., Succar, B.B., Hottz, E.D., Leal, A.C., Verçoza, B.R.F., Rodrigues, J.C.F., Bozza, P.T., Zingali, R.B., Monteiro, R.Q., 2017. Breast-cancer extracellular vesicles induce platelet activation and aggregation by tissue factor-independent and -dependent mechanisms. Thrombosis Research 159, 24–32. https://doi.org/10.1016/j.thromres.2017.09.019
Gomez, I., Ward, B., Souilhol, C., Recarti, C., Ariaans, M., Johnston, J., Burnett, A., Mahmoud, M., Luong, L.A., West, L., Long, M., Parry, S., Woods, R., Hulston, C., Benedikter, B., Niespolo, C., Bazaz, R., Francis, S., Kiss-Toth, E., van Zandvoort, M., Schober, A., Hellewell, P., Evans, P.C., Ridger, V., 2020. Neutrophil microvesicles drive atherosclerosis by delivering miR-155 to atheroprone endothelium. Nat Commun 11, 214. https://doi.org/10.1038/s41467-019-14043-y
Gomez-Garcia, M.J., Doiron, A.L., Steele, R.R.M., Labouta, H.I., Vafadar, B., Shepherd, R.D., Gates, I.D., Cramb, D.T., Childs, S.J., Rinker, K.D., 2018. Nanoparticle localization in blood vessels: dependence on fluid shear stress, flow disturbances, and flow-induced changes in endothelial physiology. Nanoscale 10, 15249–15261. https://doi.org/10.1039/C8NR03440K
Gonda, A., Kabagwira, J., Senthil, G.N., Wall, N.R., 2019. Internalization of Exosomes through Receptor-Mediated Endocytosis. Mol Cancer Res 17, 337–347. https://doi.org/10.1158/1541-7786.MCR-18-0891
Govindappa, P.K., Patil, M., Garikipati, V.N.S., Verma, S.K., Saheera, S., Narasimhan, G., Zhu, W., Kishore, R., Zhang, J., Krishnamurthy, P., 2020. Targeting exosome-associated human antigen R attenuates fibrosis and inflammation in diabetic heart. FASEB j. 34, 2238–2251. https://doi.org/10.1096/fj.201901995R
Granger, E., McNee, G., Allan, V., Woodman, P., 2014. The role of the cytoskeleton and molecular motors in endosomal dynamics. Seminars in Cell & Developmental Biology 31, 20–29. https://doi.org/10.1016/j.semcdb.2014.04.011
Gray, K.M., Stroka, K.M., 2017. Vascular endothelial cell mechanosensing: New insights gained from biomimetic microfluidic models. Seminars in Cell & Developmental Biology 71, 106–117. https://doi.org/10.1016/j.semcdb.2017.06.002
Gross, J.C., Chaudhary, V., Bartscherer, K., Boutros, M., 2012. Active Wnt proteins are secreted on exosomes. Nat Cell Biol 14, 1036–1045. https://doi.org/10.1038/ncb2574
Guo, H., Chitiprolu, M., Roncevic, L., Javalet, C., Hemming, F.J., Trung, M.T., Meng, L., Latreille, E., Tanese de Souza, C., McCulloch, D., Baldwin, R.M., Auer, R., Côté, J., Russell, R.C., Sadoul, R., Gibbings, D., 2017. Atg5 Disassociates the V1V0-ATPase to Promote Exosome Production and Tumor Metastasis Independent of Canonical Macroautophagy. Developmental Cell 43, 716-730.e7. https://doi.org/10.1016/j.devcel.2017.11.018
Gupta, D., Liang, X., Pavlova, S., Wiklander, O.P.B., Corso, G., Zhao, Y., Saher, O., Bost, J., Zickler, A.M., Piffko, A., Maire, C.L., Ricklefs, F.L., Gustafsson, O., Llorente, V.C., Gustafsson, M.O., Bostancioglu, R.B., Mamand, D.R., Hagey, D.W., Görgens, A., Nordin, J.Z., EL Andaloussi, S., 2020. Quantification of extracellular vesicles *in vitro* and *in vivo* using sensitive bioluminescence imaging. Journal of Extracellular Vesicles 9, 1800222. https://doi.org/10.1080/20013078.2020.1800222
Gurung, S., Perocheau, D., Touramanidou, L., Baruteau, J., 2021. The exosome journey: from biogenesis to uptake and intracellular signalling. Cell Commun Signal 19, 47. https://doi.org/10.1186/s12964-021-00730-1
Gustafson, C.M., Gammill, L.S., 2022. Extracellular Vesicles and Membrane Protrusions in Developmental Signaling. JDB 10, 39. https://doi.org/10.3390/jdb10040039

Hakulinen, J., Sankkila, L., Sugiyama, N., Lehti, K., Keski-Oja, J., 2008. Secretion of active membrane type 1 matrix metalloproteinase (MMP-14) into extracellular space in microvesicular exosomes. J. Cell. Biochem. 105, 1211–1218. https://doi.org/10.1002/jcb.21923

Han, J., Shuvaev, V.V., Davies, P.F., Eckmann, D.M., Muro, S., Muzykantov, V.R., 2015. Flow shear stress differentially regulates endothelial uptake of nanocarriers targeted to distinct epitopes of PECAM-1. Journal of Controlled Release 210, 39–47. https://doi.org/10.1016/j.jconrel.2015.05.006

Han, J., Zern, B.J., Shuvaev, V.V., Davies, P.F., Muro, S., Muzykantov, V., 2012. Acute and Chronic Shear Stress Differently Regulate Endothelial Internalization of Nanocarriers Targeted to Platelet-Endothelial Cell Adhesion Molecule-1. ACS Nano 6, 8824–8836. https://doi.org/10.1021/nn302687n

Hanahan, D., Coussens, L.M., 2012. Accessories to the Crime: Functions of Cells Recruited to the Tumor Microenvironment. Cancer Cell 21, 309–322. https://doi.org/10.1016/j.ccr.2012.02.022

Hanahan, D., Weinberg, R.A., 2011. Hallmarks of Cancer: The Next Generation. Cell 144, 646–674. https://doi.org/10.1016/j.cell.2011.02.013

Hanahan, D., Weinberg, R.A., 2000. The Hallmarks of Cancer. Cell 100, 57–70. https://doi.org/10.1016/S0092-8674(00)81683-9

Haraszti, R.A., Didiot, M.-C., Sapp, E., Leszyk, J., Shaffer, S.A., Rockwell, H.E., Gao, F., Narain, N.R., DiFiglia, M., Kiebish, M.A., Aronin, N., Khvorova, A., 2016. High-resolution proteomic and lipidomic analysis of exosomes and microvesicles from different cell sources. Journal of Extracellular Vesicles 5, 32570. https://doi.org/10.3402/jev.v5.32570

He, L., Zhu, W., Chen, Q., Yuan, Y., Wang, Y., Wang, J., Wu, X., 2019. Ovarian cancer cell-secreted exosomal miR-205 promotes metastasis by inducing angiogenesis. Theranostics 9, 8206–8220. https://doi.org/10.7150/thno.37455

Headley, M.B., Bins, A., Nip, A., Roberts, E.W., Looney, M.R., Gerard, A., Krummel, M.F., 2016. Visualization of immediate immune responses to pioneer metastatic cells in the lung. Nature 531, 513–517. https://doi.org/10.1038/nature16985

Hedlund, M., Stenqvist, A.-C., Nagaeva, O., Kjellberg, L., Wulff, M., Baranov, V., Mincheva-Nilsson, L., n.d. Human Placenta Expresses and Secretes NKG2D Ligands via Exosomes that Down-Modulate the Cognate Receptor Expression: Evidence for Immunosuppressive Function. The Journal of Immunology 13.

Henrich, S.E., McMahon, K.M., Plebanek, M.P., Calvert, A.E., Feliciano, T.J., Parrish, S., Tavora, F., Mega, A., De Souza, A., Carneiro, B.A., Thaxton, C.S., 2020. Prostate cancer extracellular vesicles mediate intercellular communication with bone marrow cells and promote metastasis in a cholesterol-dependent manner. Journal of Extracellular Vesicles 10. https://doi.org/10.1002/jev2.12042

Heusermann, W., Hean, J., Trojer, D., Steib, E., von Bueren, S., Graff-Meyer, A., Genoud, C., Martin, K., Pizzato, N., Voshol, J., Morrissey, D.V., Andaloussi, S.E.L., Wood, M.J., Meisner-Kober, N.C., 2016. Exosomes surf on filopodia to enter cells at endocytic hot spots, traffic within endosomes, and are targeted to the ER. J Cell Biol 213, 173–184. https://doi.org/10.1083/jcb.201506084

Hikita, T., Miyata, M., Watanabe, R., Oneyama, C., 2018. Sensitive and rapid quantification of exosomes by fusing luciferase to exosome marker proteins. Sci Rep 8, 14035. https://doi.org/10.1038/s41598-018-32535-7

Hikita, T., Uehara, R., Itoh, R.E., Mitani, F., Miyata, M., Yoshida, T., Yamaguchi, R., Oneyama, C., 2022. MEK/ERK-mediated oncogenic signals promote secretion of extracellular vesicles by controlling lysosome function. Cancer Science 113, 1264–1276. https://doi.org/10.1111/cas.15288

Hoffman, H.K., Aguilar, R.S., Clark, A.R., Groves, N.S., Pezeshkian, N., Bruns, M.M., van Engelenburg, S.B., 2022. Endocytosed HIV-1 Envelope Glycoprotein Traffics to Rab14 $^{+}$ Late Endosomes and Lysosomes to Regulate Surface Levels in T-Cell Lines. J Virol 96, e00767-22. https://doi.org/10.1128/jvi.00767-22

Hood, J.L., San, R.S., Wickline, S.A., 2011. Exosomes Released by Melanoma Cells Prepare Sentinel Lymph Nodes for Tumor Metastasis. Cancer Res 71, 3792–3801. https://doi.org/10.1158/0008-5472.CAN-10-4455

Horibe, S., Tanahashi, T., Kawauchi, S., Murakami, Y., Rikitake, Y., 2018. Mechanism of recipient cell-dependent differences in exosome uptake. BMC Cancer 18, 47. https://doi.org/10.1186/s12885-017-3958-1

Hoshino, A., Costa-Silva, B., Shen, T.-L., Rodrigues, G., Hashimoto, A., Tesic Mark, M., Molina, H., Kohsaka, S., Di Giannatale, A., Ceder, S., Singh, S., Williams, C., Soplop, N., Uryu, K., Pharmer, L., King, T., Bojmar, L., Davies, A.E., Ararso, Y., Zhang, T., Zhang, H., Hernandez, J., Weiss, J.M., Dumont-Cole, V.D., Kramer, K., Wexler, L.H., Narendran, A., Schwartz, G.K., Healey, J.H., Sandstrom, P., Jørgen Labori, K., Kure, E.H., Grandgenett, P.M., Hollingsworth, M.A., de Sousa, M., Kaur, S., Jain, M., Mallya, K., Batra, S.K., Jarnagin, W.R., Brady, M.S., Fodstad, O., Muller, V., Pantel, K., Minn, A.J., Bissell, M.J., Garcia, B.A., Kang, Y., Rajasekhar, V.K., Ghajar, C.M., Matei, I., Peinado, H., Bromberg, J., Lyden, D., 2015. Tumour exosome integrins determine organotropic metastasis. Nature 527, 329–335. https://doi.org/10.1038/nature15756

Hoshino, A., Kim, H.S., Bojmar, L., Gyan, K.E., Cioffi, M., Hernandez, J., Zambirinis, C.P., Rodrigues, G., Molina, H., Heissel, S., Mark, M.T., Steiner, L., Benito-Martin, A., Lucotti, S., Di Giannatale, A., Offer, K., Nakajima, M., Williams, C., Nogués, L., Pelissier Vatter, F.A., Hashimoto, A., Davies, A.E., Freitas, D., Kenific, C.M., Ararso, Y., Buehring, W., Lauritzen, P., Ogitani, Y., Sugiura, K., Takahashi, N., Alečković, M., Bailey, K.A., Jolissant, J.S., Wang, H., Harris, A., Schaeffer, L.M., García-Santos, G., Posner, Z., Balachandran, V.P., Khakoo, Y., Raju, G.P., Scherz, A., Sagi, I., Scherz-Shouval, R., Yarden, Y., Oren, M., Malladi, M., Petriccione, M., De Braganca, K.C., Donzelli, M., Fischer, C., Vitolano, S., Wright, G.P., Ganshaw, L., Marrano, M., Ahmed, A., DeStefano, J., Danzer, E., Roehrl, M.H.A., Lacayo, N.J., Vincent, T.C., Weiser, M.R., Brady, M.S., Meyers, P.A., Wexler, L.H., Ambati, S.R., Chou, A.J., Slotkin, E.K., Modak, S., Roberts, S.S., Basu, E.M., Diolaiti, D., Krantz, B.A., Cardoso, F., Simpson, A.L., Berger, M., Rudin, C.M., Simeone, D.M., Jain, M., Ghajar, C.M., Batra, S.K., Stanger, B.Z., Bui, J., Brown, K.A., Rajasekhar, V.K., Healey, J.H., de Sousa, M., Kramer, K., Sheth, S., Baisch, J., Pascual, V., Heaton, T.E., La Quaglia, M.P., Pisapia, D.J., Schwartz, R., Zhang, H., Liu, Y., Shukla, A., Blavier, L., DeClerck, Y.A., LaBarge, M., Bissell, M.J., Caffrey, T.C., Grandgenett, P.M., Hollingsworth, M.A., Bromberg, J., Costa-Silva, B., Peinado, H., Kang, Y., Garcia, B.A., O'Reilly, E.M., Kelsen, D., Trippett, T.M., Jones, D.R., Matei, I.R., Jarnagin, W.R., Lyden, D., 2020. Extracellular Vesicle and Particle Biomarkers Define Multiple Human Cancers. Cell 182, 1044-1061.e18. https://doi.org/10.1016/j.cell.2020.07.009

Hoshino, D., Kirkbride, K.C., Costello, K., Clark, E.S., Sinha, S., Grega-Larson, N., Tyska, M.J., Weaver, A.M., 2013. Exosome Secretion Is Enhanced by Invadopodia and Drives Invasive Behavior. Cell Reports 5, 1159–1168. https://doi.org/10.1016/j.celrep.2013.10.050

Howe, K., Clark, M.D., Torroja, C.F., Torrance, J., Berthelot, C., Muffato, M., Collins, J.E., Humphray, S., McLaren, K., Matthews, L., McLaren, S., Sealy, I., Caccamo, M., Churcher, C., Scott, C., Barrett, J.C., Koch, R., Rauch, G.-J., White, S., Chow, W., Kilian, B., Quintais, L.T., Guerra-Assunção, J.A., Zhou, Y., Gu, Y., Yen, J., Vogel, J.-H., Eyre, T., Redmond, S., Banerjee, R., Chi, J., Fu, B., Langley, E., Maguire, S.F., Laird, G.K., Lloyd, D., Kenyon, E., Donaldson, S., Sehra, H., Almeida-King, J., Loveland, J., Trevanion, S., Jones, M., Quail, M., Willey, D., Hunt, A., Burton, J., Sims, S., McLay, K., Plumb, B., Davis, J., Clee, C., Oliver, K., Clark, R., Riddle, C., Elliott, D., Threadgold, G., Harden, G., Ware, D., Begum, S., Mortimore, B., Kerry, G., Heath, P., Phillimore, B., Tracey, A., Corby, N., Dunn, M., Johnson, C., Wood, J., Clark, S., Pelan, S., Griffiths, G., Smith, M., Glithero, R., Howden, P., Barker, N., Lloyd, C., Stevens, C., Harley, J., Holt, K., Panagiotidis, G., Lovell, J., Beasley, H., Henderson, C., Gordon, D., Auger, K., Wright, D., Collins, J., Raisen, C., Dyer, L., Leung, K., Robertson, L., Ambridge, K., Leongamornlert, D., McGuire, S., Gilderthorp, R., Griffiths, C.,

Manthravadi, D., Nichol, S., Barker, G., Whitehead, S., Kay, M., Brown, J., Murnane, C., Gray, E., Humphries, M., Sycamore, N., Barker, D., Saunders, D., Wallis, J., Babbage, A., Hammond, S., Mashreghi-Mohammadi, M., Barr, L., Martin, S., Wray, P., Ellington, A., Matthews, N., Ellwood, M., Woodmansey, R., Clark, G., Cooper, J.D., Tromans, A., Grafham, D., Skuce, C., Pandian, R., Andrews, R., Harrison, E., Kimberley, A., Garnett, J., Fosker, N., Hall, R., Garner, P., Kelly, D., Bird, C., Palmer, S., Gehring, I., Berger, A., Dooley, C.M., Ersan-Ürün, Z., Eser, C., Geiger, H., Geisler, M., Karotki, L., Kirn, A., Konantz, J., Konantz, M., Oberländer, M., Rudolph-Geiger, S., Teucke, M., Lanz, C., Raddatz, G., Osoegawa, K., Zhu, B., Rapp, A., Widaa, S., Langford, C., Yang, F., Schuster, S.C., Carter, N.P., Harrow, J., Ning, Z., Herrero, J., Searle, S.M.J., Enright, A., Geisler, R., Plasterk, R.H.A., Lee, C., Westerfield, M., de Jong, P.J., Zon, L.I., Postlethwait, J.H., Nüsslein-Volhard, C., Hubbard, T.J.P., Crollius, H.R., Rogers, J., Stemple, D.L., 2013. The zebrafish reference genome sequence and its relationship to the human genome. Nature 496, 498–503. https://doi.org/10.1038/nature12111

Hsu, C., Morohashi, Y., Yoshimura, S., Manrique-Hoyos, N., Jung, S., Lauterbach, M.A., Bakhti, M., Grønborg, M., Möbius, W., Rhee, J., Barr, F.A., Simons, M., 2010. Regulation of exosome secretion by Rab35 and its GTPase-activating proteins TBC1D10A–C. Journal of Cell Biology 189, 223–232. https://doi.org/10.1083/jcb.200911018

Hsu, Y.-L., Hung, J.-Y., Chang, W.-A., Jian, S.-F., Lin, Y.-S., Pan, Y.-C., Wu, C.-Y., Kuo, P.-L., 2018. Hypoxic Lung-Cancer-Derived Extracellular Vesicle MicroRNA-103a Increases the Oncogenic Effects of Macrophages by Targeting PTEN. Molecular Therapy 26, 568–581. https://doi.org/10.1016/j.ymthe.2017.11.016

Hur, Y.H., Feng, S., Wilson, K.F., Cerione, R.A., Antonyak, M.A., 2021. Embryonic Stem Cell-Derived Extracellular Vesicles Maintain ESC Stemness by Activating FAK. Developmental Cell 56, 277-291.e6. https://doi.org/10.1016/j.devcel.2020.11.017

Hurwitz, S.N., Rider, M.A., Bundy, J.L., Liu, X., Singh, R.K., Meckes, D.G., 2016. Proteomic profiling of NCI-60 extracellular vesicles uncovers common protein cargo and cancer type-specific biomarkers. Oncotarget 7, 86999–87015. https://doi.org/10.18632/oncotarget.13569

Hwang, W.-L., Lan, H.-Y., Cheng, W.-C., Huang, S.-C., Yang, M.-H., 2019. Tumor stem-like cell-derived exosomal RNAs prime neutrophils for facilitating tumorigenesis of colon cancer. J Hematol Oncol 12, 10. https://doi.org/10.1186/s13045-019-0699-4

Hyenne, V., Apaydin, A., Rodriguez, D., Spiegelhalter, C., Hoff-Yoessle, S., Diem, M., Tak, S., Lefebvre, O., Schwab, Y., Goetz, J.G., Labouesse, M., 2015. RAL-1 controls multivesicular body biogenesis and exosome secretion. J Cell Biol 211, 27–37. https://doi.org/10.1083/jcb.201504136

Hyenne, V., Ghoroghi, S., Collot, M., Bons, J., Follain, G., Harlepp, S., Mary, B., Bauer, J., Mercier, L., Busnelli, I., Lefebvre, O., Fekonja, N., Garcia-Leon, M.J., Machado, P., Delalande, F., López, A.A., Silva, S.G., Verweij, F.J., van Niel, G., Djouad, F., Peinado, H., Carapito, C., Klymchenko, A.S., Goetz, J.G., 2019. Studying the Fate of Tumor Extracellular Vesicles at High Spatiotemporal Resolution Using the Zebrafish Embryo. Developmental Cell 48, 554-572.e7. https://doi.org/10.1016/j.devcel.2019.01.014

Imai, T., Takahashi, Y., Nishikawa, M., Kato, K., Morishita, M., Yamashita, T., Matsumoto, A., Charoenviriyakul, C., Takakura, Y., 2015. Macrophage-dependent clearance of systemically administered B16BL6-derived exosomes from the blood circulation in mice. Journal of Extracellular Vesicles 4, 26238. https://doi.org/10.3402/jev.v4.26238

Inglebert, M., Locatelli, L., Tsvirkun, D., Sinha, P., Maier, J.A., Misbah, C., Bureau, L., 2020. The effect of shear stress reduction on endothelial cells: A microfluidic study of the actin cytoskeleton. Biomicrofluidics 14, 024115. https://doi.org/10.1063/1.5143391

Jeppesen, D.K., Fenix, A.M., Franklin, J.L., Higginbotham, J.N., Zhang, Q., Zimmerman, L.J., Liebler, D.C., Ping, J., Liu, Q., Evans, R., Fissell, W.H., Patton, J.G., Rome, L.H., Burnette, D.T., Coffey, R.J., 2019. Reassessment of Exosome Composition. Cell 177, 428-445.e18. https://doi.org/10.1016/j.cell.2019.02.029

Jerabkova-Roda, K., Dupas, A., Osmani, N., Hyenne, V., Goetz, J.G., 2022. Circulating extracellular vesicles and tumor cells: sticky partners in metastasis. Trends in Cancer 8, 799–805. https://doi.org/10.1016/j.trecan.2022.05.002

Ji, Q., Zhou, L., Sui, H., Yang, L., Wu, X., Song, Q., Jia, R., Li, R., Sun, J., Wang, Z., Liu, N., Feng, Yuanyuan, Sun, X., Cai, Gang, Feng, Yu, Cai, J., Cao, Y., Cai, Guoxiang, Wang, Y., Li, Q., 2020. Primary tumors release ITGBL1-rich extracellular vesicles to promote distal metastatic tumor growth through fibroblast-niche formation. Nat Commun 11, 1211. https://doi.org/10.1038/s41467-020-14869-x

Johnsen, K.B., Gudbergsson, J.M., Andresen, T.L., Simonsen, J.B., 2019. What is the blood concentration of extracellular vesicles? Implications for the use of extracellular vesicles as blood-borne biomarkers of cancer. Biochimica et Biophysica Acta (BBA) - Reviews on Cancer 1871, 109–116. https://doi.org/10.1016/j.bbcan.2018.11.006

Joshi, B.S., de Beer, M.A., Giepmans, B.N.G., Zuhorn, I.S., 2020. Endocytosis of Extracellular Vesicles and Release of Their Cargo from Endosomes. ACS Nano 14, 4444–4455. https://doi.org/10.1021/acsnano.9b10033

Jung, T., Castellana, D., Klingbeil, P., Hernández, I.C., Vitacolonna, M., Orlicky, D.J., Roffler, S.R., Brodt, P., Zöller, M., 2009. CD44v6 Dependence of Premetastatic Niche Preparation by Exosomes. Neoplasia 11, 1093-IN17. https://doi.org/10.1593/neo.09822

Kajimoto, T., Okada, T., Miya, S., Zhang, L., Nakamura, S., 2013. Ongoing activation of sphingosine 1-phosphate receptors mediates maturation of exosomal multivesicular endosomes. Nat Commun 4, 2712. https://doi.org/10.1038/ncomms3712

Kalluri, R., LeBleu, V.S., 2020. The biology , function , and biomedical applications of exosomes. Science 367, eaau6977. https://doi.org/10.1126/science.aau6977

Kamerkar, S., LeBleu, V.S., Sugimoto, H., Yang, S., Ruivo, C.F., Melo, S.A., Lee, J.J., Kalluri, R., 2017. Exosomes facilitate therapeutic targeting of oncogenic KRAS in pancreatic cancer. Nature 546, 498–503. https://doi.org/10.1038/nature22341

Kanada, M., Bachmann, M.H., Hardy, J.W., Frimannson, D.O., Bronsart, L., Wang, A., Sylvester, M.D., Schmidt, T.L., Kaspar, R.L., Butte, M.J., Matin, A.C., Contag, C.H., 2015. Differential fates of biomolecules delivered to target cells via extracellular vesicles. Proc Natl Acad Sci USA 112, E1433–E1442. https://doi.org/10.1073/pnas.1418401112

Keup, C., Mach, P., Aktas, B., Tewes, M., Kolberg, H.-C., Hauch, S., Sprenger-Haussels, M., Kimmig, R., Kasimir-Bauer, S., 2018. RNA Profiles of Circulating Tumor Cells and Extracellular Vesicles for Therapy Stratification of Metastatic Breast Cancer Patients. Clinical Chemistry 64, 1054–1062. https://doi.org/10.1373/clinchem.2017.283531

Khanh, V.C., Yamashita, T., Ohneda, K., Tokunaga, C., Kato, H., Osaka, M., Hiramatsu, Y., Ohneda, O., 2020. Rejuvenation of mesenchymal stem cells by extracellular vesicles inhibits the elevation of reactive oxygen species. Sci Rep 10, 17315. https://doi.org/10.1038/s41598-020-74444-8

Kingston, B.R., Lin, Z.P., Ouyang, B., MacMillan, P., Ngai, J., Syed, A.M., Sindhwani, S., Chan, W.C.W., 2021. Specific Endothelial Cells Govern Nanoparticle Entry into Solid Tumors. ACS Nano 15, 14080–14094. https://doi.org/10.1021/acsnano.1c04510

Ko, S.Y., Lee, W., Kenny, H.A., Dang, L.H., Ellis, L.M., Jonasch, E., Lengyel, E., Naora, H., 2019. Cancer-derived small extracellular vesicles promote angiogenesis by heparin-bound, bevacizumab-insensitive VEGF, independent of vesicle uptake. Commun Biol 2, 386. https://doi.org/10.1038/s42003-019-0609-x

Kobayashi-Sun, J., Yamamori, S., Kondo, M., Kuroda, J., Ikegame, M., Suzuki, N., Kitamura, K., Hattori, A., Yamaguchi, M., Kobayashi, I., 2020. Uptake of osteoblast-derived extracellular vesicles promotes the differentiation of osteoclasts in the zebrafish scale. Commun Biol 3, 190. https://doi.org/10.1038/s42003-020-0925-1

Koi, Y., Tsutani, Y., Nishiyama, Y., Ueda, D., Ibuki, Y., Sasada, S., Akita, T., Masumoto, N., Kadoya, T., Yamamoto, Y., Takahashi, R., Tanaka, J., Okada, M., Tahara, H., 2020. Predicting the presence of breast cancer using circulating small RNAs, including those

in the extracellular vesicles. Cancer Sci 111, 2104–2115. https://doi.org/10.1111/cas.14393
Koles, K., Nunnari, J., Korkut, C., Barria, R., Brewer, C., Li, Y., Leszyk, J., Zhang, B., Budnik, V., 2012. Mechanism of Evenness Interrupted (Evi)-Exosome Release at Synaptic Boutons. Journal of Biological Chemistry 287, 16820–16834. https://doi.org/10.1074/jbc.M112.342667
Kong, J., Tian, H., Zhang, F., Zhang, Z., Li, J., Liu, X., Li, Xiancheng, Liu, J., Li, Xiaojie, Jin, D., Yang, X., Sun, B., Guo, T., Luo, Y., Lu, Y., Lin, B., Liu, T., 2019. Extracellular vesicles of carcinoma-associated fibroblasts creates a pre-metastatic niche in the lung through activating fibroblasts. Mol Cancer 18, 175. https://doi.org/10.1186/s12943-019-1101-4
Korkut, C., Li, Y., Koles, K., Brewer, C., Ashley, J., Yoshihara, M., Budnik, V., 2013. Regulation of Postsynaptic Retrograde Signaling by Presynaptic Exosome Release. Neuron 77, 1039–1046. https://doi.org/10.1016/j.neuron.2013.01.013
Kosaka, N., Iguchi, H., Hagiwara, K., Yoshioka, Y., Takeshita, F., Ochiya, T., 2013. Neutral Sphingomyelinase 2 (nSMase2)-dependent Exosomal Transfer of Angiogenic MicroRNAs Regulate Cancer Cell Metastasis. Journal of Biological Chemistry 288, 10849–10859. https://doi.org/10.1074/jbc.M112.446831
Kovács, Á.F., Fekete, N., Turiák, L., Ács, A., Kőhidai, L., Buzás, E.I., Pállinger, É., 2019. Unravelling the Role of Trophoblastic-Derived Extracellular Vesicles in Regulatory T Cell Differentiation. IJMS 20, 3457. https://doi.org/10.3390/ijms20143457
Kowal, J., Arras, G., Colombo, M., Jouve, M., Morath, J.P., Primdal-Bengtson, B., Dingli, F., Loew, D., Tkach, M., Théry, C., 2016. Proteomic comparison defines novel markers to characterize heterogeneous populations of extracellular vesicle subtypes. Proc Natl Acad Sci USA 113, E968–E977. https://doi.org/10.1073/pnas.1521230113
Kowal, J., Tkach, M., Théry, C., 2014. Biogenesis and secretion of exosomes. Current Opinion in Cell Biology 29, 116–125. https://doi.org/10.1016/j.ceb.2014.05.004
Kozik, P., Hodson, N.A., Sahlender, D.A., Simecek, N., Soromani, C., Wu, J., Collinson, L.M., Robinson, M.S., 2013. A human genome-wide screen for regulators of clathrin-coated vesicle formation reveals an unexpected role for the V-ATPase. Nat Cell Biol 15, 50–60. https://doi.org/10.1038/ncb2652
Krause, M., Rak-Raszewska, A., Naillat, F., Saarela, U., Schmidt, C., Ronkainen, V.-P., Bart, G., Ylä-Herttuala, S., Vainio, S.J., 2018. Exosomes as secondary inductive signals involved in kidney organogenesis. Journal of Extracellular Vesicles 7, 1422675. https://doi.org/10.1080/20013078.2017.1422675
Kriebel, P.W., Majumdar, R., Jenkins, L.M., Senoo, H., Wang, W., Ammu, S., Chen, S., Narayan, K., Iijima, M., Parent, C.A., 2018. Extracellular vesicles direct migration by synthesizing and releasing chemotactic signals. J. Cell Biol. 217, 2891–2910. https://doi.org/10.1083/jcb.201710170
Kugeratski, F.G., Santi, A., Zanivan, S., 2022. Extracellular vesicles as central regulators of blood vessel function in cancer. Sci. Signal. 15, eaaz4742. https://doi.org/10.1126/scisignal.aaz4742
Kur, I.-M., Prouvot, P.-H., Fu, T., Fan, W., Müller-Braun, F., Das, A., Das, S., Deller, T., Roeper, J., Stroh, A., Momma, S., 2020. Neuronal activity triggers uptake of hematopoietic extracellular vesicles in vivo. PLoS Biol 18, e3000643. https://doi.org/10.1371/journal.pbio.3000643
Kusama, K., Nakamura, K., Bai, R., Nagaoka, K., Sakurai, T., Imakawa, K., 2018. Intrauterine exosomes are required for bovine conceptus implantation. Biochemical and Biophysical Research Communications 495, 1370–1375. https://doi.org/10.1016/j.bbrc.2017.11.176
Kusunose, J., Zhang, H., Gagnon, M.K.J., Pan, T., Simon, S.I., Ferrara, K.W., 2013. Microfluidic System for Facilitated Quantification of Nanoparticle Accumulation to Cells Under Laminar Flow. Ann Biomed Eng 41, 89–99. https://doi.org/10.1007/s10439-012-0634-0

Lai, C.P., Kim, E.Y., Badr, C.E., Weissleder, R., Mempel, T.R., Tannous, B.A., Breakefield, X.O., 2015. Visualization and tracking of tumour extracellular vesicle delivery and RNA translation using multiplexed reporters. Nat Commun 6, 7029. https://doi.org/10.1038/ncomms8029

Lai, C.P., Mardini, O., Ericsson, M., Prabhakar, S., Maguire, C.A., Chen, J.W., Tannous, B.A., Breakefield, X.O., 2014. Dynamic Biodistribution of Extracellular Vesicles *in Vivo* Using a Multimodal Imaging Reporter. ACS Nano 8, 483–494. https://doi.org/10.1021/nn404945r

Lai, R.C., Arslan, F., Lee, M.M., Sze, N.S.K., Choo, A., Chen, T.S., Salto-Tellez, M., Timmers, L., Lee, C.N., El Oakley, R.M., Pasterkamp, G., de Kleijn, D.P.V., Lim, S.K., 2010. Exosome secreted by MSC reduces myocardial ischemia/reperfusion injury. Stem Cell Research 4, 214–222. https://doi.org/10.1016/j.scr.2009.12.003

Lam, S.S., Martell, J.D., Kamer, K.J., Deerinck, T.J., Ellisman, M.H., Mootha, V.K., Ting, A.Y., 2015. Directed evolution of APEX2 for electron microscopy and proximity labeling. Nat Methods 12, 51–54. https://doi.org/10.1038/nmeth.3179

Lange-Consiglio, A., Perrini, C., Albini, G., Modina, S., Lodde, V., Orsini, E., Esposti, P., Cremonesi, F., 2017. Oviductal microvesicles and their effect on in vitro maturation of canine oocytes. Reproduction 154, 167–180. https://doi.org/10.1530/REP-17-0117

Lanna, A., Vaz, B., D'Ambra, C., Valvo, S., Vuotto, C., Chiurchiù, V., Devine, O., Sanchez, M., Borsellino, G., Akbar, A.N., De Bardi, M., Gilroy, D.W., Dustin, M.L., Blumer, B., Karin, M., 2022. An intercellular transfer of telomeres rescues T cells from senescence and promotes long-term immunological memory. Nat Cell Biol. https://doi.org/10.1038/s41556-022-00991-z

Larios, J., Mercier, V., Roux, A., Gruenberg, J., 2020. ALIX- and ESCRT-III–dependent sorting of tetraspanins to exosomes. Journal of Cell Biology 219. https://doi.org/10.1083/jcb.201904113

Lässer, C., Seyed Alikhani, V., Ekström, K., Eldh, M., Torregrosa Paredes, P., Bossios, A., Sjöstrand, M., Gabrielsson, S., Lötvall, J., Valadi, H., 2011. Human saliva, plasma and breast milk exosomes contain RNA: uptake by macrophages. J Transl Med 9, 9. https://doi.org/10.1186/1479-5876-9-9

Latifkar, A., Ling, L., Hingorani, A., Johansen, E., Clement, A., Zhang, X., Hartman, J., Fischbach, C., Lin, H., Cerione, R.A., Antonyak, M.A., 2019. Loss of Sirtuin 1 Alters the Secretome of Breast Cancer Cells by Impairing Lysosomal Integrity. Developmental Cell 49, 393-408.e7. https://doi.org/10.1016/j.devcel.2019.03.011

Latysheva, N., Muratov, G., Rajesh, S., Padgett, M., Hotchin, N.A., Overduin, M., Berditchevski, F., 2006. Syntenin-1 Is a New Component of Tetraspanin-Enriched Microdomains: Mechanisms and Consequences of the Interaction of Syntenin-1 with CD63. Mol Cell Biol 26, 7707–7718. https://doi.org/10.1128/MCB.00849-06

Laulagnier, K., Javalet, C., Hemming, F.J., Chivet, M., Lachenal, G., Blot, B., Chatellard, C., Sadoul, R., 2018. Amyloid precursor protein products concentrate in a subset of exosomes specifically endocytosed by neurons. Cell. Mol. Life Sci. 75, 757–773. https://doi.org/10.1007/s00018-017-2664-0

Laurenzana, I., Trino, S., Lamorte, D., Girasole, M., Dinarelli, S., De Stradis, A., Grieco, V., Maietti, M., Traficante, A., Statuto, T., Villani, O., Musto, P., Sgambato, A., De Luca, L., Caivano, A., 2021. Analysis of Amount, Size, Protein Phenotype and Molecular Content of Circulating Extracellular Vesicles Identifies New Biomarkers in Multiple Myeloma. IJN Volume 16, 3141–3160. https://doi.org/10.2147/IJN.S303391

Lázaro-Ibáñez, E., Lässer, C., Shelke, G.V., Crescitelli, R., Jang, S.C., Cvjetkovic, A., García-Rodríguez, A., Lötvall, J., 2019. DNA analysis of low- and high-density fractions defines heterogeneous subpopulations of small extracellular vesicles based on their DNA cargo and topology. Journal of Extracellular Vesicles 8, 1656993. https://doi.org/10.1080/20013078.2019.1656993

Leal, A.C., Mizurini, D.M., Gomes, T., Rochael, N.C., Saraiva, E.M., Dias, M.S., Werneck, C.C., Sielski, M.S., Vicente, C.P., Monteiro, R.Q., 2017. Tumor-Derived Exosomes Induce the Formation of Neutrophil Extracellular Traps: Implications For The

Establishment of Cancer-Associated Thrombosis. Sci Rep 7, 6438. https://doi.org/10.1038/s41598-017-06893-7
Leblanc, R., Kashyap, R., Barral, K., Egea-Jimenez, A.L., Kovalskyy, D., Feracci, M., Garcia, M., Derviaux, C., Betzi, S., Ghossoub, R., Platonov, M., Roche, P., Morelli, X., Hoffer, L., Zimmermann, P., 2020. Pharmacological inhibition of syntenin PDZ2 domain impairs breast cancer cell activities and exosome loading with syndecan and EpCAM cargo. Journal of Extracellular Vesicles 10. https://doi.org/10.1002/jev2.12039
Lechertier, T., Reynolds, L.E., Kim, H., Pedrosa, A.R., Gómez-Escudero, J., Muñoz-Félix, J.M., Batista, S., Dukinfield, M., Demircioglu, F., Wong, P.P., Matchett, K.P., Henderson, N.C., D'Amico, G., Parsons, M., Harwood, C., Meier, P., Hodivala-Dilke, K.M., 2020. Pericyte FAK negatively regulates Gas6/Axl signalling to suppress tumour angiogenesis and tumour growth. Nat Commun 11, 2810. https://doi.org/10.1038/s41467-020-16618-6
Lee, B.R., Sanstrum, B.J., Liu, Y., Kwon, S.-H., 2019. Distinct role of Sirtuin 1 (SIRT1) and Sirtuin 2 (SIRT2) in inhibiting cargo-loading and release of extracellular vesicles. Sci Rep 9, 20049. https://doi.org/10.1038/s41598-019-56635-0
Leidal, A.M., Huang, H.H., Marsh, T., Solvik, T., Zhang, D., Ye, J., Kai, F., Goldsmith, J., Liu, J.Y., Huang, Y.-H., Monkkonen, T., Vlahakis, A., Huang, E.J., Goodarzi, H., Yu, L., Wiita, A.P., Debnath, J., 2020. The LC3-conjugation machinery specifies the loading of RNA-binding proteins into extracellular vesicles. Nat Cell Biol 22, 187–199. https://doi.org/10.1038/s41556-019-0450-y
Li, B., Antonyak, M.A., Zhang, J., Cerione, R.A., 2012. RhoA triggers a specific signaling pathway that generates transforming microvesicles in cancer cells. Oncogene 31, 4740–4749. https://doi.org/10.1038/onc.2011.636
Li, B., Hong, J., Hong, M., Wang, Y., Yu, T., Zang, S., Wu, Q., 2019. piRNA-823 delivered by multiple myeloma-derived extracellular vesicles promoted tumorigenesis through re-educating endothelial cells in the tumor environment. Oncogene 38, 5227–5238. https://doi.org/10.1038/s41388-019-0788-4
Li, J., Li, Z., Jiang, P., Peng, M., Zhang, X., Chen, K., Liu, H., Bi, H., Liu, X., Li, X., 2018. Circular RNA IARS (circ-IARS) secreted by pancreatic cancer cells and located within exosomes regulates endothelial monolayer permeability to promote tumor metastasis. J Exp Clin Cancer Res 37, 177. https://doi.org/10.1186/s13046-018-0822-3
Li, M., Zeringer, E., Barta, T., Schageman, J., Cheng, A., Vlassov, A.V., 2014. Analysis of the RNA content of the exosomes derived from blood serum and urine and its potential as biomarkers. Phil. Trans. R. Soc. B 369, 20130502. https://doi.org/10.1098/rstb.2013.0502
Li, S., An, N., Liu, B., Wang, S., Wang, J., Ye, Y., 2019. Exosomes from LNCaP cells promote osteoblast activity through miR-375 transfer. Oncol Lett. https://doi.org/10.3892/ol.2019.10110
Li, Y., Yang, Y., Gan, T., Zhou, J., Hu, F., Hao, N., Yuan, B., Chen, Y., Zhang, M., 2019. Extracellular RNAs from lung cancer cells activate epithelial cells and induce neutrophil extracellular traps. Int J Oncol. https://doi.org/10.3892/ijo.2019.4808
Lin, A., Sabnis, A., Kona, S., Nattama, S., Patel, H., Dong, J.-F., Nguyen, K.T., 2009. Shear-regulated uptake of nanoparticles by endothelial cells and development of endothelial-targeting nanoparticles. J. Biomed. Mater. Res. 9999A, NA-NA. https://doi.org/10.1002/jbm.a.32592
Linnemannstöns, K., Karuna M, P., Witte, L., Choezom, D., Honemann-Capito, M., Lagurin, A.S., Schmidt, C.V., Shrikhande, S., Steinmetz, L., Wiebke, M., Lenz, C., Gross, J.C., 2022. Microscopic and biochemical monitoring of endosomal trafficking and extracellular vesicle secretion in an endogenous in vivo model. J of Extracellular Vesicle 11, 12263. https://doi.org/10.1002/jev2.12263
Liu, Q., Yang, C., Wang, S., Shi, D., Wei, C., Song, J., Lin, X., Dou, R., Bai, J., Xiang, Z., Huang, S., Liu, K., Xiong, B., 2020. Wnt5a-induced M2 polarization of tumor-associated macrophages via IL-10 promotes colorectal cancer progression. Cell Commun Signal 18, 51. https://doi.org/10.1186/s12964-020-00557-2

Liu, Q., Yu, Z., Yuan, S., Xie, W., Li, C., Hu, Z., Xiang, Y., Wu, N., Wu, L., Bai, L., Li, Y., 2017. Circulating exosomal microRNAs as prognostic biomarkers for non-small-cell lung cancer. Oncotarget 8, 13048–13058. https://doi.org/10.18632/oncotarget.14369

Liu, Y., Cao, X., 2016. Characteristics and Significance of the Pre-metastatic Niche. Cancer Cell 30, 668–681. https://doi.org/10.1016/j.ccell.2016.09.011

Liu, Y., Gu, Y., Han, Y., Zhang, Q., Jiang, Z., Zhang, X., Huang, B., Xu, X., Zheng, J., Cao, X., 2016. Tumor Exosomal RNAs Promote Lung Pre-metastatic Niche Formation by Activating Alveolar Epithelial TLR3 to Recruit Neutrophils. Cancer Cell 30, 243–256. https://doi.org/10.1016/j.ccell.2016.06.021

Loyer, X., Potteaux, S., Vion, A.-C., Guérin, C.L., Boulkroun, S., Rautou, P.-E., Ramkhelawon, B., Esposito, B., Dalloz, M., Paul, J.-L., Julia, P., Maccario, J., Boulanger, C.M., Mallat, Z., Tedgui, A., 2014a. Inhibition of MicroRNA-92a Prevents Endothelial Dysfunction and Atherosclerosis in Mice. Circ Res 114, 434–443. https://doi.org/10.1161/CIRCRESAHA.114.302213

Lu, P., Takai, K., Weaver, V.M., Werb, Z., 2011. Extracellular Matrix Degradation and Remodeling in Development and Disease. Cold Spring Harbor Perspectives in Biology 3, a005058–a005058. https://doi.org/10.1101/cshperspect.a005058

Lucotti, S., Cerutti, C., Soyer, M., Gil-Bernabé, A.M., Gomes, A.L., Allen, P.D., Smart, S., Markelc, B., Watson, K., Armstrong, P.C., Mitchell, J.A., Warner, T.D., Ridley, A.J., Muschel, R.J., 2019. Aspirin blocks formation of metastatic intravascular niches by inhibiting platelet-derived COX-1/thromboxane A2. Journal of Clinical Investigation 129, 1845–1862. https://doi.org/10.1172/JCI121985

Lucotti, S., Kenific, C.M., Zhang, H., Lyden, D., 2022. Extracellular vesicles and particles impact the systemic landscape of cancer. The EMBO Journal 41. https://doi.org/10.15252/embj.2021109288

Luga, V., Zhang, L., Viloria-Petit, A.M., Ogunjimi, A.A., Inanlou, M.R., Chiu, E., Buchanan, M., Hosein, A.N., Basik, M., Wrana, J.L., 2012. Exosomes Mediate Stromal Mobilization of Autocrine Wnt-PCP Signaling in Breast Cancer Cell Migration. Cell 151, 1542–1556. https://doi.org/10.1016/j.cell.2012.11.024

Lundberg, V., Berglund, M., Skogberg, G., Lindgren, S., Lundqvist, C., Gudmundsdottir, J., Thörn, K., Telemo, E., Ekwall, O., 2016. Thymic exosomes promote the final maturation of thymocytes. Sci Rep 6, 36479. https://doi.org/10.1038/srep36479

Ma, S., McGuire, M.H., Mangala, L.S., Lee, S., Stur, E., Hu, W., Bayraktar, E., Villar-Prados, A., Ivan, C., Wu, S.Y., Yokoi, A., Dasari, S.K., Jennings, N.B., Liu, J., Lopez-Berestein, G., Ram, P., Sood, A.K., 2021. Gain-of-function p53 protein transferred via small extracellular vesicles promotes conversion of fibroblasts to a cancer-associated phenotype. Cell Reports 34, 108726. https://doi.org/10.1016/j.celrep.2021.108726

Maire, C.L., Fuh, M.M., Kaulich, K., Fita, K.D., Stevic, I., Heiland, D.H., Welsh, J.A., Jones, J.C., Görgens, A., Ricklefs, T., Dührsen, L., Sauvigny, T., Joosse, S.A., Reifenberger, G., Pantel, K., Glatzel, M., Miklosi, A.G., Felce, J.H., Caselli, M., Pereno, V., Reimer, R., Schlüter, H., Westphal, M., Schüller, U., Lamszus, K., Ricklefs, F.L., 2021. Genome-wide methylation profiling of glioblastoma cell-derived extracellular vesicle DNA allows tumor classification. Neuro-Oncology 23, 1087–1099. https://doi.org/10.1093/neuonc/noab012

Mao, Y., Wang, Y., Dong, L., Zhang, Yunjie, Zhang, Yanqiu, Wang, C., Zhang, Q., Yang, S., Cao, L., Zhang, X., Li, X., Fu, Z., 2019. Hypoxic exosomes facilitate angiogenesis and metastasis in esophageal squamous cell carcinoma through altering the phenotype and transcriptome of endothelial cells. J Exp Clin Cancer Res 38, 389. https://doi.org/10.1186/s13046-019-1384-8

Marar, C., Starich, B., Wirtz, D., 2021. Extracellular vesicles in immunomodulation and tumor progression. Nat Immunol 22, 560–570. https://doi.org/10.1038/s41590-021-00899-0

Marcoux, G., Laroche, A., Hasse, S., Bellio, M., Mbarik, M., Tamagne, M., Allaeys, I., Zufferey, A., Lévesque, T., Rebetz, J., Karakeussian-Rimbaud, A., Turgeon, J., Bourgoin, S.G., Hamzeh-Cognasse, H., Cognasse, F., Kapur, R., Semple, J.W., Hébert, M.-J., Pirenne, F., Overkleeft, H.S., Florea, B.I., Dieude, M., Vingert, B., Boilard, E., 2021. Platelet EVs

contain an active proteasome involved in protein processing for antigen presentation via MHC-I molecules. Blood 138, 2607–2620. https://doi.org/10.1182/blood.2020009957

Margolis, E., Brown, G., Partin, A., Carter, B., McKiernan, J., Tutrone, R., Torkler, P., Fischer, C., Tadigotla, V., Noerholm, M., Donovan, M.J., Skog, J., 2022. Predicting high-grade prostate cancer at initial biopsy: clinical performance of the ExoDx (EPI) Prostate Intelliscore test in three independent prospective studies. Prostate Cancer Prostatic Dis 25, 296–301. https://doi.org/10.1038/s41391-021-00456-8

Mary, B., Ghoroghi, S., Hyenne, V., Goetz, J.G., 2020. Live tracking of extracellular vesicles in larval zebrafish, in: Methods in Enzymology. Elsevier, pp. 243–275. https://doi.org/10.1016/bs.mie.2020.07.013

Massagué, J., Obenauf, A.C., n.d. Metastatic colonization by circulating tumour cells 9.

Mateescu, B., Kowal, E.J.K., van Balkom, B.W.M., Bartel, S., Bhattacharyya, S.N., Buzás, E.I., Buck, A.H., de Candia, P., Chow, F.W.N., Das, S., Driedonks, T.A.P., Fernández-Messina, L., Haderk, F., Hill, A.F., Jones, J.C., Van Keuren-Jensen, K.R., Lai, C.P., Lässer, C., di Liegro, I., Lunavat, T.R., Lorenowicz, M.J., Maas, S.L.N., Mäger, I., Mittelbrunn, M., Momma, S., Mukherjee, K., Nawaz, M., Pegtel, D.M., Pfaffl, M.W., Schiffelers, R.M., Tahara, H., Théry, C., Tosar, J.P., Wauben, M.H.M., Witwer, K.W., Nolte-'t Hoen, E.N.M., 2017. Obstacles and opportunities in the functional analysis of extracellular vesicle RNA – an ISEV position paper. Journal of Extracellular Vesicles 6, 1286095. https://doi.org/10.1080/20013078.2017.1286095

Mathieu, M., Martin-Jaular, L., Lavieu, G., Théry, C., 2019. Specificities of secretion and uptake of exosomes and other extracellular vesicles for cell-to-cell communication. Nat Cell Biol 21, 9–17. https://doi.org/10.1038/s41556-018-0250-9

Mathiyalagan, P., Liang, Y., Kim, D., Misener, S., Thorne, T., Kamide, C.E., Klyachko, E., Losordo, D.W., Hajjar, R.J., Sahoo, S., 2017. Angiogenic Mechanisms of Human CD34^{+} Stem Cell Exosomes in the Repair of Ischemic Hindlimb. Circ Res 120, 1466–1476. https://doi.org/10.1161/CIRCRESAHA.116.310557

Matsui, T., Sakamaki, Y., Nakashima, S., Fukuda, M., 2022. Rab39 and its effector UACA regulate basolateral exosome release from polarized epithelial cells. Cell Reports 39, 110875. https://doi.org/10.1016/j.celrep.2022.110875

Matsumoto, A., Takahashi, Y., Chang, H.-Y., Wu, Y.-W., Yamamoto, A., Ishihama, Y., Takakura, Y., 2020. Blood concentrations of small extracellular vesicles are determined by a balance between abundant secretion and rapid clearance. Journal of Extracellular Vesicles 9, 1696517. https://doi.org/10.1080/20013078.2019.1696517

Maus, R.L.G., Jakub, J.W., Hieken, T.J., Nevala, W.K., Christensen, T.A., Sutor, S.L., Flotte, T.J., Markovic, S.N., 2019. Identification of novel, immune-mediating extracellular vesicles in human lymphatic effluent draining primary cutaneous melanoma. OncoImmunology 8, e1667742. https://doi.org/10.1080/2162402X.2019.1667742

McKenzie, A.J., Hoshino, D., Hong, N.H., Cha, D.J., Franklin, J.L., Coffey, R.J., Patton, J.G., Weaver, A.M., 2016. KRAS-MEK Signaling Controls Ago2 Sorting into Exosomes. Cell Reports 15, 978–987. https://doi.org/10.1016/j.celrep.2016.03.085

McKiernan, J., Donovan, M.J., Margolis, E., Partin, A., Carter, B., Brown, G., Torkler, P., Noerholm, M., Skog, J., Shore, N., Andriole, G., Thompson, I., Carroll, P., 2018. A Prospective Adaptive Utility Trial to Validate Performance of a Novel Urine Exosome Gene Expression Assay to Predict High-grade Prostate Cancer in Patients with Prostate-specific Antigen 2–10 ng/ml at Initial Biopsy. European Urology 74, 731–738. https://doi.org/10.1016/j.eururo.2018.08.019

Medeiros, B., Goodale, D., Postenka, C., Lowes, L.E., Kiser, P., Hearn, S., Salmond, N., Williams, K.C., Allan, A.L., 2020. Triple-Negative Primary Breast Tumors Induce Supportive Premetastatic Changes in the Extracellular Matrix and Soluble Components of the Lung Microenvironment. Cancers 12, 172. https://doi.org/10.3390/cancers12010172

Melo, S.A., Luecke, L.B., Kahlert, C., Fernandez, A.F., Gammon, S.T., Kaye, J., LeBleu, V.S., Mittendorf, E.A., Weitz, J., Rahbari, N., Reissfelder, C., Pilarsky, C., Fraga, M.F.,

Piwnica-Worms, D., Kalluri, R., 2015. Glypican-1 identifies cancer exosomes and detects early pancreatic cancer. Nature 523, 177–182. https://doi.org/10.1038/nature14581
Men, Y., Yelick, J., Jin, S., Tian, Y., Chiang, M.S.R., Higashimori, H., Brown, E., Jarvis, R., Yang, Y., 2019. Exosome reporter mice reveal the involvement of exosomes in mediating neuron to astroglia communication in the CNS. Nat Commun 10, 4136. https://doi.org/10.1038/s41467-019-11534-w
Midekessa, G., Godakumara, K., Ord, J., Viil, J., Lättekivi, F., Dissanayake, K., Kopanchuk, S., Rinken, A., Andronowska, A., Bhattacharjee, S., Rinken, T., Fazeli, A., 2020. Zeta Potential of Extracellular Vesicles: Toward Understanding the Attributes that Determine Colloidal Stability. ACS Omega 5, 16701–16710. https://doi.org/10.1021/acsomega.0c01582
Min, L., Zhu, S., Chen, L., Liu, X., Wei, R., Zhao, L., Yang, Y., Zhang, Z., Kong, G., Li, P., Zhang, S., 2019. Evaluation of circulating small extracellular vesicles derived miRNAs as biomarkers of early colon cancer: a comparison with plasma total miRNAs. Journal of Extracellular Vesicles 8, 1643670. https://doi.org/10.1080/20013078.2019.1643670
Mirzaaghasi, A., Han, Y., Ahn, S.-H., Choi, C., Park, J.-H., 2021. Biodistribution and Pharmacokinectics of Liposomes and Exosomes in a Mouse Model of Sepsis. Pharmaceutics 13, 427. https://doi.org/10.3390/pharmaceutics13030427
Molotkov, A., Molotkova, N., Duester, G., 2006. Retinoic acid guides eye morphogenetic movements via paracrine signaling but is unnecessary for retinal dorsoventral patterning. Development 133, 1901–1910. https://doi.org/10.1242/dev.02328
Montecalvo, A., Larregina, A.T., Shufesky, W.J., Beer Stolz, D., Sullivan, M.L.G., Karlsson, J.M., Baty, C.J., Gibson, G.A., Erdos, G., Wang, Z., Milosevic, J., Tkacheva, O.A., Divito, S.J., Jordan, R., Lyons-Weiler, J., Watkins, S.C., Morelli, A.E., 2012. Mechanism of transfer of functional microRNAs between mouse dendritic cells via exosomes. Blood 119, 756–766. https://doi.org/10.1182/blood-2011-02-338004
Monypenny, J., Milewicz, H., Flores-Borja, F., Weitsman, G., Cheung, A., Chowdhury, R., Burgoyne, T., Arulappu, A., Lawler, K., Barber, P.R., Vicencio, J.M., Keppler, M., Wulaningsih, W., Davidson, S.M., Fraternali, F., Woodman, N., Turmaine, M., Gillett, C., Franz, D., Quezada, S.A., Futter, C.E., Von Kriegsheim, A., Kolch, W., Vojnovic, B., Carlton, J.G., Ng, T., 2018. ALIX Regulates Tumor-Mediated Immunosuppression by Controlling EGFR Activity and PD-L1 Presentation. Cell Reports 24, 630–641. https://doi.org/10.1016/j.celrep.2018.06.066
Morad, G., Carman, C.V., Hagedorn, E.J., Perlin, J.R., Zon, L.I., Mustafaoglu, N., Park, T.-E., Ingber, D.E., Daisy, C.C., Moses, M.A., 2019. Tumor-Derived Extracellular Vesicles Breach the Intact Blood–Brain Barrier *via* Transcytosis. ACS Nano 13, 13853–13865. https://doi.org/10.1021/acsnano.9b04397
Morishita, M., Takahashi, Y., Nishikawa, M., Sano, K., Kato, K., Yamashita, T., Imai, T., Saji, H., Takakura, Y., 2015. Quantitative Analysis of Tissue Distribution of the B16BL6-Derived Exosomes Using a Streptavidin-Lactadherin Fusion Protein and Iodine-125-Labeled Biotin Derivative After Intravenous Injection in Mice. Journal of Pharmaceutical Sciences 104, 705–713. https://doi.org/10.1002/jps.24251
Moros, M., Fergola, E., Marchesano, V., Mutarelli, M., Tommasini, G., Miedziak, B., Palumbo, G., Ambrosone, A., Tino, A., Tortiglione, C., 2021. The Aquatic Invertebrate Hydra vulgaris Releases Molecular Messages Through Extracellular Vesicles. Front. Cell Dev. Biol. 9, 788117. https://doi.org/10.3389/fcell.2021.788117
Mu, W., Rana, S., Zöller, M., 2013. Host Matrix Modulation by Tumor Exosomes Promotes Motility and Invasiveness. Neoplasia 15, 875-IN4. https://doi.org/10.1593/neo.13786
Mulcahy, L.A., Pink, R.C., Carter, D.R.F., 2014. Routes and mechanisms of extracellular vesicle uptake. Journal of Extracellular Vesicles 3, 24641. https://doi.org/10.3402/jev.v3.24641
Müller, K., Fedosov, D.A., Gompper, G., 2015. Margination of micro- and nano-particles in blood flow and its effect on drug delivery. Sci Rep 4, 4871. https://doi.org/10.1038/srep04871

Muralidharan-Chari, V., Clancy, J., Plou, C., Romao, M., Chavrier, P., Raposo, G., D'Souza-Schorey, C., 2009. ARF6-Regulated Shedding of Tumor Cell-Derived Plasma Membrane Microvesicles. Current Biology 19, 1875–1885. https://doi.org/10.1016/j.cub.2009.09.059

Nabhan, J.F., Hu, R., Oh, R.S., Cohen, S.N., Lu, Q., 2012. Formation and release of arrestin domain-containing protein 1-mediated microvesicles (ARMMs) at plasma membrane by recruitment of TSG101 protein. Proc. Natl. Acad. Sci. U.S.A. 109, 4146–4151. https://doi.org/10.1073/pnas.1200448109

Naito, Y., Yamamoto, Y., Sakamoto, N., Shimomura, I., Kogure, A., Kumazaki, M., Yokoi, A., Yashiro, M., Kiyono, T., Yanagihara, K., Takahashi, R., Hirakawa, K., Yasui, W., Ochiya, T., 2019. Cancer extracellular vesicles contribute to stromal heterogeneity by inducing chemokines in cancer-associated fibroblasts. Oncogene 38, 5566–5579. https://doi.org/10.1038/s41388-019-0832-4

Nakamura, K., Kusama, K., Bai, R., Sakurai, T., Isuzugawa, K., Godkin, J.D., Suda, Y., Imakawa, K., 2016. Induction of IFNT-Stimulated Genes by Conceptus-Derived Exosomes during the Attachment Period. PLoS ONE 11, e0158278. https://doi.org/10.1371/journal.pone.0158278

Nakase, I., Kobayashi, N.B., Takatani-Nakase, T., Yoshida, T., 2015. Active macropinocytosis induction by stimulation of epidermal growth factor receptor and oncogenic Ras expression potentiates cellular uptake efficacy of exosomes. Sci Rep 5, 10300. https://doi.org/10.1038/srep10300

Nanbo, A., Kawanishi, E., Yoshida, R., Yoshiyama, H., 2013. Exosomes Derived from Epstein-Barr Virus-Infected Cells Are Internalized via Caveola-Dependent Endocytosis and Promote Phenotypic Modulation in Target Cells. Journal of Virology 87, 10334–10347. https://doi.org/10.1128/JVI.01310-13

Nauli, S.M., Kawanabe, Y., Kaminski, J.J., Pearce, W.J., Ingber, D.E., Zhou, J., 2008. Endothelial Cilia Are Fluid Shear Sensors That Regulate Calcium Signaling and Nitric Oxide Production Through Polycystin-1. Circulation 117, 1161–1171. https://doi.org/10.1161/CIRCULATIONAHA.107.710111

Nazarenko, I., Rana, S., Baumann, A., McAlear, J., Hellwig, A., Trendelenburg, M., Lochnit, G., Preissner, K.T., Zoller, M., 2010. Cell Surface Tetraspanin Tspan8 Contributes to Molecular Pathways of Exosome-Induced Endothelial Cell Activation. Cancer Research 70, 1668–1678. https://doi.org/10.1158/0008-5472.CAN-09-2470

Nie, X., Fan, J., Li, H., Yin, Z., Zhao, Y., Dai, B., Dong, N., Chen, C., Wang, D.W., 2018. miR-217 Promotes Cardiac Hypertrophy and Dysfunction by Targeting PTEN. Molecular Therapy - Nucleic Acids 12, 254–266. https://doi.org/10.1016/j.omtn.2018.05.013

Nielsen, M.H., Beck-Nielsen, H., Andersen, M.N., Handberg, A., 2014. A flow cytometric method for characterization of circulating cell-derived microparticles in plasma. Journal of Extracellular Vesicles 3, 20795. https://doi.org/10.3402/jev.v3.20795

Nishida-Aoki, N., Tominaga, N., Kosaka, N., Ochiya, T., 2020. Altered biodistribution of deglycosylated extracellular vesicles through enhanced cellular uptake. Journal of Extracellular Vesicles 9, 1713527. https://doi.org/10.1080/20013078.2020.1713527

Nishida-Aoki, N., Tominaga, N., Takeshita, F., Sonoda, H., Yoshioka, Y., Ochiya, T., 2017. Disruption of Circulating Extracellular Vesicles as a Novel Therapeutic Strategy against Cancer Metastasis. Molecular Therapy 25, 181–191. https://doi.org/10.1016/j.ymthe.2016.10.009

Noria, S., Xu, F., McCue, S., Jones, M., Gotlieb, A.I., Langille, B.L., 2004. Assembly and Reorientation of Stress Fibers Drives Morphological Changes to Endothelial Cells Exposed to Shear Stress. The American Journal of Pathology 164, 1211–1223. https://doi.org/10.1016/S0002-9440(10)63209-9

Norouzi-Barough, L., Asgari Khosro Shahi, A., Mohebzadeh, F., Masoumi, L., Haddadi, M.R., Shirian, S., 2020. Early diagnosis of breast and ovarian cancers by body fluids circulating tumor-derived exosomes. Cancer Cell Int 20, 187. https://doi.org/10.1186/s12935-020-01276-x

Novo, D., Heath, N., Mitchell, L., Caligiuri, G., MacFarlane, A., Reijmer, D., Charlton, L., Knight, J., Calka, M., McGhee, E., Dornier, E., Sumpton, D., Mason, S., Echard, A., Klinkert, K., Secklehner, J., Kruiswijk, F., Vousden, K., Macpherson, I.R., Blyth, K., Bailey, P., Yin, H., Carlin, L.M., Morton, J., Zanivan, S., Norman, J.C., 2018. Mutant p53s generate pro-invasive niches by influencing exosome podocalyxin levels. Nat Commun 9, 5069. https://doi.org/10.1038/s41467-018-07339-y

O'Brien, K., Breyne, K., Ughetto, S., Laurent, L.C., Breakefield, X.O., 2020. RNA delivery by extracellular vesicles in mammalian cells and its applications. Nat Rev Mol Cell Biol 21, 585–606. https://doi.org/10.1038/s41580-020-0251-y

Ohue, Y., Nishikawa, H., 2019. Regulatory T (Treg) cells in cancer: Can Treg cells be a new therapeutic target? Cancer Sci 110, 2080–2089. https://doi.org/10.1111/cas.14069

Ono, M., Kosaka, N., Tominaga, N., Yoshioka, Y., Takeshita, F., Takahashi, R., Yoshida, M., Tsuda, H., Tamura, K., Ochiya, T., 2014. Exosomes from bone marrow mesenchymal stem cells contain a microRNA that promotes dormancy in metastatic breast cancer cells. Sci. Signal. 7. https://doi.org/10.1126/scisignal.2005231

Ortiz, A., Gui, J., Zahedi, F., Yu, P., Cho, C., Bhattacharya, S., Carbone, C.J., Yu, Q., Katlinski, K.V., Katlinskaya, Y.V., Handa, S., Haas, V., Volk, S.W., Brice, A.K., Wals, K., Matheson, N.J., Antrobus, R., Ludwig, S., Whiteside, T.L., Sander, C., Tarhini, A.A., Kirkwood, J.M., Lehner, P.J., Guo, W., Rui, H., Minn, A.J., Koumenis, C., Diehl, J.A., Fuchs, S.Y., 2019. An Interferon-Driven Oxysterol-Based Defense against Tumor-Derived Extracellular Vesicles. Cancer Cell 35, 33-45.e6. https://doi.org/10.1016/j.ccell.2018.12.001

Osmani, N., Follain, G., García León, M.J., Lefebvre, O., Busnelli, I., Larnicol, A., Harlepp, S., Goetz, J.G., 2019. Metastatic Tumor Cells Exploit Their Adhesion Repertoire to Counteract Shear Forces during Intravascular Arrest. Cell Reports 28, 2491-2500.e5. https://doi.org/10.1016/j.celrep.2019.07.102

Osti, D., Del Bene, M., Rappa, G., Santos, M., Matafora, V., Richichi, C., Faletti, S., Beznoussenko, G.V., Mironov, A., Bachi, A., Fornasari, L., Bongetta, D., Gaetani, P., DiMeco, F., Lorico, A., Pelicci, G., 2019. Clinical Significance of Extracellular Vesicles in Plasma from Glioblastoma Patients. Clin Cancer Res 25, 266–276. https://doi.org/10.1158/1078-0432.CCR-18-1941

Ostrowski, M., Carmo, N.B., Krumeich, S., Fanget, I., Raposo, G., Savina, A., Moita, C.F., Schauer, K., Hume, A.N., Freitas, R.P., Goud, B., Benaroch, P., Hacohen, N., Fukuda, M., Desnos, C., Seabra, M.C., Darchen, F., Amigorena, S., Moita, L.F., Thery, C., 2010. Rab27a and Rab27b control different steps of the exosome secretion pathway. Nat Cell Biol 12, 19–30. https://doi.org/10.1038/ncb2000

Palma, M.D., n.d. Microenvironmental regulation of tumour angiogenesis 18.

Palmulli, R., van Niel, G., 2018. To be or not to be... secreted as exosomes, a balance finely tuned by the mechanisms of biogenesis. Essays in Biochemistry 62, 177–191. https://doi.org/10.1042/EBC20170076

Parolini, I., Federici, C., Raggi, C., Lugini, L., Palleschi, S., De Milito, A., Coscia, C., Iessi, E., Logozzi, M., Molinari, A., Colone, M., Tatti, M., Sargiacomo, M., Fais, S., 2009. Microenvironmental pH Is a Key Factor for Exosome Traffic in Tumor Cells. Journal of Biological Chemistry 284, 34211–34222. https://doi.org/10.1074/jbc.M109.041152

Pathak, A.P., Artemov, D., Neeman, M., Bhujwalla, Z.M., 2006. Lymph Node Metastasis in Breast Cancer Xenografts Is Associated with Increased Regions of Extravascular Drain, Lymphatic Vessel Area, and Invasive Phenotype. Cancer Research 66, 5151–5158. https://doi.org/10.1158/0008-5472.CAN-05-1788

Peinado, H., Alečković, M., Lavotshkin, S., Matei, I., Costa-Silva, B., Moreno-Bueno, G., Hergueta-Redondo, M., Williams, C., García-Santos, G., Ghajar, C.M., Nitadori-Hoshino, A., Hoffman, C., Badal, K., Garcia, B.A., Callahan, M.K., Yuan, J., Martins, V.R., Skog, J., Kaplan, R.N., Brady, M.S., Wolchok, J.D., Chapman, P.B., Kang, Y., Bromberg, J., Lyden, D., 2012. Melanoma exosomes educate bone marrow progenitor cells toward a pro-metastatic phenotype through MET. Nat Med 18, 883–891. https://doi.org/10.1038/nm.2753

Peinado, H., Zhang, H., Matei, I.R., Costa-Silva, B., Hoshino, A., Rodrigues, G., Psaila, B., Kaplan, R.N., Bromberg, J.F., Kang, Y., Bissell, M.J., Cox, T.R., Giaccia, A.J., Erler, J.T., Hiratsuka, S., Ghajar, C.M., Lyden, D., 2017. Pre-metastatic niches: organ-specific homes for metastases. Nat Rev Cancer 17, 302–317. https://doi.org/10.1038/nrc.2017.6

Peng, M., Sun, R., Hong, Y., Wang, J., Xie, Y., Zhang, X., Li, J., Guo, H., Xu, P., Li, Y., Wang, X., Wan, T., Zhao, Y., Huang, F., Wang, Y., Ye, R., Liu, Q., Liu, G., Liu, X., Xu, G., 2022. Extracellular vesicles carrying proinflammatory factors may spread atherosclerosis to remote locations. Cell. Mol. Life Sci. 79, 430. https://doi.org/10.1007/s00018-022-04464-2

Pereira, E.R., Kedrin, D., Seano, G., Gautier, O., Meijer, E.F.J., Jones, D., Chin, S.-M., Kitahara, S., Bouta, E.M., Chang, J., Beech, E., Jeong, H.-S., Carroll, M.C., Taghian, A.G., Padera, T.P., 2018. Lymph node metastases can invade local blood vessels, exit the node, and colonize distant organs in mice 6.

Peters, M.M.C., Sampaio-Pinto, V., da Costa Martins, P.A., 2020. Non-coding RNAs in endothelial cell signalling and hypoxia during cardiac regeneration. Biochimica et Biophysica Acta (BBA) - Molecular Cell Research 1867, 118515. https://doi.org/10.1016/j.bbamcr.2019.07.010

Piccin, A., Murphy, W.G., Smith, O.P., 2007. Circulating microparticles: pathophysiology and clinical implications. Blood Reviews 21, 157–171. https://doi.org/10.1016/j.blre.2006.09.001

Plebanek, M.P., Angeloni, N.L., Vinokour, E., Li, J., Henkin, A., Martinez-Marin, D., Filleur, S., Bhowmick, R., Henkin, J., Miller, S.D., Ifergan, I., Lee, Y., Osman, I., Thaxton, C.S., Volpert, O.V., 2017. Pre-metastatic cancer exosomes induce immune surveillance by patrolling monocytes at the metastatic niche. Nat Commun 8, 1319. https://doi.org/10.1038/s41467-017-01433-3

Poggio, M., Hu, T., Pai, C.-C., Chu, B., Belair, C.D., Chang, A., Montabana, E., Lang, U.E., Fu, Q., Fong, L., Blelloch, R., 2019. Suppression of Exosomal PD-L1 Induces Systemic Anti-tumor Immunity and Memory. Cell 177, 414-427.e13. https://doi.org/10.1016/j.cell.2019.02.016

Pomatto, M., Gai, C., Negro, F., Cedrino, M., Grange, C., Ceccotti, E., Togliatto, G., Collino, F., Tapparo, M., Figliolini, F., Lopatina, T., Brizzi, M.F., Camussi, G., 2021. Differential Therapeutic Effect of Extracellular Vesicles Derived by Bone Marrow and Adipose Mesenchymal Stem Cells on Wound Healing of Diabetic Ulcers and Correlation to Their Cargoes. IJMS 22, 3851. https://doi.org/10.3390/ijms22083851

Prada, I., Amin, L., Furlan, R., Legname, G., Verderio, C., Cojoc, D., 2016. A new approach to follow a single extracellular vesicle–cell interaction using optical tweezers. BioTechniques 60. https://doi.org/10.2144/000114371

Prada, I., Meldolesi, J., 2016. Binding and Fusion of Extracellular Vesicles to the Plasma Membrane of Their Cell Targets. IJMS 17, 1296. https://doi.org/10.3390/ijms17081296

Pucci, F., Garris, C., Lai, C.P., Newton, A., Pfirschke, C., Engblom, C., Alvarez, D., Sprachman, M., Evavold, C., Magnuson, A., von Andrian, U.H., Glatz, K., Breakefield, X.O., Mempel, T.R., Weissleder, R., Pittet, M.J., 2016. SCS macrophages suppress melanoma by restricting tumor-derived vesicle-B cell interactions. Science 352, 242–246. https://doi.org/10.1126/science.aaf1328

Purushothaman, A., Bandari, S.K., Liu, J., Mobley, J.A., Brown, E.E., Sanderson, R.D., 2016. Fibronectin on the Surface of Myeloma Cell-derived Exosomes Mediates Exosome-Cell Interactions. J. Biol. Chem. 291, 1652–1663. https://doi.org/10.1074/jbc.M115.686295

Qiao, S., Zhang, W., Yin, Y., Wei, Z., Chen, F., Zhao, J., Sun, X., Mu, D., Xie, J., Xu, B., 2020. Extracellular vesicles derived from Krüppel-Like Factor 2-overexpressing endothelial cells attenuate myocardial ischemia-reperfusion injury by preventing Ly6C ^{high} monocyte recruitment. Theranostics 10, 11562–11579. https://doi.org/10.7150/thno.45459

Qin, X., Zhang, K., Qiu, J., Wang, N., Qu, K., Cui, Y., Huang, J., Luo, L., Zhong, Y., Tian, T., Wu, W., Wang, Y., Wang, G., 2022. Uptake of oxidative stress-mediated extracellular vesicles by vascular endothelial cells under low magnitude shear stress. Bioactive Materials 9, 397–410. https://doi.org/10.1016/j.bioactmat.2021.10.038

Quail, D.F., Joyce, J.A., 2013. Microenvironmental regulation of tumor progression and metastasis. Nat Med 19, 1423–1437. https://doi.org/10.1038/nm.3394

Raghavan, V., Rbaibi, Y., Pastor-Soler, N.M., Carattino, M.D., Weisz, O.A., 2014. Shear stress-dependent regulation of apical endocytosis in renal proximal tubule cells mediated by primary cilia. Proceedings of the National Academy of Sciences 111, 8506–8511. https://doi.org/10.1073/pnas.1402195111

Rana, S., Yue, S., Stadel, D., Zöller, M., 2012. Toward tailored exosomes: The exosomal tetraspanin web contributes to target cell selection. The International Journal of Biochemistry & Cell Biology 44, 1574–1584. https://doi.org/10.1016/j.biocel.2012.06.018

Raposo, G., Nijman, H.W., Stoorvogel, W., Liejendekker, R., Harding, C.V., Melief, C.J., Geuze, H.J., 1996. B lymphocytes secrete antigen-presenting vesicles. Journal of Experimental Medicine 183, 1161–1172. https://doi.org/10.1084/jem.183.3.1161

Record, M., Carayon, K., Poirot, M., Silvente-Poirot, S., 2014. Exosomes as new vesicular lipid transporters involved in cell–cell communication and various pathophysiologies. Biochimica et Biophysica Acta (BBA) - Molecular and Cell Biology of Lipids 1841, 108–120. https://doi.org/10.1016/j.bbalip.2013.10.004

Reginald-Opara, J.N., Svirskis, D., Paek, S.Y., Tang, M., O'Carroll, S.J., Dean, J.M., Chamley, L.W., Wu, Z., 2022. The involvement of extracellular vesicles in the transcytosis of nanoliposomes through brain endothelial cells, and the impact of liposomal pH-sensitivity. Materials Today Bio 13, 100212. https://doi.org/10.1016/j.mtbio.2022.100212

Ridder, K., Keller, S., Dams, M., Rupp, A.-K., Schlaudraff, J., Del Turco, D., Starmann, J., Macas, J., Karpova, D., Devraj, K., Depboylu, C., Landfried, B., Arnold, B., Plate, K.H., Höglinger, G., Sültmann, H., Altevogt, P., Momma, S., 2014. Extracellular Vesicle-Mediated Transfer of Genetic Information between the Hematopoietic System and the Brain in Response to Inflammation. PLoS Biol 12, e1001874. https://doi.org/10.1371/journal.pbio.1001874

Ridder, K., Sevko, A., Heide, J., Dams, M., Rupp, A.-K., Macas, J., Starmann, J., Tjwa, M., Plate, K.H., Sültmann, H., Altevogt, P., Umansky, V., Momma, S., 2015. Extracellular vesicle-mediated transfer of functional RNA in the tumor microenvironment. OncoImmunology 4, e1008371. https://doi.org/10.1080/2162402X.2015.1008371

Rikkert, L.G., de Rond, L., van Dam, A., van Leeuwen, T.G., Coumans, F.A.W., de Reijke, T.M., Terstappen, L.W.M.M., Nieuwland, R., 2020. Detection of extracellular vesicles in plasma and urine of prostate cancer patients by flow cytometry and surface plasmon resonance imaging. PLoS ONE 15, e0233443. https://doi.org/10.1371/journal.pone.0233443

Rilla, K., Mustonen, A.-M., Arasu, U.T., Härkönen, K., Matilainen, J., Nieminen, P., 2019. Extracellular vesicles are integral and functional components of the extracellular matrix. Matrix Biology 75–76, 201–219. https://doi.org/10.1016/j.matbio.2017.10.003

Ringuette Goulet, C., Bernard, G., Tremblay, S., Chabaud, S., Bolduc, S., Pouliot, F., 2018. Exosomes Induce Fibroblast Differentiation into Cancer-Associated Fibroblasts through TGFβ Signaling. Mol Cancer Res 16, 1196–1204. https://doi.org/10.1158/1541-7786.MCR-17-0784

Roberts-Dalton, H.D., Cocks, A., Falcon-Perez, J.M., Sayers, E.J., Webber, J.P., Watson, P., Clayton, A., Jones, A.T., 2017. Fluorescence labelling of extracellular vesicles using a novel thiol-based strategy for quantitative analysis of cellular delivery and intracellular traffic. Nanoscale 9, 13693–13706. https://doi.org/10.1039/C7NR04128D

Rodrigues, G., Hoshino, A., Kenific, C.M., Matei, I.R., Steiner, L., Freitas, D., Kim, H.S., Oxley, P.R., Scandariato, I., Casanova-Salas, I., Dai, J., Badwe, C.R., Gril, B., Tešić Mark, M., Dill, B.D., Molina, H., Zhang, H., Benito-Martin, A., Bojmar, L., Ararso, Y., Offer, K.,

LaPlant, Q., Buehring, W., Wang, H., Jiang, X., Lu, T.M., Liu, Y., Sabari, J.K., Shin, S.J., Narula, N., Ginter, P.S., Rajasekhar, V.K., Healey, J.H., Meylan, E., Costa-Silva, B., Wang, S.E., Rafii, S., Altorki, N.K., Rudin, C.M., Jones, D.R., Steeg, P.S., Peinado, H., Ghajar, C.M., Bromberg, J., de Sousa, M., Pisapia, D., Lyden, D., 2019. Tumour exosomal CEMIP protein promotes cancer cell colonization in brain metastasis. Nat Cell Biol 21, 1403–1412. https://doi.org/10.1038/s41556-019-0404-4

Roefs, M.T., Sluijter, J.P.G., Vader, P., 2020. Extracellular Vesicle-Associated Proteins in Tissue Repair. Trends in Cell Biology 30, 990–1013. https://doi.org/10.1016/j.tcb.2020.09.009

Ruan, Z., Pathak, D., Venkatesan Kalavai, S., Yoshii-Kitahara, A., Muraoka, S., Bhatt, N., Takamatsu-Yukawa, K., Hu, J., Wang, Y., Hersh, S., Ericsson, M., Gorantla, S., Gendelman, H.E., Kayed, R., Ikezu, S., Luebke, J.I., Ikezu, T., 2021. Alzheimer's disease brain-derived extracellular vesicles spread tau pathology in interneurons. Brain 144, 288–309. https://doi.org/10.1093/brain/awaa376

Ruhland, M.K., Roberts, E.W., Cai, E., Mujal, A.M., Marchuk, K., Beppler, C., Nam, D., Serwas, N.K., Binnewies, M., Krummel, M.F., 2020. Visualizing Synaptic Transfer of Tumor Antigens among Dendritic Cells. Cancer Cell 37, 786-799.e5. https://doi.org/10.1016/j.ccell.2020.05.002

Sabbagh, Q., Andre-Gregoire, G., Guevel, L., Gavard, J., 2020. Vesiclemia: counting on extracellular vesicles for glioblastoma patients. Oncogene 39, 6043–6052. https://doi.org/10.1038/s41388-020-01420-x

Saha, S., Aranda, E., Hayakawa, Y., Bhanja, P., Atay, S., Brodin, N.P., Li, J., Asfaha, S., Liu, L., Tailor, Y., Zhang, J., Godwin, A.K., Tome, W.A., Wang, T.C., Guha, C., Pollard, J.W., 2016. Macrophage-derived extracellular vesicle-packaged WNTs rescue intestinal stem cells and enhance survival after radiation injury. Nat Commun 7, 13096. https://doi.org/10.1038/ncomms13096

Sahai, E., Astsaturov, I., Cukierman, E., DeNardo, D.G., Egeblad, M., Evans, R.M., Fearon, D., Greten, F.R., Hingorani, S.R., Hunter, T., Hynes, R.O., Jain, R.K., Janowitz, T., Jorgensen, C., Kimmelman, A.C., Kolonin, M.G., Maki, R.G., Powers, R.S., Puré, E., Ramirez, D.C., Scherz-Shouval, R., Sherman, M.H., Stewart, S., Tlsty, T.D., Tuveson, D.A., Watt, F.M., Weaver, V., Weeraratna, A.T., Werb, Z., 2020. A framework for advancing our understanding of cancer-associated fibroblasts. Nat Rev Cancer 20, 174–186. https://doi.org/10.1038/s41568-019-0238-1

Santangelo, L., Giurato, G., Cicchini, C., Montaldo, C., Mancone, C., Tarallo, R., Battistelli, C., Alonzi, T., Weisz, A., Tripodi, M., 2016. The RNA-Binding Protein SYNCRIP Is a Component of the Hepatocyte Exosomal Machinery Controlling MicroRNA Sorting. Cell Reports 17, 799–808. https://doi.org/10.1016/j.celrep.2016.09.031

Santos, M.F., Rappa, G., Karbanová, J., Kurth, T., Corbeil, D., Lorico, A., 2018. VAMP-associated protein-A and oxysterol-binding protein–related protein 3 promote the entry of late endosomes into the nucleoplasmic reticulum. Journal of Biological Chemistry 293, 13834–13848. https://doi.org/10.1074/jbc.RA118.003725

Sardar Sinha, M., Ansell-Schultz, A., Civitelli, L., Hildesjö, C., Larsson, M., Lannfelt, L., Ingelsson, M., Hallbeck, M., 2018. Alzheimer's disease pathology propagation by exosomes containing toxic amyloid-beta oligomers. Acta Neuropathol 136, 41–56. https://doi.org/10.1007/s00401-018-1868-1

Sato, S., Vasaikar, S., Eskaros, A., Kim, Y., Lewis, J.S., Zhang, B., Zijlstra, A., Weaver, A.M., 2019. EPHB2 carried on small extracellular vesicles induces tumor angiogenesis via activation of ephrin reverse signaling. JCI Insight 4, e132447. https://doi.org/10.1172/jci.insight.132447

Saugstad, J.A., Lusardi, T.A., Van Keuren-Jensen, K.R., Phillips, J.I., Lind, B., Harrington, C.A., McFarland, T.J., Courtright, A.L., Reiman, R.A., Yeri, A.S., Kalani, M.Y.S., Adelson, P.D., Arango, J., Nolan, J.P., Duggan, E., Messer, K., Akers, J.C., Galasko, D.R., Quinn, J.F., Carter, B.S., Hochberg, F.H., 2017. Analysis of extracellular RNA in cerebrospinal fluid. Journal of Extracellular Vesicles 6, 1317577. https://doi.org/10.1080/20013078.2017.1317577

Savina, A., Fader, C.M., Damiani, M.T., Colombo, M.I., 2005. Rab11 Promotes Docking and Fusion of Multivesicular Bodies in a Calcium-Dependent Manner: Ca2+-Dependent Multivesicular Body Fusion. Traffic 6, 131–143. https://doi.org/10.1111/j.1600-0854.2004.00257.x

Schatz, D., Vardi, A., 2018. Extracellular vesicles — new players in cell–cell communication in aquatic environments. Current Opinion in Microbiology 43, 148–154. https://doi.org/10.1016/j.mib.2018.01.014

Schöneberg, J., Lee, I.-H., Iwasa, J.H., Hurley, J.H., 2017. Reverse-topology membrane scission by the ESCRT proteins. Nat Rev Mol Cell Biol 18, 5–17. https://doi.org/10.1038/nrm.2016.121

Schwartz, M., Zhang, Y., Rosenblatt, J.D., 2016. B cell regulation of the anti-tumor response and role in carcinogenesis. j. immunotherapy cancer 4, 40. https://doi.org/10.1186/s40425-016-0145-x

Scott, C.C., Vacca, F., Gruenberg, J., 2014. Endosome maturation, transport and functions. Seminars in Cell & Developmental Biology 31, 2–10. https://doi.org/10.1016/j.semcdb.2014.03.034

Sedgwick, A.E., Clancy, J.W., Olivia Balmert, M., D'Souza-Schorey, C., 2015. Extracellular microvesicles and invadopodia mediate non-overlapping modes of tumor cell invasion. Sci Rep 5, 14748. https://doi.org/10.1038/srep14748

Sedgwick, A.E., D'Souza-Schorey, C., 2018. The biology of extracellular microvesicles. Traffic 19, 319–327. https://doi.org/10.1111/tra.12558

Sheehan, C., D'Souza-Schorey, C., 2019. Tumor-derived extracellular vesicles: molecular parcels that enable regulation of the immune response in cancer. Journal of Cell Science 132, jcs235085. https://doi.org/10.1242/jcs.235085

Sheldon, H., Heikamp, E., Turley, H., Dragovic, R., Thomas, P., Oon, C.E., Leek, R., Edelmann, M., Kessler, B., Sainson, R.C.A., Sargent, I., Li, J.-L., Harris, A.L., 2010. New mechanism for Notch signaling to endothelium at a distance by Delta-like 4 incorporation into exosomes. Blood 116, 2385–2394. https://doi.org/10.1182/blood-2009-08-239228

Shelke, G.V., Yin, Y., Jang, S.C., Lässer, C., Wennmalm, S., Hoffmann, H.J., Li, L., Gho, Y.S., Nilsson, J.A., Lötvall, J., 2019. Endosomal signalling via exosome surface TGFβ-1. Journal of Extracellular Vesicles 8, 1650458. https://doi.org/10.1080/20013078.2019.1650458

Shi, J.-Y., Gao, Q., Wang, Z.-C., Zhou, J., Wang, X.-Y., Min, Z.-H., Shi, Y.-H., Shi, G.-M., Ding, Z.-B., Ke, A.-W., Dai, Z., Qiu, S.-J., Song, K., Fan, J., 2013. Margin-Infiltrating CD20+ B Cells Display an Atypical Memory Phenotype and Correlate with Favorable Prognosis in Hepatocellular Carcinoma. Clinical Cancer Research 19, 5994–6005. https://doi.org/10.1158/1078-0432.CCR-12-3497

Shurer, C.R., Kuo, J.C.-H., Roberts, L.M., Gandhi, J.G., Colville, M.J., Enoki, T.A., Pan, H., Su, J., Noble, J.M., Hollander, M.J., O'Donnell, J.P., Yin, R., Pedram, K., Möckl, L., Kourkoutis, L.F., Moerner, W.E., Bertozzi, C.R., Feigenson, G.W., Reesink, H.L., Paszek, M.J., 2019. Physical Principles of Membrane Shape Regulation by the Glycocalyx. Cell 177, 1757-1770.e21. https://doi.org/10.1016/j.cell.2019.04.017

Shurtleff, M.J., Yao, J., Qin, Y., Nottingham, R.M., Temoche-Diaz, M.M., Schekman, R., Lambowitz, A.M., 2017. Broad role for YBX1 in defining the small noncoding RNA composition of exosomes. Proc. Natl. Acad. Sci. U.S.A. 114. https://doi.org/10.1073/pnas.1712108114

Singh, A.B., Harris, R.C., 2005. Autocrine, paracrine and juxtacrine signaling by EGFR ligands. Cellular Signalling 17, 1183–1193. https://doi.org/10.1016/j.cellsig.2005.03.026

Sinha, S., Hoshino, D., Hong, N.H., Kirkbride, K.C., Grega-Larson, N.E., Seiki, M., Tyska, M.J., Weaver, A.M., 2016. Cortactin promotes exosome secretion by controlling branched actin dynamics. Journal of Cell Biology 214, 197–213. https://doi.org/10.1083/jcb.201601025

Skog, J., Würdinger, T., van Rijn, S., Meijer, D.H., Gainche, L., Curry, W.T., Carter, B.S., Krichevsky, A.M., Breakefield, X.O., 2008. Glioblastoma microvesicles transport RNA

and proteins that promote tumour growth and provide diagnostic biomarkers. Nat Cell Biol 10, 1470–1476. https://doi.org/10.1038/ncb1800
Skogberg, G., Lundberg, V., Berglund, M., Gudmundsdottir, J., Telemo, E., Lindgren, S., Ekwall, O., 2015. Human thymic epithelial primary cells produce exosomes carrying tissue-restricted antigens. Immunol Cell Biol 93, 727–734. https://doi.org/10.1038/icb.2015.33
Skotland, T., Hessvik, N.P., Sandvig, K., Llorente, A., 2019. Exosomal lipid composition and the role of ether lipids and phosphoinositides in exosome biology. Journal of Lipid Research 60, 9–18. https://doi.org/10.1194/jlr.R084343
Skotland, T., Sagini, K., Sandvig, K., Llorente, A., 2020. An emerging focus on lipids in extracellular vesicles. Advanced Drug Delivery Reviews 159, 308–321. https://doi.org/10.1016/j.addr.2020.03.002
Smyth, T., Kullberg, M., Malik, N., Smith-Jones, P., Graner, M.W., Anchordoquy, T.J., 2015. Biodistribution and delivery efficiency of unmodified tumor-derived exosomes. Journal of Controlled Release 199, 145–155. https://doi.org/10.1016/j.jconrel.2014.12.013
Sohn, W., Kim, J., Kang, S.H., Yang, S.R., Cho, J.-Y., Cho, H.C., Shim, S.G., Paik, Y.-H., 2015. Serum exosomal microRNAs as novel biomarkers for hepatocellular carcinoma. Exp Mol Med 47, e184–e184. https://doi.org/10.1038/emm.2015.68
Somiya, M., Kuroda, S., 2021. Real-Time Luminescence Assay for Cytoplasmic Cargo Delivery of Extracellular Vesicles. Anal. Chem. 93, 5612–5620. https://doi.org/10.1021/acs.analchem.1c00339
Sporn, M.B., Roberts, A.B., 1985. Autocrine growth factors and cancer. Nature 313, 745–747. https://doi.org/10.1038/313745a0
Stacker, S.A., Williams, S.P., Karnezis, T., Shayan, R., Fox, S.B., Achen, M.G., 2014. Lymphangiogenesis and lymphatic vessel remodelling in cancer. Nat Rev Cancer 14, 159–172. https://doi.org/10.1038/nrc3677
Stenqvist, A.-C., Nagaeva, O., Baranov, V., Mincheva-Nilsson, L., 2013. Exosomes Secreted by Human Placenta Carry Functional Fas Ligand and TRAIL Molecules and Convey Apoptosis in Activated Immune Cells, Suggesting Exosome-Mediated Immune Privilege of the Fetus. J.I. 191, 5515–5523. https://doi.org/10.4049/jimmunol.1301885
Stik, G., Crequit, S., Petit, L., Durant, J., Charbord, P., Jaffredo, T., Durand, C., 2017. Extracellular vesicles of stromal origin target and support hematopoietic stem and progenitor cells. Journal of Cell Biology 216, 2217–2230. https://doi.org/10.1083/jcb.201601109
Strilic, B., Offermanns, S., 2017. Intravascular Survival and Extravasation of Tumor Cells. Cancer Cell 32, 282–293. https://doi.org/10.1016/j.ccell.2017.07.001
Stuffers, S., Sem Wegner, C., Stenmark, H., Brech, A., 2009. Multivesicular Endosome Biogenesis in the Absence of ESCRTs. Traffic 10, 925–937. https://doi.org/10.1111/j.1600-0854.2009.00920.x
Suetsugu, A., Honma, K., Saji, S., Moriwaki, H., Ochiya, T., Hoffman, R.M., 2013. Imaging exosome transfer from breast cancer cells to stroma at metastatic sites in orthotopic nude-mouse models. Advanced Drug Delivery Reviews 65, 383–390. https://doi.org/10.1016/j.addr.2012.08.007
Sun, B., Zhou, Y., Fang, Y., Li, Z., Gu, X., Xiang, J., 2019. Colorectal cancer exosomes induce lymphatic network remodeling in lymph nodes. Int. J. Cancer 145, 1648–1659. https://doi.org/10.1002/ijc.32196
Sun, R., Kong, X., Qiu, X., Huang, C., Wong, P.-P., 2021. The Emerging Roles of Pericytes in Modulating Tumor Microenvironment. Front. Cell Dev. Biol. 9, 676342. https://doi.org/10.3389/fcell.2021.676342
Sung, B.H., Ketova, T., Hoshino, D., Zijlstra, A., Weaver, A.M., 2015. Directional cell movement through tissues is controlled by exosome secretion. Nat Commun 6, 7164. https://doi.org/10.1038/ncomms8164
Sung, B.H., von Lersner, A., Guerrero, J., Krystofiak, E.S., Inman, D., Pelletier, R., Zijlstra, A., Ponik, S.M., Weaver, A.M., 2020. A live cell reporter of exosome secretion and uptake

reveals pathfinding behavior of migrating cells. Nat Commun 11, 2092. https://doi.org/10.1038/s41467-020-15747-2
Sungur, C.M., Murphy, W.J., 2014. Positive and Negative Regulation by NK Cells in Cancer. Crit Rev Oncog 19, 57–66. https://doi.org/10.1615/CritRevOncog.2014010805
Svensson, K.J., Christianson, H.C., Wittrup, A., Bourseau-Guilmain, E., Lindqvist, E., Svensson, L.M., Mörgelin, M., Belting, M., 2013. Exosome Uptake Depends on ERK1/2-Heat Shock Protein 27 Signaling and Lipid Raft-mediated Endocytosis Negatively Regulated by Caveolin-1. Journal of Biological Chemistry 288, 17713–17724. https://doi.org/10.1074/jbc.M112.445403
Swartz, M.A., Fleury, M.E., 2007. Interstitial Flow and Its Effects in Soft Tissues. Annu. Rev. Biomed. Eng. 9, 229–256. https://doi.org/10.1146/annurev.bioeng.9.060906.151850
Takahashi, S., Kubo, K., Waguri, S., Yabashi, A., Shin, H.-W., Katoh, Y., Nakayama, K., 2012. Rab11 regulates exocytosis of recycling vesicles at the plasma membrane. Journal of Cell Science jcs.102913. https://doi.org/10.1242/jcs.102913
Takahashi, Y., Nishikawa, M., Shinotsuka, H., Matsui, Y., Ohara, S., Imai, T., Takakura, Y., 2013. Visualization and in vivo tracking of the exosomes of murine melanoma B16-BL6 cells in mice after intravenous injection. Journal of Biotechnology 165, 77–84. https://doi.org/10.1016/j.jbiotec.2013.03.013
Tan, A., Lam, Y.Y., Pacot, O., Hawley, A., Boyd, B.J., 2019. Probing cell–nanoparticle (cubosome) interactions at the endothelial interface: do tissue dimension and flow matter? Biomater. Sci. 7, 3460–3470. https://doi.org/10.1039/C9BM00243J
Tanaka, K., Joshi, D., Timalsina, S., Schwartz, M.A., 2021. Early events in endothelial flow sensing. Cytoskeleton 78, 217–231. https://doi.org/10.1002/cm.21652
Tanaka, Y., Okada, Y., Hirokawa, N., 2005. FGF-induced vesicular release of Sonic hedgehog and retinoic acid in leftward nodal flow is critical for left–right determination. Nature 435, 172–177. https://doi.org/10.1038/nature03494
Tang, M.K.S., Yue, P.Y.K., Ip, P.P., Huang, R.-L., Lai, H.-C., Cheung, A.N.Y., Tse, K.Y., Ngan, H.Y.S., Wong, A.S.T., 2018. Soluble E-cadherin promotes tumor angiogenesis and localizes to exosome surface. Nat Commun 9, 2270. https://doi.org/10.1038/s41467-018-04695-7
Tawil, N., Bassawon, R., Meehan, B., Nehme, A., Montermini, L., Gayden, T., De Jay, N., Spinelli, C., Chennakrishnaiah, S., Choi, D., Adnani, L., Zeinieh, M., Jabado, N., Kleinman, C.L., Witcher, M., Riazalhosseini, Y., Key, N.S., Schiff, D., Grover, S.P., Mackman, N., Couturier, C.P., Petrecca, K., Suvà, M.L., Patel, A., Tirosh, I., Najafabadi, H., Rak, J., 2021. Glioblastoma cell populations with distinct oncogenic programs release podoplanin as procoagulant extracellular vesicles. Blood Advances 5, 1682–1694. https://doi.org/10.1182/bloodadvances.2020002998
Temoche-Diaz, M.M., Shurtleff, M.J., Nottingham, R.M., Yao, J., Fadadu, R.P., Lambowitz, A.M., Schekman, R., 2019. Distinct mechanisms of microRNA sorting into cancer cell-derived extracellular vesicle subtypes. eLife 8, e47544. https://doi.org/10.7554/eLife.47544
Thakuri, B.K.C., Zhang, J., Zhao, J., Nguyen, L.N., Nguyen, L.N.T., Khanal, S., Cao, D., Dang, X., Schank, M., Wu, X.Y., Morrison, Z.D., Gazzar, M.E., Li, Z., Jiang, Y., Ning, S., Wang, L., Moorman, J.P., Yao, Z.Q., 2020. LncRNA HOTAIRM1 promotes MDSC expansion and suppressive functions through the HOXA1-miR124 axis during HCV infection. Sci Rep 10, 22033. https://doi.org/10.1038/s41598-020-78786-1
Théry, C., Duban, L., Segura, E., Véron, P., Lantz, O., Amigorena, S., 2002. Indirect activation of naïve CD4+ T cells by dendritic cell–derived exosomes. Nat Immunol 3, 1156–1162. https://doi.org/10.1038/ni854
Théry, C., Witwer, K.W., Aikawa, E., Alcaraz, M.J., Anderson, J.D., Andriantsitohaina, R., Antoniou, A., Arab, T., Archer, F., Atkin-Smith, G.K., Ayre, D.C., Bach, J.-M., Bachurski, D., Baharvand, H., Balaj, L., Baldacchino, S., Bauer, N.N., Baxter, A.A., Bebawy, M., Beckham, C., Bedina Zavec, A., Benmoussa, A., Berardi, A.C., Bergese, P., Bielska, E., Blenkiron, C., Bobis-Wozowicz, S., Boilard, E., Boireau, W., Bongiovanni, A., Borràs, F.E., Bosch, S., Boulanger, C.M., Breakefield, X., Breglio, A.M., Brennan, M.Á.,

Brigstock, D.R., Brisson, A., Broekman, M.L., Bromberg, J.F., Bryl-Górecka, P., Buch, S., Buck, A.H., Burger, D., Busatto, S., Buschmann, D., Bussolati, B., Buzás, E.I., Byrd, J.B., Camussi, G., Carter, D.R., Caruso, S., Chamley, L.W., Chang, Y.-T., Chen, C., Chen, S., Cheng, L., Chin, A.R., Clayton, A., Clerici, S.P., Cocks, A., Cocucci, E., Coffey, R.J., Cordeiro-da-Silva, A., Couch, Y., Coumans, F.A., Coyle, B., Crescitelli, R., Criado, M.F., D'Souza-Schorey, C., Das, S., Datta Chaudhuri, A., de Candia, P., De Santana, E.F., De Wever, O., del Portillo, H.A., Demaret, T., Deville, S., Devitt, A., Dhondt, B., Di Vizio, D., Dieterich, L.C., Dolo, V., Dominguez Rubio, A.P., Dominici, M., Dourado, M.R., Driedonks, T.A., Duarte, F.V., Duncan, H.M., Eichenberger, R.M., Ekström, K., EL Andaloussi, S., Elie-Caille, C., Erdbrügger, U., Falcón-Pérez, J.M., Fatima, F., Fish, J.E., Flores-Bellver, M., Försönits, A., Frelet-Barrand, A., Fricke, F., Fuhrmann, G., Gabrielsson, S., Gámez-Valero, A., Gardiner, C., Gärtner, K., Gaudin, R., Gho, Y.S., Giebel, B., Gilbert, C., Gimona, M., Giusti, I., Goberdhan, D.C., Görgens, A., Gorski, S.M., Greening, D.W., Gross, J.C., Gualerzi, A., Gupta, G.N., Gustafson, D., Handberg, A., Haraszti, R.A., Harrison, P., Hegyesi, H., Hendrix, A., Hill, A.F., Hochberg, F.H., Hoffmann, K.F., Holder, B., Holthofer, H., Hosseinkhani, B., Hu, G., Huang, Y., Huber, V., Hunt, S., Ibrahim, A.G.-E., Ikezu, T., Inal, J.M., Isin, M., Ivanova, A., Jackson, H.K., Jacobsen, S., Jay, S.M., Jayachandran, M., Jenster, G., Jiang, L., Johnson, S.M., Jones, J.C., Jong, A., Jovanovic-Talisman, T., Jung, S., Kalluri, R., Kano, S., Kaur, S., Kawamura, Y., Keller, E.T., Khamari, D., Khomyakova, E., Khvorova, A., Kierulf, P., Kim, K.P., Kislinger, T., Klingeborn, M., Klinke, D.J., Kornek, M., Kosanović, M.M., Kovács, Á.F., Krämer-Albers, E.-M., Krasemann, S., Krause, M., Kurochkin, I.V., Kusuma, G.D., Kuypers, S., Laitinen, S., Langevin, S.M., Languino, L.R., Lannigan, J., Lässer, C., Laurent, L.C., Lavieu, G., Lázaro-Ibáñez, E., Le Lay, S., Lee, M.-S., Lee, Y.X.F., Lemos, D.S., Lenassi, M., Leszczynska, A., Li, I.T., Liao, K., Libregts, S.F., Ligeti, E., Lim, R., Lim, S.K., Linē, A., Linnemannstöns, K., Llorente, A., Lombard, C.A., Lorenowicz, M.J., Lörincz, Á.M., Lötvall, J., Lovett, J., Lowry, M.C., Loyer, X., Lu, Q., Lukomska, B., Lunavat, T.R., Maas, S.L., Malhi, H., Marcilla, A., Mariani, J., Mariscal, J., Martens-Uzunova, E.S., Martin-Jaular, L., Martinez, M.C., Martins, V.R., Mathieu, M., Mathivanan, S., Maugeri, M., McGinnis, L.K., McVey, M.J., Meckes, D.G., Meehan, K.L., Mertens, I., Minciacchi, V.R., Möller, A., Møller Jørgensen, M., Morales-Kastresana, A., Morhayim, J., Mullier, F., Muraca, M., Musante, L., Mussack, V., Muth, D.C., Myburgh, K.H., Najrana, T., Nawaz, M., Nazarenko, I., Nejsum, P., Neri, C., Neri, T., Nieuwland, R., Nimrichter, L., Nolan, J.P., Nolte-'t Hoen, E.N., Noren Hooten, N., O'Driscoll, L., O'Grady, T., O'Loghlen, A., Ochiya, T., Olivier, M., Ortiz, A., Ortiz, L.A., Osteikoetxea, X., Østergaard, O., Ostrowski, M., Park, J., Pegtel, D.M., Peinado, H., Perut, F., Pfaffl, M.W., Phinney, D.G., Pieters, B.C., Pink, R.C., Pisetsky, D.S., Pogge von Strandmann, E., Polakovicova, I., Poon, I.K., Powell, B.H., Prada, I., Pulliam, L., Quesenberry, P., Radeghieri, A., Raffai, R.L., Raimondo, S., Rak, J., Ramirez, M.I., Raposo, G., Rayyan, M.S., Regev-Rudzki, N., Ricklefs, F.L., Robbins, P.D., Roberts, D.D., Rodrigues, S.C., Rohde, E., Rome, S., Rouschop, K.M., Rughetti, A., Russell, A.E., Saá, P., Sahoo, S., Salas-Huenuleo, E., Sánchez, C., Saugstad, J.A., Saul, M.J., Schiffelers, R.M., Schneider, R., Schøyen, T.H., Scott, A., Shahaj, E., Sharma, S., Shatnyeva, O., Shekari, F., Shelke, G.V., Shetty, A.K., Shiba, K., Siljander, P.R.-M., Silva, A.M., Skowronek, A., Snyder, O.L., Soares, R.P., Sódar, B.W., Soekmadji, C., Sotillo, J., Stahl, P.D., Stoorvogel, W., Stott, S.L., Strasser, E.F., Swift, S., Tahara, H., Tewari, M., Timms, K., Tiwari, S., Tixeira, R., Tkach, M., Toh, W.S., Tomasini, R., Torrecilhas, A.C., Tosar, J.P., Toxavidis, V., Urbanelli, L., Vader, P., van Balkom, B.W., van der Grein, S.G., Van Deun, J., van Herwijnen, M.J., Van Keuren-Jensen, K., van Niel, G., van Royen, M.E., van Wijnen, A.J., Vasconcelos, M.H., Vechetti, I.J., Veit, T.D., Vella, L.J., Velot, É., Verweij, F.J., Vestad, B., Viñas, J.L., Visnovitz, T., Vukman, K.V., Wahlgren, J., Watson, D.C., Wauben, M.H., Weaver, A., Webber, J.P., Weber, V., Wehman, A.M., Weiss, D.J., Welsh, J.A., Wendt, S., Wheelock, A.M., Wiener, Z., Witte, L., Wolfram, J., Xagorari, A., Xander, P., Xu, J., Yan, X., Yáñez-Mó, M., Yin, H., Yuana, Y., Zappulli,

V., Zarubova, J., Žėkas, V., Zhang, J., Zhao, Z., Zheng, L., Zheutlin, A.R., Zickler, A.M., Zimmermann, P., Zivkovic, A.M., Zocco, D., Zuba-Surma, E.K., 2018. Minimal information for studies of extracellular vesicles 2018 (MISEV2018): a position statement of the International Society for Extracellular Vesicles and update of the MISEV2014 guidelines. Journal of Extracellular Vesicles 7, 1535750. https://doi.org/10.1080/20013078.2018.1535750

Thi, M.M., Tarbell, J.M., Weinbaum, S., Spray, D.C., 2004. The role of the glycocalyx in reorganization of the actin cytoskeleton under fluid shear stress: A “bumper-car” model. Proc. Natl. Acad. Sci. U.S.A. 101, 16483–16488. https://doi.org/10.1073/pnas.0407474101

Thomas, G.M., Panicot-Dubois, L., Lacroix, R., Dignat-George, F., Lombardo, D., Dubois, C., 2009. Cancer cell–derived microparticles bearing P-selectin glycoprotein ligand 1 accelerate thrombus formation in vivo. Journal of Experimental Medicine 206, 1913–1927. https://doi.org/10.1084/jem.20082297

Thomou, T., Mori, M.A., Dreyfuss, J.M., Konishi, M., Sakaguchi, M., Wolfrum, C., Rao, T.N., Winnay, J.N., Garcia-Martin, R., Grinspoon, S.K., Gorden, P., Kahn, C.R., 2017. Adipose-derived circulating miRNAs regulate gene expression in other tissues. Nature 542, 450–455. https://doi.org/10.1038/nature21365

Tian, T., Wang, Y., Wang, H., Zhu, Z., Xiao, Z., 2010. Visualizing of the cellular uptake and intracellular trafficking of exosomes by live-cell microscopy. J. Cell. Biochem. 111, 488–496. https://doi.org/10.1002/jcb.22733

Tian, T., Zhu, Y.-L., Hu, F.-H., Wang, Y.-Y., Huang, N.-P., Xiao, Z.-D., 2013. Dynamics of exosome internalization and trafficking. J. Cell. Physiol. 228, 1487–1495. https://doi.org/10.1002/jcp.24304

Tian, T., Zhu, Y.-L., Zhou, Y.-Y., Liang, G.-F., Wang, Y.-Y., Hu, F.-H., Xiao, Z.-D., 2014. Exosome Uptake through Clathrin-mediated Endocytosis and Macropinocytosis and Mediating miR-21 Delivery. J. Biol. Chem. 289, 22258–22267. https://doi.org/10.1074/jbc.M114.588046

Toda, Y., Tsukada, J., Misago, M., Kominato, Y., Auron, P.E., Tanaka, Y., 2002. Autocrine Induction of the Human Pro-IL-1β Gene Promoter by IL-1β in Monocytes. J Immunol 168, 1984–1991. https://doi.org/10.4049/jimmunol.168.4.1984

Todorova, D., Simoncini, S., Lacroix, R., Sabatier, F., Dignat-George, F., 2017. Extracellular Vesicles in Angiogenesis. Circ Res 120, 1658–1673. https://doi.org/10.1161/CIRCRESAHA.117.309681

Tokuda, A., Miyake, T., Yasukawa, D., Ikuta, D., Mukaisho, K.-I., Murata, S., Shimizu, T., Tani, M., 2021. Cancer-derived Exosomes Activate Immune Surveillance and Suppress Peritoneal Metastasis of Murine Colonic Cancer. Anticancer Res 41, 1327–1339. https://doi.org/10.21873/anticanres.14890

Tominaga, N., Kosaka, N., Ono, M., Katsuda, T., Yoshioka, Y., Tamura, K., Lötvall, J., Nakagama, H., Ochiya, T., 2015. Brain metastatic cancer cells release microRNA-181c-containing extracellular vesicles capable of destructing blood–brain barrier. Nat Commun 6, 6716. https://doi.org/10.1038/ncomms7716

Toth, B., Nikolajek, K., Rank, A., Nieuwland, R., Lohse, P., Pihusch, V., Friese, K., Thaler, C.J., 2007. Gender-specific and menstrual cycle dependent differences in circulating microparticles. Platelets 18, 515–521. https://doi.org/10.1080/09537100701525843

Toti, A., Santi, A., Pardella, E., Nesi, I., Tomasini, R., Mello, T., Paoli, P., Caselli, A., Cirri, P., 2021. Activated fibroblasts enhance cancer cell migration by microvesicles-mediated transfer of Galectin-1. J. Cell Commun. Signal. https://doi.org/10.1007/s12079-021-00624-4

Toy, R., Hayden, E., Shoup, C., Baskaran, H., Karathanasis, E., 2011. The effects of particle size, density and shape on margination of nanoparticles in microcirculation. Nanotechnology 22, 115101. https://doi.org/10.1088/0957-4484/22/11/115101

Toyofuku, M., Nomura, N., Eberl, L., 2019. Types and origins of bacterial membrane vesicles. Nat Rev Microbiol 17, 13–24. https://doi.org/10.1038/s41579-018-0112-2

Trajkovic, K., Hsu, C., Chiantia, S., Rajendran, L., Wenzel, D., Wieland, F., Schwille, P., Brugger, B., Simons, M., 2008. Ceramide Triggers Budding of Exosome Vesicles into Multivesicular Endosomes. Science 319, 1244–1247. https://doi.org/10.1126/science.1153124

Treps, L., Edmond, S., Harford-Wright, E., Galan-Moya, E.M., Schmitt, A., Azzi, S., Citerne, A., Bidère, N., Ricard, D., Gavard, J., 2016. Extracellular vesicle-transported Semaphorin3A promotes vascular permeability in glioblastoma. Oncogene 35, 2615–2623. https://doi.org/10.1038/onc.2015.317

Treps, L., Perret, R., Edmond, S., Ricard, D., Gavard, J., 2017. Glioblastoma stem-like cells secrete the pro-angiogenic VEGF-A factor in extracellular vesicles. Journal of Extracellular Vesicles 6, 1359479. https://doi.org/10.1080/20013078.2017.1359479

Trofimenko, E., Homma, Y., Fukuda, M., Widmann, C., 2021. The endocytic pathway taken by cationic substances requires Rab14 but not Rab5 and Rab7. Cell Reports 37, 109945. https://doi.org/10.1016/j.celrep.2021.109945

Tu, F., Wang, X., Zhang, X., Ha, T., Wang, Y., Fan, M., Yang, K., Gill, P.S., Ozment, T.R., Dai, Y., Liu, L., Williams, D.L., Li, C., 2020. Novel Role of Endothelial Derived Exosomal HSPA12B in Regulating Macrophage Inflammatory Responses in Polymicrobial Sepsis. Front. Immunol. 11, 825. https://doi.org/10.3389/fimmu.2020.00825

Tzima, E., Irani-Tehrani, M., Kiosses, W.B., Dejana, E., Schultz, D.A., Engelhardt, B., Cao, G., DeLisser, H., Schwartz, M.A., 2005. A mechanosensory complex that mediates the endothelial cell response to fluid shear stress. Nature 437, 426–431. https://doi.org/10.1038/nature03952

Umakoshi, M., Takahashi, S., Itoh, G., Kuriyama, S., Sasaki, Y., Yanagihara, K., Yashiro, M., Maeda, D., Goto, A., Tanaka, M., 2019. Macrophage-mediated transfer of cancer-derived components to stromal cells contributes to establishment of a pro-tumor microenvironment. Oncogene 38, 2162–2176. https://doi.org/10.1038/s41388-018-0564-x

Umezu, T., Tadokoro, H., Azuma, K., Yoshizawa, S., Ohyashiki, K., Ohyashiki, J.H., 2014. Exosomal miR-135b shed from hypoxic multiple myeloma cells enhances angiogenesis by targeting factor-inhibiting HIF-1. Blood 124, 3748–3757. https://doi.org/10.1182/blood-2014-05-576116

Valadi, H., Ekström, K., Bossios, A., Sjöstrand, M., Lee, J.J., Lötvall, J.O., 2007. Exosome-mediated transfer of mRNAs and microRNAs is a novel mechanism of genetic exchange between cells. Nat Cell Biol 9, 654–659. https://doi.org/10.1038/ncb1596

Valapala, M., Vishwanatha, J.K., 2011. Lipid Raft Endocytosis and Exosomal Transport Facilitate Extracellular Trafficking of Annexin A2. Journal of Biological Chemistry 286, 30911–30925. https://doi.org/10.1074/jbc.M111.271155

van der Vos, K.E., Abels, E.R., Zhang, X., Lai, C., Carrizosa, E., Oakley, D., Prabhakar, S., Mardini, O., Crommentuijn, M.H.W., Skog, J., Krichevsky, A.M., Stemmer-Rachamimov, A., Mempel, T.R., El Khoury, J., Hickman, S.E., Breakefield, X.O., 2016. Directly visualized glioblastoma-derived extracellular vesicles transfer RNA to microglia/macrophages in the brain. Neuro Oncol 18, 58–69. https://doi.org/10.1093/neuonc/nov244

van Dongen, H.M., Masoumi, N., Witwer, K.W., Pegtel, D.M., 2016. Extracellular Vesicles Exploit Viral Entry Routes for Cargo Delivery. Microbiol Mol Biol Rev 80, 369–386. https://doi.org/10.1128/MMBR.00063-15

van Niel, G., D'Angelo, G., Raposo, G., 2018. Shedding light on the cell biology of extracellular vesicles. Nat Rev Mol Cell Biol 19, 213–228. https://doi.org/10.1038/nrm.2017.125

van Niel, G., Charrin, S., Simoes, S., Romao, M., Rochin, L., Saftig, P., Marks, M.S., Rubinstein, E., Raposo, G., 2011. The Tetraspanin CD63 Regulates ESCRT-Independent and -Dependent Endosomal Sorting during Melanogenesis. Developmental Cell 21, 708–721. https://doi.org/10.1016/j.devcel.2011.08.019

Verweij, F.J., Balaj, L., Boulanger, C.M., Carter, D.R.F., Compeer, E.B., D'Angelo, G., El Andaloussi, S., Goetz, J.G., Gross, J.C., Hyenne, V., Krämer-Albers, E.-M., Lai, C.P., Loyer, X., Marki, A., Momma, S., Nolte-'t Hoen, E.N.M., Pegtel, D.M., Peinado, H.,

Raposo, G., Rilla, K., Tahara, H., Théry, C., van Royen, M.E., Vandenbroucke, R.E., Wehman, A.M., Witwer, K., Wu, Z., Wubbolts, R., van Niel, G., 2021. The power of imaging to understand extracellular vesicle biology in vivo. Nat Methods 18, 1013–1026. https://doi.org/10.1038/s41592-021-01206-3

Verweij, F.J., Bebelman, M.P., Jimenez, C.R., Garcia-Vallejo, J.J., Janssen, H., Neefjes, J., Knol, J.C., de Goeij-de Haas, R., Piersma, S.R., Baglio, S.R., Verhage, M., Middeldorp, J.M., Zomer, A., van Rheenen, J., Coppolino, M.G., Hurbain, I., Raposo, G., Smit, M.J., Toonen, R.F.G., van Niel, G., Pegtel, D.M., 2018. Quantifying exosome secretion from single cells reveals a modulatory role for GPCR signaling. Journal of Cell Biology 217, 1129–1142. https://doi.org/10.1083/jcb.201703206

Verweij, F.J., Hyenne, V., Van Niel, G., Goetz, J.G., 2019. Extracellular Vesicles: Catching the Light in Zebrafish. Trends in Cell Biology 29, 770–776. https://doi.org/10.1016/j.tcb.2019.07.007

Villarroya-Beltri, C., Baixauli, F., Mittelbrunn, M., Fernández-Delgado, I., Torralba, D., Moreno-Gonzalo, O., Baldanta, S., Enrich, C., Guerra, S., Sánchez-Madrid, F., 2016. ISGylation controls exosome secretion by promoting lysosomal degradation of MVB proteins. Nat Commun 7, 13588. https://doi.org/10.1038/ncomms13588

Villarroya-Beltri, C., Gutiérrez-Vázquez, C., Sánchez-Cabo, F., Pérez-Hernández, D., Vázquez, J., Martin-Cofreces, N., Martinez-Herrera, D.J., Pascual-Montano, A., Mittelbrunn, M., Sánchez-Madrid, F., 2013. Sumoylated hnRNPA2B1 controls the sorting of miRNAs into exosomes through binding to specific motifs. Nat Commun 4, 2980. https://doi.org/10.1038/ncomms3980

Vyas, N., Walvekar, A., Tate, D., Lakshmanan, V., Bansal, D., Cicero, A.L., Raposo, G., Palakodeti, D., Dhawan, J., 2015. Vertebrate Hedgehog is secreted on two types of extracellular vesicles with different signaling properties. Sci Rep 4, 7357. https://doi.org/10.1038/srep07357

Walker, N.D., Elias, M., Guiro, K., Bhatia, R., Greco, S.J., Bryan, M., Gergues, M., Sandiford, O.A., Ponzio, N.M., Leibovich, S.J., Rameshwar, P., 2019. Exosomes from differentially activated macrophages influence dormancy or resurgence of breast cancer cells within bone marrow stroma. Cell Death Dis 10, 59. https://doi.org/10.1038/s41419-019-1304-z

Wang, G., Kostidis, S., Tiemeier, G.L., Sol, W.M.P.J., de Vries, M.R., Giera, M., Carmeliet, P., van den Berg, B.M., Rabelink, T.J., 2020. Shear Stress Regulation of Endothelial Glycocalyx Structure Is Determined by Glucobiosynthesis. ATVB 40, 350–364. https://doi.org/10.1161/ATVBAHA.119.313399

Wang, Lin, Cao, D., Wang, Ling, Zhao, J., Nguyen, L.N., Dang, X., Ji, Y., Wu, X.Y., Morrison, Z.D., Xie, Q., El Gazzar, M., Ning, S., Moorman, J.P., Yao, Z.Q., 2018. HCV-associated exosomes promote myeloid-derived suppressor cell expansion via inhibiting miR-124 to regulate T follicular cell differentiation and function. Cell Discov 4, 51. https://doi.org/10.1038/s41421-018-0052-z

Wang, T., Gilkes, D.M., Takano, N., Xiang, L., Luo, W., Bishop, C.J., Chaturvedi, P., Green, J.J., Semenza, G.L., 2014. Hypoxia-inducible factors and RAB22A mediate formation of microvesicles that stimulate breast cancer invasion and metastasis. Proceedings of the National Academy of Sciences 111, E3234–E3242. https://doi.org/10.1073/pnas.1410041111

Wang, Z., Sun, H., Provaznik, J., Hackert, T., Zöller, M., 2019. Pancreatic cancer-initiating cell exosome message transfer into noncancer-initiating cells: the importance of CD44v6 in reprogramming. J Exp Clin Cancer Res 38, 132. https://doi.org/10.1186/s13046-019-1129-8

Wang, Z., von Au, A., Schnölzer, M., Hackert, T., Zöller, M., 2016. CD44v6-competent tumor exosomes promote motility, invasion and cancer-initiating cell marker expression in pancreatic and colorectal cancer cells. Oncotarget 7, 55409–55436. https://doi.org/10.18632/oncotarget.10580

Wang, Z., Yan, X., 2013. CD146, a multi-functional molecule beyond adhesion. Cancer Letters 330, 150–162. https://doi.org/10.1016/j.canlet.2012.11.049

Webber, J., Steadman, R., Mason, M.D., Tabi, Z., Clayton, A., 2010. Cancer Exosomes Trigger Fibroblast to Myofibroblast Differentiation. Cancer Research 70, 9621–9630. https://doi.org/10.1158/0008-5472.CAN-10-1722

Webber, J.P., Spary, L.K., Sanders, A.J., Chowdhury, R., Jiang, W.G., Steadman, R., Wymant, J., Jones, A.T., Kynaston, H., Mason, M.D., Tabi, Z., Clayton, A., 2015. Differentiation of tumour-promoting stromal myofibroblasts by cancer exosomes. Oncogene 34, 290–302. https://doi.org/10.1038/onc.2013.560

Wei, D., Zhan, W., Gao, Y., Huang, L., Gong, R., Wang, W., Zhang, R., Wu, Y., Gao, S., Kang, T., 2021. RAB31 marks and controls an ESCRT-independent exosome pathway. Cell Res 31, 157–177. https://doi.org/10.1038/s41422-020-00409-1

Wei, Z., Batagov, A.O., Schinelli, S., Wang, J., Wang, Y., El Fatimy, R., Rabinovsky, R., Balaj, L., Chen, C.C., Hochberg, F., Carter, B., Breakefield, X.O., Krichevsky, A.M., 2017. Coding and noncoding landscape of extracellular RNA released by human glioma stem cells. Nat Commun 8, 1145. https://doi.org/10.1038/s41467-017-01196-x

Wen, S.W., Sceneay, J., Lima, L.G., Wong, C.S.F., Becker, M., Krumeich, S., Lobb, R.J., Castillo, V., Wong, K.N., Ellis, S., Parker, B.S., Möller, A., 2016. The Biodistribution and Immune Suppressive Effects of Breast Cancer–Derived Exosomes. Cancer Res 76, 6816–6827. https://doi.org/10.1158/0008-5472.CAN-16-0868

Wenzel, E.M., Schultz, S.W., Schink, K.O., Pedersen, N.M., Nähse, V., Carlson, A., Brech, A., Stenmark, H., Raiborg, C., 2018. Concerted ESCRT and clathrin recruitment waves define the timing and morphology of intraluminal vesicle formation. Nat Commun 9, 2932. https://doi.org/10.1038/s41467-018-05345-8

Whitham, M., Parker, B.L., Friedrichsen, M., Hingst, J.R., Hjorth, M., Hughes, W.E., Egan, C.L., Cron, L., Watt, K.I., Kuchel, R.P., Jayasooriah, N., Estevez, E., Petzold, T., Suter, C.M., Gregorevic, P., Kiens, B., Richter, E.A., James, D.E., Wojtaszewski, J.F.P., Febbraio, M.A., 2018. Extracellular Vesicles Provide a Means for Tissue Crosstalk during Exercise. Cell Metabolism 27, 237-251.e4. https://doi.org/10.1016/j.cmet.2017.12.001

Wiklander, O.P.B., Nordin, J.Z., O'Loughlin, A., Gustafsson, Y., Corso, G., Mäger, I., Vader, P., Lee, Y., Sork, H., Seow, Y., Heldring, N., Alvarez-Erviti, L., Smith, C.E., Le Blanc, K., Macchiarini, P., Jungebluth, P., Wood, M.J.A., Andaloussi, S.E., 2015. Extracellular vesicle in vivo biodistribution is determined by cell source, route of administration and targeting. Journal of Extracellular Vesicles 4, 26316. https://doi.org/10.3402/jev.v4.26316

Williams, C., Pazos, R., Royo, F., González, E., Roura-Ferrer, M., Martinez, A., Gamiz, J., Reichardt, N.-C., Falcón-Pérez, J.M., 2019. Assessing the role of surface glycans of extracellular vesicles on cellular uptake. Sci Rep 9, 11920. https://doi.org/10.1038/s41598-019-48499-1

Witwer, K.W., Théry, C., 2019. Extracellular vesicles or exosomes? On primacy, precision, and popularity influencing a choice of nomenclature. Journal of Extracellular Vesicles 8, 1648167. https://doi.org/10.1080/20013078.2019.1648167

Woith, E., Fuhrmann, G., Melzig, M.F., 2019. Extracellular Vesicles—Connecting Kingdoms. IJMS 20, 5695. https://doi.org/10.3390/ijms20225695

Wolf, M., Poupardin, R.W., Ebner-Peking, P., Andrade, A.C., Blöchl, C., Obermayer, A., Gomes, F.G., Vari, B., Maeding, N., Eminger, E., Binder, H., Raninger, A.M., Hochmann, S., Brachtl, G., Spittler, A., Heuser, T., Ofir, R., Huber, C.G., Aberman, Z., Schallmoser, K., Volk, H., Strunk, D., 2022. A functional corona around extracellular vesicles enhances angiogenesis, skin regeneration and immunomodulation. J of Extracellular Vesicle 11. https://doi.org/10.1002/jev2.12207

Wolf-Dennen, K., Gordon, N., Kleinerman, E.S., 2020. Exosomal communication by metastatic osteosarcoma cells modulates alveolar macrophages to an M2 tumor-promoting phenotype and inhibits tumoricidal functions. OncoImmunology 9, 1747677. https://doi.org/10.1080/2162402X.2020.1747677

Wong, A.J., Pollard, T.D., Herman, I.M., 1983. Actin Filament Stress Fibers in Vascular Endothelial Cells in Vivo. Science 219, 867–869. https://doi.org/10.1126/science.6681677

Wortzel, I., Dror, S., Kenific, C.M., Lyden, D., 2019. Exosome-Mediated Metastasis: Communication from a Distance. Developmental Cell 49, 347–360. https://doi.org/10.1016/j.devcel.2019.04.011

Wu, A.Y., Sung, Y., Chen, Yen-Ju, Chou, S.T., Guo, V., Chien, J.C., Ko, J.J., Yang, A.L., Huang, H., Chuang, J., Wu, S., Ho, M., Ericsson, M., Lin, W., Cheung, C.H.Y., Juan, H., Ueda, K., Chen, Yunching, Lai, C.P., 2020. Multiresolution Imaging Using Bioluminescence Resonance Energy Transfer Identifies Distinct Biodistribution Profiles of Extracellular Vesicles and Exomeres with Redirected Tropism. Adv. Sci. 7, 2001467. https://doi.org/10.1002/advs.202001467

Xie, F., Zhou, X., Su, P., Li, H., Tu, Y., Du, J., Pan, C., Wei, X., Zheng, M., Jin, K., Miao, L., Wang, C., Meng, X., van Dam, H., ten Dijke, P., Zhang, L., Zhou, F., 2022. Breast cancer cell-derived extracellular vesicles promote CD8+ T cell exhaustion via TGF-β type II receptor signaling. Nat Commun 13, 4461. https://doi.org/10.1038/s41467-022-31250-2

Xie, J., Wei, J., Lv, L., Han, Q., Yang, W., Li, G., Wang, P., Wu, S., Duan, J., Zhuo, W., Liu, P., Min, J., 2020. Angiopoietin-2 induces angiogenesis via exosomes in human hepatocellular carcinoma. Cell Commun Signal 18, 46. https://doi.org/10.1186/s12964-020-00535-8

Xu, B., Zhang, Y., Du, X.-F., Li, J., Zi, H.-X., Bu, J.-W., Yan, Y., Han, H., Du, J.-L., 2017. Neurons secrete miR-132-containing exosomes to regulate brain vascular integrity. Cell Res 27, 882–897. https://doi.org/10.1038/cr.2017.62

Xu, R., Rai, A., Chen, M., Suwakulsiri, W., Greening, D.W., Simpson, R.J., 2018. Extracellular vesicles in cancer — implications for future improvements in cancer care. Nat Rev Clin Oncol 15, 617–638. https://doi.org/10.1038/s41571-018-0036-9

Yamamoto, K., Ando, J., 2018. Emerging Role of Plasma Membranes in Vascular Endothelial Mechanosensing. Circ J 82, 2691–2698. https://doi.org/10.1253/circj.CJ-18-0052

Yan, W., Wu, X., Zhou, W., Fong, M.Y., Cao, M., Liu, J., Liu, Xiaojing, Chen, C.-H., Fadare, O., Pizzo, D.P., Wu, J., Liu, L., Liu, Xuxiang, Chin, A.R., Ren, X., Chen, Y., Locasale, J.W., Wang, S.E., 2018. Cancer-cell-secreted exosomal miR-105 promotes tumour growth through the MYC-dependent metabolic reprogramming of stromal cells. Nat Cell Biol 20, 597–609. https://doi.org/10.1038/s41556-018-0083-6

Yáñez-Mó, M., Siljander, P.R.-M., Andreu, Z., Bedina Zavec, A., Borràs, F.E., Buzas, E.I., Buzas, K., Casal, E., Cappello, F., Carvalho, J., Colás, E., Cordeiro-da Silva, A., Fais, S., Falcon-Perez, J.M., Ghobrial, I.M., Giebel, B., Gimona, M., Graner, M., Gursel, I., Gursel, M., Heegaard, N.H.H., Hendrix, A., Kierulf, P., Kokubun, K., Kosanovic, M., Kralj-Iglic, V., Krämer-Albers, E.-M., Laitinen, S., Lässer, C., Lener, T., Ligeti, E., Linē, A., Lipps, G., Llorente, A., Lötvall, J., Manček-Keber, M., Marcilla, A., Mittelbrunn, M., Nazarenko, I., Nolte-'t Hoen, E.N.M., Nyman, T.A., O'Driscoll, L., Olivan, M., Oliveira, C., Pállinger, É., del Portillo, H.A., Reventós, J., Rigau, M., Rohde, E., Sammar, M., Sánchez-Madrid, F., Santarém, N., Schallmoser, K., Stampe Ostenfeld, M., Stoorvogel, W., Stukelj, R., Van der Grein, S.G., Helena Vasconcelos, M., Wauben, M.H.M., De Wever, O., 2015. Biological properties of extracellular vesicles and their physiological functions. Journal of Extracellular Vesicles 4, 27066. https://doi.org/10.3402/jev.v4.27066

Yang, T., Martin, P., Fogarty, B., Brown, A., Schurman, K., Phipps, R., Yin, V.P., Lockman, P., Bai, S., 2015. Exosome Delivered Anticancer Drugs Across the Blood-Brain Barrier for Brain Cancer Therapy in Danio Rerio. Pharm Res 32, 2003–2014. https://doi.org/10.1007/s11095-014-1593-y

Yang, W.-W., Yang, L.-Q., Zhao, F., Chen, C.-W., Xu, L.-H., Fu, J., Li, S.-L., Ge, X.-Y., 2017. Epiregulin Promotes Lung Metastasis of Salivary Adenoid Cystic Carcinoma. Theranostics 7, 3700–3714. https://doi.org/10.7150/thno.19712

Yao, Z., Qiao, Y., Li, X., Chen, J., Ding, J., Bai, L., Shen, F., Shi, B., Liu, J., Peng, L., Li, J., Yuan, Z., 2018. Exosomes Exploit the Virus Entry Machinery and Pathway To Transmit Alpha Interferon-Induced Antiviral Activity. J Virol 92, e01578-18. https://doi.org/10.1128/JVI.01578-18

Ye, S., Li, Z.-L., Luo, D., Huang, B., Chen, Y.-S., Zhang, X., Cui, J., Zeng, Y., Li, J., 2014. Tumor-derived exosomes promote tumor progression and T-cell dysfunction through the regulation of enriched exosomal microRNAs in human nasopharyngeal carcinoma. Oncotarget 5, 5439–5452. https://doi.org/10.18632/oncotarget.2118

Yokota, Y., Noda, T., Okumura, Y., Kobayashi, S., Iwagami, Y., Yamada, D., Tomimaru, Y., Akita, H., Gotoh, K., Takeda, Y., Tanemura, M., Murakami, T., Umeshita, K., Doki, Y., Eguchi, H., 2021. Serum exosomal miR-638 is a prognostic marker of HCC via downregulation of VE-cadherin and ZO-1 of endothelial cells. Cancer Sci 112, 1275–1288. https://doi.org/10.1111/cas.14807

Yoon, T.-Y., Munson, M., 2018. SNARE complex assembly and disassembly. Current Biology 28, R397–R401. https://doi.org/10.1016/j.cub.2018.01.005

Yoon, Y.J., Kim, D.-K., Yoon, C.M., Park, J., Kim, Y.-K., Roh, T.-Y., Gho, Y.S., 2014. Egr-1 Activation by Cancer-Derived Extracellular Vesicles Promotes Endothelial Cell Migration via ERK1/2 and JNK Signaling Pathways. PLoS ONE 9, e115170. https://doi.org/10.1371/journal.pone.0115170

Yuan, X., Qian, N., Ling, S., Li, Yuheng, Sun, W., Li, J., Du, R., Zhong, G., Liu, C., Yu, G., Cao, D., Liu, Z., Wang, Y., Qi, Z., Yao, Y., Wang, F., Liu, J., Hao, S., Jin, X., Zhao, Y., Xue, J., Zhao, D., Gao, X., Liang, S., Li, Youyou, Song, J., Yu, S., Li, Yingxian, 2021. Breast cancer exosomes contribute to pre-metastatic niche formation and promote bone metastasis of tumor cells. Theranostics 11, 1429–1445. https://doi.org/10.7150/thno.45351

Yue, S., Mu, W., Erb, U., Zöller, M., 2015. The tetraspanins CD151 and Tspan8 are essential exosome components for the crosstalk between cancer initiating cells and their surrounding. Oncotarget 6, 2366–2384. https://doi.org/10.18632/oncotarget.2958

Zaborowski, M.P., Cheah, P.S., Zhang, X., Bushko, I., Lee, K., Sammarco, A., Zappulli, V., Maas, S.L.N., Allen, R.M., Rumde, P., György, B., Aufiero, M., Schweiger, M.W., Lai, C.P.-K., Weissleder, R., Lee, H., Vickers, K.C., Tannous, B.A., Breakefield, X.O., 2019. Membrane-bound Gaussia luciferase as a tool to track shedding of membrane proteins from the surface of extracellular vesicles. Sci Rep 9, 17387. https://doi.org/10.1038/s41598-019-53554-y

Zeng, Y., Tarbell, J.M., 2014. The Adaptive Remodeling of Endothelial Glycocalyx in Response to Fluid Shear Stress. PLoS ONE 9, e86249. https://doi.org/10.1371/journal.pone.0086249

Zeng, Z., Li, Y., Pan, Y., Lan, X., Song, F., Sun, J., Zhou, K., Liu, X., Ren, X., Wang, F., Hu, J., Zhu, X., Yang, W., Liao, W., Li, G., Ding, Y., Liang, L., 2018. Cancer-derived exosomal miR-25-3p promotes pre-metastatic niche formation by inducing vascular permeability and angiogenesis. Nat Commun 9, 5395. https://doi.org/10.1038/s41467-018-07810-w

Zhang, W., Zhong, W., Wang, B., Yang, J., Yang, J., Yu, Z., Qin, Z., Shi, A., Xu, W., Zheng, C., Schuchter, L.M., Karakousis, G.C., Mitchell, T.C., Amaravadi, R., Herlyn, M., Dong, H., Gimotty, P.A., Daaboul, G., Xu, X., Guo, W., 2022. ICAM-1-mediated adhesion is a prerequisite for exosome-induced T cell suppresion. Dev Cell 57, 3:329-343. https://doi/org/10.1016/j.devcel.2022.01.002.

Zhang, H., Deng, T., Liu, R., Bai, M., Zhou, L., Wang, Xia, Li, S., Wang, Xinyi, Yang, H., Li, J., Ning, T., Huang, D., Li, H., Zhang, L., Ying, G., Ba, Y., 2017. Exosome-delivered EGFR regulates liver microenvironment to promote gastric cancer liver metastasis. Nat Commun 8, 15016. https://doi.org/10.1038/ncomms15016

Zhang, R., Liang, X., Tang, S., Song, L., Zhang, J., Du, Y., 2021. Short-Term High-Intensity Treadmill Exercise Promotes Ceramide-Dependent Extracellular Vesicle Secretion in the Central Nervous System of Mice. Med Sci Monit 27. https://doi.org/10.12659/MSM.929609

Zhao, F., Cheng, L., Shao, Q., Chen, Z., Lv, X., Li, J., He, L., Sun, Y., Ji, Q., Lu, P., Ji, Y., Ji, J., 2020. Characterization of serum small extracellular vesicles and their small RNA contents across humans, rats, and mice. Sci Rep 10, 4197. https://doi.org/10.1038/s41598-020-61098-9

Zhao, H., Yang, L., Baddour, J., Achreja, A., Bernard, V., Moss, T., Marini, J.C., Tudawe, T., Seviour, E.G., San Lucas, F.A., Alvarez, H., Gupta, S., Maiti, S.N., Cooper, L., Peehl, D., Ram, P.T., Maitra, A., Nagrath, D., 2016. Tumor microenvironment derived exosomes pleiotropically modulate cancer cell metabolism. eLife 5, e10250. https://doi.org/10.7554/eLife.10250

Zhou, B., Xu, K., Zheng, X., Chen, T., Wang, J., Song, Y., Shao, Y., Zheng, S., 2020. Application of exosomes as liquid biopsy in clinical diagnosis. Sig Transduct Target Ther 5, 144. https://doi.org/10.1038/s41392-020-00258-9

Zhou, C.-F., Ma, J., Huang, L., Yi, H.-Y., Zhang, Y.-M., Wu, X.-G., Yan, R.-M., Liang, L., Zhong, M., Yu, Y.-H., Wu, S., Wang, W., 2019. Cervical squamous cell carcinoma-secreted exosomal miR-221-3p promotes lymphangiogenesis and lymphatic metastasis by targeting VASH1. Oncogene 38, 1256–1268. https://doi.org/10.1038/s41388-018-0511-x

Zhou, W., Fong, M.Y., Min, Y., Somlo, G., Liu, L., Palomares, M.R., Yu, Y., Chow, A., O'Connor, S.T.F., Chin, A.R., Yen, Y., Wang, Y., Marcusson, E.G., Chu, P., Wu, J., Wu, X., Li, A.X., Li, Z., Gao, H., Ren, X., Boldin, M.P., Lin, P.C., Wang, S.E., 2014. Cancer-Secreted miR-105 Destroys Vascular Endothelial Barriers to Promote Metastasis. Cancer Cell 25, 501–515. https://doi.org/10.1016/j.ccr.2014.03.007

Zhou, Y., Ren, H., Dai, B., Li, J., Shang, L., Huang, J., Shi, X., 2018. Hepatocellular carcinoma-derived exosomal miRNA-21 contributes to tumor progression by converting hepatocyte stellate cells to cancer-associated fibroblasts. J Exp Clin Cancer Res 37, 324. https://doi.org/10.1186/s13046-018-0965-2

Zitvogel, L., Regnault, A., Lozier, A., Wolfers, J., Flament, C., Tenza, D., Ricciardi-Castagnoli, P., Raposo, G., Amigorena, S., 1998. Eradication of established murine tumors using a novel cell-free vaccine: dendritic cell derived exosomes. Nat Med 4, 594–600. https://doi.org/10.1038/nm0598-594

Zomer, A., Maynard, C., Verweij, F.J., Kamermans, A., Schäfer, R., Beerling, E., Schiffelers, R.M., de Wit, E., Berenguer, J., Ellenbroek, S.I.J., Wurdinger, T., Pegtel, D.M., van Rheenen, J., 2015. In Vivo Imaging Reveals Extracellular Vesicle-Mediated Phenocopying of Metastatic Behavior. Cell 161, 1046–1057. https://doi.org/10.1016/j.cell.2015.04.042

Zomer, A., Steenbeek, S.C., Maynard, C., van Rheenen, J., 2016. Studying extracellular vesicle transfer by a Cre-loxP method. Nat Protoc 11, 87–101. https://doi.org/10.1038/nprot.2015.138

Zwi-Dantsis, L., Winter, C.W., Kauscher, U., Ferrini, A., Wang, B., Whittaker, T.E., Hood, S.R., Terracciano, C.M., Stevens, M.M., 2020. Highly purified extracellular vesicles from human cardiomyocytes demonstrate preferential uptake by human endothelial cells. Nanoscale 12, 19844–19854. https://doi.org/10.1039/D0NR04278A

Annexe

Resource

Developmental Cell

Studying the Fate of Tumor Extracellular Vesicles at High Spatiotemporal Resolution Using the Zebrafish Embryo

Graphical Abstract

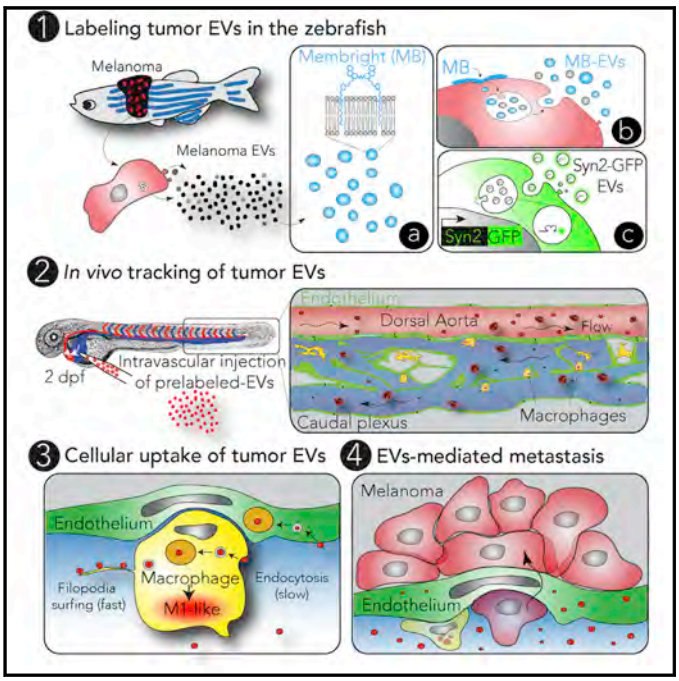

Highlights

- MemBright allows for bright and specific staining of EVs
- The zebrafish embryo allows tracking of tumor EVs at high spatiotemporal resolution
- Circulating tumor EVs are mostly taken up by endothelial cells and patrolling macrophages
- Zebrafish melanoma EVs favor metastatic outgrowth in zebrafish embryos

Authors

Vincent Hyenne, Shima Ghoroghi, Mayeul Collot, ..., Christine Carapito, Andrey S. Klymchenko, Jacky G. Goetz

Correspondence

hyenne@unistra.fr (V.H.), jacky.goetz@inserm.fr (J.G.G.)

In Brief

Tumor extracellular vesicles (EVs) promote tumor progression. However, their behavior in body fluids remains mysterious. Hyenne et al. show that the zebrafish embryo can be used to track and assess the function of circulating tumor EVs *in vivo* and provide a high-resolution description of their dissemination and uptake.

Hyenne et al., 2019, Developmental Cell *48*, 1–19
February 25, 2019
https://doi.org/10.1016/j.devcel.2019.01.014

CellPress

Please cite this article in press as: Hyenne et al., Studying the Fate of Tumor Extracellular Vesicles at High Spatiotemporal Resolution Using the Zebrafish Embryo, Developmental Cell (2019), https://doi.org/10.1016/j.devcel.2019.01.014

Developmental Cell
Resource

Studying the Fate of Tumor Extracellular Vesicles at High Spatiotemporal Resolution Using the Zebrafish Embryo

Vincent Hyenne,[1,2,3,4,12,*] Shima Ghoroghi,[1,2,3] Mayeul Collot,[5] Joanna Bons,[6] Gautier Follain,[1,2,3] Sébastien Harlepp,[1,2,3] Benjamin Mary,[1,2,3] Jack Bauer,[1,2,3] Luc Mercier,[1,2,3] Ignacio Busnelli,[1,2,3] Olivier Lefebvre,[1,2,3] Nina Fekonja,[1,2,3] Maria J. Garcia-Leon,[1,2,3] Pedro Machado,[7] François Delalande,[6] Ana Amor López,[8] Susana Garcia Silva,[8] Frederik J. Verweij,[9,10] Guillaume van Niel,[9,10] Farida Djouad,[11] Héctor Peinado,[8] Christine Carapito,[6] Andrey S. Klymchenko,[5] and Jacky G. Goetz[1,2,3,*]

[1]INSERM UMR_S1109, Strasbourg 67200, France
[2]Université de Strasbourg, Strasbourg 67200, France
[3]Fédération de Médecine Translationnelle de Strasbourg, Strasbourg 67200, France
[4]CNRS SNC5055, Strasbourg 67200, France
[5]Laboratoire de Biophotonique et Pharmacologie, UMR CNRS 7213, Université de Strasbourg, Illkirch 67000, France
[6]CNRS, Laboratoire de Spectrométrie de Masse Bio-Organique (LSMBO), IPHC, UMR 7178, Université de Strasbourg, Strasbourg 67087, France
[7]Electron Microscopy Core Facility, European Molecular Biology Laboratory, Heidelberg 69117, Germany
[8]Microenvironment and metastasis group. Department of Molecular Oncology, Spanish National Cancer Research Center (CNIO), Madrid, Spain
[9]Institut Curie, PSL Research University, CNRS UMR144, Paris 75005, France
[10]Center for Psychiatry and Neuroscience, Hôpital Saint-Anne, Université Descartes, INSERM U894, Paris 75014, France
[11]IRMB, Université de Montpellier, INSERM, Montpellier, France
[12]Lead Contact
*Correspondence: hyenne@unistra.fr (V.H.), jacky.goetz@inserm.fr (J.G.G.)
https://doi.org/10.1016/j.devcel.2019.01.014

SUMMARY

Tumor extracellular vesicles (EVs) mediate the communication between tumor and stromal cells mostly to the benefit of tumor progression. Notably, tumor EVs travel in the bloodstream, reach distant organs, and locally modify the microenvironment. However, visualizing these events *in vivo* still faces major hurdles. Here, we describe an approach for tracking circulating tumor EVs in a living organism: we combine chemical and genetically encoded probes with the zebrafish embryo as an animal model. We provide a first description of tumor EVs' hemodynamic behavior and document their intravascular arrest. We show that circulating tumor EVs are rapidly taken up by endothelial cells and blood patrolling macrophages and subsequently stored in degradative compartments. Finally, we demonstrate that tumor EVs activate macrophages and promote metastatic outgrowth. Overall, our study proves the usefulness and prospects of zebrafish embryo to track tumor EVs and dissect their role in metastatic niches formation *in vivo*.

INTRODUCTION

Over the past two decades, extracellular vesicles (EVs) have emerged as novel mediators of cell-cell communication due to their capacity to carry functional molecules coupled with their ability to travel in biological fluids (Raposo and Stoorvogel, 2013). EVs are heterogeneous in content and origin, as they can either arise from plasma membrane budding (then called microvesicles) or originate from a late endosomal compartment, the multi-vesicular body (MVB) (i.e., exosomes) (van Niel et al., 2018). EVs are known to be important in tumor progression and metastasis, where the complex tumor microenvironment requires a permanent cross-communication between cells (Hyenne et al., 2017). EVs secreted by tumor cells are enriched in pro-tumoral and pro-metastatic factors (proteins, mRNAs, miRNAs, and other non-coding RNAs) and can modify the phenotype of both tumor and stromal cells, mostly to the benefit of tumor growth and metastasis formation (Hyenne et al., 2017). For instance, tumor EVs were shown to transfer oncogenic traits from more aggressive to less aggressive tumor cells (Al-Nedawi et al., 2008). Importantly, tumor EVs can differentiate macrophages or fibroblasts into tumor-associated macrophages or fibroblasts, thereby promoting tumor growth and invasion (Chow et al., 2014; Gu et al., 2012; Paggetti et al., 2015). This pro-metastatic EV-mediated communication can occur within the primary tumor or at distance in physically far-off organs (Peinado et al., 2017). Remarkably, repeated injection of EVs isolated from metastatic cells into the mouse blood circulation induces the formation of a pre-metastatic niche, even in the absence of tumor cells (Costa-Silva et al., 2015; Grange et al., 2011; Hoshino et al., 2015; Liu et al., 2016; Peinado et al., 2012). The ability of circulating tumor EVs to alter the microenvironment of a given organ is particularly relevant with regard to (1) the increased amounts of tumor EVs present in the blood circulation of patients with cancer (Baran et al., 2010; Galindo-Hernandez et al., 2013;

Logozzi et al., 2009), and (2) the fact that elevated levels of EV proteins have been associated with poor prognosis in metastatic melanoma patients (Peinado et al., 2012). Therefore, it is crucial to precisely understand the mechanisms governing tumor EV dispersion and uptake in the blood circulation.

However, local or distant dissemination of tumor EVs has only been sparsely characterized in living organisms (Hoshino et al., 2015; Lai et al., 2015; Pucci et al., 2016). In particular, how EVs circulate in the blood flow and how specifically they are internalized by stromal cells during the priming of pre-metastatic niches remain poorly understood. EVs are nanoscale objects and are thus difficult to track *in vivo*. Moreover, mouse models are not fully suited for real time and *in vivo* EV tracking. In mice, EVs can either be followed after bulk injections (Lai et al., 2014; Takahashi et al., 2013) or with increased resolution through intravital imaging procedures (Lai et al., 2015; Van Der Vos et al., 2016; Zomer et al., 2015). However, such approaches have not yet been able to describe the behavior of tumor EVs in the blood circulation. An ideal animal model suited to accurately dissect the behavior of tumor EVs *in vivo* would allow their tracking in the circulation and their uptake and, at the same time, be amenable for modeling tumor and metastasis progression.

Interestingly, the zebrafish embryo largely complies with all these needs. Indeed, zebrafish has recently emerged as a potent model in cancer biology (White et al., 2013). The molecular pathways driving cancer progression and the anatomo-pathological features of tumorigenesis are essentially conserved between human and fish. In addition, the zebrafish embryo is transparent, possesses a stereotyped vasculature, a maturating immune system and is therefore perfectly suited for intravital imaging with high spatial and temporal resolution. For these reasons, the zebrafish embryo appears as an adequate model to study tumor EVs *in vitro*.

Here, we show that zebrafish melanoma EVs are similar to human melanoma EVs and demonstrate how their fate can be tracked in the zebrafish embryo. For efficient staining of EVs, we used MemBright, a recently developed cyanine-based membrane probe with improved brightness and specificity (Collot et al., 2019). Using this tool, and EVs from genetically engineered cells in parallel, we provide the first description of EVs' dynamics in the blood circulation. We subsequently examined the transit routes and arrest sites of tumor EVs and identified endothelial cells and patrolling macrophages as major EVs-recipient cells. Importantly, these cells have also been identified in a parallel study describing endogenous EVs dispersion in the zebrafish embryo (Verweij et al., 2019). We further show that these cell types have increased uptake efficiency toward tumor EVs, and found that patrolling macrophages internalize tumor EVs through at least two distinct endocytic mechanisms, before storing them in acidic compartments. Using correlated light and electron microscopy (CLEM), we precisely identified the cells uptaking EVs and finely described their morphology as well as the storage or degradative compartments at the electron microscopy level. In addition, we demonstrate that it is possible to track naturally released EVs *in vivo* in the zebrafish embryo using either pre-labeling with MemBright or genetically engineered cells. Finally, we show that melanoma EVs activate macrophages and promote metastatic outgrowth in zebrafish.

RESULTS

Zebrafish Melanoma EVs Are Similar to Human and Mouse Melanoma EVs

To study tumor EVs in zebrafish, we first characterized EVs released by a melanoma cell line (Zmel1) derived from a transgenic mitfa-BRAF(V600E);p53(−/−) zebrafish line (Heilmann et al., 2015) (Figure 1A). EVs were isolated from a cell culture supernatant following an established protocol of differential centrifugation (Théry et al., 2006), and EVs present in the 100.000 g pellet were characterized by nanoparticle tracking analysis (NTA) and electron microscopy. We found that Zmel1 EVs have an average diameter of 150 nm in solution and 90 nm after chemical fixation (Figures 1B and 1C). Subsequently, we characterized the protein content of these EVs by mass spectrometry and identified 794 proteins present in Zmel1 EVs (Table S1A). This list includes several proteins typically found in extracellular vesicles, such as ALIX, CD81, Flotillin 1, TSG101, CD9, RalA, Hsc70, HSP90, syntenin 2, integrins α5 and β1, and others (of note, CD63 was absent from Zmel1 EVs) (Figure 1D; Table S1A). We then wondered whether the content of zebrafish melanoma EVs was comparable to the ones of human or mouse melanoma EVs. We compared proteins present in Zmel1 EVs with proteins identified in the EVs isolated from six human (451-LU, SK-Mel28, SK-Mel147, SK-Mel103, WM35, and WM164) (Tables S1B–S1G) and three mouse (B16-F0, B16-F1, and B16-F10) (Tables S1H–S1J) melanoma cell lines. Protein content comparison revealed that 65% and 40% of Zmel1 proteins were also identified in human or mouse melanoma EVs, respectively (Figure 1E). Zmel1 EVs are closer to human melanoma EVs than to mouse melanoma EVs. We identified a core list of 82 proteins found in melanoma EVs from either zebrafish, mice, or human (Table S1K). Altogether, these data demonstrate that Zmel1 EVs derived from an established zebrafish melanoma cell line are highly similar to mammalian melanoma EVs and therefore constitute a good model to study human melanoma EVs.

In addition, we compared proteins present in Zmel1 EVs with proteins present in two other types of zebrafish EVs identified in a parallel study (Verweij et al., 2019). First, 17% of Zmel1 EVs proteins are also present in EVs from AB9 fibroblastic cell line (Table S1L). Then, we compared Zmel1 EVs with CD63-positive EVs secreted by a zebrafish embryonic epithelium, the yolk syncytial layer (YSL), and isolated from zebrafish embryos (Verweij et al., 2019). Interestingly, we found a relatively low similarity between these two types of zebrafish EVs (1–2% of Zmel1 EV proteins are present in YSL CD63+EVs; 10% of YSL CD63+EV proteins are present in Zmel1 EVs) (Table S1M). This difference illustrates the cell-type specificity of EV cargo enrichment. However, the mechanism of biogenesis of these two EV types could be partially similar, as 5 of the 12 proteins common to Zmel1 EVs and YSL EVs have been shown to affect, positively or negatively, exosome secretion in mammalian cells: TSG101, ALIX, Syntenin 2, Flotillin 1, and Rab2 (Baietti et al., 2012; Colombo et al., 2013; Okabayashi and Kimura, 2010; Ostrowski et al., 2010).

The MemBright Dye Specifically and Brightly Labels Tumor EVs

In order to fluorescently label Zmel1 EVs and follow them *in vivo*, we used new membrane probes, MemBright (Collot et al., 2019).

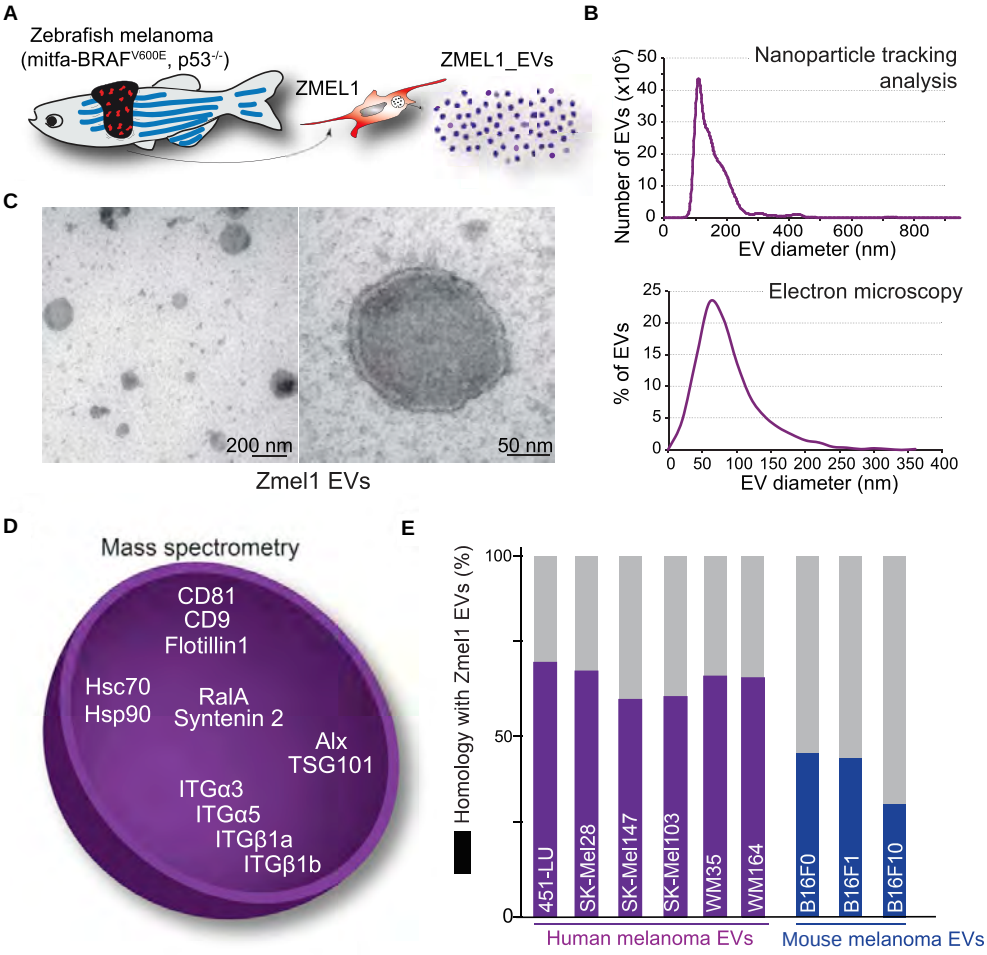

Figure 1. EVs Secreted by Zmel1 Zebrafish Melanoma Cells Are Similar to Mouse and Human Melanoma EVs

(A) Zebrafish melanoma EVs were isolated from Zmel1 cells by differential centrifugation (Heilmann et al., 2015).

(B) Histogram of a nanoparticle tracking analysis of Zmel1 EVs showing the number of EVs (y axis) versus their diameter (nm, x axis).

(C) Electron microscopy images of Zmel1 EVs and a histogram showing the percentage of total EVs (y axis) versus their diameter (nm, x axis).

(D) Illustration of some of the classical EV proteins present among the 794 proteins identified in ZMel1 EVs by mass spectrometry (see Table S1).

(E) Histogram showing the percentage of Zmel1 EVs proteins common with EV proteins from various human or mouse cell lines (using human orthologs).

They differ significantly from existing commercial dyes because they bear two amphiphilic groups composed of zwitterions and alkyl chains, which insert the dye into the membrane bilayer (Figure 2A). Moreover, MemBright is available in several colors, which therefore enables multi-color approach in EV imaging (Figures S2G–S2I). To assess the value of MemBright in EV labeling, we first globally compared the MemBright-labeled EVs to identical EVs labeled with PKH-26, a commercially available and widely used dye for EV labeling (Hoshino et al., 2015; Imai et al., 2015). Zmel1 EVs were incubated with MemBright-Cy3 (at 0.2 μM) or with PKH-26 (at 2 μM, according to manufacturer's instructions), washed and isolated by ultracentrifugation. Using fluorescence spectroscopy, we observed that PKH-labeled EVs display a broad absorption spectrum, with a blue shifted peak typically indicating the presence of H-aggregation (Figure 2B) (Würthner et al., 2011). By contrast, MemBright-labeled EVs show an absorption spectrum identical to the solubilized form of the probe (Figures 2B and S1A), revealing that the MemBright is efficiently embedded in EV membranes. MemBright-labeled EVs are as bright as PKH-labeled EVs even though the MemBright was 10-fold less concentrated than PKH (Figures 2B, 2C, and S1D). When both dyes were used at similar dilutions (0.2 μM), the MemBright labeled EVs were much brighter than the PKH ones (Figure S1E). Indeed, MemBright displays >20-fold higher quantum yield than the PKH: 0.42 versus 0.02 (Table S2). Since MemBright-Cy3 and

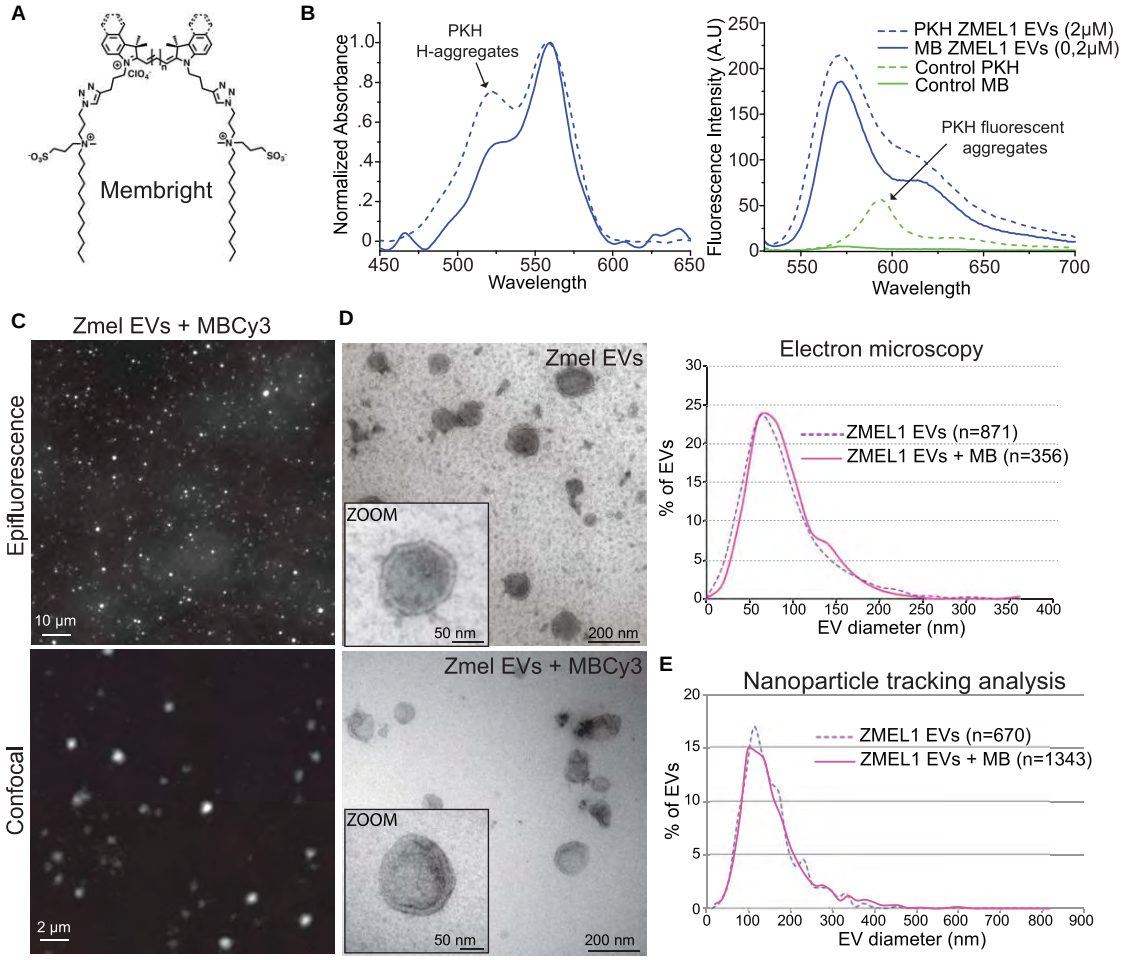

Figure 2. EVs Can Be Brightly and Specifically Labeled with MemBright

(A) Molecular structure of the membrane binding probe MemBright.

(B) Histograms showing a spectroscopy analysis of MemBright (MB) and PKH labeled Zmel1 EVs describing the absorbance (left histogram, y axis) and the fluorescence intensity (right histogram, y axis) versus the wavelength (nm, x axis). Arrows indicate the presence of PKH aggregates in labeled EVs (left) as well as in control PKH alone (right).

(C) Zmel1 EVs labeled with MemBright Cy3 (MBCy3) observed by Epifluorescence (upper) and confocal (lower).

(D) Electron microscopy of non-labeled (upper) and labeled (lower) Zmel1 EVs and histogram showing the percentage of labeled and non-labeled Zmel1 EVs (y axis) versus their diameter (x axis, nm) by electron microscopy (right graph).

(E) Nanoparticle tracking analysis of MemBright-labeled and non-labeled Zmel1 EVs showing the number of EVs (y axis) versus their diameter (nm, x axis).

PKH26 contain the same Cy3-based fluorophore, such remarkable difference in the quantum yield suggests inefficient partitioning of PKH into EV membranes. This poor partitioning probably arises from the aggregation of PKH in aqueous media, in line with characteristic short-wavelength shoulder in the absorption spectrum in the samples of EVs (Figure S1B). This is not the case for MemBright. Interestingly, a similar spectroscopic experiment conducted without EVs reveals the presence of a red-shifted fluorescence peak with PKH alone but not with MemBright alone (Figure S1C). These fluorescent PKH aggregates have an average diameter of 80 nm (± 10 nm), as analyzed by fluorescence correlation spectroscopy (FCS), which is in the range of EVs and therefore could lead to artifacts. To complement these studies, we analyzed MemBright-labeled EVs by electron microscopy and NTA and found that neither their morphology nor their size was affected, when compared to non-labeled EVs (Figure 2D). Importantly, no larger size aggregates were detected in MemBright-labeled EVs (Figure 2E). Finally, we demonstrated the versatility of MemBright by labeling EVs isolated from 4T1 mouse mammary carcinoma cells. Spectroscopy (Figure S1B; Table S2) and electron microscopy analysis (data not shown) confirmed the advantages of the

Please cite this article in press as: Hyenne et al., Studying the Fate of Tumor Extracellular Vesicles at High Spatiotemporal Resolution Using the Zebrafish Embryo, Developmental Cell (2019), https://doi.org/10.1016/j.devcel.2019.01.014

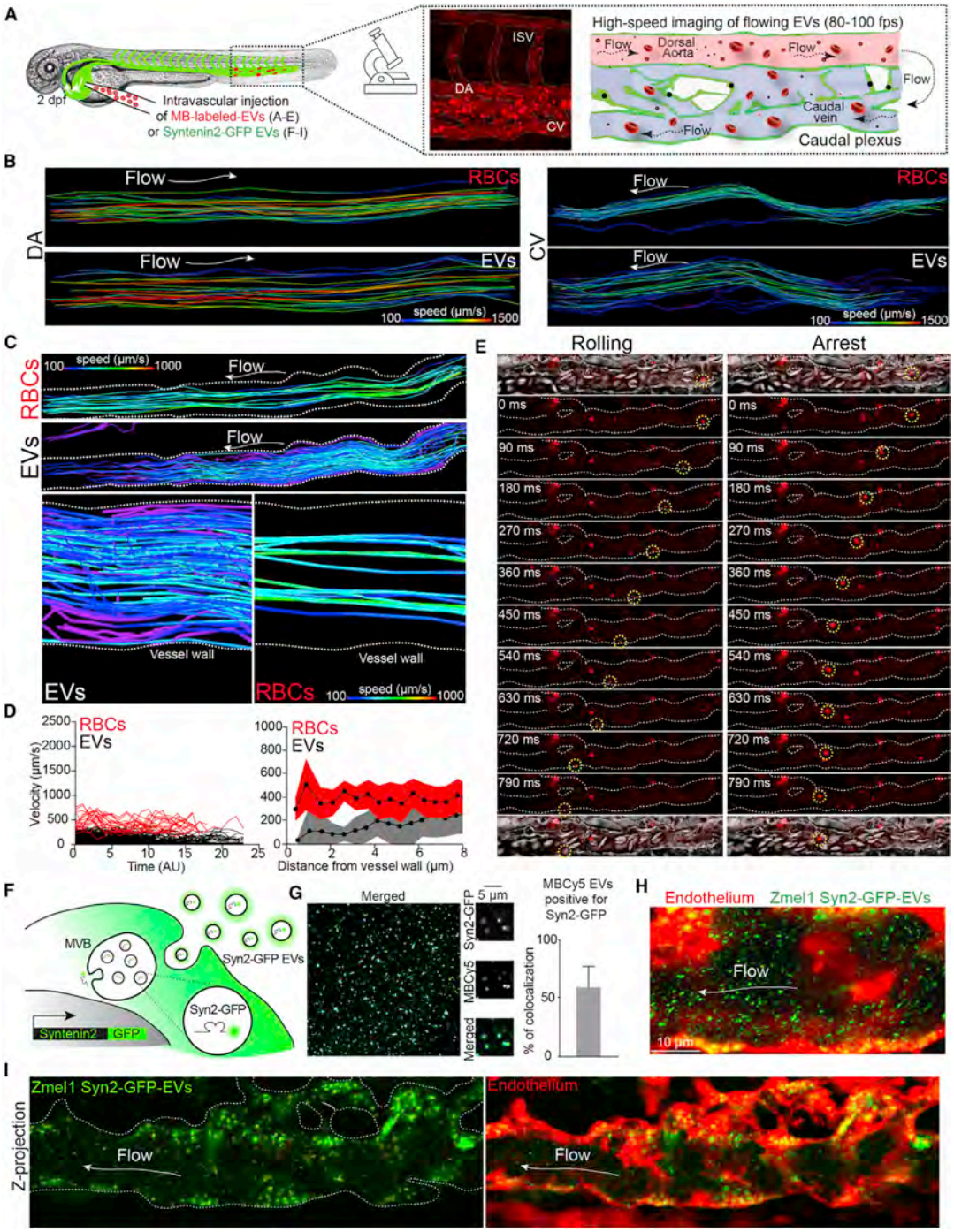

(legend on next page)

MemBright probes. Furthermore, separation of MemBright-labeled 4T1 EVs by density gradient revealed that the majority of the fluorescent MemBright is present in the fractions where most EVs are found, as confirmed by the presence of ALIX and TSG101 (Figure S1F). Altogether, these experiments prove that labeling EVs with MemBright does not lead to soluble fluorescent aggregates that can be confounded with labeled EVs. In addition, given its high quantum yield, MemBright can be used at a relatively low concentration to efficiently label isolated EVs.

Tumor EVs Can Be Individually Tracked in the Living Zebrafish Embryo

We next investigated whether MemBright labeling could be used for tracking tumor EVs *in vivo*. We injected zebrafish embryos at 2 days post-fertilization with MemBright-labeled EVs in the blood circulation. Fluorescent EVs were observed essentially in the tail region of the embryo, which is composed of the dorsal aorta and the venous caudal plexus (Figure 3A). Minutes following injection, we observed several fluorescent EVs that were either still flowing or that were already arrested along the endothelium (Figure 3A; Video S1A). We first assessed the apparent size of EVs by comparing them to 100 nm fluorescent polystyrene beads. *In vitro* and upon injection in the circulation of zebrafish embryos, we found that MemBright-labeled EVs and 100 nm fluorescent beads display similar apparent sizes, which correspond to the resolution limits of confocal microscopy (Figures S2A–S2D). Furthermore, MemBright-labeled EVs do not adhere to red blood cells (RBCs), and no leakage of MemBright from EVs to RBCs could be observed *in vitro* or *in vivo* (Figures S2E and S2F). These observations suggest that MemBright in combination with our microscopy set-up allow imaging of fluorescent objects of the size of an individual EV. At this stage, however, we cannot assess whether bigger spots result from bigger EVs or clusters of small EVs. In addition, MemBright can be used to co-inject different types of EVs labeled with different colors (Cy3, Cy5) and specifically track their fate. As a proof of concept, we co-injected Zmel1 tumor EVs (labeled with MemBright-Cy5) with 4T1 mouse tumor EVs (labeled with MemBright-Cy3) in zebrafish embryos and observed both specific localizations for each EVs population as well as a common uptake in isolated cells (Figures S2H and S2I). This suggests that MemBright could be used to follow specific internalization routes of distinct types of EVs that might be on the basis of their function and message delivery.

We then aimed to describe the over-looked behavior of tumor EVs in the blood circulation. To do that, we performed high-speed confocal acquisitions of flowing tumor EVs (and of co-flowing RBCs) in different regions of the vasculature of living zebrafish embryos (Figure 3A; Videos S1B and S1C). When tracking both tumor EVs and RBCs, we first found that EVs have a higher velocity in the aorta than in the caudal veins, in accordance with the hydrodynamic profiles previously described in this region of the zebrafish embryo vasculature (Figure 3B) (Follain et al., 2018a). Second, when analyzing co-motion of tumor EVs and RBCs in a single vessel, we noticed that EVs have a reduced velocity compared to RBCs. These observations are not restricted to Zmel1 EVs since 4T1 EVs display a higher velocity in the dorsal aorta than in the caudal veins but a slower velocity than RBCs (Figures 3C and 3D). Interestingly, we observed that the hemodynamic behavior of tumor EVs differs in regions close to the vessel wall, from which RBCs are mostly excluded. Indeed, when we plotted the velocity of tumor EVs as a function of their position with regards to vessel walls, we observed that tumor EVs explore the vicinity of vessel walls with a reduced velocity (Figures 3C and 3D). Thus, it seems that tumor EVs follow a Poiseuille flow, which predicts that objects displaced by a laminar flow would have a reduced velocity because of frictional forces, along the border of the vessel wall. Such a behavior, in addition to their potential adhesive capacity, could thus favor the arrest of tumor EVs. Indeed, individual inspection of EVs in close proximity to the vessel wall reveals that they are either flowing, rolling on the surface of the endothelium, or arresting (Figure 3E). We observed arrest of EVs following a rolling behavior, suggesting that it could be driven by progressive activation of adhesion molecules, as well as the sharp arrest of flowing EVs, without a rolling phase (Video S2). A very similar behavior was observed for endogenous EVs (Verweij et al., 2019). Altogether, we provide the first accurate description of circulating tumor EVs in the vasculature.

In addition, we used a complementary genetic approach. We expressed Syntenin2 (a major cargo detected in Zmel1 EVs by mass spectrometry, Figure 1D) fused to GFP in Zmel1 cells and showed that these cells secrete GFP-positive EVs (Figures 3F and 3G). Upon intravascular injection in zebrafish embryos, the Syntenin2-GFP EVs can be tracked in the circulation similar to MemBright-labeled EVs (Figures 3H and 3I). Altogether, we document that both genetically and chemically labeled tumor

Figure 3. Hemodynamic Characterization of Individual EVs Tracked in the Circulation of Zebrafish Embryo

(A) Experimental setup used to track circulating EVs: two days post-fertilization zebrafish embryos are injected in the duct of Cuvier with fluorescent EVs (left) and observed in the caudal plexus with high-speed confocal microscopy. Middle: *Z* projection of MemBright-Cy3 Zmel1 EVs in the caudal plexus right after injection. Right: schematic representation of the caudal plexus showing the direction of the blood flow in the dorsal aorta (pink) and the venous plexus (blue).

(B) Individual tracks of red blood cells (RBC) or Zmel1 EVs in the dorsal aorta (DA, left) and in the caudal vein (CV, right).

(C) Upper: Individual tracks of red blood cells (RBC) or 4T1 EVs in the CV. Lower: Zoom on individual tracks of red blood cells (RBC, right) or 4T1 EVs (left) in the CV in proximity of the vessel wall (white lines). (B) and (C): Color coding represents velocities.

(D) Left: histogram showing the velocity (y axis, μm/s) versus the time (x axis, AU) of RBCs (red) and EVs (black) in the CV. Right: histogram showing the velocity (y axis, μm/s) versus the distance to the vessel wall (x axis, μm) of RBCs (red) and EVs (gray) in the CV.

(E) Examples of individual EVs rolling (left) or arresting (right) in the circulation of the CV.

(F) Schematic representation of Zmel1 cells expressing Syntenin2-GFP.

(G) EVs isolated from Zmel1 Syntenin2-GFP cells and labeled with MemBright; the diagram indicates the colocalization between GFP and MemBright (mean and standard deviation).

(H) Temporal projection of a time-lapse of *Tg(Fli:Gal4, UAS:RFP)* embryos injected with Zme1 Syntenin2-GFP EVs imaged immediately after injection.

(I) *Z*-projection of *Tg(Fli:Gal4, UAS:RFP)* embryos injected with Zme1 Syntenin2-GFP EVs imaged 1h after injection.

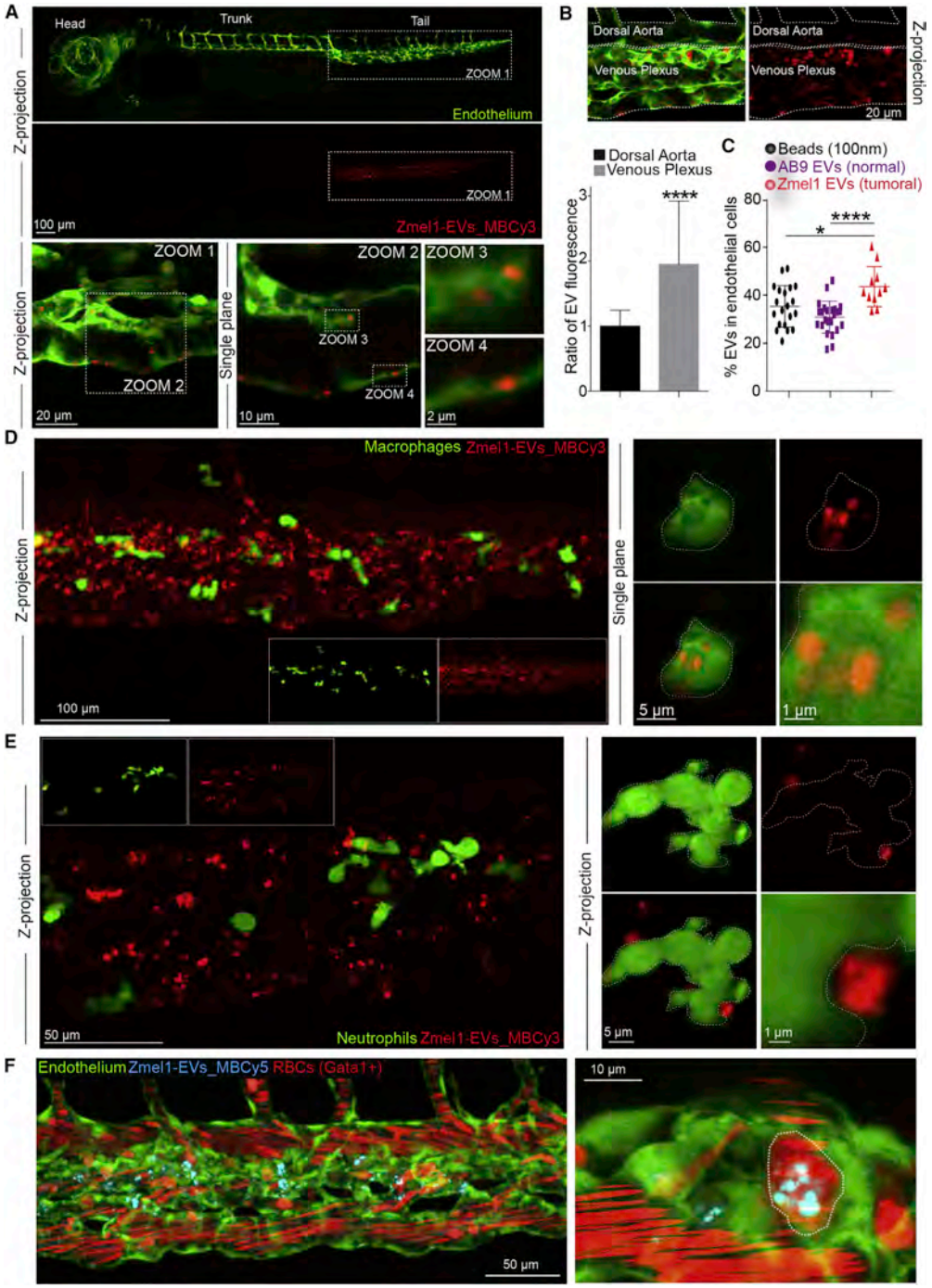

Figure 4. Zmel1 EVs Are Mainly Taken Up by Endothelial Cells, Macrophages, and Hematopoietic Stem Cells but Not by Neutrophils

(A) Confocal images of MemBright-Cy3 labeled Zmel1 EVs 3 h post-injection (hpi) in *Tg(Fli1:GFP)* embryos (endothelium specific expression). The upper panels were stitches from several individual images to allow a large region to be visualized.

(legend continued on next page)

EVs can be tracked in the bloodstream of zebrafish embryos, allowing the study of their hemodynamic behavior and intravascular arrest.

Circulating Tumor EVs Are Mostly Taken Up by Endothelial Cells and Patrolling Macrophages

How circulating tumor EVs target specific cell types at distance remains a mystery, mostly because this step could not be captured before. Here, most of the tumor EVs are found arrested, exclusively in the tail region of the fish, only 10 to 15 min following injection (Figure 4A). In addition, we found that most of the uptake by endothelial cells occurs in the venous region (Figure 4B), suggesting that the permissive flow profiles of this particular region favor arrest and uptake of tumor EVs, as they do for circulating tumor cells (Follain et al., 2018a). Syntenin2-GFP EVs arrest similarly in *Tg(Fli:Gal4, UAS:RFP)* embryos (Figure 3I) and similar observations have been done for endogenous EVs (Verweij et al., 2019). To assess which cell types could uptake tumor EVs, we used four transgenic zebrafish lines with different tissue-specific fluorescent expression *Tg(Fli1:GFP)* for the endothelium (Figure 4A), *Tg(mpeg1:GFP)* for macrophages (Figure 4D), *Tg(mpo:GFP)* for neutrophils (Figure 4E), and *Tg(gata1:dsRed)* for RBCs and putative hematopoietic stem cells (Figure 4F). We found that tumor EVs are rapidly taken up by endothelial cells, macrophages, and immobile Gata1-positive cells (putative hematopoietic stem cells) but not by neutrophils that are known to have a reduced phagocytic activity (Figures 4A, 4D, 4E, and 4F) (Le Guyader et al., 2008). Embryos injected with the MemBright dye alone do not show any signal that could arise from soluble fluorescent aggregates (Figure S3). In addition, endothelial cells and macrophages take up equivalent proportions of Zmel1 EVs, 43% (n = 19 fish) and 38% (n = 11) respectively. Together, this represents the large majority of arrested EVs in the zebrafish embryo at that stage. Importantly, a similar behavior is observed for endogenous CD63-positive EVs (Verweij et al., 2019), suggesting again that circulating EVs of different origins share common mechanisms of arrest *in vivo*. Interestingly, although inert polystyrene beads and non-tumoral EVs (from AB9 zebrafish fibroblasts) can be taken up by macrophages and endothelial cells, they show a reduced accumulation compared to Zmel1 EVs (Figures 4C and 5C). This suggests that both unspecific and specific uptake mechanisms co-exist *in vivo*.

In mice, tumor EVs are internalized by different types of monocytes and macrophages (Whiteside, 2016). In the zebrafish embryo, we noticed that tumor EVs are mostly taken up by small round mpeg1-positive cells (Figures 5A and 5B). In non-injected embryos, these round cells are in direct contact with the blood flow (Figure 5A), which they scan using long protrusions (Figure 5D; Video S3). They also display a reduced velocity (Figure 5E; Video S4). Therefore, the morphology, location, and dynamics of these cells are reminiscent of patrolling monocytes, which are known to play an important role in tumor progression and metastasis in mice and humans (Auffray et al., 2007; Carlin et al., 2013; Hanna et al., 2015). To confirm this observation and gain insight into the ultrastructure of these cells, we used our established CLEM procedure (Goetz et al., 2014; Karreman et al., 2016b) in *Tg(mpeg1:GFP)* embryos injected with tumor EVs labeled with MemBright-Cy3 (Figure 5F; Video S5). We targeted two typical mpeg1:GFP positive cells that have taken up circulating tumor EVs in the living zebrafish embryo (see STAR Methods; Figures S4A and S4B). Fine segmentation of EM images revealed that macrophages localize in a cavity of the lumen of the vessel, where they form tight contacts with the endothelium and extend wide protrusions in the lumen (Figure 5F; Video S5). Interestingly, the region of the endothelium that contacts the macrophages is enriched of endocytic structures, suggesting active exchange between those two cell types (Figure 5G). The macrophages that have taken up tumor EVs extend long and dynamic protrusions in the lumen of the vessel (Figures 5D and 5H), as shown for patrolling monocytes in mice (Carlin et al., 2013). Surprisingly, analysis of the serial sections reveals that their height can be >3 μm and that these protrusions are actually forming large flat sheets deployed in the lumen. Altogether, our data show that circulating tumor EVs are rapidly taken up by patrolling macrophages in the zebrafish embryo, which suggests that it can be used to track the mechanisms of delivery of tumor EVs at high spatiotemporal resolution.

Internalized Tumor EVs Are Targeted to Late Endosomal Compartments

To gain further insight into the mechanisms through which patrolling macrophages uptake tumor EVs, we then imaged the dynamics of circulating tumor EVs (Video S6A). On one hand, EVs arrest at the surface of the macrophage and undergo a slow internalization that can be tracked at optimal spatiotemporal resolution (Figures 6A and 6C; Video S6B). The timing of this uptake (∼ 30 s) is in the range of classical endocytosis (Figure 6A) (Idrissi and Geli, 2014; Taylor et al., 2011). On the other hand, tumor EVs are first caught by a protrusion extending from the macrophage, and then crawl back toward the cell center before being internalized at the basis of the protrusion (Figures 6B and 6C; Video S6C). This second mechanism of internalization is significantly faster (< 5 s) (Figure 6C).

Next, we wondered which intracellular compartments are targeted by uptaken EVs. For this, we incubated *Tg(mpeg1:GFP)* zebrafish embryos with the LysoTracker to label late endosome-lysosomes (LELs). Rapidly after injection, several Zmel1 EVs already colocalize with LysoTracker, although the majority does not (Figure 6D). This colocalization increases over time and 3 h post-injection (hpi), most EV signal is found in

(B) *Z*-projections showing the borders of the dorsal aorta (DA) and the venous plexus (VP), and a histogram showing the EV fluorescence per surface in DA and VP (mean and standard deviation; $p < 0.0001$; Mann-Whitney test).
(C) Quantification of the proportion of 100 nm polystyrene beads, fibroblasts AB9 Evs, or Zmel1 melanoma EVs taken up by endothelial cells 3 hpi (Zmel1 EVs Vs beads: $p = 0.015$, unpaired t test; Zmel1 EVs Vs AB9 EVs: $p < 0.0001$, unpaired t test).
(D) Confocal images of MemBright-Cy3 labeled Zmel1 EVs 3 hpi in *Tg(mpeg1:GFP)* (macrophage specific expression).
(E) Confocal images of MemBright-Cy3 labeled Zmel1 EVs 3 hpi in *Tg(mpo1:GFP)* (neutrophil-specific expression).
(F) Confocal images of MemBright-Cy5 labeled Zmel1 EVs 3 hpi in *Tg(Fli1:GFP; Gata1:RFP)* (GFP: endothelium; *Gata1*: red blood cells and hematopoietic stem cells).

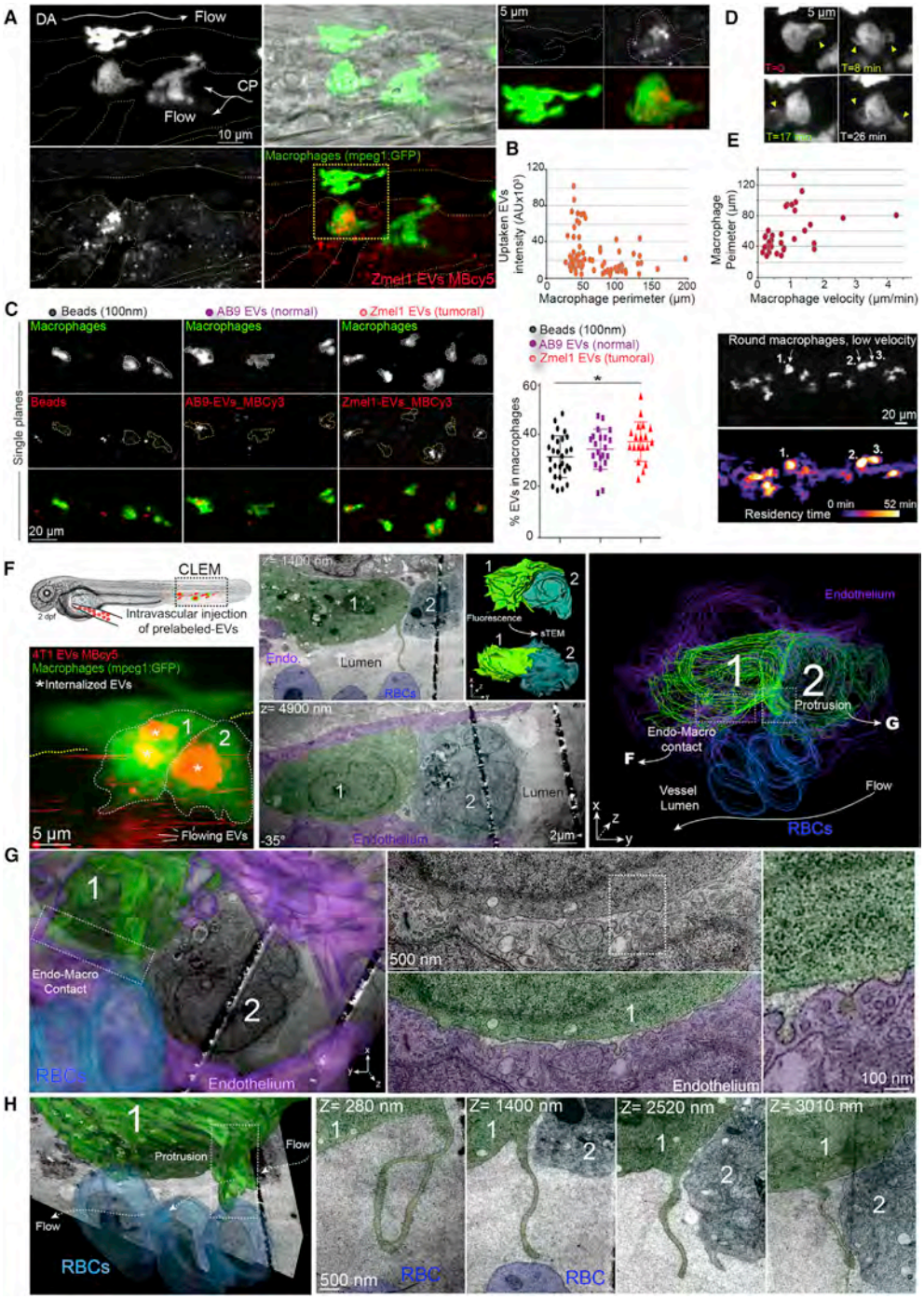

Figure 5. Circulating EVs Are Taken Up by Patrolling Macrophages

(A) Confocal Z projection images of MemBright-Cy3 labeled Zmel1 EVs injected in *Tg(mpeg1:GFP)* (left) with zoom on elongated macrophages devoid of EVs and round macrophages accumulating EVs (right).

(legend continued on next page)

endosome-lysosome compartments (Figure 6D). Of note, 24 hpi, the MemBright signal is still visible and fully colocalizes with LysoTracker (Figure 6D). Although this approach provides a dynamic view of EVs trafficking in zebrafish embryos, LysoTracker labeling does not distinguish between MVBs, late endosomes, and lysosomes. To complement this study, we again exploited our established CLEM procedure on *Tg(mpeg1:GFP)* embryos injected with tumor EVs (Figures 5F–5H and 6E). We generated a 3D model of MemBright-labeled EVs in each macrophage, based on the confocal fluorescent data (called fluorescent 3D model, Figure 6F, upper panel). In parallel, based on TEM serial sections of the same cells, we segmented all the MVBs, late endosomes, and lysosomes that we could locate, and generated a 3D model of these compartments (called TEM 3D model) (Figure 6F, lower panel; Video S5). When comparing the two models, we found that the 3D model created from the fluorescent tumor EVs overlaps with the model from serial TEM sections of LELs (Video S5). This suggests that the internalized tumor EVs are stored within these MVBs, LELs compartments that we imaged at high-resolution (Figure 6E, lower panels). Besides, close examination of the EM stack revealed EVs present in the lumen of the vessel, in close proximity of macrophage protrusions, as well as putative EVs present in endosomes (Figures S4C–S4E). Altogether, this demonstrates the power of the zebrafish embryo to track, at multiple scales, the fate of nanometer-sized objects such as tumor EVs.

Tracking the Release of EVs *In Vivo* Using MB and Genetically Engineered Cells

We focused so far on tumor EVs that were previously isolated and labeled *in vitro* and subsequently tracked *in vivo*. This strategy, however, does not allow tracking of tumor EVs shed from *in-vivo*-grown tumors. Interestingly, we noticed that EVs can be labeled by incubating the secreting cells with the MemBright dye. MemBright quickly and exclusively accumulates in late endosomal compartments of Zmel1 cells in culture (Figure 7A). Upon extensive washing, these cells release fluorescently labeled EVs (Figure 7B) whose morphologies and diameters are similar to EVs from non-labeled cells (Figure 7B). When this approach was used on 4T1 cells expressing CD63-GFP, we could detect EVs positive for both MemBright and CD63, proving that the MemBright can label exosomes (Figure S5). We observed puncta positive for CD63-GFP but not for MemBright and vice-versa. This suggests that the MemBright dye does not label all EVs equally and illustrates the heterogeneity of EVs, which has recently been described (Kowal et al., 2016). Altogether, these experiments suggest that the MemBright is rapidly endocytosed, targeted to MVBs, and incorporated into the membrane of intra-luminal vesicles before being subsequently released outside of the cells attached to the membrane of exosomes. Such a behavior is extremely useful since it allows labeling and tracking of naturally released EVs by pre-incubating cells with MemBright. To prove this, we co-cultured Zmel1 pre-labeled with MemBright-Cy5 with Zmel1 cells expressing cytoplasmic tdTomato. After a week, we observed several Cy5 fluorescent puncta accumulating in the cytoplasm of Zmel1 tdTomato cells, suggesting that indirectly labeled EVs successfully transferred between neighboring cells (Figure 7B). Such a result opens the door to *in vivo* experiments where pre-labeled tumor cells would be grafted in zebrafish embryos (Figures 7C and 7D). To test local EVs transfer, tdTomato Zmel1 cells were pre-labeled with MemBright-Cy5 and subsequently injected into the circulation of *Tg(mpeg1:GFP)* zebrafish embryos. We observed macrophages crawling around arrested Zmel1 tumor cells, and containing Cy5-positive fluorescent puncta (Figure 7C; Video S7), suggesting local EVs transfer between tumor cells and macrophages. These puncta are negative for tdTomato, revealing a different mechanism than the transfer of cytoplasmic material between melanoma cells and macrophages (Roh-Johnson et al., 2017). In addition, we tested the distant transfer of EVs by injecting tdTomato Zmel1 cells pre-labeled with MemBright-Cy5 in the yolk region and imaging macrophages present in the caudal plexus. Similar to the previous experiment, we detected Cy5 fluorescence in macrophages, suggesting the existence of a distant transfer of EVs that exploits the blood circulation for shedding and targeting at distance (Figure 7D). We further validated the ability to detect secreted EVs *in vivo* by intravascular injection of Syntenin2-GFP expressing Zmel1 cells. Upon injection of these cells in the bloodstream, we followed successful extravasation and metastatic outgrowth overtime, which was accompanied by an increased secretion of tumor EVs. While the release of fluorescent EVs was not observed around recently extravasated cells (4 hpi), growing metastatic foci gradually released increasing amounts of Syn2-GFP EVs, which were either mobile or immobile (Figure 7E). Altogether, these experiments demonstrate that the zebrafish embryo allows tracking of the release and transfer of chemically and genetically labeled EVs from tumor to stromal cells *in vivo*.

Tumor EVs Activate Macrophages and Promote Metastatic Growth in Zebrafish

In contrast to inert objects, tumor EVs are loaded with signaling molecules that are likely to affect the fate or behavior of cells that

(B) EVs are mostly taken up by small macrophages. Histogram showing the intensity of taken up EVs (y axis, arbitrary units) versus the perimeter of the macrophages (x axis, μm). Each dot represents one macrophage.
(C) Macrophages internalize tumor EVs more efficiently than 100 nm polystyrene beads (mean and standard deviation; p = 0.016, unpaired t test).
(D) Individual time points of single plane confocal images showing the dynamics of the protrusions in round macrophages.
(E) Histogram showing the perimeter of macrophages (y axis, μm) versus their velocity (x axis, μm/s) (left) and images at the beginning (T = 0) and the end (T = 60 min) of a representative time-lapse. Velocities of migration of *Tg(mpeg1:GFP)*-positive cells are represented with a color code. Three round *Tg(mpeg1:GFP)*-positive cells (1, 2, and 3) show very little displacement during one h.
(F) CLEM experiment on *Tg(mpeg1:GFP)* embryos injected with MemBright-Cy3 4T1 EVs imaged by confocal right after injection (left, *Z* projection). Middle: electron microscopy images on two different *Z* planes showing the same cells. Right: 3D model showing the two macrophages (green), the endothelium (purple), and three red blood cells (blue).
(G) Electron microscopy images of the contact between the endothelium and the macrophage, showing the accumulation of endocytic structures on the endothelium side.
(H) 3D model and electron microscopy images of one protrusion sent by the macrophage into the lumen. This protrusion is visible over several microns in *Z*.

Please cite this article in press as: Hyenne et al., Studying the Fate of Tumor Extracellular Vesicles at High Spatiotemporal Resolution Using the Zebrafish Embryo, Developmental Cell (2019), https://doi.org/10.1016/j.devcel.2019.01.014

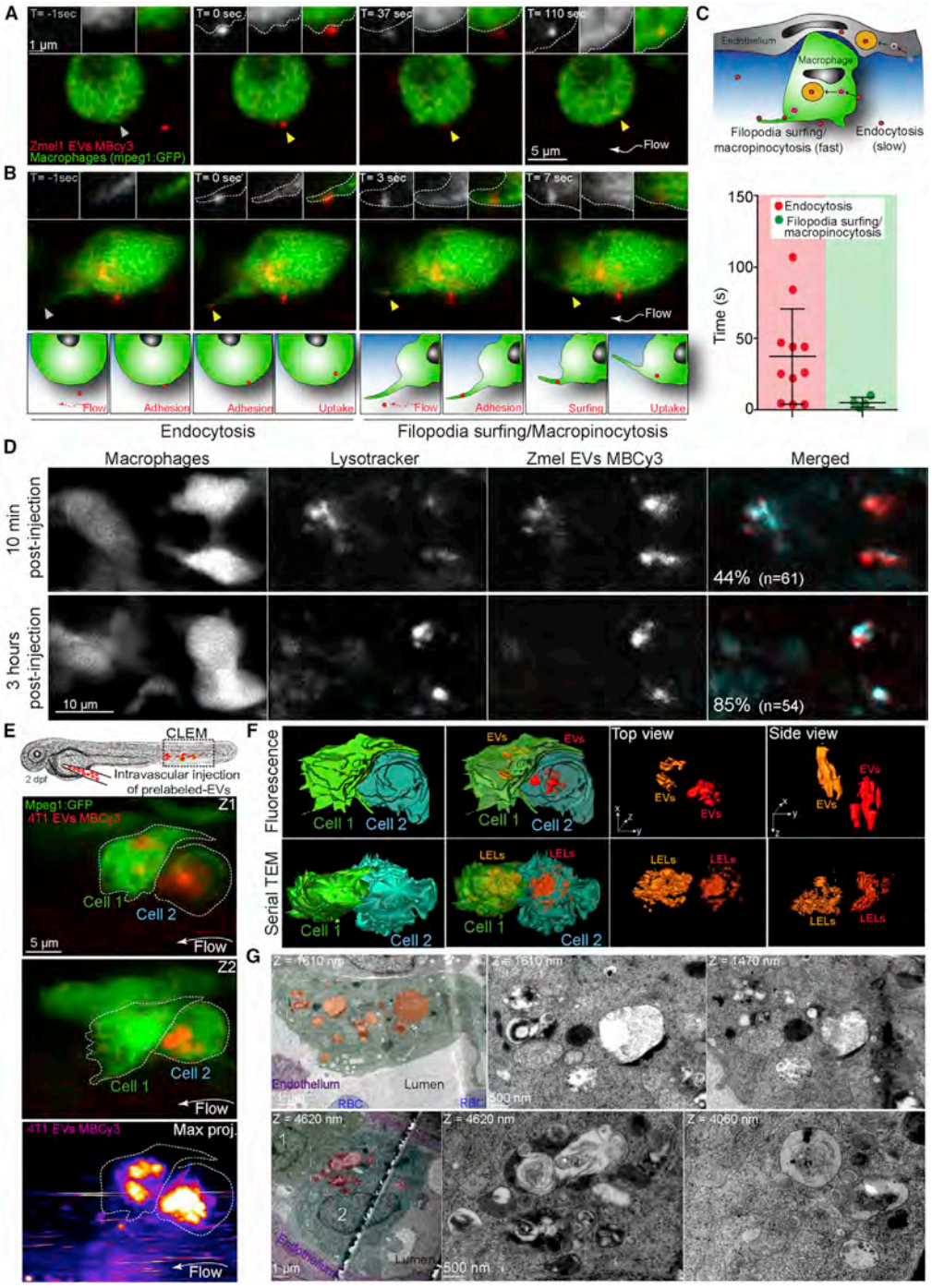

(legend on next page)

internalize them. We thus assessed whether Zmel1 EVs could modify the behavior of receiving cells. We focused on macrophages, which are taking up most of the circulating EVs, and first analyzed their velocities upon uptake. The uptake of tumor EVs by patrolling macrophages significantly reduced their motility when compared to macrophages that had internalized control beads (Figure 8A). Since macrophage velocity has been associated with their activation status *in vitro* (Vogel et al., 2014), we chose to evaluate the impact of Zmel1 EVs on macrophage activation. To do this, we used a recently described transgenic line that relies on the expression of TNF-α to discriminate between pro-inflammatory "M1-like" and "M2-like" polarized macrophages (Nguyen-Chi et al., 2015). Strikingly, most embryos injected with Zmel1 EVs showed M1 activated macrophages 20 hpi (Figures 8B and 8C). Such switches were rarely observed when embryos were injected with 100 nm control polystyrene beads, which clearly demonstrates that circulating Zmel1 EVs can modify the behavior of receiving cells at distance. Tumor EVs can educate receiving cells and confer them pro-metastatic characteristics (Peinado et al., 2017). Inspired by such experiments mostly performed in mice, we next assessed whether circulating tumor EVs could tune metastatic outgrowth. We first "primed" embryos with intravascular injection of either Zmel1 EVs (or 100 nm polystyrene beads). After 12 h, the same embryos were injected with Zmel1 cells in a classical experimental metastasis assay as previously performed (Follain et al., 2018a). Metastatic growth was assessed 7 days later by measuring fluorescence in the caudal plexus. We observed a marked and significant increase in metastatic outgrowth when embryos were primed with Zmel EVs, and not with inert beads (Figure 8D). Furthermore, metastatic foci of embryos primed with tumor Zmel EVs were strikingly more invasive and displayed colonization of the fin parenchyma (Figures 8D and 8E). Altogether, these experiments demonstrate that (1) tumor EVs transform the phenotypes of macrophages and (2) favor metastatic outgrowth and invasiveness by modifying the microenvironment. In addition to demonstrating that labeling EVs with MemBright does not perturb their function, this further validates the use of zebrafish embryos to dissect, with high spatiotemporal resolution, the cascade of events induced by circulating tumor EVs and leading to pre-metastatic niche formation *in vivo*.

DISCUSSION

The work presented here establishes the zebrafish embryo as a new animal model to study tumor EVs *in vivo*. It demonstrates the proximity of zebrafish melanoma EVs to human melanoma EVs and shows how a new membrane probe, the MemBright, specifically and brightly labels EVs. Using this probe, but also genetically labeled EVs, we were able to precisely track their fate and behavior at high spatiotemporal resolution *in vivo*. This allowed us to provide a description of the behavior of tumor EVs circulating in the blood flow and to track their fate upon arrest. We identify the three main cell types taking up circulating tumor EVs (endothelial cells, patrolling macrophages, and putative hematopoietic stem cells) and unravel their uptake mechanisms. Besides, we describe two complementary methods, a conventional genetic approach and the pre-labeling of secreting cells by MemBright, allowing to track the release and transfer of EVs *in vivo*. Finally, we provide evidence for a functional role of tumor EVs in altering the metastatic microenvironment and promoting metastatic outgrowth in zebrafish embryos.

In a parallel study, Verweij and colleagues examine the fate of CD63 positive EVs secreted by the YSL in zebrafish embryo (Verweij et al., 2019). They track endogenous EVs, genetically labeled and naturally secreted during zebrafish development, while we tracked exogenous MemBright-labeled injected tumor EVs. Yet, both studies reach similar conclusions. They both show that (1) endogenous and tumor EVs mainly arrest in the caudal plexus, in regions of low blood flow, (2) EVs are mostly taken up by endothelial cells and patrolling macrophages, and (3) EVs are stored in acidic compartments. Together, our reports establish the zebrafish embryo (*Danio rerio*) as a new model to study fundamental aspects of EVs biology *in vivo*. It thus represents a precious and complementary tool to invertebrate models *Drosophila* and *C. elegans*, which already contributed to better understand the mechanisms of EV secretion as well as their function (Beer and Wehman, 2017).

In addition, we propose the zebrafish embryo as a new and complementary model to murine and human cell culture systems for studying the fate and the function of tumor EVs during the priming of metastatic niches at distance. Compared to *in vitro* systems, zebrafish embryo offers an invaluable complex microenvironment, where different cell types known to contribute to tumor progression are present and can be tracked using established fluorescent transgenic lines. Its transparency allows visualization of individual tumor EVs dispersion and uptake in living zebrafish with unprecedented spatiotemporal resolution, which represents a major advantage over the mouse, where more complex intravital imaging procedures are required in order to visualize single EVs (Lai et al., 2015; Van Der Vos et al., 2016; Zomer et al., 2015). The zebrafish embryo is also amenable to CLEM,

Figure 6. EVs Are Taken Up through Different Mechanisms and Accumulate in Late Endosomal Compartments

(A and B) Single-plane confocal images of *Tg(mpeg1:GFP)* embryos injected with Zmel1 MemBright-Cy3 (MBCy3) EVs extracted from time-lapses generated immediately after injection and showing: (A) the attachment and uptake of EVs by endocytosis and (B) the sliding of EVs on the macrophage protrusion and its fast internalization.

(C) Schematic representation of the modes of uptake by macrophages (upper) and histogram showing the duration (y axis, s) of those two mechanisms (mean and standard deviation).

(D) Single plane confocal images of *Tg(mpeg1:GFP)* embryos injected with Zmel1 MBCy3 EVs and incubated with LysoTracker.

(E) CLEM experiment on *Tg(mpeg1:GFP)* embryos injected with MemBright-Cy3 4T1 EVs imaged by confocal (2 single confocal planes of the GFP and the MBCy3 channels and Z projection of the EV channel (lower)).

(F) 3D model of the two cells and the taken up EVs generated from the confocal data (upper panel, fluorescence), and 3D model of the two cells and the MVBs-late endosomes-lysosomes compartments (LELs) generated from the serial transmission electron microscopy data (lower panel, serial TEM).

(G) Global view of each macrophage highlighting the MVBs-late endosomes-lysosomes compartments (orange and red, left). Zooms of those compartments are shown on the right in two different *Z* positions of the same region.

Please cite this article in press as: Hyenne et al., Studying the Fate of Tumor Extracellular Vesicles at High Spatiotemporal Resolution Using the Zebrafish Embryo, Developmental Cell (2019), https://doi.org/10.1016/j.devcel.2019.01.014

CellPress

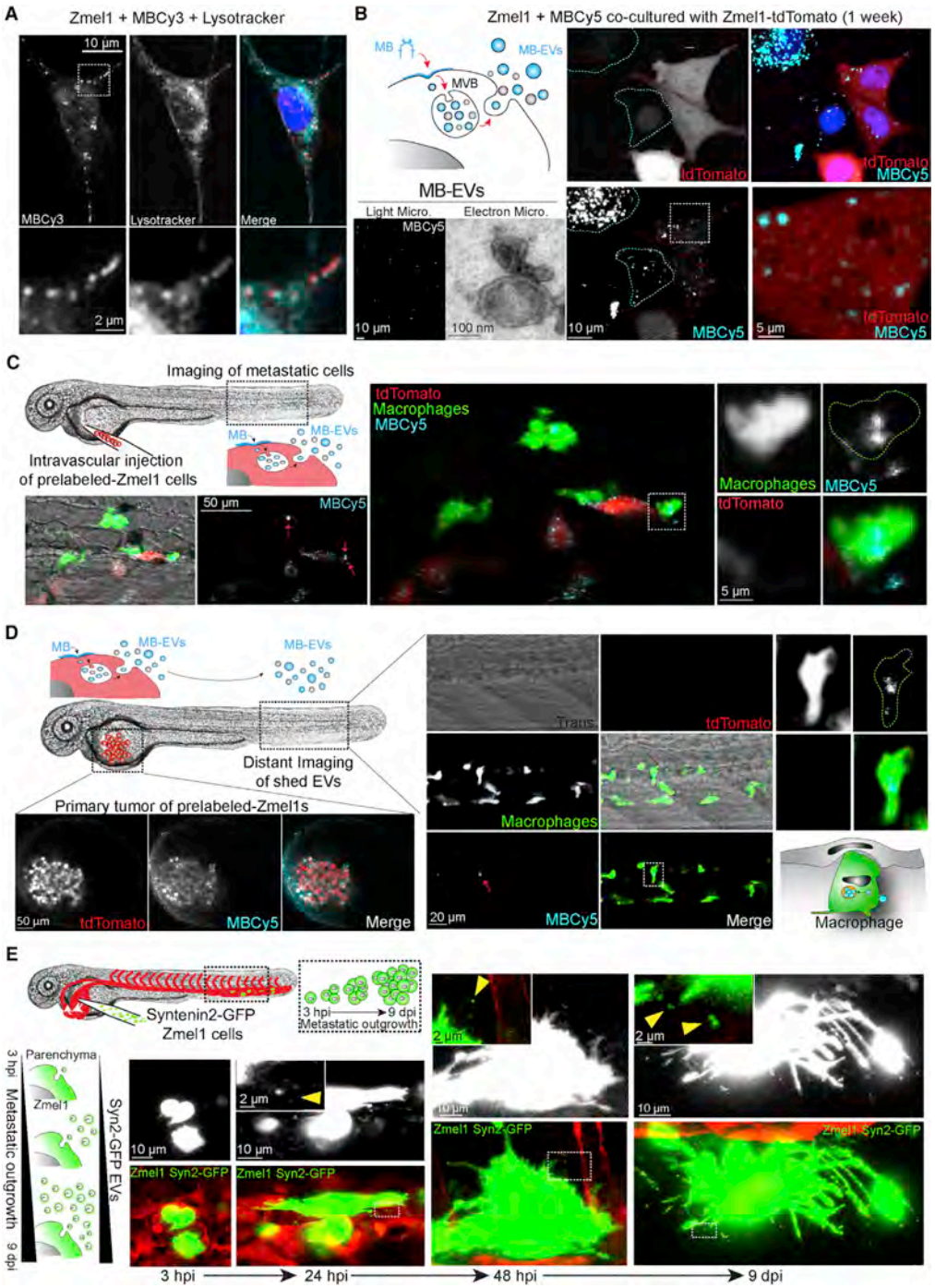

(legend on next page)

through procedures which are simplified compared to the mouse (Goetz et al., 2015; Karreman et al., 2016b). In the future, nanoscale imaging should unravel how tumor EVs secreted by a primary tumor reach the blood circulation before crossing the endothelium when reaching a given organ but also to grasp the details of their uptake and trafficking at a subcellular level.

Here, we show that most tumor EVs are internalized by a subset of macrophages. We consider these cells as functionally similar to murine and human patrolling monocytes for the following reasons: (1) they are positive for the mpeg1 promoter, which is expressed both by monocytes and macrophages in human (Spilsbury et al., 1995), (2) they are small, round and have a slow migration velocity when compared to elongated differentiated macrophages, and (3) they are sending highly dynamic protrusions toward the lumen of the vessels and show areas of direct cell-cell contacts with the endothelial wall, as previously shown (Murayama et al., 2006). These last two aspects match the main characteristics of human and mice patrolling monocytes (Auffray et al., 2007; Carlin et al., 2013). Notably, CLEM analysis reveals that the dynamic protrusions observed in live imaging are actually flat sheets of several microns that scan the vessel lumen and could function as butterfly nets to catch tumor EVs deep in the vessel lumen. Such structures are specific to macrophages, allowing them to internalize fluid-borne objects, unlike neutrophils that only phagocytose surface-bound ones (Colucci-Guyon et al., 2011). Once they have contacted the protrusion, the EVs quickly slide toward the cell body through unknown mechanisms, which could be similar to the filopodia surfing recently described (Heusermann et al., 2016). Those protrusions could also participate in macropinocytic uptake of EVs, similar to what has been observed by microglia (Fitzner et al., 2011). EVs are then internalized at the basis of the protrusions, probably in regions of active endocytosis. Interestingly, our EM data revealed several EVs present at the basis of protrusions (see Figure S4C). Alternatively, circulating EVs can directly bind to the macrophage surface before being endocytosed. The capacity of patrolling macrophages to rapidly uptake circulating EVs explains the very short half-life (10–20 min) of circulating EVs after their injection in the blood circulation of either mouse (Morishita et al., 2015; Saunderson et al., 2014; Takahashi et al., 2013) or zebrafish (our work). This is in agreement with the observation that chemical depletion of monocytes and macrophages in mice dramatically increases the stability of circulating EVs (Imai et al., 2015).

Tumor EVs are then rapidly stored in acidic degradative compartments, similar to what has been described for macrophages *in vitro* (Feng et al., 2010). Determining whether and how internalized EVs deliver signaling molecules to the receiving cell, although they are mostly targeted to degradative compartments, is a central question in the EV field. It will be particularly important to address it in the case of tumor EVs taken up by patrolling macrophages. It is interesting to note that uptake mechanisms and compartments are similar between exogenous tumor EVs (this study) and endogenous EVs (Verweij et al., 2019). This suggests that tumor EVs are internalized using universal mechanisms and further demonstrates that the zebrafish embryo is a perfect model for dissecting such behavior.

In addition, the zebrafish embryo allows a direct comparison of EVs with distinct sizes, contents, or origins. This will be essential to better understand the heterogeneity of EVs, as it is now clear that multiple sub-populations (or sizes) of EVs co-exist with different cargo contents and presumably different functions (Kowal et al., 2016). Co-injection of different types of EVs can, for instance, be used to precisely dissect the involvement of one given EV transmembrane or cargo protein, or to compare tumor EVs from patients at different stages of tumor progression. Using multi-color MemBright probes (Cy3, 5, or 7) to label EVs, it is possible to directly compare the behavior of co-injected populations of EVs. Labeling EVs with membrane probes after their isolation is fast and allows obtaining bright fluorescent EVs regardless of their origin. It is particularly relevant for EVs isolated from cell lines reluctant to gene expression manipulation, from animal body fluids, or, importantly, in the case of tumor EVs from samples of cancer patients. However, the use of membrane probes requires the assurance of labeling specificity. This is particularly essential for studies aiming to track EVs dispersion and uptake, as dye aggregates can easily be confounded with EVs, due to their small sizes (Lai et al., 2015; Takov et al., 2017). Here, using spectroscopic and microscopic approaches, we have shown that the MemBright does not form such fluorescent aggregates, in contrast to commonly used PKH. In addition, it is brighter and can therefore be used at reduced concentrations, minimizing again the risk of false-positive results. The key difference of MemBright from PKH is the presence of amphiphilic groups, which favor efficient transfer of the fluorophore from aqueous media to lipid membranes (Collot et al., 2015; Kucherak et al., 2010). Therefore, MemBright can be used to confidently track EV dispersion and uptake.

Finally, our work demonstrates that zebrafish can be used to dissect the causal relationship between circulating tumor EVs uptake and formation of metastatic niches. While most studies performed in mice demonstrate correlations between bulk injection of EVs and emergence of a pre-metastatic niche, the zebrafish embryo, by allowing continuous imaging, allows direct

Figure 7. Tracking EVs Released by Zebrafish Melanoma Cells

(A) Confocal images of Zmel1 cells incubated with MemBright-Cy3 and stained with LysoTracker.

(B) Schematic representation of the experimental procedure: MemBright added to cells in culture accumulates in MVBs and is subsequently released in exosomes. Such EVs can be observed by electron microscopy. Confocal images of Zmel1 cells pre-labeled with MemBright-Cy5 and co-cultured with Zmel1 tdTomato cells, showing the transfer of MemBright in *Z* projections (left) and single planes (right).

(C) Confocal images of tdTomato Zmel1 cells pre-labeled with MemBright-Cy5 injected in the circulation of *Tg(mpeg1:GFP)* embryos and imaged in the caudal plexus two days post-injection, showing the local transfer of MemBright-Cy5 to macrophages.

(D) Confocal images of tdTomato Zmel1 cells pre-labeled with MemBright Cy5 injected above the yolk of *Tg(mpeg1:GFP)* embryos and imaged in the yolk region (primary tumor, left) and in the caudal plexus (distant imaging of shed EVs, right) two days post-injection, showing the long distance transfer of MemBright-Cy5 to macrophages.

(E) *In vivo* release of Syntenin2-GFP EVs. Zmel1 Syntenin2-GFP cells injected in the circulation of *Tg(Fli:Gal4, UAS:RFP)* embryos and imaged by confocal in the following days.

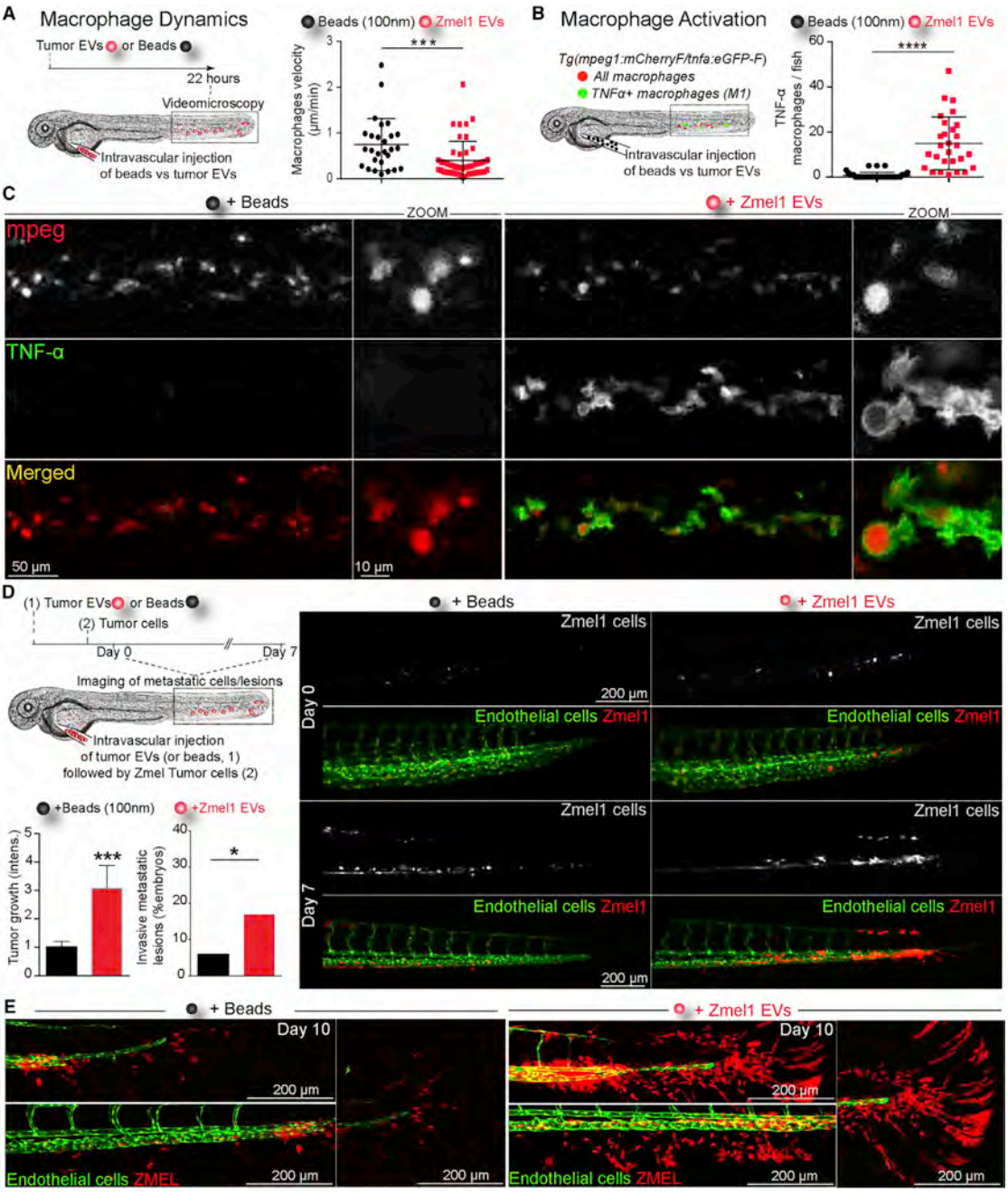

Figure 8. Melanoma EVs Activate Macrophages and Promote Tumor Growth in Zebrafish

(A) 22 h following injection of Zmel1 EVs or 100 nm beads, the dynamics of mpeg1:GFP macrophages was measured by time-lapse. Histogram showing that the velocity of macrophages 22 h after injection (one dot represents one macrophage; mean and standard deviation; $p = 0.0009$, Mann-Whitney test).

(B) *Tg(mpeg1:mCherry/TNFa:eGFP)* injected with Zmel1 EVs or 100 nm beads and imaged 20 h post-injection. Histogram showing the number of TNFa:GFP positive cells per fish caudal plexus (one dot represents one embryo; mean and standard deviation; $p < 0.0001$, Mann-Whitney test).

(C) Confocal images of *Tg(mpeg1:mCherry/TNFa:eGFP)* injected with Zmel1 EVs or 100 nm beads and imaged 20 h post-injection.

(legend continued on next page)

quantitative assessment of how metastatic niches are formed and how they can contribute to metastatic outgrowth. In this work, we show that injection of tumor EVs in the circulation is rapidly followed by expression of TNFα, reminiscent of their activation into a pro-inflammatory "M1-like" phenotype. These results are consistent with *in vitro* studies showing that EVs from breast cancer cells or oral squamous carcinoma cells stimulate an M1 macrophage inflammatory response (including TNF induction) (Xiao et al., 2018; Chow et al., 2014). Other studies, however, show that tumor EVs, for instance from prostate tumors, induce an M2 activation (Halin Bergström et al., 2016). Although the M1/M2 binary polarization model of macrophages has been challenged (Aras and Zaidi, 2017), pro-inflammatory macrophages have been reported to exert pro- or anti-tumoral effects depending on the context (Engblom et al., 2016). Further work is thus needed to better understand how tumor EVs tune macrophages' fate during metastatic progression. Here, the zebrafish model offers the opportunity to revisit the interactions between tumor EVs, macrophages and other immune cells (and their activation status), and tumor cells during extravasation and metastatic outgrowth. Recent work performed in mice, which exploited intravital imaging, revealed close interactions between tumor cells arrested in the circulation and myeloid cells and the exchange of microvesicles promoting extravasation (Headley et al., 2016). Complementary usage of these two models, based on intravital imaging, is thus likely to bring important insights into how tumor EVs can tune metastatic outgrowth.

Importantly, we show that pre-treatment of zebrafish with Zmel1 tumor EVs enhances metastatic outgrowth, leading to a more invasive phenotype. This phenotype is reminiscent of several mice studies showing that pre-injection of EVs from either melanoma, pancreatic ductal adenocarcinoma, or breast tumors promotes metastasis of their respective tumors cells injected in the circulation (Costa-Silva et al., 2015; Hoshino et al., 2015; Plebanek et al., 2017). In Zmel1 EVs pre-treated fish, we also observed that tumor cells were more efficient at actively invading the caudal fin. Such a phenotype could result from increased extravasation efficiency or from EV-mediated increased proliferation. Alternatively, it could arise from tumor EVs that can directly alter the extracellular matrix in pre-metastatic niches (Costa-Silva et al., 2015), or induce the secretion of pro-migratory factors by activated pro-inflammatory macrophages (Xiao et al., 2018).

Altogether, our work on the tracking of exogenous tumor EVs (this study) and of endogenous EVs (Verweij et al., 2019) set the zebrafish embryo as a new and highly attractive *in vivo* model to track EVs at the single EV scale. Interestingly, both studies identified similar mechanisms of transit and uptake for physiological and pathological extracellular vesicles, which further validate the zebrafish embryo as a reliable animal model for studying the biology of EVs. Finally, we believe that the zebrafish embryo will open new avenues for EV biology, as it offers adapted time and space scales to the study of small organelles *in vivo*.

STAR★METHODS

Detailed methods are provided in the online version of this paper and include the following:

- KEY RESOURCES TABLE
- CONTACT FOR REAGENT AND RESOURCE SHARING
- EXPERIMENTAL MODEL AND SUBJECT DETAILS
  - Zmel1, Zmel1 tdTomato and Zmel1 Syntenin2-GFP
  - AB9 Cells
  - 4T1 Cells and 4T1 CD63-GFP
  - B16-F0, F1 and F10
  - 451-LU, SK-Mel28, SK-Mel147, SK-Mel103, WM35 and WM164
  - Zebrafish
- METHOD DETAILS
  - Cell Line Generation
  - EV Isolation and Analysis
  - Shotgun Proteomics
  - Protein Comparisons
  - MemBright and PKH Labeling of EVs
  - Spectroscopy
  - Fluorescence Correlation Spectroscopy (FCS)
  - MemBright Labeling of Cells
  - Intravascular Injection of Zebrafish Embryo
  - Confocal Imaging and Analysis
  - Semi-automated Method to Determine the Proportion of Internalized EVs
  - Quantification of EVs in Aorta vs Vein Regions
  - Flow Analysis for Red Blood Cells
  - Flow Analysis of EVs
  - EVs and RBCs Distance and Velocity from the Endothelial Barrier
  - Sample Preparation for Correlative Light and Electronic Microscopy of ZF Embryos
- QUANTIFICATION AND STATISTICAL ANALYSIS
  - Statistical Tests
  - Zebrafish Experiments
  - EVs Experiments
- DATA AND SOFTWARE AVAILABILITY

SUPPLEMENTAL INFORMATION

Supplemental Information includes five figures, two tables, and seven videos and can be found with this article online at https://doi.org/10.1016/j.devcel.2019.01.014.

ACKNOWLEDGMENTS

We thank all members of the Goetz Lab for helpful discussions. We are indebted to K. Richter and F. Peri (EMBL, Heidelberg, Germany) as well as to P. Hanns and C. Lengerke (University Hospital Basel, Switzerland) for supplying zebrafish embryos. We are grateful to R. White (MSKCC, New York, USA) for the Zmel1 (native and tdTomato) cells, to Dr. D.C. Bennett (St. George's University of London, U.K.) and Dr. M. Soengas (CNIO, Madrid, Spain) for mammalian melanoma cells, and to P. Zimmerman (CRCM,

(D) Zmel1-tdTomato tumor growth is enhanced in *Tg(Fli1:GFP)* embryos that were pre-injected with Zmel1 EVs. Histograms showing tumor growth at 7 days (left; $p = 0.0004$, Mann-Whitney test) and invasive lesions at 10 days (right; $p < 0.05$; chi-squared test). Epifluorescent images of tumor growth in the caudal plexus, right panels.

(E) Confocal images of tumor cell invasion in embryos.

Marseille, France) for the Syntenin-2 construct. We thank A. Michel (EFS, Strasbourg, France) and C. Spiegelhalter (IGBMC, Illkirch, France) for EM assistance, Y.Schwab for advice during CLEM analysis (EMBL, Heidelberg), E. Guiot and Y. Lutz (IGBMC, Illkirch, France) for advice on confocal imaging, and A. Audfray (Malvern Instruments) for NTA. We thank the CNIO proteomics core for performing the mass spectrometry on mouse and human melanoma EVs. We thank P. Herbomel for critical reading of the manuscript. This work was supported by a fellowship from IDEX (University of Strasbourg) to S.G.; by grants from La Ligue contre le Cancer, Canceropole Grand-Est, INCa (MetaCLEM) and Roche to J.G.G.; and by institutional funds from University of Strasbourg, INSERM, and ANR (to CC, French Proteomics Infrastructure ProFI; ANR-10-INBS-08-03).

AUTHOR CONTRIBUTIONS

V.H. and J.G.G. planned the project. V.H. designed and conducted most of the experiments with contributions from S.G., B.M., G.F., M.J.G-L., and J.B. M.C. synthesized the MemBright and led the spectroscopy experiments, with A.S.K. S.H. designed the automated EV tracking and the EV colocalization analysis. O.L. engineered the fluorescent cell lines. F.De., J.B., and C.C. conducted the mass spectrometry on Zmel1 EVs. A.I.A., S.G.S., and H.P. lead the mass spectrometry analysis on human and mice melanoma EVs. F.V. and G.v.N. generated the mass spectrometry data on AB9 and endogenous zebrafish EVs. N.F. prepared the samples for CLEM and P.M. did the serial sectioning and the microCT. F.Dj. provided the *Tg(mpeg:mCherry,tnf:GFP)* zebrafish line and advised its use. L.M. and I.B. performed image analysis. V.H. and J.G.G. wrote the manuscript with insights from all authors.

DECLARATION OF INTERESTS

The authors declare no competing interests.

Received: March 15, 2018
Revised: October 19, 2018
Accepted: January 10, 2019
Published: February 7, 2019

REFERENCES

Al-Nedawi, K., Meehan, B., Micallef, J., Lhotak, V., May, L., Guha, A., and Rak, J. (2008). Intercellular transfer of the oncogenic receptor EGFRvIII by microvesicles derived from tumour cells. Nat. Cell Biol. *10*, 619–624.

Aras, S., and Zaidi, M.R. (2017). TAMeless traitors: macrophages in cancer progression and metastasis. Br. J. Cancer *117*, 1583–1591.

Auffray, C., Fogg, D., Garfa, M., Elain, G., Join-Lambert, O., Kayal, S., Sarnacki, S., Cumano, A., Lauvau, G., and Geissmann, F. (2007). Monitoring of blood vessels and tissues by a population of monocytes with patrolling behavior. Science *317*, 666–670.

Baietti, M.F., Zhang, Z., Mortier, E., Melchior, A., Degeest, G., Geeraerts, A., Ivarsson, Y., Depoortere, F., Coomans, C., Vermeiren, E., et al. (2012). Syndecan–syntenin–ALIX regulates the biogenesis of exosomes. Nat. Cell Biol. *14*, 677–685.

Baran, J., Baj-Krzyworzeka, M., Weglarczyk, K., Szatanek, R., Zembala, M., Barbasz, J., Czupryna, A., Szczepanik, A., and Zembala, M. (2010). Circulating tumour-derived microvesicles in plasma of gastric cancer patients. Cancer Immunol. Immunother. *59*, 841–850.

Beer, K.B., and Wehman, A.M. (2017). Mechanisms and functions of extracellular vesicle release in vivo-what we can learn from flies and worms. Cell Adh. Migr. *11*, 135–150.

Carapito, C., Burel, A., Guterl, P., Walter, A., Varrier, F., Bertile, F., and Van Dorsselaer, A. (2014). MSDA, a proteomics software suite for in-depth mass spectrometry Data Analysis using grid computing. Proteomics *14*, 1014–1019.

Cardona, A., Saalfeld, S., Schindelin, J., Arganda-Carreras, I., Preibisch, S., Longair, M., Tomancak, P., Hartenstein, V., and Douglas, R.J. (2012). TrakEM2 software for neural circuit reconstruction. PLoS One *7*, e38011.

Carlin, L.M., Stamatiades, E.G., Auffray, C., Hanna, R.N., Glover, L., Vizcay-Barrena, G., Hedrick, C.C., Cook, H.T., Diebold, S., and Geissmann, F. (2013). Nr4a1-dependent Ly6C(low) monocytes monitor endothelial cells and orchestrate their disposal. Cell *153*, 362–375.

Chow, A., Zhou, W., Liu, L., Fong, M.Y., Champer, J., Van Haute, D., Chin, A.R., Ren, X., Gugiu, B.G., Meng, Z., et al. (2014). Macrophage immunomodulation by breast cancer-derived exosomes requires Toll-like receptor 2-mediated activation of NF-κB. Sci. Rep. *4*, 5750.

Collot, M., Kreder, R., Tatarets, A.L., Patsenker, L.D., Mely, Y., and Klymchenko, A.S. (2015). Bright fluorogenic squaraines with tuned cell entry for selective imaging of plasma membrane vs. endoplasmic reticulum. Chem. Commun. *51*, 17136–17139.

Collot, M., Ashokkumar, P., Anton, H., Boutant, E., Faklaris, O., Galli, T., Mély, Y., Danglot, L., and Klymchenko, A.S. (2019). MemBright: a family of red to near-infrared fluorescent membrane probes for advanced cellular imaging and neuroscience. Cell Chem. Biol. *26*, https://doi.org/10.1016/j.chembiol.2019.01.009.

Colombo, M., Moita, C., van Niel, G., Kowal, J., Vigneron, J., Benaroch, P., Manel, N., Moita, L.F., Théry, C., and Raposo, G. (2013). Analysis of ESCRT functions in exosome biogenesis, composition and secretion highlights the heterogeneity of extracellular vesicles. J. Cell Sci. *126*, 5553–5565.

Colucci-Guyon, E., Tinevez, J.Y., Renshaw, S.A., and Herbomel, P. (2011). Strategies of professional phagocytes in vivo: unlike macrophages, neutrophils engulf only surface-associated microbes. J. Cell Sci. *124*, 3053–3059.

Costa-Silva, B., Aiello, N.M., Ocean, A.J., Singh, S., Zhang, H., Thakur, B.K., Becker, A., Hoshino, A., Mark, M.T., Molina, H., et al. (2015). Pancreatic cancer exosomes initiate pre-metastatic niche formation in the liver. Nat. Cell Biol. *17*, 816–826.

Cox, J., Hein, M.Y., Luber, C.A., Paron, I., Nagaraj, N., and Mann, M. (2014). Accurate Proteome-wide label-free quantification by delayed normalization and maximal peptide ratio extraction, termed MaxLFQ. Mol. Cell Proteomics *13*, 2513–2526.

Van Deun, J., Mestdagh, P., Sormunen, R., Cocquyt, V., Vermaelen, K., Vandesompele, J., Bracke, M., De Wever, O., and Hendrix, A. (2014). The impact of disparate isolation methods for extracellular vesicles on downstream RNA profiling. J. Extracell. Vesicles *3*, 1–14.

EV-TRACK Consortium, Van Deun, J., Mestdagh, P., Agostinis, P., Akay, Ö., Anand, S., Anckaert, J., Martinez, Z.A., Baetens, T., Beghein, E., et al. (2017). EV-TRACK: transparent reporting and centralizing knowledge in extracellular vesicle research. Nat. Methods *14*, 228–232.

Engblom, C., Pfirschke, C., and Pittet, M.J. (2016). The role of myeloid cells in cancer therapies. Nat. Rev. Cancer *16*, 447–462.

Feng, D., Zhao, W.L., Ye, Y.Y., Bai, X.C., Liu, R.Q., Chang, L.F., Zhou, Q., and Sui, S.F. (2010). Cellular internalization of exosomes occurs through phagocytosis. Traffic *11*, 675–687.

Fitzner, D., Schnaars, M., van Rossum, D., Krishnamoorthy, G., Dibaj, P., Bakhti, M., Regen, T., Hanisch, U.K., and Simons, M. (2011). Selective transfer of exosomes from oligodendrocytes to microglia by macropinocytosis. J. Cell Sci. *124*, 447–458.

Follain, G., Osmani, N., Azevedo, A.S., Allio, G., Mercier, L., Karreman, M.A., Solecki, G., Garcia Leòn, M.J., Lefebvre, O., Fekonja, N., et al. (2018a). Hemodynamic forces tune the arrest, adhesion, and extravasation of circulating tumor cells. Dev. Cell *45*, 33–52.

Follain, G., Osmani, N., Fuchs, C., Allio, G., Harlepp, S., and Goetz, J.G. (2018b). Using the zebrafish embryo to dissect the early steps of the metastatic cascade. Methods Mol. Biol. *1749*, 195–211.

Galindo-Hernandez, O., Villegas-Comonfort, S., Candanedo, F., González-Vázquez, M.C., Chavez-Ocaña, S., Jimenez-Villanueva, X., Sierra-Martinez, M., and Salazar, E.P. (2013). Elevated concentration of microvesicles isolated from peripheral blood in breast cancer patients. Arch. Med. Res. *44*, 208–214.

Goetz, J.G., Steed, E., Ferreira, R.R., Roth, S., Ramspacher, C., Boselli, F., Charvin, G., Liebling, M., Wyart, C., Schwab, Y., et al. (2014). Endothelial cilia mediate low flow sensing during zebrafish vascular development. Cell Rep. *6*, 799–808.

Goetz, J.G., Monduc, F., Schwab, Y., and Vermot, J. (2015). Using correlative light and electron microscopy to study zebrafish vascular morphogenesis. Methods Mol. Biol. *1189*, 31–46.

Grange, C., Tapparo, M., Collino, F., Vitillo, L., Damasco, C., Deregibus, M.C., Tetta, C., Bussolati, B., and Camussi, G. (2011). Microvesicles released from human renal cancer stem cells stimulate angiogenesis and formation of lung premetastatic niche. Cancer Res. *71*, 5346–5356.

Gu, J., Qian, H., Shen, L., Zhang, X., Zhu, W., Huang, L., Yan, Y., Mao, F., Zhao, C., Shi, Y., et al. (2012). Gastric cancer exosomes trigger differentiation of umbilical cord derived mesenchymal stem cells to carcinoma-associated fibroblasts through TGF-β/Smad pathway. PLoS One *7*, e52465.

Le Guyader, D., Redd, M.J., Colucci-Guyon, E., Murayama, E., Kissa, K., Briolat, V., Mordelet, E., Zapata, A., Shinomiya, H., and Herbomel, P. (2008). Origins and unconventional behavior of neutrophils in developing zebrafish. Blood *111*, 132–141.

Halin Bergström, S., Hägglöf, C., Thysell, E., Bergh, A., Wikström, P., and Lundholm, M. (2016). Extracellular vesicles from metastatic rat prostate tumors prime the normal prostate tissue to facilitate tumor growth. Sci. Rep. *6*, 31805.

Hanna, R.N., Cekic, C., Sag, D., Tacke, R., Thomas, G.D., Nowyhed, H., Herrley, E., Rasquinha, N., McArdle, S., Wu, R., et al. (2015). Patrolling monocytes control tumor metastasis to the lung. Science *350*, 985–990.

Headley, M.B., Bins, A., Nip, A., Roberts, E.W., Looney, M.R., Gerard, A., and Krummel, M.F. (2016). Visualization of immediate immune responses to pioneer metastatic cells in the lung. Nature *531*, 513–517.

Heilmann, S., Ratnakumar, K., Langdon, E.M., Kansler, E.R., Kim, I.S., Campbell, N.R., Perry, E.B., McMahon, A.J., Kaufman, C.K., Van Rooijen, E., et al. (2015). A quantitative system for studying metastasis using transparent zebrafish. Cancer Res. *75*, 4272–4282.

Heusermann, W., Hean, J., Trojer, D., Steib, E., von Bueren, S., Graff-Meyer, A., Genoud, C., Martin, K., Pizzato, N., Voshol, J., et al. (2016). Exosomes surf on filopodia to enter cells at endocytic hot spots and shuttle within endosomes to scan the ER. J. Cell Biol. *213*, 173–184.

Hoshino, A., Costa-Silva, B., Shen, T.L., Rodrigues, G., Hashimoto, A., Tesic Mark, M., Molina, H., Kohsaka, S., Di Giannatale, A., Ceder, S., et al. (2015). Tumour exosome integrins determine organotropic metastasis. Nature *527*, 329–335.

Hyenne, V., Lefebvre, O., and Goetz, J.G. (2017). Going live with tumor exosomes and microvesicles. Cell Adh. Migr. *11*, 173–186.

Idrissi, F.Z., and Geli, M.I. (2014). Zooming in on the molecular mechanisms of endocytic budding by time-resolved electron microscopy. Cell. Mol. Life Sci. *71*, 641–657.

Imai, T., Takahashi, Y., Nishikawa, M., Kato, K., Morishita, M., Yamashita, T., Matsumoto, A., Charoenviriyakul, C., and Takakura, Y. (2015). Macrophage-dependent clearance of systemically administered B16BL6-derived exosomes from the blood circulation in mice. J. Extracell. Vesicles *4*, 26238.

Karreman, M.A., Mercier, L., Schieber, N.L., Solecki, G., Allio, G., Winkler, F., Ruthensteiner, B., Goetz, J.G., and Schwab, Y. (2016a). Fast and precise targeting of single tumor cells in vivo by multimodal correlative microscopy. J. Cell Sci. *129*, 444–456.

Karreman, M.A., Hyenne, V., Schwab, Y., and Goetz, J.G. (2016b). Intravital correlative microscopy: imaging life at the nanoscale. Trends Cell Biol. *26*, 848–863.

Kowal, J., Arras, G., Colombo, M., Jouve, M., Morath, J.P., Primdal-Bengtson, B., Dingli, F., Loew, D., Tkach, M., and Théry, C. (2016). Proteomic comparison defines novel markers to characterize heterogeneous populations of extracellular vesicle subtypes. Proc. Natl. Acad. Sci. USA *113*, E968–E977.

Kucherak, O.A., Oncul, S., Darwich, Z., Yushchenko, D.A., Arntz, Y., Didier, P., Mély, Y., and Klymchenko, A.S. (2010). Switchable Nile red-based probe for cholesterol and lipid order at the outer leaflet of biomembranes. J. Am. Chem. Soc. *132*, 4907–4916.

Lai, C.P., Mardini, O., Ericsson, M., Prabhakar, S., Maguire, C.A., Chen, J.W., Tannous, B.A., and Breakefield, X.O. (2014). Dynamic biodistribution of extracellular vesicles in vivo using a multimodal imaging reporter. ACS Nano *8*, 483–494.

Lai, C.P., Kim, E.Y., Badr, C.E., Weissleder, R., Mempel, T.R., Tannous, B.A., and Breakefield, X.O. (2015). Visualization and tracking of tumour extracellular vesicle delivery and RNA translation using multiplexed reporters. Nat. Commun. *6*, 7029.

Liu, Y., Gu, Y., Han, Y., Zhang, Q., Jiang, Z., Zhang, X., Huang, B., Xu, X., Zheng, J., and Cao, X. (2016). Tumor exosomal RNAs promote lung pre-metastatic niche formation by activating alveolar epithelial TLR3 to recruit neutrophils. Cancer Cell *30*, 243–256.

Logozzi, M., De Milito, A., Lugini, L., Borghi, M., Calabrò, L., Spada, M., Perdicchio, M., Marino, M.L., Federici, C., Iessi, E., et al. (2009). High levels of exosomes expressing CD63 and caveolin-1 in plasma of melanoma patients. PLoS One *4*, e5219.

Magde, D., Rojas, G.E., and Seybold, P.G. (1999). Solvent dependence of the fluorescence lifetimes of xanthene dyes. Photochem. Photobiol. *70*, 737–744.

Morishita, M., Takahashi, Y., Nishikawa, M., Sano, K., Kato, K., Yamashita, T., Imai, T., Saji, H., and Takakura, Y. (2015). Quantitative analysis of tissue distribution of the B16BL6-derived exosomes using a streptavidin-lactadherin fusion protein and iodine-125-Labeled biotin derivative after intravenous injection in mice. J. Pharm. Sci. *104*, 705–713.

Müller, P., Schwille, P., and Weidemann, T. (2014). PyCorrFit - generic data evaluation for fluorescence correlation spectroscopy. Bioinformatics *30*, 2532–2533.

Murayama, E., Kissa, K., Zapata, A., Mordelet, E., Briolat, V., Lin, H.F., Handin, R.I., and Herbomel, P. (2006). Tracing hematopoietic precursor migration to successive hematopoietic organs during zebrafish development. Immunity *25*, 963–975.

Nguyen-Chi, M., Laplace-Builhe, B., Travnickova, J., Luz-Crawford, P., Tejedor, G., Phan, Q.T., Duroux-Richard, I., Levraud, J.P., Kissa, K., Lutfalla, G., et al. (2015). Identification of polarized macrophage subsets in zebrafish. Elife *4*, e07288.

van Niel, G., D'Angelo, G., and Raposo, G. (2018). Shedding light on the cell biology of extracellular vesicles. Nat. Rev. Mol. Cell Biol. *19*, 213–228.

Okabayashi, S., and Kimura, N. (2010). LGI3 interacts with flotillin-1 to mediate APP trafficking and exosome formation. NeuroReport *21*, 606–610.

Oliveros, J.C. (2007). VENNY. An Interactive Tool for Comparing Lists with Venn Diagrams. BioinfoGP of CNB-CSIC, http://bioinfogp.cnb.csic.es/tools/venny/.

Ostrowski, M., Carmo, N.B., Krumeich, S., Fanget, I., Raposo, G., Savina, A., Moita, C.F., Schauer, K., Hume, A.N., Freitas, R.P., et al. (2010). Rab27a and Rab27b control different steps of the exosome secretion pathway. Nat. Cell Biol. *12*, 19–30.

Paggetti, J., Haderk, F., Seiffert, M., Janji, B., Distler, U., Ammerlaan, W., Kim, Y.J., Adam, J., Lichter, P., Solary, E., et al. (2015). Exosomes released by chronic lymphocytic leukemia cells induce the transition of stromal cells into cancer-associated fibroblasts. Blood *126*, 1106–1117.

Peinado, H., Aleckovic, M., Lavotshkin, S., Matei, I., Costa-Silva, B., Moreno-Bueno, G., Hergueta-Redondo, M., Williams, C., García-Santos, G., Ghajar, C.M., et al. (2012). Melanoma exosomes educate bone marrow progenitor cells toward a pro-metastatic phenotype through MET. Nat. Med. *18*, 883–891.

Peinado, H., Zhang, H., Matei, I.R., Costa-Silva, B., Hoshino, A., Rodrigues, G., Psaila, B., Kaplan, R.N., Bromberg, J.F., Kang, Y., et al. (2017). Pre-metastatic niches: organ-specific homes for metastases. Nat. Rev. Cancer *17*, 302–317.

Plebanek, M.P., Angeloni, N.L., Vinokour, E., Li, J., Henkin, A., Martinez-Marin, D., Filleur, S., Bhowmick, R., Henkin, J., Miller, S.D., et al. (2017). Pre-metastatic cancer exosomes induce immune surveillance by patrolling monocytes at the metastatic niche. Nat. Commun. *8*, 1319.

Pucci, F., Garris, C., Lai, C.P., Newton, A., Pfirschke, C., Engblom, C., Alvarez, D., Sprachman, M., Evavold, C., Magnuson, A., et al. (2016). SCS macrophages suppress melanoma by restricting tumor-derived vesicle-B cell interactions. Science *1328*, 242–246.

Raposo, G., and Stoorvogel, W. (2013). Extracellular vesicles: exosomes, microvesicles, and friends. J. Cell Biol. *200*, 373–383.

Roh-Johnson, M., Shah, A.N., Stonick, J.A., Poudel, K.R., Kargl, J., Yang, G.H., di Martino, J., Hernandez, R.E., Gast, C.E., Zarour, L.R., et al. (2017). Macrophage-dependent cytoplasmic transfer during melanoma invasion in vivo. Dev. Cell *43*, 549–562.e6.

Saunderson, S.C., Dunn, A.C., Crocker, P.R., and McLellan, A.D. (2014). CD169 mediates the capture of exosomes in spleen and lymph node. Blood *123*, 208–216.

Schindelin, J., Arganda-Carreras, I., Frise, E., Kaynig, V., Longair, M., Pietzsch, T., Preibisch, S., Rueden, C., Saalfeld, S., Schmid, B., et al. (2012). Fiji: an open-source platform for biological-image analysis. Nat. Methods *9*, 676–682.

Spilsbury, K., O'Mara, M.A., Wu, W.M., Rowe, P.B., Symonds, G., and Takayama, Y. (1995). Isolation of a novel macrophage-specific gene by differential cDNA analysis. Blood *85*, 1620–1629.

Stoletov, K., Kato, H., Zardouzian, E., Kelber, J., Yang, J., Shattil, S., and Klemke, R. (2010). Visualizing extravasation dynamics of metastatic tumor cells. J. Cell Sci. *123*, 2332–2341.

Takahashi, Y., Nishikawa, M., Shinotsuka, H., Matsui, Y., Ohara, S., Imai, T., and Takakura, Y. (2013). Visualization and in vivo tracking of the exosomes of murine melanoma B16-BL6 cells in mice after intravenous injection. J. Biotechnol. *165*, 77–84.

Takov, K., Yellon, D.M., and Davidson, S.M. (2017). Confounding factors in vesicle uptake studies using fluorescent lipophilic membrane dyes. J. Extracell. Vesicles *6*, 1388731.

Taylor, M.J., Perrais, D., and Merrifield, C.J. (2011). A high precision survey of the molecular dynamics of mammalian clathrin-mediated endocytosis. PLoS Biol. *9*, e1000604.

Théry, C., Amigorena, S., Raposo, G., and Clayton, A. (2006). Isolation and characterization of exosomes from cell culture supernatants. Curr. Protoc. Cell Biol. 3.22.1–3.22.29.

Thomas, P.D., Campbell, M.J., Kejariwal, A., Mi, H., Karlak, B., Daverman, R., Diemer, K., Muruganujan, A., and Narechania, A. (2003). PANTHER: A library of protein families and subfamilies indexed by function. Genome Res. *13*, 2129–2141.

Verweij, F., Revenu, C., Arras, G., Dingli, F., Loew, D., Pegtel, M., Follain, G., Allio, G., Goetz, J.G., Zimmermann, P., et al. (2019). Live tracking of inter-organ communication by endogenous exosomes in vivo. Dev. Cell *48*. Published online February 7, 2019. https://doi.org/10.1016/j.devcel.2019.01.004.

Vogel, D.Y.S., Heijnen, P.D.A.M., Breur, M., de Vries, H.E., Tool, A.T.J., Amor, S., and Dijkstra, C.D. (2014). Macrophages migrate in an activation-dependent manner to chemokines involved in neuroinflammation. J. Neuroinflamm. *11*, 1–11.

Van Der Vos, K.E., Abels, E.R., Zhang, X., Lai, C., Carrizosa, E., Oakley, D., Prabhakar, S., Mardini, O., Crommentuijn, M.H.W., Skog, J., et al. (2016). Directly visualized glioblastoma-derived extracellular vesicles transfer RNA to microglia/macrophages in the brain. Neuro. Oncol. *18*, 58–69.

White, R., Rose, K., and Zon, L. (2013). Zebrafish cancer: the state of the art and the path forward. Nat. Rev. Cancer *13*, 624–636.

Whiteside, T.L. (2016). Exosomes and tumor-mediated immune suppression. J. Clin. Invest. *126*, 1216–1223.

Würthner, F., Kaiser, T.E., and Saha-Möller, C.R. (2011). J-aggregates: From serendipitous discovery to supramolecular engineering of functional dye materials. Angew. Chem. Int. Ed. *50*, 3376–3410.

Xiao, M., Zhang, J., and Chen, W., Chen W. (2018). M1-like tumor-associated macrophages activated by exosome-transferred THBS1 promote malignant migration in oral squamous cell carcinoma. J. Exp. Clin. Cancer Res. *37*, 1–15.

Zomer, A., Maynard, C., Verweij, F.J., Kamermans, A., Schäfer, R., Beerling, E., Schiffelers, R.M., De Wit, E., Berenguer, J., Ellenbroek, S.I.J., et al. (2015). In vivo imaging reveals extracellular vesicle-mediated phenocopying of metastatic behavior. Cell *161*, 1046–1057.

Please cite this article in press as: Hyenne et al., Studying the Fate of Tumor Extracellular Vesicles at High Spatiotemporal Resolution Using the Zebrafish Embryo, Developmental Cell (2019), https://doi.org/10.1016/j.devcel.2019.01.014

CellPress

STAR★METHODS

KEY RESOURCES TABLE

REAGENT OR RESOURCE	SOURCE	IDENTIFIER
Chemicals, Peptides and Recombinant proteins		
MemBright	Collot et al. (2019)	N/A
PKH-26	Sigma-Aldrich	MINI26
100nm fluorescent beads	Phosphorex	2211
Antibodies		
Mouse monoclonal anti-Alix antibody	BD Biosciences	Cat# 611621; RRID: AB_2236941
Mouse monoclonal anti-TSG-101 antibody	GeneTex	Cat# GTX70255; RRID: AB373239
Anti-mouse IgG coupled to HRP	Fisher scientific	Cat# NC9491974
Deposited Data		
EV related experimental details	EV-track consortium	EV180078
EV proteomics	Exocarta	TBD
Experimental Models: Cell lines		
Zmel1	White lab (MSKCC)	N/A
Zmel1 tdTomato	White lab (MSKCC)	N/A
Zmel1 Syntenin2-GFP	This paper	N/A
AB9	ATCC	ATCC-CRL-2298
4T1		RRID: CVCL_0125
4T1 CD63-GFP	This paper	N/A
B16F0	ATCC	ATCC CRL-6322; RRID: CVCL_0604
B16F1	ATCC	ATCC CRL-6323; RRID: CVCL_0158
B16F10	ATCC	ATCC CRL-6475; RRID: CVCL_0159
451-LU	Soengas lab (CNIO)	RRID: CVCL_6357
SK-Mel28	Soengas lab (CNIO)	RRID: CVCL_0526
SK-Mel147	Soengas lab (CNIO)	RRID: CVCL_3876
SK-Mel103	Soengas lab (CNIO)	RRID: CVCL_6069
WM35	Soengas lab (CNIO)	RRID: CVCL_0580
WM164	Soengas lab (CNIO)	RRID: CVCL_7928
Experimental Models: Organisms/strains		
Zebrafish: *Tg(Fli1a:eGFP)*	Peri lab; EMBL zebrafish facility	N/A
Zebrafish: *Tg(mpeg1a:eGFP)*	Lengerke lab; Basel University zebrafish facility	N/A
Zebrafish: *Tg(mpo:eGFP)*	Lengerke lab; Basel University zebrafish facility	N/A
Zebrafish: *Tg(Fli1a:Gal4; UAS:RFP)*	Lengerke lab; Basel University zebrafish facility	N/A
Zebrafish: Casper *Tg(Flk:eGFP; Gata1:RFP)*	Vermot lab; IGBMC zebrafish facility	N/A
Zebrafish: *Tg(mpeg1:mCherry; TNFa:eGFP)*	Djouad lab; IRMB zebrafish facility	N/A
Recombinant DNA		
pSyntenin2-eGFP	Zimmermann lab (CRCM)	N/A
pCS2 Zf-Syntenin2-eGFP	This paper	N/A
pLenti CMV-CD63-AcGFP	This paper	N/A
Software and Algorithms		
Fiji / Image J	NIH	N/A
IMOD	University of Colorado	N/A
Amira for Life Sciences	ThermoFisher Scientific	N/A
GraphPad PRISM	GraphPad Software	N/A
MaxQuant	Max Planck Institute of Biochemistry	N/A
PyCorrFit software	Max Planck Institute of Biochemistry	N/A

(*Continued on next page*)

Continued

REAGENT OR RESOURCE	SOURCE	IDENTIFIER
Other		
Transmitted electron microscope CM12	Philips	N/A
Transmitted electron microscope CM120	Philips	N/A
Biotwin CM120 (FEI) TEM	Philips	
Nanosight NS300	Malvern Instruments	N/A
ZetaView	Particle Metrix	N/A
NanoAcquity UPLC device	Waters	N/A
NanoLC-Ultra 1D+ system	Eksigent	N/A
Cary 400 Scan ultraviolet–visible spectrophotometer	Varian	N/A
FluoroMax-4 spectrofluorometer	Horiba Jobin Yvon	N/A
M205 FA stereomicroscope	Leica	N/A
Inverted TCS SP5 confocal microscope	Leica	N/A
Upright SP8 confocal microscope	Leica	N/A

CONTACT FOR REAGENT AND RESOURCE SHARING

Further information and requests for resources and reagents should be directed to and will be fulfilled by the Lead Contact, Vincent Hyenne (hyenne@unistra.fr).

EXPERIMENTAL MODEL AND SUBJECT DETAILS

Zmel1, Zmel1 tdTomato and Zmel1 Syntenin2-GFP

Zebrafish melanoma Zmel1 and Zmel1 td Tomato Kindly provided by Richard White (Memorial Sloan Kettering Cancer Center, New York) (Heilmann et al., 2015). Zmel1 Syntenin2-GFP generated in the laboratory. Culture condition: 28°C, 5% CO_2. DMEM high glucose (HG), 10% FBS, 1% NEAA-MEM, 1% penicillin-streptomycin.

AB9 Cells

Zebrafish fibroblasts obtained from the caudal fin of an adult AB strain zebrafish (ATCC CRL-2298). Culture condition: 28°C, 5% CO_2. DMEM HG, 10% FBS, 1% NEAA-MEM, 1% Penstrep.

4T1 Cells and 4T1 CD63-GFP

Mouse mammary gland carcinoma (BALB/c female) (CVCL_0125). 4T1 CD63-GFP generated in the laboratory. Culture condition: 37°C, 5%CO_2. RPMI 1640 with 10% FBS, 1% penicillin-streptomycin. Authentication: Injection in the nipple of mammary gland of BALB/c mice lead to mammary tumor.

B16-F0, F1 and F10

Mouse melanoma cell lines, purchased from ATCC (ATCC CRL-6322; ATCC CRL-6323; ATCC CRL-6475). Culture condition: 37°C, 5%CO_2. DMEM supplemented with 10% (v/v) EV-depleted fetal bovine serum (EV-d-FBS), glutamine 2mM and gentamicin

451-LU, SK-Mel28, SK-Mel147, SK-Mel103, WM35 and WM164

Human melanoma cells, kindly provided by Dr. M. Soengas (CNIO, Madrid). Culture condition: 37°C, 5%CO_2. DMEM with 10% EV-d-FBS.

Zebrafish

Zebrafish embryos were obtained from the following strains: *Tg(fli1a:eGFP), Tg(mpeg1:eGFP)*, *Tg(mpo:eGFP), Tg(Fli1:Gal4; UAS:RFP), Casper Tg(Gata1:RFP; flk:GFP), Tg(mpeg:mCherry*; TNF-α:GFP). Embryos were grown in our laboratory or kindly provided by F. Peri's (EMBL, Heidelberg, Germany) and C. Lengerke's laboratories (University Hospital Basel, Switzerland). Embryos were maintained at 28° in Danieau 0.3X medium, supplemented with 1-Phenyl-2-thiourea (Sigma-Aldrich) after 24 h post fertilization (hpf). For all Zebrafish experiments, the offspring of one single cross was selected, based on anatomical/developmental good health. Embryos were split randomly between experimental groups. All injection experiments were carried at 48 hpf and imaged between 48 hpf and 72 hpf. All animal procedures were performed in accordance with French and European Union animal welfare guidelines and supervised by local ethics committee (Animal facility #A6748233; APAFIS #2018092515234191).

METHOD DETAILS

Cell Line Generation

To generate Zmel1 cells expressing Syntenin2-GFP, Syntenin2 (a gift from P.Zimmerman) was first cloned in pCS2 eGFP Ires Blast vector. Then, 2 millions of Zmel dark cells were transfected with 2 μg of plasmid pCS2 Zf-Syntenin2-eGFP Ires Blast cut with NotI using 4 μl of JetPrime according to manufactory instructions (PolyPlus, Illkirch, France). After 1 week, cells with stable integration of the construct were selected using 4μg/ml of blasticidin (Sigma Aldrich, St. Quentin Fallavier, France). 4T1 cells expressing CD63-GFP were generated as follows. Briefly, human CD63 cDNA was fused to AcGFP cDNA by In-Fusion cloning (Takara, Ozyme, Saint-Quentin-en-Yvelines, France) and introduced in pLenti CMV-MABBXXS mPGK-Blast vector. Lentiviruses were obtained by HEK293T cells (ATCC CRL-3216; cultured in DMEM, 10% FCS, 1% penicillin-streptomycin) transfection (Invitrogen, Life Technologies, Saint Aubin, France) with pLenti CMV-CD63-acGFP mPGK-Blast together with pLP1, pLP2 and pLP/VSVG lentiviral packaging plasmids to obtain lentiviral particles. After 48 hours, conditioned media was collected, filtered through a 0.22 μm filter to remove cell debris, and used to transduce 4T1 cells cultured in DMEM supplemented with 10% fetal calf serum and 1% penicillin-streptomycin (Gibco, USA) in the presence of 5μg/mL polybrene (Sigma Aldrich, Lyon, France), followed by selection with puromycin (1 μg/mL, Sigma Aldrich, Lyon, France). Human blood was collected from healthy donors using 3.8% (v/v) sodium citrate (1:9) as anticoagulant. Human erythrocyte rich pellet was obtained by centrifugation at 250 rpm during 15 minutes at room temperature.

EV Isolation and Analysis

For Zmel1 and 4T1 EVs isolation, cells were cultured in EV depleted medium (obtained by overnight ultracentrifugation at 100,000g, using a Beckman, XL-70 centrifuge with a Ti70 rotor) for 24h before supernatant collection. Extracellular medium was concentrated using a Centricon Plus-70 centrifugal filter (10k; Millipore) and EVs were isolated by successive centrifugation at 4°C: 5 minutes at 300 g, 10 minutes at 2,000 g, 30 minutes at 10,000 g and 70 minutes at 100,000 g (using a Beckman XL-70 centrifuge with a SW28 rotor). EVs pellets were washed in PBS, centrifuged again at 100,000 g for 70 minutes, resuspended in PBS and stored at 4°C. For *in vivo* experiments, EVs were used immediately after isolation or kept 4°C at and used the next day.

For mouse and human melanoma EVs isolation, cells were cultured in media supplemented with 10% EV-depleted FBS (FBS, Hyclone). FBS was depleted of bovine EVs by ultracentrifugation at 100,000xg for 70 min. EVs were isolated from conditioned media collected after 72 h of cell cultures by successive centrifugation at 10°C: 5 minutes at 300 g, 10 minutes at 500 g, 20 minutes at 12,000 g and 70 minutes at 100,000 g (using a Beckman Optima X100 with a Beckman 70Ti rotor). EVs pellets were washed in PBS, centrifuged again at 100,000 g for 70 minutes, and resuspended in PBS. Protein content was measured by bicinchoninic acid assay (BCA assay).

For transmitted electron microscopy analysis, 3 μl of EV extracts were allowed to dry on formvar coated grids for 20 minutes, fixed in 3% PFA for 10 minutes, rinsed in water and contrasted in a uranyl acetate (0,4%)/ methylcellulose (2%) mix for 10 minutes on ice. EVs were observed either with an Orius 100 charge-coupled device camera (Gatan) mounted on a Philips CM12 microscope operated at 80kV or with a Veleta 2kx2k side-mounted TEM CDD Camera (Olympus Soft Imaging Solutions) mounted on a Philips CM120 microscope operated at 120kV.

NTA was performed on Zmel1 EVs diluted 10 times with sterile PBS, using a Nanosight NS300 (Malvern Instruments) or a ZetaView (Particle Metrix). The measurement was repeated three times.

For density gradient analysis, EVs isolated in the 100,000 g pellet were loaded on top of a 5-40% iodixanol (Optiprep) density gradient prepared as previously described (Van Deun et al., 2014). The gradient was centrifuged for 18 hours at 100,000g and 4°C (using a Beckman XL-70 centrifuge with a SW28 rotor). Gradient fractions of 1ml were collected from the top of the gradient. Fractions 1 to 4, 5 to 10 and 11 to 16 were pooled, diluted to 16 ml in PBS and centrifuged for 3 hours at 100,000g and 4°C. The resulting pellet was resuspended in 50 μl of PBS. For western blotting analysis, 10 μl of EV extracts were loaded on 4-20% polyacrylamide gels (Biorad), under denaturing conditions. The following antibodies were used: Alix (BD Biosciences 611621) and TSG101 (GeneTex GTX70255). Acquisitions were done using a PXi system (Syngene).

Shotgun Proteomics

Sample Preparation of Zmel1 EVs Protein Content

After having determined protein concentration (RC-DC™; Bio-Rad, Hercules, CA), 20 μg samples were denaturated at 95°C for 5 min in Laemmli buffer and then concentrated in one stacking band using a 5% SDS-PAGE gel. The gel was fixed with 50% ethanol/3% phosphoric acid and stained with colloidal Coomassie Brilliant Blue. Each band was excised, cut in five pieces, and transferred into a 96-well microtiter plate. Gel slices were washed with 3 cycles of incubations in 100 μL of 50:50 (v/v) 25 mM NH_4HCO_3/ACN for 10 min. Gel bands were then dehydrated with 50 μL 100% ACN and then reduced with 50 μL 10 mM DTT for 30 min at 60°C, followed by 30 min at RT. Proteins were then alkylated with 50 μL 55 mM iodoacetamide for 20 min in the dark at RT, and then 100 μL ACN were added for 5 min. Samples were washed with 50 μL 25 mM NH_4HCO_3 for 10 min, and then 50 μL ACN for 5 min, before being dehydrated with two cycles of incubations in 50 μL ACN for 5 min. Proteins were digested overnight with a modified porcine trypsin (Promega, Madison, WI) solution at a 1:100 (w/w) enzyme/protein ratio at 37°C. Tryptic peptides were extracted under agitation at RT with 60 μL 60% ACN/0.1% FA for 45 min, and then 100% ACN for 10 min. The extraction supernatants were pooled and vacuum-dried, before re-suspension in 40 μL 2% ACN/0.1% FA.

Nano-LC-MS/MS Analysis of Zmel1 EVs Protein Content

Nano-LC-MS/MS analysis was performed on a nanoAcquity UPLC device (Waters, Milford, MA) coupled to a Q-Exactive Plus mass spectrometer (Thermo Fisher Scientific, Bremen, Germany). The solvents consisted of 0.1% FA in H_2O (solvent A) and 0.1% in ACN (solvent B). 1 μL of the samples was loaded onto a Symmetry C18 pre-column (20 mm × 180 μm, 5 μm diameter particles; Waters, Milford, MA) over 3 min at 5 μL/min with 1% solvent B. Peptides were eluted on a Acquity UPLC BEH130 C18 column (250 mm × 75 μm, 1.7 μm particles; Waters, Milford, MA) at 450 μL/min with the following gradient of solvent B: linear from 1% to 8 % in 2 min, linear from 8% to 35% in 77 min, linear from 35% to 90% in 1 min, isocratic at 90% for 5 min, down to 1% in 2 min, isocratic at 1% for 2 min.

The Q-Exactive Plus was operated in data-dependent acquisition mode by automatically switching between full MS and consecutive MS/MS acquisitions. Full-scan MS spectra were collected from 300-1,800 m/z at a resolution of 70,000 at 200 m/z with an automatic gain control target fixed at 3×10^6 ions and a maximum injection time of 50 ms. The top 10 precursor ions with an intensity exceeding 2×10^5 ions and charge states ≥ 2 were selected on each MS spectrum for fragmentation by higher-energy collisional dissociation. MS/MS spectra were collected at a resolution of 17,500 at 200 m/z with a fixed first mass at 100 m/z, an automatic gain control target fixed at 1×10^5 ions and a maximum injection time of 100 ms. A dynamic exclusion time was set to 60 s.

Sample Preparation of Mammalian EVs Cargo

Proteins were solubilized using 8 M urea in 100 mM Tris-HCl pH 8.0. Samples (7.5 μg) were digested by means of the standard FASP protocol. Briefly, proteins were reduced (10 mM DTT, 30 min, RT), alkylated (55 mM IA, 20 min in the dark, RT) and sequentially digested with Lys-C (Wako) (protein:enzyme ratio 1:50, o/n at RT) and trypsin (Promega) (protein:enzyme ratio 1:100, 6 h at 37° C). Resulting peptides were desalted using C_{18} stage-tips.

Nano-LC-MS/MS Analysis of Mammalian EVs Cargo

LC-MS/MS was done by coupling a nanoLC-Ultra 1D+ system (Eksigent) to a LTQ Orbitrap Velos mass spectrometer (Thermo Fisher Scientific) via a Nanospray Flex source (Thermo Fisher Scientific). Peptides were loaded into a trap column (NS-MP-10 BioSphere C18 5 μm, 20 mm length, Nanoseparations) for 10 min at a flow rate of 2.5 μl/min in 0.1% FA. Then peptides were transferred to an analytical column (ReproSil Pur C18-AQ 2.4 μm, 500 mm length and 0.075 mm ID) and separated using a 120 min linear gradient (buffer A: 4% ACN, 0.1% FA; buffer B: 100% ACN, 0.1% FA) at a flow rate of 250 nL/min. The gradient used was: 0-2 min 6% B, 2-103 min 30% B, 103-113 min 98% B, 113-120 min 2% B. The peptides were electrosprayed (1.8 kV) into the mass spectrometer with a PicoTip emitter (360/20 Tube OD/ID μm, tip ID 10 μm) (New Objective), a heated capillary temperature of 325°C and S-Lens RF level of 60%. The mass spectrometer was operated in a data-dependent mode, with an automatic switch between MS and MS/MS scans using a top 15 method (threshold signal $\geq$ 800 counts and dynamic exclusion of 60 s). MS spectra (350-1500 m/z) were acquired in the Orbitrap with a resolution of 60,000 FWHM (400 m/z). Peptides were isolated using a 1.5 Th window and fragmented using collision induced dissociation (CID) with linear ion trap read out at a NCE of 35% (0.25 Q-value and 10 ms activation time). The ion target values were 1E6 for MS (500 ms max injection time) and 5000 for MS/MS (100 ms max injection time).

Nano-LC-MS/MS Data Interpretation

Raw files were processed with MaxQuant (versions 1.6.0.16) (Cox et al., 2014) against an in-house concatenated *Danio rerio-Bos taurus* (UniProtKB, February 2017, 90,922 entries) supplemented with contaminants for Zmel1 EVs proteins and generated with the database toolbox from MSDA (Carapito et al., 2014), or a human protein database (UniProtKB/Swiss-Prot, August 2014, 20,187 sequences) supplemented with contaminants for mammalian EVs cargo. Label-free quantification was done with the match between runs option activated (match window of 0.7 min and alignment window of 20 min). Carbamidomethylation of cysteines was set as a fixed modification whereas oxidation of methionines and protein N-term acetylation were set as variable modifications. Minimal peptide length was set to 7 amino acids and a maximum of two tryptic missed-cleavages were allowed.

Protein Comparisons

To compare the Zmel1 protein content with mammalian EV content, each protein list was concatenated and duplicate proteins were deleted. Ortholog proteins were searched using the ortholog protein files predicted by the PANTHER classification system (ftp://ftp.pantherdb.org/ortholog/13.0/ (Thomas et al., 2003)). Only proteins referred as "Least diverged ortholog" or "Ortholog" were considered. All comparisons between Zmel1 EVs and mammalian EVs were done using human orthologs and the lists of common proteins was obtained using Venny 2.1 (Oliveros, 2007).

MemBright and PKH Labeling of EVs

Isolated EVs were incubated with MemBright-Cy3 or Cy5 at 200nM (final concentration) in PBS for 30 minutes at room temperature in the dark. They were then rinsed in 15ml of PBS and centrifuged at 100,000g with a SW28 rotor in a Beckman XL-70 centrifuge. Pellets were resuspended in 50 μl PBS and stored at 4°C. For *in vivo* experiments, EVs were used immediately after isolation or stored overnight at 4°C and injected the next day. For PKH-26 labeling EVs were treated according to the manufacturer's instructions (2 μM final concentration). Briefly, EVs in 200 μl of PBS were first mixed with 300 μl of Diluent C, then with 500μl of Diluent C containing 4 μl of PKH and finally incubated for 30 minutes at room temperature in the dark. PKH labeled EVs were then processed as MemBright labeled EVs. As a control, PBS alone was processed similarly to EVs, labeled with MemBright or PKH and analysed by microscopy or spectroscopy.

For photonic microscopy analysis, 3 μl of labeled EV extracts were allowed to settle on poly-L lysine coated coverslips and then imaged on a Zeiss Imager Z2 with a 63X objective (N.A. 1.4) or with a SP5 confocal (Leica) with a 40X objective (N.A. 1.25).

Spectroscopy

EVs labeled with either MemBright-Cy3 or PKH-26, or control MemBright-Cy3 or control PKH (diluted in PBS as described above), as well as the dyes directly diluted in Milli-Q water (Millipore) or ethanol were analyzed by spectroscopy. Absorption and emission spectra were recorded at 20°C in quartz cuvettes on a Cary 400 Scan ultraviolet–visible spectrophotometer (Varian) and a FluoroMax-4 spectrofluorometer (Horiba Jobin Yvon) equipped with a thermostated cell compartment, respectively. For standard recording of fluorescence spectra, excitation was at 520 nm and the emission was collected 10 nm after the excitation wavelength (530 nm to 700 nm). All the spectra were corrected from wavelength-dependent response of the detector. The scattering due to the EVs was corrected with a baseline correction using Origin software. Quantum yields were determined using rhodamine B in water (QY= 0.31) as a reference (Magde et al., 1999).

Fluorescence Correlation Spectroscopy (FCS)

To characterize the size of PKH aggregates, FCS measurements were performed on PKH26 (diluted at 5 μM) using a home-built confocal set-up based on a Nikon inverted microscope with a Nikon 60x 1.2NA water immersion objective. Excitation was provided by a cw laser diode (532 nm, Oxxius) and photons were detected with a fibered Avalanche Photodiode (APD SPCM-AQR-14-FC, Perkin Elmer) connected to an on-line hardware correlator (ALV7000-USB, ALV GmbH, Germany). Typical acquisition time was 5 min (10 × 30 s) with an excitation power of 1.1 μW at the sample level. The data were analyzed using the PyCorrFit software (Müller et al., 2014).

MemBright Labeling of Cells

Sub-confluent cells in 10cm culture dishes were rinsed twice with warm serum free medium and then incubated for 30 minutes at 28°C (Zmel1 cells) or at 37°C (4T1 cells) with MemBright quickly diluted in serum free medium (200nM final). To eliminate all possible traces of unbound MemBright, cells were then rinsed three times with serum free medium, rinsed with EDTA and trypsinated. Cells were then either injected in zebrafish embryos, seeded in a triple flask for EV production, or seeded in glass bottom microwell dishes (MatTek Corporation) pre-coated with fibronectin from bovine plasma at 10μg/ml (Sigma F-1141) for imaging.

Intravascular Injection of Zebrafish Embryo

At 48h post-fertilization (hpf), zebrafish embryos were dechorionated and mounted in 0.8% low melting point agarose pad containing 650 μM of tricaine (ethyl-3-aminobenzoate-methanesulfonate) to immobilize them. Pre-labelled EVs, polystyrene beads (Phosphorex) or tumors cells were injected with a Nanoject microinjector 2 (Drummond) and microforged glass capillaries (25 to 30 μm inner diameter) filled with mineral oil (Sigma). 27,6 nL of a EV, beads or cell suspension (at 100.10^6 cells) per ml were injected into the duct of Cuvier of the embryos under the M205 FA stereomicroscope (Leica), as previously described (Follain et al., 2018b; Stoletov et al., 2010). For the priming experiments, 32hpf embryos were injected with either Zmel1 EVs or 100nm polystyrene beads (together with fluorescent dextran to assess the efficiency of injection). 14h post-injection, embryos were injected in the circulation with Zmel1 tdTomato tumor cells. Larvae were grown for a week and imaged at 7 days post-injection. For late endosome/lysosome labeling, embryos were incubated with Lysotracker Deep Red (Thermo Fisher Scientific) diluted at 5μM in Danieau 0,3X medium for 2 hours at 28°C before injection.

Confocal Imaging and Analysis

Confocal imaging was alternatively performed with an inverted TCS SP5 with HC PL APO 20X/0,7 IMM CORR CS objective (Leica) or an upright SP8 confocal microscope with a HC FLUOTAR L 25X/0,95 W VISIR objective (Leica). For high speed imaging of EVs in the blood flow, embryos were imaged right after injection; acquisitions were done at 80-100 frames per second for 1 minute, using the resonant scanner in a single Z plane, with an opened pinhole of more than 1 airy unit. To identify the cell types uptaking EVs, the caudal plexus region of mpeg1:GFP, mpo:GFP or Fli1a:GFP was imaged 3h post-injection with a z-step of 1 μm. To quantify the proportion of EVs arrested in the dorsal aorta *vs* venous plexus regions, images were acquired similarly in Fli1:GFP embryos. For each case, quantification is described in the next paragraphs. To image the dynamics of macrophage protrusions, short time lapses of mpeg1:GFP embryos were acquired at 5 to 10 Z stacks per minute (z-step of 0,5 μm, stack covering the macrophage). To image the dynamics of macrophages, long time lapses of mpeg1:GFP embryos were acquired at 1 Z stack per minute for one hour in (z-step of 2 μm, stack covering the venous plexus). To image the uptake of EVs by macrophage, mpeg1:GFP embryos short time lapses were generated right after injection at 3 to 8 images per second on single Z planes. Image analysis and processing were performed using Fiji (Schindelin et al., 2012) as described in the following paragraphs.

Semi-automated Method to Determine the Proportion of Internalized EVs

To determine the proportion of EVs internalized by either endothelial or macrophages, we used the Z-stacks obtained from either Fli1:GFP or mpeg1:GFP embryos injected with Zmel1-MemBright EVs. Using Fiji, we split the cell and EVs channels and merged them in a single RGB image. From the merged channel, we made a binary stack followed by a Z-projection with maximal intensity. We used this as a reference image where all the EVs and cells are apparent. After normalizing this image to 1 we multiplied each stack (respectively EVs and Cell) by this projection. In both stacks, we thus kept only the positions that colocalize either with the EV position or the Cells position (all other positions possess a null value). We then made a binary from the Cell stack, applied close and dilated before normalizing it to 1. The multiplication of this stack with the EV one lead to a new stack that keeps only the particle enclosed in

the cellular compartments. Getting back to the Cell stack, we apply an inversion of the intensity values before substracting 254. The resulting stack was then multiplied by the EV stack and the created new stack let only apparent the EVs that did not colocalize with the cells. Further analyses of the intensities from the two stacks allowed us to access the ratiometric values of EVs uptaken by the different cell lines.

Quantification of EVs in Aorta vs Vein Regions

Each region (dorsal aorta and venous plexus) was manually delimited on Z-projections, using vessels visible in Fli1:GFP channels. Total EV intensity was then measured in each region and reported to the area. A ratio of EV fluorescence in the venous plexus over dorsal aorta was then measured for each fish.

Flow Analysis for Red Blood Cells

Flow analysis of red blood cells

We first globally enhanced the contrast of the whole stack. Then we performed a Z-projection with the average intensity and subtracted the obtained image to the stack. The remaining stack exhibits only the moving objects i.e. the red blood cells in this case. Then we applied a binarisation to the stack before applying a bandpass filter with the correct values to remove the background noise and keeping only the flowing blood cells. This stack was then further analyzed with the Mosaic 2D/3D particle tracker plugin. We thus accessed the positions of each blood cell for the different frames and we computed the velocities of each individual track.

Flow Analysis of EVs

Time-lapses of EVs were first thresholded and binarized. We then inverted the stack before running the 2D spot enhancing Filter plugin. We used the resulting stack to perform a second binarisation and then launched the Mosaic 2D/3D particle tracker plugin. We thus accessed the positions of each EV for the different frames and we computed the velocities of each individual track

EVs and RBCs Distance and Velocity from the Endothelial Barrier

In order to access to the distance of the EVs or red blood cells to the endothelial barrier, we first drew the endothelial wall using the transmitted light and extracted its coordinates to a table. From the analysis described in the previous paragraph, we extracted the coordinates and the velocity EVs and red blood cells. We ran a macro where we compared for all the position X_{EV} and Y_{EV} of the EV the closest position X_{endo} and Y_{endo} by comparing all the possible distances d by calculating :

$$d = \sqrt{(x_{EV} - x_{endo})^2 + (y_{EV} - y_{endo})^2}$$

and keeping the smallest distance.

This allowed us to plot the EV or the red blood cells velocities as a function of the distance from the endothelial wall.

Sample Preparation for Correlative Light and Electronic Microscopy of ZF Embryos

Correlative Light and Electron Microscopy was performed as previously described (Goetz et al., 2014; Karreman et al., 2016a). Transgenic mpeg1:GFP embryos were injected with MemBright-Cy3 4T1 EVs and imaged alive with a Leica SP8 confocal microscope (see "Confocal imaging and analysis section"). Z stack was performed on two patrolling macrophages having uptaken EVs. After imaging, the embryo was chemically fixed with 2,5% glutaraldehyde and 4% paraformaldehyde in 0.1 M Cacodylate buffer (the fish tail was cut off in the fixative). The sample was kept in fixative at room temperature for 1-2h and stored in fixative at 4°C overnight or until further processing. The sample was rinsed in 0.1M Cacodylate buffer for 2x5min and post-fixed using 1% OsO4 in 0.1 M Cacodylate buffer, for 1h at 4°C. Then, sample was rinsed for 2x10 min in 0.1M Cacodlyate buffer and secondary post-fixed with 4% water solution of uranyl acetate, 1h at room temperature. Rotation was used at all steps of sample processing. Followed by 5 min wash in MiliQ water, the sample was stepwise dehydrated in Ethanol (25%, 50% each 15min, 95%, 3X100% each 20 min) and infiltrated in a graded series of Epon (Ethanol/Epon 3/1, 1/1, 1/3, each 45 min). Sample was left in absolute Epon (EmBed812) overnight. The following day, sample was placed in a fresh absolute Epon for 1h and polymerized (flat embedded) at 60°C for 24-48h. Once polymerized, most surrounding Epon was cut off using razorblade and sample was mounted on empty Epon blocks (samples flat on the top of the blocks) and left at 60°C for 24h-48h. Samples were attached to an imaging pin with dental wax and mounted into the Brukker Skyscan 1272 for microCT imaging. Data were acquired over 188° with 0.2° angular step and a pixel size of 9 μm. Karreman et al. thoroughly details the process of how the microCT data enables the correlation of fluorescent imaging to 3D EM of voluminous samples (Karreman et al., 2016a). Retrieval of the region of interest is described in Figure S4. The region of interest was targeted by ultramicrotome, sections stained with toluidine blue and compared with the MicroCT and LM datasets. After targeting, serial 70nm sections were collected in formvar coated slot grids. The sections were post stained with uranyl acetate (4%) and lead citrate. The sections were imaged in a Biotwin CM120 Philips (FEI) TEM at 80kV with a SIS 1K KeenView. Stitches of the 70 sections were aligned using the Track EM plugin in Fiji (Cardona et al., 2012). Segmentation and 3D reconstruction were done using the IMOD software package (Boulder Laboratory, University of Colorado) and Amira.

Please cite this article in press as: Hyenne et al., Studying the Fate of Tumor Extracellular Vesicles at High Spatiotemporal Resolution Using the Zebrafish Embryo, Developmental Cell (2019), https://doi.org/10.1016/j.devcel.2019.01.014

QUANTIFICATION AND STATISTICAL ANALYSIS

Statistical Tests

Statistical analysis of the results was performed using the GraphPad Prism program version 5.04. The Shapiro-Wilk normality test was used to confirm the normality of the data. The statistical difference of Gaussian data sets was analyzed using the Student unpaired two-tailed t test, with Welch's correction in case of unequal variances. For data not following a Gaussian distribution, the Mann-Whitney test was used. Illustrations of these statistical analyses are displayed as the mean +/- standard deviation (SD). p-values smaller than 0.05 were considered as significant. *, $p<0.05$, **, $p < 0.01$, ***, $p < 0.001$, ****, $p < 0.0001$.

Zebrafish Experiments

Measurements of EVs displacement in the dorsal aorta and in the caudal vein of zebrafish embryos (Figures 3B–3E) was performed on four zebrafish embryos. Measurements of EV uptake in aorta versus venous plexus was repeated three times (n=17; Figure 4B). Comparison of the uptake of beads, AB9 EVs and Zmel1 EVs by endothelial cells (n=20, 24 and 11 respectively; Figure 4C) and macrophages (n=28, 21 and 19 respectively; Figure 5C) was repeated three times each. The correlation between Zmel1 uptake intensity and macrophages perimeter was done on 73 macrophages (13 embryos; Figure 5B). The velocity of non-injected macrophages was measured on 35 macrophages (6 embryos; Figure 5E). The colocalization between uptaken EVs and lysotracker in macrophages at 10 min and 3h post-injection was performed on 61 and 54 puncta, respectively (n=6 and 7 fish, respectively; Figure 6D). The dynamics of macrophages injected with either beads or Zmel1 EVs was measured on 27 and 47 macrophages, respectively (5 and 8 embryos; Figure 8A). The activation of M1 macrophages after beads or Zmel1 EVs injection was repeated twice (n=38 and 28 fish, respectively; Figures 8B and 8C). The metastatic outgrowth of Zmel1 cells in zebrafish embryos injected with either beads or Zmel1 EVs was repeated five times (n=55 and 57 fish, respectively; Figure 8D).

EVs Experiments

Measurements of the diameters of Zmel1 EVs (Figure 1B) and Zmel1 EVs labeled with MemBright (Figure 2E) by NTA was repeated three times. Analysis of Zmel1 EVs (Figures 1C and 2D) and Zmel1 EVs labeled with MemBright (Figure 2D) by TEM was repeated each three times (n= 871 and 356, respectively). Spectroscopic analysis of PKH and MemBright labeled EVs (Figure 1B) was performed once, at different concentrations. Measurements of the fluorescence of PKH or MemBright labeled EVs was repeated three times (Figures S2A and S2B). The number of puncta measured is indicated in the graph bars. The density gradient isolation of EVs was repeated twice (Figure S1F). The measurements of the apparent EV diameter Vs beads diameter by confocal was repeated three times *in vitro* and *in vivo* (Figure S2). The number of individual puncta measured is indicated in the graphs. Mass spectrometry of EVs was performed on triplicates (Figure 1E; Table S1).

DATA AND SOFTWARE AVAILABILITY

The proteomics data have been deposited on Exocarta. All relevant data regarding the EVs experiments have been deposited on the EV-TRACK knowledgebase (EV-Track ID:EV180078) (Van Deun et al., 2017).

Developmental Cell, Volume *48*

Supplemental Information

Studying the Fate of Tumor Extracellular Vesicles at High Spatiotemporal Resolution Using the Zebrafish Embryo

Vincent Hyenne, Shima Ghoroghi, Mayeul Collot, Joanna Bons, Gautier Follain, Sébastien Harlepp, Benjamin Mary, Jack Bauer, Luc Mercier, Ignacio Busnelli, Olivier Lefebvre, Nina Fekonja, Maria J. Garcia-Leon, Pedro Machado, François Delalande, Ana Amor López, Susana Garcia Silva, Frederik J. Verweij, Guillaume van Niel, Farida Djouad, Héctor Peinado, Christine Carapito, Andrey S. Klymchenko, and Jacky G. Goetz

Supplementary figure legends

Supplementary Figure 1 (Related to Figure 2): Analysis of MemBright labeled EVs (A) Histograms showing a spectroscopy analysis of MemBright and PKH describing the absorbance (left, y axis) and the fluorescence intensity (right, y axis) versus the wavelength (nm, x axis) of the two probes in water or methanol. The presence of aggregates of PKH in water is visible. Arrows indicate the presence of PKH aggregates in labeled EVs (left) as well as in control PKH alone (right). **(B)** Histograms showing the absorbance (left, y axis) and the normalized absorbance (right, y axis) of Zmel1 or 4T1 EVs labeled with PKH or MemBright versus the wavelength (nm, x axis). PKH aggregates are denoted with an arrow. **(C)** Histograms showing the intensity of the emitted fluorescence (left, y axis) and the normalized fluorescence intensity (right, y axis) of Zmel1 or 4T1 EVs labeled with PKH or MemBright versus the versus the wavelength (nm, x axis). PKH fluorescent aggregates are denoted with an arrow. **(D)** Representative fluorescent images of Zmel1 EVs labeled with PKH (at 2µM) or MemBright (at 200nM) and histogram showing the relative fluorescent intensity of individual puncta (p=0,001; Mann-Whitney test). **(E)** Representative fluorescent images of 4T1 EVs labeled with PKH (at 200nM) or MemBright (at 200nM) and histogram showing a higher fluorescent intensity of Zmel1-MemBright individual puncta compared to Zmel1-PKH puncta (p<0,0001; Mann-Whitney test). **(F)** Western blot on EVs labeled with MembrightCy3, or MemBright alone, separated on a density gradient (Left). It shows the presence of Alix and TSG-101 in the fractions 5-10 exclusively. No signal is observed in the control MemBright alone. Representative fluorescent images at low (upper) and high (lower) magnifications of the same samples than the western blots (right). Fluorescent MemBrightCy3 puncta accumulate in fractions 5-10.

Supplementary Figure 2 (Related to Figure 3): Characterization of MemBright EVs *in vivo*. (A) Representative confocal images of Zmel1 EVs labeled with MemBright-Cy5 and incubated with 100nm red fluorescent polystyrene beads *in vitro*. **(B)** Representative confocal Z projections of *Tg(pu1:GFP)* (lymphoid, monocytes/macrophages) embryos co-injected with Zmel1 EVs labeled with MemBright-Cy5 and with 100nm red fluorescent polystyrene beads imaged 3 hours post-injection. **(C)** Single plane zoom on embryos co-injected with Zmel1 EVs labeled with MemBright-Cy5 and with 100nm red fluorescent polystyrene beads. **(D)** Histogram showing the apparent diameters (left, nm) of MemBright labeled Zmel1 EVs and 100nm beads measured in confocal images *in vitro* and *in vivo* in zebrafish embryos (*in vitro*: p<0,0001; *in vivo*: p=0,6; Mann-Whitney test). **(E)** Confocal images from three different Z planes of Zmel1 EVs labeled with MemBright-Cy5 and incubated with human red blood cells *in vitro* for 10 minutes. **(F)** Confocal images from rapid time-lapses of *Tg(Gata1:RFP; Fli1:GFP)* embryos injected with MemBright-Cy5 labeled Zmel1 EVs, showing examples of EVs far (upper panel) or close (lower panel) from RBCs in the circulation. **(G)** Representative confocal Z projections of *Tg(Fli1:GFP)* embryos co-injected with Zmel1 EVs labeled with MemBright-Cy3 and with 4T1 EVs labeled with MemBright-Cy5. **(H)** Representative confocal single planes from a time-lapse imaged right after injection of *Tg(Fli1:GFP)* embryos co-injected with Zmel1 EVs labeled with MemBright-Cy3 and with 4T1 EVs labeled with MemBright-Cy5. **(I)** Time projection over 10 seconds of a time-lapse

imaged right after injection of *Tg(Fli1:GFP)* embryos co-injected with Zmel1 EVs labeled with MemBright-Cy3 and with 4T1 EVs labeled with MemBright-Cy5.

Supplementary Figure 3 (Related to Figure 4): Control Zebrafish embryo injected with MemBright-labeled EVs or with control MemBright alone. Representative confocal Z-projections of *Tg(mpeg1:GFP)* (macrophages) embryos injected with either 4T1 EVs labeled with MemBright-Cy3 or with MemBright-Cy3 without EVs and imaged 3 hours post injection.

Supplementary Figure 4 (Related to Figure 5): Retrieval of the cells by CLEM and the putative journey of EVs in macrophages by electron microscopy (A) *Tg(mpeg1:GFP)* embryos were injected with 4T1 MemBright-Cy3 labeled EVs and imaged by confocal (upper panels). The upper right panel shows the position of the Region Of Interest (ROI) containing the two target cells, with respect to several embryonic landmarks imaged by confocal at low magnification. The lower left image shows the tail of the embryo after fixation and resin embedding imaged by microCT. The lower right image shows the position of the ROI in an electron microscopy section. **(B)** Higher magnification of the ROI imaged by confocal and electron microscopy. Common features between transmitted light in the living fish and electron microscopy on fixed fish are highlighted to allow a precise positioning of the ROI. The electron microscopy panel is stitched together from several individual images to allow a larger region to be visualized with better resolution. The asterisk points to a dirt speck on the EM section. **(C)** Electron microscopy images of EVs observed in the lumen of the vessel, in the close proximity of protrusions extending from the macrophage plasma membrane, which were identified by CLEM. **(D)** Electron microscopy images of putative EVs present in early endosomes close to the surface of macrophages. **(E)** Electron microscopy images of putative EVs present in MVBs.

Supplementary Figure 5 (Related to Figure 7): 4T1 CD63-GFP cells pre-labeled with MemBright. (A) Representative confocal images of 4T1 CD63-GFP cells labeled with MemBright-Cy3 at different times before and after MemBright addition. **(B)** Zooms on confocal images of 4T1 CD63-GFP cells labeled with MemBright-Cy3 at 3h and 24h after MemBright addition. **(C)** Representative images of EVs isolated from the extracellular medium of 4T1 CD63-GFP cells pre-labeled with MemBright-Cy3.

Supplementary tables

Table 1 (Related to Figure 1): proteins identified in EVs by mass spectrometry (A) proteins identified in EVs isolated from Zmel1 zebrafish melanoma cells (page 1-20); **(B-G)** proteins identified in EVS isolated from human melanoma 451-LU cells (page 21-68) **(B)**, SK-Mel28 cells (page 69-125) **(C)**, SK-Mel147 cells (page 126-167) **(D)**, SK-Mel103 cells (page 168-215) **(E)**, WM35 (page 216-258) **(F)** and WM164 cells (page 259-307) **(G)**; **(H-J)** proteins identified in EVs isolated from mouse melanoma B16-F0 cells (page 308-322) **(H)**, B16-F1 cells (page 323-349) **(I)** and B16-F10 cells (page 350-364) **(J)**; **(K)** proteins common to zebrafish, mouse and human melanoma EVs (page 365-367); **(L)** proteins common to Zmel1 EVs and AB9 EVs (page 368-371); **(M)** proteins common to Zmel1 EVs and YSL CD63-GFP positive EVs (page 372).

Table 2 (Related to Figure 2): Quantum yield of MemBright and PKH labeled EVs.

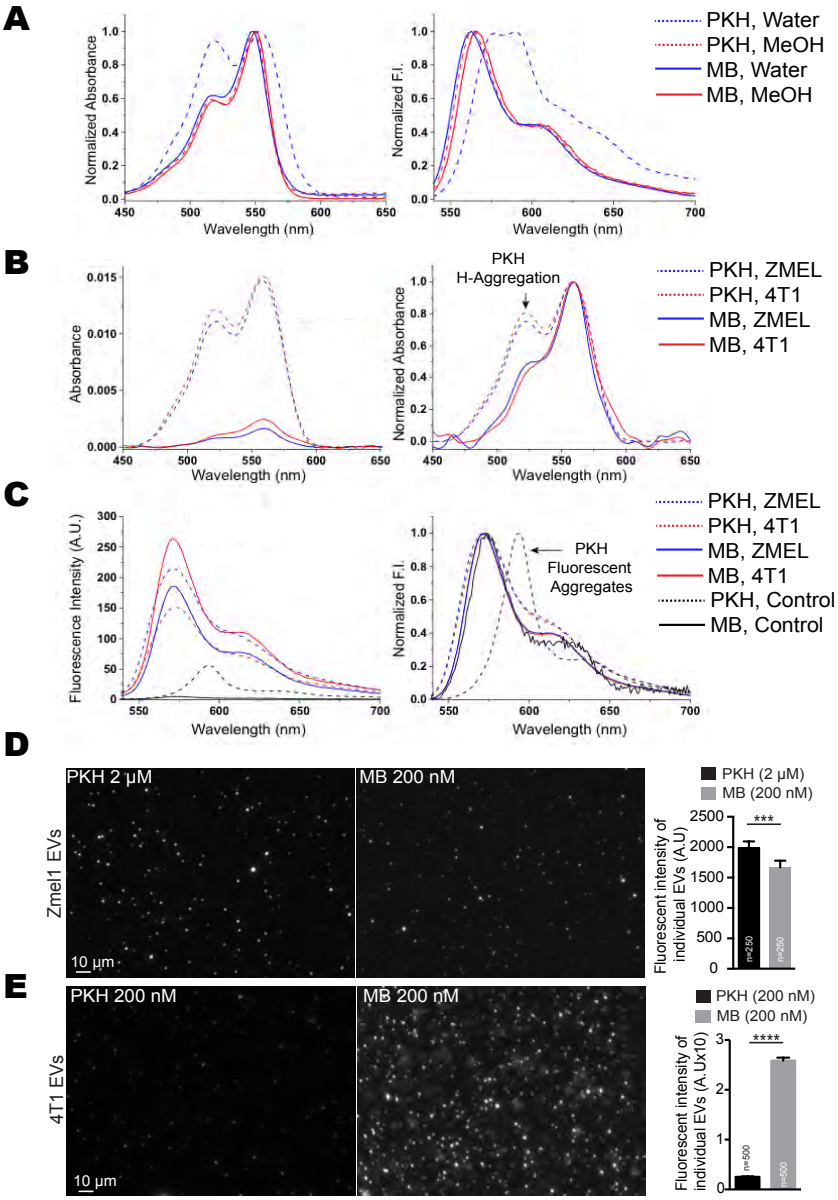

Supplementary Figure 1_Hyenne et al.

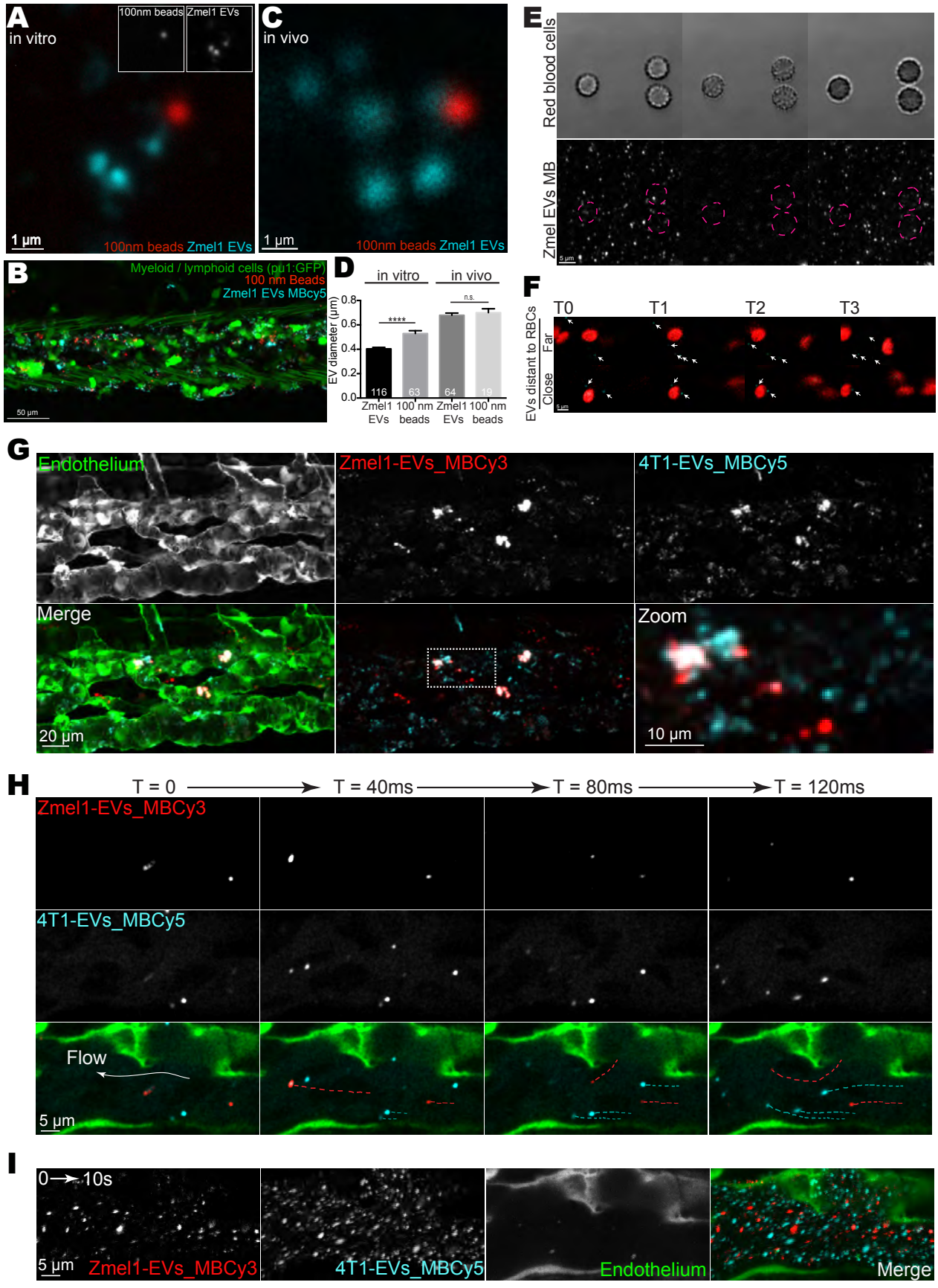

Supplementary Figure 2_Hyenne et al.

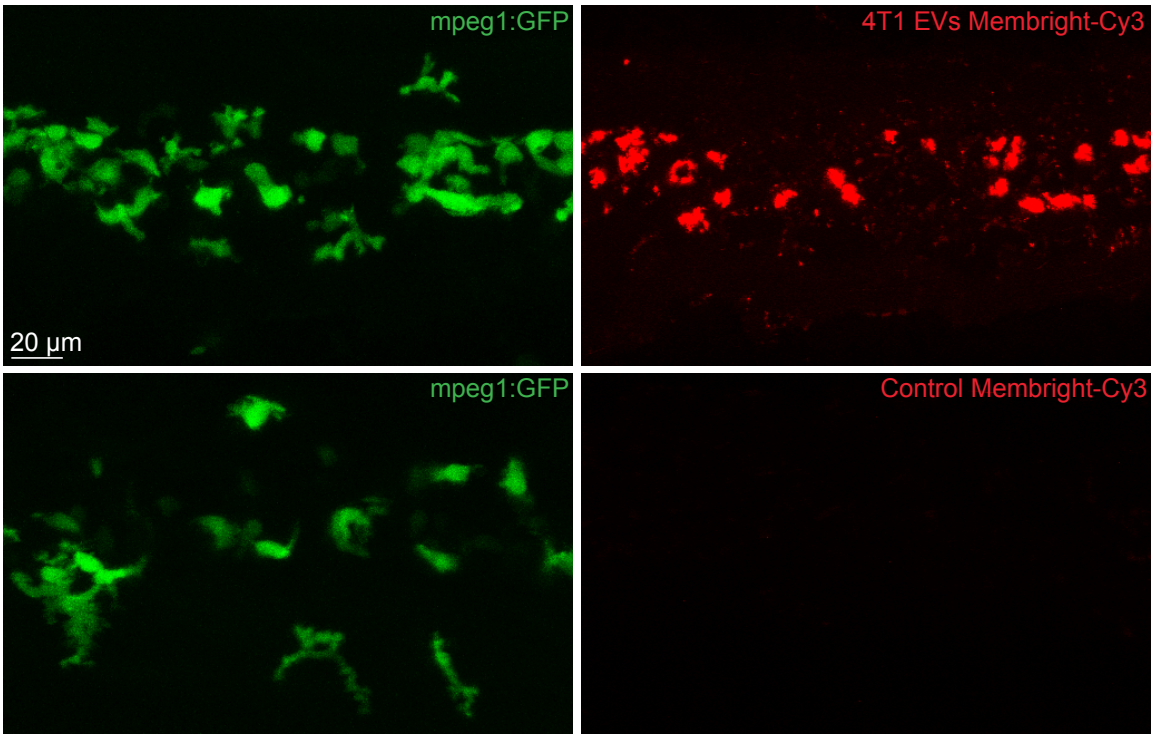

Supplementary Figure 3_Hyenne et al.

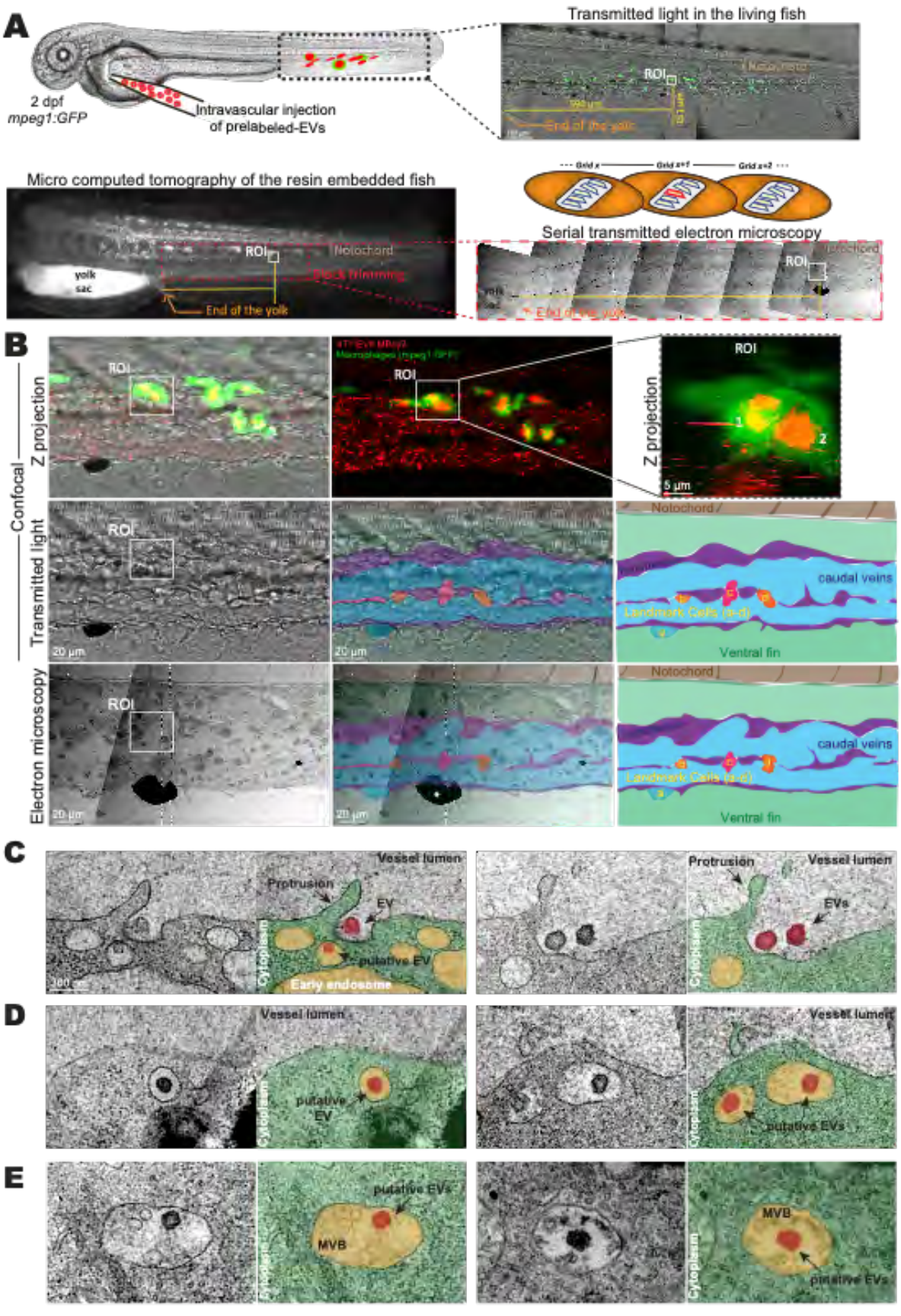

Supplementary Figure 4_Hyenne et al.

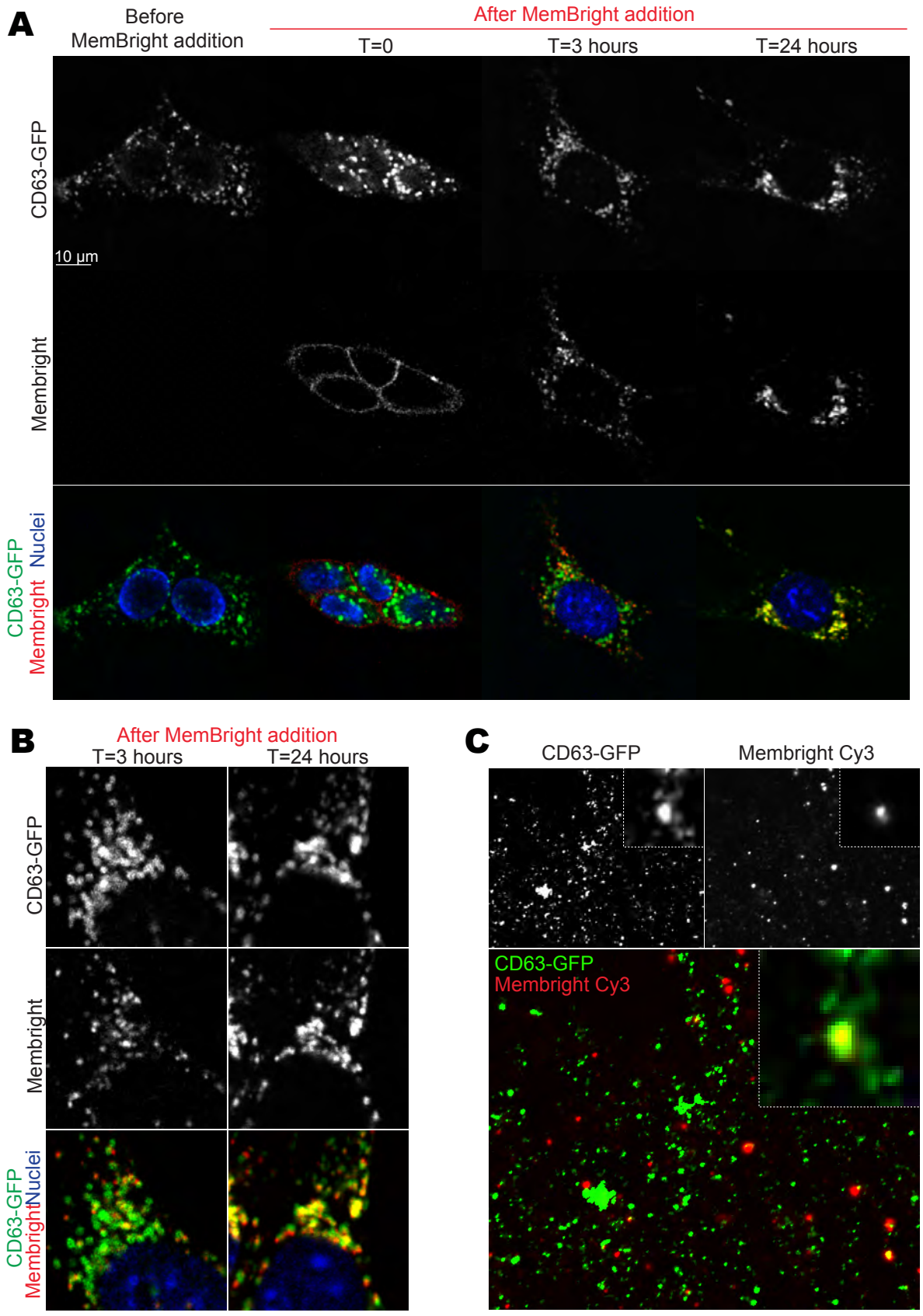

Supplementary Figure 5_Hyenne et al.

Table S2, related to Figure 2 : Photo-physical properties of labelled EVs.

	λ Abs (nm)	FWHM Abs (nm)	λ Em (nm)	FWHM Em (nm)	QY (ϕ)
PKH 4T1	559[a]	72	574	47	0.02
PKH Zmel1	558[a]	71	572	50	0.04
MB 4T1	559	42	572	33	0.42
MB Zmel1	560	42	571	34	0.41

[a] A second H-aggregation peak was observed at 522nm.

Université de Strasbourg

Benjamin MARY

École Doctorale des Sciences de la Vie et de la Santé STRASBOURG

Disséquer l'impact des forces hémodynamiques dans l'internalisation, le destin et la fonction des vésicules extracellulaires tumorales circulantes

Résumé

Parmi les multiples messagers sécrétés par une tumeur, les vésicules extracellulaires tumorales (VEt) sont connues pour modifier l'environnement des organes à distance de leur lieu de sécrétion. Via leur dissémination par le sang, elles favorisent la croissance de tumeurs secondaires (métastases) au sein de l'organisme. Néanmoins, le rôle du flux sanguin et des forces hémodynamiques dans ce modèle est mal connu. Mon travail de thèse montre qu'une vitesse de flux modérée, présente dans les petits vaisseaux (e.g. les vénules/capillaires), favorise l'internalisation des VEs tumorales par les cellules des parois vasculaires (les cellules endothéliales) et modifie leur destin intracellulaire. Elles sont redirigées vers des compartiments moins acides, échappent ainsi en partie à la dégradation et favorisent une activité pro-angiogénique localement. In fine, ce mécanisme dépendant du flux pourrait être impliqué dans les processus de formation des métastases médiés par les VEs tumorales.

Mots clés :

Vésicules extracellulaires, cancer, métastases, hémodynamique, endolysosomes

Résumé en anglais

Tumor masses secrete plethora of molecular and cellular messengers that mediate tumor growth. Among them, tumor Extracellular Vesicles (tEVs) are known to modify distant microenvironment and participate to the formation of pre-metastatic niche, a favorable soil for metastasis development. tEVs disseminate via the vascular system, nonetheless, the role of blood flow and hemodynamic forces in this model is not known. My work shows that moderate flow speed similar to what is measured in venule and capillaries, enhances tEVs internalization in endothelial cells and modifies their intracellular fate. tEVs are redirected toward less acidic and less degradative compartments. This redirection allows part of internalized tEVs to avoid degradation and favors a pro-angiogenic activity. Finally, this newly identified flow-dependent mechanism could participate to tEV-mediated metastasis formation.

Keywords :

Extracellular vesicles, cancer, metastasis, hemodynamic, endolysosomes